Experimental Investigation into the Cyclic Response of A1085 HSS Braces

Joe Kaldestad

A thesis
submitted in partial fulfillment of the
requirements for the degree of

Master of Science in Civil Engineering

University of Washington
2022

Reading Committee:

Dawn E. Lehman

Jeffrey W. Berman

Charles W. Roeder

Program Authorized to Offer Degree:
Civil and Environmental Engineering

University of Washington

Abstract

Experimental Investigation into the Cyclic Response of A1085 HSS Braces

Joe Kaldestad

Co-Chairs of the Supervisory Committee:

Professor Dawn E. Lehman
Civil and Environmental Engineering

Professor Jeffrey W. Berman
Civil and Environmental Engineering

Concentrically braced frames (CBFs) are commonly used as the seismic force-resisting system in buildings, where the ordinary (OCBFs) and special concentrically braced frames (SCBFs) provide moderate and high ductility, respectively. In both OCBFs and SCBFs, the braces are the primary yielding component and square HSS sections are commonly used for braces. One of the most important design constraints to provide ductility is the upper limit on the width to thickness ratio, *b/t*, for braces. Prior research has verified that braces that meet the highly-ductile *b/t* limit for ASTM A500 square HSS braces have the required stable cyclic behavior and strength for SCBFs. In 2013, a new specification for square HSS was introduced: ASTM A1085 which has tighter control on material properties and dimensions. As a result, A1085 HSS have smaller width-to-thickness ratios than the same nominal A500 HSS section. Previous research has used A1085 HSS braces within a full SCBF and identified that they may have increased ductility relative to A500. To understand the full benefits of A1085 braces, a multi-phase, large-scale testing program of full-size braces subjected to cyclic loading was undertaken. Ten reference A500 HSS braces were tested along with 31 A1085 HSS braces. In

the initial phase of the study, the response of the A500 and A1085 sections was compared; the response of the two brace types was similar. A second phase was conducted to study the impact of geometric and material properties, steel type, HSS producer, and loading protocol for the A1085 sections alone. The *b/t* ratios ranged from 9 to 25.7; the global slenderness ratios ranged from 60 to 127. As such, most of the studied braces met the compactness limits for OCBFs, some met the limits for SCBFs and others did not meet either. The structural response of each brace specimen was quantified using the axial deformation range, the equivalent story-drift range, and energy dissipation capacity. The findings indicate that deformability of the brace, and therefore the frame, is determined by the local compactness and global slenderness ratios. Specifically, deformability increased with smaller local compactness ratios and larger global slenderness ratios. Current design provisions do not recognize the interdependence of the story drift capacity on both the local compactness and global slenderness. Evaluation of the current local slenderness limits for SCBFs and OCBFs showed that the current highly ductile limit is sufficient, but the moderately ductile limit is too conservative. The brace response did not depend on HSS producer, toughness, or type (A500 or A1085). The story-drift range was independent of load history, while the maximum deformation in either direction (tension or compression) does depend on the load history.

TABLE OF CONTENTS

Chapter 1. Introduction 1

1.1 Background and Motivation 1
1.2 Research Objectives 5
1.3 Document Overview 5

Chapter 2. Literature Review 7

2.1 Introduction 7
2.2 Design Requirements for Braces in CBFs 7
2.3 Cyclic Testing and Behavior of Steel Bracing Members 9
2.4 Experimental Investigation to Compare the Cyclic Response of A500 and A1085 HSS Braces (Bergendahl, 2021) 17
2.5 Summary of Findings 22

Chapter 3. Test Setup And Specimen Design 23

3.1 Introduction 23
3.2 Test Setup Overview 23
3.3 Test Specimen Design 38
3.4 Test Specimen Properties 46
3.5 Loading Protocol 71
3.6 Test Instrumentation 75
3.7 Pre-Testing Procedure 80

Chapter 4. Experimental Results 82

4.1 Introduction 82
4.2 Test Results 84

Chapter 5. Data Analysis And interpretation 116

5.1 Introduction 116
5.2 Data Processing 116
5.3 A1085 Test Comparisons 120
5.4 Summary of Findings 149

Chapter 6. Evaluation of Design Provisions and Performance-based engineering tools 151
6.1 Introduction 151
6.2 Evaluation of the Requirements for Braces AISC 341-16 Seismic Provisions 151
6.3 Evaluation of AISC 342 Nonlinear Models for Braces 156
Chapter 7. Summary, Conclusions, and Future Work 180
7.1 Summary 181
7.2 Conclusions 183
7.3 Recommendations for Future Work 184
Appendix A. Test Setup & Specimen Drawings 188
Appendix B. Sample Calculations 195
Appendix C. Appendix 3: Material properties 216
Appendix D. MATLAB SCRIPTS 224
Appendix E. Additional Tables and Figures 231
Appendix F. Brace Test Reports 238

LIST OF FIGURES

Figure 1.1. Concentrically Braced Frame Configurations (Sabelli et al., 2013) 1
Figure 1.2. Progression of Brace Deformation and Damage at Center 2
Figure 2.1. Hysteretic Behavior of Chevron 3 (A1085) and Chevron 5 (A500) 10
Figure 2.2 Chevron 4 Measured Brace Axial Force vs. Axial Deformation 11
Figure 2.3. Test Frame and Loading Sequence.....12
Figure 2.4. Comparison of Energy Dissipation Capacity 13
Figure 2.5. Comparison of RHS Seismic Performance 14
Figure 2.6. Loading Protocol: (a) Standard and (b) Compression Dominated 15
Figure 2.7. Effect of Local Compactness on Fracture Drift and Energy Dissipation.....16
Figure 2.8 Series 1 Symmetric Displacement Protocol 18
Figure 2.9 Axial Displacement Range vs. Local Compactness (Bergendahl, 2021).....20
Figure 2.10 Axial Displacement Range vs. Global Slenderness (Bergendahl, 2021) 21
Figure 3.1. Overview of Test Frame for 237.5" Specimens 25
Figure 3.2. Overview of Test Frame for 165.5" Specimens 26
Figure 3.3. Configuration of Test Frame for 237.5" Brace Specimen.....27
Figure 3.4 Configuration of Test Frame for 183.5" Brace Specimen.....27
Figure 3.5. Layout of South End of Test Frame 28
Figure 3.6. End Reaction Block – Before (a) and After (b) Being Moved Into Place.....28
Figure 3.7. Orientation of Actuators and Sliding Beam 29
Figure 3.8. Layout of Actuators and Sliding Beam 30
Figure 3.9. Actuator Base Plate Design 31
Figure 3.10. Actuator Assembly and Connections 32
Figure 3.11 Sliding Beam - Original (a) and In Upright Position (b).....33
Figure 3.12 Sliding Beam Dimensions 33
Figure 3.13 Cross-Sectional View of Sliding Beam and Vertical Restraint System 34
Figure 3.14. Keyway Plate Dimensions (a) and Keyway Plate Welded in Place (b) 35
Figure 3.15. Sliding Beam Connection Plate - During Testing (a) and Elevation (b).....36
Figure 3.16. End Connection Plate Details.....37
Figure 3.17 Configuration of South Connection with Added Reaction Block.....38
Figure 3.18 Test Specimen Layout 43

Figure 3.19 Gusset Plate Design - General 45
Figure 3.20 Net Section Reinforcement at End Connection 45
Figure 3.21. Range of Global Slenderness and Local Compactness Ratios 49
Figure 3.22. Ratio of Measured to Nominal Wall Thickness – A1085 Specimens 51
Figure 3.23 Ratio of Measured to Nominal Wall Thickness – A500 Specimens 52
Figure 3.24 Producer Comparison of Measured Thickness – A1085 52
Figure 3.25. Measured Yield Strength Ratios – A1085 Specimens 58
Figure 3.26 Measured Yield Strength Ratios – A500 Specimens 59
Figure 3.27 Producer Comparison of Yield Strength – A1085 HSS 60
Figure 3.28 Measured Ultimate Tensile Strength Ratios – A1085 Specimens 62
Figure 3.29 Measured Ultimate Tensile Strength Ratios – A500 Specimens 62
Figure 3.30 Producer Comparison of Tensile Strength – A1085 HSS 63
Figure 3.31 Measured ultimate-to-yield strength ratio – A1085 Specimens 64
Figure 3.32 Measured ultimate-to-yield strength ratio – A500 Specimens 65
Figure 3.33 Producer Comparison of Percent Elongation 65
Figure 3.34 Modified CVN Toughness – A1085 Specimens 68
Figure 3.35 Modified CVN Toughness – A500 Specimens 69
Figure 3.36. Symmetric Displacement Protocol 72
Figure 3.37 Chevron Displacement Protocol 73
Figure 3.38 Near Fault Tension Dominant Displacement Protocol 73
Figure 3.39 Short Brace Symmetric Displacement Protocol 74
Figure 3.40. String (a and b) and Duncan Potentiometers (c) 76
Figure 3.41. String Potentiometer Layout 76
Figure 3.42. Duncan Potentiometer Layout 78
Figure 3.43. Strain Gauge Layout 78
Figure 3.44. Optotrak LED Layout 79
Figure 3.45. Test Specimen Prior to Welding (a) and Fully Welded (b) 80
Figure 4.1 Assumed Brace Configuration in Chevron 85
Figure 4.2 Brace Hysteretic Response: 5x5x3/8 A1085 R 95
Figure 4.3 Brace Hysteretic Response: 5x5x3/8 A1085 W 96
Figure 4.4 Brace Hysteretic Response: 5x5x3/8 A1085 B 97

Figure 4.5 Brace Hysteretic Response: 6x6x3/8 A1085 R 98
Figure 4.6 Brace Hysteretic Response: 6x6x3/8 A1085 W 99
Figure 4.7 Brace Hysteretic Response: 6x6x3/8 A1085 B 100
Figure 4.8 Brace Hysteretic Response: 8x8x3/8 A1085 R 101
Figure 4.9 Brace Hysteretic Response: 8x8x3/8 A1085 W 102
Figure 4.10 Brace Hysteretic Response: 8x8x3/8 A1085 B 103
Figure 4.11 Brace Hysteretic Response: 8x8x1/2 A1085 R 104
Figure 4.12 Brace Hysteretic Response: 8x8x1/2 A1085 W 105
Figure 4.13 Brace Hysteretic Response: 8x8x1/2 A1085 B 106
Figure 4.14 Brace Hysteretic Response: 5x5x3/8 A1085 Y Chevron 107
Figure 4.15 Brace Hysteretic Response: 5x5x3/8 A1085 Y Near Fault 108
Figure 4.16 Brace Hysteretic Response: 7x7x3/8 A1085 Y Chevron 109
Figure 4.17 Brace Hysteretic Response: 7x7x3/8 A1085 Y Near Fault 110
Figure 4.18 Brace Hysteretic Response: 8x8x3/8 A1085 Y Chevron 111
Figure 4.19 Brace Hysteretic Response: 8x8x3/8 A1085 Y Near Fault 112
Figure 4.20 Brace Hysteretic Response: 5x5x3/8 A1085 Y Short 113
Figure 4.21 Brace Hysteretic Response: 7x7x3/8 A1085 Y Short 114
Figure 4.22 Brace Hysteretic Response: 8x8x3/8 A1085 Y Short 115
Figure 5.1 Examples of (a) Raw and (b) Processed LabVIEW Data.....117
Figure 5.2 Effects of String Potentiometer Rigid-Body Rotation (a) original position (b) rotated position.....118
Figure 5.3 Original (Blue), Corrected (Red), and Total (Green) Axial Displacement 119
Figure 5.4 Producer Comparison of Normalized Axial Deformation Range 124
Figure 5.5 Producer Comparison of Accumulated Axial Deformation 125
Figure 5.6 Producer Comparison of Normalized Energy Dissipation 126
Figure 5.7 Effect of Displacement Protocol on Normalized Axial Deformation Range 128
Figure 5.8 Effect of Displacement Protocol on Story Drift Range.....129
Figure 5.9 Effect of Displacement Protocol on Normalized Energy Dissipation.....130
Figure 5.10 Axial Deformation Range vs. Measured Yield Strength Ratio 131
Figure 5.11 Axial Deformation Range vs. Measured Ultimate-to-Yield Strength Ratio 131
Figure 5.12 Axial Deformation Range vs. Unmodified CVN Toughness.....132

Figure 5.13 Axial Deformation Range vs. Local Compactness – Long Braces 134
Figure 5.14 Axial Deformation Range vs. Local Compactness – Short Braces 135
Figure 5.15 Axial Deformation Range vs. Measured Local Compactness, b_{nom}/t_{meas} 136
Figure 5.16 Axial Deformation Range vs. Measured Local Compactness, $(b/t)_{meas}$ 136
Figure 5.17 Story Drift Range vs. Local Compactness 137
Figure 5.18 Maximum Story Drift vs. Local Compactness 138
Figure 5.19 Axial Deformation at Local Cupping vs. Local Compactness 139
Figure 5.20 Accumulated Axial Deformation vs. Local Compactness 140
Figure 5.21 Normalized Energy Dissipation vs. Local Compactness 141
Figure 5.22 Axial Deformation Range vs. Global Slenderness 142
Figure 5.23 Story Drift Range vs. Global Slenderness 143
Figure 5.24 Maximum Story Drift Range vs. Global Slenderness 144
Figure 5.25 Axial Deformation at Local Cupping vs. Global Slenderness 144
Figure 5.26 Accumulated Axial Deformation Range vs. Global Slenderness 145
Figure 5.27 Normalized Energy Dissipation vs. Global Slenderness 146
Figure 5.28 Global Slenderness vs. Local Compactness vs. Axial Deformation Range 148
Figure 5.29 Global Slenderness vs. Local Compactness vs. Story Drift Range 148
Figure 5.30 Global Slenderness vs. Local Compactness vs. Maximum Story Drift 149
Figure 6.1 Story Drift Range vs. Normalized Width-to-Thickness Ratio 153
Figure 6.3 Story Drift Range vs. Global Slenderness 153
Figure 6.4 Global Slenderness vs. Local Compactness with Story Drift Range Indicated: A1085 Specimens 155
Figure 6.5 Global Slenderness vs. Local Compactness with Story Drift Range Indicated: A500 Specimens 155
Figure 6.6 Generalized Brace Force-Deformation Response (AISC, Draft 2021) 156
Figure 6.7 Backbone Curve – 5x5x3/8 A500 Y 161
Figure 6.8 Backbone Curve – 5x5x3/8 A1085 Y 161
Figure 6.9 Backbone Curve – 5x5x3/8 A1085 W 162
Figure 6.10 Backbone Curve – 5x5x3/8 A1085 B 162
Figure 6.11 Backbone Curve – 5x5x3/8 A1085 R 162
Figure 6.12 Backbone Curve – 6x6x5/16 A500 R 162

Figure 6.13 Backbone Curve – 6x6x5/16 A1085 Y 162
Figure 6.14 Backbone Curve – 6x6x3/8 A500 R.....162
Figure 6.15 Backbone Curve – 6x6x3/8 A1085 Y 163
Figure 6.16 Backbone Curve – 6x6x3/8 A1085 R.....163
Figure 6.17 Backbone Curve – 6x6x3/8 A1085 W.....163
Figure 6.18 Backbone Curve – 6x6x3/8 A1085 B.....163
Figure 6.19 Backbone Curve – 6x6x1/2 A500 R.....163
Figure 6.20 Backbone Curve – 6x6x1/2 A1085 Y 163
Figure 6.21 Backbone Curve – 7x7x5/16 A500 Y 164
Figure 6.22 Backbone Curve – 7x7x5/16 A1085 Y 164
Figure 6.23 Backbone Curve – 7x7x3/8 A500 Y 164
Figure 6.24 Backbone Curve – 7x7x3/8 A1085 Y 164
Figure 6.25 Backbone Curve – 7x7x1/2 A500 B.....164
Figure 6.26 Backbone Curve – 7x7x1/2 A1085 Y 164
Figure 6.27 Backbone Curve – 8x8x3/8 A500 W.....165
Figure 6.28 Backbone Curve – 8x8x3/8 A1085 Y 165
Figure 6.29 Backbone Curve – 8x8x3/8 A1085 R.....165
Figure 6.30 Backbone Curve – 8x8x3/8 A1085 W.....165
Figure 6.31 Backbone Curve – 8x8x3/8 A1085 B.....165
Figure 6.32 Backbone Curve – 8x8x1/2 A500 W.....165
Figure 6.33 Backbone Curve – 8x8x1/2 A1085 Y 166
Figure 6.34 Backbone Curve – 8x8x1/2 A1085 R.....166
Figure 6.35 Backbone Curve – 8x8x1/2 A1085 W.....166
Figure 6.36 Backbone Curve – 8x8x1/2 A1085 B.....166
Figure 6.37 Backbone Curve – 10x10x3/8 A500 W.....166
Figure 6.38 Backbone Curve – 10x10x3/8 A1085 Y 166
Figure 6.39 Backbone Curve – 5x5x3/8 A1085 Y-S.....167
Figure 6.40 Backbone Curve – 7x7x3/8 A1085 Y-S.....167
Figure 6.41 Backbone Curve – 8x8x3/8 A1085 Y-S.....168
Figure 6.42 Backbone Curve – 5x5x3/8 A1085 Y-C 169
Figure 6.43 Backbone Curve – 7x7x3/8 A1085 Y-C 169

Figure 6.44 Backbone Curve – 8x8x3/8 A1085 Y-C 169
Figure 6.45 Backbone Curve – 5x5x3/8 A1085 Y-NF 170
Figure 6.46 Backbone Curve – 7x7x3/8 A1085 Y-NF 170
Figure 6.47 Backbone Curve – 8x8x3/8 A1085 Y-NF 170
Figure 6.48 Predicted vs. Measured Tensile Deformation Capacity 174
Figure 6.49 Predicted vs. Measured Compressive Deformation Capacity 174
Figure 6.50 Predicted vs. Measured Deformation Range Capacity 175

LIST OF TABLES

Table 1.1. Comparison of HSS Specifications....3
Table 1.2. Width-to-thickness limits for HSS with different steels....4
Table 2.1 Brace Requirements in Braced Frames (Hsiao, 2012)....8
Table 2.2 Test Specimens – Test Series 1....17
Table 2.3 Summary of Series 1 Test Specimens Performance....19
Table 3.1 Available HSS Shapes....39
Table 3.2 Test Specimens – Test Series 1....39
Table 3.3 Test Specimens – Test Series 2....40
Table 3.4 Test Specimens – Test Series 3....41
Table 3.5. Expected Tensile and Compressive HSS Member Capacity....42
Table 3.6. Gusset Plate and Fillet Weld Design....44
Table 3.7 Net Section Reinforcement Design....46
Table 3.8. Test Specimen Width-to-Thickness Ratios....47
Table 3.9 Test Specimen Global Slenderness Ratios....48
Table 3.10. Wall Thickness Measurements....50
Table 3.11 Summary of Wall Thickness Ratios....53
Table 3.12. Measured and Nominal Local Slenderness Ratios....55
Table 3.13. Material Properties from Tension Coupon Testing....57
Table 3.14 Summary of Measured Yield Strengths....61
Table 3.15 Summary of Measured Tensile Strengths....64
Table 3.16. Charpy V-Notch Test Results....67
Table 3.17 Summary of Measured Unmodified Charpy V-Notch Data....70
Table 4.1. Brace Performance States....83
Table 4.2 Summary of Nominal and Measured Geometric Properties....87
Table 4.3 Summary of Material Properties....88
Table 4.4 Summary of Expected and Measured Loads....89
Table 4.5 Summary of Test Specimen Performance....90
Table 4.6 Summary of Measured Axial Deformation Limits....94

Table 5.1 Summary of Test Specimen Performance – Series 1 (Bergendahl, 2021).....121
Table 5.2 Summary of Test Specimen Performance – Series 2, 3, & 4.....122
Table 5.3 Summary of Brace Axial Deformation Ranges 124
Table 5.4 Summary of Accumulated Axial Deformations 125
Table 5.5 Summary of Energy Dissipation Capacities 126
Table 6.1 Test Specimen Modeling Parameters 158
Table 6.2 Comparison of Predicted and Measured Brace Axial Deformation 171
Table 6.3 Summary of Measured and Predicted Behavior 173
Table 6.7 Modified Equations for Calculation of n-factor in AISC 342 Nonlinear Model.....178
Table 6.8 RMSE of Modified Models 179
Table 7.1 Summary of Experimental Test Specimens.....182

Acknowledgements

I would like to start by acknowledging my advisors, Professors Dawn Lehman, Jeffrey Berman, Charles Roeder, and Andrew Sen for providing me with the opportunity and funding for this research. Thank you all for being reliable sources of knowledge and advice throughout the many phases of this project. Your guidance and feedback for this thesis was invaluable.

Most of my time on this project was spent in the lab and I would like to thank everyone that helped me with construction and testing. First, I am extremely grateful for lab manager and professional jerry-rigger, Vince Chaijaroen, who is a master of all things mechanical, electrical, and hydraulic. He taught me many skills and made the lab a fun workplace. A huge thank you also goes to Will Bergendahl, who I worked alongside throughout construction and the first series of testing. His work ethic is admirable and greatly appreciated. Additionally, I am grateful for the help in the lab from fellow grad students Will Krause, Spencer Lindsley, and Austin Anderson.

Thank you to the American Institute of Steel Construction for funding this research project. Additionally, thank you to all four steel producers Atlas Tube, Nucor Tubular Products, Searing Industries, and Maruichi American Corporation for providing the materials for experimental testing.

Finally, I would like to thank my family for their constant love and support throughout all of my endeavors.

Chapter 1. INTRODUCTION

1.1 BACKGROUND AND MOTIVATION

Concentrically braced frames (CBFs) are commonly used as the seismic force-resisting system in buildings, where ordinary (OCBFs) and special concentrically braced frames (SCBFs) provide moderate and high ductility, respectively. CBF systems consist of braces, beams, and columns; the beams and columns are connected using bolted or welded beam-column joints and braces are connected at the beam-column through a gusset-plate connection. SCBFs have more stringent design requirements than OCBFs for the brace geometry and connection design. Typical configurations are shown in Figure 1.1. In SCBFs and OCBFs, HSS sections are often used as the diagonal bracing members, which act as the primary source of lateral strength, stiffness, and deformability.

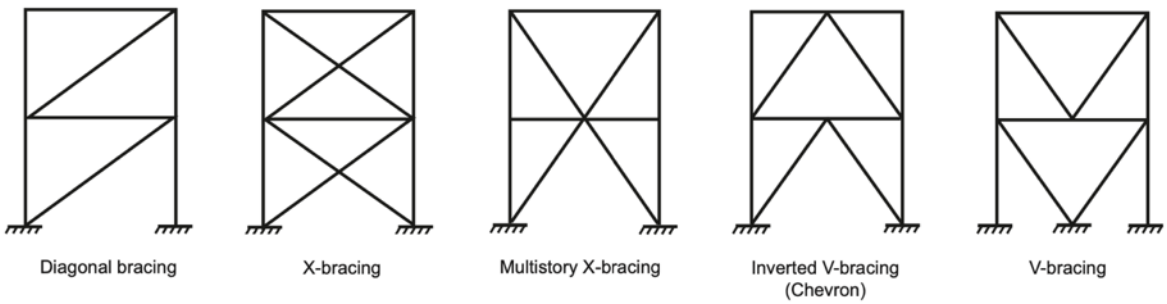

Figure 1.1. Concentrically Braced Frame Configurations (Sabelli et al., 2013)

HSS braces resist lateral loads and dissipate energy through inelastic yielding in tension and buckling in compression. As the brace experiences large axial deformations due to story drift, the brace forms a plastic hinge and develops large strains as a result of localized deformations. Once the brace develops these local deformations (often referred to as cupping), the brace is susceptible to tearing and fracture in tension. This progression of damage is shown in Figure 1.2. Preventing the formation of local deformations delays brace fracture, which improves the performance of the brace and the OCBF/SCBF. Ideally, the HSS brace will sustain large, cyclic axial deformations without local damage to maximize the system deformability. Research has shown that the local compactness ratio (b/t) and global slenderness ratio (KL/r) determine the

deformability of HSS braces. In these geometric parameters, *b* is the flat wall width, *t* is the wall thickness, *K* is the effective length factor, *L* is the brace length, and *r* is the radius of gyration. An HSS brace with low *b/t* ratio and high *KL/r* ratio exhibits greater deformability than a brace with a higher *b/t* ratio and a lower *KL/r*; the latter is more prone to premature brace fracture.

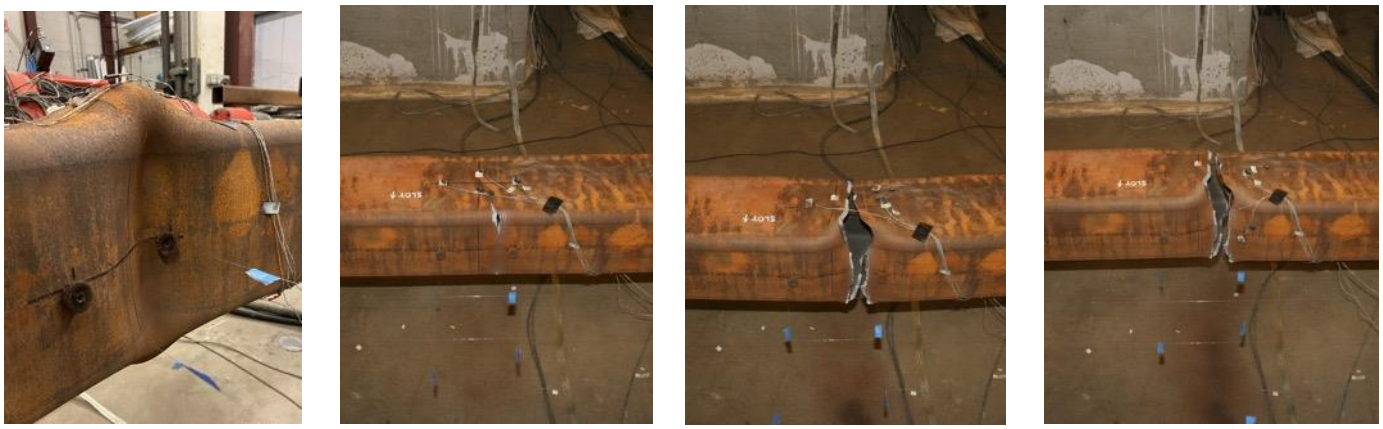

Figure 1.2. Progression of Brace Deformation and Damage at Center

Since OCBFs and SCBFs were first introduced, ASTM 500 Grade B or C have typically been used for HSS bracing members. In 2013, a new specification for HSS sections was introduced – ASTM 1085; at this time a dual grade of A500 B/C was used. The new A1085 specification is similar to A500; however, it has tighter tolerances on some geometric properties and has additional requirements for some material properties. As a result of more stringent material and geometric requirements, A1085 HSS provides various potential advantages.

Table 1.1 shows the requirements for the ASTM A500 and A1085 HSS specifications. The table shows differences in the material and geometric requirements. The A500 specification permits a minimum wall thickness of 0.9*t*. Consequently, the design thickness is reduced to 0.93*t* (AISC, 2010). The A1085 specification has a minimum wall thickness 0.95*t*; the design thickness is the full thickness of 1.0*t*. Additionally, the A1085 specification has a minimum corner radius while A500 does not. This prevents tubes with overly tight corners, which can cause cracking and limited deformability.

In addition to the minimum thickness requirements, there are differences in the maximum yield strength and CVN requirements. The A1085 specification limits the maximum yield stress to 70 ksi, while A500 does not have a maximum yield stress limit. The maximum yield stress

aims to prevent over strength and to reduce material variability. As a result of the maximum permitted yield stress, A1085 has a smaller expected yield strength ratio, R_y, than A500. A1085 also has a minimum toughness requirement which calls for a minimum Charpy V-Notch test value of 25 ft-lbs at 40^o F.

Table 1.1. Comparison of HSS Specifications

Property	ASTM A500 Gr. C	ASTM A1085
Yield Stress	50 ksi (min) No limit on max	50 ksi (min) 70 ksi (max)
Yield Strength Ratio, R_y	1.3	1.25
Tensile Stress	62 ksi (min)	65 ksi (min)
Wall Thickness Tolerance	-10%	-5%
Design Thickness	$0.93*t_{nom}$	$1.0*t_{nom}$
Mass Tolerance	N/A	-3.5%
Corner Radii	$r < 3t$	$t < 0.4$": $1.6t < r < 3t$ $t > 0.4$": $1.8t < r < 3t$
CVN Toughness	N/A	25 lb-ft at 40^o F

Today, the seismic design of SCBFs and OCBFs is provided in AISC 341-16, *Seismic Provisions for Structural Steel Buildings* (AISC, 2016). As shown in Table 1.2, AISC 341-16 provides maximum width-to-thickness limits where OCBFs are limited by the moderately ductile criteria and SCBFs are limited by the highly ductile criteria. Since the limits are a function of the expected yield strength ratio, R_y, A1085 has slightly higher values for the same equation. Additionally, the larger design thickness for A1085 results in lower *b/t* ratios than the same section of HSS A500. The combination of lower *b/t* ratios and higher *b/t* limits allows larger A1085 HSS shapes to meet the design criteria for local compactness. The ability to use larger braces, provides efficiency structurally, architecturally, and financially.

Table 1.2. Width-to-thickness limits for HSS with different steels

HSS Steel	F_y (ksi)	R_y	AISC 341-16 *b/t* Limits	
			Moderately Ductile ($0.76\sqrt{E/(R_yF_y)}$)	Highly Ductile ($0.65\sqrt{E/(R_yF_y)}$)
A500 Gr. C	50	1.3	16.1	13.7
A1085	50	1.25	16.4	14.0

Previous research has used A1085 HSS braces within a full SCBF and identified that they may have increased ductility relative to A500. Additionally, the geometric and material properties of A1085 provide potential benefits over A500. However, there is limited research on the structural performance of A1085 HSS as it is still relatively new to the market. Understanding the cyclic behavior of A1085 HSS is critical to fully realize the benefits of A1085 HSS. Furthermore, it is important that the seismic design provisions are validated for the A1085 specification.

To understand the full benefits of A1085 braces, a multi-phase, large scale testing program of full-size braces subjected to cyclic loading was undertaken. Ten reference A500 HSS braces were tested along with 31 A1085 HSS braces. The study examined square HSS of various sizes and lengths with a keen eye towards the effect of the following parameters: (1) HSS specification (A500 vs. A1085), (2) local slenderness ratio, *b/t*, (3) global slenderness ratio, *KL/r*, (4) displacement history, and (5) HSS producer. Previous testing has shown that the deformability of HSS braces is strongly related to the *b/t* and *KL/r* ratios. Consequently, a wide range of HSS sizes were selected based on these factors and were provided by four different steel HSS producers. The specimens tested included members both meeting and exceeding the current compactness limits. The test frame – designed and built at the UW SRL – consisted of two hydraulic actuators acting in parallel, with a combined capacity of 1000 kips in tension, 700 kips in compression and axial displacement range of ±10 inches. The test frame was able to accommodate a range of HSS sizes and was designed to test a range of specimen lengths.

The experimental testing was organized into four test series, each focused on studying specific brace parameters. Series 1 consisted of twenty brace tests – ten A500 HSS braces and ten A1085 braces. The purpose of this series was to examine the effect of *b/t* and *KL/r*, and compare the performance of A500 and A1085 HSS under cyclic loading. The results from Series

1 were presented and analyzed by Bergendahl (2021) and will be incorporated in the data analysis chapter of this document. In Test Series 2, 3, and 4, the primary brace parameters were HSS producer, displacement history, and global slenderness, respectively. This document presents the experimental data from Test Series 2, 3, and 4, and includes data from all four test series in analysis and discussions of design implications.

1.2 Research Objectives

The Goal of this thesis is to evaluate the performance of A1085 HSS for CBFs through an extensive experimental research program. The objectives of this research project are as follows:

- Compare the structural response of A500 and A1085 HSS subjected to cyclic loading through component testing (completed by Bergendahl (2021)).
- Examine the material and geometric properties of A500 and A1085 HSS through material testing of HSS members.
- Compare the properties and structural response of A1085 HSS from different producers.
- Investigate the effects of local slenderness and global slenderness on brace behavior.
- Investigate the effect of displacement history on the structural performance of A1085 HSS.
- Evaluate the AISC 341-16 design provisions for HSS braces in CBFs.
- Evaluate performance-based engineering tools used to model the inelastic behavior of HSS braces.

1.3 Document Overview

This document describes a multiphase experimental research program which investigates the cyclic behavior of A1085 HSS braces. The following chapters are organized as follows:

- Chapter 2 provides background information for this research, including a discussion of the A1085 specification and requirements for SCBFs. This chapter also includes a review

of literature describing previous experimental research on the inelastic response of steel HSS under cyclic loading.

- Chapter 3 provides an overview of the test frame constructed for this project, as well as a description of the specimens tested. The instrumentation and testing procedure is also presented in this chapter.
- Chapter 4 provides the measured results and visual performance observations from each test in Test Series 2, 3, and 4.
- Chapter 5 provides analysis of the experimental data. First, the data is processed to fundamental responses including deflections, local forces, local deformations and other important experimental data for each specimen. Then the performance of the test series are analyzed, assessed, and compared. The effects of the various test parameters are evaluated in this chapter.
- Chapter 6 evaluates current design provisions and performance-based engineering tools. The design and evaluation of braces in AISC 341-16 and AISC 342-22, respectively, are investigated using experimental data from all test series conducted as part of research program.
- Chapter 7 provides a summary of and conclusions of the research program; and recommendations for future work.

Chapter 2. LITERATURE REVIEW

2.1 INTRODUCTION

This chapter will provide a background on CBFs and a review of previous research projects to provide the motivation for this project. Section 2.2 provides a background on the history and evolution of CBFs and discusses the current design requirements for OCBFs and SCBFs. Section 2.3 describes in summary, the experimental setup, test results, and conclusions of previous related research that informed the design and implementation of the research program in this thesis. The reviews provided here will summarize the research and findings; additional depth on some previous research can be found in Bergendahl (2021). Section 2.4 will provide a summary of the results and findings from Bergendahl (2021), which was Series 1 of this same research project. The same test frame at the UW SRL was used for each testing series in this research program. The experimental results and data analysis presented later will build on the results presented by Bergendahl (2021).

2.2 DESIGN REQUIREMENTS FOR BRACES IN CBFS

Braces in OCBFs and SCBFs are the primary source of lateral force resistance and energy dissipation. The brace is designed to act as the "fuse" by exhibiting ductile behavior through adequate inelastic deformation during the event of an earthquake. This is achieved by designing a brace that can withstand yielding in tension and buckling in compression at adequate story drifts without brace fracture. This design approach aims to concentrate the inelastic damage within the brace. The principle of capacity design is to design the other members to remain elastic in an event where the brace develops its maximum force. Although it is not explicitly considered in design, SCBFs may also exhibit additional yielding in the beams, columns, and gusset plates.

This principle of capacity-based design was introduced in the 1988 Uniform Building Code (ICBO, 1988). Prior to this, components within braced frames were designed for the expected seismic loads without consideration of brace capacity. This prior approach creates systems less capable of ductile behavior, which can result in failure at low deformations. If such failure occurs prior to inelastic deformations in the brace, the system is incapable of dissipating energy and withstanding lateral loads. Additionally, there were no design requirements for the

geometry of the brace which is now controlled by compactness and slenderness requirements. The design requirements for braces in CBFs are presented in Table 2.1.

Table 2.1 Brace Requirements in Braced Frames (Hsiao, 2012)

Component	**Non-Seismic CBFs** (R = 3)	**OCBFs** (R = 3.25)	**SCBFs** (R = 6)
Brace Global Slenderness	No limit	$KL/r < 4\sqrt{E/F_Y} \approx 100$	$KL/r < 200$
Brace Local Slenderness	No limit	Compactness ratio < λ_{md}	Compactness ratio < λ_{hd}
Net Section	Design for factored loads	Design for factored loads	Design for $R_yF_yA_g$ of brace
Brace Connection Design	Design for factored loads	Design for minimum of $R_yF_yA_g$ of brace or amplified seismic load	Design for $R_yF_yA_g$ and $1.1R_yP_n$ of brace & permit end rotation of brace

The design requirements for braced frames are intended to ensure ductile behavior in the event of an earthquake. In OCBFs and SCBFs, there are design requirements for the brace as well as the connections and the surrounding members which must carry the expected brace forces. The ductility of the brace is primarily dependent on the brace global and local slenderness. Brace global slenderness is quantified by the global slenderness ratio, *KL/r*, while brace local slenderness is quantified by the compactness ratio (also known as the width-to-thickness ratio), *b/t*. Braces with low compactness ratios have been shown to exhibit much greater ductility than those with high ratios. Braces with high compactness ratios tend to develop local damage and fracture at much lower drift demands. This effect is represented in the current code by the limits for compactness ratios shown in Table 1.2. These were determined through research which showed that braces with compactness ratios larger than these limits are unlikely to withstand the drift demands in a large earthquake (Fell et al., 2009). The compactness limits are dependent on the expected yield stress, R_yF_y, of the brace. The two steel HSS specifications used today, A500 and A1085, have a nominal yield stress of 50 ksi, however, A1085 has a lower R_y due to a maximum yield strength requirement. The R_y value for A1085 is 1.25, while that of A500 is 1.3. The lower R_y value for A1085 produces compactness limits which are slightly higher than those for A500. The increased compactness and tighter wall thickness tolerance for

A1085 HSS permits larger HSS sections to be used for OCBFs and SCBFs. The ability to use larger braces can lead to more efficient lateral systems which is beneficial structurally and architecturally.

The deformability of the brace is also dependent on the global slenderness ratio, *KL/r*. Braces with larger global slenderness ratios generally provide more ductility because brace buckling remains elastic at larger story drifts. This effect, however, is not represented in the code. There is a design requirement stating that the global slenderness ratio must not exceed 200, however this is not intended to ensure greater ductility but rather to prevent unbalanced forces caused by very slender bracing members within SCBFs (AISC, 2016). Increased slenderness decreases the compressive capacity of the brace which can lead to an inefficient design because SCBFs are designed to provide lateral resistance through the deployment of compression and tension braces in pairs. Therefore, the slenderness ratio for braces in practice are not likely to approach such a high value as 200.

Ductility in an SCBF is also provided by the connections which are typically designed to allow for rotations under brace buckling. In this case, the gusset plates connecting the brace to the frame must be designed to permit the formation of plastic hinges to allow this rotation. The connection detailing requirements improve the inelastic deformation capacity of SCBFs therefore improving the performance. Alternatively, the brace connections can be designed as fully restrained moment connections however this is less common and is primarily in cases where large compressive resistance is necessary. Either method is required to provide connections capable of developing the expected brace forces.

2.3 Cyclic Testing and Behavior of Steel Bracing Members

This section will review previous experimental research programs that influenced the research in this thesis. The papers reviewed motivated the testing and influenced the design of the test frame and test specimens. As stated in Section 2.1, the major points from each paper will be provided here, however, more detailed reviews, findings, and commentary can be found in Bergendahl (2021).

2.3.1 *Effect of Beam Yielding on Chevron Braced Frames (Roeder et al., 2019)*

Six single story chevron SCBFs were tested in this research program to investigate the effect of beam strength in chevron configured SCBFs. The program studied braced frames with different beam strengths to understand the effect of beam yielding on the strength and drift capacity of the system under cyclic loading. Of the six braced frames tested, five used A1085 HSS braces while only one used A500 HSS braces. Chevron specimens 3 and 5 used identical configurations and were subjected to identical displacement protocols however, Chevron 3 had A1085 braces and Chevron 5 had A500 braces. The hysteretic response of these two specimens are shown in Figure 2.1 below. Chevron 3 reached a story drift range of 7.2% while chevron 5 reached a story drift range of 6.6% prior to brace fracture. Therefore, the specimen with the A1085 braces exhibited more ductility as it reached a 9% greater story drift range. The greater deformability of the A1085 braces encouraged futher testing of A1085 braces and comparison to A500. Most previous full-scale component testing of square HSS braces has been on A500 however, the lack of data for A1085 braces motivated the testing in this thesis.

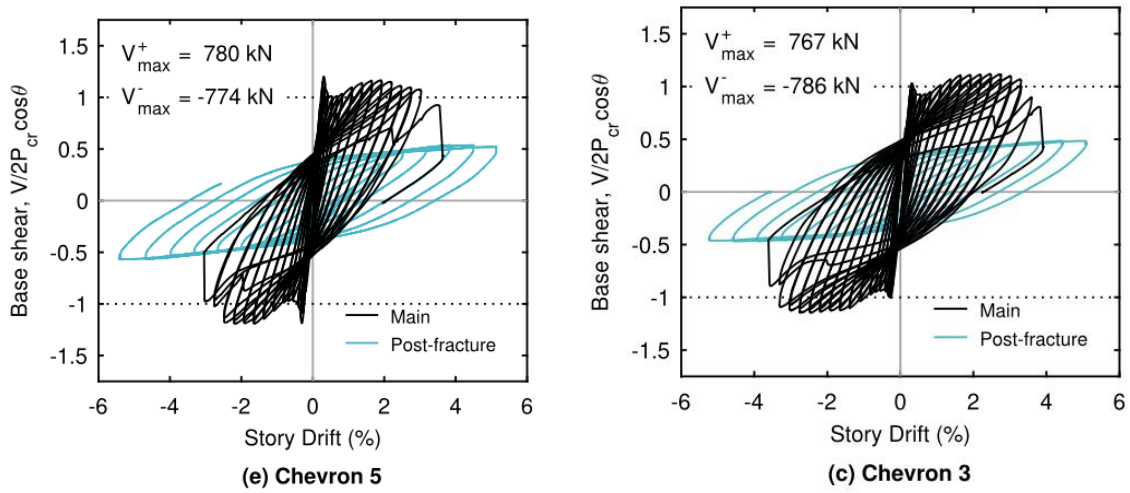

Figure 2.1. Hysteretic Behavior of Chevron 3 (A1085) and Chevron 5 (A500)

The results also indicated that chevron configured SCBFs with yielding beams reached greater story drifts than those without yielding beams prior to brace fracture. The increased downward deflection in beams resulted in increased compressive brace deformations and decreased tensile brace deformations. This effect can be seen in Figure 2.2 which provides the measured brace axial force-deformation curve for Chevron 4. Chevron 4 had the lowest beam strength and

stiffness of all six specimens. The specimen showed very little tensile brace elongation, and the maximum tensile force was approximately the same magnitude as the buckling load. This observation was the motivation behind the chevron displacement protocol formulated for the testing in this thesis.

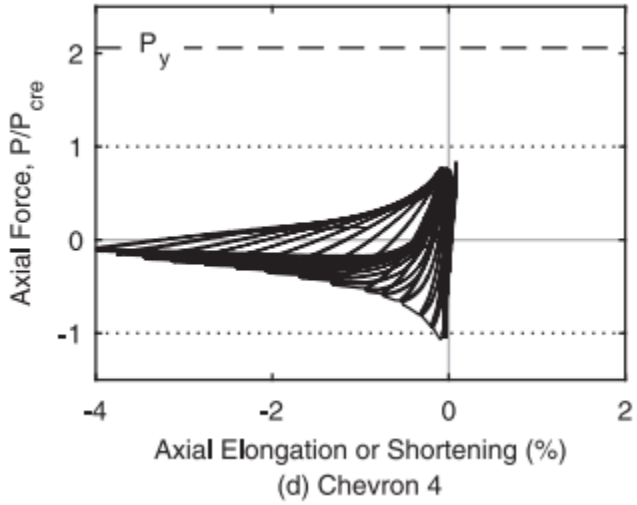

Figure 2.2 Chevron 4 Measured Brace Axial Force vs. Axial Deformation

2.3.2 *Inelastic Seismic Response of Steel Bracing Members (Tremblay, 2002)*

Trembley et al. (2002) studied the performance of steel bracing members subjected to cyclic loading to provide an understanding of the inelastic response of bracing members. The paper includes the results from 9 previous experimental programs providing a total 76 test specimens, 38 of which were rectangular A500 HSS (RHS). The RHS specimens varied in size and length to provide a range of local and global slenderness ratios. In the tests, brace damage occurred as follows: local deformations formed in the plastic hinge region under increased compressive displacement demands, followed by tearing at the corners of the cross section in the plastic hinge region, followed by tearing across the full cross-section leading to fracture. It was found that the local deformations were the first sign leading to fracture and that these local deformations were strongly influenced by the local compactness and the global slenderness.

The paper concluded that the local compactness was more critical for less slender braces and that a minimum global slenderness could improve ductility. This paper stressed the

importance of global slenderness on the ductility of RHS bracing members. It has been shown that there is a relationship between the effects of local compactness and global slenderness however there is currently no design requirement that represents this. This study provided a comprehensive review of the performance of A500 HSS, however, the A1085 specification was not established at the time and the lack of data for A1085 HSS motivated the testing in this thesis.

2.3.3 *Behaviour of Square Hollow Structural Steel Braces with End Connections Under Reversed Cyclic Axial Loading (Shaback and Brown, 2003)*

In this research study, nine square HSS specimens were tested under cyclic loading at the University of Calgary. The goal of this research was to evaluate the effects of various parameters on the ductility and seismic performance of square HSS braces. The parameters studied include local compactness, global slenderness, and end connection type. The test frame used for these experimental tests, shown in Figure 2.3 below, is similar to the setup used at the UW SRL which is described in Chapter 3.

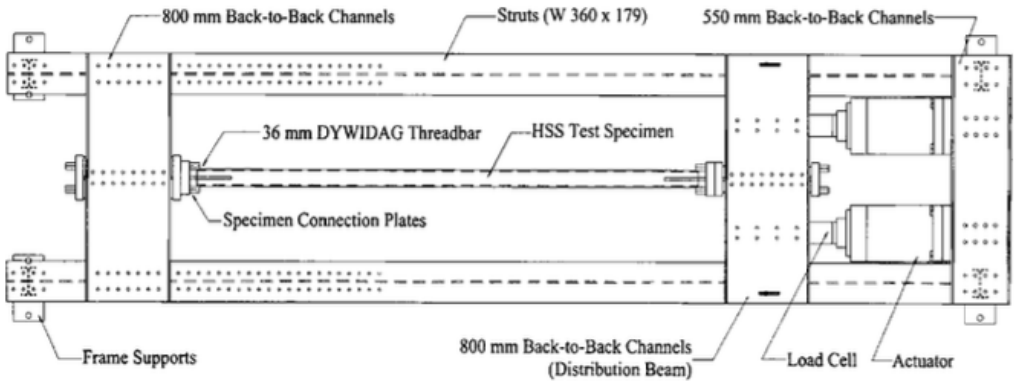

Figure 2.3. Test Frame and Loading Sequence

The results from these tests were analyzed to understand the controlling parameters of brace deformability and energy dissipation efficiency and capacity. The results showed that local compactness had the most significant effect on brace fracture life. More compact sections with lower compactness ratios developed local cupping deformations at larger axial

deformations and therefore fractured at larger deformations. Global slenderness and yield strength also affected the brace deformation capacity but to a lesser extent.

While it was concluded that brace local compactness most strongly influences fracture life, it was determined that the global slenderness ratio, *KL/r*, had the most significant influence on the hysteretic behavior. As shown in Figure 2.4 below, the hysteric responses were analyzed to assess the energy dissipation efficiency and energy dissipation capacity. The results showed that braces with lower global slenderness ratios provide more efficient energy dissipation at early cycles due to increased compressive force capacity. However, braces with higher global slenderness ratios were more ductile and could withstand more inelastic cycles, therefore providing higher energy dissipation capacities prior to brace fracture.

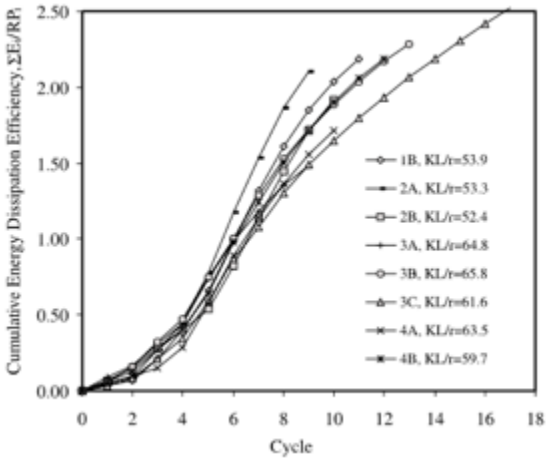

Figure 2.4. Comparison of Energy Dissipation Capacity

All of the specimens in this study were subjected to a compression dominant displacement protocol. The applied displacements may affect the performance of the brace so alternative displacement protocols should be studied to understand the effect on brace deformability and hysteretic behavior. Additionally, all of the specimens in this study met the design criteria for braced frames. Specimens that exceed the requirements should also be studied to gain a better understanding of the effects of local compactness and global slenderness.

2.3.4 *Inelastic Cyclic Testing of Large Size Steel Bracing Members (Tremblay, 2008)*

In this research project, 34 steel bracing members were tested under cyclcic loading at the Hydro-Quebec Structural Engineering Lab at Ecole Polytechnique of Montreal. Of the 34 tests, 19 test specimens were A500 rectangular HSS. The project focused on studying the behavior of stocky braces with a wide range of compactness ratios. The braces tested included sections with compactness ratios less than, equal to, and greater than the AISC highly ductile limit. The global slenderness ratios ranged from 40 to 60, which is at the stocky end of the spectrum.

Consistent with previous research, the results from these tests showed that low local compactness ratios and high global slenderness ratios lead to increased deformation capacity. The effect of these parameters is shown in Figure 2.5 below which shows the hysteretic response of three RHS specimens of different shapes. Of the three specimens shown, RHS-19 has the lowest *b/t* ratio and the highest *KL/r* ratio, and it exhibited the greatest deformability. RHS-4 had the highest *b/t* ratio and the lowest *KL/r* ratio, and it exhibited the least deformability. The research also showed that even if a brace is compliant with local compactness requirements, it may not sustain the expected seismic demands if the member is too stocky (low *KL/r*). Stocky bracing members are prone to early local cupping and fracture which can prevent the brace from achieving sufficient ductility. Current AISC design requirements do not include a minimum global slenderness ratio, but this research shows that such requirements could ensure sufficient ductility. These results were motivation for testing a wide range of *b/t* and *KL/r* ratios as part of this thesis.

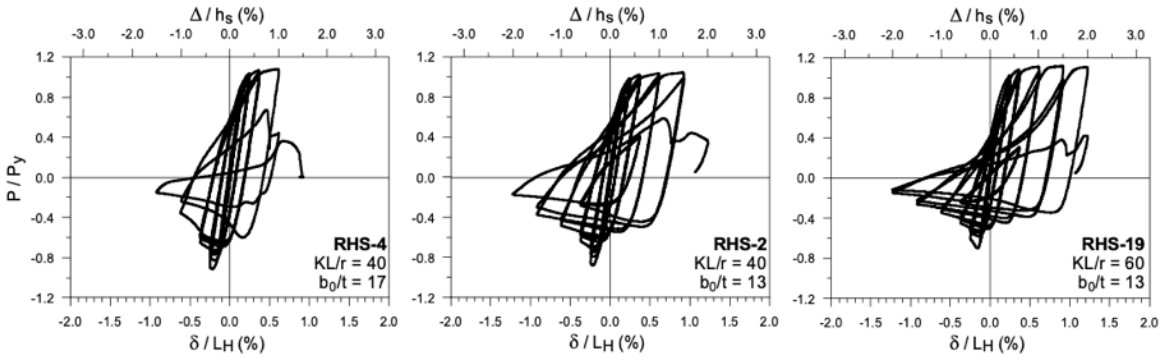

Figure 2.5. Comparison of RHS Seismic Performance

2.3.5 *Experimental Investigation of Inelastic Cyclic Buckling and Fracture of Steel Braces (Fell et al., 2009)*

In this research program, 18 steel braces were tested to investigate the inelastic behavior under cyclic loading and to evaluate the design requirements for braced frames. The experimental program studied the effects of local compactness, global slenderness, brace shape, displacement history, and load rate. Of the 18 total tests, five were hollow square HSS specimens which pertain to this thesis. Four of the hollow square HSS specimens were subjected to a symmetric cyclic loading protocol with increasing displacements, while one was subjected to a compression dominant near fault loading protocol. These loading protocols, shown in Figure 2.6, influenced the loading protocols used at the UW SRL.

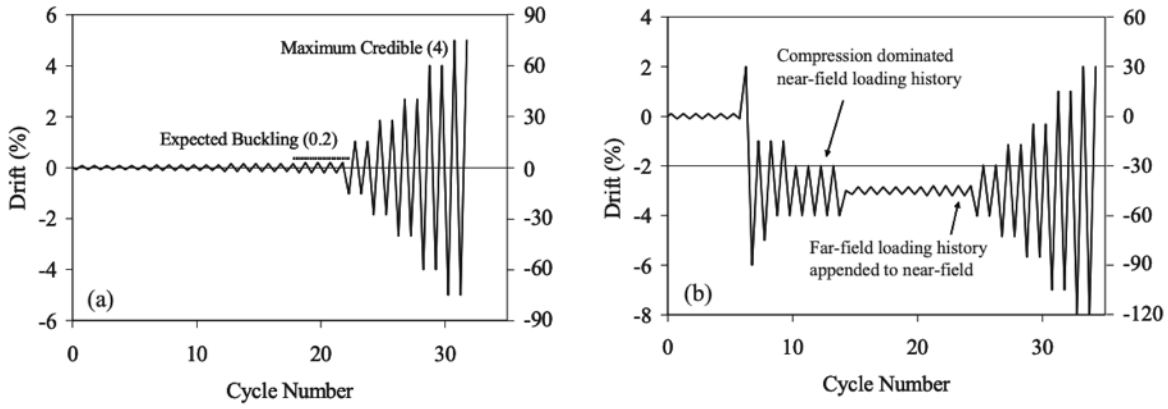

(a) (b)

Figure 2.6. Loading Protocol: (a) Standard and (b) Compression Dominated

In these tests, the brace behavior and development of damage looked generally the same as previous research except several test specimens without net section reinforcement at the end connections fractured prior to the development of local deformations in the brace. In cases where brace damage developed in the plastic hinge region, it was found that the symmetric loading protocol was more damaging than the compression dominant near fault loading protocol. However, only one test was completed using the compression dominant near fault loading protocol so the need for further research motivated the testing in this thesis.

The results from Fell et al. (2009) are shown in Figure 2.7 below, with horizontal lines at 2% and 4% story drifts. Although not explicitly stated in design provisions, it is often assumed

that SCBFs should be designed to achieve a minimum 2% drift prior to fracture. The 4% limit comes from previous research that showed braced frame drift demands may exceed 4%. The results from this research showed that not all HSS specimens which met the AISC local compactness requirements achieved a 4% drift. On the basis that braces should achieve a maximum story drift of 4%, the authors suggested that the design limits for compactness were nonconservative and that reducing the compactness limits for CBFs by 25% would ensure the capability to achieve a 4% drift. Although the research also showed improved ductility with increased global slenderness, local compactness was shown to have the most significant effect on brace ductility.

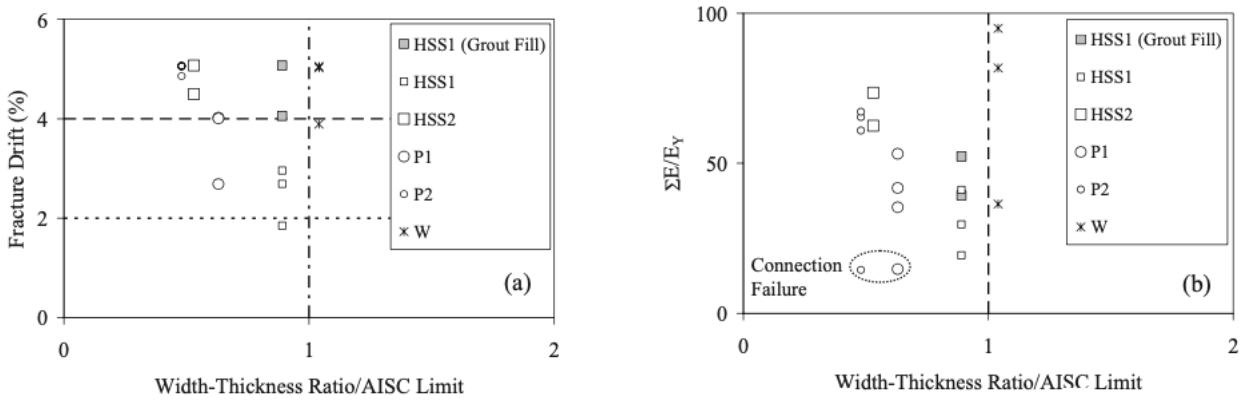

Figure 2.7. Effect of Local Compactness on Fracture Drift and Energy Dissipation

In 2010, following the results from this research and others, AISC adjusted the compactness limit for highly ductile HSS bracing members from $0.64\sqrt{\frac{E}{F_y}}$ to $0.55\sqrt{\frac{E}{F_y}}$. In 2016, the AISC width-to-thickness limits were adjusted to account for the expected yield strength of the member. AISC 341-16 provides a *b/t* limit of $0.65 \cdot \sqrt{\frac{E}{R_y F_y}}$. The inclusion of the expected strength, R_yF_y, did not change the compactness limit for A500 HSS but it does increase the limit for A1085.

2.4 EXPERIMENTAL INVESTIGATION TO COMPARE THE CYCLIC RESPONSE OF A500 AND A1085 HSS BRACES (BERGENDAHL, 2021)

The results presented by Bergendahl (2021) were part of the same research program as the current thesis. The research program consisted of four series of component brace tests to investigate the cyclic response of A1085 and A500 HSS braces. The first series consisted of twenty brace tests – ten A500 HSS braces and ten A1085 braces. The results from the first series were presented and analyzed by Bergendahl (2021) and will be referred to as Series 1 throughout this document. A summary of the test specimens and results from Series 1 will be provided here.

The sections tested during Series 1 are shown in green in Table 2.2 below. The purpose of this series was to compare the performance of A500 and A1085 HSS under cyclic loading. The A500 HSS braces tested were provided by four different producers, denoted by the colors in Table 2.2 (Yellow, Red, Blue, and White), while the ten A1085 HSS tested were provided by the Yellow producer.

Table 2.2 Test Specimens – Test Series 1

	ASTM A500				**ASTM A1085**
HSS Shape	**YELLOW**	**RED**	**BLUE**	**WHITE**	**YELLOW**
10x10x3/8					
8x8x1/2					
8x8x3/8					
7x7x1/2					
7x7x3/8					
7x7x5/16					
6x6x1/2					
6x6x3/8					
6x6x5/16					
5x5x3/8					

The same test setup was used for all four series and is detailed in Chapter 3. The twenty braces in Series 1 were 237.5” long and were subjected to a symmetric cyclic loading protocol with increasing displacements as shown in Figure 2.8 below. This symmetric displacement protocol was developed based on previous research at the UW SRL and recommendations for testing components of steel structures (ATC, 1992, Krawinkler, 2009). In this displacement protocol, two full cycles were conducted for each target displacement. The first six target displacements were in increments of 1/8”, starting at 0.125” and increasing to 0.75”. These small

displacements were applied to capture elastic behavior of the brace as well as initial global buckling and yielding. After the 0.75” displacements, the subsequent target displacements were increased in 0.5” increments until the specimen fractured.

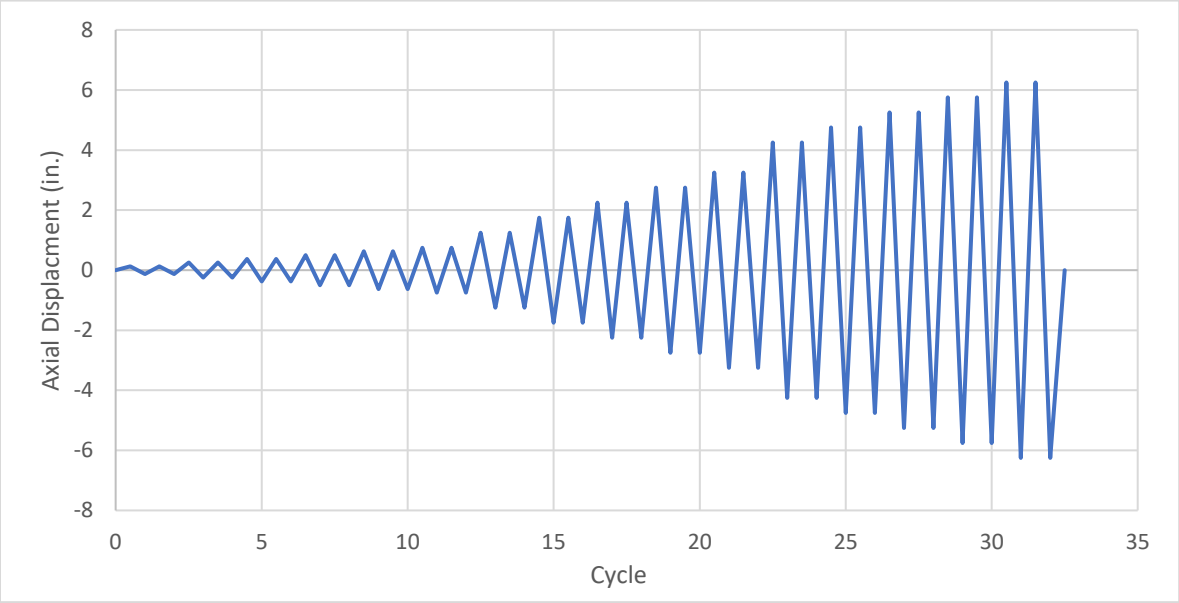

Figure 2.8 Series 1 Symmetric Displacement Protocol

A summary of the test specimen performance is shown below in Table 2.3. The table includes the maximum tensile and compressive forces, $P_{T,max}$ and $P_{C,max}$, as well as the ratio of these maximum forces to the measured yield and critical buckling forces, P_Y and P_C. These forces were calculated using the measured yield stress, $F_{y,m}$, the measured cross-sectional area, $A_{g,m}$, and the nominal *KL/r* ratio. The measured cross-sectional area, $A_{g,m,}$ was taken as the nominal area, A_g, multiplied by the ratio of measured to nominal wall thickness. Additionally, the table provides the maximum tensile and compressive axial brace deformations, $\Delta_{T,max}$ and $\Delta_{C,max}$. The deformation range, Δ_{range}, is the difference between the peak tensile and compressive deformations. Additionally, the table provides the approximate story drift percentage for each corresponding axial brace deformation. The story drifts were calculated following the procedure described in Section 4.2.1 which assumes a 45˚ brace configuration. The table also includes accumulated axial brace deformation, Δ_{Acc}, which is the summation of all of the brace axial deformations prior to fracture. Finally, the table includes the energy dissipation capacity, $\sum E_{Diss}$, normalized by the measured cross-sectional area and the measured yield strength, $A_{g,m}$ and $F_{y,m}$, respectively. Further analysis of these results will be included in Chapter 6.

Table 2.3 Summary of Series 1 Test Specimens Performance

HSS Section	$P_{T,max}$ (kips) ($P_{T,max}/P_y$)	$P_{C,max}$ (kips) ($P_{C,max}/P_{Cr}$)	$\Delta_{T,max}$ (in.) (Drift %)	$\Delta_{C,max}$ (in.) (Drift %)	Δ_{range} (in.) (Drift %)	Δ_{Acc} (in.) (Drift %)	$\frac{\sum E_{Diss}}{A_{g,m}F_{y,m}}$
5x5x3/8 A500 Y	432.50 *(1.04)*	-95.30 *(0.96)*	5.13 *(4.28)*	4.89 *(4.07)*	10.02 *(8.35)*	119.54 *(99.65)*	20.57
5x5x3/8 A1085 Y	443.60 *(1.02)*	-98.38 *(0.97)*	5.25 *(4.38)*	5.50 *(4.59)*	10.75 *(8.96)*	132.02 *(110.05)*	21.74
6x6x5/16 A500 R	409.70 *(1.06)*	-125.75 *(0.79)*	3.06 *(2.55)*	3.26 *(2.71)*	6.31 *(5.26)*	52.34 *(43.63)*	13.29
6x6x5/16 A1085 Y	456.40 *(1.07)*	139.80 *(0.87)*	3.13 *(2.61)*	3.12 *(2.60)*	6.25 *(5.21)*	51.33 *(42.79)*	12.57
6x6x3/8 A500 R	511.00 *(1.05)*	-168.70 *(0.92)*	3.74 *(3.12)*	3.72 *(3.10)*	7.46 *(6.22)*	65.80 *(54.85)*	16.45
6x6x3/8 A1085 Y	547.90 *(1.01)*	-180.00 *(0.97)*	3.52 *(2.93)*	3.52 *(2.93)*	7.04 *(5.87)*	56.61 *(47.19)*	13.63
6x6x1/2 A500 R	646.20 *(1.02)*	-218.70 *(0.98)*	4.45 *(3.71)*	4.06 *(3.39)*	8.51 *(7.10)*	80.64 *(67.22)*	17.25
6x6x1/2 A1085 Y	727.20 *(1.06)*	-218.60 *(1.00)*	4.67 *(3.89)*	5.12 *(4.27)*	9.79 *(8.16)*	97.41 *(81.21)*	22.36
7x7x5/16 A500 Y	496.60 *(1.05)*	-209.80 *(0.89)*	1.73 *(1.44)*	1.83 *(1.53)*	3.56 *(2.97)*	20.29 *(16.91)*	5.82
7x7x5/16 A1085 Y	478.10 *(1.05)*	-201.50 *(0.84)*	1.99 *(1.66)*	2.31 *(1.92)*	4.29 *(3.58)*	27.94 *(23.30)*	8.01
7x7x3/8 A500 Y	570.90 *(1.06)*	-231.80 *(0.87)*	2.51 *(2.09)*	2.79 *(2.33)*	5.30 *(4.42)*	35.26 *(29.40)*	10.49
7x7x3/8 A1085 Y	615.90 *(1.07)*	-254.90 *(0.90)*	2.36 *(1.97)*	2.85 *(2.38)*	5.21 *(4.35)*	37.42 *(31.20)*	9.76
7x7x1/2 A500 B	710.40 *(1.06)*	-278.80 *(0.83)*	3.59 *(2.99)*	4.16 *(3.47)*	7.75 *(6.46)*	70.86 *(59.08)*	19.31
7x7x1/2 A1085 Y	805.10 *(1.04)*	-305.70 *(0.86)*	3.48 *(2.90)*	4.41 *(3.68)*	7.89 *(6.58)*	70.13 *(58.46)*	18.21
8x8x3/8 A500 W	702.70 *(1.02)*	359.98 *-(0.92)*	1.24 *(1.04)*	1.90 *(1.58)*	3.14 *(2.62)*	18.10 *(15.09)*	4.97
8x8x3/8 A1085 Y	672.60 *(1.02)*	-328.80 *(0.84)*	2.18 *(1.82)*	2.18 *(1.82)*	4.36 *(3.63)*	27.43 *(22.87)*	9.18
8x8x1/2 A500 W	905.97 *(1.03)*	-434.72 *(0.89)*	2.71 *(2.26)*	2.80 *(2.34)*	5.51 *(4.60)*	38.25 *(31.89)*	12.66
8x8x1/2 A1085 Y	921.90 *(1.02)*	-418.20 *(0.83)*	2.96 *(2.46)*	3.32 *(2.77)*	6.28 *(5.23)*	44.07 *(36.74)*	13.29
10x10x3/8 A500 W	785.40 *(1.01)*	-480.10 *(0.85)*	2.10 *(1.75)*	2.48 *(2.07)*	4.58 *(3.81)*	25.71 *(21.43)*	5.96
10x10x3/8 A1085 Y	812.80 *(1.01)*	-507.60 *(0.87)*	1.60 *(1.33)*	1.84 *(1.53)*	3.44 *(2.87)*	15.66 *(13.05)*	4.67

In table above, direct comparisons can be made between test specimens of the same shape in A500 and A1085. The results from the twenty tests in Series 1 showed relatively minimal differences between the performance of A500 and A1085 HSS. For six of the ten HSS shapes tested, the A1085 exhibited a greater deformation range, while for the other four HSS shapes, the A500 exhibited a greater deformation range. Bergendahl concluded that this was likely due to the similarities in the measured geometric and material properties between the two specifications.

Figure 2.9 shows the axial displacement range versus local compactness. In the figure, the axial displacement range is normalized by the initial brace length and the width-to-thickness ratio is normalized by the AISC highly ductile limit. From Figure 2.9 it is evident that a decrease in local compactness ratio is associated with an increase in axial displacement range. This trend is consistent with the data from previous research and is reflected by the AISC maximum *b/t* limits. The power regression curve in this plot has an R^2 value of 0.82 which expresses that local compactness accounts for a significant amount of the variation in deformation range. The figure shows a strong correlation between local compactness and ductility, but it is difficult to draw a clear conclusion about the effect of HSS ASTM specification.

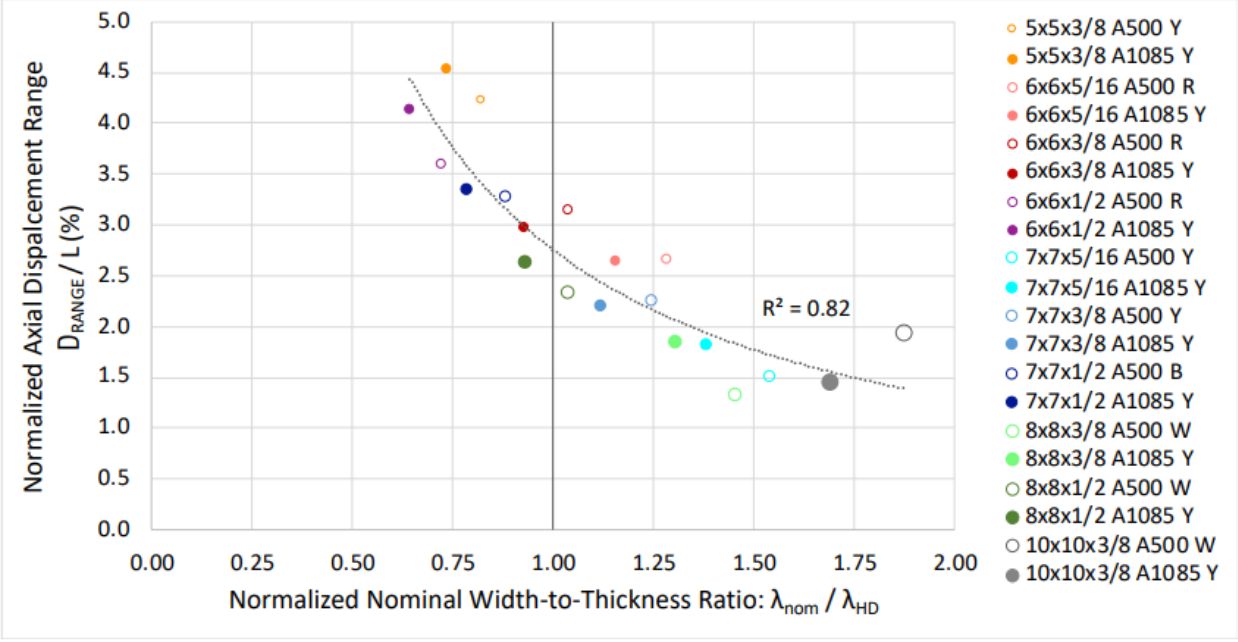

Figure 2.9 Axial Displacement Range vs. Local Compactness (Bergendahl, 2021)

The normalized maximum axial displacement range is plotted versus the global slenderness ratio, *KL/r*, in Figure 2.10 below. The dataset provided a wide range of *KL/r* ratios; from about 60 to 127. The plot shows a clear relationship between increased global slenderness and increased maximum displacement range. Specifically, there is a clear correlation between brace width and deformation capacity. It is evident that much of the variation within each group of brace widths is due to the compactness ratio, *b/t*. The power regression curve accounts for a significant amount of the variation with an R^2 of 0.71, however much of the variation is due to other factors such as *b/t*.

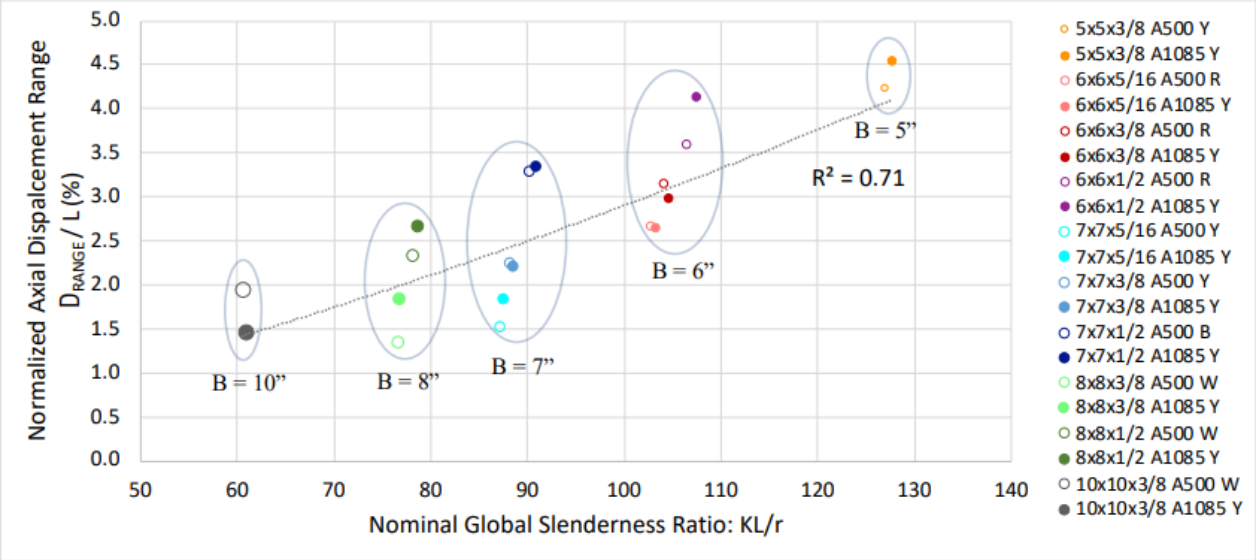

Figure 2.10 Axial Displacement Range vs. Global Slenderness (Bergendahl, 2021)

Overall, the results showed that local compactness and global slenderness are the most influential factors for brace ductility. The data showed that deformability and energy dissipation capacity increased with decreased *b/t* and increased *KL/r* ratios. Additionally, the effect of CVN toughness on brace performance was studied however there was no clear relationship between them. The similarity in cyclic performance between A500 and A1085 was found to be likely due to similarities in the measured geometric and stress-strain properties. The A1085 specification has tighter tolerances on some geometric requirements and a few material requirements that the A500 specification does not require. Many of A500 specimens met or were close to meeting the A1085 specification.

Parameters not studied in Bergendahl's thesis were the effects of steel producer displacement protocol. These parameters were investigated in Series 2 and 3 described in the current thesis. Additionally, shorter length braces were tested in Series 4 to further investigate the effect of brace length and global slenderness.

2.5 SUMMARY OF FINDINGS

The previous research presented above has shown that brace ductility is strongly associated with local compactness and global slenderness. Generally, braces with low width-to-thickness ratios and high global slenderness ratios exhibit greater deformability. Additionally, brace behavior is affected by other factors such as braced frame configuration and displacement history. Previous research may have indicated potential benefits of A1085 HSS over A500 HSS, however, the results from Series 1 of this testing series did not indicate any clear differences. It appears that A500 is being produced very closely to the specified requirements for A1085. Currently, AISC enforces local compactness limits for SCBFs, however, there is no minimum global slenderness requirement. Previous research has shown that braces with increased global slenderness generally exhibit greater ductility. The results of the experimental program in this thesis will be useful in evaluating the design requirements for SCBFs with A1085 HSS braces. The effects of local compactness, global slenderness, steel type, steel producer, and displacement protocol will be investigated in this thesis.

Chapter 3. TEST SETUP AND SPECIMEN DESIGN

3.1 INTRODUCTION

This chapter will describe the design and construction of the test frame and test specimens. The loading protocols and test instrumentation will also be detailed in this chapter. Forty-one square HSS braces were tested to investigate the performance of A1085 HSS subjected to cyclic loading and to compare the cyclic response of A500 and A1085. The application of cyclic loading was achieved by a testing rig capable of ±10 inches of axial displacement and total axial forces up to 1000 kips in tension and 700 kips in compression. The design of the testing rig also aimed to incorporate the ability to test HSS specimens of various sizes and lengths, while allowing for an efficient testing process.

The first series of testing in this program consisted of 20 brace tests – ten A500 HSS braces and ten A1085 HSS braces. The results from series one were compiled by Bergendahl (Bergendahl, 2021). Bergendahl's thesis includes a complete description of the design of the test setup. The same exact setup was used throughout testing, so, this chapter will provide an overview of the test setup and specimen design.

3.2 TEST SETUP OVERVIEW

This section will provide an overview of the test setup and how it was designed. The section will start with a description of the overall layout and then detail the design process and considerations of various components. Although this section will provide descriptions to understand the test setup, more detail regarding the test setup design can be found in Bergendahl (2021).

3.2.1 *Overall Layout*

Figure 3.1 and Figure 3.2 show the test frame used for this experimental research program for the 237.5” and 183.5” length braces, respectively. Note that the difference between these two figures is that Figure 3.2 includes a second end block for the testing of shorter braces. The rig was designed using the available equipment within the constraints of the strong floor in the UW SRL. The geometry and capacity of the test frame was designed to accommodate various sizes and lengths of HSS braces to study a wide range of compactness and slenderness ratios. In this setup, cyclic loads were applied by two hydraulic actuators acting in parallel.

The capacity of each component was designed based on the maximum combined actuator forces of 1000 kips in tension and 700 kips in compression. The actuators operated in unison under displacement control to apply cyclic displacements to the sliding beam which was able to slide on a near frictionless surface. The north gusset plate of each specimen was bolted to the sliding beam so that cyclic displacements of the sliding beam were applied to the specimen. The south gusset remained stationary as it was bolted to a connection plate which was attached to a concrete reaction block fixed to the floor. The test frame was designed to utilize the full stroke of the actuators, allowing for displacements of 10” in compression and tension.

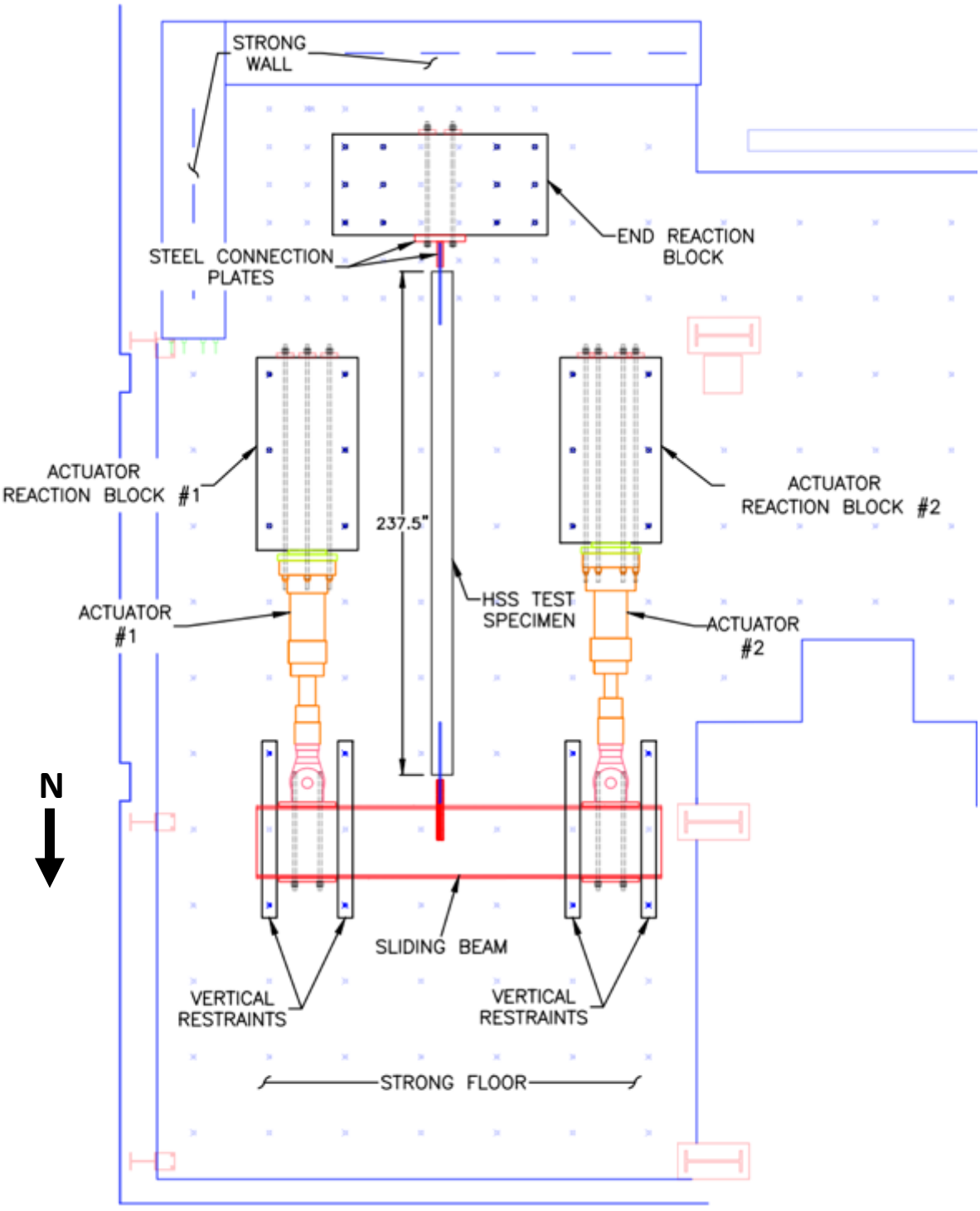

Figure 3.1. Overview of Test Frame for 237.5” Specimens

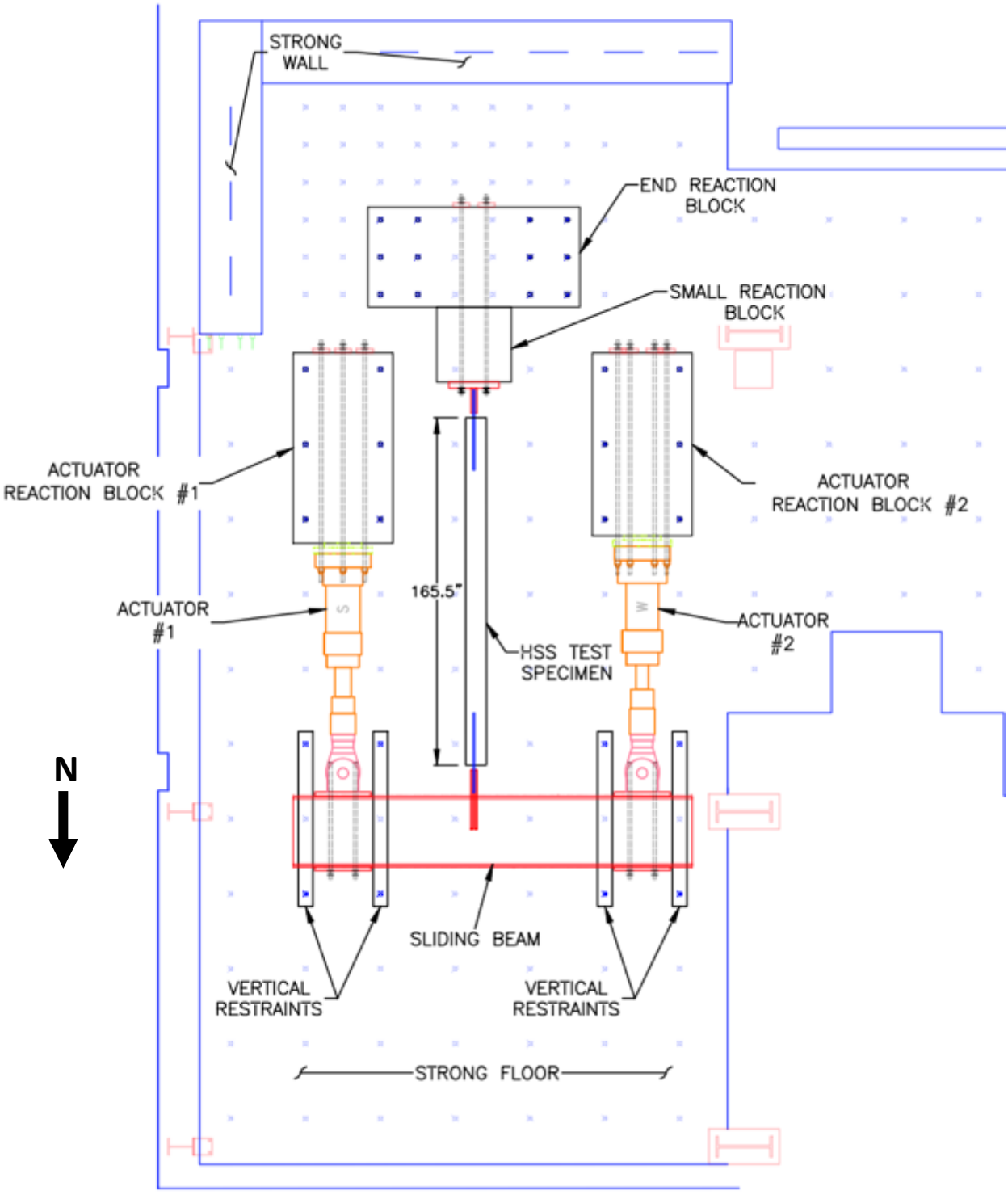

Figure 3.2. Overview of Test Frame for 165.5" Specimens

In this testing program, brace specimens were 237.5” and 183.5” in length. Figure 3.3 below shows the test frame configuration for a 237.5” long specimen – the maximum brace length the rig was capable of testing. Figure 3.4 shows the configuration for a 183.5” specimen. The shorter length was achieved by moving the end reaction block 18” north and adding a 36” deep block on the north side of the larger end block.

Figure 3.3. Configuration of Test Frame for 237.5” Brace Specimen

Figure 3.4 Configuration of Test Frame for 183.5” Brace Specimen

The end reaction block shown in Figure 3.5 and Figure 3.6 needed to resist the combined actuator force of 1000 kips which required twelve 1-3/4" diameter 150 ksi threaded tie down bars. The end block was placed at the south end of the strong floor where there is a higher density of anchor holes providing enough inserts for the twelve tie down rods. Additionally, the closer spacing of anchor holes made it possible to move the block in smaller increments to test braces of different lengths.

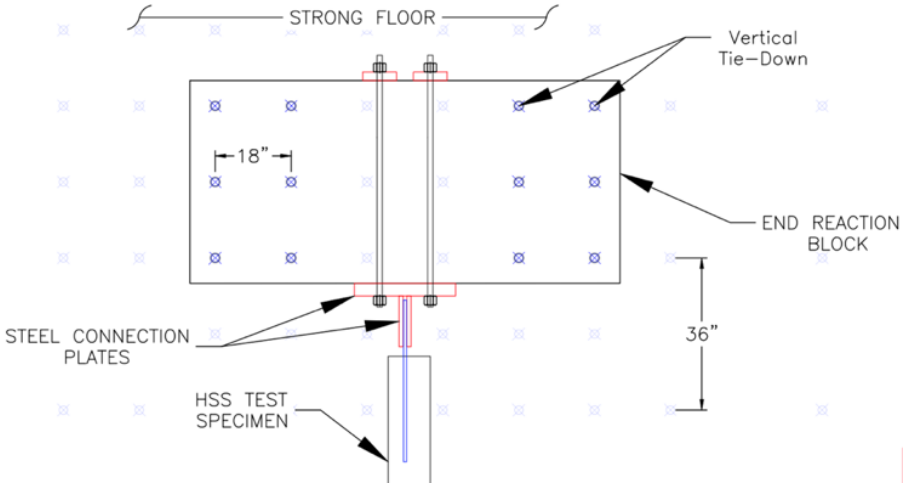

Figure 3.5. Layout of South End of Test Frame

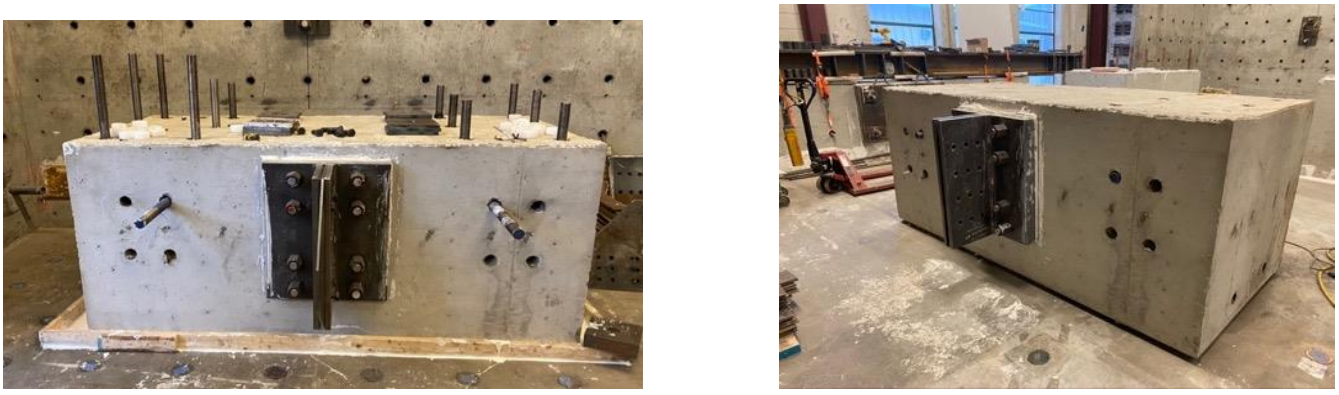

(a) (b)

Figure 3.6. End Reaction Block – Before (a) and After (b) Being Moved Into Place

3.2.2 *Horizontal Loading System*

As mentioned in the overall layout described in Section 3.2.1, two hydraulic actuators acting in parallel were used to apply axial forces on the test specimens. The two actuators were spaced at 12’ on center and were oriented parallel to the test specimen in the north-south direction. The spacing of the actuators allowed space for the expected out of plane buckling displacements of the test specimens.

Figure 3.7. Orientation of Actuators and Sliding Beam

The two hydraulic actuators had different capacities. At a hydraulic pressure of 3000 psi, the stronger actuator had a capacity of 450 kips in compression and 375 kips in tension, while the smaller actuator had a capacity of 350 kips in compression and 275 kips in tension (a 9:7 actuator capacity ratio). Note that the compressive capacity of the actuators is the tensile brace loading capacity and vice versa. In order to test the larger specimens, the hydraulic pump pressure needed to be increased. Doing so, the combined loading capacity achievable by the system was nearly 1000 kips in tension and 700 kips in compression. Because the actuators had different capacities, the actuators were placed asymmetrically about the HSS specimen in order to utilize the capacity of the two actuators. The spacing of the actuators about the center of the specimen is shown in Figure 3.8 below, where the stronger actuator is 63” from the center of the

specimen and the weaker actuator is 81” from the center of the specimen. Matching the actuator spacing ratio to the actuator strength ratio ensured that the full capacity could be utilized and that only axial horizontal forces were applied without causing any rotations of the sliding beam.

The two actuators were attached to a sliding beam which transferred the loads from the actuators to the test specimen. This sliding member was a built up steel beam filled with concrete. The sliding beam was placed on four supports with sliding surfaces and vertical restraints.

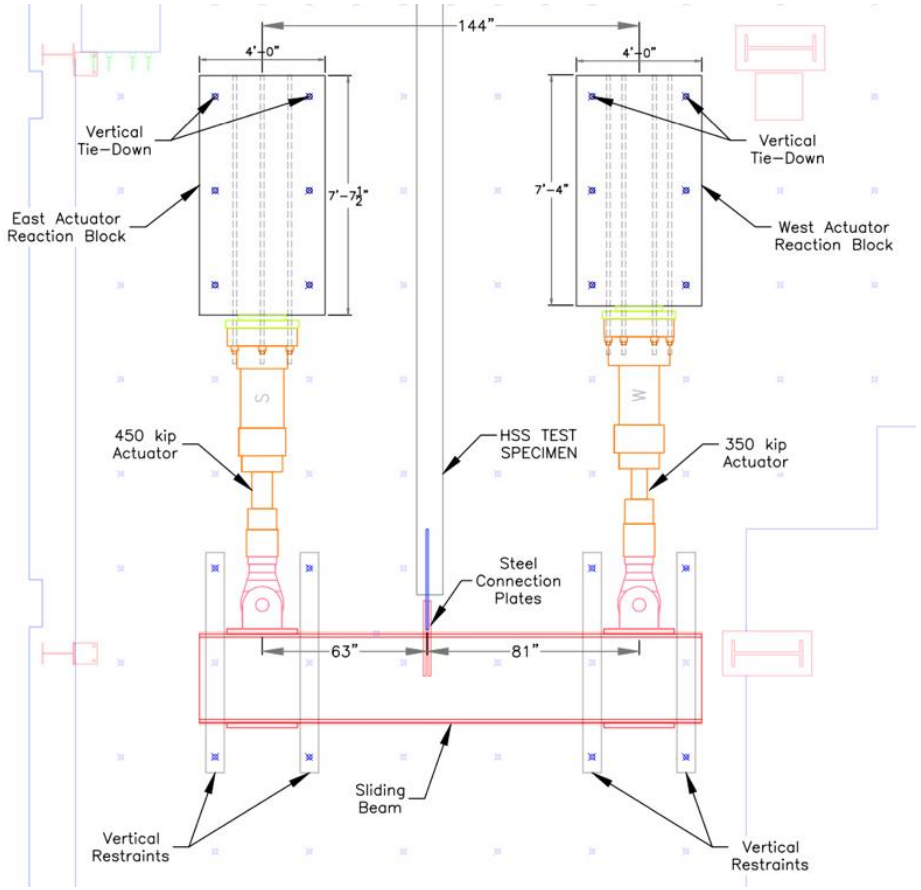

Figure 3.8. Layout of Actuators and Sliding Beam

The bases of the actuators were connected to concrete reaction blocks to provide a stationary base anchored to the strong floor. The reaction blocks were placed over a layer of hydrostone which provided a monolithic surface between the reaction block and the floor. After the hydrostone cured, each block was anchored to the strong floor with six 1-3/4” diameter 150

ksi threaded bars post-tensioned to 200 kips each for a total of 1200 kips. Drawings of the actuator reaction blocks, and the respective reinforcement can be found in Appendix A.

The actuators were tied to concrete reaction blocks using six 1-1/4” diameter 150 ksi threaded bars post-tensioned to 100 kips each. 600 kips of prestressing force ensured the base of the actuators would stay anchored to the block and prevented fatigue in the threaded bars while the actuators were loaded to their capacity in tension. The interface between the base of the actuators and the side of the reaction block consisted of a steel plate and a cotton duct pad. The 3” thick steel plates were designed specifically for each respective actuator base bolt hole layout. The plates were designed to provide a solid bearing surface at the base of each actuator. Between the steel plate and the reaction block was a circular 2” thick elastomeric cotton duct pad to allow for small actuator rotations. Additionally, the swivel heads of the actuators were oriented horizontally to accommodate small rotations of the sliding beam.

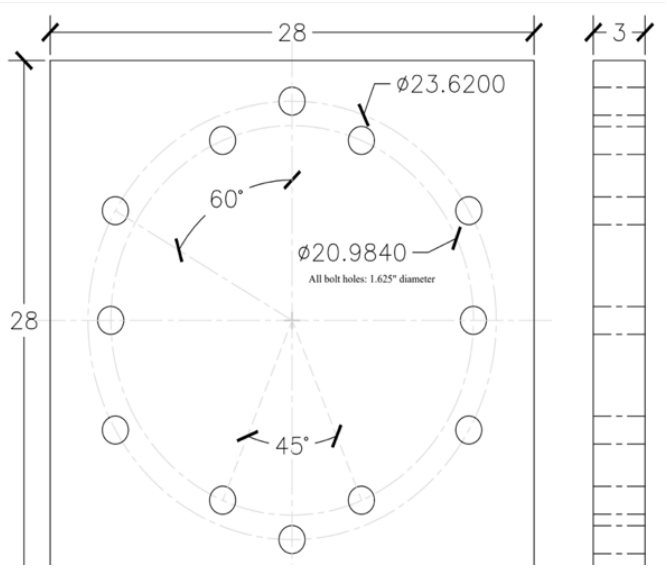

Figure 3.9. Actuator Base Plate Design

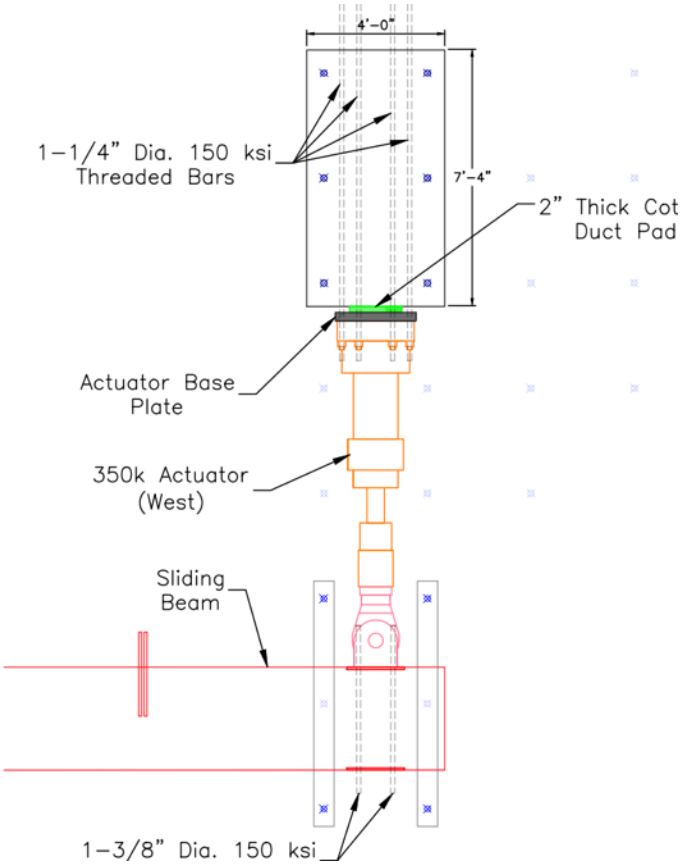

Figure 3.10. Actuator Assembly and Connections

3.2.3 *Sliding Beam Design*

As described above in the test setup overview, the sliding beam transferred the applied actuator displacements to the test specimen. The sliding beam was designed to be very stiff in order to withstand the large bending demands so that the brace axial displacements would equal the actuator displacements. The member was a concrete filled steel beam built up of a 16’ long W33x201 beam with 3/4” thick steel plates welded to its flanges. The design created a box section seen below in Figure 3.11. The box section was then filled with concrete to increase the bending stiffness. The member was greatly overdesigned for the 1000 kip maximum potential combined actuator force to guarantee durability and stiffness over many loading cycles. The actuators were connected to the sliding beam using 1-3/8” 150 ksi threaded rods which ran through the width of the sliding beam. Figure 3.12 shows the dimensions for the overall geometry of the sliding beam. More detail regarding the design can be found in Bergendahl (2021). Additionally, detailed calculations for the sliding beam can be found in Appendix A.

(a) (b)

Figure 3.11 Sliding Beam - Original (a) and In Upright Position (b)

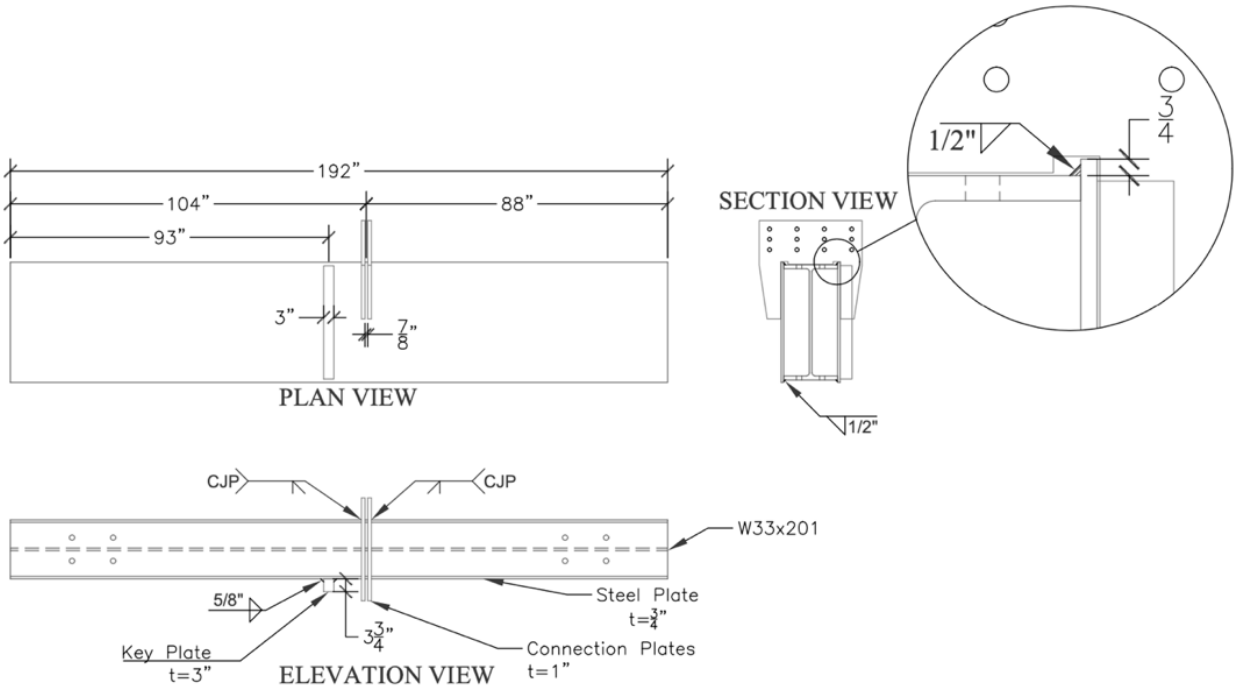

Figure 3.12 Sliding Beam Dimensions

As displayed in Figure 3.8, four vertical restraints were used to support the sliding beam and resist any vertical movement. The vertical support system also provided a sliding surface on the top and bottom of the sliding beam. The bottom support consisted of a 4x4x3/8 HSS welded to the top of a 14” deep wide-flange which was anchored to strong floor using 1” diameter steel threaded rods. A 6x6x1/4 HSS was used as the top restraint and was tied to the bottom support using 1” threaded rods. 1-1/4” diameter holes were cut in the top HSS, bottom HSS, and wide flange to connect the threaded rods from the top of the top HSS through the bottom HSS to the bottom of the top flange of the wide flange. The geometry of the vertical support system is shown in the cross-section elevation view in Figure 3.13.

The sliding surface on the top and bottom of the sliding beam consisted of a greased Polytetrafluoroethylene (PTFE) and stainless steel interface – a system used in many previous experiments in the UW SRL. Strips of PTFE were attached to the top of the bottom HSS and the bottom of the top HSS where the sliding surfaces are shown in Figure 3.13. Strips of stainless steel were welded to the top and bottom of the sliding beam in alignment with the top and bottom HSS. This interface provided a nearly frictionless surface so that the total actuator force would be directly applied to the test specimen. While moving the sliding beam without a test specimen, the resistance due to friction was less than 1 kip.

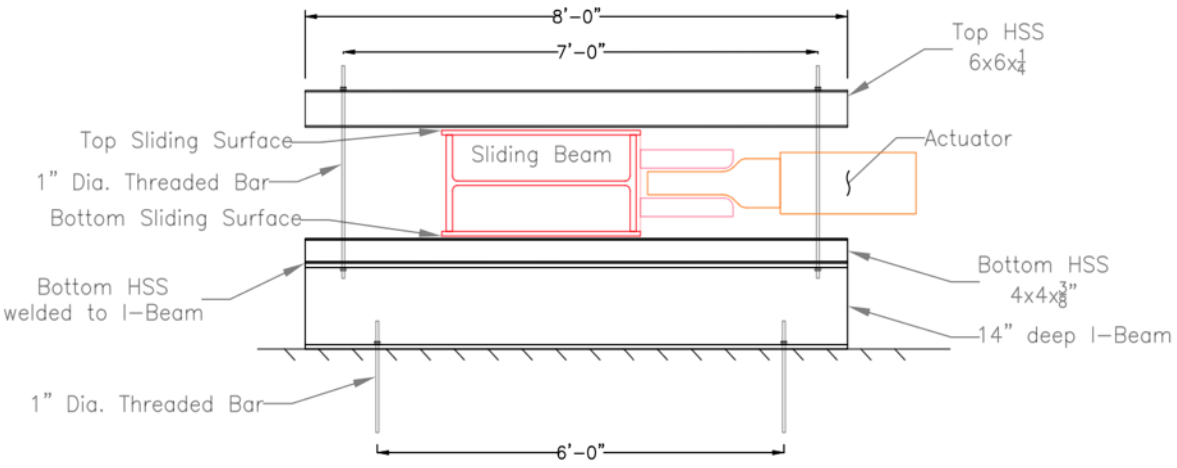

Figure 3.13 Cross-Sectional View of Sliding Beam and Vertical Restraint System

The two actuators were operated under displacement control so that they would apply the same displacements. This prevented rotation of the sliding beam, but additional measures were taken to prevent unwanted lateral movement of the sliding beam. The key and keyway system shown in Figure 3.14 below was designed to mitigate lateral movement. The "key" was a 3" thick, 3.5" deep, rectangular steel section welded to the bottom of the sliding beam. The "keyway" was a 4" thick steel plate shown in Figure 3.14. The keyway was welded to a 3" thick floor plate which was fixed to the strong floor using four 1-3/4" diameter 150 ksi threaded bars prestressed to 200 kips each. With this system, the key would move north-south through the keyway with a 3/8" gap on both sides to avoid frictional resistance but if the sliding beam were to move laterally east-west, the key would hit the keyway to prevent lateral movement. Fortunately, the keyway was never hit throughout the testing for this project. Detailed calculations for the design of the key and keyway are provided in Appendix A.

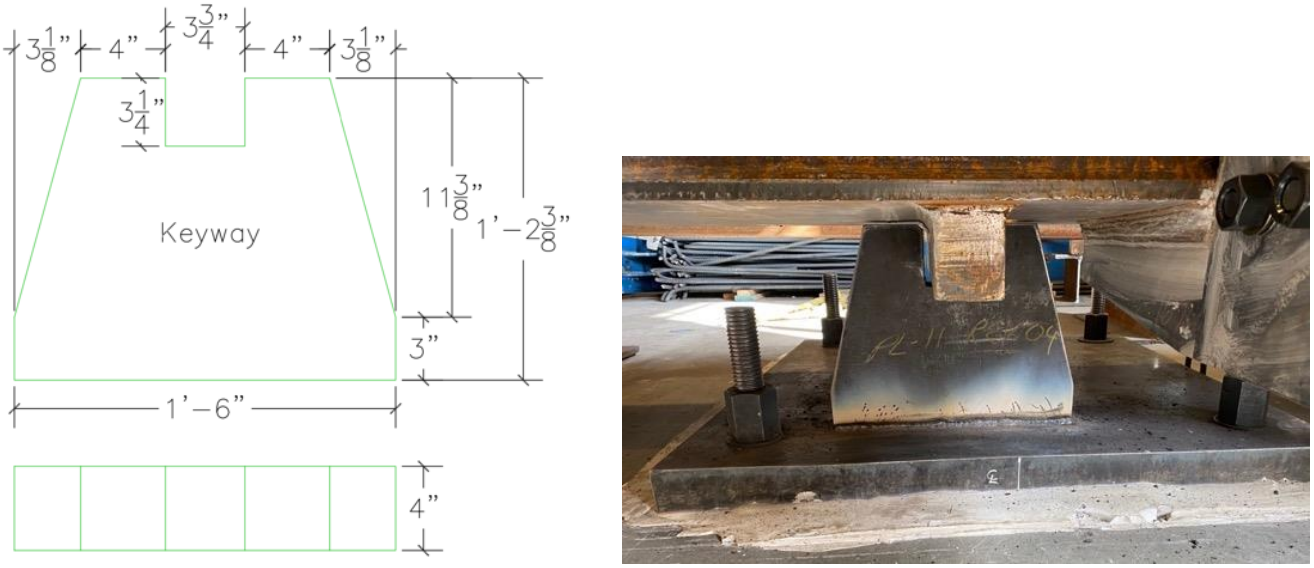

(a) (b)

Figure 3.14. Keyway Plate Dimensions (a) and Keyway Plate Welded in Place (b)

The test specimens were connected to the sliding beam via two 1" thick steel connection plates as shown below in Figure 3.15. The two plates were welded to the sliding beam along the top, bottom, and front side of the sliding beam. There was a 7/8" gap between the two connection plates to allow space for the various sized gusset plates. The additional space between the gusset plates and the connection plates was filled using steel shim plates to provide a tight connection. Twelve 1-1/8" diameter bolt holes were drilled into each connection plate, matching the bolt

pattern of the gusset plate. These connection plates were designed to ensure any deformation in the connection during testing would occur in the gusset plates and not the connection plates.

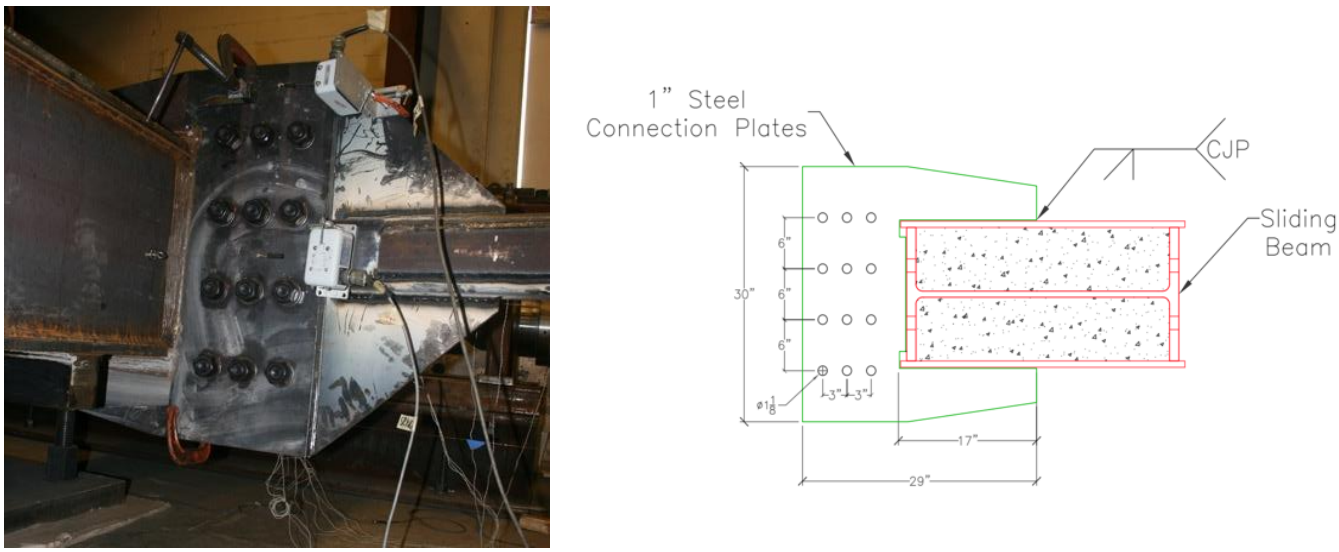

(a) (b)

Figure 3.15. Sliding Beam Connection Plate - During Testing (a) and Elevation (b)

3.2.4 *End Connection Plate and Reaction Block Design*

The south gusset plate of the test specimen was connected to two 1" connection plates anchored to the south end reaction block. The two 1" plates were constructed similarly to the north connection plates where there was a 7/8" gap between the two plates and the same twelve bolt hole layout. The two connection plates were welded to a 3" thick steel plate which was anchored to the reaction block using eight 1-3/8" diameter 150 ksi threaded bars prestressed to 180 kips each. This provided a total prestressing force of 1440 kips which exceeded the maximum demand of 1000 kips in order to prevent movement of the connection plate relative to the block and to prevent fatigue in the threaded bars during cyclic loading. The geometry of this built up connection plate is shown in Figure 3.16.

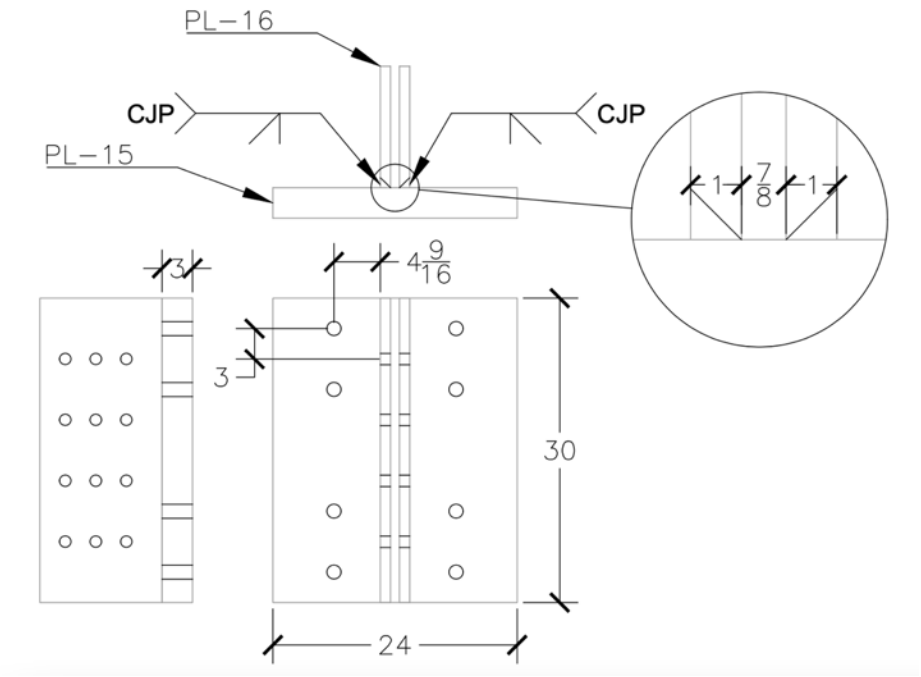

Figure 3.16. End Connection Plate Details

The south end reaction block was designed for a maximum demand of 1000 kips from the combined force of the actuators. The block was prestressed to the floor using twelve 1-3/4" diameter 150 ksi threaded bars, stressed to 200 kips each. Prior to stressing, the reaction blocks were placed over a layer of hydrostone which provided a uniform surface between the reaction block and the floor. Detailed drawings of the reinforcement layout for the reaction block are provided in Appendix A.

A second smaller concrete reaction block was also used at the south end to permit the testing of shorter length brace specimens. The smaller block was used in test series four for the testing of 183.5" long brace specimens. The smaller block was 36" wide by 36" long, with a height of 41", and was placed in front of the larger block on the north side. The smaller block was not prestressed to the strong floor but rather anchored to the larger reaction block. Eight horizontal conduits ran through both of the reaction blocks which aligned with the layout of the south end connection plate. The connection plate was connected to the north side of the smaller block using eight 1-3/8" diameter 150 ksi threaded bars which ran through to the south side of the larger block. Figure 3.17 below shows the configuration of the south connection using the smaller reaction block.

Figure 3.17 Configuration of South Connection with Added Reaction Block

3.3 TEST SPECIMEN DESIGN

3.3.1 *Overview*

Four test series, totaling 41 tests, were completed at the University of Washington Structural Research Lab (UW SRL). Four different steel producers provided the HSS used in this experimental program. In order to maintain anonymity, these four producers will be referred to here as “Yellow”, “Red”, “Blue”, and “White”. These manufacturers provided a combined ten different HSS shapes in both A500 Grade C and A1085. The specimen section size was constrained by the capacity of the actuators which acting in parallel were capable of outputting axial forces of 1000 kips in tension and 700 kips in compression. The tubes provided by each producer are shown in Table 3.1. The green cells represent a section provided by the corresponding producer. Two 40’ long sections were provided for each section shown in Table 3.1. These sections allowed for multiple tests on each section as well as enough for material

testing. The various HSS sections were selected based on their local compactness ratio, global slenderness ratio, predicted capacity, and availability from the various producers.

Table 3.1 Available HSS Shapes

	ASTM A500				ASTM A1085			
HSS Shape	**YELLOW**	**RED**	**BLUE**	**WHITE**	**YELLOW**	**RED**	**BLUE**	**WHITE**
10x10x3/8								
8x8x1/2								
8x8x3/8								
7x7x1/2								
7x7x3/8								
7x7x5/16								
6x6x1/2								
6x6x3/8								
6x6x5/16								
5x5x3/8								

The sections tested during Series 1 are shown below in Table 3.2. The purpose of this series was to compare the performance of A500 and A1085 HSS under cyclic loading. The A500 HSS tested was provided by four different producers, while the ten A1085 HSS tested was provided by the Yellow producer. The braces in this series were subjected to a symmetric cyclic loading protocol with increasing displacements as described in Section 3.5.

Table 3.2 Test Specimens – Test Series 1

	ASTM A500				ASTM A1085
HSS Shape	**YELLOW**	**RED**	**BLUE**	**WHITE**	**YELLOW**
10x10x3/8					
8x8x1/2					
8x8x3/8					
7x7x1/2					
7x7x3/8					
7x7x5/16					
6x6x1/2					
6x6x3/8					
6x6x5/16					
5x5x3/8					

The HSS sections tested in Series 2 are shown in Table 3.3. The purpose of this series was to compare the performance of A1085 HSS from different producers. Four sections were tested from producers Red, Blue, and White (Yellow was tested in Series 1). The specimens were subjected to a symmetric cyclic loading protocol identical to that used in Series 1.

Table 3.3 Test Specimens – Test Series 2

	ASTM A1085		
HSS Shape	**RED**	**BLUE**	**WHITE**
10x10x3/8			
8x8x1/2			
8x8x3/8			
7x7x1/2			
7x7x3/8			
7x7x5/16			
6x6x1/2			
6x6x3/8			
6x6x5/16			
5x5x3/8			

The sections tested in Series 3 are shown in Table 3.4. The purpose of this series was to study the performance of A1085 HSS with different displacement histories. Three different sections from the Yellow producer were tested. The sections were selected to provide an array of varying compactness compliance. The sections range from highly-ductile to moderately-ductile to non-ductile. Each HSS shape was tested under three different loading protocols. The first loading protocol was that used in Series 1 and 2. The two alternative loading protocols used in this series were called “chevron” and “near fault”. The chevron loading protocol was compression dominant and intended to represent the behavior of a brace within an SCBF with a chevron configuration where vertical beam deformation occurs. The near fault loading protocol was tension dominant and intended to represent the pulse demands of a near fault ground motion. These loading protocols are further detailed in Section 3.5.

Table 3.4 Test Specimens – Test Series 3

	ASTM A1085
HSS Shape	**YELLOW**
10x10x3/8	
8x8x1/2	
8x8x3/8	
7x7x1/2	
7x7x3/8	
7x7x5/16	
6x6x1/2	
6x6x3/8	
6x6x5/16	
5x5x3/8	

The HSS sections tested in Series 4 were the same as in Series 3 shown in Table 3.4 above. The purpose of this series was to explore the effect of global slenderness on the performance of A1085 HSS under cyclic loading. The tests in this series were conducted on 183.5" long braces, while all previous tests were 237.5" long braces. The specimens in this test series were subjected to a symmetric cyclic loading protocol with increasing displacements. The loading protocol was the same as Series 1 and 2, but the magnitude of displacements was scaled down based on the proportional brace length. Again, the loading protocols are described in detail in Section 3.5.

The expected yield and critical buckling loads of all the specimens tested in this research project are shown below in Table 3.5. For the expected critical buckling forces, the values shown are for the 237.5" long specimens tested in Series 1-3, while the values shown in parentheses are for the 183.5" long specimens tested in Series 4. The yield force is the same for both brace lengths. The expected yield force, $P_{y,e}$, was calculated by taking the product of the nominal cross-sectional area, A_g, and the expected yield strength, R_yF_y. The overstrength factor, R_y, is 1.3 for A500 Grade C HSS and 1.25 for A1085 HSS. The nominal yield strength, F_y, is 50 ksi for both specifications. The presented critical buckling force, $P_{cr,e}$, is calculated based on the nominal material and geometric properties of each test specimen. The measured material properties are presented in Section 3.4.2.

Table 3.5. Expected Tensile and Compressive HSS Member Capacity

	Expected Yield Force, $P_{y,e}$ (kips)		**Expected Critical Buckling Force, $P_{cr,e}$ (kips)**	
HSS Shape	**A500**	**A1085**	**A500**	**A1085**
10x10x3/8	858	917	605	628
8x8x1/2	878	936	491	511
8x8x3/8	676	722	387	404 (503)
7x7x1/2	754	806	347	364
7x7x3/8	583	623	278	292 (390)
7x7x5/16	493	528	239	252
6x6x1/2	633	673	216	225
6x6x3/8	493	525	175	185
6x6x5/16	418	447	153	157
5x5x3/8	402	428	96	101 (169)

3.3.2 *Test Specimen Layout and Connections*

The specimens tested in this program were square HSS members welded to trapezoidal gusset plates at each end. The HSS tubes were cut to length and slotted at each end using a plasma cutter. The gusset plates were then installed and welded into the slots. The gusset plates were connected to the reaction block and sliding beam via steel connection plates and twelve 1” diameter A490 bolts. To prevent net section rupture at the reduced slotted cross-section, net section reinforcement plates were welded to the sides of the HSS tubes. An annotated diagram of the overall layout is shown in Figure 3.18. The connection design will be presented below, however, Bergendahl (2021) has more detail regarding the design process and calculations.

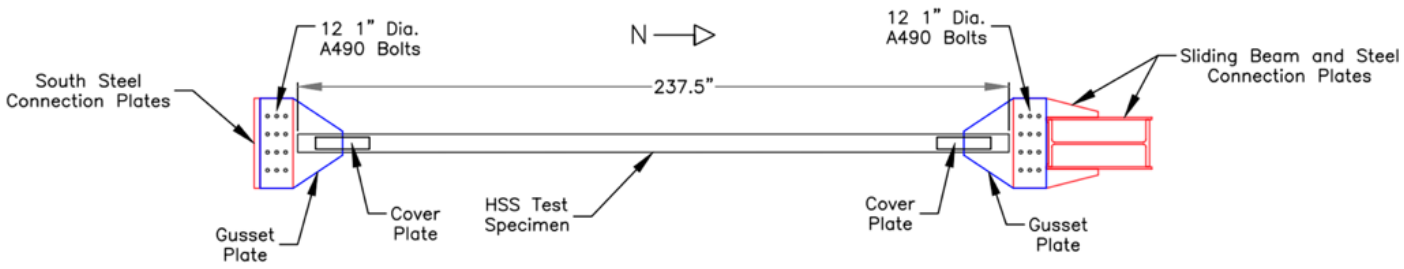

Figure 3.18 Test Specimen Layout

The exact length of the specimens was determined by the final as-built dimensions of the test frame. The two brace lengths tested were 237.5" and 183.5" and this is the end-to-end brace length as shown in Figure 3.18. The dimensions of the gusset plates and fillet welds for each of the specimens are displayed below in Table 3.6. The steel connection plates on both ends consisted of two 1" steel plates where the gusset plate would go between to create a double-shear connection. The gap between the connection plates was 0.875" and due to varying gusset plate thicknesses, shim plates were used to fill the gaps and create a tight fit.

The gusset plates were designed to create pseudo-pinned ends to allow the brace ends to rotate while buckling in compression. A gap was provided between the ends of the HSS and the connection plate to allow for rotation. This gap was three times the thickness of the gusset plate. The gusset plates were designed considering the following limit states: yielding on the gross area, tensile rupture, block shear, bearing and tear out, and buckling. The final design details of the gusset plates, fillet welds, and slots are provided in Table 3.6 below. Figure 3.19 displays the typical details of the gusset plates with annotations for the varying dimensions. Drawings of each specific gusset plate design can be found in Appendix A and calculations for the design on the gusset plates and corresponding fillet welds can be found in Appendix B.

The gusset plate was connected to the HSS member with an intentional eccentricity in order to control the direction of out of plane buckling. This was necessary to prevent the specimen from hitting the actuator reaction blocks during large displacements in compression. Additionally, controlling the direction of buckling allowed for a more efficient instrumentation layout where the string potentiometers used to capture out of plane displacements could remain unobstructed. The eccentricity of the connection was designed to control the direction of out of

plane buckling without sacrificing the strength of the member. The eccentricity was determined following previous research conducted at the UW SRL where a ratio of slot eccentricity to radius of gyration (*e/r*) equal to 0.1 was used. The same ratio was used in this project. This magnitude of eccentricity ensured the direction of buckling without significantly reducing the compressive capacity of the member.

Table 3.6. Gusset Plate and Fillet Weld Design

	Gusset Plate		Fillet Weld		Slot
Section	**Length (in.)**	**Thickness (in.)**	**Length (in.)**	**Size (in.)**	**Slot Eccentricity (in.)**
10x10x3/8	38.25	0.75	25.0	0.5	0.375
8x8x1/2	32.25	0.75	19.0	0.625	0.3125
8x8x3/8	32.875	0.625	20.0	0.5	0.3125
7x7x1/2	29.875	0.625	17.0	0.5	0.25
7x7x3/8	29.5	0.5	17.0	0.5	0.25
7x7x5/16	30.5	0.5	18.0	0.5	0.25
6x6x1/2	26.875	0.625	14.0	0.5	0.25
6x6x3/8	27.5	0.5	15.0	0.4375	0.25
6x6x5/16	27.125	0.375	15.0	0.4375	0.25
5x5x3/8	24.125	0.375	12.0	0.375	0.1875

As mentioned above, the connection between the gusset plates and the connection plates, consisted of twelve 1” diameter A490 bolts in double-shear. The bolt layout is shown below in Figure 3.19. This connection was designed considering the following limit states: block shear, tear out, and bolt shear. Using a hydraulic wrench, the bolts were pretensioned to a minimum of 64 kips which was verified using load-indicating washers. The prestressed bolted connection made the connection slip-critical, however due to large cyclic axial loads, the bolts did slip during each test. Typically, the connection only slipped once in tension, however for some of the larger members, the connection slipped multiple times due to large forces in tension and compression. Calculations for the design of this connection are in Appendix B.

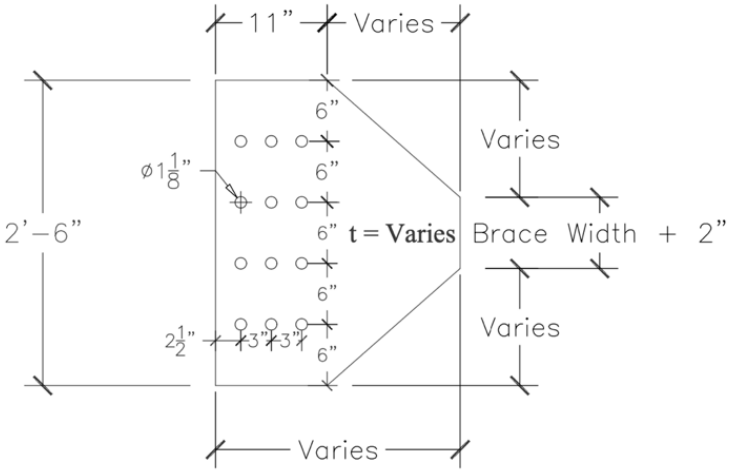

Figure 3.19 Gusset Plate Design - General

Net section reinforcement was provided at the HSS to gusset plate connection where there was a reduced net section due to the slot in the HSS. The net section reinforcement was provided by welding rectangular steel plates on both sides of the tube at each connection as shown in Figure 3.20. These plates increased the net effective area to be greater than the gross area of the HSS brace. This prevented tensile net-section rupture which may occur prior to brace yielding if unreinforced. The net section reinforcement plates for each brace section were 3/8” thick and were welded along both longitudinal sides with ¼” fillet welds. These welds were designed to have a capacity equal to that of the reinforcement plate on each side of the end of the slot. The dimensions of the net section reinforcement plates are shown below in Table 3.7. Complete calculations for the design of the net section reinforcement are in Appendix B.

Figure 3.20 Net Section Reinforcement at End Connection

Table 3.7 Net Section Reinforcement Design

	Net Section Reinforcement Plate	
Section	**Length (in.)**	**Width (in.)**
10x10x3/8	24	5.25
8x8x1/2	24	5.25
8x8x3/8	20	4.25
7x7x1/2	20	4.25
7x7x3/8	20	4.25
7x7x5/16	18	3.25
6x6x1/2	18	3.25
6x6x3/8	18	3.25
6x6x5/16	18	3.25
5x5x3/8	16	2.75

3.4 TEST SPECIMEN PROPERTIES

Prior research has proven that the inelastic behavior of HSS braces is strongly dependent on the cross-sectional compactness and the global slenderness ratios. The ductility of HSS braces is reliant on the ability to withstand inelastic deformations without excessive loss of resistance or premature fracture. As braces buckle under large compressive displacements, a plastic hinge forms at the center of the brace. Significant local deformations develop at the center of this plastic hinge region (a phenomenon often referred to in this thesis as “local cupping”). These large local deformations and high strains are quickly followed by fracture in tension. Resisting the development of these deformations and high local strains is therefore critical to the inelastic performance of HSS braces. Research has shown that the deformations causing the development of these local strains is strongly related to *b/t* and *KL/r* ratios. Braces with high compactness ratios typically develop local cupping deformations at smaller axial deformations which leads to premature fracture of the brace. The *b/t* limits provided in Table 1.2 are currently required to prevent braces from experiencing concentrated local strains at low drift displacements, therefore allowing the brace to perform in a ductile manner during an earthquake. One objective of this

research project was to evaluate the AISC 341-16 width-to-thickness limits. To do this, braces with a wide range of compactness ratios were tested.

The nominal local compactness ratios of the specimens tested in this research program are provided in Table 3.8. The nominal width-to-thickness ratios shown in this table are color coded according to the specimen's adherence with the width-to-thickness limits in *The Seismic Provisions*. In the table, green is for HSS that satisfy the limits for highly ductile braces, orange for HSS that satisfy the limits for is moderately ductile braces, and red is for HSS that do not meet either of limits in *The Seismic Provisions*.

Table 3.8. Test Specimen Width-to-Thickness Ratios

	Nominal Width-to-Thickness Ratio	
HSS Shape	**A500 Gr. C**	**A1085**
10x10x3/8	*25.7*	23.7
8x8x1/2	14.2	13
8x8x3/8	19.9	18.3
7x7x1/2	12.1	11
7x7x3/8	17.1	15.7
7x7x5/16	21.1	19.4
6x6x1/2	9.9	9
6x6x3/8	14.2	13
6x6x5/16	17.6	16.2
5x5x3/8	11.3	10.3

The nominal global slenderness ratios (*KL/r*) of the specimens tested in this research program are provided in Table 3.9. The values shown are for the 237.5" long brace specimens, while the values in parentheses are for the 183.5" long brace specimens. AISC 341-16 states that the global slenderness ratio of HSS braces in SCBF's must be limited to $Lc/r \leq 200$. This limit is much higher than all of the specimens tested in this program. Braces in SCBFs are designed to provide resistance in tension and compression. The compressive capacity decreases as *Lc/r* increases so the upper limit prevents unbalanced forces in SCBFs. It is interesting to note that AISC does not enforce a lower limit on global slenderness because stocky braces with lower slenderness ratios typically buckle inelastically at lower compressive displacements, exhibiting less ductility than those with larger slenderness ratios as described in several previous studies

reviewed in Chapter 2. Slender braces with higher *KL/r* ratios have a larger inelastic deformation capacity therefore providing a more ductile performance under cyclic loads, albeit at a smaller compressive capacity. Therefore, in practice, many braced frames are designed using braces with global slenderness ratios in the range of 40 to 100 to get adequate ductility without compromising compressive force capacity (Sabelli et al., 2013).

The global slenderness ratios for ordinary concentrically braced frames (OCBFs) are limited by the equation:

$$Lc/r \leq 4\sqrt{E/F_Y}$$

This requirement limits the *KL/r* ratio for A500 and A1085 HSS braces in OCBFs to be under about 96 which is much more restrictive than the limits for SCBFs. The lower limit is to ensure sufficient compressive force capacity in order to avoid unbalanced forces in a braced frames (AISC, 2016).

Table 3.9 Test Specimen Global Slenderness Ratios

	Nominal Global Slenderness Ratio	
Section	**A500 Gr. C**	**A1085**
10x10x3/8	60.6	60.9
8x8x1/2	78.1	78.6
8x8x3/8	76.6	76.9 (59.4)
7x7x1/2	90.3	91.0
7x7x3/8	88.3	88.6 (68.5)
7x7x5/16	87.3	87.6
6x6x1/2	106.5	107.5
6x6x3/8	104.2	104.6
6x6x5/16	102.8	103.3
5x5x3/8	127.0	127.7 (98.7)

The ranges of local compactness and global slenderness ratios are shown below in Figure 3.21. The HSS test specimens had width-to-thickness ratios ranging from of 9 to 25.7, and global slenderness ratios ranging from about 60 to 127. This range provided braces that meet the compactness limits for SCBFs and OCBFs as well as many that do not meet the requirements for either.

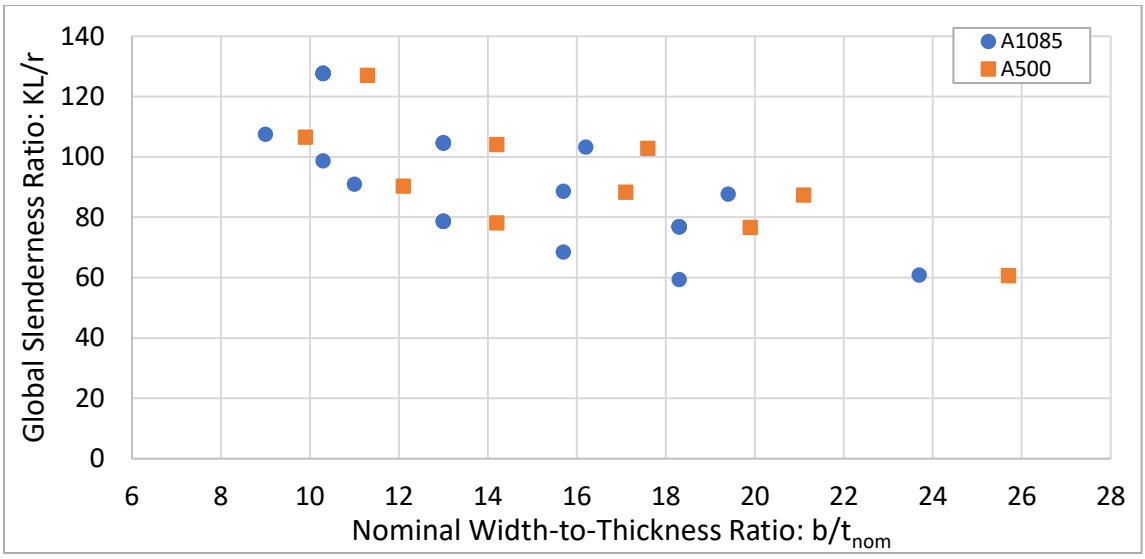

Figure 3.21. Range of Global Slenderness and Local Compactness Ratios

3.4.1 *Geometric Properties*

Geometric properties of each specimen were measured to make comparisons between specimens as well as comparisons to the specified values. The properties presented in this section are from the test specimens in all four test series. Two different thicknesses are specified for HSS – the nominal thickness, t_{nom}, and the design thickness, t_{des}. The nominal thickness is that noted in the name of the HSS shape. The design thickness is the thickness used in design calculations and for calculating properties such as the gross area and *b/t* ratio. The specified wall thickness tolerance for A500 is ±10%, while that for A1085 is +10%, -5%. As a result of this, there is a 7% reduction in the design thickness for A500 HSS, while there is no reduction for A1085. Furthermore, the larger design thickness for A1085 provides compactness ratios less than that of A500 HSS of the same shape. Therefore, more A1085 HSS sections meet the highly ductile criteria provided in *The Seismic Provisions*.

The wall thickness of each specimen was measured using a micrometer. Two measurements were recorded for each of the four side walls at both ends of the provided HSS tube, for a total of 16 measurements per specimen. The average of these thickness measurements is denoted as t_{meas}. The wall thickness measurements are provided below in Table 3.10. This table also compares the measured thicknesses to the specified nominal thickness, t_{nom}, design thickness, t_{des}, and required thickness, $t_{req,A1085}$. $t_{req,A1085}$ is taken as 95% of t_{nom} due to the 5% wall thickness tolerance for the A1085 specification.

Table 3.10. Wall Thickness Measurements

Test Specimen	Nominal Wall Thickness, t_{nom} (in)	Design Wall Thickness, t_{des} (in)	Measured Wall Thickness, t_{meas} (in)	t_{meas} / t_{nom}	t_{meas} / t_{des}	$t_{meas} / t_{req,A1085}$
5x5x3/8 A500 Y	0.375	0.349	0.360	0.960	1.032	1.01
5x5x3/8 A1085 Y	0.375	0.375	0.376	1.003	1.003	1.06
6x6x5/16 A500 R	0.3125	0.291	0.305	0.976	1.048	1.03
6x6x5/16 A1085 Y	0.3125	0.313	0.313	1.002	1.000	1.05
6x6x3/8 A500 R	0.375	0.349	0.367	0.979	1.052	1.03
6x6x3/8 A1085 Y	0.375	0.375	0.375	1.000	1.000	1.05
6x6x1/2 A500 R	0.5	0.465	0.479	0.958	1.030	1.01
6x6x1/2 A1085 Y	0.5	0.500	0.486	0.972	0.972	1.02
7x7x5/16 A500 Y	0.3125	0.291	0.290	0.928	0.997	0.98
7x7x5/16 A1085 Y	0.3125	0.313	0.305	0.976	0.974	1.03
7x7x3/8 A500 Y	0.375	0.349	0.342	0.912	0.980	0.96
7x7x3/8 A1085 Y	0.375	0.375	0.365	0.973	0.973	1.02
7x7x1/2 A500 B	0.5	0.465	0.464	0.928	0.998	0.98
7x7x1/2 A1085 Y	0.5	0.500	0.484	0.968	0.968	1.02
8x8x3/8 A500 W	0.375	0.349	0.350	0.933	1.003	0.98
8x8x3/8 A1085 Y	0.375	0.375	0.370	0.987	0.987	1.04
8x8x1/2 A500 W	0.5	0.465	0.461	0.922	0.991	0.97
8x8x1/2 A1085 Y	0.5	0.500	0.488	0.976	0.976	1.03
10x10x3/8 A500 W	0.375	0.349	0.347	0.925	0.994	0.97
10x10x3/8 A1085 Y	0.375	0.375	0.366	0.976	0.976	1.03
5x5x3/8 A1085 R	0.375	0.375	0.375	1.000	1.000	1.053
5x5x3/8 A1085 W	0.375	0.375	0.374	0.997	0.997	1.050
5x5x3/8 A1085 B	0.375	0.375	0.381	1.016	1.016	1.069
6x6x3/8 A1085 R	0.375	0.375	0.371	0.989	0.989	1.041
6x6x3/8 A1085 W	0.375	0.375	0.376	1.003	1.003	1.055
6x6x3/8 A1085 B	0.375	0.375	0.380	1.013	1.013	1.067
8x8x3/8 A1085 R	0.375	0.375	0.368	0.981	0.981	1.033
8x8x3/8 A1085 W	0.375	0.375	0.374	0.997	0.997	1.050
8x8x3/8 A1085 B	0.375	0.375	0.375	1.000	1.000	1.053
8x8x1/2 A1085 R	0.5	0.500	0.465	0.930	0.930	0.979
8x8x1/2 A1085 W	0.5	0.500	0.499	0.998	0.998	1.051
8x8x1/2 A1085 B	0.5	0.500	0.501	1.002	1.002	1.055

Note: Data shown above the line is from Bergendahl (2021)

The ratio of the measured wall thickness to the specified nominal wall thickness for the A1085 HSS specimens is plotted in Figure 3.22. Included in the figure is a dashed line for the nominal specified wall thickness and a solid line for the minimum required wall thickness for A1085. The figure shows that all of the A1085 test specimens met the minimum required thickness except for the 8x8x1/2 A1085 R specimen. All but one of the specimens which met the specification were within 3% of the nominal wall thickness.

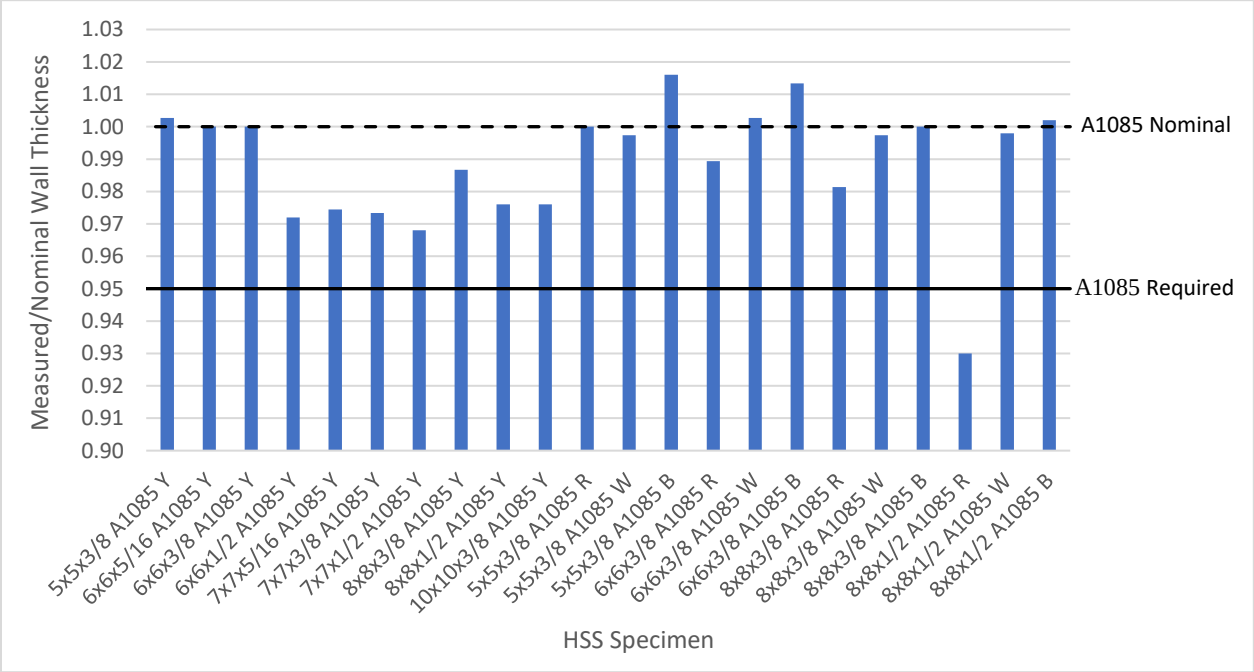

Figure 3.22. Ratio of Measured to Nominal Wall Thickness – A1085 Specimens

The ratio of the measured wall thickness to the specified nominal wall thickness for the A500 HSS specimens is plotted in Figure 3.23. Included in the figure are horizontal lines to show the specified nominal, design, and minimum thicknesses. The figure shows that all of the A500 test specimens met the 10% wall thickness tolerance for A500 Grade C and four of the A500 test specimens met the 5% wall thickness tolerance for A1085. On average, the wall thickness for the A500 test specimens was right around the design thickness for A500.

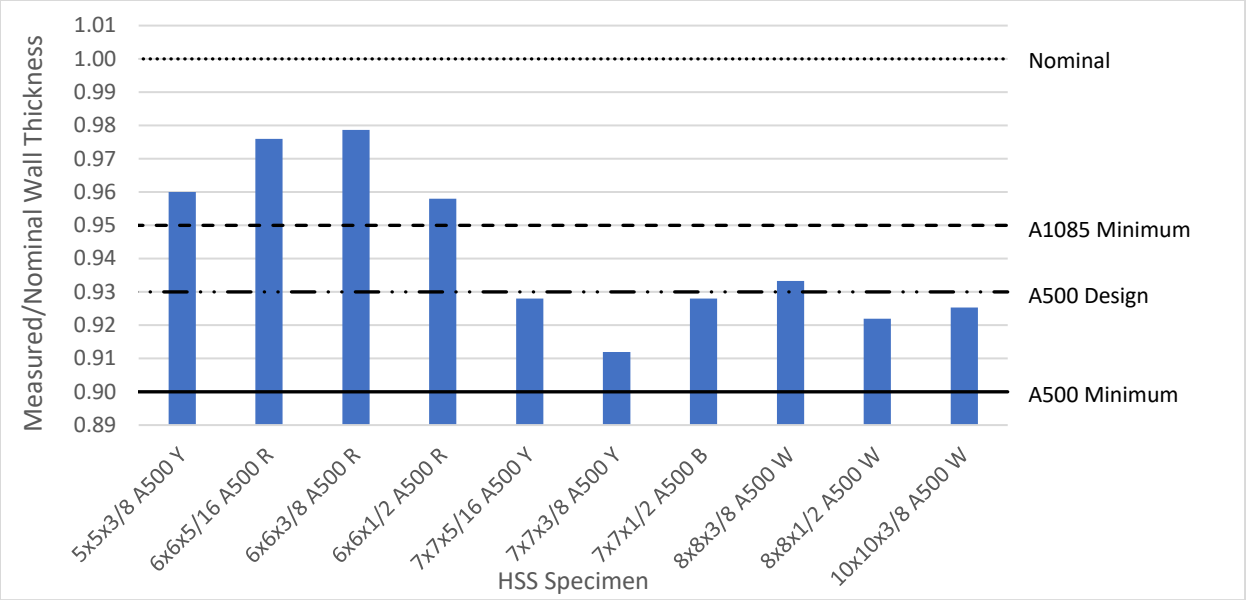

Figure 3.23 Ratio of Measured to Nominal Wall Thickness – A500 Specimens

The measured wall thicknesses are presented again Figure 3.24 below to compare between the different producers of A1085. In the figure, it is evident that the Red producer is the most variable and the 8x8x1/2 A1085 R specimen which does not meet the A1085 specification for wall thickness is the main source of variability.

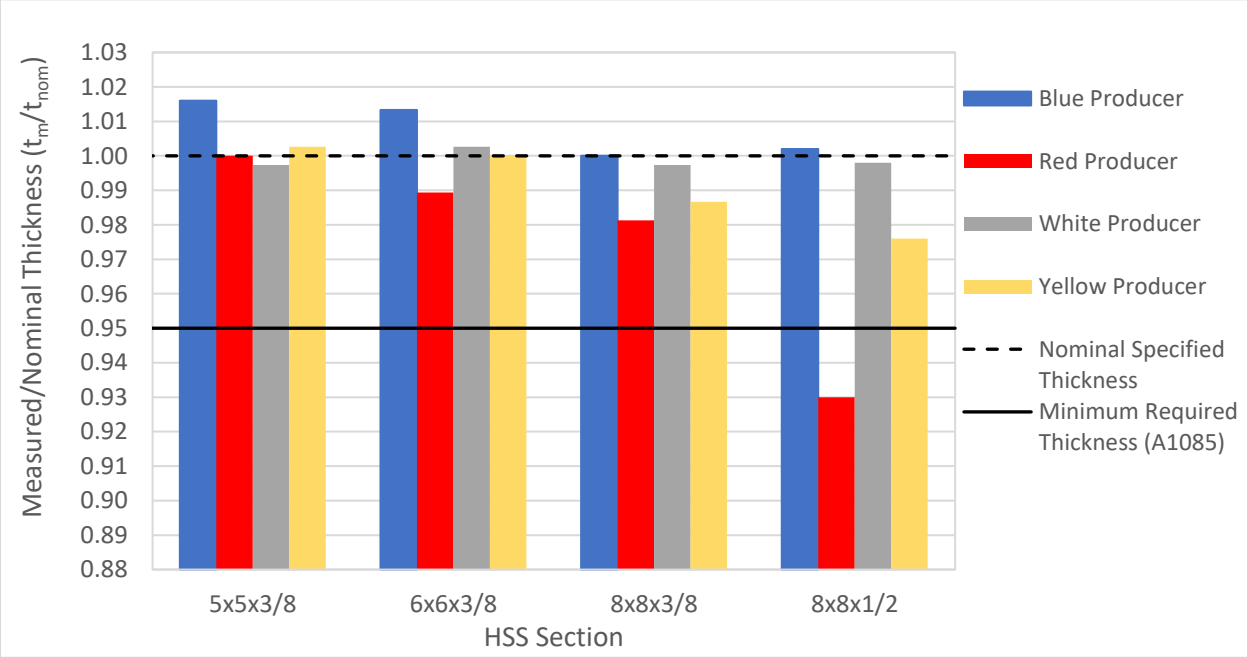

Figure 3.24 Producer Comparison of Measured Thickness – A1085

Table 3.11 shows a summary of the measured to nominal wall thickness ratios for each producer. For the A1085 specimens, the average thickness from each producer was within 2% of the nominal thickness. The Red producer was the most variable with a standard deviation of 0.03, while producers Blue, White and Yellow had standard deviations of 0.01, 0.00, and 0.01, respectively. The higher standard deviation for the Red producer is largely due to the 8x8x1/2 A1085 R specimen which was 7% thinner than the nominal thickness.

The average wall thickness ratio for all of the A500 specimens was 0.94, which is just slightly higher than the specified design thickness ratio of 0.93. This indicates that the 7% reduction in design thickness for A500 HSS is quite accurate. The standard deviation for all of the A1085 specimens was 9.2% less than that of all the A500 specimens, indicating that there is less variability in the thickness of A1085 HSS due to the tighter tolerance on wall thickness.

Table 3.11 Summary of Wall Thickness Ratios

t_{meas}/t_{nom}	**# of HSS Specimens**	**Average**	**Standard Deviation**
ALL	32	0.97	0.030
ALL A1085	22	0.99	0.019
A1085 B	4	1.01	0.008
A1085 R	4	0.98	0.031
A1085 W	4	1.00	0.003
A1085 Y	10	0.98	0.013
ALL A500	10	0.94	0.024
A500 B	1	0.93	-
A500 R	3	0.97	0.011
A500 W	3	0.93	0.006
A500 Y	3	0.93	0.024

The measured and nominal local slenderness ratios are shown in Table 3.12. Shown in the table are two different measured width to thickness ratios, $(b/t)_{meas}$ and b_{nom}/t_{meas}. $(b/t)_{meas}$ uses the measured flat width and the measured thickness, while b_{nom}/t_{meas} uses the nominal flat width and the measured thickness. The nominal flat width, b_{nom} is calculated as the brace width minus 3 times the design thickness. The measured flat width, b_{meas} was calculated as the brace width minus two times the measured corner radius. The corner radius was measured using a framing square set on the corner of the HSS such that the inside edges of the framing square were snug to adjacent sidewalls. The radius was then measured from the corner of the square to the point where the corner started (taken as the tangent of the side wall where the square was no longer in contact with the side wall). It is important to note that determination of the point where the corner starts is somewhat subjective so the $(b/t)_{meas}$ values should be considered with that in mind. The table below shows that the values for b_{nom}/t_{meas} are generally very similar to the nominal b/t values, however the $(b/t)_{meas}$ values are all less than the nominal values. This indicates that the actual corner radii were typically larger than the minimum specified leading to cross-sections that were more compact than expected.

Table 3.12. Measured and Nominal Local Slenderness Ratios

HSS SECTION	$(b/t)_{nom}$	$(b/t)_{meas}$	b_{nom}/t_{meas}	$(b/t)_{meas} / (b/t)_{nom}$	$(b_{nom}/t_{meas}) / (b/t)_{nom}$
5x5x3/8 A500 Y	11.3	9.7	11.0	0.86	0.97
5x5x3/8 A1085 Y	10.3	9.4	10.3	0.91	1.00
6x6x5/16 A500 R	17.6	15.8	16.8	0.90	0.95
6x6x5/16 A1085 Y	16.2	14.8	16.2	0.92	1.00
6x6x3/8 A500 R	14.2	12.3	13.5	0.86	0.95
6x6x3/8 A1085 Y	13	12.2	13.0	0.94	1.00
6x6x1/2 A500 R	9.9	8.4	9.6	0.85	0.97
6x6x1/2 A1085 Y	9	8.9	9.3	0.99	1.03
7x7x5/16 A500 Y	21.1	19.6	21.2	0.93	1.00
7x7x5/16 A1085 Y	19.4	18.6	19.9	0.96	1.03
7x7x3/8 A500 Y	17.1	15.6	17.5	0.91	1.02
7x7x3/8 A1085 Y	15.7	14.2	16.1	0.91	1.03
7x7x1/2 A500 B	12.1	11.0	12.1	0.91	1.00
7x7x1/2 A1085 Y	11	10.1	11.4	0.92	1.03
8x8x3/8 A500 W	19.9	18.3	19.8	0.92	1.00
8x8x3/8 A1085 Y	18.3	15.9	18.5	0.87	1.01
8x8x1/2 A500 W	14.2	13.5	14.3	0.95	1.01
8x8x1/2 A1085 Y	13	11.7	13.3	0.90	1.02
10x10x3/8 A500 W	25.7	24.4	25.8	0.95	1.01
10x10x3/8 A1085 Y	23.7	23.1	24.3	0.98	1.02
5x5x3/8 A1085 R	11.3	9.7	11.0	0.86	0.97
5x5x3/8 A1085 W	10.3	9.4	10.3	0.91	1.00
5x5x3/8 A1085 B	17.6	15.8	16.8	0.90	0.95
6x6x3/8 A1085 R	16.2	14.8	16.2	0.92	1.00
6x6x3/8 A1085 W	14.2	12.3	13.5	0.86	0.95
6x6x3/8 A1085 B	13	12.2	13.0	0.94	1.00
8x8x3/8 A1085 R	9.9	8.4	9.6	0.85	0.97
8x8x3/8 A1085 W	9	8.9	9.3	0.99	1.03
8x8x3/8 A1085 B	21.1	19.6	21.2	0.93	1.00
8x8x1/2 A1085 R	19.4	18.6	19.9	0.96	1.03
8x8x1/2 A1085 W	17.1	15.6	17.5	0.91	1.02
8x8x1/2 A1085 B	15.7	14.2	16.1	0.91	1.03

Note: Data shown above the line is from Bergendahl (2021)

3.4.2 *Material Properties*

Tension tests and Charpy V-Notch tests were conducted at the UW SRL to measure the material properties of the test specimens. The tables presented in this section include the material properties from all four test series, including both A1085 and A500 test specimens. Flat plates were taken from the walls of the HSS specimens to use for material tension testing. Two tension tests were completed for each specimen to measure the material yield strength, ultimate tensile strength, and percent elongation. The tension coupons were cut out of the flat plates using a waterjet cutter, and the procedure for the tension tests followed ASTM Standard Test Methods and Definitions for Mechanical Testing of Steel Products (ASTM, 2017). The measured material properties from the tension tests are provided in Table 3.13

Table 3.13. Material Properties from Tension Coupon Testing

HSS Section	Measured Yield Strength, *Fy,m* (ksi)	Measured Yield Strength Ratio, *Ry,m*	Measured Tensile Strength, *Fu,m* (ksi)	Measured Tensile Strength Ratio, *Rt,m*	Percent Elongation (%)
5x5x3/8 A500 Y	65.38	1.31	71.9	1.16	30.79
5x5x3/8 A1085 Y	66.04	1.32	74.6	1.15	32.83
6x6x5/16 A500 R	57.37	1.15	72.8	1.17	34.65
6x6x5/16 A1085 Y	62.07	1.24	71.9	1.11	34.11
6x6x3/8 A500 R	61.19	1.22	76.4	1.23	35.36
6x6x3/8 A1085 Y	66.81	1.34	72.6	1.12	31.86
6x6x1/2 A500 R	62.84	1.26	67.1	1.08	33.48
6x6x1/2 A1085 Y	67.85	1.36	72.0	1.11	34.88
7x7x5/16 A500 Y	62.71	1.25	70.0	1.13	31.16
7x7x5/16 A1085 Y	57.70	1.15	64.1	0.99	33.12
7x7x3/8 A500 Y	61.35	1.23	72.2	1.16	30.76
7x7x3/8 A1085 Y	61.89	1.24	70.1	1.08	31.32
7x7x1/2 A500 B	57.82	1.16	69.1	1.11	29.6
7x7x1/2 A1085 Y	64.38	1.29	71.7	1.10	32.7
8x8x3/8 A500 W	66.19	1.32	76.5	1.23	34.44
8x8x3/8 A1085 Y	60.37	1.21	72.1	1.11	34.2
8x8x1/2 A500 W	65.47	1.31	72.0	1.16	34.27
8x8x1/2 A1085 Y	64.42	1.29	75.4	1.16	32.23
10x10x3/8 A500 W	59.02	1.18	69.5	1.12	34.2
10x10x3/8 A1085 Y	58.34	1.17	73.8	1.14	34.94
5x5x3/8 A1085 R	68.82	1.38	77.52	1.19	34.92
5x5x3/8 A1085 W	69.53	1.39	75.03	1.15	38.06
5x5x3/8 A1085 B	78.15	1.56	87.62	1.35	27.90
6x6x3/8 A1085 R	60.41	1.21	74.29	1.14	33.26
6x6x3/8 A1085 W	67.66	1.35	73.22	1.13	37.53
6x6x3/8 A1085 B	69.05	1.38	73.59	1.13	34.75
8x8x3/8 A1085 R	61.20	1.22	75.42	1.16	32.44
8x8x3/8 A1085 W	63.19	1.26	70.67	1.09	40.55
8x8x3/8 A1085 B	68.24	1.36	71.63	1.10	37.18
8x8x1/2 A1085 R	58.54	1.17	64.27	0.99	34.43
8x8x1/2 A1085 W	58.54	1.17	64.27	0.99	42.02
8x8x1/2 A1085 B	66.36	1.33	70.51	1.08	39.56

Note: Data shown above the line is from Bergendahl (2021)

Figure 3.25 below shows the measured yield strength ratios for the A1085 test specimens. The measured yield strength ratio, $R_{y,m}$, is calculated by dividing the measured yield strength by the nominal yield strength. For A1085 HSS, the nominal yield strength is 50 ksi and the maximum permitted yield strength is 70 ksi. The figure includes horizontal lines at 1.25 and 1.4 which represent the expected yield strength ratio and maximum permitted yield strength ratio, respectively. This figure shows that all of the A1085 test specimens met the minimum specified yield strength and most of the specimens were close to the expected yield strength. The outlier is the 5x5x3/8 A1085 B specimen which had a higher than expected yield strength. Not only is it higher than expected but it also exceeds the maximum specified yield strength for A1085 HSS.

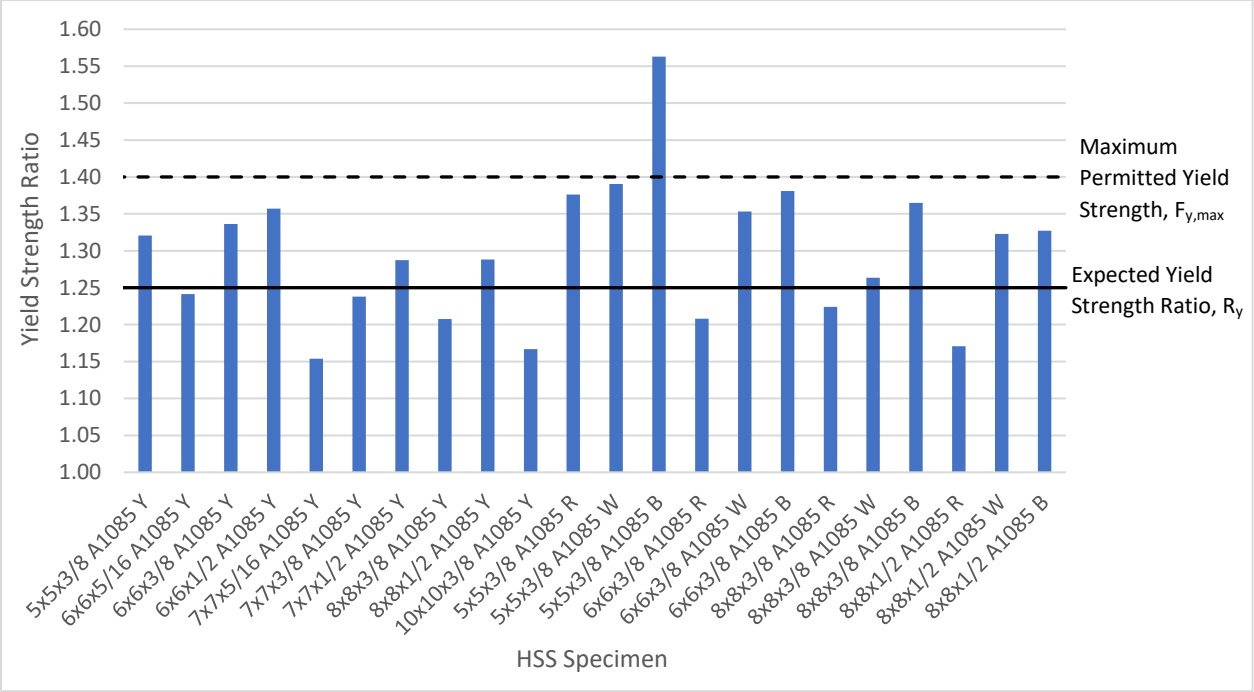

Figure 3.25. Measured Yield Strength Ratios – A1085 Specimens

Figure 3.26 below shows the measured yield strength ratios for the A500 test specimens. For A500 HSS, the nominal yield strength is 50 ksi and contrary to A1085, there is no maximum specified yield strength. The figure includes a horizontal line at 1.30 which represents the expected yield strength ratio, R_y. This figure shows that all of the A500 test specimens met the minimum specified yield strength. Many of the specimens were close to the expected yield

strength, however, the average yield strength ratio for the A500 test specimens was notably less than the expected value. Additionally, although there is no maximum yield strength requirement for A500, none of the A500 test specimens exceeded the maximum yield strength specified for A1085.

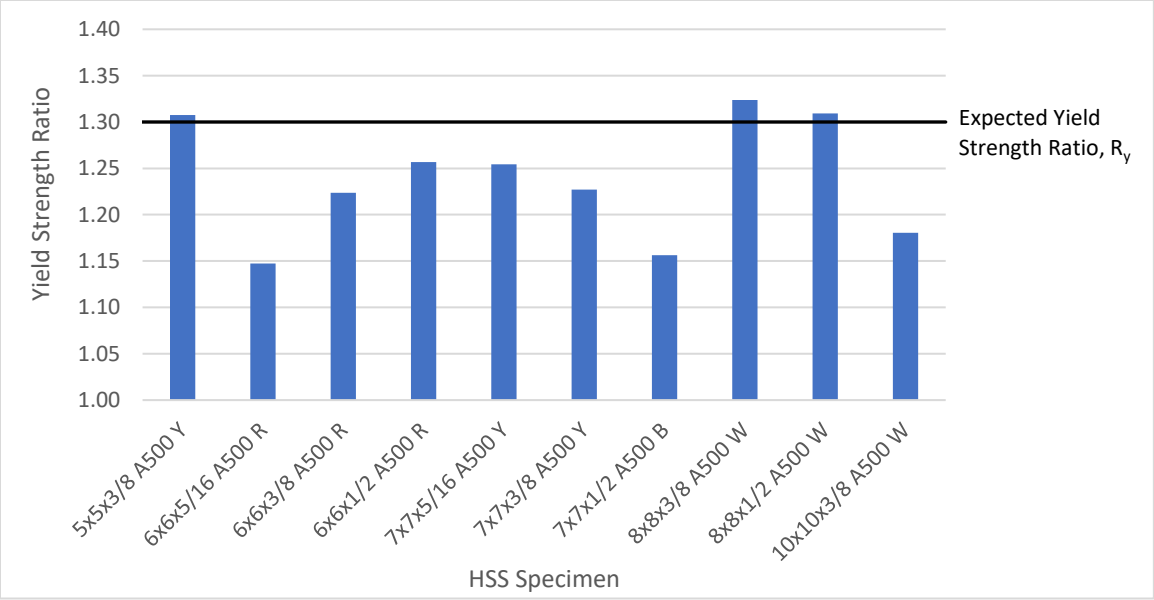

Figure 3.26 Measured Yield Strength Ratios – A500 Specimens

Figure 3.27 compares the yield strength ratios of the different producers. The figure shows that generally, the measured yield strengths were close to the expected value, R_yF_y. For all four of the HSS sections, the Blue producer had the highest yield strength. For three of the four, the Blue producer was only slightly above the others, but the 5x5x3/8 A1085 B specimen had a yield strength of 1.56 times the nominal which is considerably higher than second highest (1.39) and is also higher than the maximum specified by the A1085 specification (1.40).

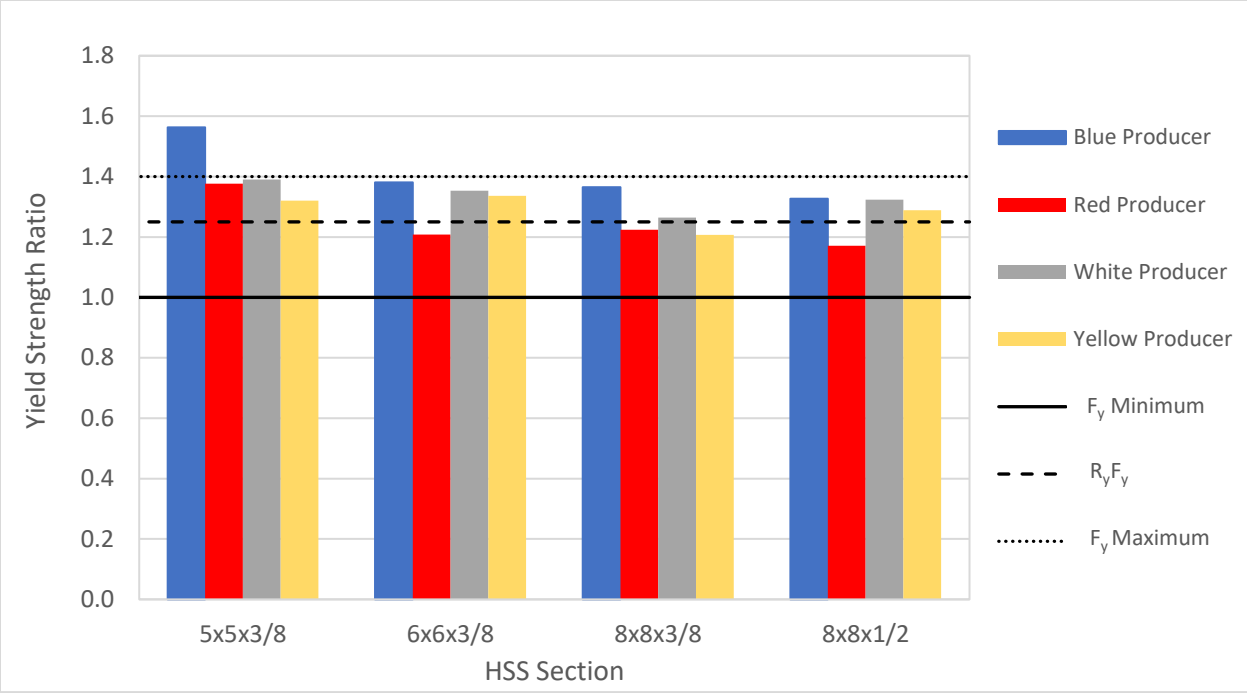

Figure 3.27 Producer Comparison of Yield Strength – A1085 HSS

The yield strength data is summarized in Table 3.14. The average measured yield strength for the A1085 specimens was 64.87 ksi, while that of the A500 specimens was 61.93 ksi. These values are relatively similar, but it is surprising that the A1085 is higher considering A1085 has a maximum specified yield strength while A500 does not. The average measured yield strength ratio for all the A1085 specimens was 1.30 which is slightly higher than the specified expected yield strength ratio of 1.25. For the A1085 specimens, the Blue producer has the highest standard deviation meaning it was the most variable. This variability was largely due to the very high yield strength of the 5x5x3/8 A1085 B specimen. Aside from this outlier, the other variations in yield strength across the different producers is minimal and close to the expected values for A1085.

Table 3.14 Summary of Measured Yield Strengths

	# of HSS Specimens	Measured Yield Strength, $F_{y,m}$ (ksi)		Measured Yield Strength Ratio, $R_{y,m}$	
		Average	Standard Deviation	Average	Standard Deviation
ALL	32	63.95	4.49	1.28	0.090
ALL A1085	22	64.87	4.76	1.30	0.095
A1085 B	4	70.45	5.26	1.41	0.105
A1085 R	4	62.24	4.52	1.24	0.090
A1085 W	4	66.63	2.68	1.33	0.054
A1085 Y	10	62.99	3.50	1.26	0.070
ALL A500	10	61.93	3.18	1.24	0.064
A500 B	1	57.82	-	1.16	-
A500 R	3	60.47	2.81	1.21	0.056
A500 W	3	63.56	3.95	1.27	0.079
A500 Y	3	63.15	2.05	1.26	0.041

The measured tensile strength ratios for the A1085 HSS specimens are shown below in Figure 3.28. This ratio is the measured ultimate tensile strength divided by the minimum required tensile strength of 65 ksi for A1085. The figure shows that most of the values are close to the expected value, however there are two outliers. The first notable difference is the very high tensile strength of the 5x5x3/8 A1085 B specimen. The high tensile strength is not an issue, but the corresponding exceedingly high yield strength does not meet the specification. The other notable outlier is the 8x8x1/2 A1085 R which did not meet the minimum tensile strength for the A1085 specification.

The measured tensile strength ratios for the A500 test specimens are shown below in Figure 3.29. This ratio is the measured ultimate tensile strength divided by the minimum required tensile strength of 62 ksi for A500. This figure shows that all of the A500 test specimens met the minimum tensile strength requirement for A500 and only two specimens exceeded the expected tensile strength ratio of 1.20.

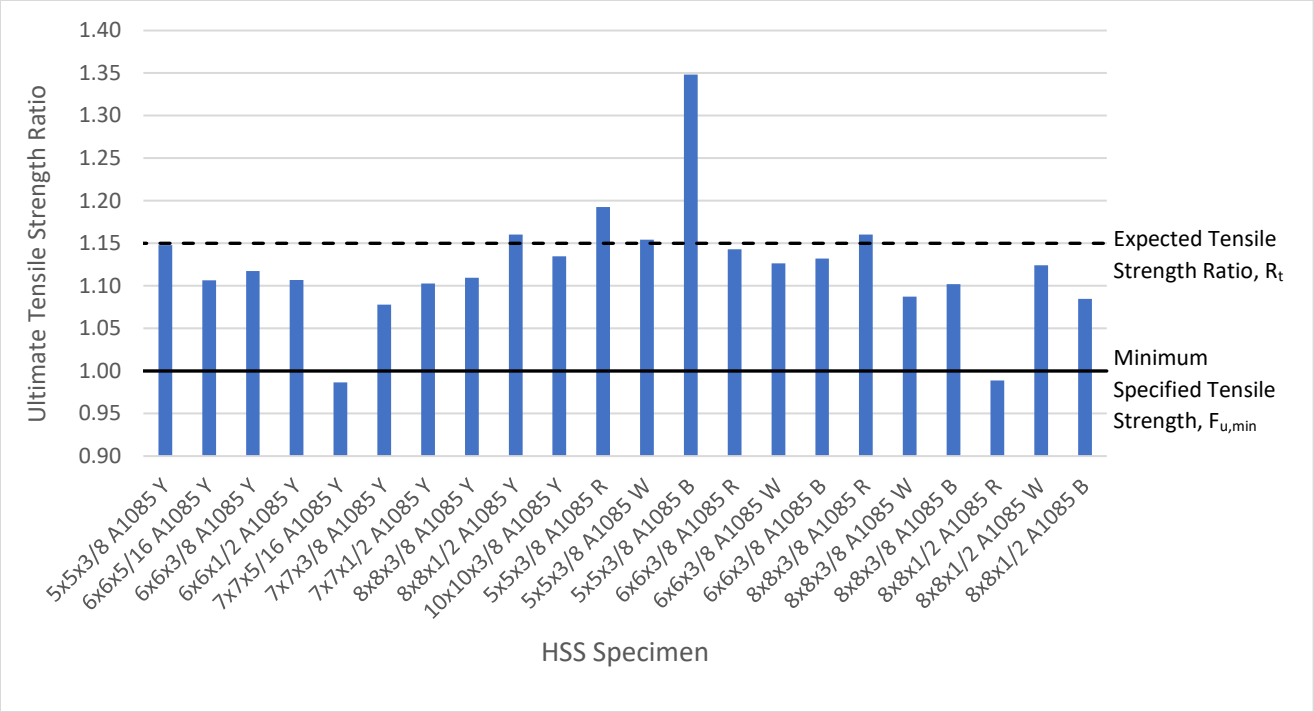

Figure 3.28 Measured Ultimate Tensile Strength Ratios – A1085 Specimens

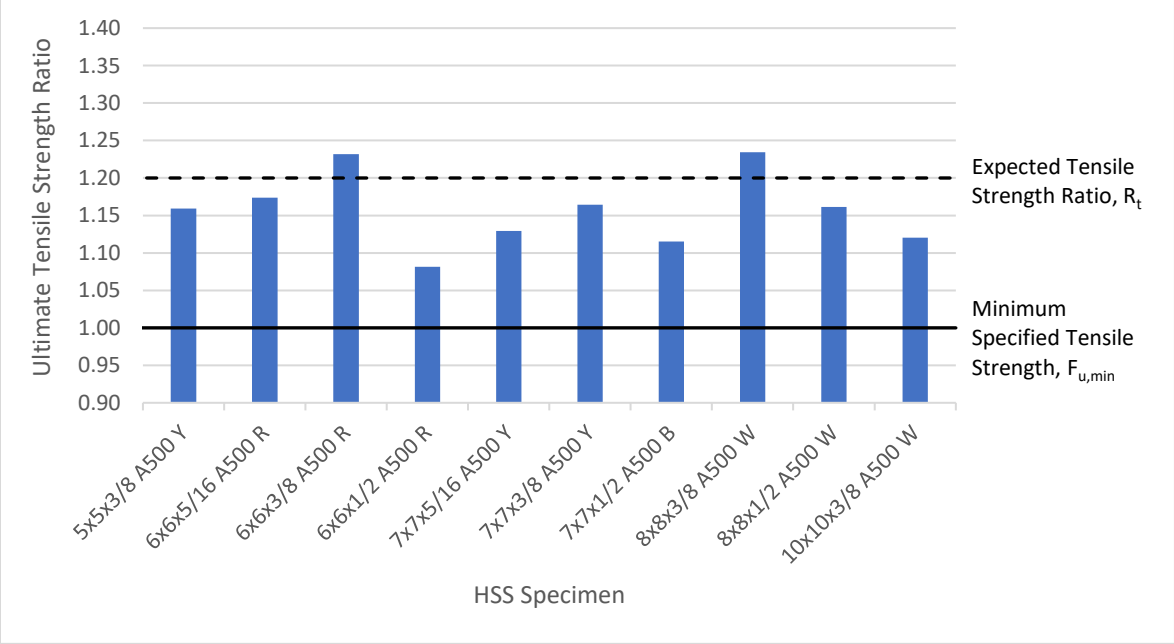

Figure 3.29 Measured Ultimate Tensile Strength Ratios – A500 Specimens

The results for measured ultimate strength are presented again in Figure 3.30 below to compare between the different A1085 producers. In the figure, it is evident that the ultimate tensile strengths for the Blue and Red producers were more variable than the White and Yellow producers. Most of the measured ultimate strengths are near or slightly below the expected tensile strength for A1085, however two specimens stand out as outliers. First, the 5x5x3/8 A1085 B specimen had an ultimate strength ratio of 1.35 which is much higher than the second highest (1.19) and much higher than the expected tensile strength ratio (1.15). The second outlier is the 8x8x1/2 A1085 R specimen which fell slightly below the minimum tensile strength for A1085 with an ultimate tensile strength ratio of 0.99.

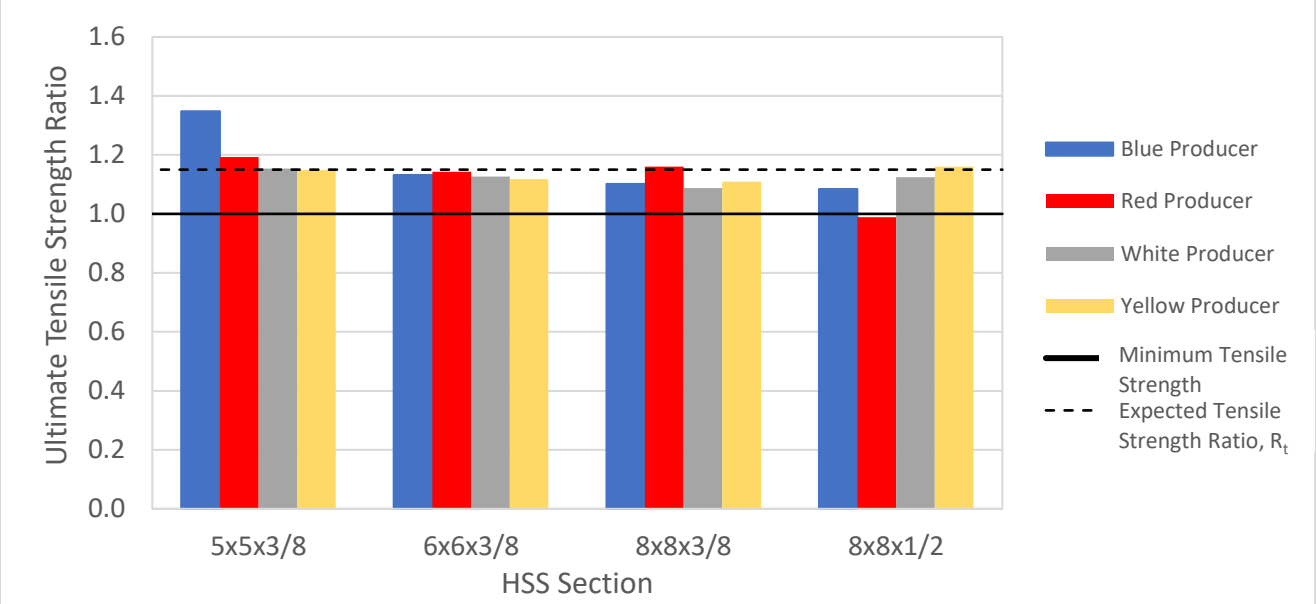

Figure 3.30 Producer Comparison of Tensile Strength – A1085 HSS

A summary of the measured tensile strengths is shown in Table 3.1. Regarding the A1085 test specimens, this table shows that the four producers were very similar with the exception of the Blue producer. For A1085, the Blue producer had an average measured tensile strength ratio of 1.17 while the Red, White, and Yellow producers had average measured tensile strength ratios of 1.12, 1.12, and 1.11, respectively. The Blue producer also had the highest variation with a standard deviation of measured tensile strength of 7.96. Again, the variation of the Blue producer is largely due to the very high tensile strength of the 5x5x3/8 A1085 B specimen.

Table 3.15 Summary of Measured Tensile Strengths

	# of HSS Specimens	Measured Tensile Strength, $F_{u,m}$ (ksi)		Measured Tensile Strength Ratio, $R_{t,m}$	
		Average	Standard Deviation	Average	Standard Deviation
ALL	32	72.58	4.13	1.13	0.066
ALL A1085	22	72.96	4.56	1.12	0.070
A1085 B	4	75.84	7.96	1.17	0.122
A1085 R	4	72.87	5.89	1.12	0.091
A1085 W	4	73.00	1.79	1.12	0.027
A1085 Y	10	71.83	3.12	1.11	0.048
ALL A500	10	71.75	3.02	1.16	0.049
A500 B	1	69.10	-	1.11	-
A500 R	3	72.10	4.69	1.16	0.076
A500 W	3	72.67	3.55	1.17	0.057
A500 Y	3	71.37	1.19	1.15	0.019

Figure 3.31 and Figure 3.32 show the measured ultimate-to-yield strength ratio, $F_{u,m}/F_{y,m}$, for A1085 and A500, respectively. The figures show variability across the test specimens with ratios ranging from 1.05 to 1.26.

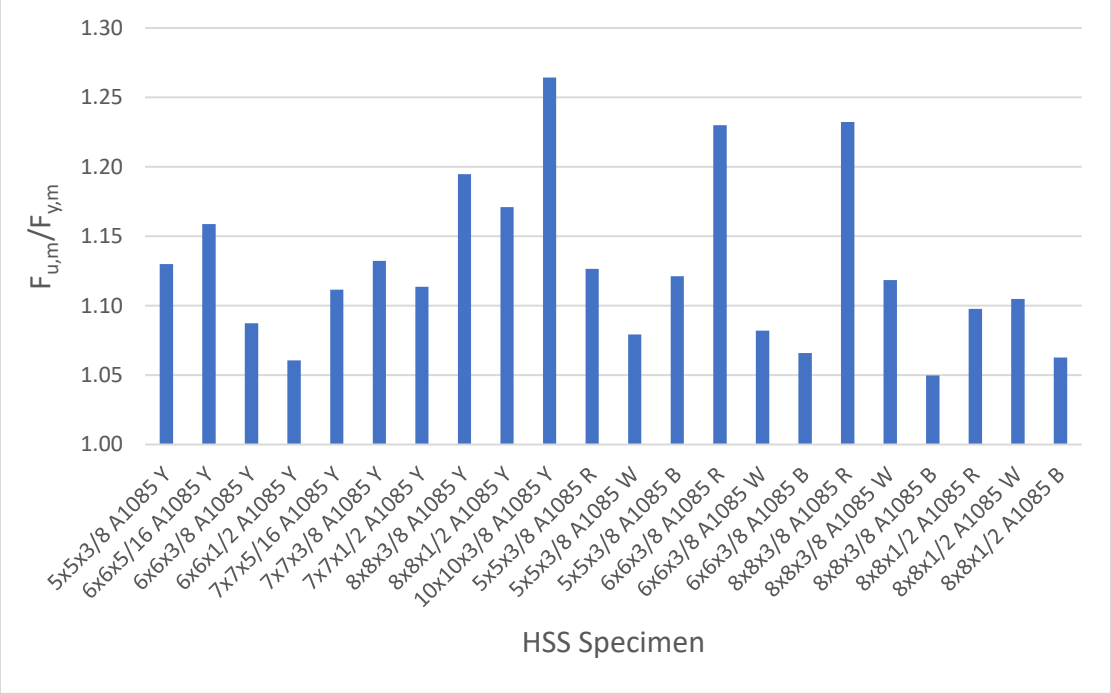

Figure 3.31 Measured ultimate-to-yield strength ratio – A1085 Specimens

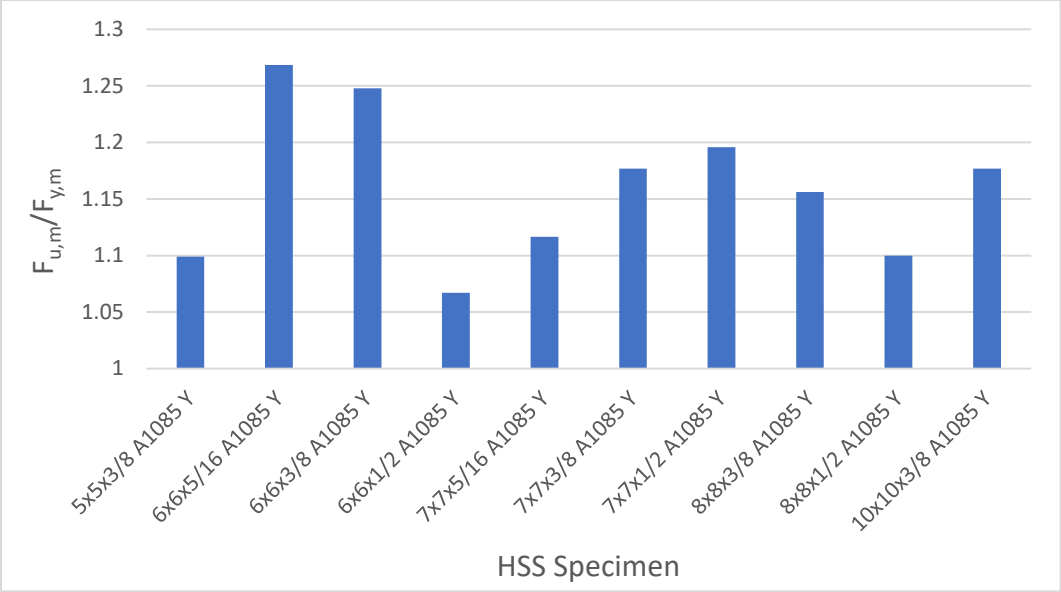

Figure 3.32 Measured ultimate-to-yield strength ratio – A500 Specimens

The results for percent elongation are presented in Figure 3.33 below to compare between the different A1085 producers. The figure shows that all of the producers consistently exceeded the minimum percent elongation requirement for the A1085 specification. All of the specimens were above 30% elongation except for the 5x5x3/8 A1085 B specimens which had the lowest percent elongation at 27.9%. This is the same specimen that exceeded the maximum specified yield strength for A1085.

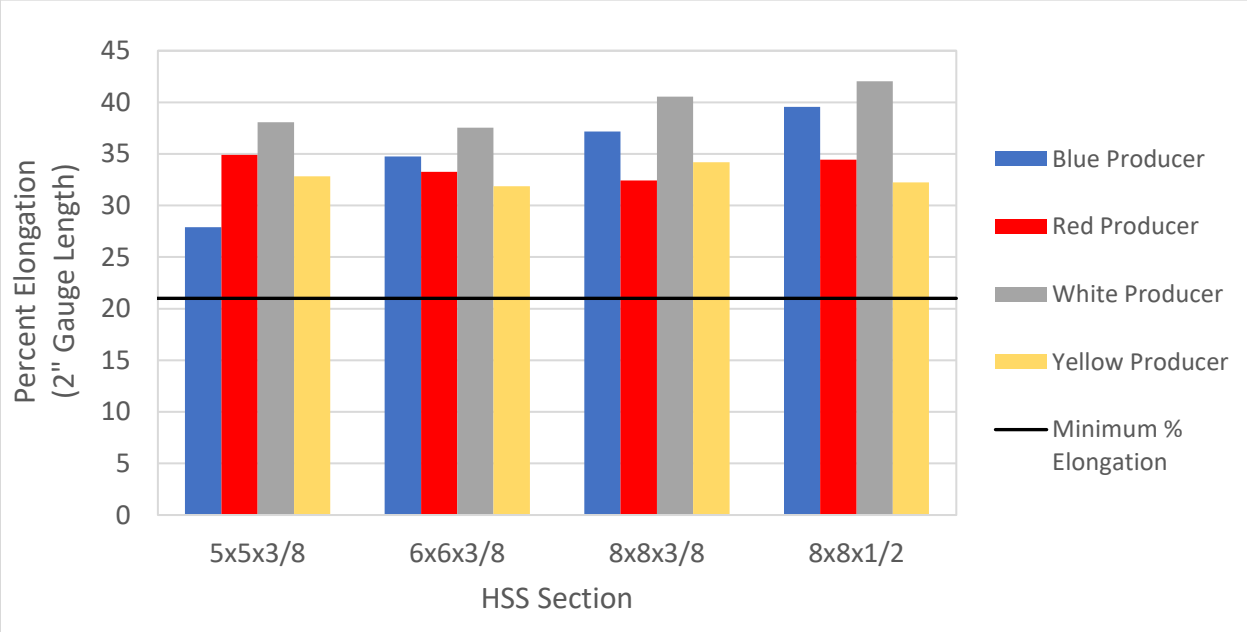

Figure 3.33 Producer Comparison of Percent Elongation

Three Charpy V-Notch (CVN) specimens were tested for each HSS test specimen to determine the toughness and energy absorption capacity of the steel. The A1085 specification requires a minimum CVN toughness of 25 ft-lbs at 40 F, while the A500 specification does not have a minimum toughness requirement. The CVN specimens were tested in the UW SRL using a Charpy Machine and using the procedure set by ASTM E23. The Charpy machine was calibrated following the NIST Charpy Verification program and this process was detailed by Bergendahl (2021). The CVN specimens were machined by Laboratory Testing, Inc in accordance with ASTM Standard Test Methods for Notched Bar Impact Testing of Metallic Materials (ASTM, 2007). The CVN specimens were machined from flat plates cut out of the side walls of the HSS specimens. The standard size Charpy specimen is 55mm x 10mm x 10mm. Standard size specimens were used for the 1/2" thick HSS tubes however, sub-sized specimens had to be used for the thinner HSS tubes. 55mm x 10mm x 7.5mm Charpy specimens were used for 3/8” thick tubes and 55mm x 10mm x 5mm Charpy specimens were used for the 5/16” thick tubes.

Table 3.16 below shows the Charpy specimen size and absorbed energy for each HSS test specimen. The CVN tests were conducted from the high energy position on the Charpy machine which has a potential energy of 120 lb-ft. Many specimens did not fully fracture under the impact of the Charpy machine pendulum. For each material that this occurred, all three of the specimens in a given set did not fracture and the absorbed energy was recorded as 120+. Although direct comparison of the absorbed energy results from specimens of varying size is not feasible, there are recommended methods to convert the results from sub-sized specimens to correlate with the results from standard sized specimens (Wallin, 2016). The most basic conversion is multiplying the energy absorbed by a sub-sized specimen by the proportion of a standard size to the sub-sized specimen. For example, for a 55mm x 10mm x 5mm specimen, the energy is multiplied by 2.0 to make it correspond to a standard size specimen. Although this correlation method is not completely accurate, the method is also recommended by ASTM 370 for modifying CVN criteria for various sub-size specimens. This methodology was used to calculate the modified absorbed energy provided in Table 3.16.

Table 3.16. Charpy V-Notch Test Results

Test Specimen	CVN Specimen Width (mm)	Absorbed Energy (ft-lbs)	Modified Absorbed Energy (ft-lbs)
5x5x3/8 A500 Y	7.5	12.8	17.0
5x5x3/8 A1085 Y	7.5	18.8	25.0
6x6x5/16 A500 R	5	40.8	81.6
6x6x5/16 A1085 Y	5	23.0	46.0
6x6x3/8 A500 R	7.5	42.5	56.5
6x6x3/8 A1085 Y	7.5	18.8	25.0
6x6x1/2 A500 R	10	120 +	120 +
6x6x1/2 A1085 Y	10	27.8	27.8
7x7x5/16 A500 Y	5	15.7	23.6
7x7x5/16 A1085 Y	5	18.5	27.8
7x7x3/8 A500 Y	7.5	14.3	19.0
7x7x3/8 A1085 Y	7.5	17.3	23.0
7x7x1/2 A500 B	10	42.0	42.0
7x7x1/2 A1085 Y	10	28.7	28.7
8x8x3/8 A500 W	7.5	65.5	87.1
8x8x3/8 A1085 Y	7.5	8.5	11.3
8x8x1/2 A500 W	10	67.3	67.3
8x8x1/2 A1085 Y	10	40.3	40.3
10x10x3/8 A500 W	7.5	120 +	120 +
10x10x3/8 A1085 Y	7.5	20.7	27.5
8x8x1/2 A1085 Y *C	10	89.5	89.5
8x8x1/2 A500 W *C	10	120 +	120 +
5x5x3/8 A1085 R	7.5	23.17	30.9
5x5x3/8 A1085 W	7.5	76.83	102.4
5x5x3/8 A1085 B	7.5	30.67	40.9
6x6x3/8 A1085 R	7.5	40.5	54.0
6x6x3/8 A1085 W	7.5	82.67	110.2
6x6x3/8 A1085 B	7.5	120+	120+
8x8x3/8 A1085 R	7.5	58.33	77.8
8x8x3/8 A1085 W	7.5	70.5	94.0
8x8x3/8 A1085 B	7.5	120+	120+
8x8x1/2 A1085 R	10	120+	120+
8x8x1/2 A1085 W	10	120+	120+
8x8x1/2 A1085 B	10	120+	120+

Note: Data shown above the line is from Bergendahl (2021)

Figure 3.34 and Figure 3.35 below show the modified absorbed energy normalized by the minimum CVN toughness requirement for A1085 (25 ft-lbs). Figure 3.34 shows data from the A1085 test specimens, while Figure 3.35 shows data from the A500 test specimens. The figures show significant variance among the test specimens. All of the A1085 test specimens meet the minimum toughness requirement for A1085 except for the 7x7x3/8 and 8x8x3/8 A1085 test specimens from the Yellow producer. The 7x7x3/8 A1085 Y specimens provided an average absorbed energy of 23.1 ft-lbs, just under the requirement of 25 ft-lbs. The 8x8x3/8 A1085 Y specimen had an average absorbed energy of 11.3 ft-lbs which is less than half of the required value. The proportional correlation method may be the cause of the 7x7 specimen not meeting the requirement but the 8x8 is short of the meeting requirement. Although there is no minimum CVN requirement for A500 HSS, eight out of the ten A500 test specimens met the CVN minimum for A1085.

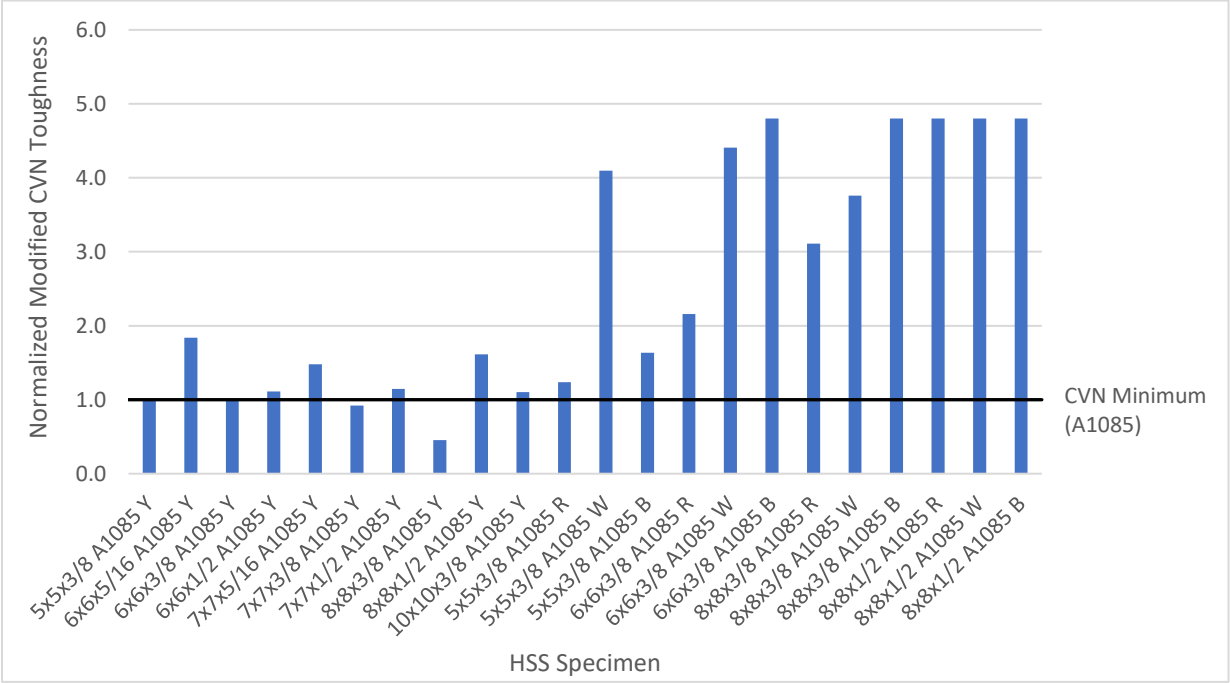

Figure 3.34 Modified CVN Toughness – A1085 Specimens

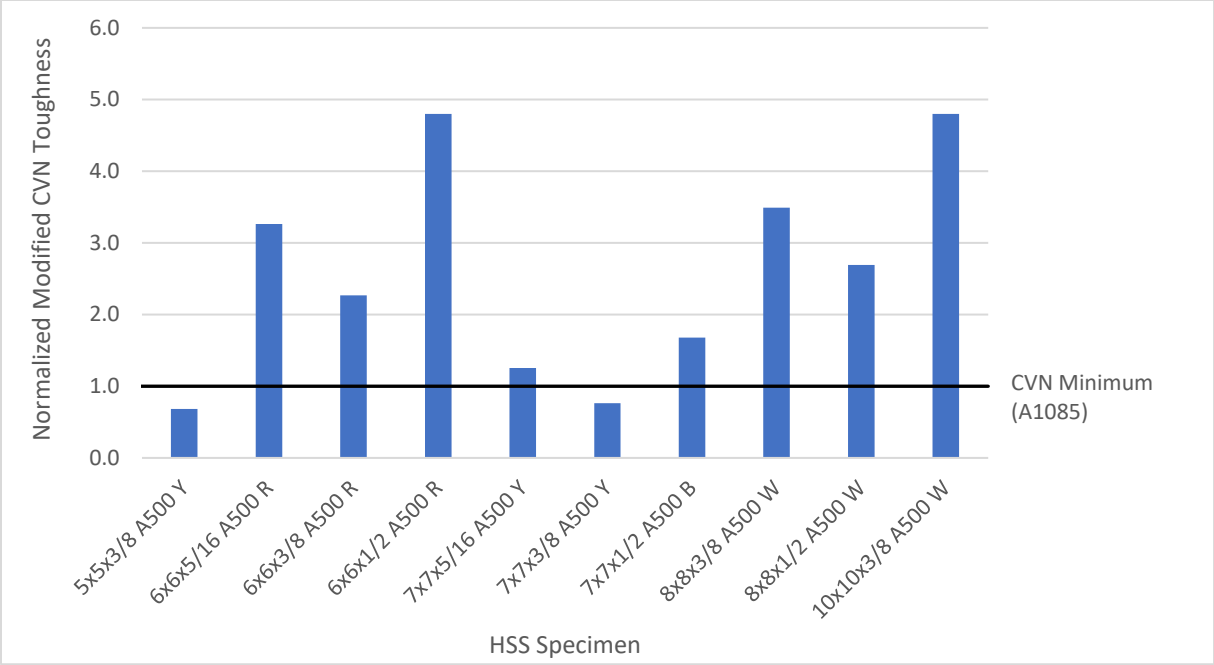

Figure 3.35 Modified CVN Toughness – A500 Specimens

Table 3.17 below provides a summary of the measured unmodified CVN toughness results. This table separates the results by Charpy specimen size so comparisons can be made between same sized specimens.

Table 3.17 Summary of Measured Unmodified Charpy V-Notch Data

	# of Specimens	Width (mm)	Average (ft-lbs)	Standard Deviation
All A1085	6	10	76.1	48.26
	14	7.5	50.5	38.09
	2	5	20.8	3.18
A1085 B	1	10	120.0	-
	3	7.5	90.2	51.57
A1085 R	1	10	120.0	-
	3	7.5	40.7	17.58
A1085 W	1	10	120.0	-
	3	7.5	76.7	6.09
A1085 Y	3	10	32.3	6.97
	5	7.5	16.8	4.79
	2	5	20.8	3.18
ALL A500	3	10	76.4	39.79
	5	7.5	51.0	44.30
	3	5	76.4	39.79
A500 B	1	10	42.0	-
	1	10	120.0	-
A500 R	1	7.5	42.5	-
	1	5	40.8	-
A500 W	1	10	67.3	-
	2	7.5	92.8	38.54
A500 Y	2	7.5	13.6	1.06
	1	5	15.7	-
	6	10	76.1	48.26

3.4.3 *Summary of Test Specimen Properties*

Generally, the measured geometric and material properties show minor variations, however, there were a few results that stood out and were not in compliance with the A1085 specification requirements. All of the A1085 test specimens met the 5% wall thickness tolerance for A1085 except for the 8x8x3/8 A1085 R specimen which had a measured wall thickness 7% less than the nominal. All of the measured flat widths were smaller than the nominal values. This generated $(b/t)_{meas}$ values smaller than the nominal width-to-thickness ratios. Generally, the ratio

of the $(b/t)_{meas}$ to the $(b/t)_{nom}$ was between 0.85 and 0.95, showing that the HSS specimens were more compact than specified.

The measured properties from the tension tests showed that there was some variation between producers. The Blue and Red producers were more variable than the White and Yellow producers. The measured material properties of two specific specimens stood out. The 5x5x3/8 A1085 B specimen had a yield stress exceeding the maximum specified value for A1085 and an ultimate stress much higher than the rest of the specimens. Additionally, the 8x8x1/2 A1085 R specimen did not meet the minimum specified ultimate strength for A1085, although it was only 1% shy of the limit.

3.5 LOADING PROTOCOL

The tests in this program were conducted by applying quasi-static cyclic axial displacements to one end of the specimen while the other end stayed pinned in place. The displacements were applied using two hydraulic actuators acting in parallel. The actuators were programmed to run under displacement control using MTS MultiPurpose Testware (MPT) Software. Under actuator displacement control, the two actuators would apply identical axial displacements ensuring no applied rotations on the end of the brace. Prior to each test, two cycles of $\pm$1/16" displacements were applied to the specimen. This was done to ensure proper functioning of the instrumentation prior to running the actual displacement procedure. For each of the displacement load histories, the procedure was followed until the test specimen fractured. Pauses were made frequently throughout testing to take pictures and make observations.

The displacement loading protocol for each testing series is shown in the following figures. The majority of the tests in this research program were from Series 1 and Series 2. In these testing series, 237.5" long braces were subjected to a symmetric cyclic loading protocol with increasing displacements as shown in Figure 3.36. This symmetric displacement protocol was developed based on previous research at the UW SRL and recommendations for testing components of steel structures (ATC, 1992, Krawinkler, 2009). In this displacement protocol, two full cycles were conducted for each target displacement. A cycle started by pulling the brace in tension to a target displacement. Once the target tension displacement was reached, the loading was reversed, and the specimen was pushed into compression towards a target

compressive displacement of the same magnitude. The first six target displacements were in increments of 1/8”, starting at 0.125” and increasing to 0.75”. These small displacements were applied to capture the elastic behavior of the brace as well as initial global buckling and yielding. After the 0.75” displacements, the subsequent target displacements were increased in 0.5” increments until the specimen fractured.

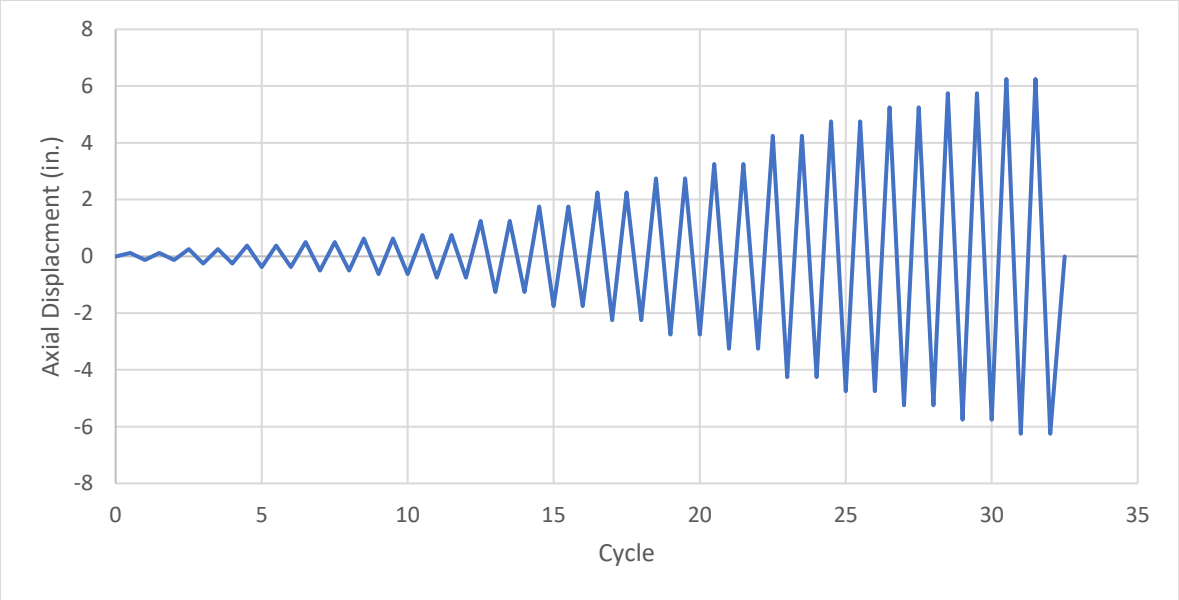

Figure 3.36. Symmetric Displacement Protocol

In Series 3, two alternative displacement protocols were used. The “chevron” displacement protocol, shown in Figure 3.37, was developed to represent the behavior of a brace in a braced frame with a chevron configuration. Previous research has shown that the deflection of beams in chevron configurations results in increased compressive deformations and decreased tensile deformations (Roeder et al., 2019). In this displacement protocol, the target compressive displacements increased in the same progression as the symmetric protocol. The target tensile displacements increased in the same progression from the beginning until the tensile load reached the magnitude of the buckling load. From this point forward, the tension cycles were controlled by load rather than displacement. In each tension cycle forward, the specimen was pulled to a tensile load equal to the magnitude of the actual buckling load. In the figure below, the plateaued tensile displacements show an approximate displacement for a tensile load equivalent to the magnitude of the buckling load.

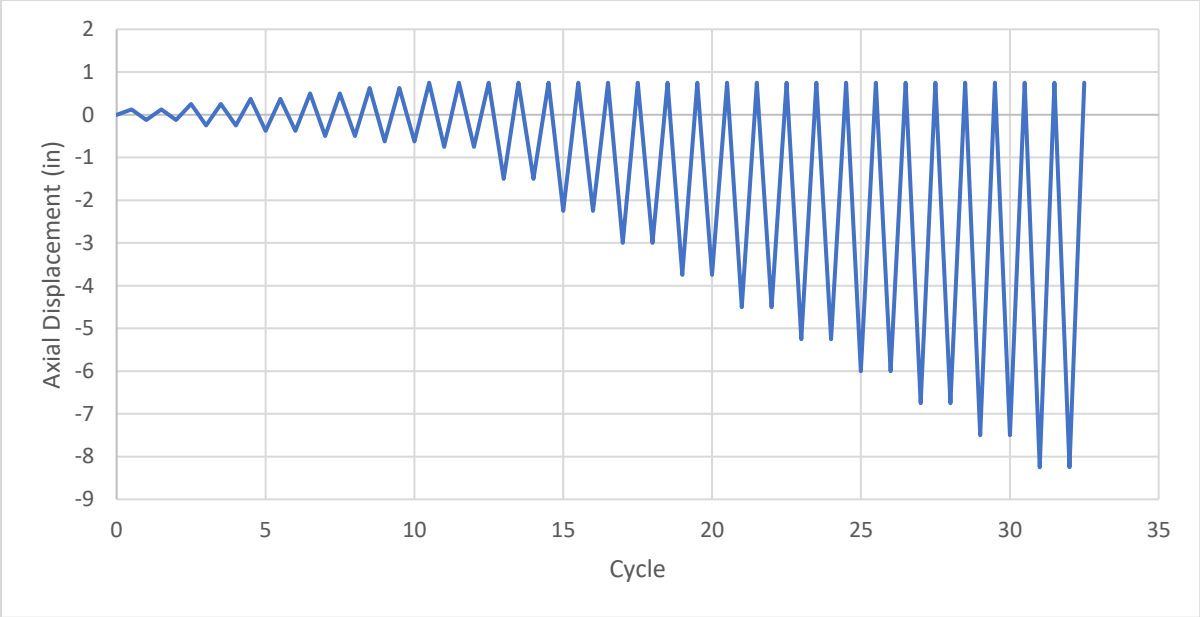

Figure 3.37 Chevron Displacement Protocol

The “near fault” displacement protocol, shown in Figure 3.38, was developed as a modified version of a loading protocol used in previous research to represent non-symmetric pulse type demands for a braced frame subjected to near-fault ground motions (Fell et al., 2009). This protocol follows the shape of the compression dominated near-field loading protocol used by Fell, but this protocol was flipped to be tension dominated and the magnitude of displacements was modified.

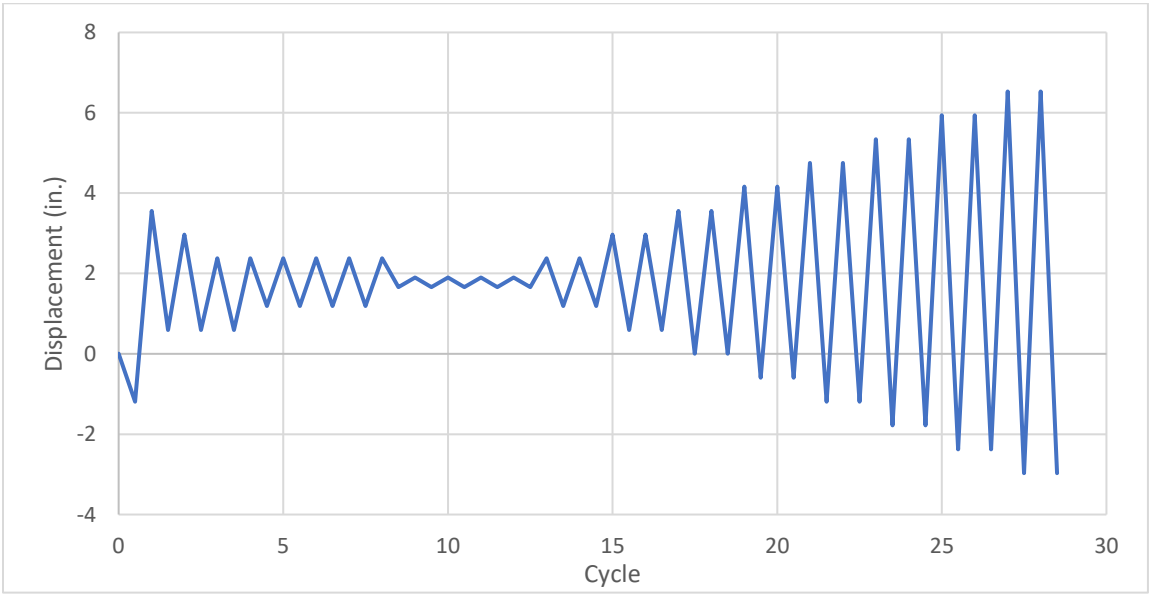

Figure 3.38 Near Fault Tension Dominant Displacement Protocol

In Series 4 of this testing program, the specimen brace length was shortened from 237.5” to 183.5”. The goal of this series was to explore the effects of brace length and global slenderness. The results from this series would be compared to Series 1 and 2 so the specimens were subjected to the same symmetric loading protocol scaled down by the short to long brace length ratio (183.5:237.5). The short brace symmetric displacement protocol for series 4 is shown in Figure 3.39.

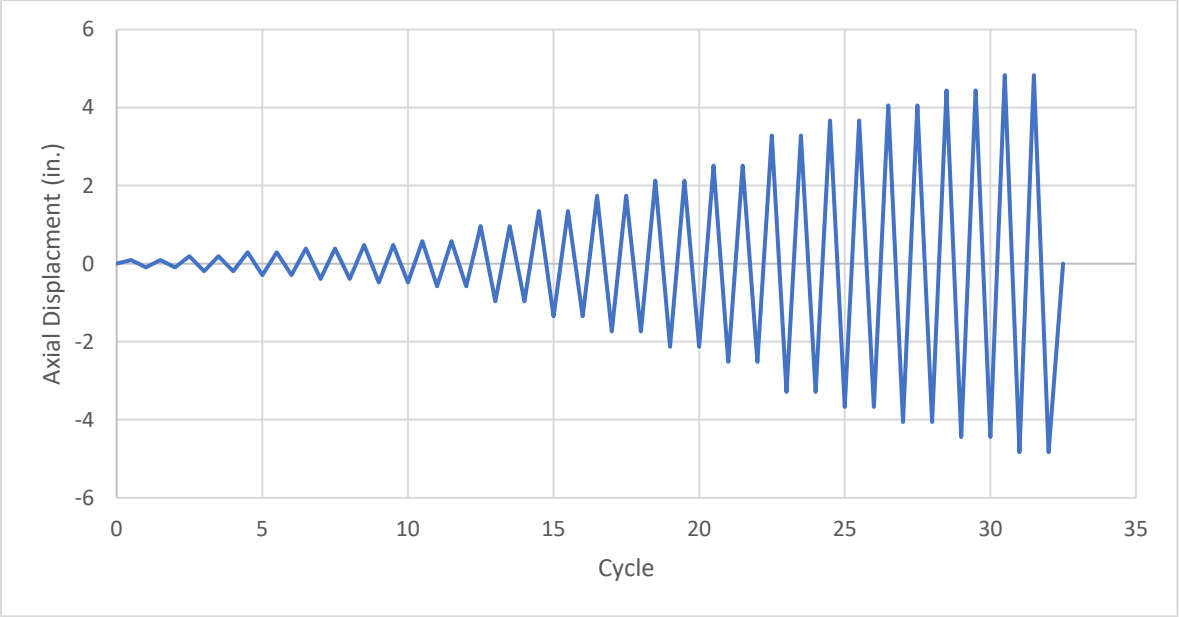

Figure 3.39 Short Brace Symmetric Displacement Protocol

3.6 TEST INSTRUMENTATION

Various data collection instruments were used to collect quantitative data of the forces, displacements, and strains during testing. The following instruments were used in testing: string potentiometers, Duncan potentiometers, strain gauges, load cells, Linear Variable Differential Transformers (LVDTs), and Optotrak sensors. Data from the potentiometers, strain gauges, load cells, and LVDTs was collected using LabVIEW software, developed by National Instruments. Data from the Optotrak sensors was collected using NDI First Principles software. Further detail regarding the instruments and the location of instruments is detailed in this section.

3.6.1 *Actuators – Load Cell and LVDT*

The displacements and loads applied by the two actuators were recorded using internal LVDTs and load cells, respectively. The loads collected by the load cells were used to determine the axial brace forces in the test specimens. The LVDT data was used to ensure the proper functioning of the dual actuator displacement control. The displacement of the two actuators could be checked in real time to make sure they were moving in sync, applying the same displacements to the sliding beam. Additionally, the data from both of the load cells could be checked to ensure the intended actuator load ratio of 9:7.

3.6.2 *Potentiometers*

Potentiometers were strategically placed to measure critical displacements of the test specimens as well as displacements of components of the test frame. Two types of potentiometers were used to measure displacements during testing – UniMeasure P510 string potentiometers and BEI Duncan 600 Series linear conductive potentiometers. Generally, string potentiometers were used to measure displacements that would exceed 2” or where rotation was expected. The locations of the string potentiometers are displayed in Figure 3.41. Duncan potentiometers were typically used to measure the movement of various components in the test frame where much smaller displacements were expected. The locations of the Duncan potentiometers are displayed in Figure 3.42.

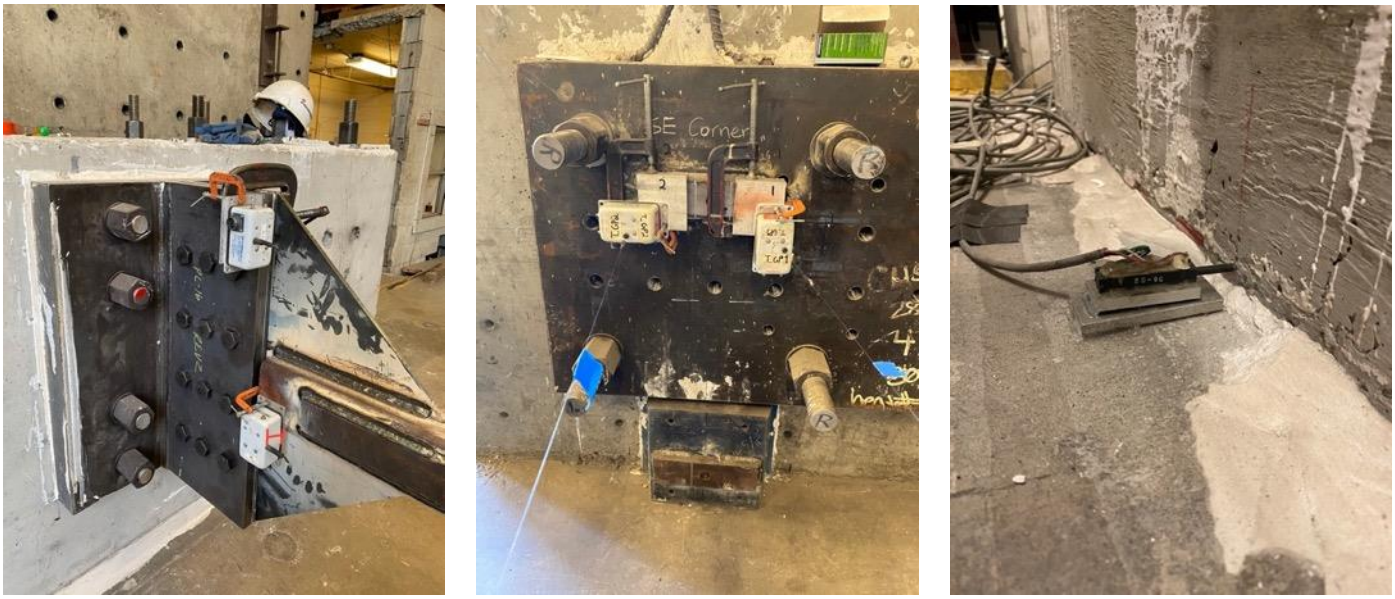

(a) (b) (c)

Figure 3.40. String (a and b) and Duncan Potentiometers (c)

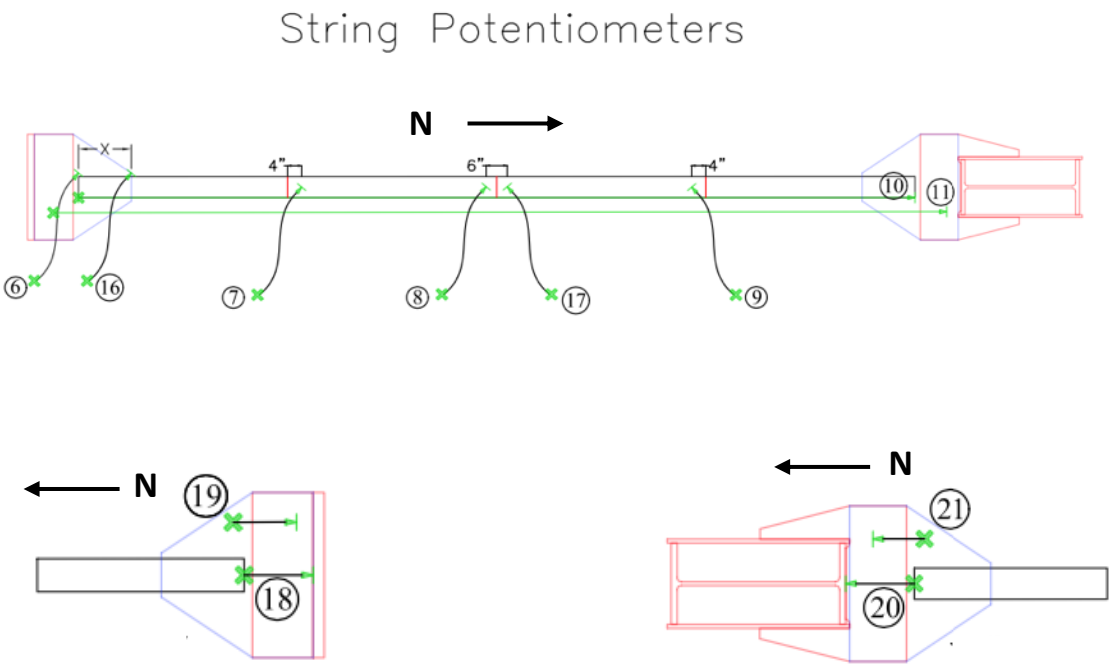

Figure 3.41. String Potentiometer Layout

The axial brace deformation used in analysis was measured using string potentiometers 10 and 11. String potentiometer 10 was attached to the south end of the brace using a C-clamp and the string ran along the side of the brace to the north end of the specimen. This directly measured the axial deformation of the specimen; however, the data needed to be corrected as detailed in Chapter 5. String potentiometer 11 also measured axial deformation but it was attached to the south connection plate and ran to the north connection plate, so the measured displacements included bolt slip and deformation of the gusset plates.

The lateral deformation along the specimen was measured by string potentiometers 6, 7, 8, 9, 16, and 17. String potentiometers 6 and 16 were located 10" apart on the south gusset plate and were used to calculate the end rotation. This was useful when correcting for the impact of rigid body gusset rotation on the axial deformation data. String potentiometers 7 and 9 measured the lateral displacements of the quarter points of the specimen and potentiometers 8 and 17 measured the out-of-plane displacement at the center of the brace.

String potentiometers 18-21 were placed on the north and south connections to measure bolt slip and gusset plate elongation. Potentiometers 18 and 20 were connected to the side of the HSS brace and the string ran parallel to the connection plates where the end was attached to the bearing plate using a magnet. Potentiometers 19 and 20 were attached to the gusset plates and the string ran parallel to the gusset plate to where the end was clamped to the side of the connection plate.

The Duncan potentiometers were used to monitor the movement of various components in the test frame to ensure there was no significant unwanted movement. A Duncan potentiometer was attached at the base of each reaction block to measure sliding of the blocks during testing. Duncan potentiometers 12, 13, and 14 measured the east, west, and end reaction blocks, respectively. Potentiometer 22 was attached to the top of the south connection plate to measure the movement of the connection plate relative to the end reaction block. The layout of the Duncan potentiometers is shown below in Figure 3.42.

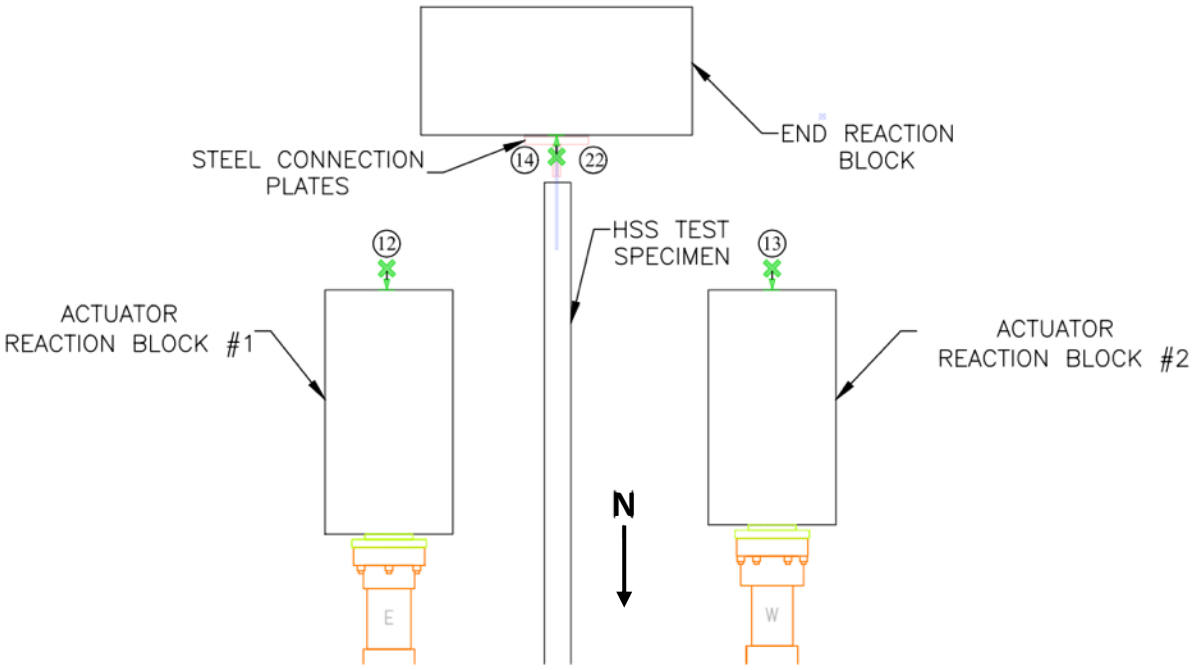

Figure 3.42. Duncan Potentiometer Layout

3.6.3 *Strain Gauges*

Eight total strain gauges were attached to each test specimen – four at each quarter point. The strain gauges were placed at the center of each side wall and were oriented longitudinally. The strain gauges were used to measure the axial force in the specimen, which provided redundancy to the axial force aquired by the actuator load cells. The layout of the strain gauges is shown in Figure 3.43.

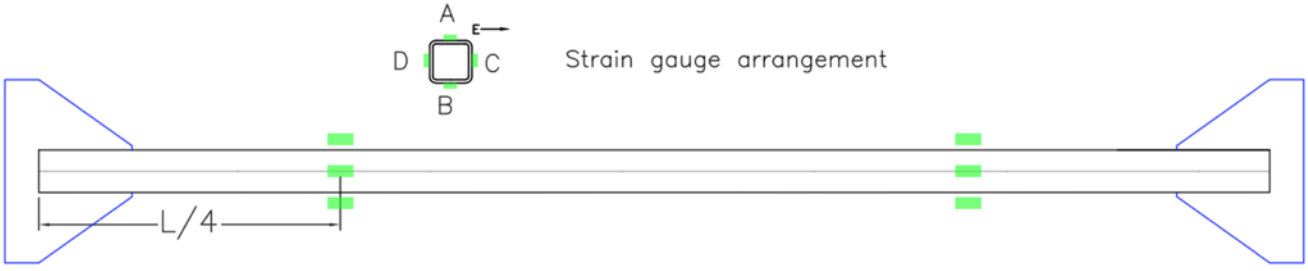

Figure 3.43. Strain Gauge Layout

3.6.4 *Optotrak System*

The Optrotrak system uses a series of three cameras to measure 3-dimensional displacement at the locations of LED sensors. The measurements acquired by the Optrotrak system are accurate to within a millimeter. The Optotrak camera was placed on the north side of the test frame and 20 LED sensors were placed at the locations shown in Figure 3.44. The data collected by this system could be used to measure the rotation of the north gusset plate and any axial or lateral displacement of the test specimen. Additionally, the data could be used to determine axial and transverse displacements of the sliding beam.

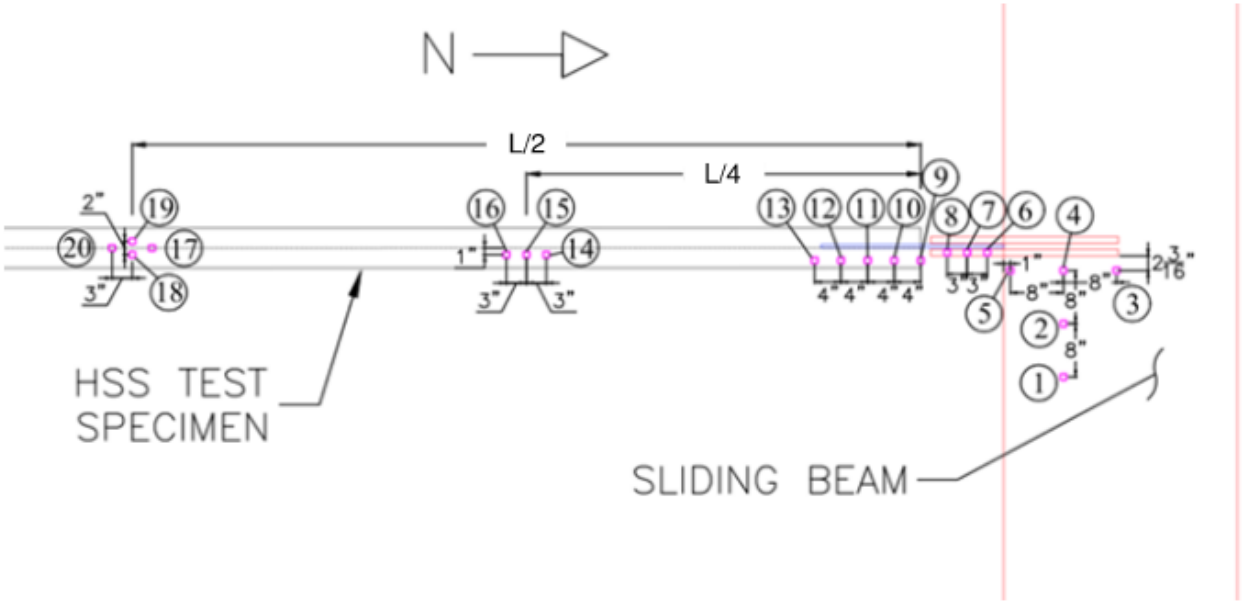

Figure 3.44. Optotrak LED Layout

3.7 PRE-TESTING PROCEDURE

The following procedure was used to prepare the specimen, test frame, and instrumentation for testing. First, the HSS specimen was cut to length using a plasma cutter. The tubes were provided in 40’ sections so the specimens needed to be cut to the intended length. Next, slots were cut at both ends of the specimen using a plasma cutter. These slots allowed for connection of the gusset plates. Next, the gusset plates were attached to the HSS brace using the testing rig as a jig. The gusset plates were bolted to the connection plates of the testing rig, and the brace was placed into the rig using a box crane to lower the tube into place with the slots aligned with the gusset plates. Once the positioning of the tube was verified to ensure alignment and connection spacing, the brace was tack welded to the gusset plates at both ends. The brace was then pulled out of the test frame and set aside. The net section reinforcement plates were then tack welded to the sides of the specimen. The tack welds on the gusset plates and net section reinforcement held all members in the correct position until a certified structural welder completed the full welds. Figure 3.45 shows a specimen before and after welding of the gusset plate to brace connection.

(a) (b)

Figure 3.45. Test Specimen Prior to Welding (a) and Fully Welded (b)

After all welds were completed, eight strain gauges were attached to the locations detailed in section 3.6.3. Then the specimen was moved back into the test frame and bolted using twelve 1” diameter A490 bolts at both ends. The bolts were then tightened using a hydraulic wrench to achieve the intended bolt tension.

Once the brace was fully connected to the test frame, all instrumentation was attached to the specimen and connected to the data acquisition system. Two digital cameras were set up around the specimen – one on the end block capturing the entire specimen, and one on east side of the specimen capturing the local damage at the center of the brace. The cameras were controlled using a remote trigger to capture photos on both cameras at the same time. A third mobile camera was also used to take photos at different locations and from different perspectives not captured by the stationary cameras.

Chapter 4. EXPERIMENTAL RESULTS

4.1 INTRODUCTION

This chapter presents the experimental test results to detail the performance of each brace test specimen. As described in Chapter 3, this experimental program consisted of four testing series. Results from series two, three, and four are provided in this chapter (results from series one can be found in Bergendahl (2021)). The test specimens for each test series are shown in Section 3.3.

To define each test specimen, a naming convention is used. The naming convention, adopted from Bergendahl (2021), includes the following information in the order it is listed: (1) HSS shape, (2) steel specification (ASTM A1085 or A500), and (3) producer (Y-Yellow, R-Red, B-Blue, and W-White). Unless noted otherwise, the brace specimen was 237.5” in length and subjected to a symmetric loading protocol which was the case for all of the braces tested in Series 1 and 2 (32 of the 41 total tests). In Series 3, the loading protocol was changed, and in Series 4, the brace length was changed. For these tests, the convention also indicates (1) loading protocol or (2) brace length. Specimens subjected to alternate loading protocols include the name of the protocol (Chevron or Near Fault). Specimens tested at the shorter length of 183.5” are named “Short”. For example, a 7x7x3/8 HSS specimen made of A1085 steel, produced by the Yellow manufacturer, subjected to the near fault load protocol, would be named “7x7x3/8 A1085 Y Near Fault”. Although long, this naming convention distinguishes each test specimen uniquely.

The behavior of each brace is described using observations of the response of the brace as well as measured axial and out of plane deflections and quantitative data recorded during testing. Additionally, the behavior will be described using a set of performance states which were adopted from previous research on SCBFs with a focus on the brace alone (Swatosh, 2016). The terminology for these performance states is provided in Table 4.1 below.

Table 4.1. Brace Performance States

Sketch/Photograph of Damage State	Abbreviation	Performance State	Description
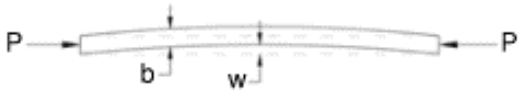	B1	Initial Global Buckling	Brace mid-span deflection, ***w***, is visible but less than the brace depth, **b**. Begins when maximum compressive load is reached.
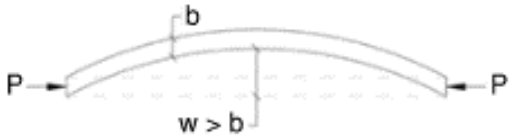	B2	Moderate Global Buckling	Brace mid-span deflection, ***w***, exceeds the brace depth, **b**.
	B3 – C	Local Cupping Deformations	Visible Local Cupping deformations (also termed **C**upping) near midpoint of the brace.
	B3 – T	Striations and Tearing	Striation lines begin in the cupping region (plastic hinge region) of the brace.
	B4	Brace Fracture	Brace fractures through the entire cross section.

Section 4.2 presents the observations for all of the tests and is organized as described here. First, summary tables are presented in Section 4.2.1. These tables summarize the measured geometric and material properties as well as the performance of each test specimen.

The remaining sections (Sections 4.2.2 through 4.2.22), provide the brace axial force versus deformation curves and provide a brief summary of the observations made during the testing of each of the twenty specimens. In each figure showing the individual, normalized force-deformation behavior, the brace axial force is normalized by the measured brace yield force (shown in Table 4.3), and the brace axial deformation is expressed as a percentage of the initial brace length. The axial force was measured by the actuator load cells. The axial brace deformation was measured by a string potentiometer along the length of the brace as described in Section 3.7. The initiation of each performance state listed in Table 4.1 during testing is indicated by a symbol on the hysteretic curve.

In addition to the damage states and the force displacement response, there is a brief test summary recapping the critical events and observations as well as any unexpected behavior/loading/response that may have occurred during testing. These summaries use the brace axial deformation to describe the state of the specimen at the various events, while the target displacements and cycle numbers are used to describe cycle at which the event occurred. Photographs are included as well to show the damage states. Appendix F provides more extensive summaries which further detail the brace properties and brace performance through additional tables, plots, and photos.

4.2 TEST RESULTS

This section includes several tables which provide the nominal and measured properties of each brace as well as deformation corresponding to the performance states provided in Table 4.1. Nominal and measured geometric properties of each specimen are provided in Table 4.2. The methods for determining the measured properties such as wall thickness and compactness ratio are described in Chapter 3. The nominal *b/t* ratios are color coded to indicate compliance with the AISC-341 *b/t* limits. The corresponding colors are as follows: green for highly ductile, orange for moderately ductile, and red for non-ductile (does not meet the requirements for highly or moderately ductile).

Table 4.3 provides the measured material properties for each specimen. The measured yield and ultimate strengths were determined through coupon tension tests at the UW SRL. The yield stress obtained from tension testing was used to determine the brace yield force. This table also includes CVN toughness values which was determined using the methods detailed in Section 3.3.

The expected and measured brace forces are provided in Table 4.4. The measured brace yield force was determined by multiplying the measured yield stress, $F_{y,m}$, and the measured cross-sectional area, $A_{g,m}$. The measured cross-sectional area, $A_{g,m,}$ was taken as the nominal area, A_g, multiplied by the ratio of measured to nominal wall thickness. The expected critical buckling load is calculated using R_yF_y as the yield stress, while the measured critical buckling is calculated using $F_{y,m}A_{g,m}$ as the yield stress.

A summary of the axial deformations corresponding to each performance state of each specimen is provided in Table 4.6. The table also provides other critical events such as brace yielding and peak tensile force. Here, brace yielding is defined as the point when the applied axial load first meets the predicted yield force, $F_{y,m}A_{g,m}$. The tabulated brace axial deformations note the axial deformation at the initiation of the specified performance state (the point at which the performance state was first observed). Provided in parentheses is the approximate drift ratio at the tabulated axial deformation. The approximate drift ratio was calculated based on a chevron configuration with a brace angle of 45°, as shown in Figure 4.1 below. In the figure, L_i denotes the initial brace length, while L_f denotes the final deformed brace length.

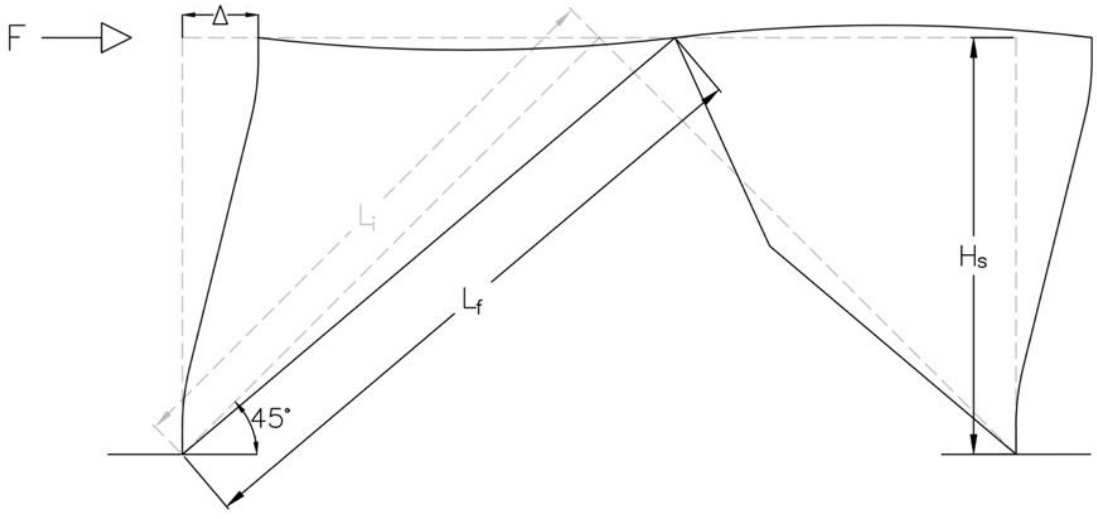

Figure 4.1 Assumed Brace Configuration in Chevron

Based on the configuration above, the corresponding story height, H_s, is calculated as follows:

$$H_s = \sqrt{\frac{{L_i}^2}{2}} \tag{4.1}$$

The story lateral displacement, Δ_s, can be approximated using the axial brace deformation, L_f - L_i , where L_i is the initial, undeformed length of the brace and L_f is the final, deformed length of the brace corresponding to the performance state. As such, L_f depends on the current axial deformation of the brace and L_i is constant.

$$\Delta_s = (L_f - L_i) \cdot 2 \cdot \cos(45°) = 1.41 \cdot (L_f - L_i) \tag{4.2}$$

The drift ratios are provided as percentages of story height using the simple calculation:

$$\frac{\Delta_s}{H_s} \cdot 100 \tag{4.3}$$

All drift ratios provided in this thesis are calculated using this same approach.

Table 4.5 also provides the target axial displacement of the cycle, *d*, corresponding to the initiation of each performance state. The target displacement, which is the peak applied actuator displacement in a given cycle, differs from the measured brace axial deformation due to factors such as bolt slip, gusset plate deformation, bolt bearing, and elastic deformations in the test frame. The number in parentheses under the target displacement indicates whether the event occurred during the first or second cycle to the target displacement. Table 4.5 also provides the axial force at the initiation of each damage state. Shown in parentheses is the ratio of the axial force to either the yield load or critical buckling load from Table 4.3. Tensile forces are shown as a ratio of the yield load and compressive forces are shown as a ratio of the critical buckling load. This is also indicated under each performance state title. Typically, the specimens would fracture in tension, however, there were several specimens that fractured in compression following tearing in tension. In these cases, noted by an asterisk, the axial force ratio at fracture is shown as a ratio of the force at fracture to the expected critical buckling load.

The maximum tensile and compressive axial deformations experienced by the brace are shown in Table 4.6 with the corresponding approximate drift ratios in parentheses. This table also includes the deformation and drift ranges – summations of the maximum tensile and compressive deformations and story drifts.

4.2.1 *Summary Tables*

Table 4.2 Summary of Nominal and Measured Geometric Properties

			Wall Thickness		Brace Compactness		
Test Specimen	**Nominal Area, A_g (in²)**	**Moment of Inertia, I (in⁴)**	**Nominal, t_{nom} (in)**	**Measured, t_{meas} (in)**	**Nominal, b/t_{nom}**	**Measured, b/t_{meas}**	**Global Slenderness, KL/r**
5x5x3/8 A1085 R	6.58	22.8	0.375	0.375	10.30	9.23	127.7
5x5x3/8 A1085 W	6.58	22.8	0.375	0.374	10.30	9.50	127.7
5x5x3/8 A1085 B	6.58	22.8	0.375	0.381	10.30	9.27	127.7
6x6x3/8 A1085 R	8.08	41.6	0.375	0.371	13.00	12.30	104.6
6x6x3/8 A1085 W	8.08	41.6	0.375	0.376	13.00	11.74	104.6
6x6x3/8 A1085 B	8.08	41.6	0.375	0.380	13.00	11.41	104.6
8x8x3/8 A1085 R	11.1	106.0	0.375	0.368	18.30	17.43	76.9
8x8x3/8 A1085 W	11.1	106.0	0.375	0.374	18.30	17.26	76.9
8x8x3/8 A1085 B	11.1	106.0	0.375	0.375	18.30	16.77	76.9
8x8x1/2 A1085 R	14.4	131.0	0.500	0.465	13.00	12.82	78.6
8x8x1/2 A1085 W	14.4	131.0	0.500	0.499	13.00	12.20	78.6
8x8x1/2 A1085 B	14.4	131.0	0.500	0.501	13.00	11.68	78.6
5x5x3/8 A1085 Y Chevron	6.58	22.8	0.375	0.376	10.3	9.42	127.7
5x5x3/8 A1085 Y Near Fault	6.58	22.8	0.375	0.376	10.3	9.42	127.7
7x7x3/8 A1085 Y Chevron	9.58	68.7	0.375	0.365	15.7	14.21	88.6
7x7x3/8 A1085 Y Near Fault	9.58	68.7	0.375	0.365	15.7	14.21	88.6
8x8x3/8 A1085 Y Chevron	11.1	106.0	0.375	0.370	18.3	15.89	76.9
8x8x3/8 A1085 Y Near Fault	11.1	106.0	0.375	0.370	18.3	15.89	76.9
5x5x3/8 A1085 Y Short	6.58	22.8	0.375	0.376	10.3	9.42	98.7
7x7x3/8 A1085 Y Short	9.58	68.7	0.375	0.365	15.7	14.21	68.5
8x8x3/8 A1085 Y Short	11.1	106.0	0.375	0.370	18.3	15.89	59.4

Table 4.3 Summary of Material Properties

Test Specimen	Measured Yield Strength, F_y (ksi)	Measured Ultimate Strength, F_u (ksi)	CVN Absorbed Energy (ft-lbs)
5x5x3/8 A1085 R	68.82	77.52	23.17
5x5x3/8 A1085 W	69.53	75.03	76.83
5x5x3/8 A1085 B	78.14	87.62	30.67
6x6x3/8 A1085 R	60.40	74.29	40.5
6x6x3/8 A1085 W	67.66	73.22	82.67
6x6x3/8 A1085 B	69.05	73.59	120+
8x8x3/8 A1085 R	61.2	75.42	58.33
8x8x3/8 A1085 W	63.18	70.67	70.5
8x8x3/8 A1085 B	68.23	71.63	120+
8x8x1/2 A1085 R	58.54	64.27	120+
8x8x1/2 A1085 W	58.54	64.27	120+
8x8x1/2 A1085 B	66.35	70.51	120+
5x5x3/8 A1085 Y Chevron	66.04	74.62	18.8
5x5x3/8 A1085 Y Near Fault	66.04	74.62	18.8
7x7x3/8 A1085 Y Chevron	61.89	70.07	17.3
7x7x3/8 A1085 Y Near Fault	61.89	70.07	17.3
8x8x3/8 A1085 Y Chevron	60.37	72.12	8.5
8x8x3/8 A1085 Y Near Fault	60.37	72.12	8.5
5x5x3/8 A1085 Y Short	66.04	74.62	18.8
7x7x3/8 A1085 Y Short	61.89	70.07	17.3
8x8x3/8 A1085 Y Short	60.37	72.12	8.5

Table 4.4 Summary of Expected and Measured Loads

Test Specimen	Yield Load		Critical Buckling Load	
	Expected, $P_{y,e}$ ($R_yF_yA_g$) (kips)	**Measured, $P_{y,m}$ ($F_{y,m}A_{g,m}$) (kips)**	**Expected, $P_{cr,e}$ (kips)**	**Measured, $P_{cr,m}$ (kips)**
5x5x3/8 A1085 R	427.7	452.8	101.3	101.3
5x5x3/8 A1085 W	427.7	456.3	101.3	101.3
5x5x3/8 A1085 B	427.7	522.4	101.3	101.3
6x6x3/8 A1085 R	525.2	482.9	185.3	185.3
6x6x3/8 A1085 W	525.2	548.2	185.3	185.3
6x6x3/8 A1085 B	525.2	565.4	185.3	185.3
8x8x3/8 A1085 R	721.5	666.6	404.3	400.4
8x8x3/8 A1085 W	721.5	699.5	404.3	406.3
8x8x3/8 A1085 B	721.5	757.4	404.3	420.1
8x8x1/2 A1085 R	936.0	784.0	511.4	496.5
8x8x1/2 A1085 W	936.0	784.0	511.4	523.7
8x8x1/2 A1085 B	936.0	957.4	511.4	524.4
5x5x3/8 A1085 Y Chevron	427.7	435.7	101.3	101.3
5x5x3/8 A1085 Y Near Fault	427.7	435.7	101.3	101.3
7x7x3/8 A1085 Y Chevron	622.7	577.1	292.2	291.4
7x7x3/8 A1085 Y Near Fault	622.7	577.1	292.2	291.4
8x8x3/8 A1085 Y Chevron	721.5	661.2	404.3	397.8
8x8x3/8 A1085 Y Near Fault	721.5	661.2	404.3	397.8
5x5x3/8 A1085 Y Short	427.7	435.7	168.9	169.7
7x7x3/8 A1085 Y Short	622.7	577.1	390.1	387.9
8x8x3/8 A1085 Y Short	721.5	661.2	404.3	490.8

Table 4.5 Summary of Test Specimen Performance

HSS Section	B1: Global Buckling			B2: Moderate Buckling		
	Target, *d* (in.) (*Cycle*)	Deformation (in.) (*Approx. Drift (%)*)	Force (k) ($P/P_{critical}$)	Target, *d* (in.) (*Cycle*)	Deformation (in.) (*Approx. Drift (%)*)	Force (k) ($P/P_{critical}$)
5x5x3/8 A1085 R	0.25 *(1)*	-0.13 *-(0.11)*	-114.2 *(1.13)*	1.25 *(1)*	-0.34 *-(0.28)*	-104.8 *(1.03)*
5x5x3/8 A1085 W	0.25 *(1)*	-0.14 *-(0.12)*	-110.2 *(1.09)*	0.625 *(1)*	-0.39 *-(0.33)*	-102.8 *(1.02)*
5x5x3/8 A1085 B	0.25 *(1)*	-0.15 *-(0.13)*	-126.4 *(1.25)*	0.5 *(1)*	-0.38 *-(0.32)*	-110.6 *(1.09)*
6x6x3/8 A1085 R	0.25 *(1)*	-0.19 *-(0.16)*	-178.8 *(0.97)*	0.75 *(1)*	-0.53 *-(0.44)*	-147.6 *(0.80)*
6x6x3/8 A1085 W	0.375 *(1)*	-0.23 *-(0.19)*	-185.8 *(1.00)*	0.625 *(1)*	-0.57 *-(0.47)*	-148.4 *(0.80)*
6x6x3/8 A1085 B	0.325 *(1)*	-0.18 *-(0.15)*	-177.9 *(0.96)*	0.625 *(1)*	-0.55 *-(0.45)*	-152.0 *(0.82)*
8x8x3/8 A1085 R	0.5 *(1)*	-0.12 *-(0.10)*	-323.7 *(0.80)*	1.25 *(1)*	-0.69 *-(0.57)*	-205.4 *(0.51)*
8x8x3/8 A1085 W	0.5 *(1)*	-0.24 *-(0.20)*	-361.0 *(0.89)*	1.25 *(1)*	-0.78 *-(0.65)*	-219.8 *(0.54)*
8x8x3/8 A1085 B	0.625 *(1)*	-0.34 *-(0.28)*	-363.9 *(0.90)*	1.25 *(1)*	-1.06 *-(0.88)*	-249.1 *(0.62)*
8x8x1/2 A1085 R	0.625 *(1)*	-0.13 *-(0.11)*	-425.3 *(0.83)*	1.25 *(1)*	-0.57 *-(0.47)*	-275.5 *(0.54)*
8x8x1/2 A1085 W	0.625 *(1)*	-0.35 *-(0.29)*	-446.3 *(0.87)*	1.25 *(1)*	-0.95 *-(0.79)*	-299.9 *(0.59)*
8x8x1/2 A1085 B	0.75 *(1)*	-0.12 *-(0.10)*	-478.6 *(0.94)*	1.25 *(1)*	-0.70 *-(0.59)*	-318.6 *(0.62)*
5x5x3/8 A1085 Y Chevron	0.375 *(1)*	-0.19 *-(0.15)*	-93.3 *(0.92)*	0.625 *(1)*	-0.35 *-(0.29)*	-87.3 *(0.86)*
5x5x3/8 A1085 Y Near Fault	1.19 - [1]	-0.18 *-(0.15)*	-95.4 *(0.94)*	1.19 - [1]	-0.36 *-(0.30)*	-88.9 *(0.88)*
7x7x3/8 A1085 Y Chevron	0.5 *(1)*	-0.23 *-(0.19)*	-257.4 *(0.88)*	1.50 *(1)*	-0.74 *-(0.62)*	-186.1 *(0.64)*
7x7x3/8 A1085 Y Near Fault	1.19 - [1]	-0.23 *-(0.19)*	-255.2 *(0.87)*	1.19 - [1]	-0.72 *-(0.60)*	-188.7 *(0.65)*
8x8x3/8 A1085 Y Chevron	0.5 *(1)*	-0.27 *-(0.22)*	-320.7 *(0.79)*	1.50 *(1)*	-1.06 *-(0.88)*	-213.6 *(0.53)*
8x8x3/8 A1085 Y Near Fault	1.19 - [1]	-0.31 *-(0.25)*	-308.4 *(0.76)*	0.59 - [1]	1.38 *(1.15)*	-194.3 *(0.48)*
5x5x3/8 A1085 Y Short	0.290 *(1)*	-0.19 *-(0.20)*	-140.8 *(0.83)*	0.579 *(1)*	-0.41 *-(0.44)*	-113.7 *(0.67)*
7x7x3/8 A1085 Y Short	0.386 *(1)*	-0.23 *-(0.25)*	-327.9 *(0.84)*	0.966 *(1)*	-0.84 *-(0.91)*	-193.6 *(0.50)*
8x8x3/8 A1085 Y Short	0.483 *(1)*	-0.29 *-(0.32)*	-393.6 *(0.78)*	1.352 *(1)*	-0.88 *-(0.95)*	-212.1 *(0.42)*

Table 4.4 Continued

HSS Section	B3-C: Local Cupping			B3-T: Striations/Tearing		
	Target, *d* (in.) (*Cycle*)	Deformation (in.) (*Approx. Drift (%)*)	Force (k) ($P/P_{critical}$)	Target, *d* (in.) (*Cycle*)	Deformation (in.) (*Approx. Drift (%)*)	Force (k) (P/P_{yield})
5x5x3/8 A1085 R	4.25 *(1)*	-4.14 *-(3.45)*	-29.1 *(0.29)*	5.75 *(1)*	4.21 *(3.51)*	108.5 *(0.24)*
5x5x3/8 A1085 W	4.25 *(1)*	-4.27 *-(3.56)*	-30.1 *(0.30)*	5.25 *(1)*	4.01 *(3.34)*	165.2 *(0.36)*
5x5x3/8 A1085 B	3.75 *(1)*	-3.95 *-(3.29)*	-33.7 *(0.33)*	4.75 *(1)*	3.70 *(3.09)*	332.3 *(0.64)*
6x6x3/8 A1085 R	3.25 *(1)*	-3.09 *-(2.58)*	-51.0 *(0.28)*	4.25 *(1)*	2.99 *(2.49)*	107.6 *(0.22)*
6x6x3/8 A1085 W	3.25 *(1)*	-3.17 *-(2.65)*	-47.8 *(0.26)*	4.25 *(1)*	3.05 *(2.54)*	370.1 *(0.68)*
6x6x3/8 A1085 B	2.25 *(1)*	-2.30 *-(1.92)*	-60.2 *(0.32)*	3.75 *(1)*	2.13 *(1.77)*	156.5 *(0.28)*
8x8x3/8 A1085 R	1.75 *(1)*	-1.27 *-(1.06)*	-146.1 *(0.36)*	2.25 *(1)*	2.06 *(1.72)*	630.7 *(0.95)*
8x8x3/8 A1085 W	1.75 *(1)*	-1.66 *-(1.39)*	-149.0 *(0.37)*	2.25 *(1)*	1.70 *(1.42)*	673.7 *(0.96)*
8x8x3/8 A1085 B	1.25 *(1)*	-1.34 *-(1.12)*	-212.3 *(0.53)*	2.25 *(1)*	1.26 *(1.05)*	561.9 *(0.74)*
8x8x1/2 A1085 R	1.75 *(1)*	-1.45 *-(1.21)*	-176.3 *(0.34)*	2.75 *(1)*	2.35 *(1.96)*	793.5 *(1.01)*
8x8x1/2 A1085 W	1.75 *(1)*	-1.75 *-(1.46)*	-202.8 *(0.40)*	3.25 *(1)*	2.38 *(1.98)*	943.5 *(0.99)*
8x8x1/2 A1085 B	1.75 *(1)*	-1.39 *-(1.16)*	-221.4 *(0.43)*	3.25 *(1)*	2.40 *(2.00)*	694.0 *(0.72)*
5x5x3/8 A1085 Y Chevron	8.25 *(1)*	-7.74 *-(6.45)*	-20.6 *(0.20)*	4.5 *(1)*	3.23 *(2.69)*	168.2 *(0.39)*
5x5x3/8 A1085 Y Near Fault	2.38 - [1]	-2.62 *-(2.18)*	-25.3 *(0.25)*	8.31 - [1]	6.64 *(5.53)*	38.0 *(0.09)*
7x7x3/8 A1085 Y Chevron	2.25 *(1)*	-2.01 *-(1.68)*	-106.3 *(0.36)*	4.50 *(1)*	0.09 *(0.08)*	256.6 *(0.44)*
7x7x3/8 A1085 Y Near Fault	0 - [1]	-0.27 *-(0.22)*	-98.7 *(0.34)*	4.75 - [1]	3.32 *(2.76)*	194.3 *(0.34)*
8x8x3/8 A1085 Y Chevron	2.25 *(1)*	-2.03 *-(1.69)*	-139.2 *(0.34)*	3.75 *(1)*	0.14 *(0.11)*	320.6 *(0.48)*
8x8x3/8 A1085 Y Near Fault	0 - [1]	0.13 *(0.11)*	-126.6 *(0.31)*	4.16 - [1]	3.25 *(2.71)*	352.5 *(0.53)*
5x5x3/8 A1085 Y Short	2.511 *(1)*	-2.32 *-(2.50)*	-43.3 *(0.26)*	3.670 *(1)*	3.30 *(3.56)*	388.6 *(0.89)*
7x7x3/8 A1085 Y Short	1.352 *(1)*	-1.33 *-(1.43)*	-145.0 *(0.37)*	1.738 *(1)*	1.12 *(1.21)*	473.6 *(0.82)*
8x8x3/8 A1085 Y Short	1.352 *(1)*	-1.24 *-(1.34)*	-157.5 *(0.31)*	1.738 *(1)*	1.32 *(1.42)*	663.1 *(1.00)*

Table 4.4 Continued

HSS Section	B4: Fracture			Brace Yielding		
	Target, *d* (in.) (*Cycle*)	Deformation (in.) (*Approx. Drift (%)*)	Force (k) (P/P_{yield})	Target, *d* (in.) (*Cycle*)	Deformation (in.) (*Approx. Drift (%)*)	Force (k)
5x5x3/8 A1085 R	5.75 *(1)*	4.91 *(4.09)*	125.3 *(0.28)*	5.75 *(1)*	4.91 *(4.09)*	452.8
5x5x3/8 A1085 W*	5.25 *(1)*	2.05 *(1.71)*	-23.0 *(0.23)**	1.75 *(1)*	1.01 *(0.84)*	456.3
5x5x3/8 A1085 B	5.25 *(1)*	3.74 *(3.11)*	117.5 *(0.22)*	2.25 *(1)*	1.18 *(0.98)*	522.4
6x6x3/8 A1085 R	4.25 *(1)*	3.96 *(3.30)*	125.1 *(0.26)*	1.25 *(1)*	0.77 *(0.64)*	482.9
6x6x3/8 A1085 W*	4.25 *(1)*	1.44 *(1.20)*	-22.5 *(0.12)**	1.75 *(1)*	1.23 *(1.02)*	548.2
6x6x3/8 A1085 B	3.75 *(1)*	2.97 *(2.48)*	182.0 *(0.32)*	1.75 *(1)*	1.07 *(0.89)*	565.4
8x8x3/8 A1085 R	2.75 *(1)*	2.68 *(2.23)*	95.1 *(0.14)*	- [2] - [2]	- [2] - [2]	666.6
8x8x3/8 A1085 W	2.75 *(1)*	2.31 *(1.93)*	180.4 *(0.26)*	1.75 *(1)*	1.04 *(0.87)*	699.5
8x8x3/8 A1085 B	2.75 *(1)*	1.74 *(1.45)*	170.6 *(0.23)*	1.75 *(1)*	0.87 *(0.73)*	757.4
8x8x1/2 A1085 R	3.75 *(1)*	3.31 *(2.76)*	168.3 *(0.21)*	1.75 *(1)*	1.12 *(0.93)*	784.0
8x8x1/2 A1085 W	3.75 *(1)*	2.83 *(2.36)*	221.3 *(0.23)*	1.75 *(1)*	0.89 *(0.74)*	950.7
8x8x1/2 A1085 B	3.25 *(1)*	2.20 *(1.83)*	11.8 *(0.01)*	- [2] - [2]	- [2] - [2]	957.4
5x5x3/8 A1085 Y Chevron	4.50 *(1)*	3.64 *(3.03)*	125.0 *(0.29)*	- [2] - [2]	- [2] - [2]	435.7
5x5x3/8 A1085 Y Near Fault	8.31 - [1]	7.88 *(6.57)*	84.6 *(0.19)*	3.56 - [1]	1.14 *(0.95)*	435.7
7x7x3/8 A1085 Y Chevron	5.25 *(1)*	1.16 *(0.97)*	127.1 *(0.22)*	- [2] - [2]	- [2] - [2]	577.1
7x7x3/8 A1085 Y Near Fault	4.75 - [1]	4.08 *(3.40)*	185.8 *(0.32)*	3.56 *(1)*	0.65 *(0.54)*	577.1
8x8x3/8 A1085 Y Chevron	4.50 *(1)*	1.10 *(0.92)*	86.5 *(0.13)*	- [2] - [2]	- [2] - [2]	661.2
8x8x3/8 A1085 Y Near Fault	4.16 - [1]	3.95 *(3.29)*	132.1 *(0.20)*	3.56 - [1]	0.85 *(0.71)*	661.2
5x5x3/8 A1085 Y Short	4.056 *(1)*	3.64 *(3.93)*	78.1 *(0.18)*	1.738 *(1)*	1.32 *(1.43)*	435.7
7x7x3/8 A1085 Y Short	2.125 *(1)*	1.56 *(1.68)*	104.8 *(0.82)*	1.352 *(1)*	0.53 *(0.57)*	577.1
8x8x3/8 A1085 Y Short	2.125 *(1)*	1.61 *(1.74)*	124.2 *(0.19)*	1.352 *(1)*	0.77 *(0.83)*	661.2

Table 4.4 Continued

HSS Section	Peak Tensile Force		
	Target, *d* (in.) (*Cycle*)	Deformation (in.) (*Approx. Drift (%)*)	Force (kips) (P/P_{yield})
5x5x3/8 A1085 R	2.25	1.72	456.6
	(1)	*(1.44)*	*(1.01)*
5x5x3/8 A1085 W	2.25	1.54	468.3
	(1)	*(1.29)*	*(1.03)*
5x5x3/8 A1085 B	2.75	1.66	538.2
	(1)	*(1.39)*	*(1.03)*
6x6x3/8 A1085 R	2.25	1.78	521.0
	(1)	*(1.49)*	*(1.08)*
6x6x3/8 A1085 W	1.75	1.26	549.5
	(1)	*(1.05)*	*(1.00)*
6x6x3/8 A1085 B	2.25	1.62	581.7
	(1)	*(1.35)*	*(1.03)*
8x8x3/8 A1085 R	2.25	1.98	660.4
	(1)	*(1.65)*	*(0.99)*
8x8x3/8 A1085 W	1.75	1.21	712.0
	(1)	*(1.01)*	*(1.02)*
8x8x3/8 A1085 B	2.25	1.40	763.0
	(1)	*(1.17)*	*(1.01)*
8x8x1/2 A1085 R	1.75	1.37	819.2
	(1)	*(1.14)*	*(1.04)*
8x8x1/2 A1085 W	2.25	1.40	964.7
	(1)	*(1.17)*	*(1.01)*
8x8x1/2 A1085 B	1.75	1.21	938.6
	(1)	*(1.01)*	*(0.98)*
5x5x3/8 A1085 Y Chevron	- [1]	3.53	409.1
	- [1]	*(2.94)*	*(0.94)*
5x5x3/8 A1085 Y Near Fault	3.56	3.16	464.2
	- [1]	*(2.63)*	*(1.07)*
7x7x3/8 A1085 Y Chevron	- [1]	0.01	258.3
	- [1]	*(0.01)*	*(0.45)*
7x7x3/8 A1085 Y Near Fault	3.56	2.74	670.9
	- [1]	*(2.29)*	*(1.16)*
8x8x3/8 A1085 Y Chevron	- [1]	0.08	332.9
	- [1]	*(0.07)*	*(0.50)*
8x8x3/8 A1085 Y Near Fault	3.56	3.10	716.3
	- [1]	*(2.58)*	*(1.08)*
5x5x3/8 A1085 Y Short	1.738	1.37	438.6
	(1)	*(1.48)*	*(1.01)*
7x7x3/8 A1085 Y Short	1.738	1.20	617.5
	(1)	*(1.29)*	*(1.07)*
8x8x3/8 A1085 Y Short	1.352	0.92	666.4
	(1)	*(1.00)*	*(1.01)*

[1] Target displacement cycle does not apply for the corresponding alternate displacement protocol.
[2] The specimen did not reach the calculated measured yield force.

Table 4.6 Summary of Measured Axial Deformation Limits

Test Specimen	**Tension** Deformation (in) *Approx. Drift (%)*	**Compression** Deformation (in) *Approx. Drift (%)*	**Range** Deformation (in) *Approx. Drift (%)*
5x5x3/8 A1085 R	4.91 *(4.09)*	5.14 *(4.29)*	10.05 *(8.38)*
5x5x3/8 A1085 W	4.72 *(3.93)*	5.27 *(4.39)*	9.99 *(8.32)*
5x5x3/8 A1085 B	3.93 *(3.28)*	5.07 *(4.23)*	9.00 *(7.51)*
6x6x3/8 A1085 R	3.96 *(3.30)*	4.14 *(3.45)*	8.09 *(6.75)*
6x6x3/8 A1085 W	3.66 *(3.05)*	4.04 *(3.37)*	7.70 *(6.42)*
6x6x3/8 A1085 B	2.97 *(2.48)*	3.26 *(2.72)*	6.23 *(5.19)*
8x8x3/8 A1085 R	2.68 *(2.23)*	1.77 *(1.48)*	4.45 *(3.71)*
8x8x3/8 A1085 W	2.31 *(1.93)*	2.28 *(1.90)*	4.59 *(3.83)*
8x8x3/8 A1085 B	1.74 *(1.45)*	2.55 *(2.12)*	4.29 *(3.57)*
8x8x1/2 A1085 R	3.31 *(2.76)*	2.95 *(2.46)*	6.26 *(5.21)*
8x8x1/2 A1085 W	2.83 *(2.36)*	3.28 *(2.73)*	6.10 *(5.09)*
8x8x1/2 A1085 B	3.03 *(2.53)*	3.05 *(2.55)*	6.08 *(5.07)*
5x5x3/8 A1085 Y Chevron	3.64 *(3.03)*	7.82 *(6.52)*	11.46 *(9.55)*
5x5x3/8 A1085 Y Near Fault	7.88 *(6.57)*	4.34 *(3.62)*	12.22 *(10.19)*
7x7x3/8 A1085 Y Chevron	1.16 *(0.97)*	4.24 *(3.54)*	5.41 *(4.51)*
7x7x3/8 A1085 Y Near Fault	4.08 *(3.40)*	1.50 *(1.25)*	5.57 *(4.65)*
8x8x3/8 A1085 Y Chevron	1.10 *(0.92)*	3.58 *(2.98)*	4.68 *(3.90)*
8x8x3/8 A1085 Y Near Fault	3.95 *(3.29)*	1.03 *(0.86)*	4.98 *(4.15)*
5x5x3/8 A1085 Y Short	3.64 *(3.93)*	3.45 *(3.73)*	7.10 *(7.66)*
7x7x3/8 A1085 Y Short	1.56 *(1.68)*	1.74 *(1.88)*	3.30 *(3.57)*
8x8x3/8 A1085 Y Short	1.61 *(1.74)*	1.65 *(1.78)*	3.27 *(3.52)*

4.2.2 *5x5x3/8 A1085 R*

Specimen 5x5x3/8 A1085 R reached initial global buckling at a compressive axial deformation of 0.13” which corresponds to a maximum compressive force of 114.23 kips (1.13 times the expected critical buckling load). The specimen reached a peak tension load of 456.59 kips at an axial deformation of 1.72”. As local damage in the plastic hinge region developed, the peak tension load of each subsequent cycle slightly decreased. Local cupping was first observed in compression at an axial brace deformation of 4.14”. The severity of cupping increased each compression cycle going forward. In the final tension cycle, the specimen started tearing at a brace axial deformation of 4.21”. Tearing continued across the cross-section and the specimen eventually fractured at an axial deformation of 4.91”.

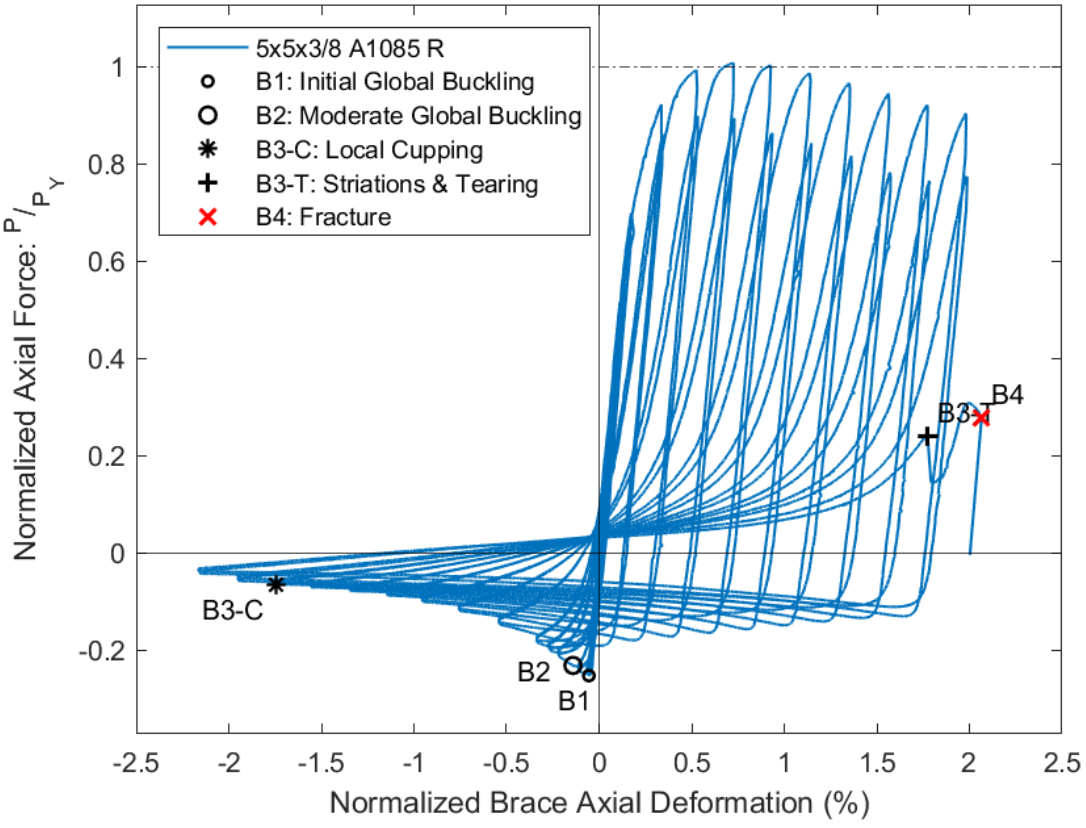

Figure 4.2 Brace Hysteretic Response: 5x5x3/8 A1085 R

4.2.3 *5x5x3/8 A1085 W*

Global buckling of the 5x5x3/8 A1085 W specimen was first observed at a compressive axial deformation of 0.14” at which point the buckling load was 110.2 kips (1.09 times the expected critical buckling load). The specimen reached a maximum tensile force of 468.3 kips at an axial deformation of 1.54”. Following this, the peak tension load of each cycle slowly decreased. Initial signs of local cupping were observed at the center of brace at a compressive axial deformation of 4.27”. These local cupping deformations grew in each subsequent cycle which led to tearing. The specimen tore through three of the side walls during the second tension cycle of 5.25” target displacements. As the brace buckled out of plane in the following compression cycle, tearing continued through the final wall and the specimen fractured.

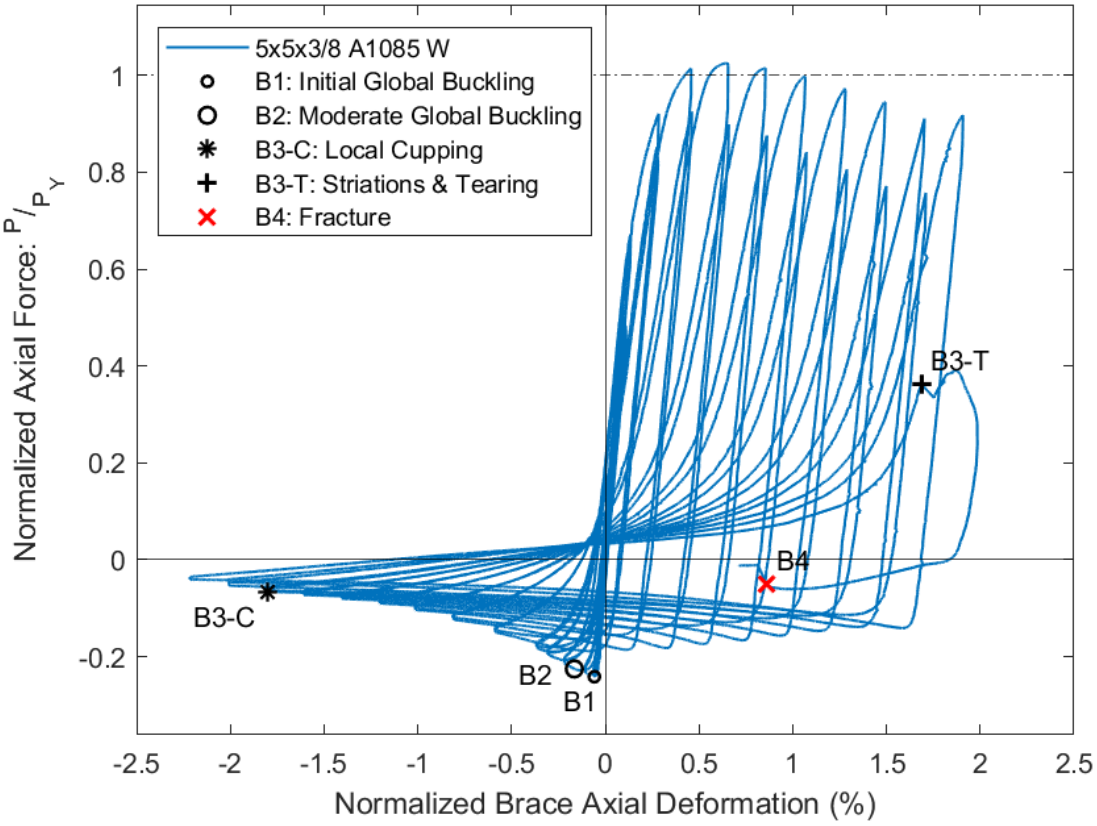

Figure 4.3 Brace Hysteretic Response: 5x5x3/8 A1085 W

4.2.4 *5x5x3/8 A1085 B*

The specimens in this research project were design to buckle out of plane in the West direction. However, the 5x5x3/8 A1085 B specimen began to buckle in the East direction during initial elastic cycles, so instrumentation was moved to capture the necessary data without obstruction. The reverse buckling may have been caused by initial camber in the specimen or construction issues regarding the eccentricity of the gusset plates. The specimen exhibited global buckling when it reached a maximum compressive force of 126.4 kips (1.25 times the expected critical buckling load) at an axial brace deformation of 0.15”. During the first 2.25” target cycle, the brace switched out of plane buckling directions (now buckling west). Again, string potentiometers were moved to the other side of the specimen to avoid obstruction during out of plane buckling. The specimen reached a maximum tensile force of 538.2 kips at an axial brace deformation of 1.66”. This maximum tensile load is notably greater than the previous tests of 5x5x3/8 A1085 specimens. Cupping began to develop near the center of the brace at an axial brace deformation of 3.95” in compression and the severity of cupping increased each subsequent cycle. The specimen tore through three walls during the second 4.75” tension cycle and fractured during the next cycle at an axial brace deformation of 3.74”.

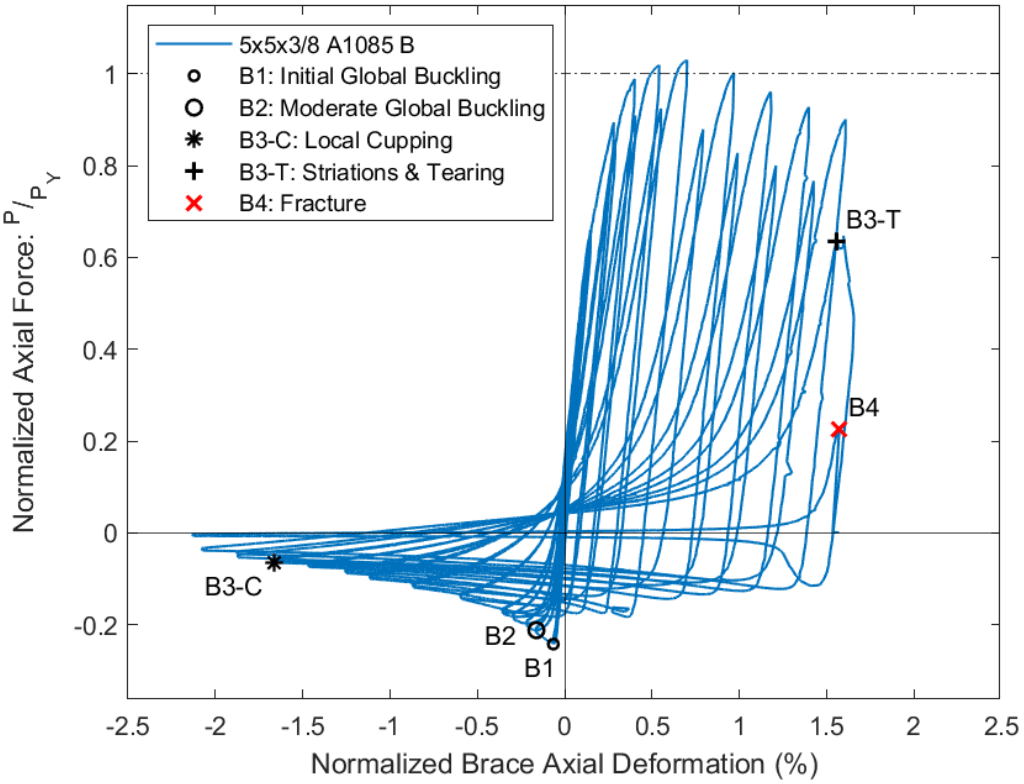

Figure 4.4 Brace Hysteretic Response: 5x5x3/8 A1085 B

4.2.5 *6x6x3/8 A1085 R*

The 6x6x3/8 A1085 R specimen experienced global buckling at an axial brace deformation of 0.19” when it reached a maximum compressive force of 178.8 kips (0.97 times the expected critical buckling load). The specimen reached a maximum tensile force of 521.0 kips at an axial brace deformation of 1.78” during the first 2.25” target cycle. The peak tensile forces remained relatively the same over the following cycles. Local cupping was first observed at the center of the specimen at an axial brace deformation of 3.09”. During the first 4.25” target cycle, tearing began and quickly propagated across the specimen leading to fracture at an axial brace deformation of 3.96”.

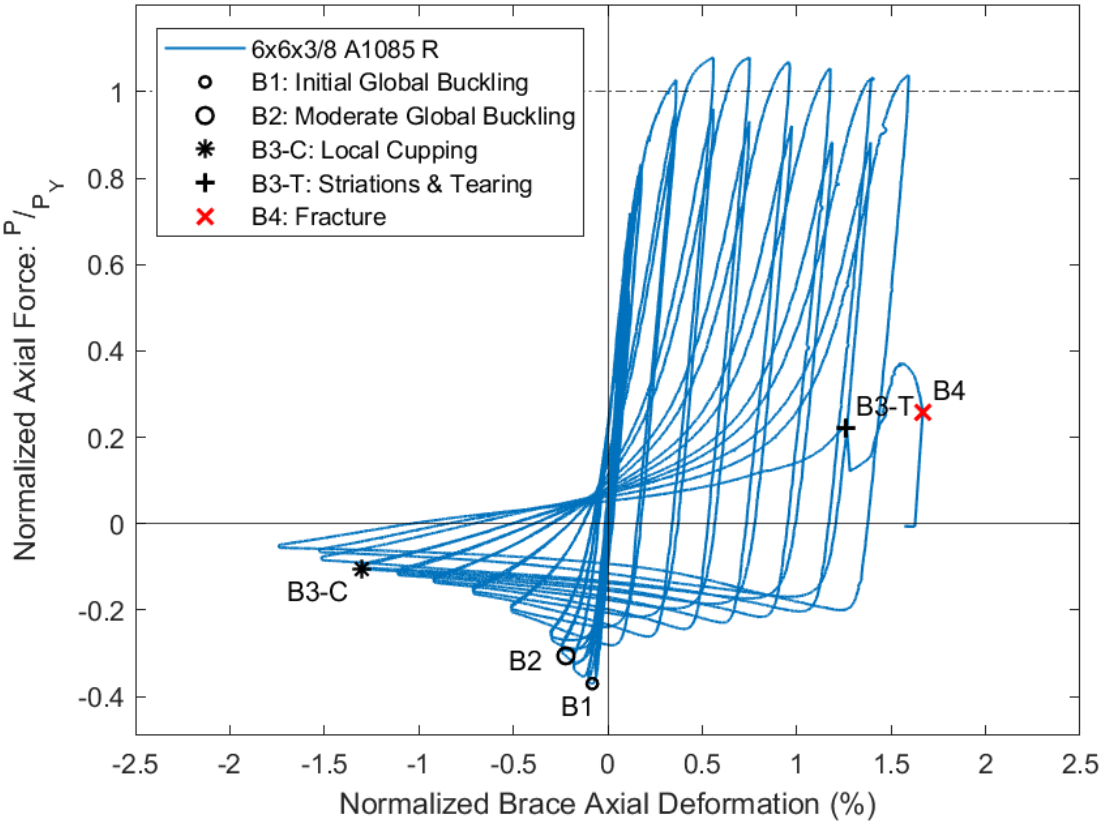

Figure 4.5 Brace Hysteretic Response: 6x6x3/8 A1085 R

4.2.6 *6x6x3/8 A1085 W*

Global buckling of the 6x6x3/8 A1085 W specimen was observed at a compressive deformation of 0.23”. At this moment, the specimen reached a maximum compressive load of 185.8 kips (equal to the expected critical buckling load). The maximum tensile force experienced by the specimen was 549.5 kips, which occurred at an axial brace deformation of 1.26”. The specimen began to exhibit local cupping when it reached a compressive deformation of 3.17”, and the severity of cupping increased in the following cycles. During the first 4.25” target tension cycle, the specimen tore through most of the cross-section, leaving only one corner intact. The brace then fractured as it buckled going into the next compression cycle.

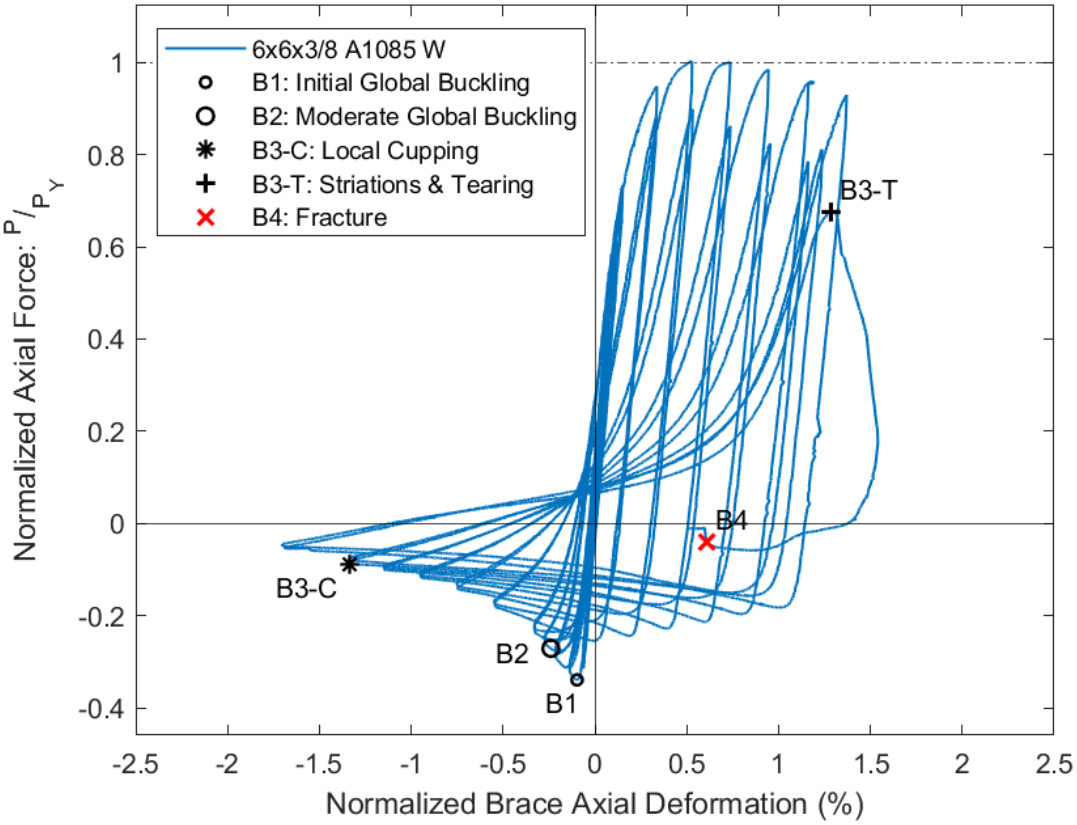

Figure 4.6 Brace Hysteretic Response: 6x6x3/8 A1085 W

4.2.7 *6x6x3/8 A1085 B*

Global buckling of the 6x6x3/8 A1085 B specimen occurred at an axial brace deformation of 0.18” with a corresponding compressive force of 177.9 kips (0.96 times the expected critical buckling load). The maximum tensile force was 581.7 kips, experienced at an axial deformation of 1.62”. Local cupping was first observed when the specimen reached an axial brace deformation of 2.30”. The severity of local damage increased and led to tearing and fracture during the first 3.25” target tension cycle. The maximum tensile axial brace deformation was 2.97” – lower than previous 6x6x3/8 A1085 specimens.

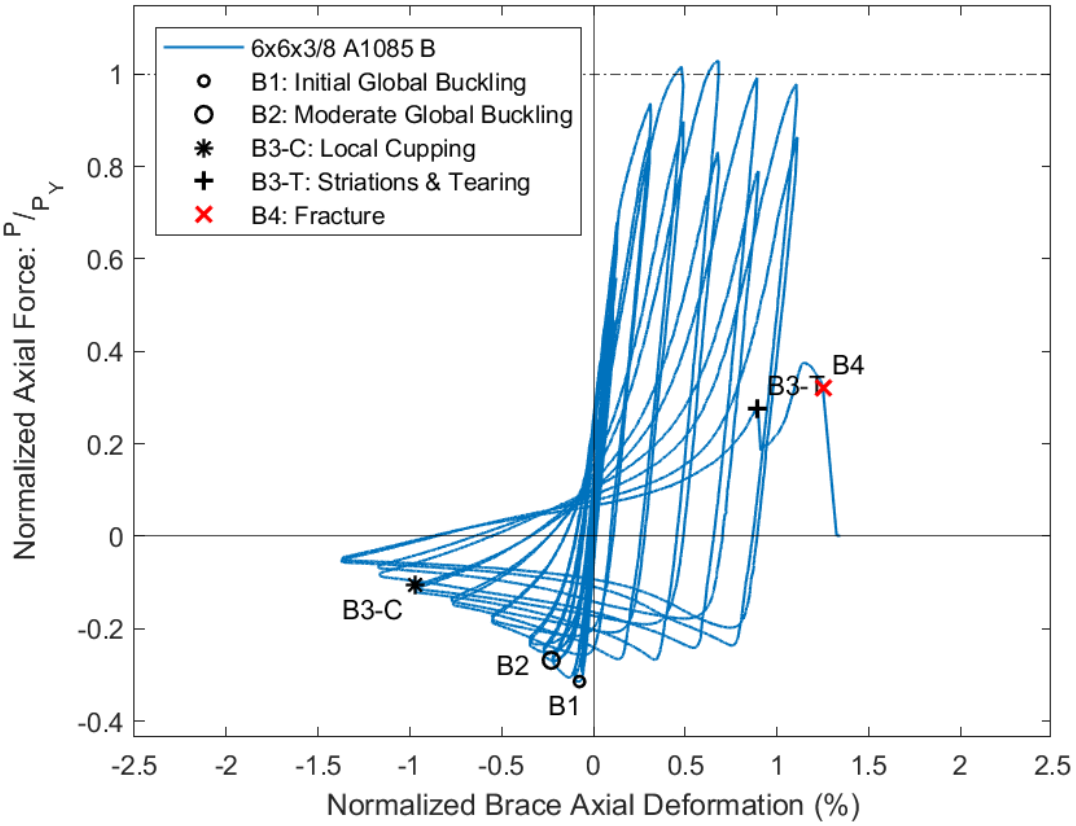

Figure 4.7 Brace Hysteretic Response: 6x6x3/8 A1085 B

4.2.8 *8x8x3/8 A1085 R*

The 8x8x3/8 A1085 R specimen exhibited global buckling at an axial brace deformation of 0.12” during the first 0.5” target displacement cycle. The global buckling load was 323.7 kips (0.80 times the expected critical buckling load). Due to large forces in tension and compression, the specimen experienced bolt slips multiple times in tension and compression. This is evident in the hysteresis response below. The maximum tensile force reached was 660.4 kips. Initial minor cupping deformations were first observed at an axial brace deformation of 1.27” in compression and the severity quickly increased in each subsequent cycle leading to tearing and fracture. The specimen fractured reaching a maximum axial brace deformation of 2.68” in tension.

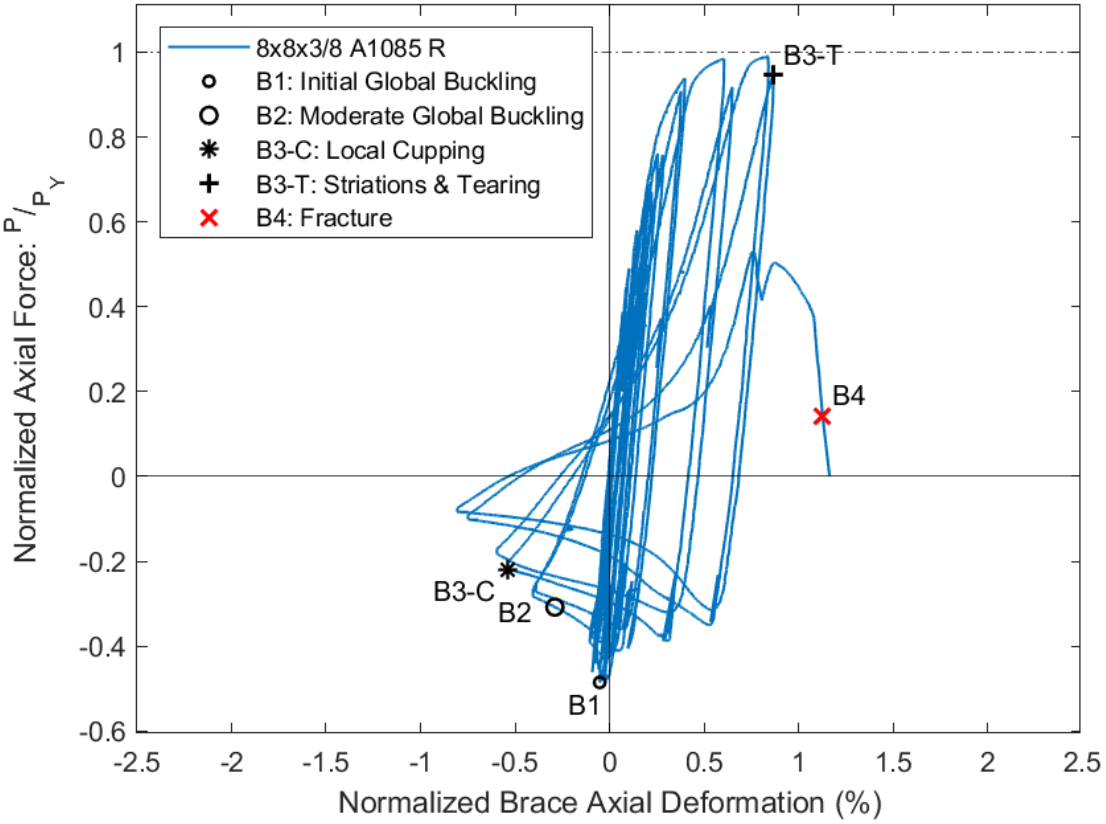

Figure 4.8 Brace Hysteretic Response: 8x8x3/8 A1085 R

4.2.9 *8x8x3/8 A1085 W*

Global buckling of the 8x8x3/8 A1085 W specimen occurred at an axial brace deformation of 0.24” and a compressive force of 361.0 kips (0.89 times the expected critical buckling load). As with the other 8x8x3/8 test specimens, bolt slip occurred multiple times due to slipping in tension and compression. Bolt slip occurred in the 0.5” and 0.625” target cycles but resided following that. Local cupping deformations were first observed 3.5” north of the center of brace while the brace was at an axial deformation of 1.66”. The local deformations grew in each subsequent cycle, quickly followed by visible striations and minor tearing on the corners at the peak of the second 2.25” target tension cycle. The specimen fractured during the next tension cycle at an axial brace deformation of 2.31”.

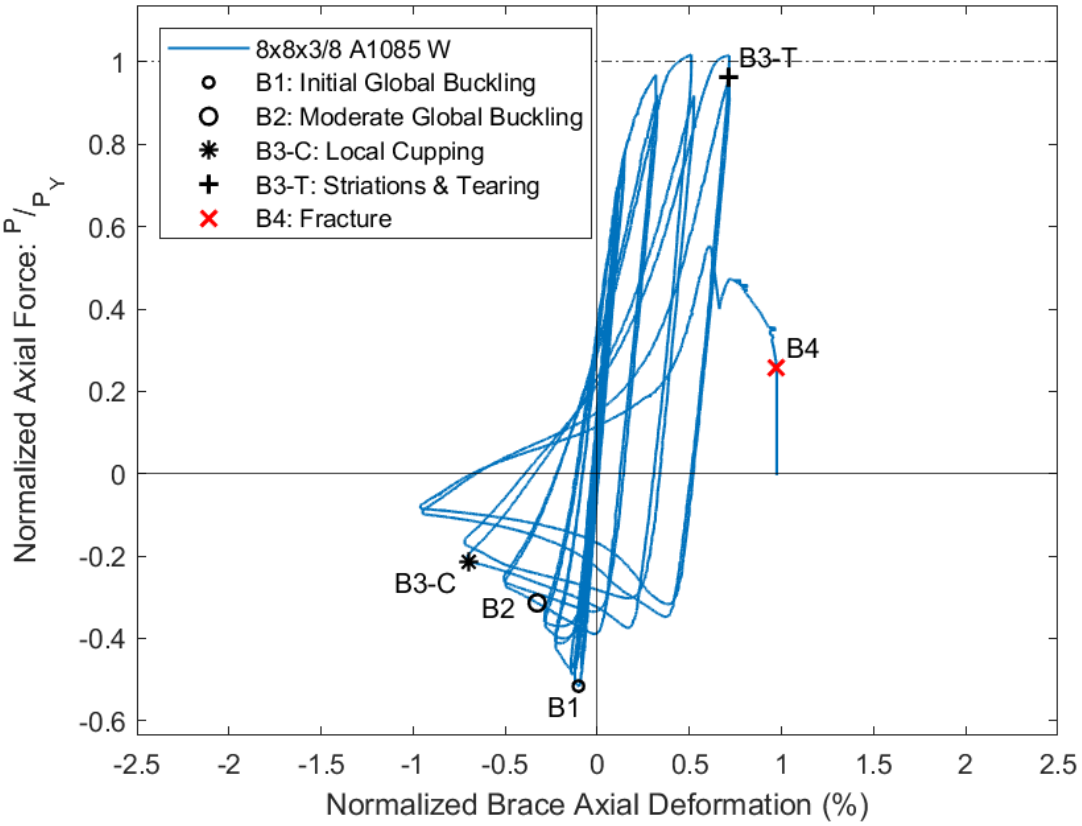

Figure 4.9 Brace Hysteretic Response: 8x8x3/8 A1085 W

4.2.10 *8x8x3/8 A1085 B*

The 8x8x3/8 A1085 B test specimen reached a maximum compressive force of 363.9 kips (0.90 times the expected critical buckling load). Global buckling under this load was observed at an axial deformation of 0.34”. A maximum tensile force of 763.0 kips was reached during the first 2.25” target displacement cycle where the specimen reached an axial deformation of 1.40”. Bolt slip occurred multiple time in tension and compression throughout the test. This is evident in the hysteresis response where there is a cluster of overlapping cycles near the zero deformation axis. Cupping at the center of the specimen was first observed at the peak of the second compressive cycle targeting 2.25”, at which point the axial deformation was 1.34”. Larger cupping deformations were observed during each following compression cycle. During the second tension cycle of the 2.25” target displacements, the specimen tore halfway through. Complete fracture was observed during the next tension cycle at an axial brace deformation of 1.74”.

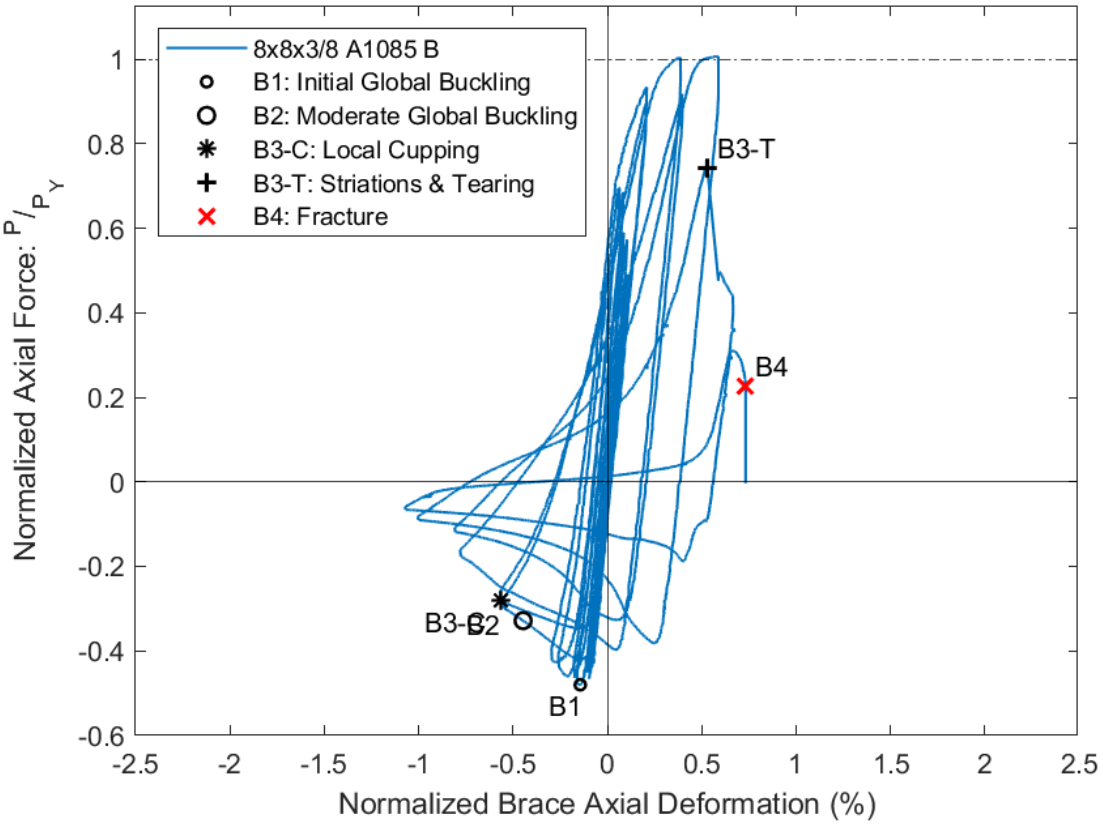

Figure 4.10 Brace Hysteretic Response: 8x8x3/8 A1085 B

4.2.11 *8x8x1/2 A1085 R*

The 8x8x1/2 A1085 R test specimen reached a maximum compressive force of 425.3 kips (0.83 times the expected critical buckling load), at which point the specimen exhibited global buckling. The maximum tensile force was 819.2 kips, which was reached at an axial brace deformation of 1.37”. The peak tensile loads remained relatively the same in the subsequent cycles prior to tearing. Local cupping at the center of the specimen was observed during the first compression cycle targeting 2.25”, at which point the axial brace deformation was 1.45”. From there on, the severity of local cupping damage increased each cycle leading to tearing. The specimen tore through the east, top, and bottom walls during the first 3.25” target cycle. The specimen survived one more tension cycle and eventually fractured during the first 3.75” target cycle. The brace fractured at an axial deformation of 3.31”.

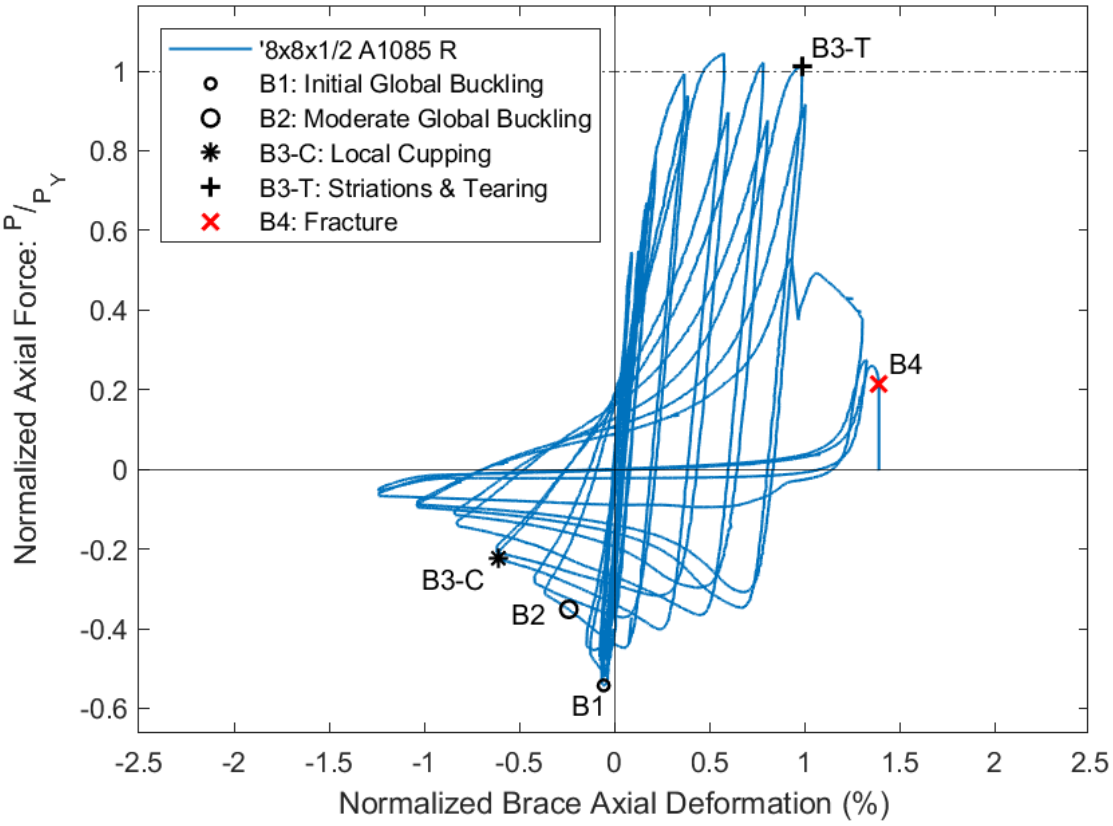

Figure 4.11 Brace Hysteretic Response: 8x8x1/2 A1085 R

4.2.12 *8x8x1/2 A1085 W*

Global buckling of the 8x8x1/2 A1085 W test specimen occurred at an axial brace deformation of 0.35” when it reached a maximum compressive force of 446.3 kips (0.87 times the expected critical buckling load). The specimen reached a maximum tensile force of 964.7 kips at an axial deformation of 1.40” and continued to reach a similar force for each subsequent cycle prior to tearing. The first observation of local cupping occurred during the first cycle of 2.25” target displacements. The severity of the local deformations increased each cycle going forward. Striations and minor tearing at the corners of the side wall was observed at an axial deformation of 2.38”. During the following tension cycle, tearing propagated through the east, top, and bottom walls of the specimen. The specimen fractured during the next tension cycle at an axial brace deformation of 2.83”.

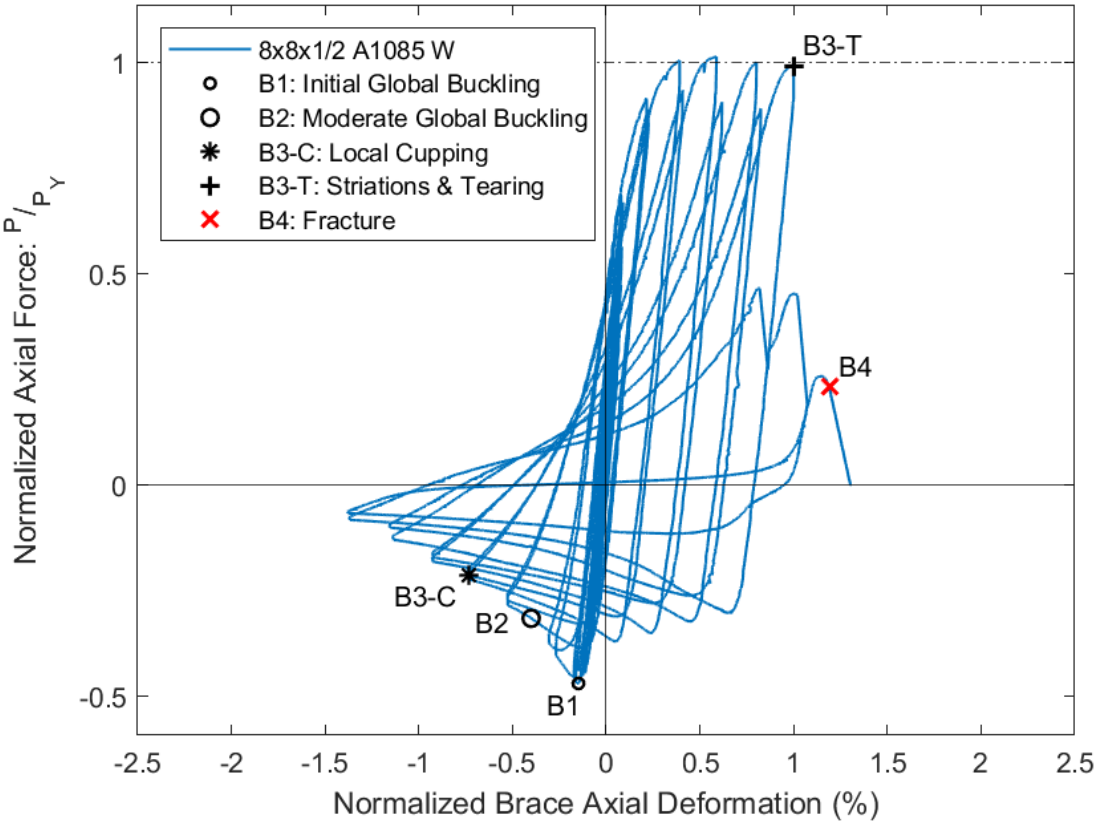

Figure 4.12 Brace Hysteretic Response: 8x8x1/2 A1085 W

4.2.13 *8x8x1/2 A1085 B*

The 8x8x1/2 A1085 B test specimen exhibited initial global buckling when it reached a compressive deformation of 0.12” and a compressive load of 478.6 kips (0.94 times the expected critical buckling load). During the first tension cycle of 1.75” target displacements, the smaller actuator reached its maximum capacity causing a lag between the two actuators of about 0.2”. The test was briefly paused while the hydraulic pump pressure was increased. Following the adjustment, testing continued smoothly, and the actuators were capable of applying the necessary loads. The maximum tensile force reached was 938.6 kips at an axial deformation of 1.21”. Local cupping deformations began to develop at an axial brace deformation of 1.39” and the severity of cupping continued to increase each following cycle. During the first tension cycle at 3.25” target displacements, the specimen tore halfway through. As the specimen buckled out of plane in the following compression cycle, tearing propagated through the specimen, leaving one corner intact. The specimen eventually fractured as it was pulled back into tension.

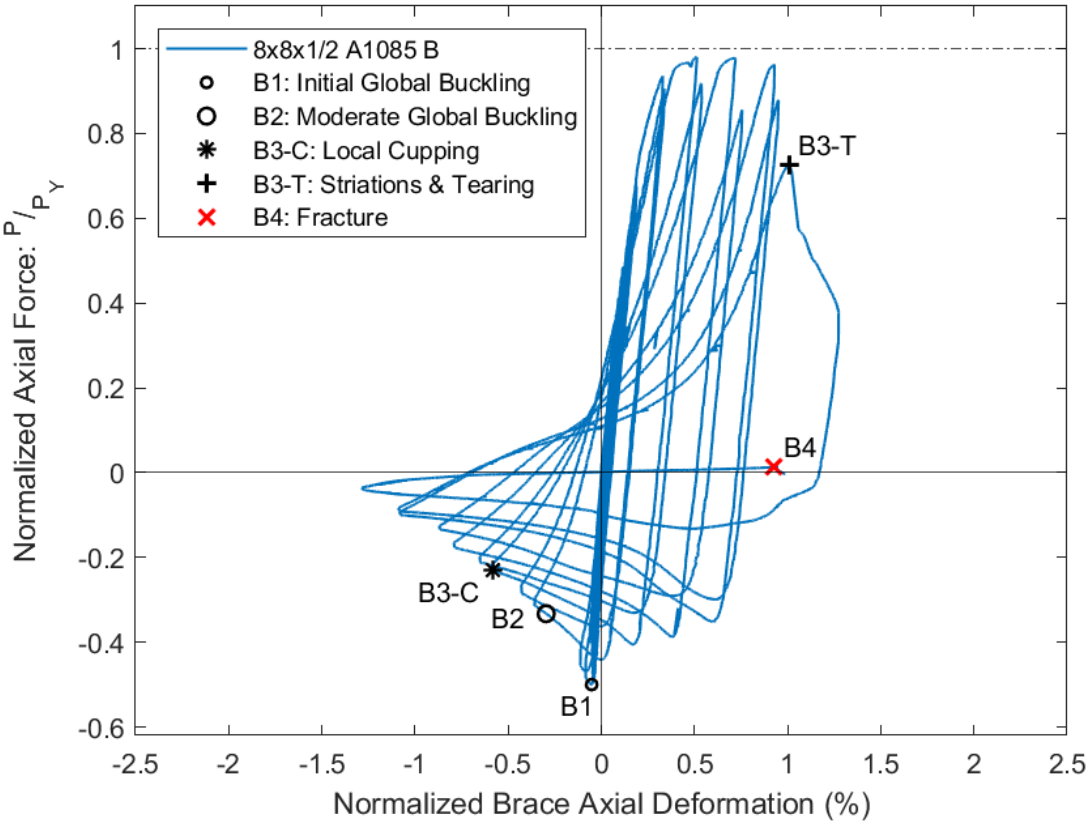

Figure 4.13 Brace Hysteretic Response: 8x8x1/2 A1085 B

4.2.14 *5x5x3/8 A1085 Y Chevron*

The 5x5x3/8 A1085 Y Chevron test specimen was subjected to the "chevron" load protocol. The procedure for this involves increasing the compressive displacements, while only pulling the specimen to a tensile force equal to the magnitude of the critical buckling load. During this test, the actuators reached the maximum stroke at 8.25". Cycles at this displacement did not cause any damage so the specimen was then subjected to increasing tensile displacement demands while continuing to target 8.25" displacements in compression.

The test specimen reached a maximum compressive force of 93.3 kips (0.92 times the expected critical buckling load) at an axial brace deformation of 0.19". The out of plane displacement increased with each cycle but the brace did not show any severe local cupping until after the increased tension loads were applied. Local cupping was first observed at an axial deformation of 7.74" in compression. The severity of local damage slightly increased each subsequent cycle. The brace reached a maximum tensile force of 409.1 kips at an axial deformation of 3.53". At this point, no striations were observed but there was visual necking at the center of the specimen. In the subsequent tension cycle targeting a 4.5" displacement, the specimen fractured when the specimen reached an axial brace deformation of 3.64".

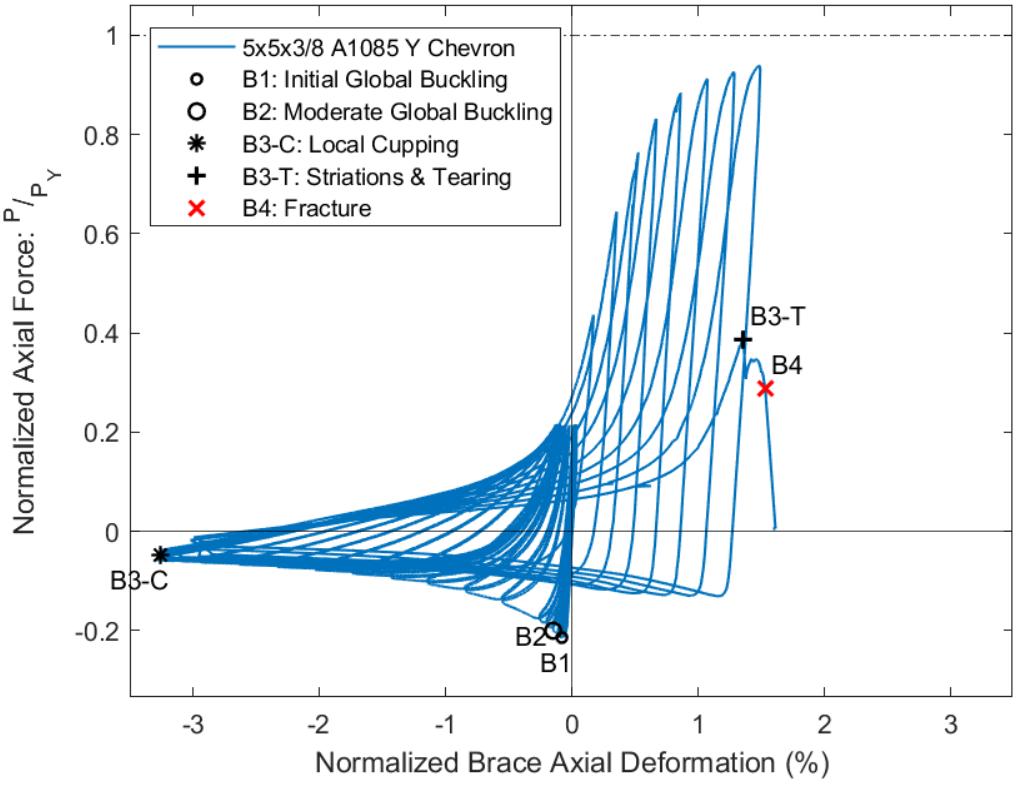

Figure 4.14 Brace Hysteretic Response: 5x5x3/8 A1085 Y Chevron

4.2.15 *5x5x3/8 A1085 Y Near Fault*

In the first compression cycle, the 5x5x3/8 A1085 Y Near Fault specimen exhibited global buckling as it reached a maximum compressive force of 95.4 kips (0.94 times the expected critical buckling load) at an axial brace deformation of 0.18”. In the same cycle, the specimen reached an out of plane displacement of just over 9”. The specimen was then subjected to a large target tensile displacement of 3.56” where it reached a maximum tensile force of 464.2 kips at an axial deformation of 3.16”. Local cupping was first observed at a compressive axial deformation of 2.62”. The severity of cupping increased during each subsequent cycle and the center of the brace became very hot to the touch. Necking was observed at the peak of the 7.72” target tension cycles, however, striations and tearing did not develop until the final cycle. In the final tension cycle, the specimen began to tear at an axial deformation of 6.64” and ultimately fractured at an axial deformation of 7.88”.

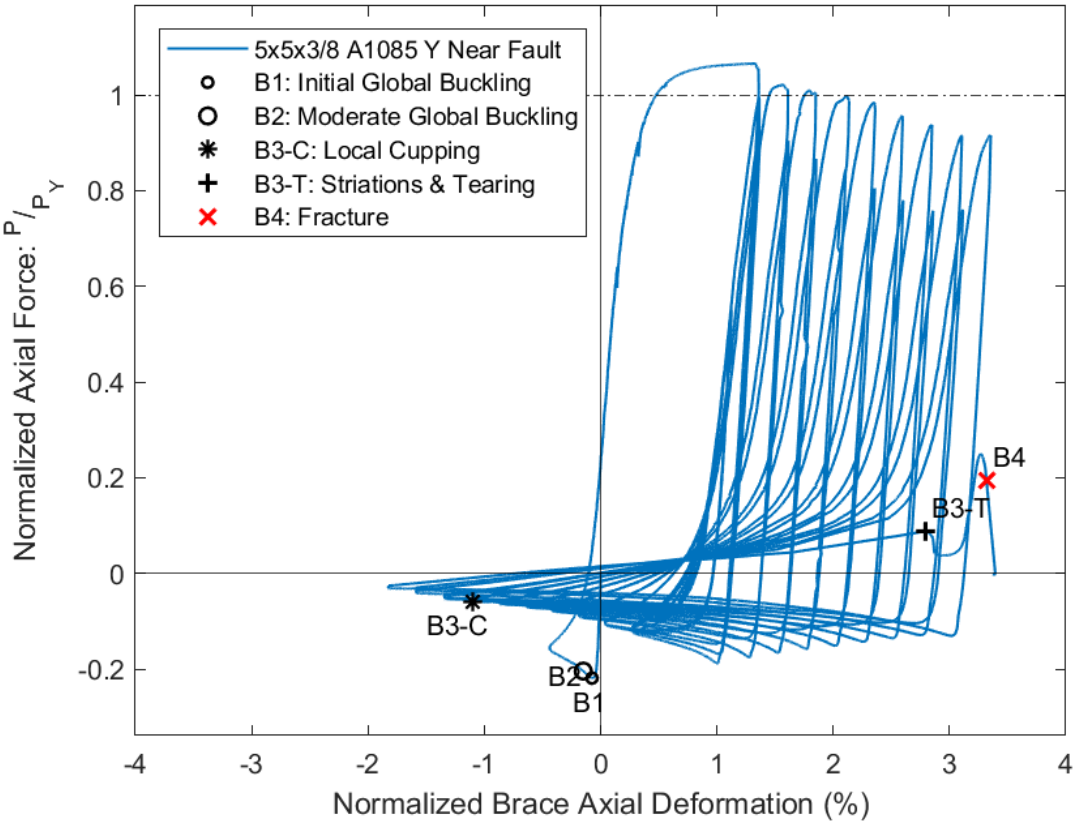

Figure 4.15 Brace Hysteretic Response: 5x5x3/8 A1085 Y Near Fault

4.2.16 *7x7x3/8 A1085 Y Chevron*

The 7x7x3/8 A1085 Y Chevron specimen reached a maximum compressive load of 257.4 kips (0.88 times the expected critical buckling load) at an axial brace deformation of 0.23". Adhering to the chevron compression dominant displacement protocol, the brace only reached a maximum tension load of 258.3 kips. Local cupping was first observed during the second 2.25" target cycle at which point the brace axial deformation was 2.01". The severity of local cupping deformations increased each subsequent cycle. Striations and very minor tearing were observed during the tension cycle following the first 4.50" target compressive displacement. As the specimen was loaded in tension following the second 4.50" target compressive cycle, the specimen started tearing and then fractured at an axial deformation of 1.16".

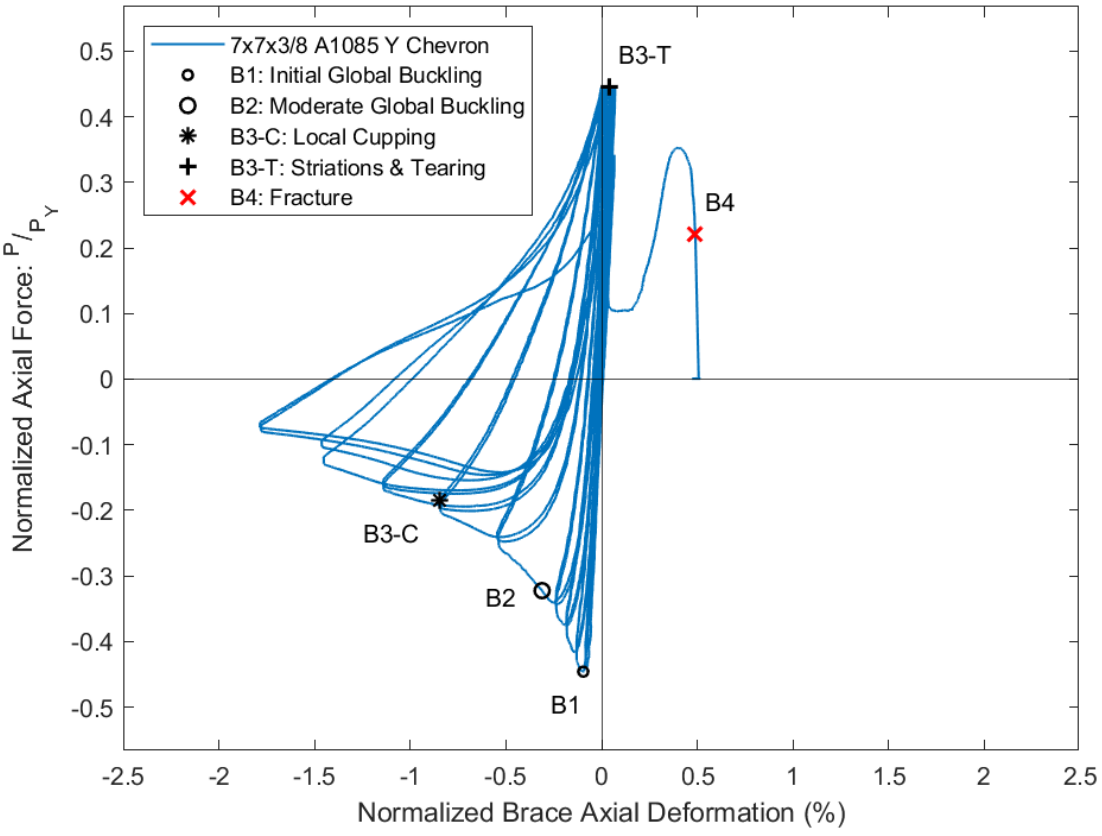

Figure 4.16 Brace Hysteretic Response: 7x7x3/8 A1085 Y Chevron

4.2.17 *7x7x3/8 A1085 Y Near Fault*

The 7x7x3/8 A1085 Y Near Fault specimen experienced initial global buckling and moderate global buckling during the first compression cycle. The global buckling load was 255.2 kips (0.87 times the expected critical buckling load) with a corresponding axial deformation of 0.23”. During the first tension cycle, the specimen yielded in tension and reached a maximum tensile load of 670.9 kips. Following this large tension cycle, the specimen switched out of plane buckling directions. Instrumentation was moved to the other side of the specimen to record data without obstruction. The specimen continued to buckle east throughout the rest of the test. Initial cupping deformations were first observed at an axial deformation of 0.27”. The cupping deformations became very severe at a compressive axial brace deformation of 1.75” which was quickly followed by tearing and fracture. The specimen fractured at an axial deformation of 4.08”.

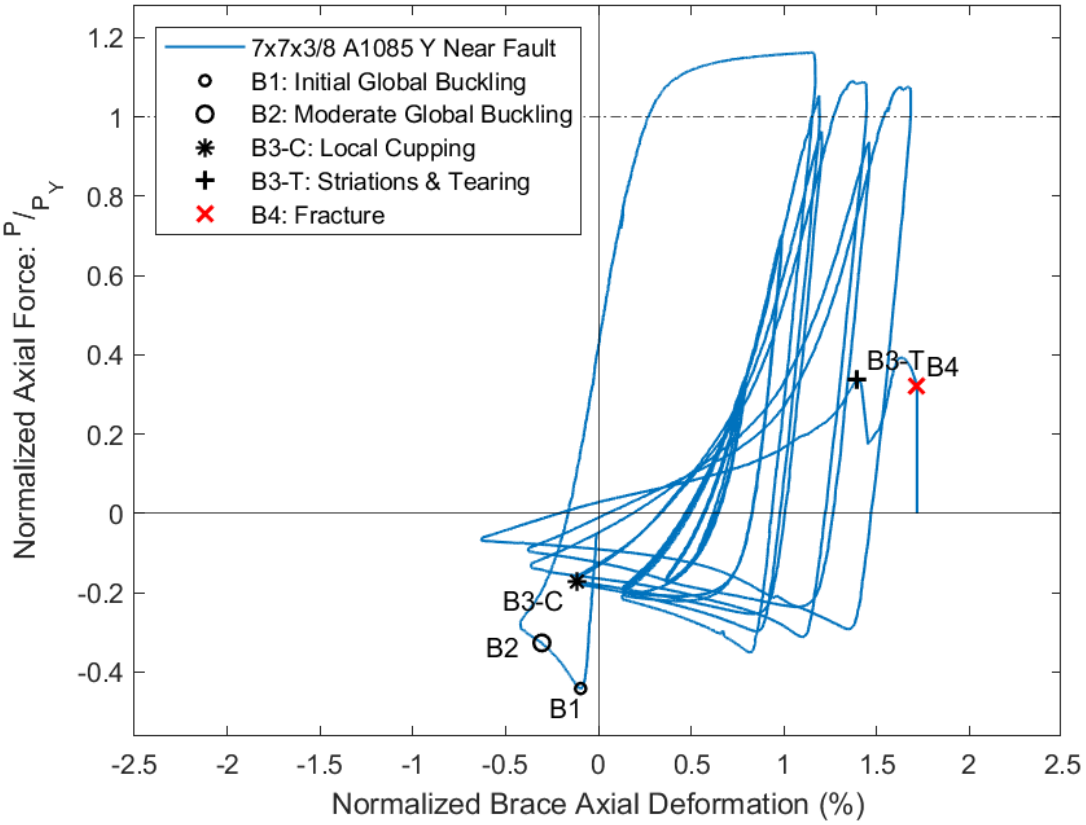

Figure 4.17 Brace Hysteretic Response: 7x7x3/8 A1085 Y Near Fault

4.2.18 *8x8x3/8 A1085 Y Chevron*

Global buckling of the 8x8x3/8 A1085 Y Chevron occurred at an axial deformation of 0.27” and a compressive load of 320.7 kips (0.79 times the expected critical buckling load). The global buckling load was the target load for each subsequent tension cycle so the maximum tensile load experienced by the specimen was 332.9 kips. Initial local cupping deformations were first observed at the peak of the 2.25” target displacements. The specimen started tearing on the corners of the east wall following the first 3.75” target compression displacement. The specimen then fractured during the next tension cycle, reaching a maximum tensile deformation of 1.09”.

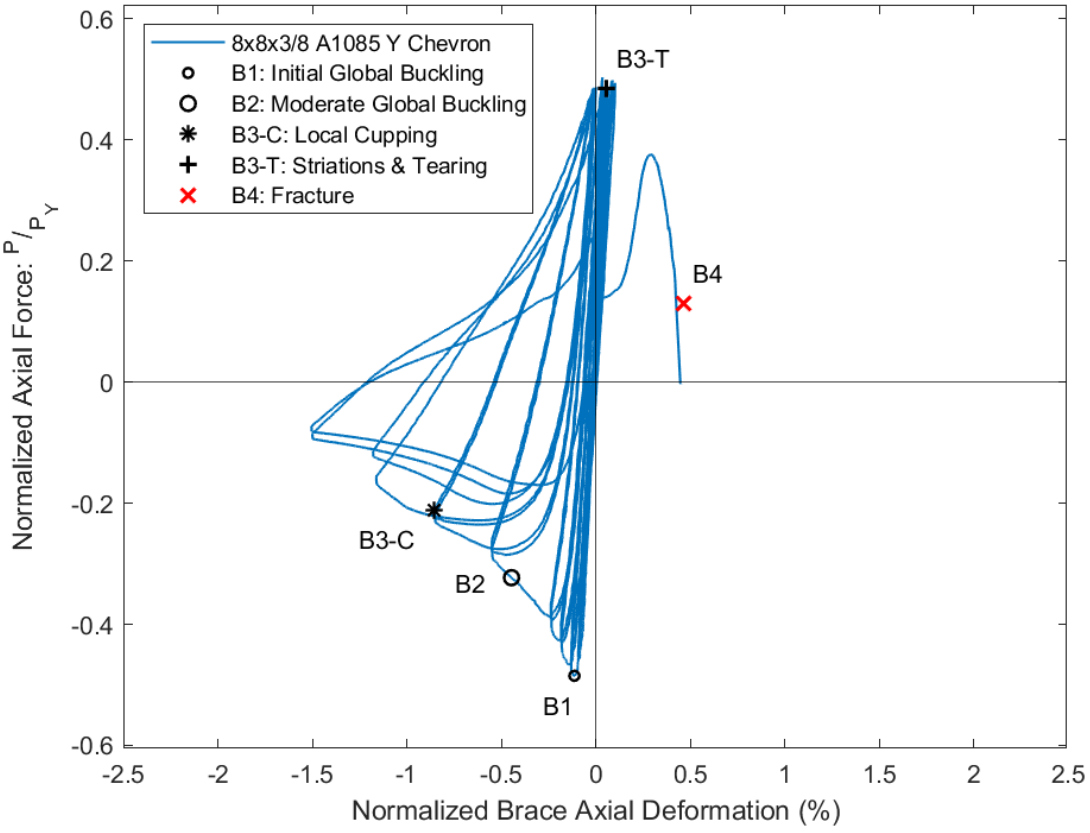

Figure 4.18 Brace Hysteretic Response: 8x8x3/8 A1085 Y Chevron

4.2.19 *8x8x3/8 A1085 Y Near Fault*

In the first compression cycle, the 8x8x3/8 A1085 Y Near Fault specimen exhibited initial global buckling at an axial deformation of 0.31” and a compressive force of 308.4 kips (0.76 times the expected critical buckling load). In the first tension cycle, the specimen experienced excessive yielding and reached a maximum tensile force of 716.3 kips. Due to the large amount yielding in tension, the brace experienced global and local cupping at positive axial deformations as seen on the hysteretic response plotted below in Figure 4.19. Once local cupping was observed, the local deformations quickly grew in each following cycle. The specimen started to tear at an axial brace deformation of 3.25” which was followed by fracture at an axial brace deformation of 3.95”.

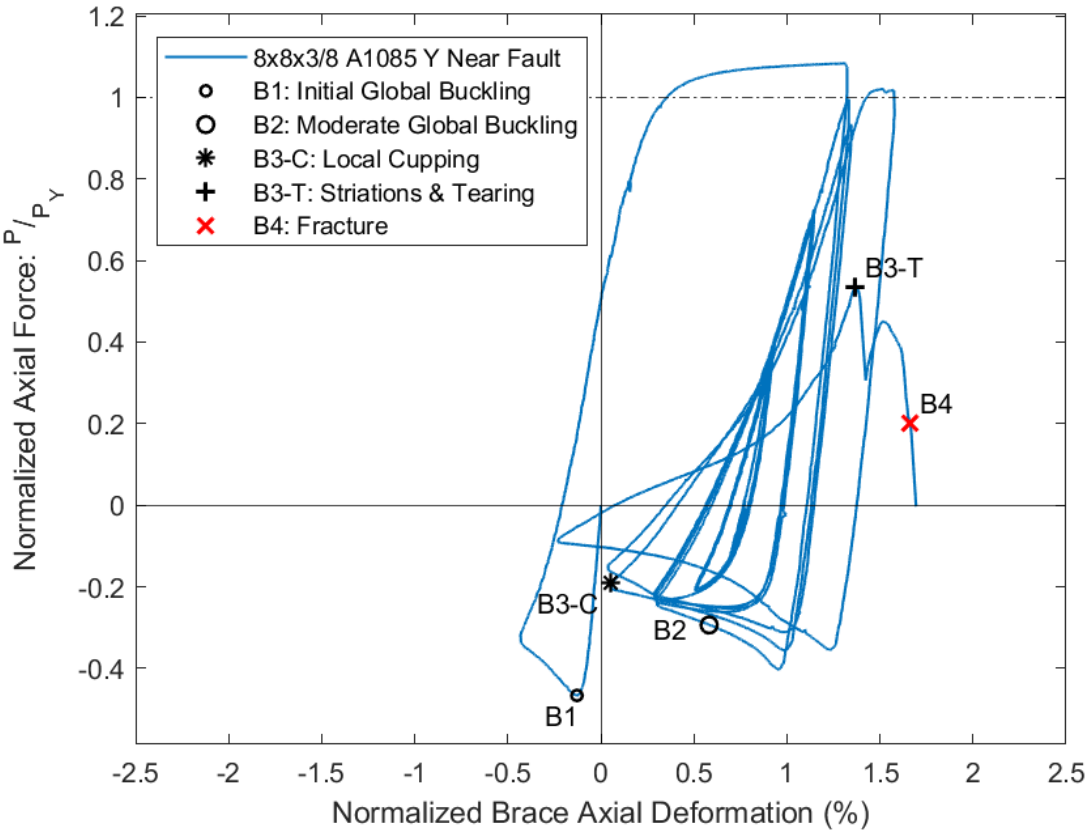

Figure 4.19 Brace Hysteretic Response: 8x8x3/8 A1085 Y Near Fault

4.2.20 *5x5x3/8 A1085 Y Short*

The 5x5x3/8 A1085 Y Short test specimen was subjected to a symmetric load protocol proportionate to that of the longer specimens. Initial global buckling occurred at an axial brace deformation of 0.19”, and a compressive force of 140.8 kips (0.83 times the expected critical buckling load). The specimen reached a maximum tensile force of 438.6 kips, just over the calculated yield load. Local cupping deformations were first observed at an axial compressive deformation of 2.32”. This cupping behavior became more severe as the compressive displacements increased. Striations were observed at the corner of the cupping region during the first 3.30” target cycle. In the next tension cycle, the specimen tore halfway through the section. In the subsequent cycle, the specimen ultimately fractured at an axial brace deformation of 3.64” during the first 4.056” target cycle.

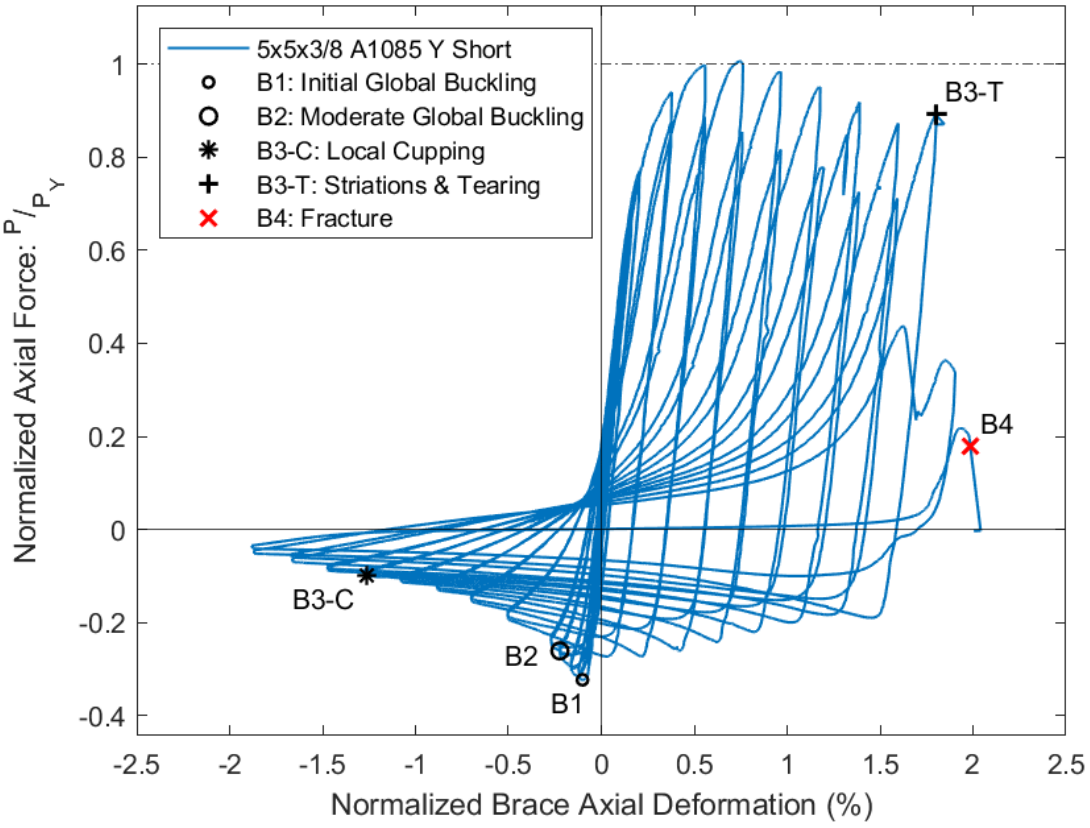

Figure 4.20 Brace Hysteretic Response: 5x5x3/8 A1085 Y Short

4.2.21 *7x7x3/8 A1085 Y Short*

Global buckling was observed in the 7x7x3/8 A1085 Y Short test specimen at a compressive deformation of 0.23”, at which point the brace reached a maximum compressive force of 327.9 kips (0.84 times the expected critical buckling load). The maximum tensile force was 617.5 kips which corresponded to an axial brace deformation of 1.20”. Local cupping deformations were first observed at an axial brace deformation of 1.33” during the first 1.35” target cycle. During the 1.738” target displacement cycles, cupping became more severe, and striations were observed on the top east corner of the specimen. During the first 2.125” target tension cycle, the brace fractured at an axial deformation of 1.56”.

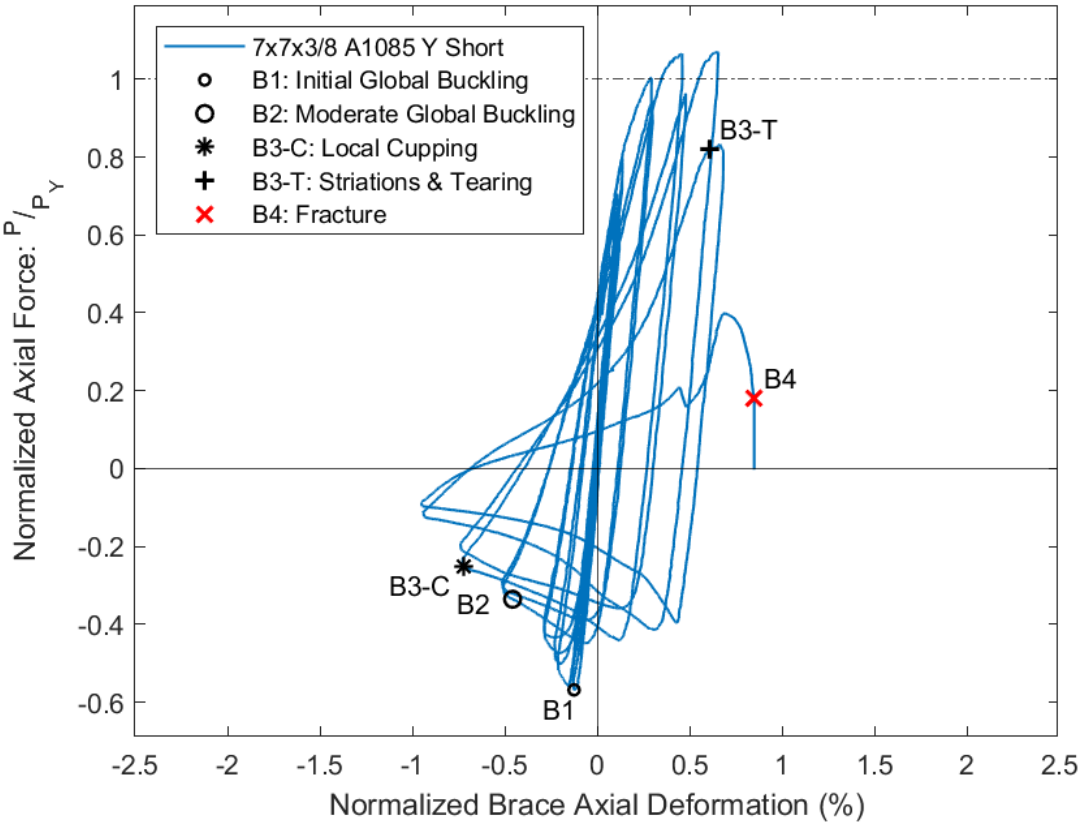

Figure 4.21 Brace Hysteretic Response: 7x7x3/8 A1085 Y Short

4.2.22 *8x8x3/8 A1085 Y Short*

The 8x8x3/8 A1085 Y Short specimen exhibited initial global buckling at an axial deformation of 0.29” and a compressive force of 393.6 kips (0.78 times the expected critical buckling load). The tensile force increased with each increase in displacement prior to fracture, obtaining a maximum tensile force of 666.4 kips. The specimen started to show local cupping deformations at an axial deformation of 1.24” in compression during the first 1.352” target cycle. The severity of cupping deformations increased drastically each subsequent cycle. Striations were observed during the first tension cycle of the 1.738” target cycles. During the next tension cycle, the brace tore through the east, top, and bottom walls, and ultimately fractured during the subsequent tension cycle. The specimen fractured at an axial deformation of 1.61”.

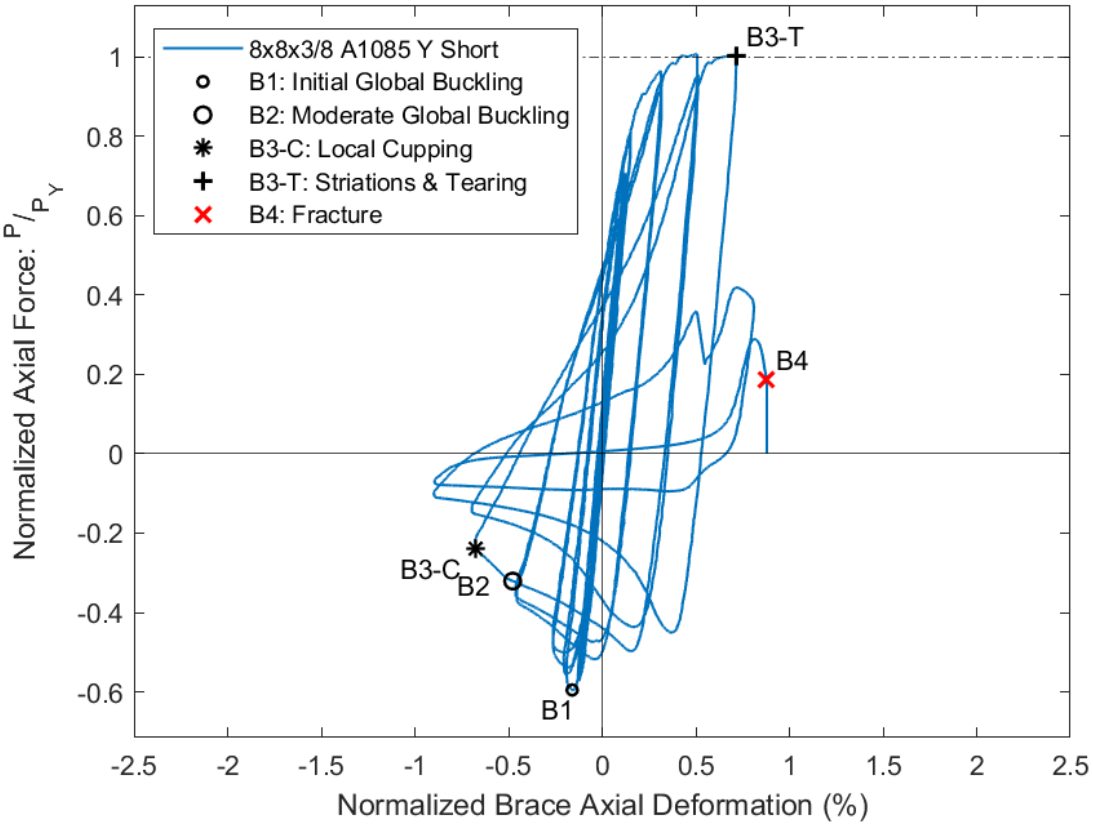

Figure 4.22 Brace Hysteretic Response: 8x8x3/8 A1085 Y Short

Chapter 5. DATA ANALYSIS AND INTERPRETATION

5.1 INTRODUCTION

Chapter 5 presents analysis and interpretation of the test data. Section 5.2 describes the methods used for processing the data recorded during cyclic testing. The raw data collected during testing required trimming and correcting to produce clean, accurate, and comparable plots. The process is detailed in Section 5.2.

The analyzed data is presented in Section 5.3 to investigate the effects of HSS producer, loading protocol, local compactness, and global slenderness. Section 5.3.7 examines the relationship between local and global slenderness leading to recommendations for design provisions. The analysis in this chapter includes data from all four Tests Series in this experimental program. This includes the data presented in Chapter 4, as well as the data from Series 1 presented by Bergendahl (2021).

5.2 DATA PROCESSING

The data collected during experimental testing was collected using the LabVIEW software by National Instruments. Data was collected throughout testing at a frequency of 5 Hz. The acquisition of the data was not paused during the test, and was only stopped following fracture of the specimen.

The raw data files from each test were processed to remove aberrant data spikes and excess data during holds. Figure 5.1 provides a generic example of raw (a) and processed (b) datasets. The processing was done via several Matlab scripts which were built to remove data points during hold periods where the actuators were not moving. The scripts also remove random spikes which were inaccurate data points. The processed dataset was used directly for all measurements except for the brace axial deformation which required data correction as described in Section 5.2.1.

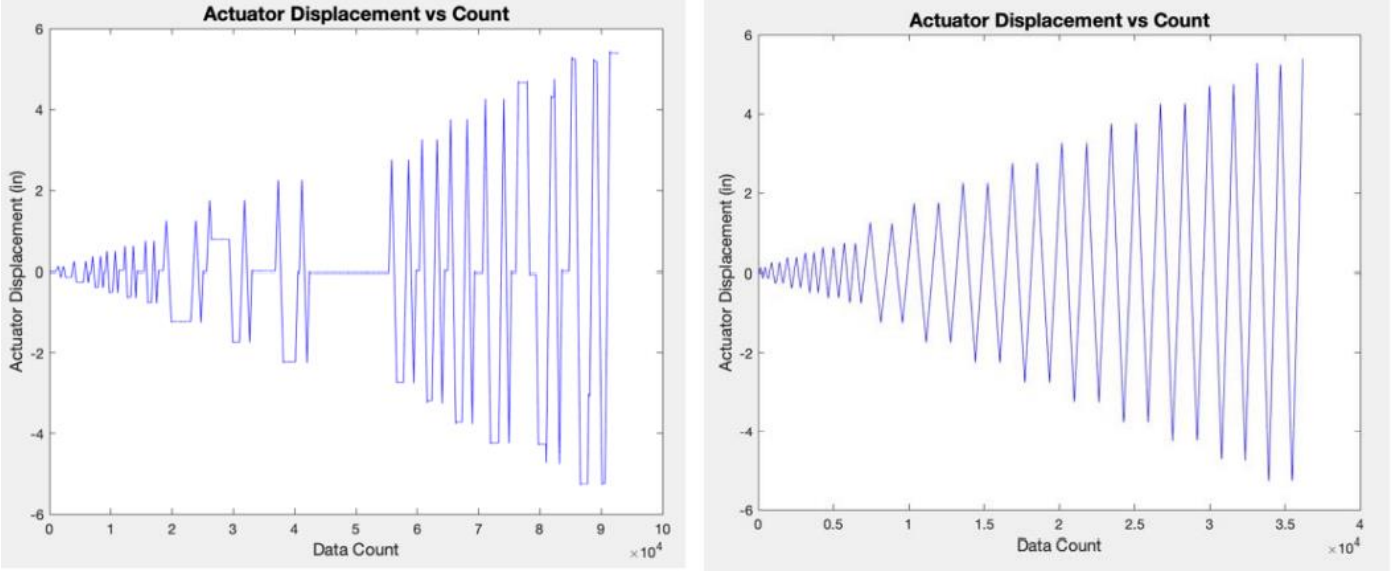

(a) (b)

Figure 5.1 Examples of (a) Raw and (b) Processed LabVIEW Data

5.2.1 *Brace Axial Deformation*

To determine the measured brace axial deformation, the measurement from the string potentiometer along the length of the brace was corrected to remove the additional compressive displacement due to end rotation (Figure 5.2). As the specimen buckled out of plane with respect to the gusset plate, the string potentiometer attached to the side of specimen rotated; this rotation was measured by the instrument resulting in a larger measured than the actual axial compressive deformations. As such, a correction was applied. The angle of rotation of the string pot was calculated using the measured rotation of the gusset plates. The angle of the gusset plates was calculated using the transverse displacement measured by two string potentiometers at two points along the gusset plate. This rigid body rotation is displayed in Figure 5.2. The script, provided in Appendix D, uses the geometry of the string pot and the test specimen to calculate what additional axial deformation is caused by the rotation.

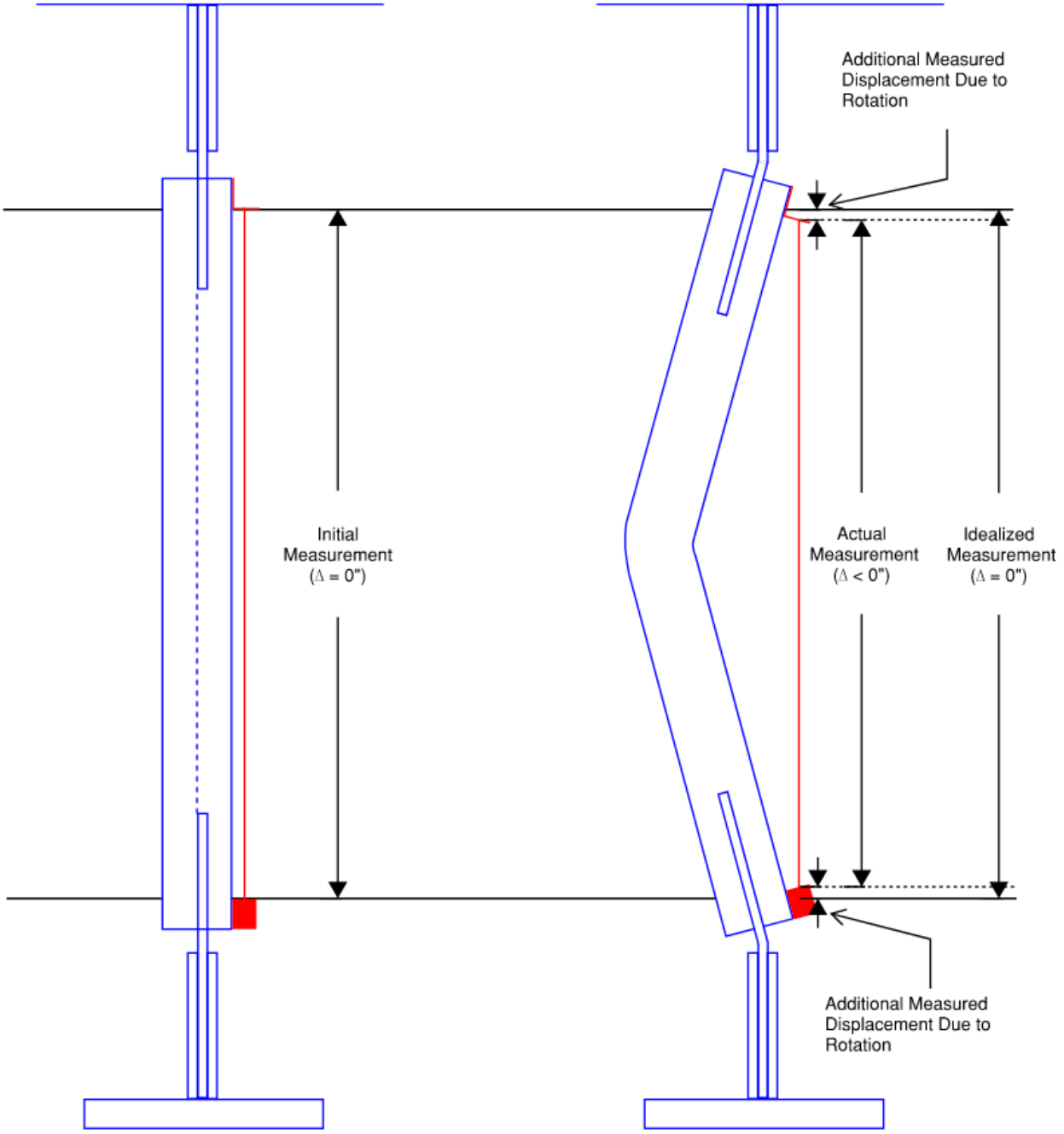

Figure 5.2 Effects of String Potentiometer Rigid-Body Rotation (a) original position (b) rotated position

Figure 5.3 shows the axial brace deformation data before and after corrections for rigid body rotation of the string potentiometer. The figure includes the total displacement of the system measured by a string potentiometer which measured the displacement between the end connection plates. The corrected data was compared to the total displacement to ensure the accuracy of the corrections. The total displacement could not be used for brace axial deformation because it includes gusset plate deformations, bolt bearing, and bolt slip.

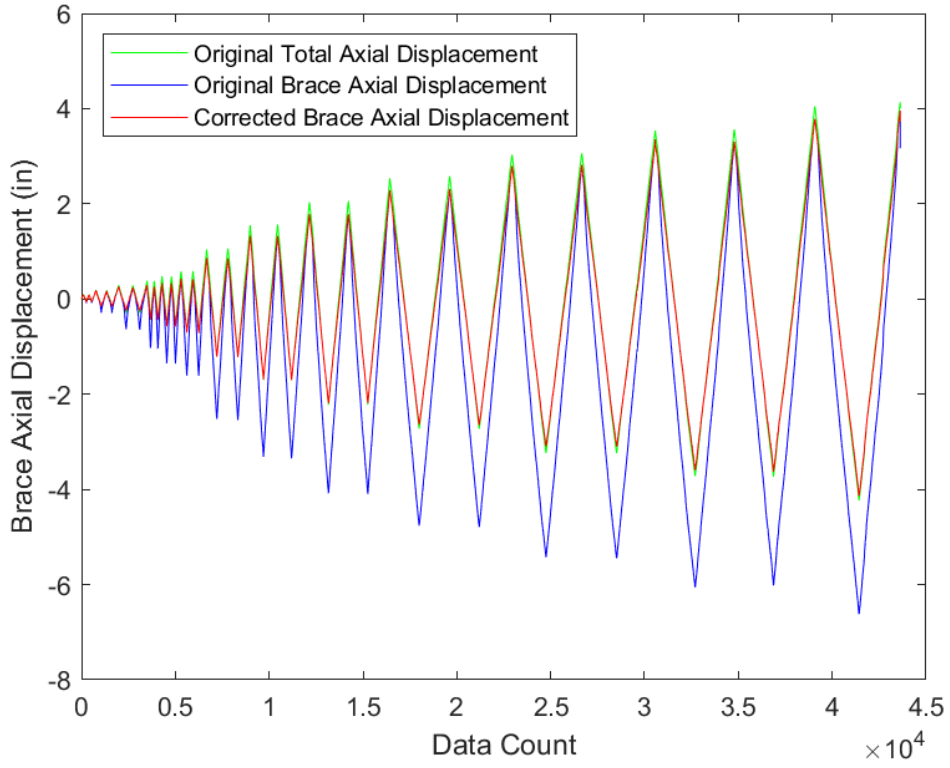

Figure 5.3 Original (Blue), Corrected (Red), and Total (Green) Axial Displacement

In addition to the axial deformation, the test results were used to compare the energy dissipation capacity. In the event of an earthquake, the brace in a concentrically braced frame (SCBF or OCBF) is the primary source of energy dissipation. This occurs as the brace endures inelastic deformations through inelastic buckling in compression and yielding in tension. The energy dissipation capacity is determined by calculating the cumulative energy dissipated prior to fracture (the total area under the force-deformation curve). The cumulative energy dissipation of each test specimen was calculated using trapezoidal integration over the entire force-deformation curve. This integration follows the equation below. Here, W is the total energy

dissipated during the full cyclic testing protocol, F is the brace axial force, Δ is the axial brace deformation, and n is the number of data points for the entire test.

$$W = \sum_{i=1}^{n} \frac{F_i + F_{i-1}}{2} (\Delta_i - \Delta_{i-1}) \quad (5.1)$$

5.3 A1085 TEST COMPARISONS

In this section, the analyzed data is presented to investigate the effects of material and geometric properties as well as HSS producer and loading protocol. The section is organized as follows. First, Section 5.3.1 presents summary tables which quantify the performance each test specimen. The remaining subsections (5.3.2 through 5.3.6) examine the effects of various parameters in the order that follows: (1) HSS producer, (2) displacement history, (3) material properties, (4) cross-sectional compactness ratio, (5) global slenderness ratio (6) relationship of *KL/r* and *b/t*.

5.3.1 *Summary Tables*

A summary of tabulated values which quantify the performance of each test specimen are presented here. Table 5.1 presents data from Test Series 1 which was compiled by Bergendahl (2021). Table 5.2 presents the data from Test Series 2, 3, and 4. The tables include the following information:

- Maximum tensile and compressive forces, $P_{T,max}$ and $P_{C,max}$, as well as the ratio of these maximum forces to the predicted yield and critical buckling forces, P_Y and P_C.
- Maximum tensile and compressive axial brace deformations, $\Delta_{T,max}$ and $\Delta_{C,max}$.
- The deformation range, Δ_{range}, which is the sum of the peak tensile and compressive deformations.
- Approximate story drift percentage for each corresponding axial brace deformation. The story drifts were calculated following the procedure described in Section 4.2.1.
- Accumulated axial brace deformation, Δ_{Acc}, which is the summation of all of the brace axial deformations prior to fracture.
- The energy dissipation capacity, $\sum E_{Diss}$, normalized by the measured cross-sectional area and the measured yield strength, $A_{g,m}$ and $F_{y,m}$, respectively.

Table 5.1 Summary of Test Specimen Performance – Series 1 (Bergendahl, 2021)

HSS Section	$P_{T,max}$ (kips) ($P_{T,max}/P_y$)	$P_{C,max}$ (kips) ($P_{C,max}/P_{Cr}$)	$\Delta_{T,max}$ (in.) (Drift %)	$\Delta_{C,max}$ (in.) (Drift %)	Δ_{range} (in.) (Drift %)	Δ_{Acc} (in.) (Drift %)	$\frac{\sum E_{Diss}}{A_{g,m}F_{y,m}}$
5x5x3/8 A500 Y	432.50 *(1.04)*	-95.30 *(0.99)*	5.13 *(4.28)*	4.89 *(4.07)*	10.02 *(8.35)*	119.54 *(99.65)*	20.57
5x5x3/8 A1085 Y	443.60 *(1.02)*	-98.38 *(0.97)*	5.25 *(4.38)*	5.50 *(4.59)*	10.75 *(8.96)*	132.02 *(110.05)*	21.74
6x6x5/16 A500 R	409.70 *(1.06)*	-125.75 *(0.82)*	3.06 *(2.55)*	3.26 *(2.71)*	6.31 *(5.26)*	52.34 *(43.63)*	13.29
6x6x5/16 A1085 Y	456.40 *(1.07)*	139.80 *(0.87)*	3.13 *(2.61)*	3.12 *(2.60)*	6.25 *(5.21)*	51.33 *(42.79)*	12.57
6x6x3/8 A500 R	511.00 *(1.05)*	-168.70 *(0.96)*	3.74 *(3.12)*	3.72 *(3.10)*	7.46 *(6.22)*	65.80 *(54.85)*	16.45
6x6x3/8 A1085 Y	547.90 *(1.01)*	-180.00 *(0.97)*	3.52 *(2.93)*	3.52 *(2.93)*	7.04 *(5.87)*	56.61 *(47.19)*	13.63
6x6x1/2 A500 R	646.20 *(1.02)*	-218.70 *(1.01)*	4.45 *(3.71)*	4.06 *(3.39)*	8.51 *(7.10)*	80.64 *(67.22)*	17.25
6x6x1/2 A1085 Y	727.20 *(1.06)*	-218.60 *(0.97)*	4.67 *(3.89)*	5.12 *(4.27)*	9.79 *(8.16)*	97.41 *(81.21)*	22.36
7x7x5/16 A500 Y	496.60 *(1.05)*	-209.80 *(0.88)*	1.73 *(1.44)*	1.83 *(1.53)*	3.56 *(2.97)*	20.29 *(16.91)*	5.82
7x7x5/16 A1085 Y	478.10 *(1.05)*	-201.50 *(0.80)*	1.99 *(1.66)*	2.31 *(1.92)*	4.29 *(3.58)*	27.94 *(23.30)*	8.01
7x7x3/8 A500 Y	570.90 *(1.06)*	-231.80 *(0.83)*	2.51 *(2.09)*	2.79 *(2.33)*	5.30 *(4.42)*	35.26 *(29.40)*	10.49
7x7x3/8 A1085 Y	615.90 *(1.07)*	-254.90 *(0.87)*	2.36 *(1.97)*	2.85 *(2.38)*	5.21 *(4.35)*	37.42 *(31.20)*	9.76
7x7x1/2 A500 B	710.40 *(1.06)*	-278.80 *(0.80)*	3.59 *(2.99)*	4.16 *(3.47)*	7.75 *(6.46)*	70.86 *(59.08)*	19.31
7x7x1/2 A1085 Y	805.10 *(1.04)*	-305.70 *(0.84)*	3.48 *(2.90)*	4.41 *(3.68)*	7.89 *(6.58)*	70.13 *(58.46)*	18.21
8x8x3/8 A500 W	702.70 *(1.02)*	359.98 *-(0.93)*	1.24 *(1.04)*	1.90 *(1.58)*	3.14 *(2.62)*	18.10 *(15.09)*	4.97
8x8x3/8 A1085 Y	672.60 *(1.02)*	-328.80 *(0.81)*	2.18 *(1.82)*	2.18 *(1.82)*	4.36 *(3.63)*	27.43 *(22.87)*	9.18
8x8x1/2 A500 W	905.97 *(1.03)*	-434.72 *(0.88)*	2.71 *(2.26)*	2.80 *(2.34)*	5.51 *(4.60)*	38.25 *(31.89)*	12.66
8x8x1/2 A1085 Y	921.90 *(1.02)*	-418.20 *(0.82)*	2.96 *(2.46)*	3.32 *(2.77)*	6.28 *(5.23)*	44.07 *(36.74)*	13.29
10x10x3/8 A500 W	785.40 *(1.01)*	-480.10 *(0.79)*	2.10 *(1.75)*	2.48 *(2.07)*	4.58 *(3.81)*	25.71 *(21.43)*	5.96
10x10x3/8 A1085 Y	812.80 *(1.01)*	-507.60 *(0.81)*	1.60 *(1.33)*	1.84 *(1.53)*	3.44 *(2.87)*	15.66 *(13.05)*	4.67

Table 5.2 Summary of Test Specimen Performance – Series 2, 3, & 4

HSS Section	$P_{T,max}$ (kips) ($P_{T,max}/P_y$)	$P_{C,max}$ (kips) ($P_{C,max}/P_{Cr}$)	$\Delta_{T,max}$ (in.) (Drift %)	$\Delta_{C,max}$ (in.) (Drift %)	Δ_{range} (in.) (Drift %)	Δ_{Acc} (in.) (Drift %)	$\frac{\sum E_{Diss}}{A_{g,m}F_{y,m}$
5x5x3/8 A1085 R	456.59 *(1.01)*	-114.23 *(1.13)*	4.91 *(4.09)*	5.14 *(4.29)*	10.05 *(8.38)*	*120.09 (100.11)*	18.79
5x5x3/8 A1085 W	468.27 *(1.03)*	-110.19 *(1.09)*	4.72 *(3.93)*	5.27 *(4.39)*	9.99 *(8.32)*	*109.31 (91.13)*	17.64
5x5x3/8 A1085 B	538.20 *(1.03)*	-126.44 *(1.25)*	3.93 *(3.28)*	5.07 *(4.23)*	9.00 *(7.51)*	*98.28 (81.93)*	15.50
6x6x3/8 A1085 R	521.04 *(1.08)*	-178.82 *(0.97)*	3.96 *(3.30)*	4.14 *(3.45)*	8.09 *(6.75)*	*73.05 (60.89)*	17.30
6x6x3/8 A1085 W	549.55 *(1.00)*	-185.84 *(1.00)*	3.66 *(3.05)*	4.04 *(3.37)*	7.70 *(6.42)*	*65.74 (54.81)*	14.62
6x6x3/8 A1085 B	581.67 *(1.03)*	-177.88 *(0.96)*	2.97 *(2.48)*	3.26 *(2.72)*	6.23 *(5.19)*	*50.27 (41.91)*	10.74
8x8x3/8 A1085 R	660.41 *(0.99)*	-323.69 *(0.80)*	2.68 *(2.23)*	1.77 *(1.48)*	4.45 *(3.71)*	*25.76 (21.48)*	8.17
8x8x3/8 A1085 W	711.95 *(1.02)*	-361.03 *(0.89)*	2.31 *(1.93)*	2.28 *(1.90)*	4.59 *(3.83)*	*26.46 (22.06)*	8.30
8x8x3/8 A1085 B	763.00 *(1.01)*	-363.94 *(0.90)*	1.74 *(1.45)*	2.55 *(2.12)*	4.29 *(3.57)*	*24.55 (20.47)*	6.71
8x8x1/2 A1085 R	819.18 *(1.04)*	-425.29 *(0.83)*	3.31 *(2.76)*	2.95 *(2.46)*	6.26 *(5.21)*	*47.25 (39.39)*	11.77
8x8x1/2 A1085 W	964.72 *(1.01)*	-446.26 *(0.87)*	2.83 *(2.36)*	3.28 *(2.73)*	6.10 *(5.09)*	*45.42 (37.86)*	13.10
8x8x1/2 A1085 B	938.58 *(0.98)*	-478.57 *(0.94)*	3.03 *(2.53)*	3.05 *(2.55)*	6.08 *(5.07)*	*39.67 (33.07)*	10.93
5x5x3/8 A1085 Y Chevron	409.06 *(0.94)*	-93.31 *(0.92)*	3.64 *(3.03)*	7.82 *(6.52)*	11.46 *(9.55)*	*229.47 (191.30)*	23.12
5x5x3/8 A1085 Y Near Fault	464.24 *(1.07)*	-95.36 *(0.94)*	7.88 *(6.57)*	4.34 *(3.62)*	12.22 *(10.19)*	*152.72 (127.32)*	24.92
7x7x3/8 A1085 Y Chevron	258.35 *(0.45)*	-257.40 *(0.88)*	1.16 *(0.97)*	4.24 *(3.54)*	5.41 *(4.51)*	*34.04 (28.37)*	5.81
7x7x3/8 A1085 Y Near Fault	670.92 *(1.16)*	-255.17 *(0.87)*	4.08 *(3.40)*	1.50 *(1.25)*	5.57 *(4.65)*	*42.55 (35.47)*	12.78
8x8x3/8 A1085 Y Chevron	332.92 *(0.50)*	-320.72 *(0.79)*	1.10 *(0.92)*	3.58 *(2.98)*	4.68 *(3.90)*	*25.74 (21.46)*	5.32
8x8x3/8 A1085 Y Near Fault	716.32 *(1.08)*	-308.41 *(0.76)*	3.95 *(3.29)*	1.03 *(0.86)*	4.98 *(4.15)*	*32.37 (26.98)*	11.43
5x5x3/8 A1085 Y Short	438.58 *(1.01)*	-140.80 *(0.83)*	3.64 *(3.93)*	3.45 *(3.73)*	7.10 *(7.66)*	*76.29 (63.60)*	15.94
7x7x3/8 A1085 Y Short	617.53 *(1.07)*	-327.91 *(0.84)*	1.56 *(1.68)*	1.74 *(1.88)*	3.30 *(3.57)*	*19.88 (16.57)*	7.10
8x8x3/8 A1085 Y Short	666.42 *(1.01)*	-393.60 *(0.78)*	1.61 *(1.74)*	1.65 *(1.78)*	3.27 *(3.52)*	*19.70 (16.42)*	6.98

5.3.2 *HSS Producers*

This subsection compares the performance of HSS specimens of the same shapes from different producers. Four different A1085 square HSS shapes were supplied from each of the four producers: 5x5x3/8, 6x6x3/8, 8x8x3/8, and 8x8x1/2. The geometric and material properties of these HSS specimens were compared in Chapter 3. This section will make comparisons based on cyclic response and structural performance. To analyze the performance of the different producers, comparisons will be made based on deformability and energy dissipation capacity.

Figure 5.4 and Table 5.3 investigate the consistency of the response of different HSS sections among different producers based on axial deformation range. The figure shows that there is consistency in the responses. There is very little variation in the deformation range of the 8x8x3/8 and 8x8x1/2 specimens (coefficients of variation of 0.03 and 0.02, respectively). There is, however, slightly more variation in the 5x5x3/8 and 6x6x3/8 specimens (coefficients of variation of 0.07 and 0.11, respectively). For both the 5x5x3/8 and 6x6x3/8 HSS sections, the Blue producer exhibited notably lower deformation ranges causing the increased variability. The 5x5x3/8 A1085 B test specimen is difficult to compare because this specimen exhibited unique behavior when it flipped buckling directions during testing as described in Chapter 4. This behavior was not observed in any of the other tests. Aside from the unique buckling behavior, the measured yield may be the cause for the lacking performance of the Blue specimens. As discussed in Chapter 3, the 5x5x3/8 A1085 B specimen had the highest measured yield strength, the highest measured ultimate strength, and lowest measured percent elongation of all the specimens tested.

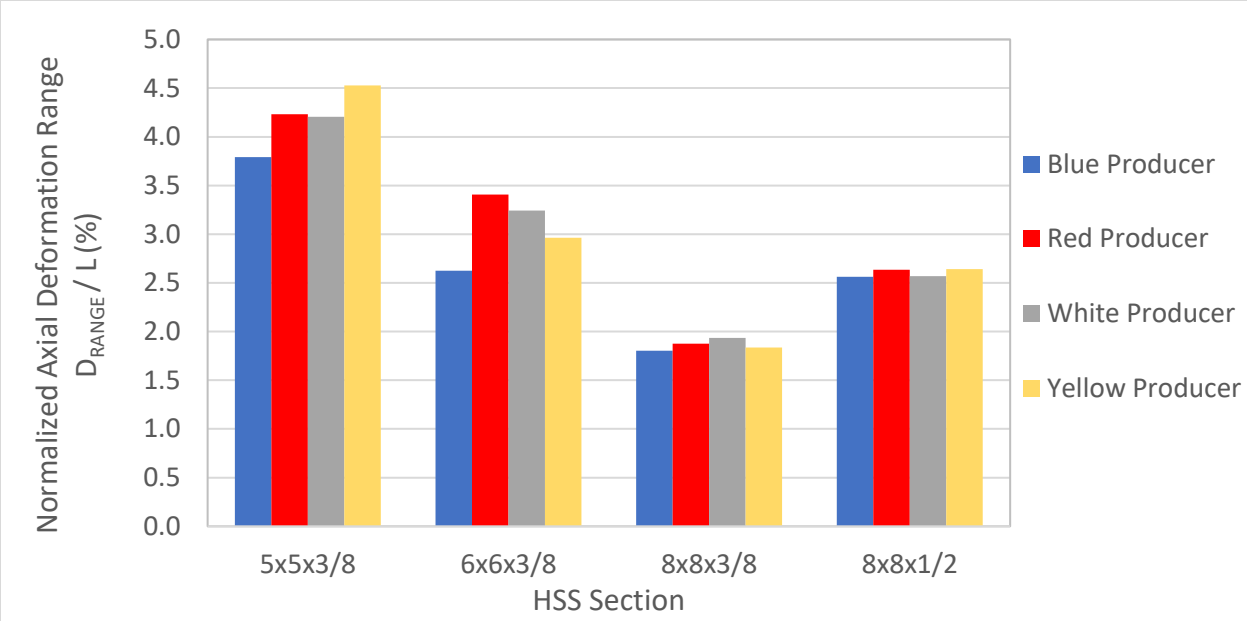

Figure 5.4 Producer Comparison of Normalized Axial Deformation Range

Table 5.3 Summary of Brace Axial Deformation Ranges

	Average (%)	**Standard Deviation (%)**	**Coefficient of Variance**
5x5x3/8	4.19	0.30	0.07
6x6x3/8	3.06	0.34	0.11
8x8x3/8	1.86	0.06	0.03
8x8x1/2	2.60	0.04	0.02

Brace deformability can also be quantified by accumulated axial deformation prior to fracture. The accumulated axial deformation for each specimen is shown in Figure 5.5. Unlike the other measurements of deformability such as deformation range and story drift range, the accumulated axial deformation accounts for the difference between a brace fracturing during the first or second cycle of a specified target displacement. Two specimens could have the same deformation range but different accumulated axial deformations. Generally, the figure shows similar trends as the Figure 5.4, however, there are minor differences to be noted. For example, the 5x5x3/8 A1085 Red and White had relatively the same deformation range however the Red brace achieved a 9.86% greater accumulated axial deformation. This is because the Red

specimen withstood one more cycle of the 5.25” target displacements prior to fracture. Again, the 5x5x3/8 and 6x6x3/8 HSS sections show more variability than the 8x8 HSS sections, however there is not a clear trend between HSS producer and brace deformability.

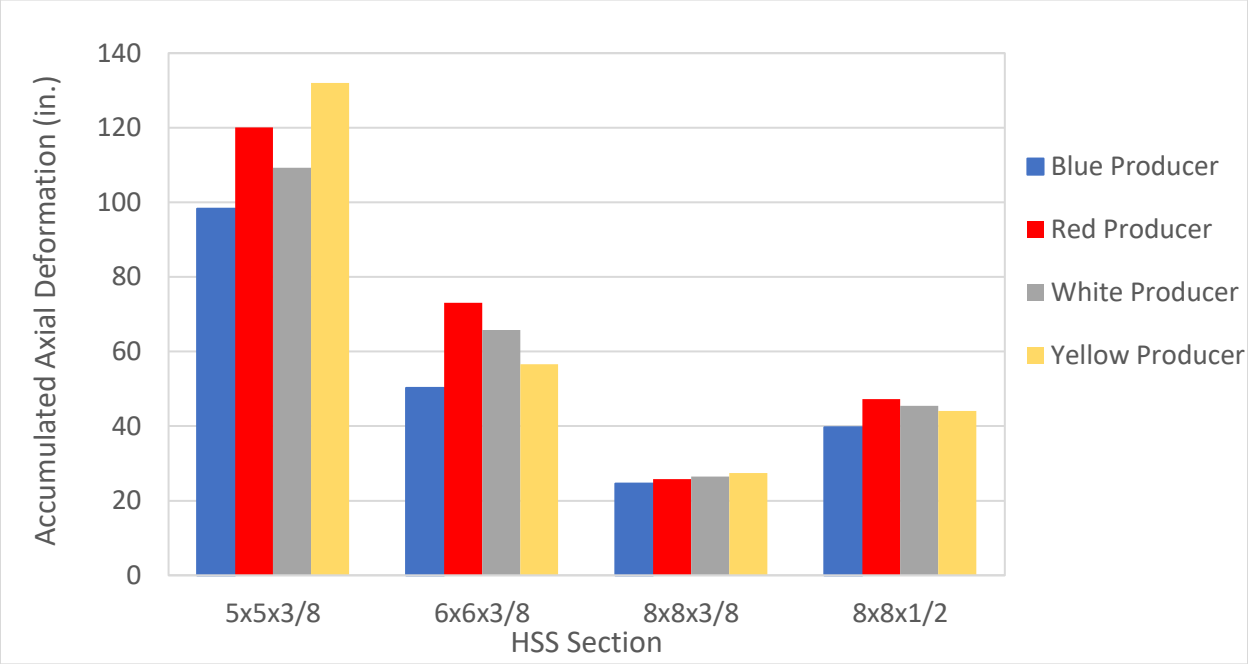

Figure 5.5 Producer Comparison of Accumulated Axial Deformation

Table 5.4 Summary of Accumulated Axial Deformations

	Average (in.)	**Standard Deviation (in.)**	**Coefficient of Variance**
5x5x3/8	114.93	14.46	0.13
6x6x3/8	61.42	10.02	0.16
8x8x3/8	26.05	1.21	0.05
8x8x1/2	44.10	3.23	0.07

Figure 5.6 compares the steel producers based on the normalized energy dissipation capacity. In this plot, the energy dissipation capacity is normalized by the measured yield force, $A_{g,m} F_{y,m}$. This comparison shows more variation between the 8x8x3/8 and 8x8x1/2 specimens from the different manufacturers than when comparing the deformation ranges. For example, the 8x8x3/8 A1085 Y specimen achieved an axial deformation range 3.16% greater than the 8x8x3/8

A1085 B specimen, however the Yellow specimen exhibited a normalized energy dissipation capacity of 21.59% greater than the Blue specimen. This increase in variation for normalized energy dissipation is likely due to differences in material properties.

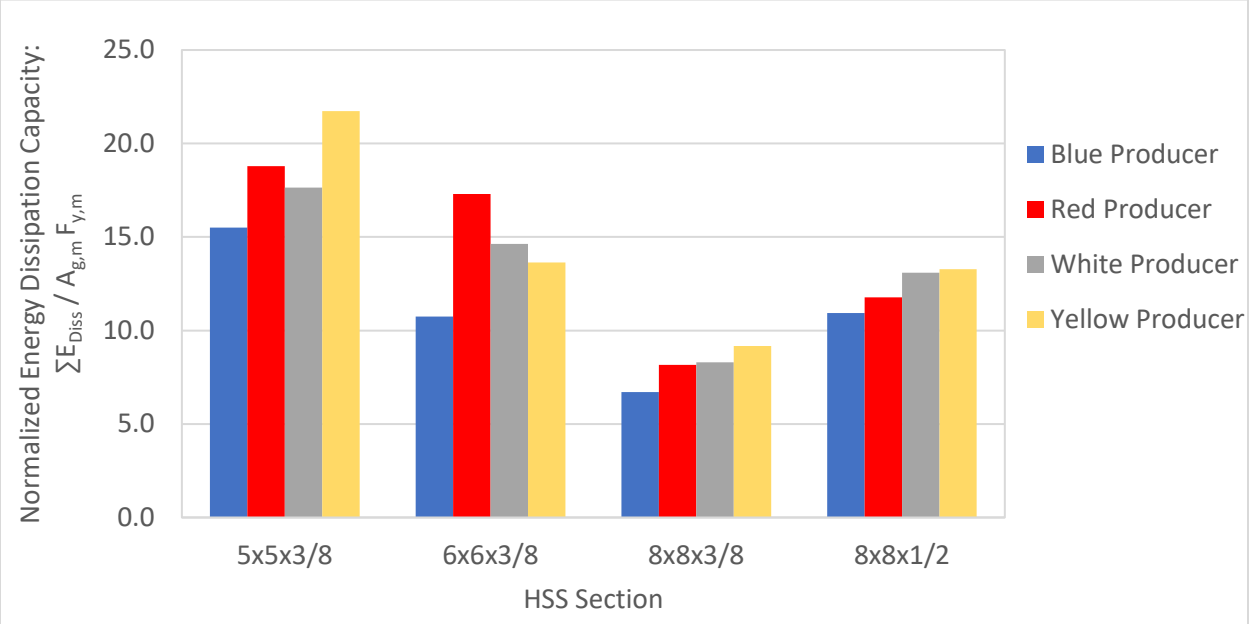

Figure 5.6 Producer Comparison of Normalized Energy Dissipation

Table 5.5 Summary of Energy Dissipation Capacities

	Average (in.)	**Standard Deviation (in.)**	**Coefficient of Variance**
5x5x3/8	18.42	2.60	0.14
6x6x3/8	14.08	2.71	0.19
8x8x3/8	8.09	1.02	0.13
8x8x1/2	12.27	1.12	0.09

5.3.3 *Displacement Protocol*

This section investigates the effect of the applied loading protocol on the cyclic response of A1085 HSS bracing members. A symmetric cyclic loading protocol was used for the majority of the experimental tests conducted for this research project. In order to study the effect of displacement history on the performance of HSS braces, two alternative displacement protocols were studied on the following HSS shapes: 5x5x3/8, 7x7x3/8, and 8x8x3/8. The first alternative displacement protocol, called “chevron”, was a compression biased displacement protocol intended to represent the deformation demands in a chevron configured braced frame. The second, called “near fault”, was a tension dominant displacement protocol intended to represent the non-symmetric pulse type demands for a braced frame subjected to near-fault ground motions. These displacement protocols are described in detail in Chapter 3. HSS sections from the same producer and same heat were used for each of the three displacement protocols allowing direct comparison of the effect of displacement protocol.

Figure 5.7 compares the normalized axial deformation ranges achieved by brace specimens subjected to the various displacement protocols. In the figure, the columns are stacked to show the maximum tensile and compressive range for each specimen. Although there is minor variation in the brace axial deformation range between the different displacement protocols, they are generally very similar. It is evident that maximum tensile and compressive axial deformations are strongly dependent on the displacement protocol but the deformation range is not significantly impacted by displacement protocol. This shows that deformation range is a more indicative parameter for brace deformation capacity than maximum deformation in one direction.

For each of the three HSS sections, the achieved deformation ranges ranked lowest to highest in the following order: symmetric, chevron, near fault. Although the variation is small, the specimens subjected to the symmetric loading protocol reached the smallest deformation range for each HSS section. This indicates that the symmetric loading protocol is more damaging than the compression or tension dominant protocols. The investigation into the effects of local compactness and global slenderness in later sections is based on specimens that were subjected to the symmetric displacement protocol. The observations made in those sections could be considered conservative considering the symmetric loading protocol is the most damaging.

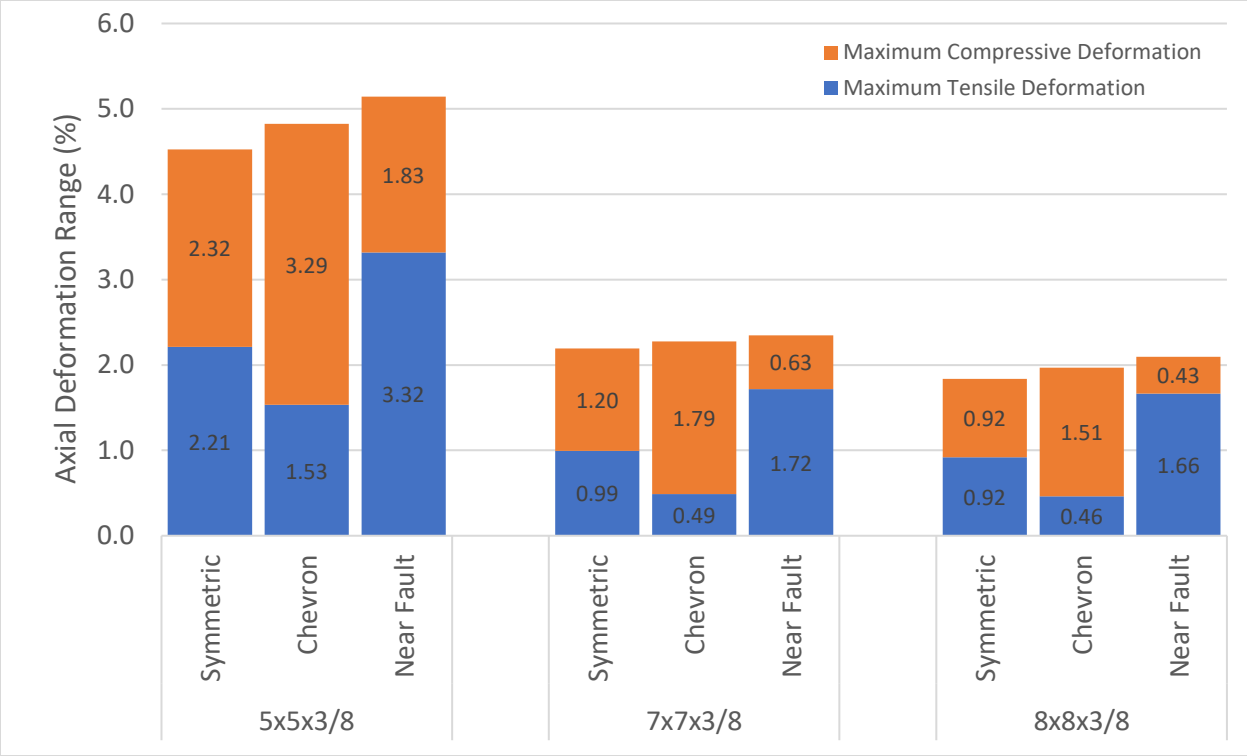

Figure 5.7 Effect of Displacement Protocol on Normalized Axial Deformation Range

Another comparison for brace deformability is shown in Figure 5.8 where the story drift range is plotted to explore the effect of displacement history. The story drift ranges in this figure were approximated using the methodology described in Chapter 4 which assumes a 45˚ brace configuration. This figure shows the same trends as Figure 5.7, however deformation demands for lateral force resisting systems are often written in terms of story drift so it is included here. The target story drift capacity for SCBFs is considered to be 2.5%, however, this figure indicates that story drift range is a better indicator of brace deformability than maximum story drift in one direction. For example, the 7x7x3/8 braces subjected to the symmetric and chevron displacement protocols achieved maximum story drifts of 2.38% 3.54%, respectively. Looking at maximum story drift alone, the brace subjected to the chevron protocol sounds much more ductile, however, both specimens achieved relatively the same story drift range (4.35% and 4.51%). Therefore, the deformation range is more indicative of brace deformability than the maximum deformation. Deformation range should be used as the primary parameter for brace demand and capacity.

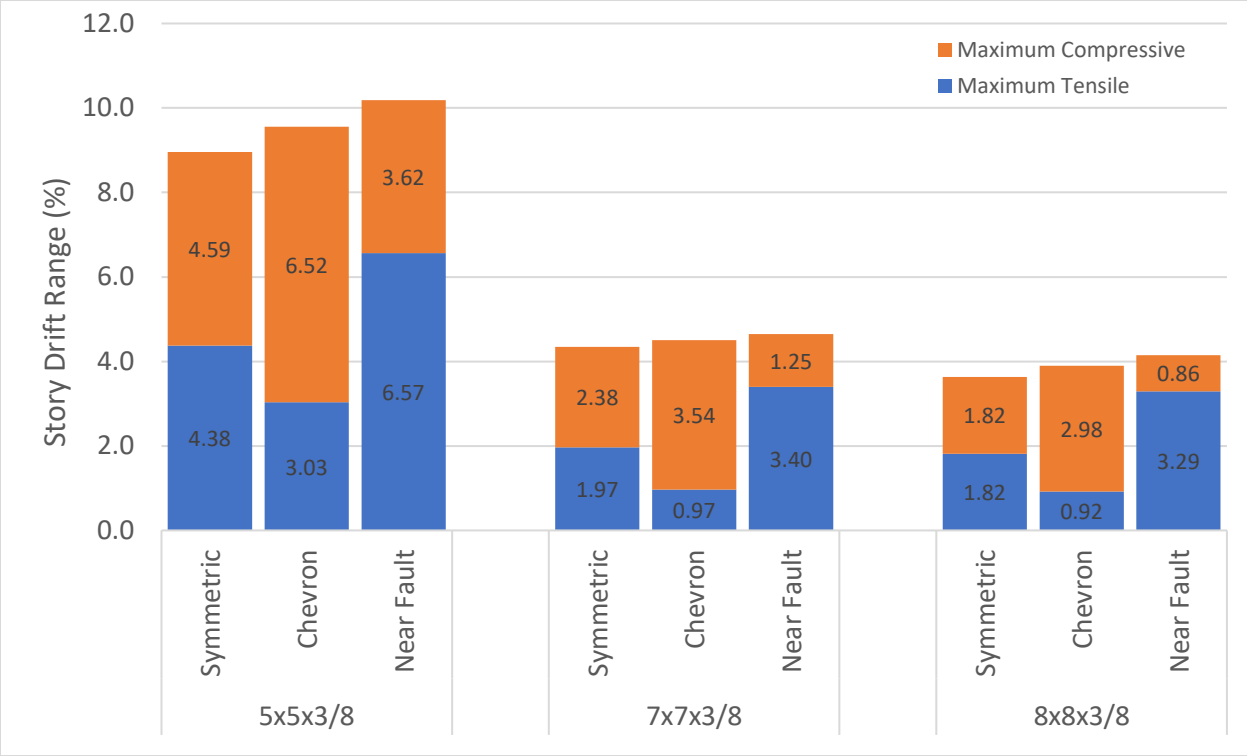

Figure 5.8 Effect of Displacement Protocol on Story Drift Range

The displacement protocols can also be compared based on energy dissipation capacity, as shown in Figure 5.9. It is evident that for the 7x7x3/8 and 8x8x3/8 test specimens, the specimen subjected to the chevron protocol exhibited a much lower energy dissipation capacity. This is because the chevron protocol was compression dominant, and the brace tensile force never exceeded the magnitude of the buckling load. Therefore, the brace did not experience the inelastic tension cycles like those subjected to the symmetric and near fault protocols. The inelastic tension cycles are the primary source of energy dissipation due to yielding occurring during the large tensile forces. This trend, however, does not apply to the 5x5x3/8 chevron specimen shown in Figure 5.9. As discussed in Chapter 4, during the 5x5x3/8 A1085 Y Chevron test, the actuators reached the maximum stroke in compression and increased tension demands had to be applied to fracture the specimen. During the increasing tension demands the specimen withstood multiple inelastic tension cycles therefore dissipating much more energy than the other chevron tests.

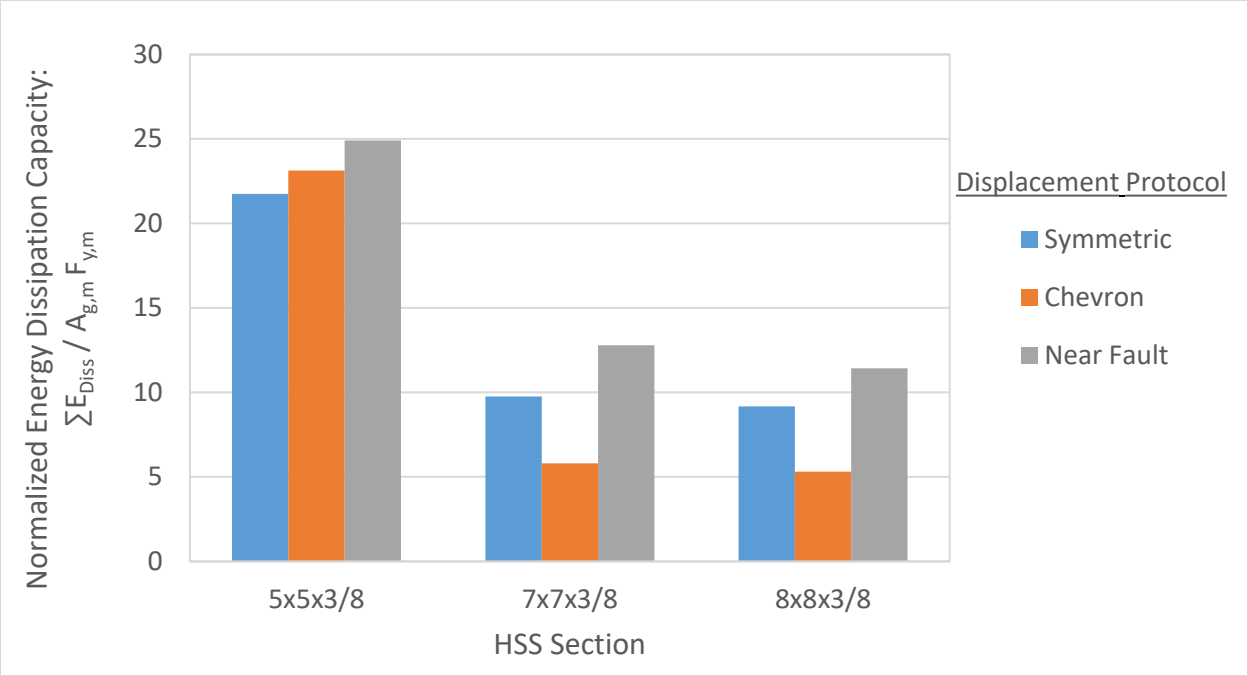

Figure 5.9 Effect of Displacement Protocol on Normalized Energy Dissipation

5.3.4 *Material Properties*

As discussed in Chapter 3, material properties were measured via tension tests and CVN toughness tests. This section will investigate the effect of the measured material properties on the deformability of the HSS brace specimens. The figures shown in this section include three A1085 HSS sections from four different producers: 5x5x3/8, 6x6x3/8, and 8x8x3/8. In the figures, the markers are grouped by HSS shape so that the effect of only the material properties can be analyzed. In each of the plots, the axial deformation range is normalized by the brace initial brace length.

Figure 5.10 plots the axial deformation range versus the measured yield strength ratio to show the effect of the measured yield strength. The measured yield strength ratio, $R_{y,m}$, is taken as the measured yield strength divided by the minimum nominal yield strength (50 ksi for A1085 and A500). The figure shows that for the 5x5x3/8 and 6x6x3/8 specimens (both classified as highly ductile), the axial deformation range decreased with increases in yield strength. However, this trend is not apparent with the 8x8x3/8 specimens.

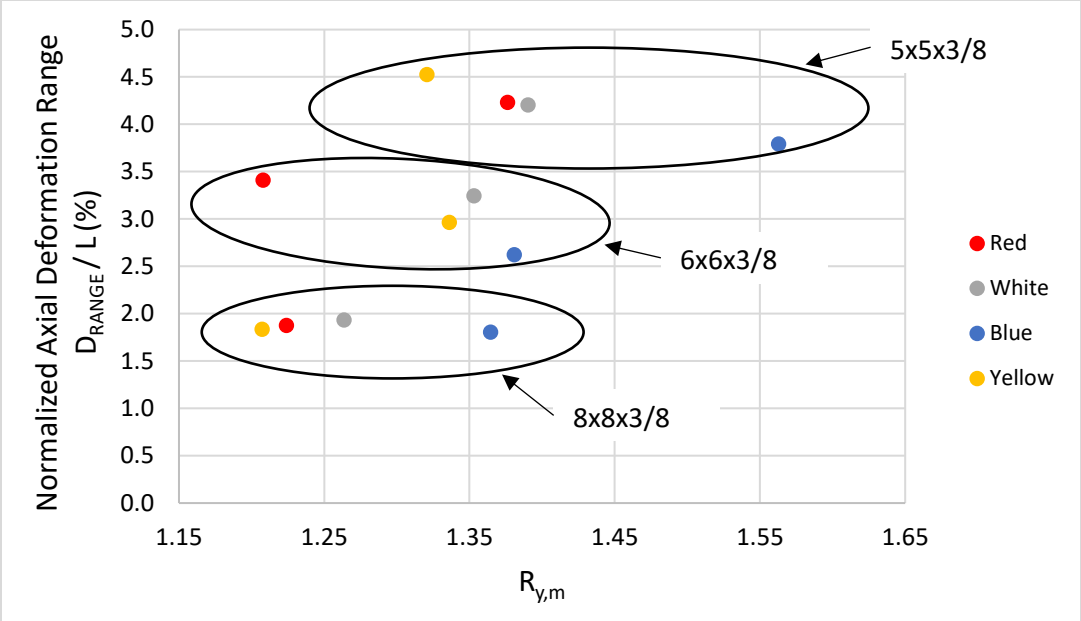

Figure 5.10 Axial Deformation Range vs. Measured Yield Strength Ratio

Figure 5.11 shows the normalized axial deformation range plotted against the measured ultimate-to-yield strength ratio, $F_{u,m}/F_{y,m}$. The ultimate-to-yield strength ratio does not prove to be a significant parameter affecting the deformability of HSS braces. For the 6x6x3/8 specimens, the specimen with the highest ultimate-to-yield strength ratio achieved the largest deformation range but this observation is not consistent with any trend across the dataset.

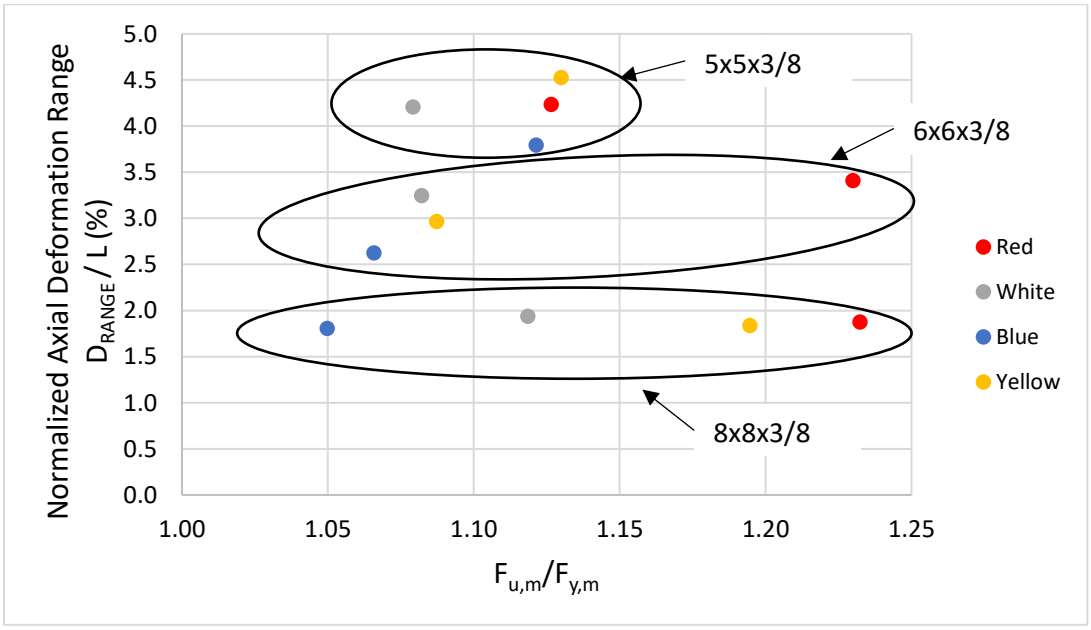

Figure 5.11 Axial Deformation Range vs. Measured Ultimate-to-Yield Strength Ratio

Figure 5.12 displays the axial deformation range plotted against the unmodified measured CVN toughness values. Analysis of the CVN toughness in Chapter 3 showed significant variation across all of the A1085 specimens. In this figure, it is apparent for each of the HSS sections that there is no relationship between CVN toughness and brace deformability.

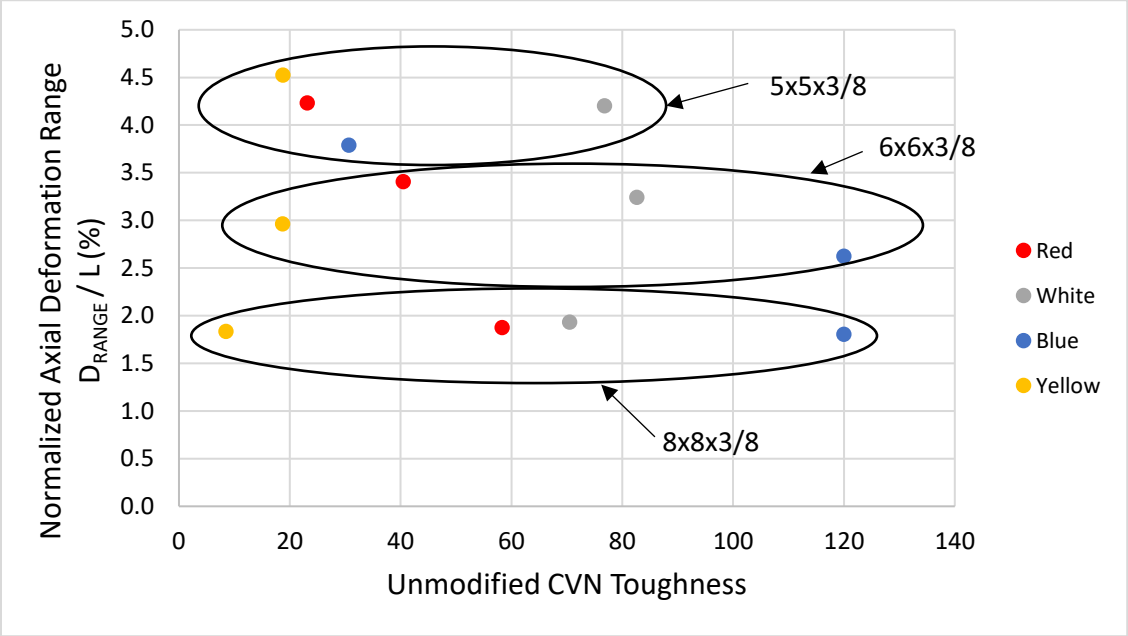

Figure 5.12 Axial Deformation Range vs. Unmodified CVN Toughness

5.3.5 *Local Compactness Ratio, b/t*

Previous research has proven that local compactness is a critical parameter controlling the structural response of HSS braces. This section will investigate the effect of local compactness on various measurements of performance and ductility such as axial deformation range, maximum story drift, accumulated axial deformation, and cumulative energy dissipation. In this section, the effects of local compactness will only be analyzed for the A1085 HSS specimens subjected to the symmetric loading protocol.

In the following plots, the AISC width-to-thickness limits are shown as vertical lines. Specimens plotted to the left of the solid line represent HSS braces that meet the AISC criteria for highly ductile, while specimens plotted to the left of the dashed line represent HSS braces that meet the moderately ductile criterial. Axial deformation range is normalized by the brace length in the figures below. The values for approximated story drift in the following figures were calculated following the procedure described in Section 4.1.

Figure 5.13 shows the relationship between the nominal compactness ratio, *b/t*, and the normalized axial deformation range. The normalized axial deformation range is a quantitative measure of the deformability of the test specimen. It represents the sum of the magnitudes of the maximum compressive deformation and the maximum tensile deformation. In this plot, it is evident that a decrease in local compactness ratio is associated with an increase in axial deformation range. This trend is consistent with the data from previous research and is reflected by the AISC maximum *b/t* limits. The power regression curve in this plot has an R^2 value of 0.91 which expresses that local compactness accounts for a significant amount of the variation in deformation range. The figure shows that the effect of compactness ratio is exponential – at lower compactness ratios, a change in *b/t* causes a larger change in deformation range. This is evident in the plotted best fit line where the slope to the left of the highly ductile limit is much steeper than the slope to the right of the moderately ductile limit. All of the specimens which met the AISC highly ductile limit achieved an axial deformation range of at least 2.5%. The more compact specimens, with width-to-thickness ratios less than 12, reached axial deformation ranges of at least 3.25%. All of the specimens which met the AISC moderately ductile limit reached an axial deformation range of at least 2.2%.

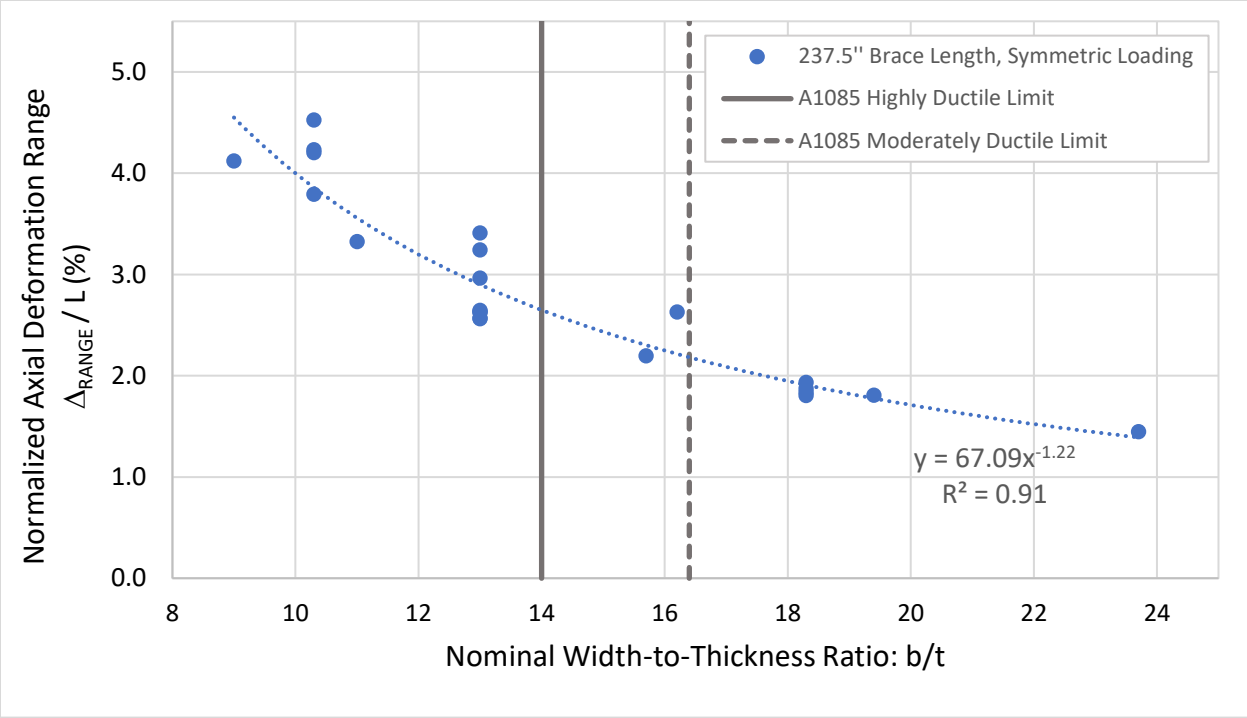

Figure 5.13 Axial Deformation Range vs. Local Compactness – Long Braces

Axial deformation range versus local compactness is plotted for the shorter, 183.5" long brace specimens, in Figure 5.14. Although only three specimens were tested at the shorter length, a similar relationship between local compactness and axial deformation range is evident in this figure for the shorter braces. The 5x5x3/8 specimen was the only short specimen that is classified as highly-ductile by AISC's compactness limits. This specimen exhibited much greater ductility than the specimens which classify as moderately ductile and non-ductile. It is interesting that although the 7x7x3/8 is significantly more compact than the 8x8x3/8, both specimens exhibited the same deformation range. There was a larger difference between the same two HSS sections at the longer length. The effect of brace length and global slenderness is investigated in further detail in Section 5.3.6.

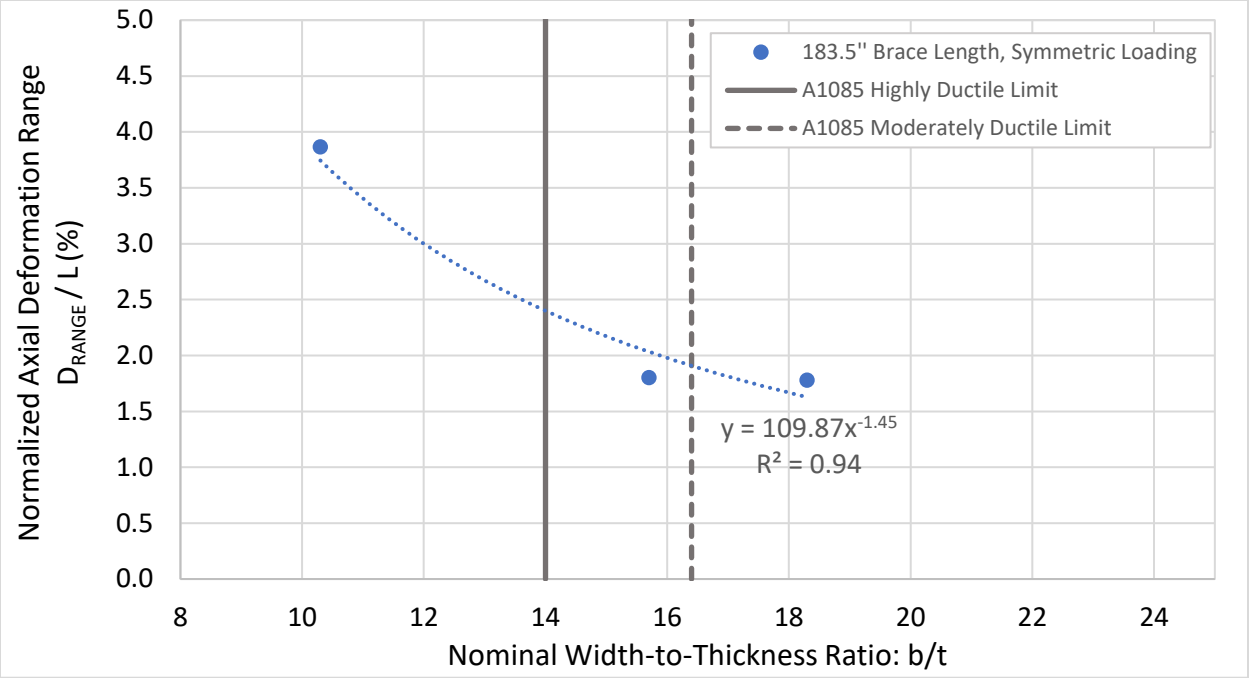

Figure 5.14 Axial Deformation Range vs. Local Compactness – Short Braces

In Figure 5.15 and Figure 5.16, the axial deformation range is plotted against the measured width-to-thickness ratios, rather than the nominal width-to-thickness ratio. Figure 5.15 uses the nominal width to measured thickness ratio, b_{nom}/t_{meas}, while Figure 5.16 uses the measured width to measured thickness ratio, $(b/t)_{meas}$. Both plots are included because the method described in Chapter 3 for measuring the flat width, b, was somewhat subjective. The measurement of the wall thickness, however, was quite accurate. Both figures show the same trend as Figure 5.13 where the braces with lower compactness ratios reach larger deformation ranges.

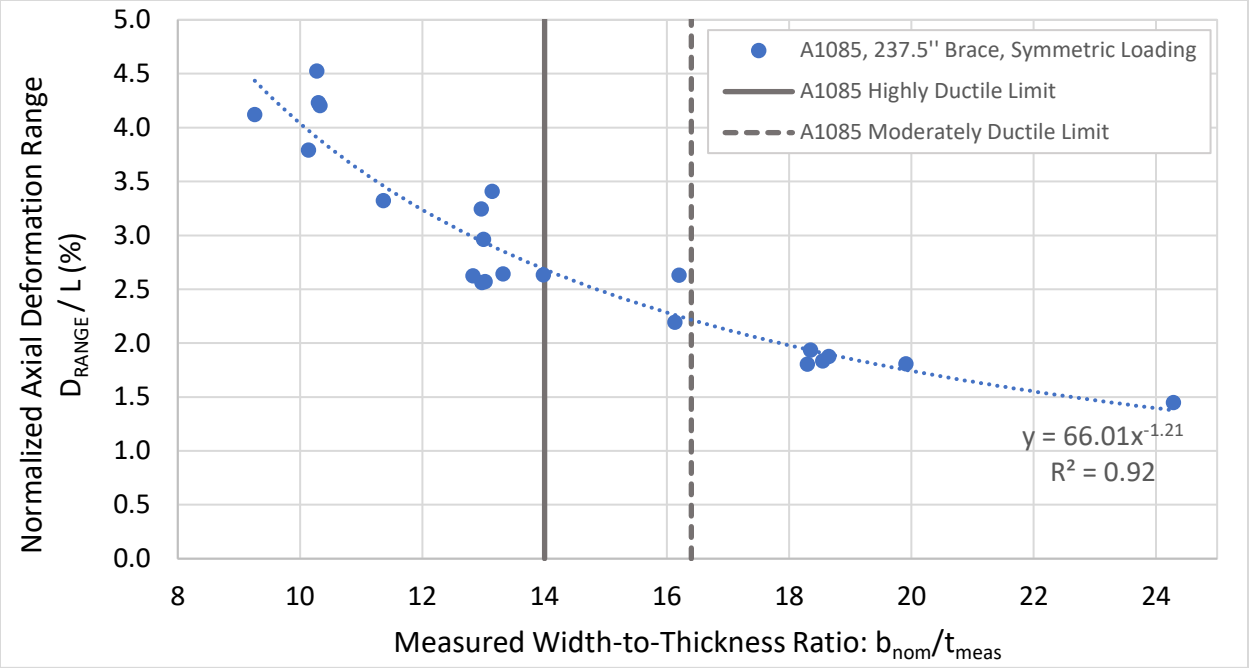

Figure 5.15 Axial Deformation Range vs. Measured Local Compactness, b_{nom}/t_{meas}

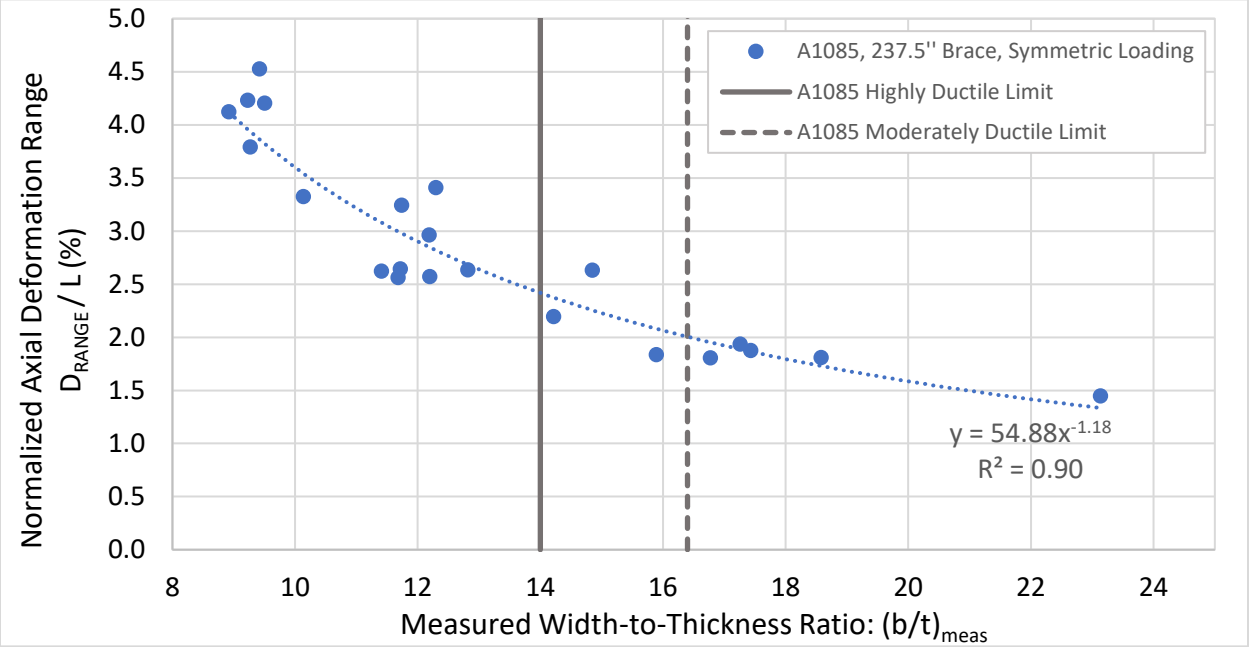

Figure 5.16 Axial Deformation Range vs. Measured Local Compactness, $(b/t)_{meas}$

Brace deformability is investigated again in Figure 5.17 where the story drift range is plotted versus the nominal width-to-thickness ratio. The story drift ranges in this figure were approximated using the methodology described in Chapter 4 which assumes a 45˚ brace configuration. The same trends shown in Figure 5.13 are seen here, however, story drift is often

used to assess the ductility of braced frames, so it is included here. All of the brace specimens which classify as highly ductile according to the seismic provisions achieved a story drift range of at least 5%. All of the brace specimens which classify as moderately ductile achieved a story drift range of at least 4%.

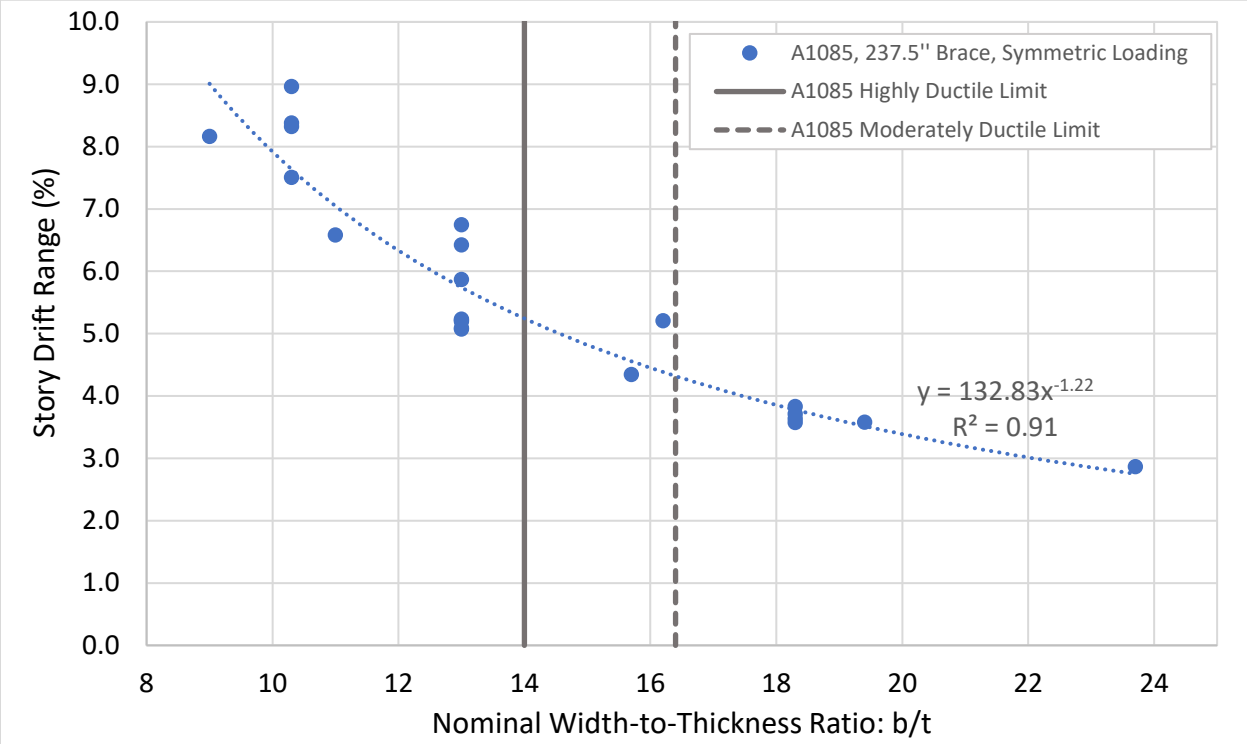

Figure 5.17 Story Drift Range vs. Local Compactness

The maximum story drift is plotted against the nominal local compactness ratio in Figure 5.20. All of the specimens in this plot were subjected to the same symmetric displacement protocol, making it possible to compare the maximum story drifts. Due to the symmetry of the loading protocol, the maximum story drift is generally about half of the story drift range shown in Figure 5.17, however the maximum story drift was not always exactly half of the range due to the effects of bolt slip or fracture at the first peak tension displacement cycle. The figure displays the same trend as the figures above.

The figure shows that all of the specimens that classify as highly ductile bracing members reached a story drift of at least 2.5% prior to fracture. It is commonly assumed that the target inelastic deformation for SCBFs prior to brace fracture is about 2.5% (Sabelli et al., 2013). All of the specimens that classify as highly ductile meet this deformation standard. Additionally, all

of the brace specimens that classify as moderately ductile achieved a maximum story drift of at least 2.38%, just slightly lower than the standard target of 2.5% for SCBFs. This indicates that the moderately ductile limit is conservative considering the drift demands for OCBFs are smaller than those for SCBFs.

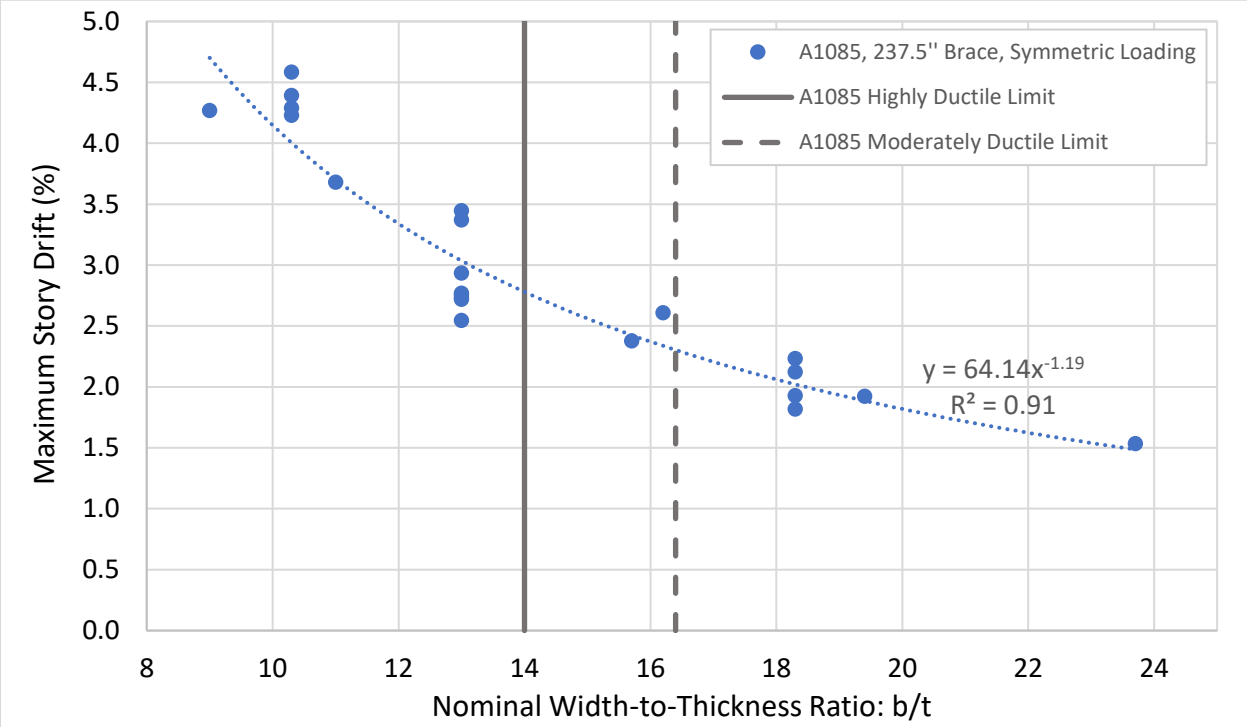

Figure 5.18 Maximum Story Drift vs. Local Compactness

As HSS braces buckle under large compressive displacements, a plastic hinge forms at the center of the brace. Significant local deformations develop at the center of this plastic hinge region (a phenomenon often referred to in this thesis as “local cupping”). As a result of these large local deformations and high strains, the brace becomes susceptible to fracture in tension. Resisting the development of these deformations and high local strains is therefore critical to the inelastic performance of HSS braces. In each of the brace tests, local cupping deformations were observed prior to fracture. Figure 5.19 shows the axial brace deformation at the initiation of local cupping plotted against the local compactness ratio, *b/t*. The figure shows that the formation of local deformations is dependent on the local compactness. The development of local cupping is delayed in more compact braces. This delay in local cupping leads to increase in axial deformation range and therefore fracture life.

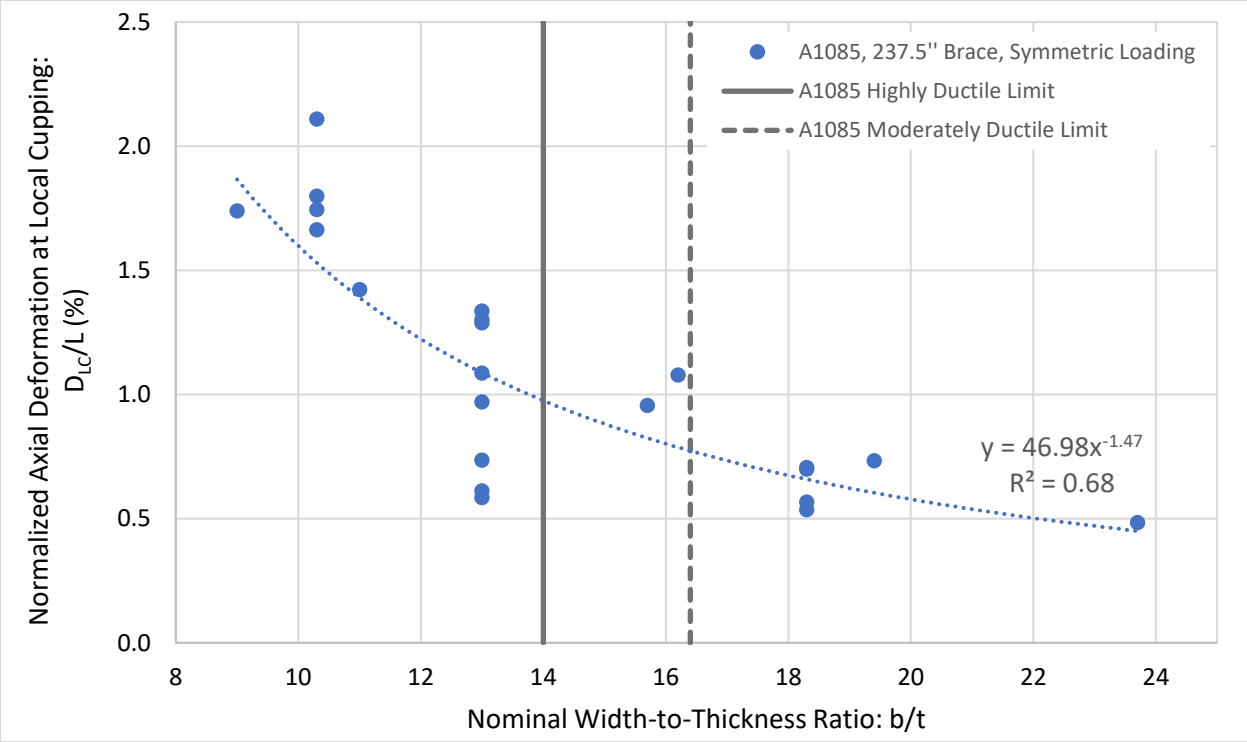

Figure 5.19 Axial Deformation at Local Cupping vs. Local Compactness

Brace ductility can also be quantified by accumulated axial deformation prior to fracture. The effect of the nominal width-to-thickness ratio on accumulated axial deformation is shown in Figure 5.20. Unlike the other measurements of ductility such as deformation range and maximum story drift, the accumulated axial deformation accounts for the difference between a brace fracturing during the first or second cycle of a specified target displacement. Two specimens could have the same range but different accumulated axial deformation ranges. The accumulated axial deformation is highly dependent on the deformation protocol. All of the specimens in this figure were subjected to the same displacement protocol which makes it possible to make comparisons. Similar to the effect of local compactness on axial deformation range, a decrease in the width-to-thickness ratio is associated with an increase in accumulated axial deformation. The power regression curve in this plot has an R^2 value of 0.88 which is lower than the R^2 value in the plot for axial deformation range versus local compactness which had an R^2 value of 0.91. This indicates that that local compactness accounts for less of the variation in accumulated axial deformation. The greater variation in accumulated axial deformations is likely due to differences in post tearing ductility. As stated above, accumulated axial deformation accounts for difference between a brace fracturing during the first cycle or the second cycle of a

specified target displacement. The difference between a brace fracturing during the first or second cycle of a specified target displacement is likely determined by post-tearing ductility of the brace which is strongly influenced by the material properties. Therefore, although local compactness determines the deformation range, material properties are likely to influence post tearing ductility which is accounted for in accumulated axial deformation.

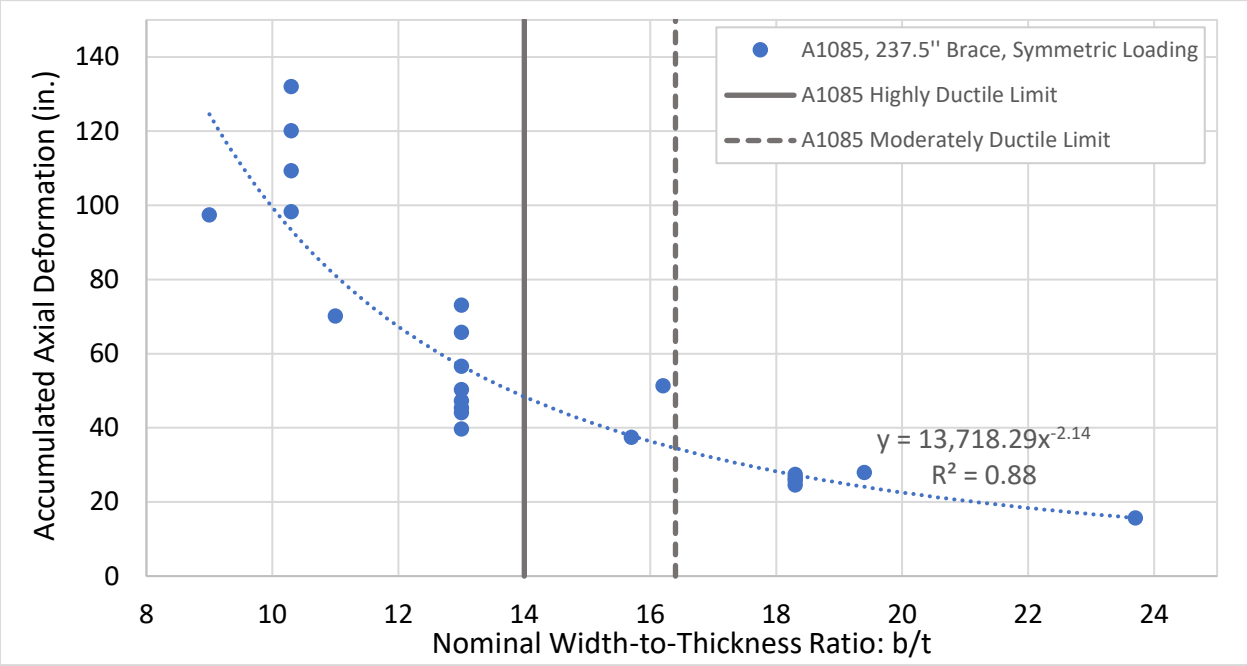

Figure 5.20 Accumulated Axial Deformation vs. Local Compactness

In Figure 5.21, the normalized energy dissipation capacity is plotted against the nominal local compactness ratio. In this plot, the energy dissipation capacity is normalized by the measured cross-sectional area and the measured yield strength to account for differences in geometric and material properties. The plot shows a clear correlation between more locally compact braces and increased energy dissipation capacity. The power regression curve accounts for a significant amount of the variation with an R^2 value of 0.88. The general trend of increased energy dissipation capacity with decreased width-to-thickness ratio is a product of braces with lower compactness ratios being able to withstand more inelastic cycles at larger axial deformations. There is however more variation between members of the same size in this plot than in the axial deformation range plot. As discussed in the producer comparisons, there was

more variation in energy dissipation capacity than in deformation range. This is likely due to minor differences in material properties.

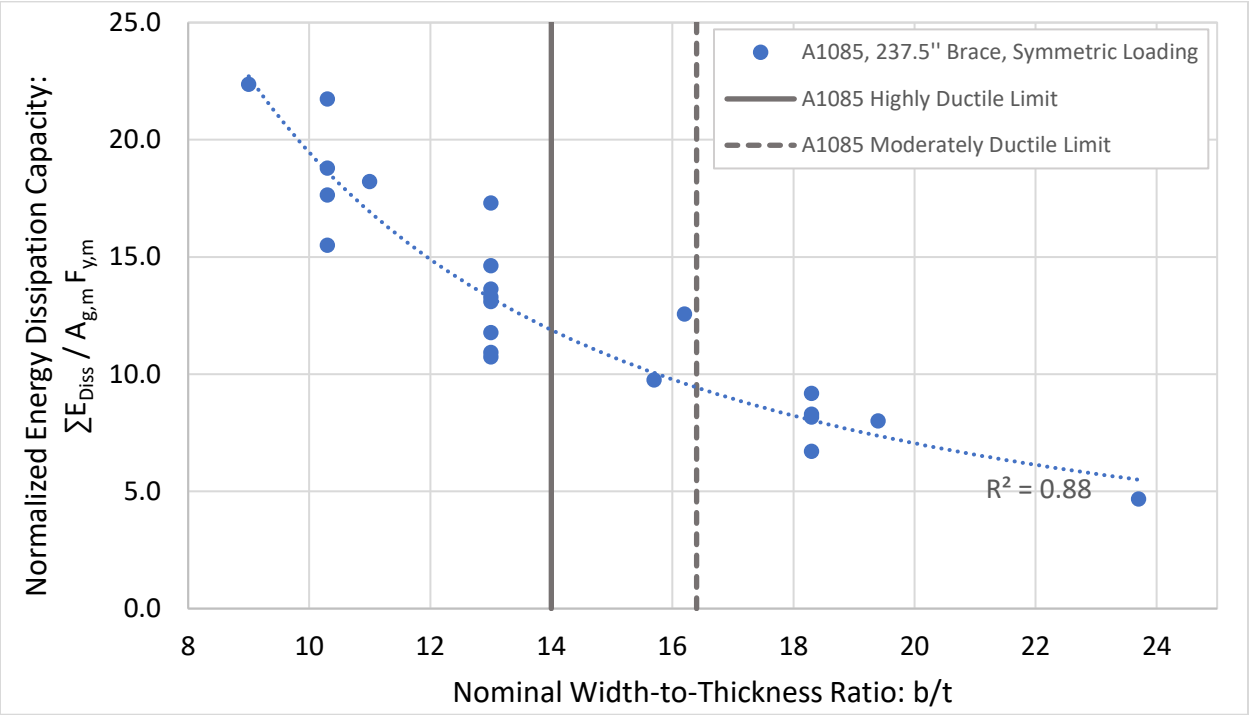

Figure 5.21 Normalized Energy Dissipation vs. Local Compactness

5.3.6 *Slenderness Ratio, KL/r*

This section investigates the effect of global slenderness on the ductility and structural performance of A1085 HSS braces subjected to cyclic loading. The structural response parameters studied will include quantitative measures such as axial deformation range, story drift range, maximum story drift, accumulated axial deformation, and energy dissipation capacity. The plots in this section include data from all of the A1085 HSS test specimens subjected to the symmetric displacement protocol. This includes the specimens at both lengths, 237.5” and 183.5”. Previous research has shown that the global slenderness ratio, *KL/r*, is a primary parameter effecting brace ductility, and this trend will be investigated in this section.

Figure 5.22 shows the relationship between brace axial deformation range and global slenderness ratio, *KL/r*. The dataset provided a wide range of *KL/r* ratios ranging from about 60 to 127. The plot shows a clear relationship between increased global slenderness and increased deformation range. The power regression curve accounts for a significant amount of the variation with an R^2 of 0.77, however, much of the other variation is due to other factors such as local compactness. HSS shapes of the same width have relatively the same global slenderness ratio but can have very different local compactness ratios depending on the wall thickness. It was shown in Section 5.3.3 that the local compactness has a significant effect on brace deformability which is the reason for most of the unaccounted for variability in Figure 5.22. For example, the 7x7x5/16 and 7x7x1/2 have very similar *KL/r* values of 88 and 91, respectively, however, the 7x7x1/2 had an 83% greater axial deformation range largely due to being more locally compact.

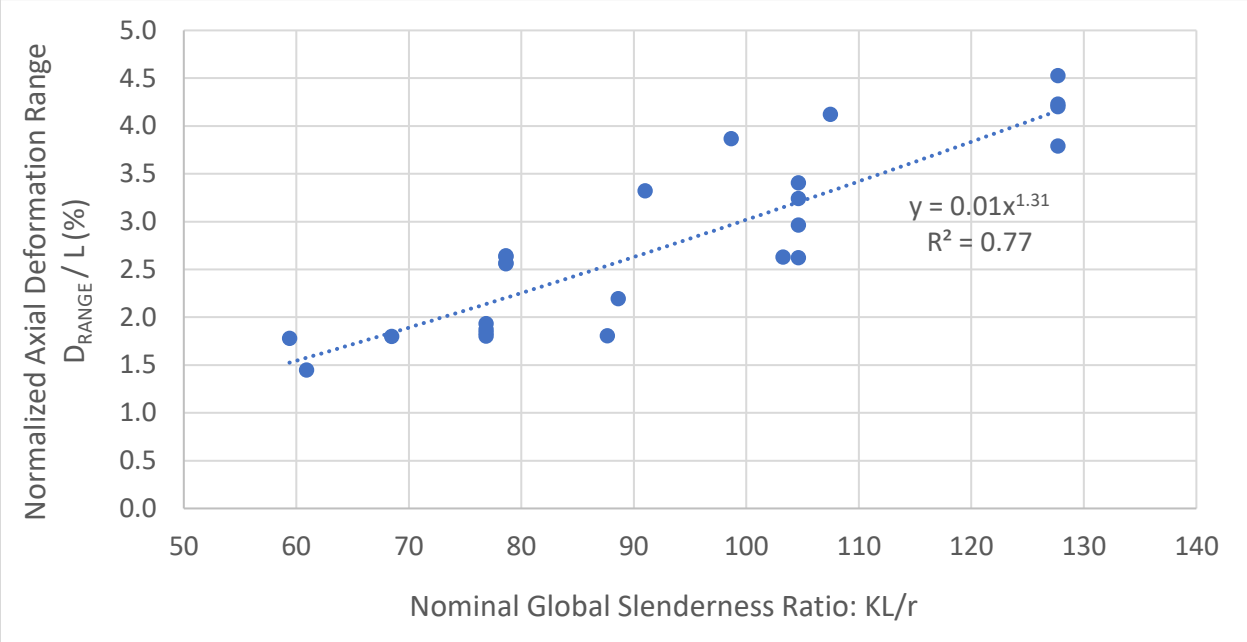

Figure 5.22 Axial Deformation Range vs. Global Slenderness

In Figure 5.23, the story drift range is plotted versus the nominal width-to-thickness ratio. The story drift ranges in this figure were approximated using the methodology described in Chapter 4 which assumes a 45˚ brace configuration. The same trends shown in Figure 5.22 are seen here. The figure shows that all of the specimens with a global slenderness ratio above 90, achieved a story drift range of at least 5%.

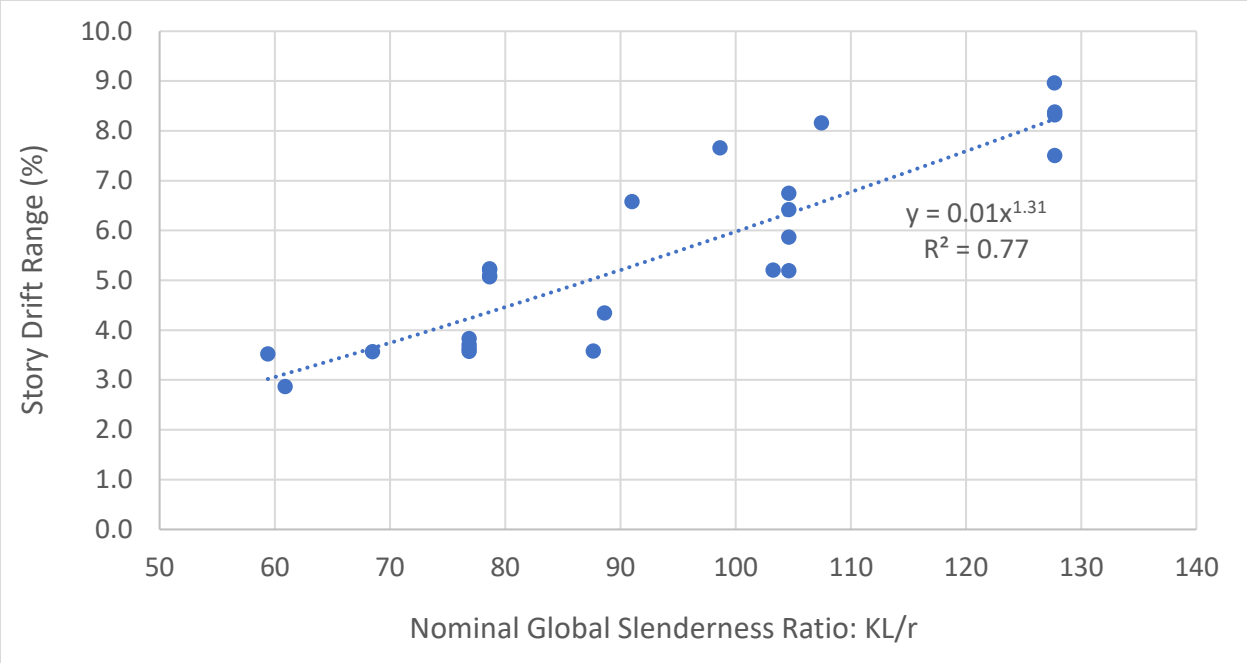

Figure 5.23 Story Drift Range vs. Global Slenderness

The maximum story drift is plotted against the global slenderness ratio in Figure 5.24. The maximum story drift is strongly dependent on the applied displacement protocol. All of the specimens in this plot were subjected to the same symmetric displacement protocol, making it possible to compare the maximum story drifts. Due to the symmetry of the loading protocol, the maximum story drift is generally about half of the story drift range shown in Figure 5.23, however the maximum story drift is not always exactly half of the range due to the effects of bolt slip or fracture at the first peak tension displacement cycle. The figure displays the same trend as the figures above, however the regression curve shows a an R^2 value of 0.77 which is the same as the curve for story drift range. In this figure, all of the specimens with a global slenderness ratio above 90, achieved a maximum story drift of at least 2.5%.

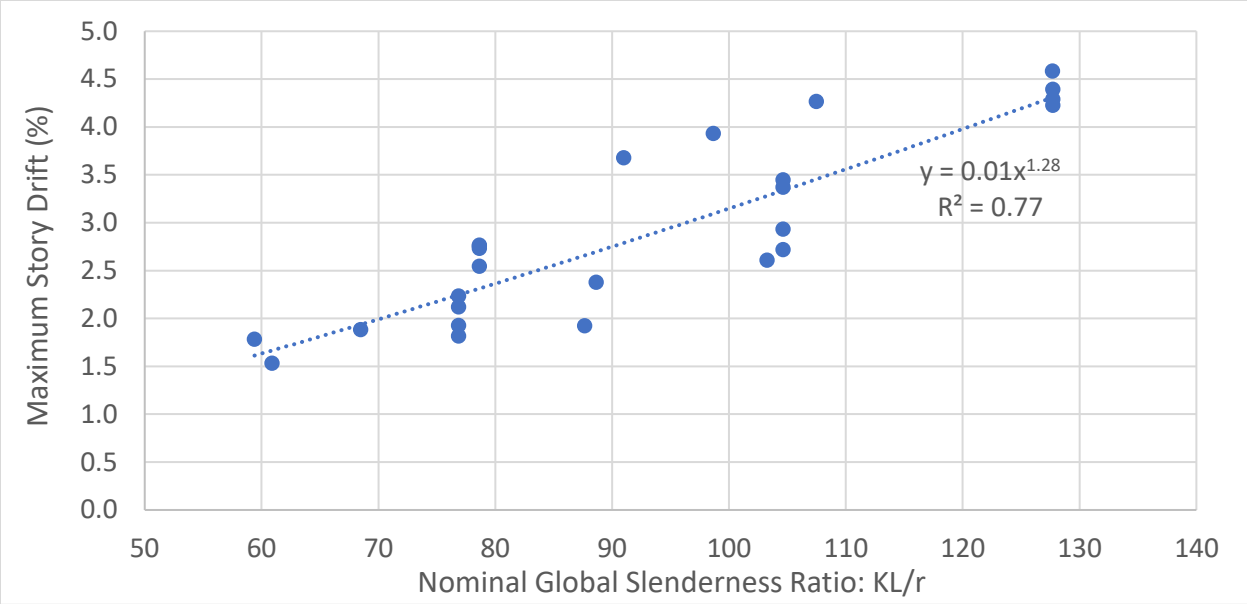

Figure 5.24 Maximum Story Drift Range vs. Global Slenderness

As described earlier, the fracture life of HSS braces is highly dependent on the formation local cupping deformation. Figure 5.25 shows the axial brace deformation at the initiation of local cupping plotted against the global slenderness ratio, *KL/r*. It is evident that development of local cupping occurs earlier for more stocky braces (lower *KL/r*). Stocky braces with lower slenderness ratios typically buckle inelastically at lower compressive displacements, therefore exhibiting less ductility than those with larger slenderness ratios.

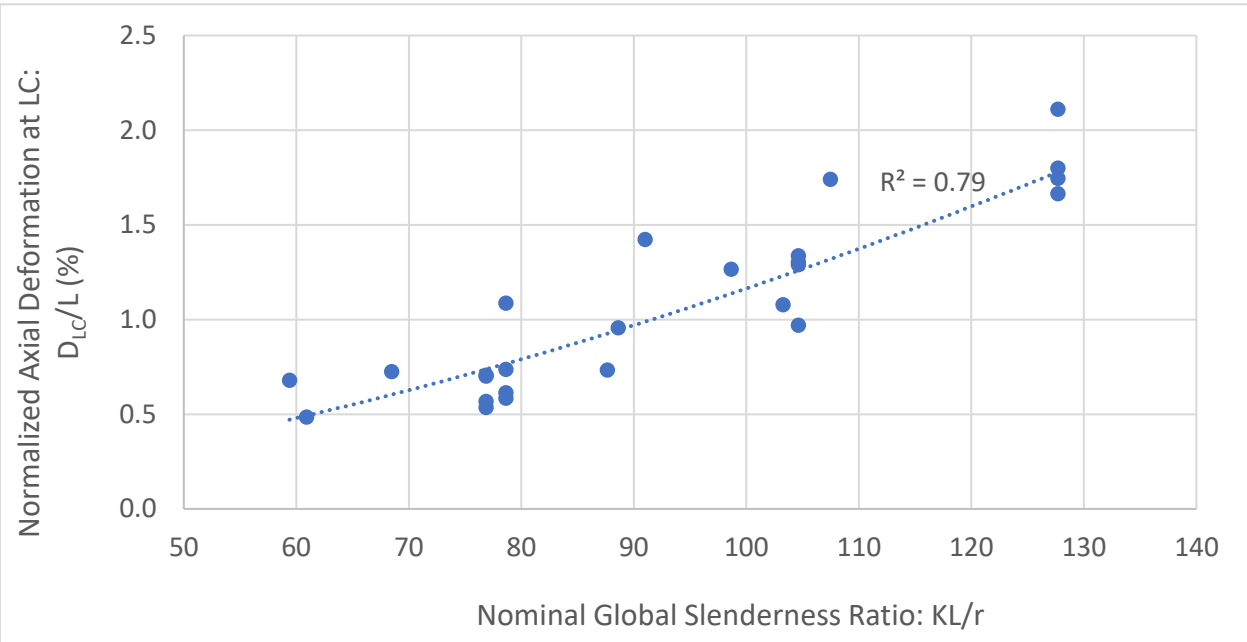

Figure 5.25 Axial Deformation at Local Cupping vs. Global Slenderness

The effect of the nominal global slenderness ratio on accumulated axial deformation is shown in Figure 5.20. As described in the previous section, accumulated axial deformation accounts for whether the specimen fractured at the first or second cycle. The accumulated axial deformation is highly dependent on the displacement protocol. All of the specimens in this figure were subjected to the same displacement protocol which makes it possible to make comparisons. Additionally, the accumulated axial deformation is normalized by the brace length so that brace specimens of both lengths, 237.5" and 183.5", can be compared. Similar to the effect of global slenderness on axial deformation range, an increase in slenderness is associated with an increase in accumulated axial deformation. The power regression curve in this plot has an R^2 value of 0.81 which is higher than that in plot for axial deformation range versus global slenderness which had an R^2 value of 0.77.

In Figure 5.27, normalized energy dissipation capacity is plotted versus the nominal global slenderness ratio, *KL/r*. Consistent with the effect of *KL/r* on deformation range, this plot shows a positive relationship between global slenderness and energy dissipation capacity. Although increases in *KL/r* causes a decrease in compressive force capacity, it causes an increase in deformability. Evidently, the brace energy dissipation capacity is more dependent on deformation capacity than force capacity.

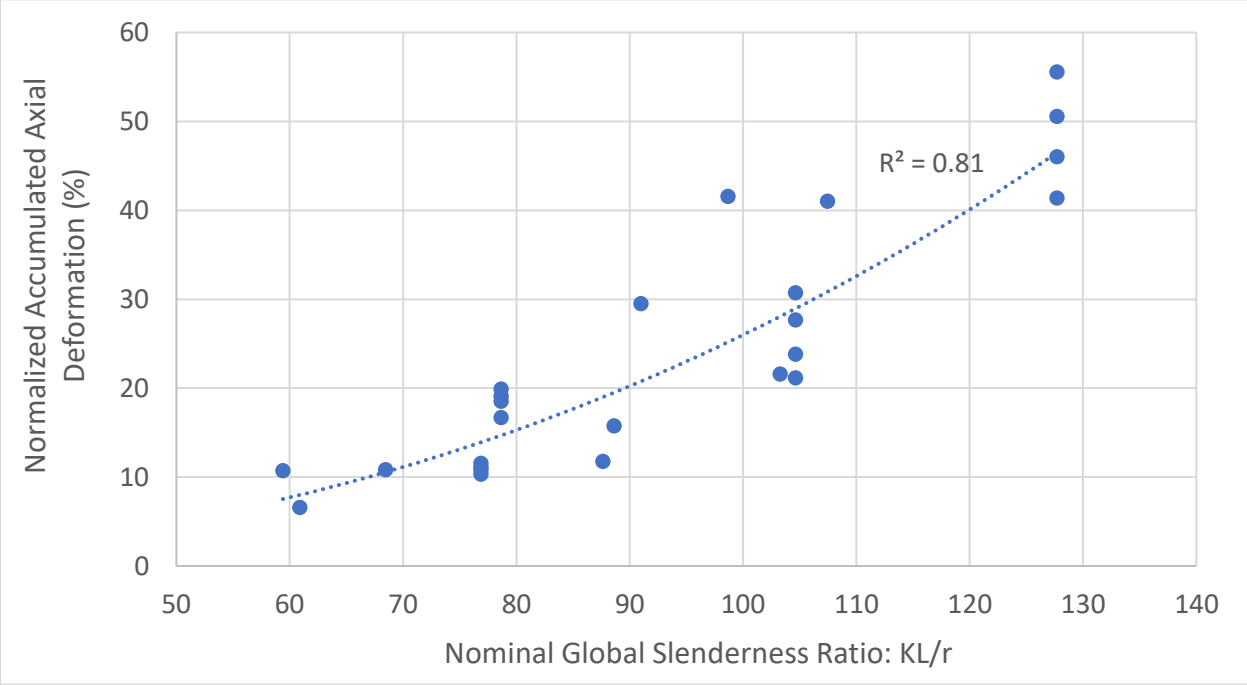

Figure 5.26 Accumulated Axial Deformation Range vs. Global Slenderness

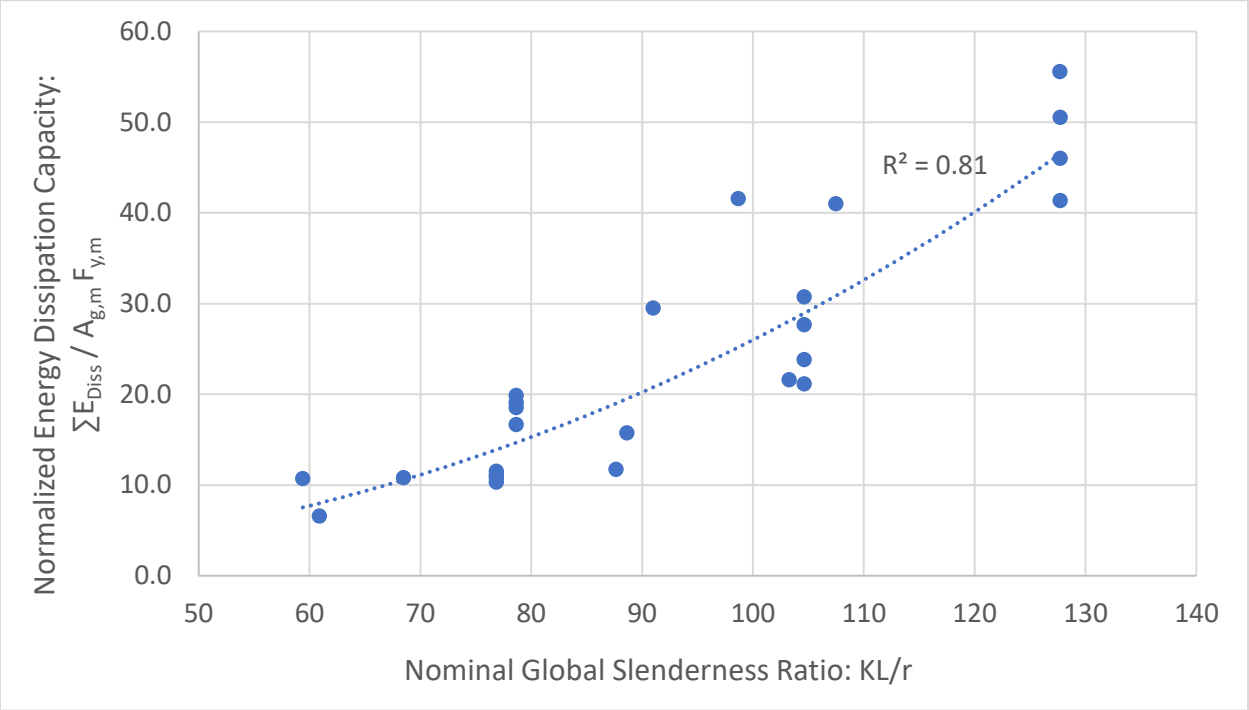

Figure 5.27 Normalized Energy Dissipation vs. Global Slenderness

5.3.7 *Relationship between b/t and KL/r*

As shown in the previous sections, the deformability of HSS bracing members is highly dependent on both the local compactness ratio, *b/t*, and the global slenderness ratio, *KL/r*. The effects of these ratios are, however, not independent of one another, and the relationship between these parameters will be investigated in this section. Currently, the AISC design provisions provide limits on local compactness however there is no minimum requirement for global slenderness. Although, the AISC provisions do not currently include a minimum *KL/r* requirement, the idea of introducing one will be explored here.

This section will provide a series of figures that plot the global slenderness ratio, *KL/r*, versus the local compactness ratio, *b/t*. These figures include all of A1085 HSS specimens from the yellow producer subjected to the symmetric loading protocol. The plotted points are labeled with various measures of brace deformability. In Figure 5.28, the normalized brace axial deformation range is labeled. In Figure 5.29, the approximated story drift range is labeled. In Figure 5.30, the maximum story drift range is labeled.

Consistent with prior research, the figures show that deformability increases as the width-to-thickness ratio decreases and as the global slenderness ratio increases. The circled specimens in the figures show groups indicating the effect of global slenderness. In each group the specimens have the same or nearly the same compactness ratio, but they show increased deformability with increased *KL/r*. In the left circle, as *KL/r* increases, the deformability increases much more than when *KL/r* is increased in the right circle. This indicates that the effect of *KL/r* is more significant at lower *b/t* ratios.

In the right circle, the three specimens have the same or nearly the same *b/t* ratio. Although they all classify as moderately ductile bracing members, they exhibited different levels of deformability. The brace at a *KL/r* ratio of 70 provided a story drift range of 3.57%, while the brace at a *KL/r* ratio of 103 provided a story drift range of 5.21%.

A story drift of 2.5% is often considered the demand for SCBFs. All of the specimens that meet the AISC highly ductile compactness requirement achieved a maximum story drift of at least 2.5%. Additionally, one specimen that meets the AISC moderately ductile limit requirement achieved a maximum story drift greater than 2.5%. This moderately ductile member had a global slenderness ratio of 103.26 – the highest of all the moderately ductile members. This indicates that an additional provision could be made to allow the use of moderately ductile members in SCBFs if they have a global slenderness ratio above a minimum limit. This figure indicates that minimum limit could be 100. The introduction of a minimum global slenderness would recognize the importance of global slenderness on the ductility of HSS braces and would allow the use of more HSS shapes in SCBFs.

Further investigation into design implications is provided in Chapter 6.

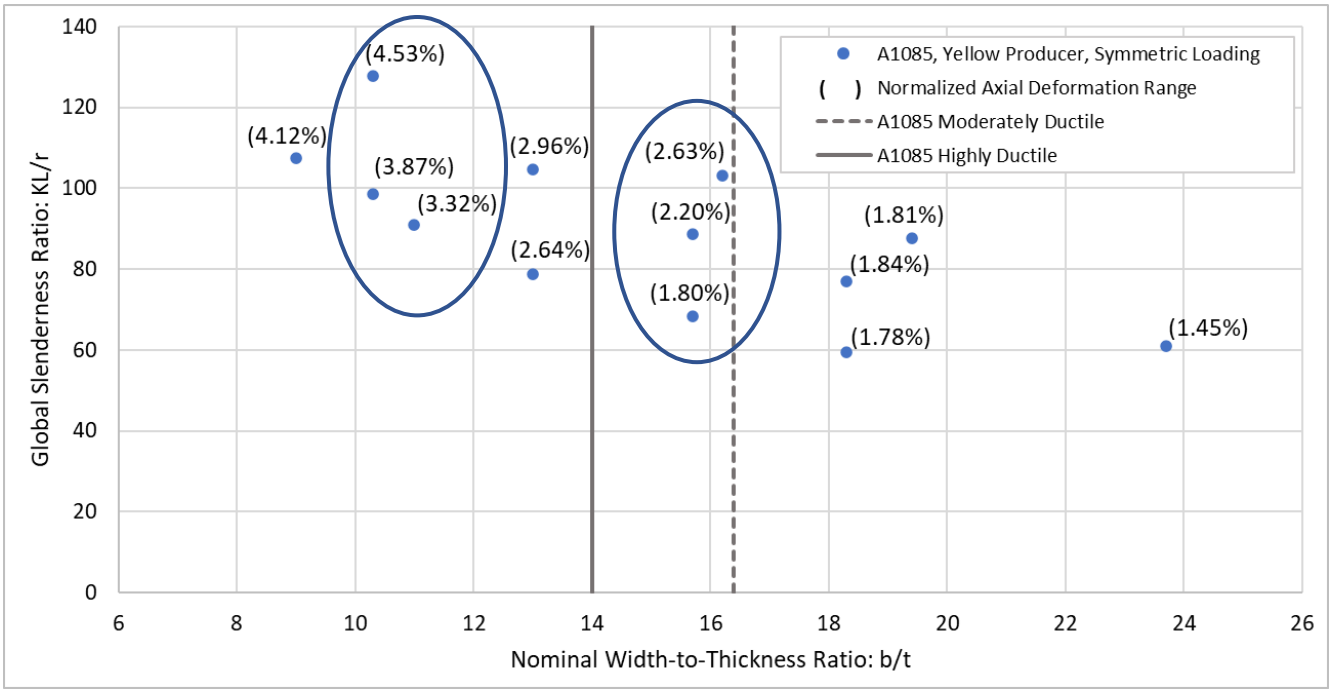

Figure 5.28 Global Slenderness vs. Local Compactness vs. Axial Deformation Range

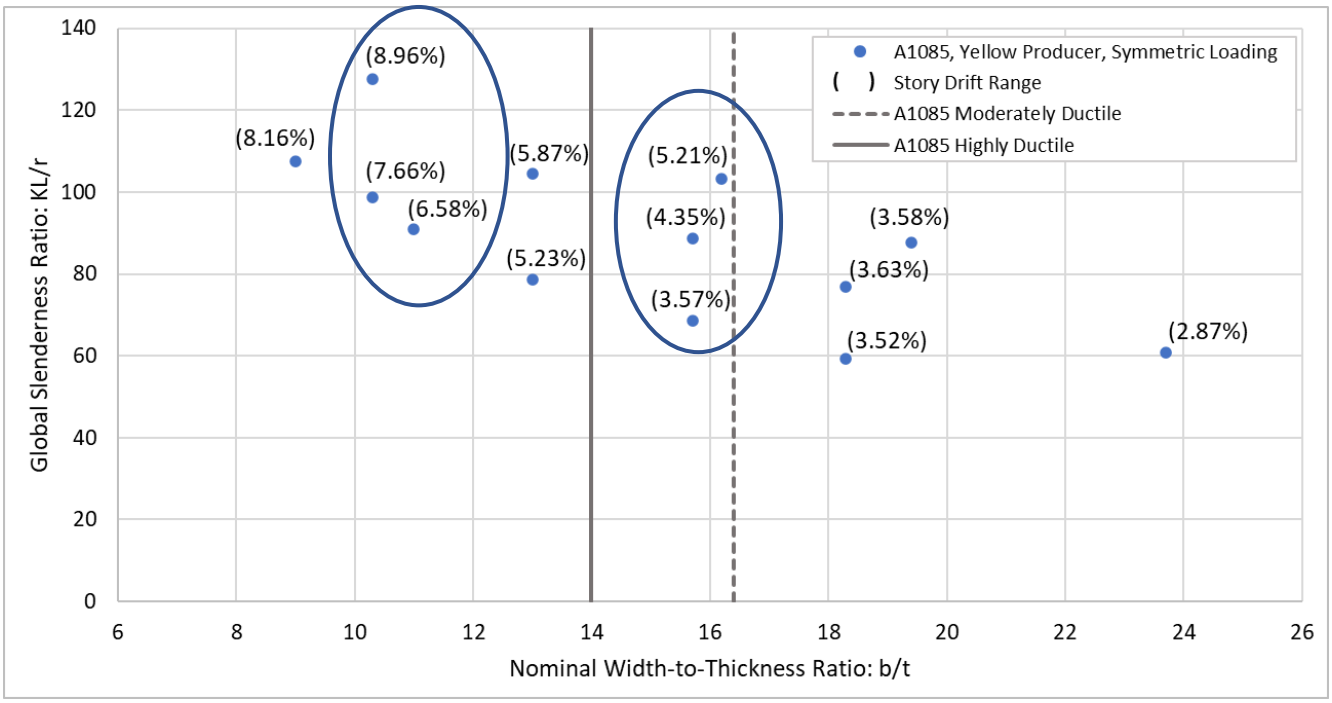

Figure 5.29 Global Slenderness vs. Local Compactness vs. Story Drift Range

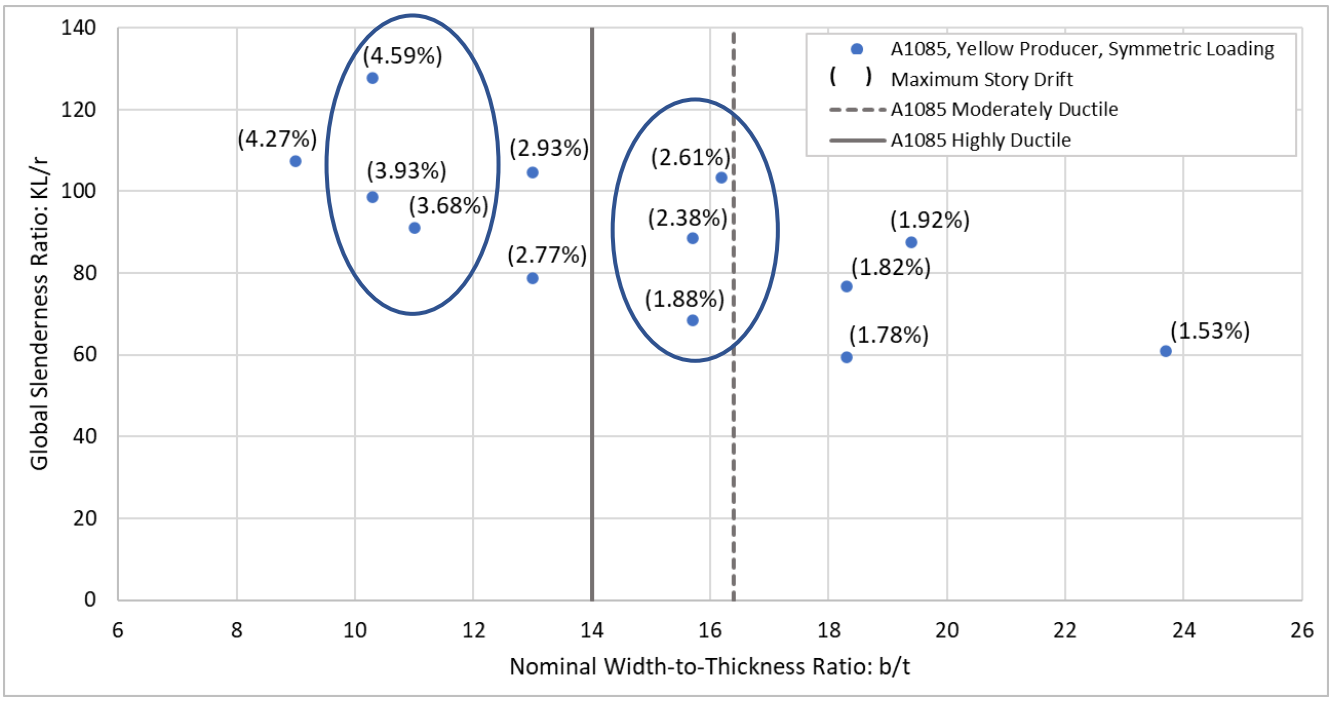

Figure 5.30 Global Slenderness vs. Local Compactness vs. Maximum Story Drift

5.4 SUMMARY OF FINDINGS

This chapter investigated the effect of various parameters on the cyclic performance of HSS braces. The conclusions drawn from this investigation are summarized below:

- Analysis of the results in this experimental study indicates that ductility and energy dissipation capacity of HSS bracing members are most significantly impacted by the local compactness and global slenderness ratios. Deformability and energy dissipation was shown to increase with decreased local compactness ratios and increased global slenderness ratios. This is consistent with previous research.

- Overall, there was minor variability between the producers of A1085 HSS, however, there was no clear trend between HSS producer and brace performance. The test specimens from the Blue producer, most notably the 5x5x3/8 and 6x6x3/8, did not perform as well as the other producers. This may have been a result of differences in material properties. As seen in the results from tension testing, the Blue producer had the highest yield strength for each of the four HSS sizes tested in the producer comparison test series.

- In the study of various applied displacement protocols, it was evident that the maximum tensile and compressive deformations were highly dependent on displacement history, however, the deformation range was not significantly impacted by displacement history. Therefore, to characterize the seismic response of OCBFs and SCBFs, story drift range should be used, rather than the maximum drift in a single direction.

- Results from material testing showed little correlation with structural response and brace deformability. For more locally compact sections, high yield strength may cause decreased deformability but there is no relationship between deformability and CVN toughness or F_u/F_y.

- Although there is not currently a design provision that recognizes the effect of global slenderness on the deformability of HSS braces, introducing minimum global slenderness ratio requirements could ensure sufficient ductility of SCBFs. Additionally, it could allow for the use of more HSS shapes in SCBFs. There is a relationship between global slenderness, local compactness, and deformability and it should be recognized by the design provisions.

- As concluded by Bergendahl, there were no significant differences between the performance of A500 and A1085 as they both exhibited similar responses. This may be due to the similarities between the geometric and material properties of A500 and A1085 specimens (Bergendahl, 2021). No new data for A500 HSS braces was presented in this paper to draw further conclusions.

Chapter 6. EVALUATION OF DESIGN PROVISIONS AND PERFORMANCE-BASED ENGINEERING TOOLS

6.1 INTRODUCTION

Today, the design criteria for CBFs are provided by AISC 341-16, *Seismic Provisions for Structural Steel Buildings* (AISC, 2016). Additionally, AISC 342, which is under development at the time of this writing, provides guidelines for seismic evaluation and retrofit of steel buildings (AISC, Draft 2021). The AISC 342 standard is intended to effectively replace the previous provisions provided by Chapter 9 of ASCE/SEI 41 (ASCE, 2017) that dealt with force and deformation capacities of steel structural systems and components. The treatment of braces in AISC 341 and 342 are evaluated in this chapter through comparisons with experimental data from this research program. Section 6.2 compares experimental results with the brace requirements in the AISC 341-16 seismic provisions. Section 6.3 compares the nonlinear modeling methods for braces provided by AISC 342 with the experimental results. Throughout this chapter, the experimental data is from all four phases of testing, a total of 41 individual brace tests.

6.2 EVALUATION OF THE REQUIREMENTS FOR BRACES AISC 341-16 SEISMIC PROVISIONS

Deformation demands for CBFs are often stated in terms of story drift. For SCBFs, this story drift demand is often considered to be 2.5% in one direction (which is the allowable story drift limit in ASCE 7-16 for risk category II structures). Analysis of the experimental data in Chapter 5 showed that story drift range is much a stronger indicator of the deformation capacity of an HSS brace and therefore story drift range is a better demand parameter. This means that rather than targeting a 2.5% story drift in one direction, targeting a story drift range of 5% would better ensure sufficient ductility in an SCBF. There is no specific target for OCBFs but it must be much less than that for SCBFs and a 3% drift range may be considered a sufficient threshold for a moderately ductile system.

Consistent with previous research, the analysis provided in Chapter 5 showed that the primary parameters affecting the deformability of HSS braces are the local slenderness ratio, *b/t*, and the global slenderness ratio, *KL/r*. The current AISC 341-16 seismic provisions specify requirements for maximum local slenderness and global slenderness ratios. It is interesting to note that AISC does not enforce a lower limit on global slenderness because stocky braces with lower global slenderness ratios typically buckle inelastically at lower compressive displacements and exhibit less overall ductility than those with larger slenderness ratios. Braces with higher *KL/r* ratios have lower strains in outer fibers of the cross section during buckling and have a larger inelastic deformation capacity under cyclic loads, albeit at a smaller compressive capacity.

In the following figures, the current width-to-thickness limits can be evaluated based on the story drift limits for SCBFs and OCBFs of 5% and 3%, respectively. Additionally, the effect of global slenderness on brace deformability is shown which leads to a discussion about potential minimum *KL/r* requirements.

Figure 6.1 shows the relationship between local compactness and story drift range. Here, the story drift was calculated following the methodology presented in Chapter 4 which assumes a 45 degree brace configuration. In this plot, it is evident that a decrease in the local compactness ratio is associated with an increase in story drift range. The strong correlation in this figure reinforces the use of compactness limits for ensuring ductility in CBFs. All of the specimens meeting the highly ductile limit achieved a story drift range of above 5% indicating that the current highly ductile limit is sufficient. Additionally, all of the specimens that classify as moderately ductile achieved a story drift range of at least 4%. While exceptional, if the demand for OCBFs is 3% or even 3.5%, the figure shows that many more HSS sections have sufficient ductility and would meet the moderately ductile limit for OCBF braces if that limit was increased to $0.90\sqrt{\frac{E}{R_y F_y}}$.

Figure 6.2 shows the relationship between the global slenderness ratio and the story drift range. This figure includes all of the test specimens subjected to a symmetric loading protocol, including A500 and A1085 HSS, and brace lengths of 237.5” and 183.5”. The figure shows a clear relationship between increased global slenderness and increased deformation range which is currently neglected in the AISC Seismic Provisions.

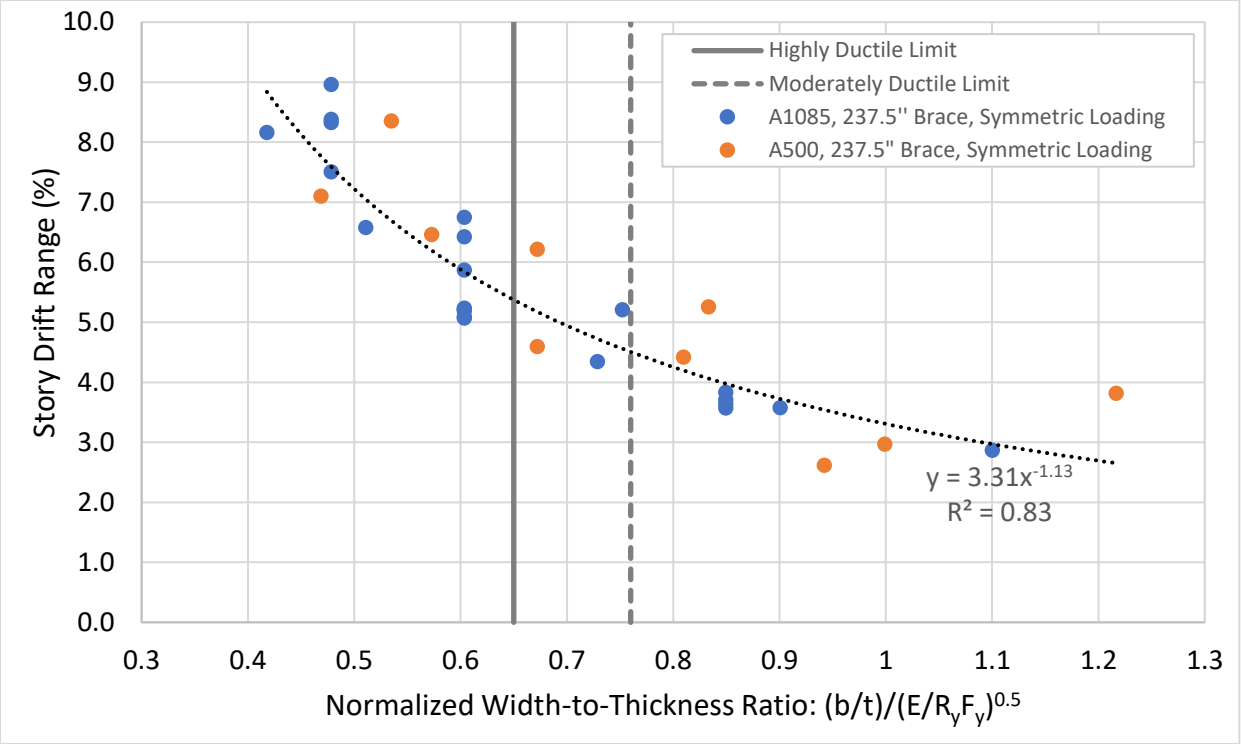

Figure 6.1 Story Drift Range vs. Normalized Width-to-Thickness Ratio

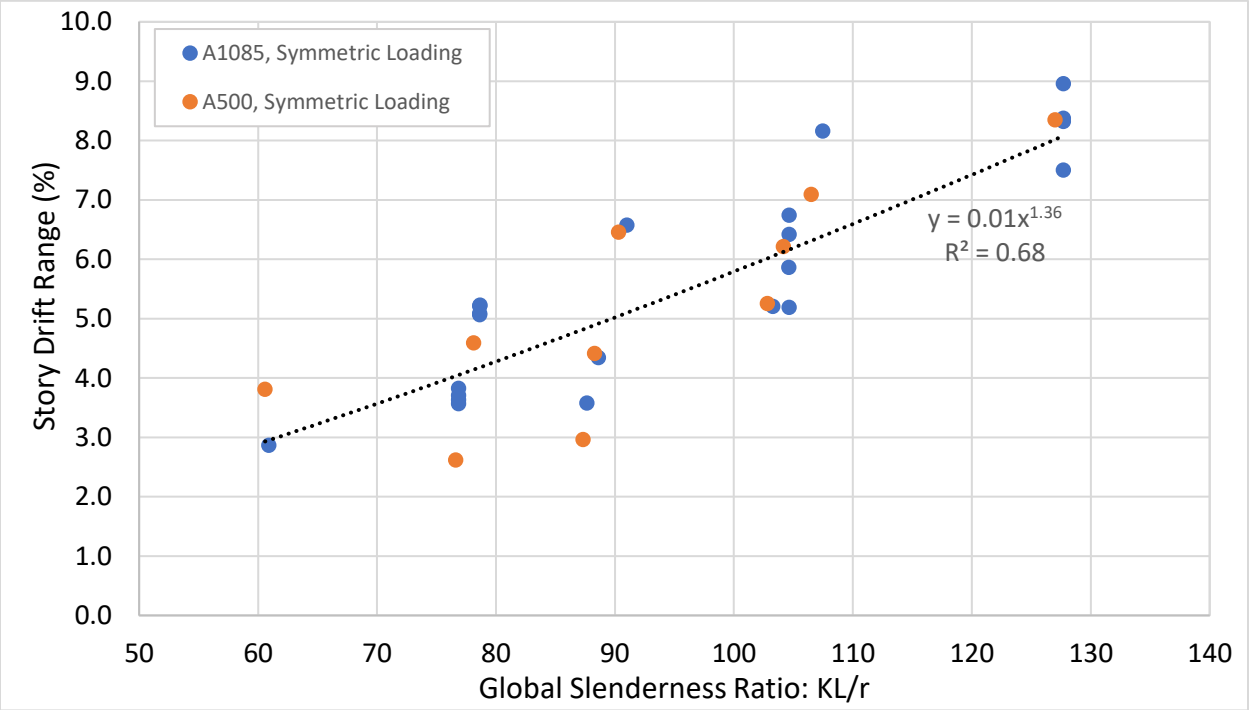

Figure 6.2 Story Drift Range vs. Global Slenderness

As shown above, the deformability of HSS bracing members is highly dependent on both the local compactness ratio, *b/t*, and the global slenderness ratio, *KL/r*. The effects of these ratios are, however, not independent of one another, and the relationship between these parameters will be investigated in this section next. Currently, the AISC design provisions provide limits on local compactness however there is no minimum requirement for global slenderness. Although, the AISC provisions do not currently include a minimum *KL/r* requirement, the idea of introducing one will be explored here.

In Figure 6.3 and Figure 6.4, the global slenderness ratio is plotted against the local compactness ratio. Figure 6.3 includes the 13 A1085 HSS specimens from the yellow producer subjected to the symmetric loading protocol. Figure 6.4 includes the ten A500 specimens subjected to the symmetric loading protocol. In these figures, the markers are labeled with their achieved story drift range.

Consistent with prior research, the figures show that deformability increases as the width-to-thickness ratio decreases and as the global slenderness ratio increases. The circled specimens in Figure 6.3 show groups that emphasize the effect of global slenderness. In each group the specimens have the same or nearly the same compactness ratio, but they show increased deformability with increased *KL/r*. In the left circle, as *KL/r* increases, the deformability increases much more than when *KL/r* is increased in the right circle. This indicates that the effect of *KL/r* is more significant at lower *b/t* ratios.

All of the A500 and A1085 specimens that meet the AISC highly ductile compactness requirement achieved a story drift range of at least 5%. Additionally, three specimens that do not meet the highly ductile requirement but have *KL/r* ratios greater than 100 achieved story drift ranges greater than 5%. This indicates that an additional provision could be made to allow the use of moderately ductile members in SCBFs if they have a global slenderness ratio above a minimum limit. This figure indicates that minimum limit could be 100. The introduction of a minimum global slenderness would recognize the importance of global slenderness on the ductility of HSS braces and would allow the use of more HSS shapes in SCBFs.

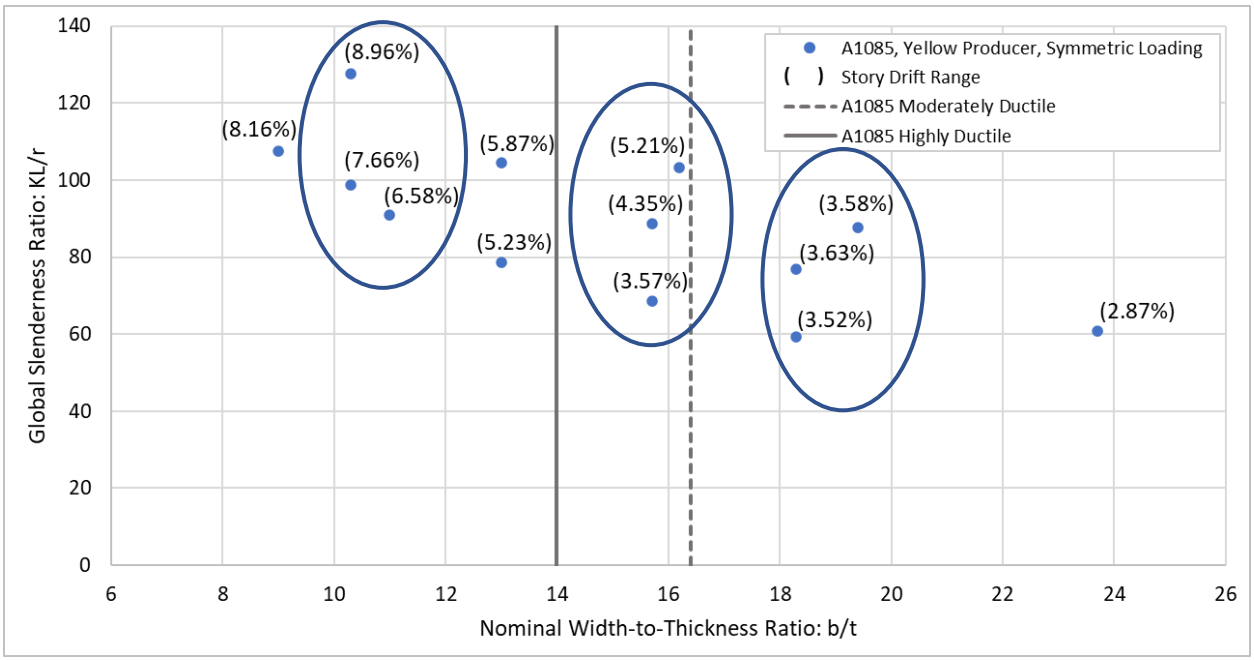

Figure 6.3 Global Slenderness vs. Local Compactness with Story Drift Range Indicated: A1085 Specimens

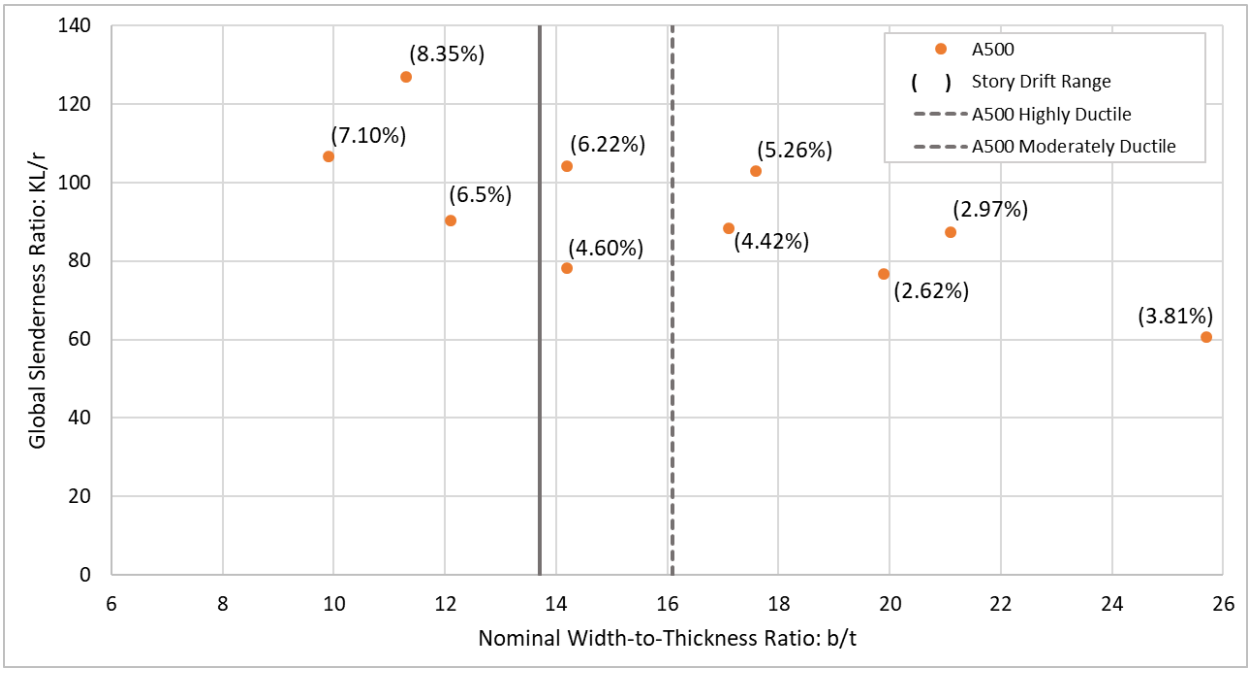

Figure 6.4 Global Slenderness vs. Local Compactness with Story Drift Range Indicated: A500 Specimens

6.3 EVALUATION OF AISC 342 NONLINEAR MODELS FOR BRACES

This section presents an evaluation of performance-based engineering tools used to model the nonlinear behavior of steel braced frames with rectangular HSS braces. AISC 342, which is under development at the time of this writing, provides guidelines for seismic evaluation and retrofit of steel buildings (AISC, Draft 2022). The AISC 342 standard is intended to effectively replace the previous provisions provided by Chapter 9 of ASCE/SEI 41 (ASCE, 2017). The nonlinear modeling procedure for rectangular HSS braces presented in Section C3 of AISC 342 will be evaluated in this chapter through comparisons with the experimental results from this research project. AISC 342 provides the methodology to construct generalized force-deformation curves (backbone curves) based on the geometric and material properties of a brace. Separate backbone curves are computed for the tensile and compressive force-deformation behaviors. Figure 6.5 below shows the generalized force-deformation response for a steel brace, representing the predicted nonlinear response. The modeling parameters used to construct the generalized backbone curve will be compared to the experimental results to evaluate the accuracy of the AISC 342 modeling methods.

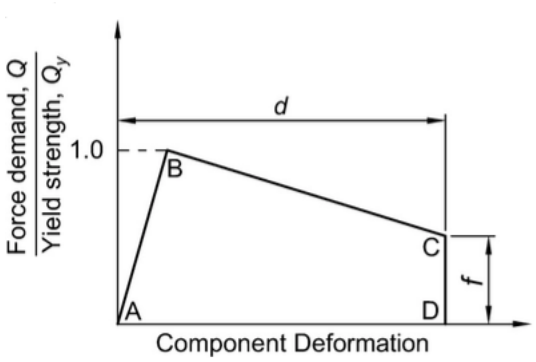

Figure 6.5 Generalized Brace Force-Deformation Response (AISC, Draft 2021)

6.3.1 *Nonlinear Modeling of Bracing Members*

The modeling parameters used for developing the backbone curves are presented in Table 6.1. This table includes the modeling parameters for each of the HSS brace specimens tested in this research project. The modeling parameters were calculated following the procedure provided in Section C3 of AISC 342. The methodology and equations will be presented here, however, a

full example calculation can be found in Appendix B. The modeling parameters were calculated following the equations below, which are provided in Table C3.4 of AISC 342. These equations are used to calculate the predicted axial deformation capacity, *d*, and the strength ratio at the maximum deformation, *f*, which models the predicted strength degradation due to nonlinear deformation demands. For rectangular HSS braces, the strength ratio, *f*, is taken as 1.0 for tension and 0.2 for compression. The much lower value for compression is representative of the post-buckling strength degradation. The n-factors, calculated as shown below, are used to predict the maximum brace deformation in tension and compression. The n-factor is dependent on the tabulated local compactness ratio (λ), AISC 341-16 highly ductile local slenderness ratio (λ_{hd}), global slenderness ratio (L_c/r), and expected yield strength (F_{ye}), all of which have been proven to affect the ductility of HSS braces. Per AISC 342, F_{ye} shall be taken as the measured yield stress ($F_{y,m}$) when established by testing. Tensile tests were performed for each brace specimen so the measured yield stress is used here. Additionally, R_yF_y in the limiting local slenderness ratio, λ_{hd}, is replaced by F_{ye}.

For tension of a rectangular HSS brace:

$$n = 4.7\left(\frac{\lambda}{\lambda_{hd}}\right)^{-1.0}\left(\frac{\left(\frac{L_c}{r}\right)}{\sqrt{\frac{E}{F_{ye}}}}\right)^{0.24} \tag{6.1}$$

For compression of a rectangular HSS brace:

$$n = 3.0\left(\frac{\lambda}{\lambda_{hd}}\right)^{-1.0}\left(\frac{\left(\frac{L_c}{r}\right)}{\sqrt{\frac{E}{F_{ye}}}}\right)^{1.0} \tag{6.2}$$

The predicted maximum tensile and compressive deformations, *d*, are calculated by multiplying the n-factor by the yield deformation and buckling deformation, respectively.

For tension of a rectangular HSS brace:

$$\Delta_T = \frac{(P_{ye} \cdot L_c)}{A_g \cdot E} \quad (6.3)$$

$$d = n \cdot \Delta_T \quad (6.4)$$

For compression of a rectangular HSS brace:

$$\Delta_C = \frac{(P_{ce} \cdot L_c)}{A_g \cdot E} \quad (6.5)$$

$$d = n \cdot \Delta_C \quad (6.6)$$

The modeling parameters for the predicted tensile and compressive behavior of each of the HSS test specimens are provided in Table 6.1 below. Test specimens subjected to a non-symmetric loading protocol are shown in grey. This is consistent throughout this chapter. In this table, the total axial deformation, *d*, is provided for both tension and compression. The residual strength, *f* *P, shown in the table was calculated as the strength ratio, *f*, multiplied by the expected tensile yield strength and the expected compressive buckling load.

Table 6.1 Test Specimen Modeling Parameters

			n-factor		***d* (in.)**		***f* * P (k)**	
Test Specimen	**Δ_T (in.)**	**Δ_C (in.)**	**Tens.**	**Comp.**	**Tens.**	**Comp.**	**Tens.**	**Comp.**
5x5x3/8 A500 Y	0.54	0.13	8.76	21.92	4.69	2.79	417	20
6x6x5/16 A500 R	0.47	0.19	5.62	11.39	2.64	2.21	387	32
6x6x3/8 A500 R	0.50	0.19	6.82	14.31	3.42	2.71	488	37
6x6x1/2 A500 R	0.51	0.18	9.73	20.98	5.01	3.80	630	44
7x7x5/16 A500 Y	0.51	0.26	4.36	8.07	2.24	2.06	474	47
7x7x3/8 A500 Y	0.50	0.25	5.44	10.07	2.73	2.51	539	54
7x7x1/2 A500 B	0.47	0.24	7.90	14.55	3.74	3.46	669	67
8x8x3/8 A500 W	0.54	0.31	4.39	7.51	2.38	2.31	690	78
8x8x1/2 A500 W	0.54	0.30	6.20	10.73	3.33	3.21	876	98
10x10x3/8 A500 W	0.48	0.35	3.35	4.60	1.62	1.62	775	113
5x5x3/8 A1085 Y	0.54	0.13	9.59	24.18	5.19	3.05	436	20
6x6x5/16 A1085 Y	0.51	0.19	5.93	12.43	3.02	2.40	426	32

			n-factor		*d* (in.)		*f* * P (k)	
Test Specimen	**Δ_T (in.)**	**Δ_C (in.)**	**Tens.**	**Comp.**	**Tens.**	**Comp.**	**Tens.**	**Comp.**
6x6x3/8 A1085 Y	0.55	0.19	7.21	15.69	3.95	2.95	540	37
6x6x1/2 A1085 Y	0.56	0.18	10.42	23.29	5.79	4.14	683	44
7x7x5/16 A1085 Y	0.47	0.25	4.90	8.81	2.31	2.18	457	48
7x7x3/8 A1085 Y	0.51	0.25	5.91	11.00	2.99	2.74	577	57
7x7x1/2 A1085 Y	0.53	0.24	8.36	16.13	4.41	3.90	773	71
8x8x3/8 A1085 Y	0.49	0.29	4.94	8.19	2.44	2.40	661	78
8x8x1/2 A1085 Y	0.53	0.29	6.83	11.80	3.60	3.48	905	101
10x10x3/8 A1085 Y	0.48	0.35	3.66	5.01	1.75	1.74	803	117
5x5x3/8 A1085 R	0.56	0.13	9.44	24.18	5.32	3.05	453	20
5x5x3/8 A1085 W	0.57	0.13	9.40	24.18	5.36	3.05	456	20
5x5x3/8 A1085 B	0.64	0.13	9.00	24.18	5.76	3.05	522	21
6x6x3/8 A1085 R	0.49	0.19	7.49	15.69	3.71	2.95	483	37
6x6x3/8 A1085 W	0.55	0.19	7.18	15.69	3.98	2.95	548	37
6x6x3/8 A1085 B	0.57	0.19	7.12	15.69	4.03	2.95	565	38
8x8x3/8 A1085 R	0.50	0.30	4.92	8.19	2.47	2.42	667	79
8x8x3/8 A1085 W	0.52	0.30	4.86	8.19	2.51	2.46	699	81
8x8x3/8 A1085 B	0.56	0.31	4.72	8.19	2.64	2.54	757	84
8x8x1/2 A1085 R	0.48	0.28	7.08	11.80	3.39	3.33	784	92
8x8x1/2 A1085 W	0.54	0.30	6.76	11.80	3.66	3.51	951	105
8x8x1/2 A1085 B	0.54	0.30	6.75	11.80	3.67	3.52	957	105
5x5x3/8 A1085 Y [S]	0.42	0.16	9.01	18.68	3.77	3.05	436	34
7x7x3/8 A1085 Y [S]	0.39	0.26	5.55	8.50	2.17	2.18	577	76
8x8x3/8 A1085 Y [S]	0.38	0.28	4.65	6.33	1.78	1.77	661	97
5x5x3/8 A1085 Y [C]	0.54	0.13	9.59	24.18	5.19	3.05	436	20
7x7x3/8 A1085 Y [C]	0.51	0.25	5.91	11.00	2.99	2.74	577	57
8x8x3/8 A1085 Y [C]	0.49	0.29	4.94	8.19	2.44	2.40	661	78
5x5x3/8 A1085 Y [NF]	0.54	0.13	9.59	24.18	5.19	3.05	436	20
7x7x3/8 A1085 Y [NF]	0.51	0.25	5.91	11.00	2.99	2.74	577	57
8x8x3/8 A1085 Y [NF]	0.49	0.29	4.94	8.19	2.44	2.40	661	78

Note: Data shown above the line is from Bergendahl (Bergendahl, 2021)

[C] Chevron Compression Dominant Loading Protocol

[NF] Near Fault Tension Dominant Loading Protocol

[S] Short Brace Test

6.3.2 *Evaluation of Predicted Brace Performance*

This section will provide comparisons between the predicted nonlinear behavior and the measured behavior from the experiments in the four phases of testing in order to evaluate the accuracy of the nonlinear modeling methods provided in Section C3 of AISC 342 for the tested specimens. Notably, the models in AISC 342 were developed from a data set that did not have a substantial variation in both local and global slenderness as the data was extracted from tests focused on other aspects of brace and braced frame behavior. In the following figures, the computed backbone curves are plotted on top of the measured force-deformation response for the specimens reported here and in Bergendahl (2021). The backbone curves correspond to the values provided in Section 6.2. These figures allow for comparisons between the measured and predicted behavior of individual braces; however, further analysis of the complete dataset is provided later in this chapter.

6.3.1.a Symmetric Loading, 237.5" Long Braces

This section provides figures comparing the measured force-deformation response and the AISC backbone curve for the 237.5" HSS braces subjected to a symmetric loading protocol (Figure 6.7 through 6.38). This includes tests from Series 1 and Series 2 for a total of 32 test specimens. Generally, the backbone curve provides a similar shape to measured force-deformation response, however, the following observations can be made:

- The compressive deformation capacities for the 5x5x3/8 specimens are significantly underestimated.
- The accuracy of the predicted tensile deformation capacity is strongly dependent on the measured yield stress. The tensile deformation capacity for the 5x5x3/8 specimens are accurately predicted when $F_{y,m}$ is similar to R_yF_y but the inaccuracy increases as $F_{y,m}$ increases. For example, the 5x5x3/8 A1085 Y ($F_{y,m}$ of 66 ksi) predicted tensile behavior almost perfectly matches the measured behavior. However, the 5x5x3/8 A1085 B ($F_{y,m}$ of 78 ksi) tensile deformation capacity is considerably over-predicted due to its large measured yield stress. Although the 5x5x3/8 A1085 B specimen had a greater yield stress, the specimen achieved a maximum tensile deformation less than

that of all four 5x5x3/8 A1085 test specimens indicating that an increase in yield stress does not directly correspond with an increase in deformation capacity. Similarly, the 6x6x3/8 A1085 B tensile capacity is over predicted due to large measured F_y.

- The predicted maximum tensile force is accurate across all of the specimens in this section. This is expected since the measured yield strength was used to calculate the maximum tensile force capacity.
- The predicted maximum compressive force is generally accurate. As the brace width increases, the measured-to-predicted ratio of maximum compressive force tends to decrease. This is likely due to the larger connection eccentricity in the wider test specimens rather than an inaccuracy in the model.
- For cases where the compressive deformation capacity is accurately predicted (such as the 6x6 and 7x7 specimens), the strength degradation amount and rate is accurately predicted. It is difficult to assess the accuracy of the strength degradation amount and rate when the maximum compressive deformation is not accurately predicted.
- The nonlinear model shows no strength degradation in tension. This is consistent with the measured force-deformation response where in most cases, the measured maximum tensile force is sustained until tearing. There are, however, a few cases where the tensile force diminishes as axial tensile deformations increase (such as the 6x6x1/2 A500 Y, 6x6x1/2 A1085 Y, and 5x5x3/8 A1085 B brace specimens).

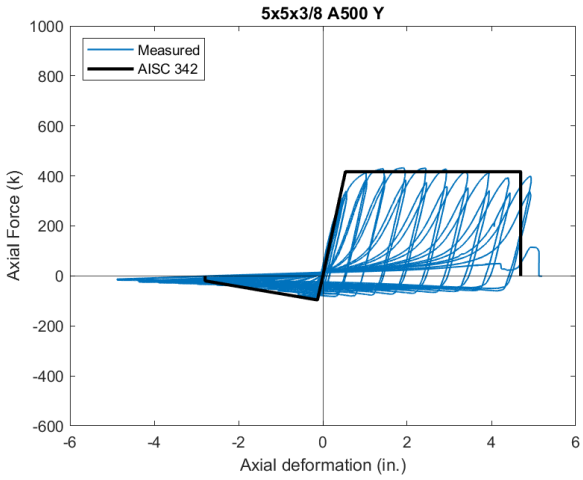

Figure 6.6 Backbone Curve – 5x5x3/8 A500 Y

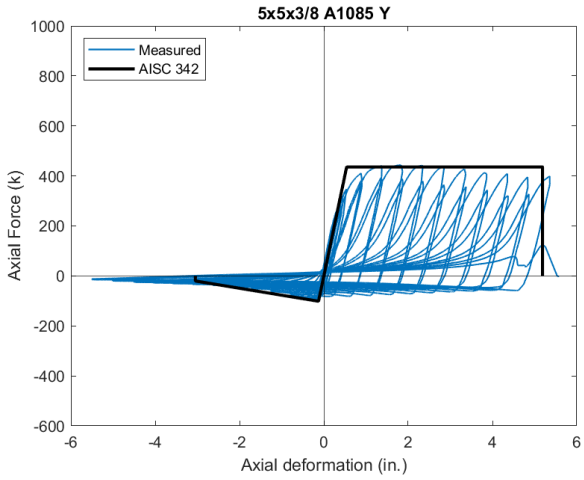

Figure 6.7 Backbone Curve – 5x5x3/8 A1085 Y

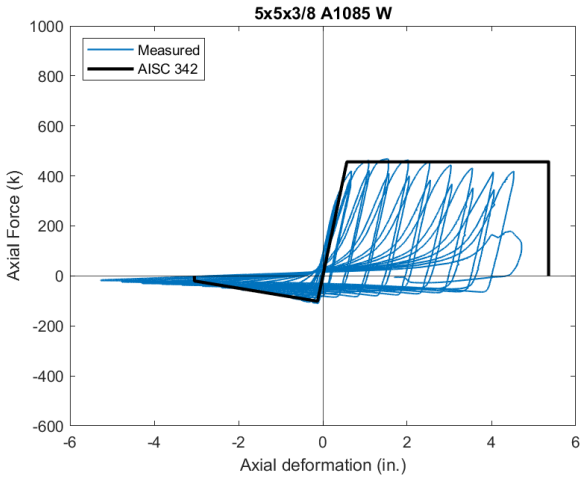

Figure 6.8 Backbone Curve – 5x5x3/8 A1085 W

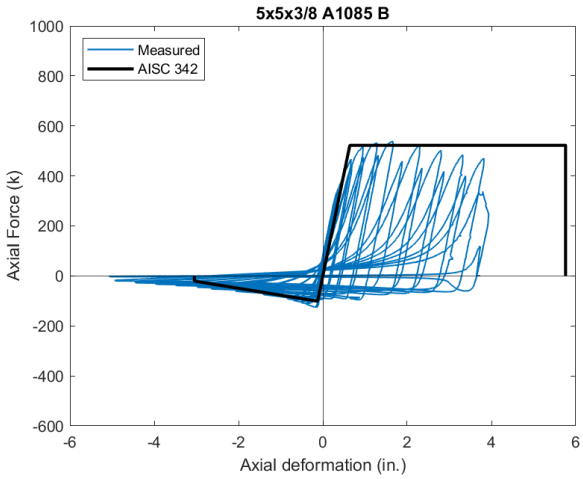

Figure 6.9 Backbone Curve – 5x5x3/8 A1085 B

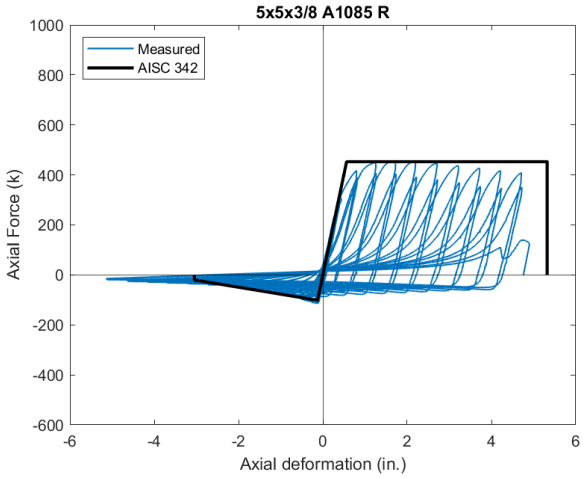

Figure 6.10 Backbone Curve – 5x5x3/8 A1085 R

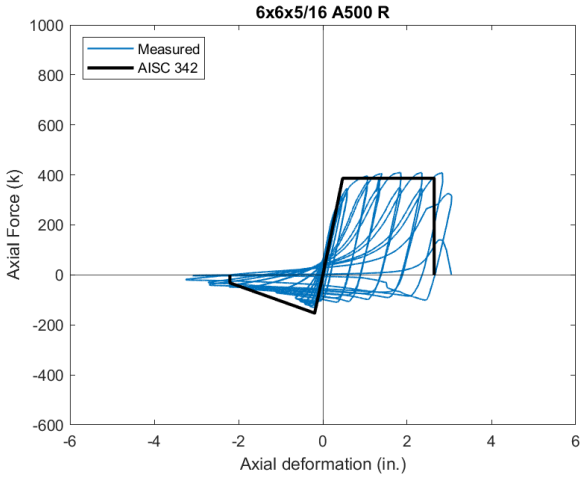

Figure 6.11 Backbone Curve – 6x6x5/16 A500 R

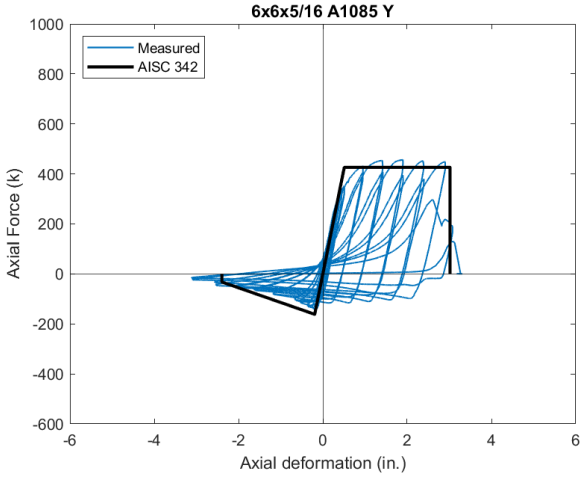

Figure 6.12 Backbone Curve – 6x6x5/16 A1085 Y

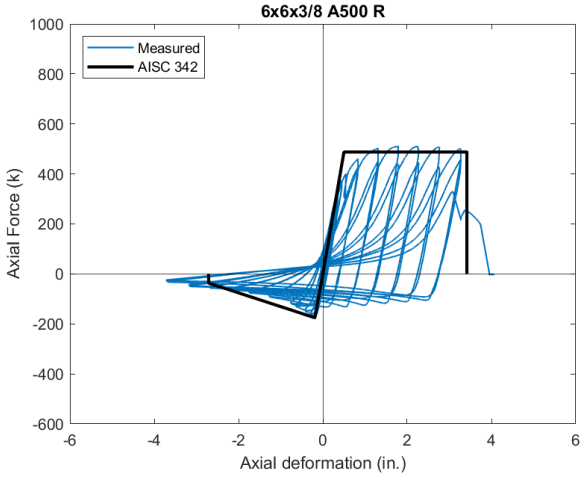

Figure 6.13 Backbone Curve – 6x6x3/8 A500 R

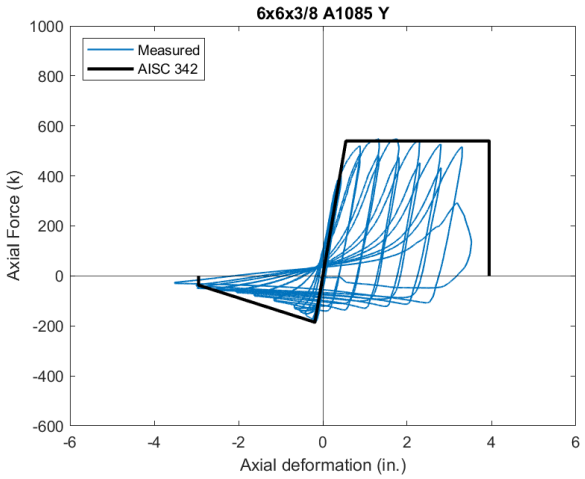

Figure 6.14 Backbone Curve – 6x6x3/8 A1085 Y

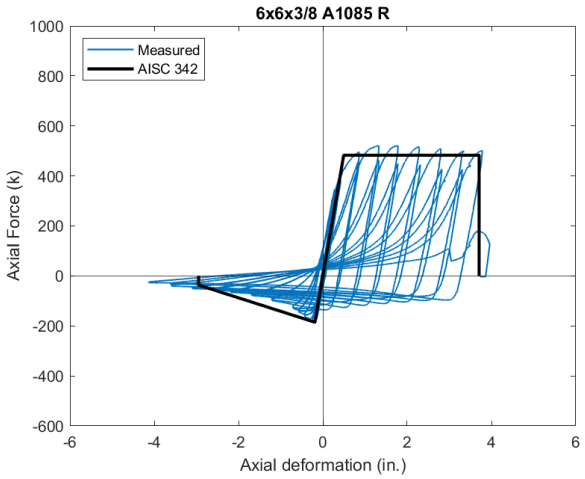

Figure 6.15 Backbone Curve – 6x6x3/8 A1085 R

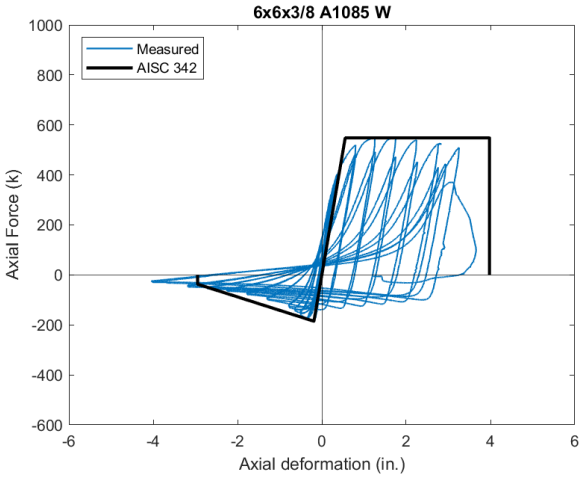

Figure 6.16 Backbone Curve – 6x6x3/8 A1085 W

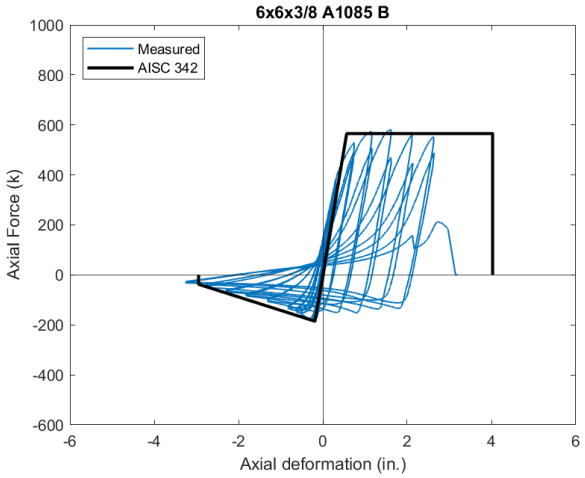

Figure 6.17 Backbone Curve – 6x6x3/8 A1085 B

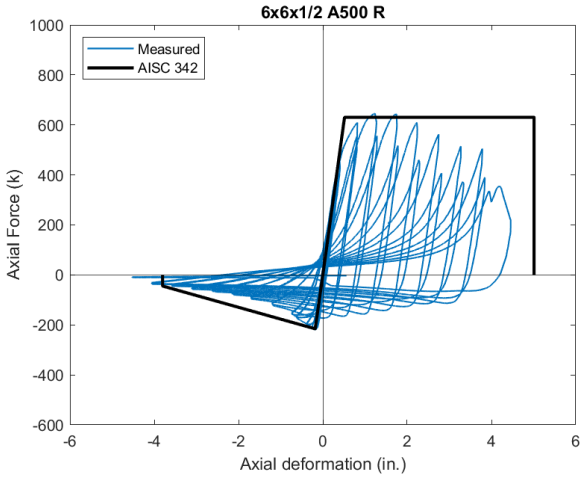

Figure 6.18 Backbone Curve – 6x6x1/2 A500 R

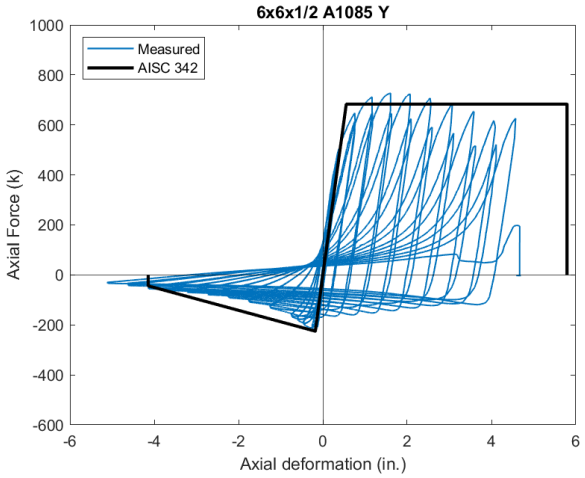

Figure 6.19 Backbone Curve – 6x6x1/2 A1085 Y

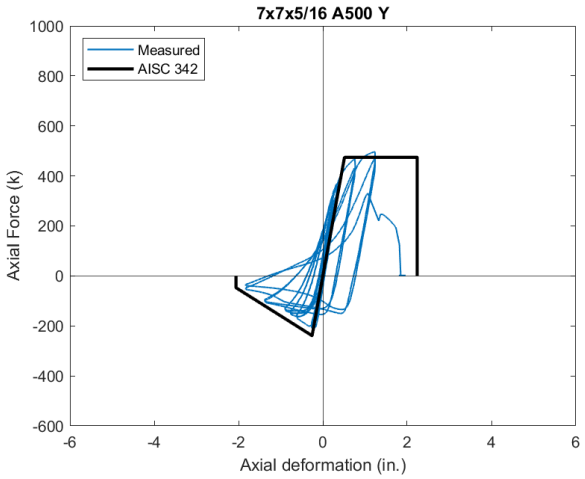

Figure 6.20 Backbone Curve – 7x7x5/16 A500 Y

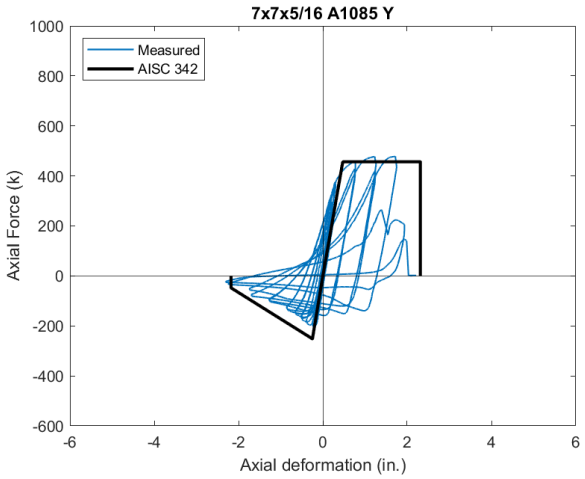

Figure 6.21 Backbone Curve – 7x7x5/16 A1085 Y

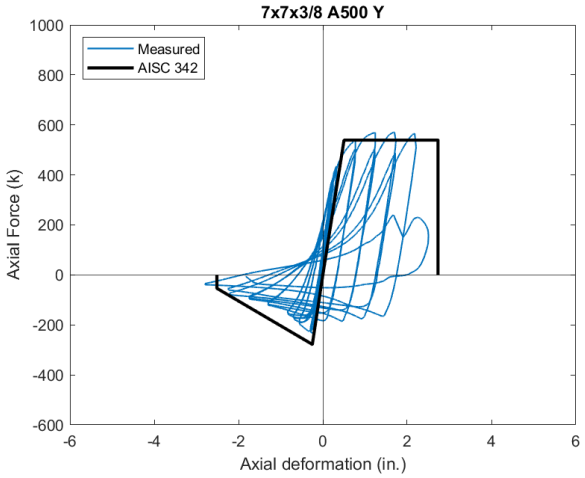

Figure 6.22 Backbone Curve – 7x7x3/8 A500 Y

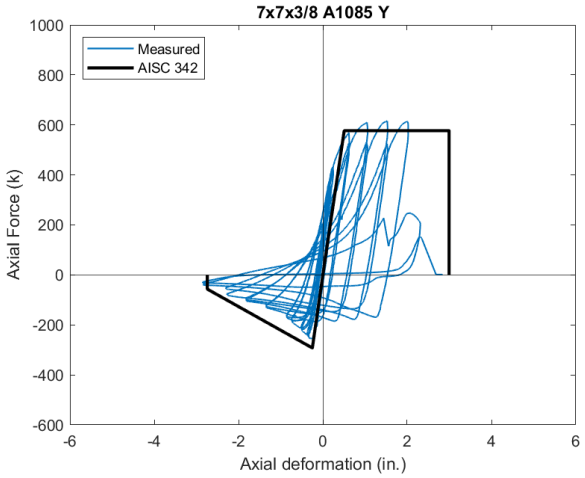

Figure 6.23 Backbone Curve – 7x7x3/8 A1085 Y

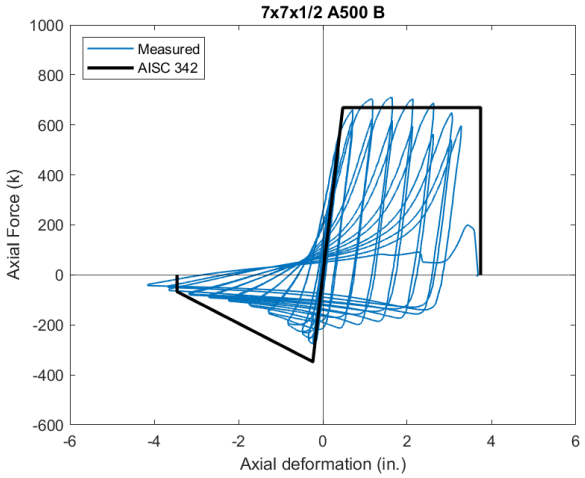

Figure 6.24 Backbone Curve – 7x7x1/2 A500 B

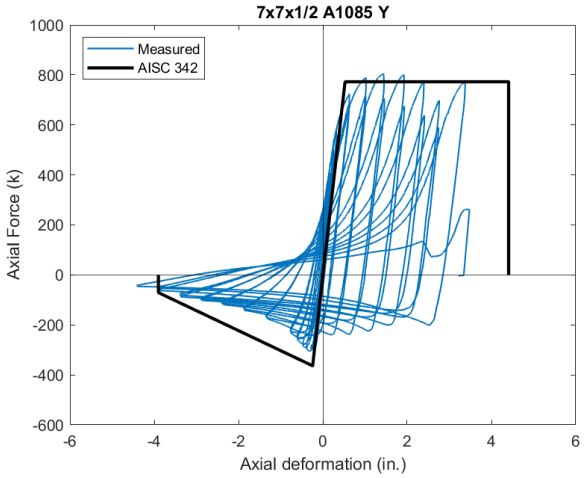

Figure 6.25 Backbone Curve – 7x7x1/2 A1085 Y

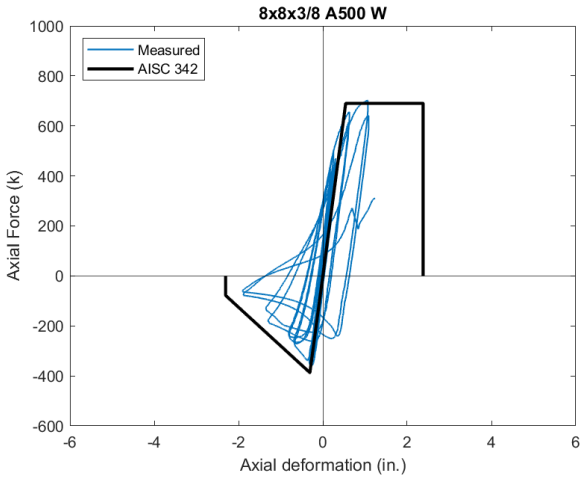

Figure 6.26 Backbone Curve – 8x8x3/8 A500 W

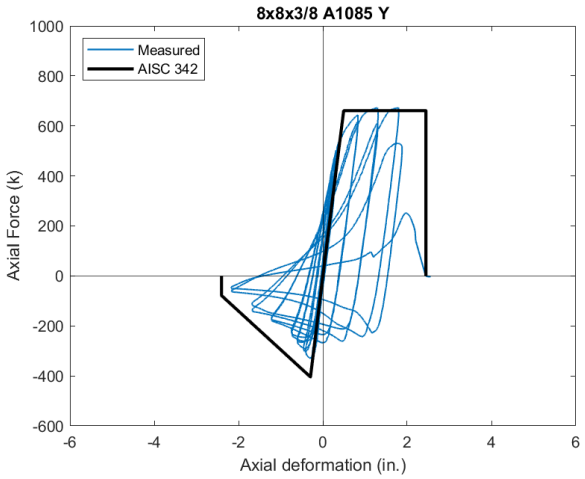

Figure 6.27 Backbone Curve – 8x8x3/8 A1085 Y

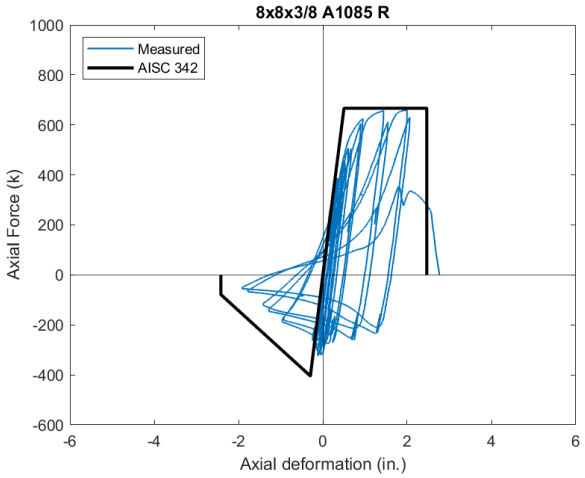

Figure 6.28 Backbone Curve – 8x8x3/8 A1085 R

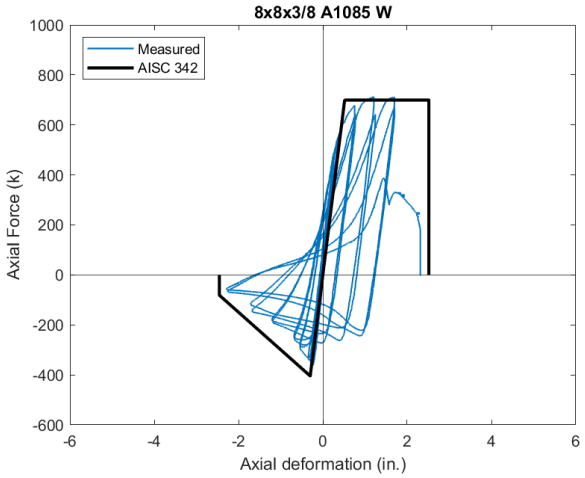

Figure 6.29 Backbone Curve – 8x8x3/8 A1085 W

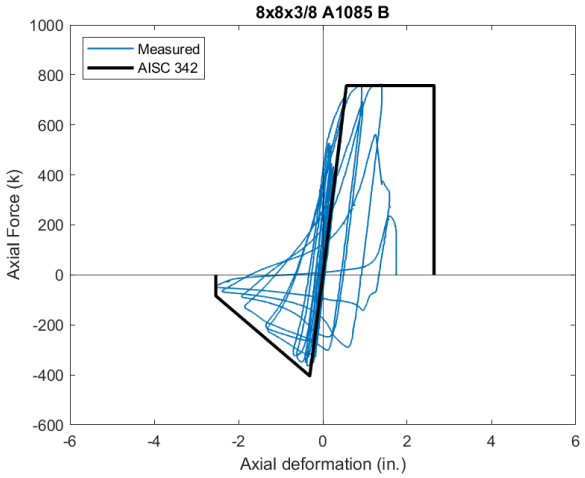

Figure 6.30 Backbone Curve – 8x8x3/8 A1085 B

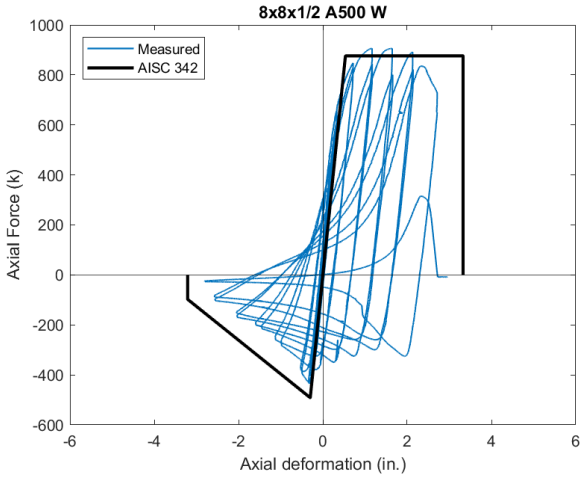

Figure 6.31 Backbone Curve – 8x8x1/2 A500 W

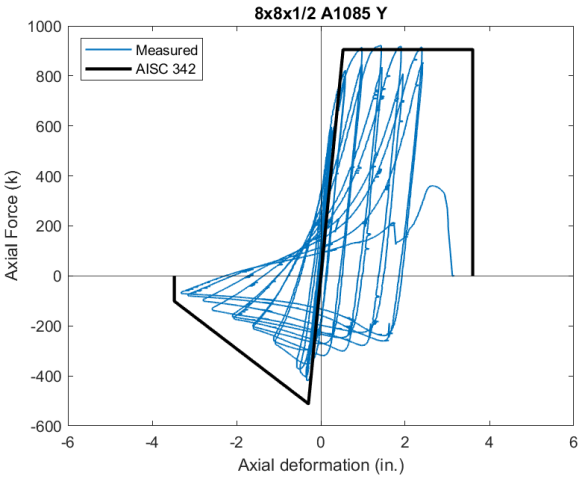

Figure 6.32 Backbone Curve – 8x8x1/2 A1085 Y

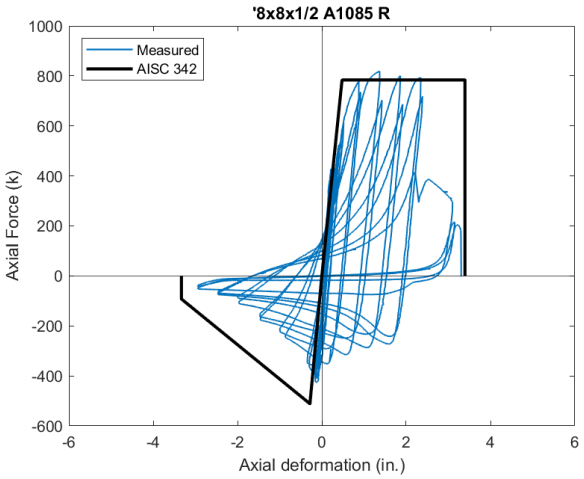

Figure 6.33 Backbone Curve – 8x8x1/2 A1085 R

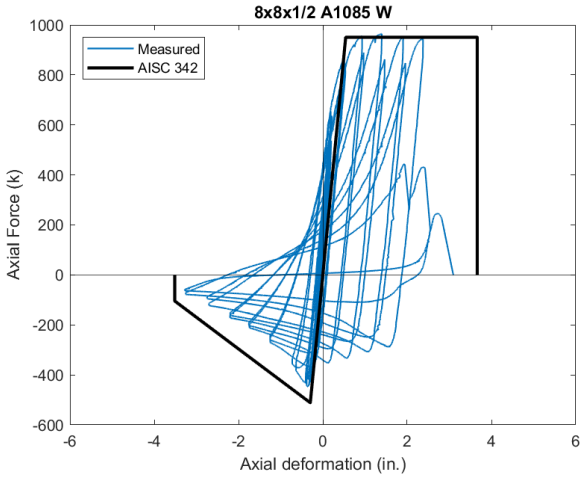

Figure 6.34 Backbone Curve – 8x8x1/2 A1085 W

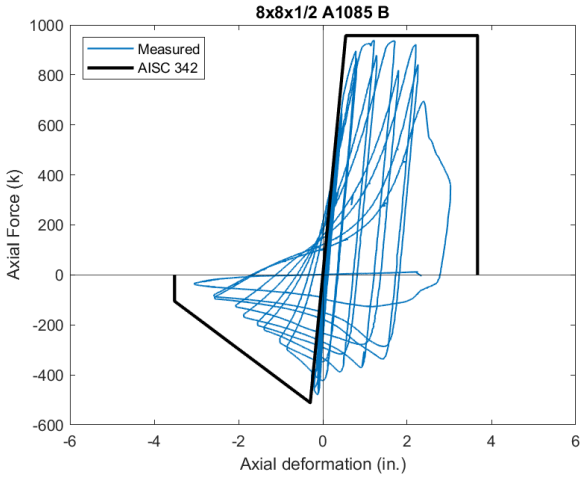

Figure 6.35 Backbone Curve – 8x8x1/2 A1085 B

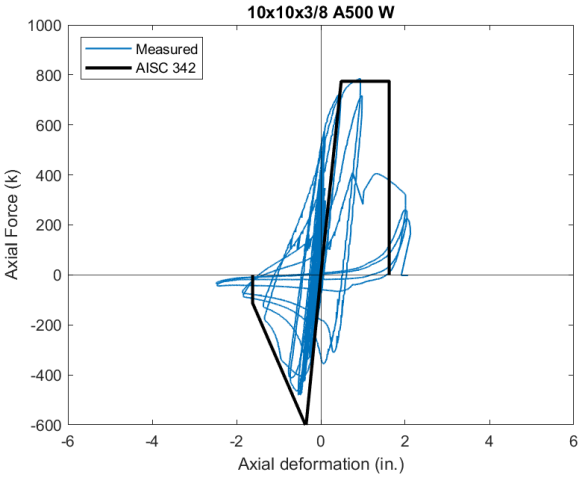

Figure 6.36 Backbone Curve – 10x10x3/8 A500 W

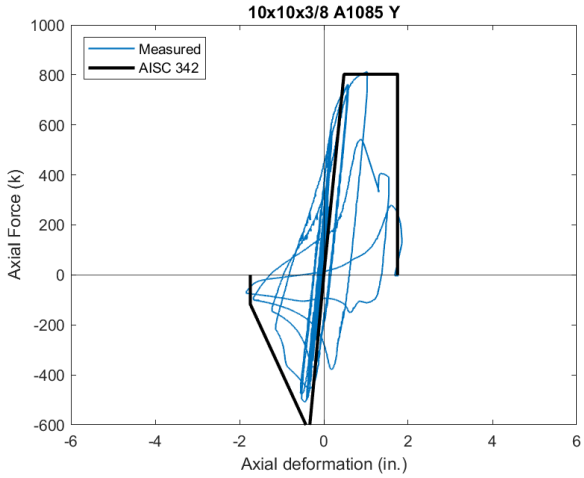

Figure 6.37 Backbone Curve – 10x10x3/8 A1085 Y

6.3.1.b Symmetric Loading, 183.5" Long Braces

In this experimental research program, three HSS specimens were tested at a shorter brace length to investigate the effect of brace length and to provide a wider range the global slenderness ratio, *KL/r*. These specimens were subjected to the same symmetric loading protocol scaled down by the short to long brace length ratio (183.5:237.5). Figures 6.39 through 6.41 compare the measured force-deformation response to the AISC backbone curve for these test specimens.

The compressive deformation capacity is more accurately predicted for the 5x5x3/8 A1085 Y 183.5" long brace specimen (*KL/r* of 99) than the 5x5x3/8 A1085 Y 237.5" long brace specimen (*KL/r* of 128) shown in Section 6.3.1.a. This indicates that the model underestimates the compressive capacity at higher *KL/r* ratios. This is understandable considering the model was calibrated based on previous research where *KL/r* ratios over 100 were not tested.

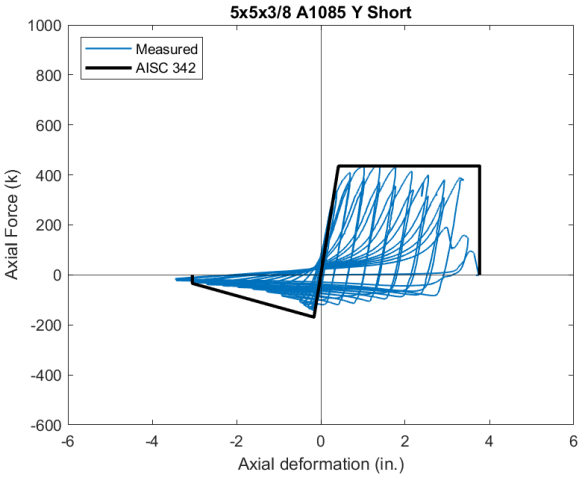

Figure 6.38 Backbone Curve – 5x5x3/8 A1085 Y-S

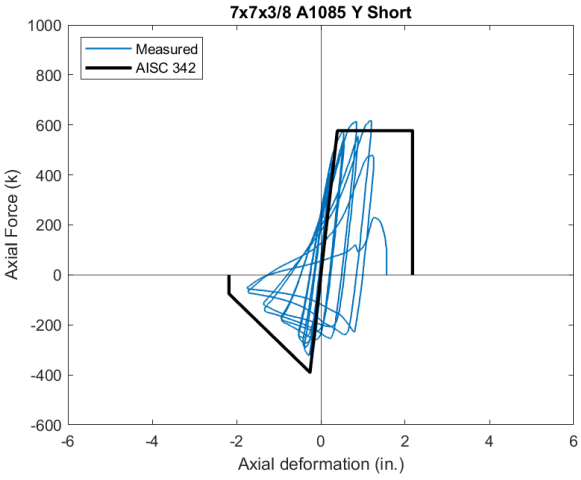

Figure 6.39 Backbone Curve – 7x7x3/8 A1085 Y-S

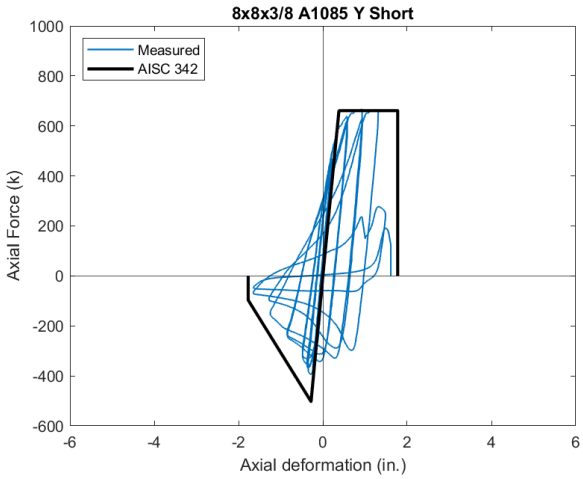

Figure 6.40 Backbone Curve – 8x8x3/8 A1085 Y-S

6.3.1.c Chevron Compression-Dominant Loading, 237.5" Long Braces

In this experimental research program, three HSS test specimens were subjected to a compression-biased loading protocol used to represent the behavior of braces in a chevron-configured SCBF. Figures 6.42 through 6.45 compare the measured force-deformation response to the AISC backbone curve for these test specimens. The following observations are drawn from the figures shown in this section:

- The measured compressive deformation significantly exceeds the predicted compressive deformation capacity, consistent with the trend noted in previous sections of this chapter.
- Discrepancies in deformation capacity are more notable between the AISC 342 nonlinear model and nonsymmetrical loading protocols.
- In the 5x5x3/8 A1085 Y Chevron test, the maximum compressive actuator stroke was reached so tensile demands were increased leading to fracture. Figure 6.41 shows that the post-buckling reloading stiffness in tension is strongly affected and this is not simulated with the simple bilinear backbone curve in tension.
- For the 7x7x3/8 and 8x8x3/8 specimens, the predicted deformation range is similar to the measured deformation range.

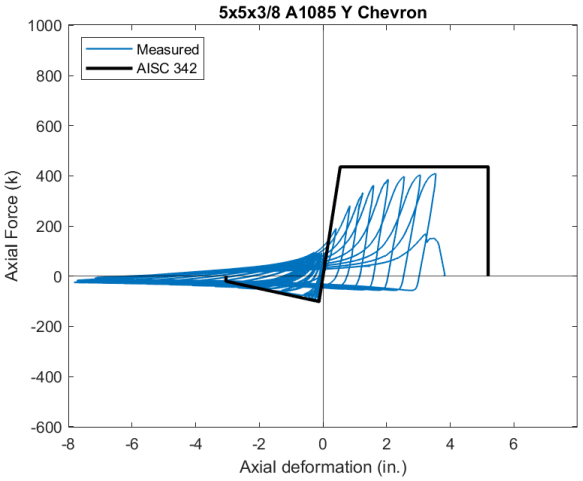

Figure 6.41 Backbone Curve – 5x5x3/8 A1085 Y-C

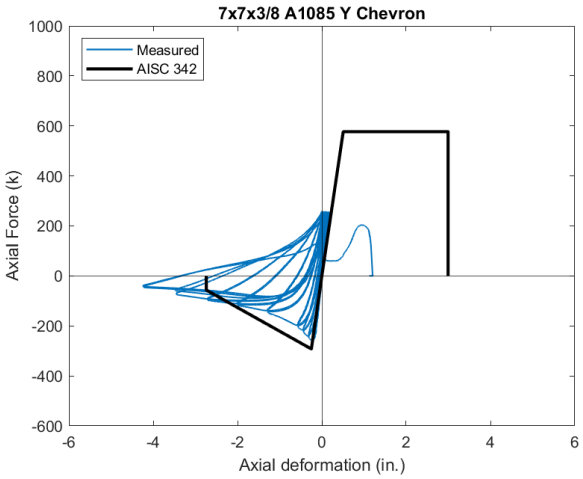

Figure 6.42 Backbone Curve – 7x7x3/8 A1085 Y-C

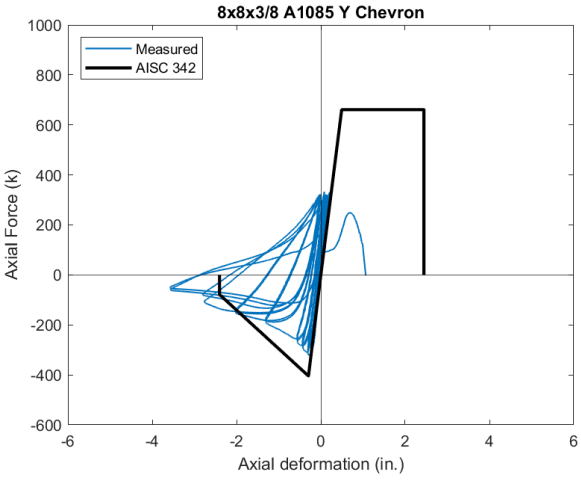

Figure 6.43 Backbone Curve – 8x8x3/8 A1085 Y-C

6.3.1.d Near-Fault Tension Dominant Loading, 237.5" Long Braces

In this experimental research program, three HSS braces were subjected to a tension-dominant loading protocol used to represent the non-symmetric pulse type demands for a braced frame subjected to near-fault ground motions. Figures 6.45-6.47 compare the measured force-deformation response to the AISC backbone curve for these test specimens. The following observations are made:

- The shift in the force-deformation responses in the positive deformation direction is representative of the tension bias in the applied loading.
- Here the maximum measured tensile deformation is notably larger than the predicted value for all three test specimens.
- For the 7x7x3/8 and 8x8x3/8 specimens, the predicted deformation range is similar to the measured deformation range.

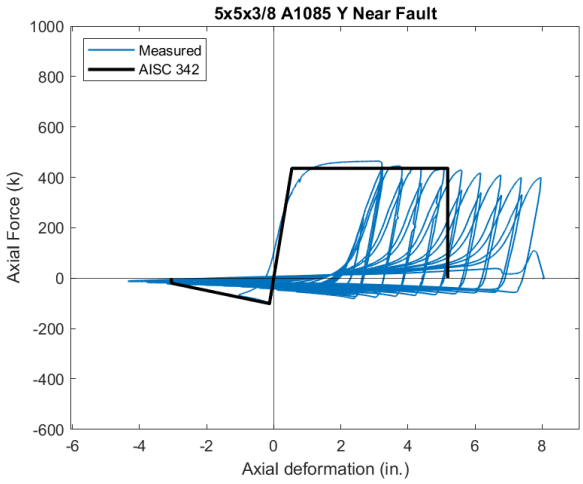

Figure 6.44 Backbone Curve – 5x5x3/8 A1085 Y-NF

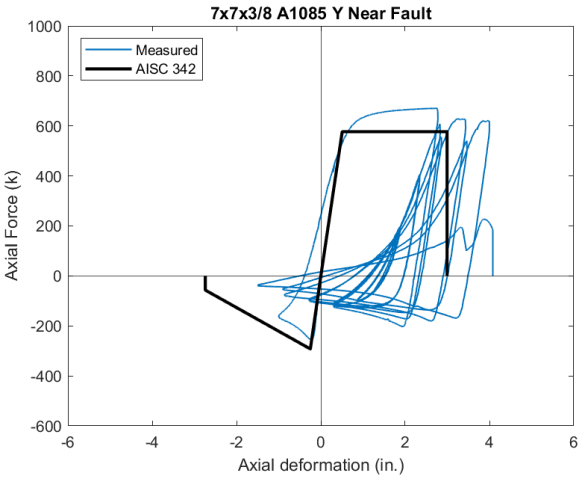

Figure 6.45 Backbone Curve – 7x7x3/8 A1085 Y-NF

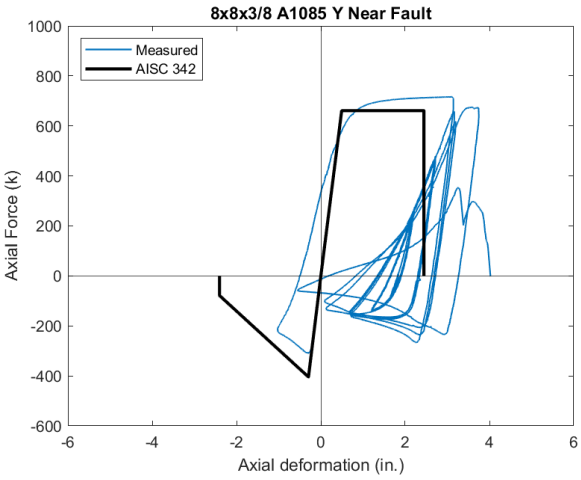

Figure 6.46 Backbone Curve – 8x8x3/8 A1085 Y-NF

6.3.3 *Comparison of Predicted and Measured Deformation Capacities*

In Section 6.3.2, it was apparent that the AISC 342 models accurately predicted the tensile and compressive force capacities and strength degredation, however, there were inaccuracies in the predicted deformation capacities. In this section, a series of tables and figures will be presented to further evaluate the accuracy of the AISC 342 predicted deformation capacities.

Table 6.2 below shows the predicted and measured maximum deformations for each of the HSS brace specimens tested in this experimental program. The table also includes the ratio of measured to predicted deformation capacity in order to evaluate the accuracy of the AISC 342 nonlinear model.

A summary of the measured-to-predicted deformation ratios is provided in Table 6.3. The table provides statistics which allow for the evaluation of the accuracy of the backbone curves based on various variables such as steel type, local compactness, global slenderness, and loading protocol. The table also includes the ratios for deformation range which is the sum of the maximum compressive and tensile deformations.

Table 6.2 Comparison of Predicted and Measured Brace Axial Deformation

	Predicted Maximum Deformation (in.) $\Delta_{predicted}$		**Measured Maximum Deformation (in.)** $\Delta_{measured}$		**Ratio of Measured-to-Predicted Capacity** $\Delta_{measured} : \Delta_{predicted}$	
Test Specimen	**Tens.**	**Comp.**	**Tens.**	**Comp.**	**Tens.**	**Comp.**
5x5x3/8 A500 Y	4.69	2.79	5.13	4.89	1.09	1.75
6x6x5/16 A500 R	2.64	2.21	3.05	3.26	1.15	1.48
6x6x3/8 A500 R	3.42	2.71	3.74	3.72	1.09	1.37
6x6x1/2 A500 R	5.01	3.80	4.45	4.06	0.89	1.07
7x7x5/16 A500 Y	2.24	2.06	1.73	1.83	0.77	0.89
7x7x3/8 A500 Y	2.73	2.51	2.51	2.79	0.92	1.11
7x7x1/2 A500 B	3.74	3.46	3.59	4.16	0.96	1.20
8x8x3/8 A500 W	2.38	2.31	1.24	1.90	0.52	0.82
8x8x1/2 A500 W	3.33	3.21	2.71	2.80	0.82	0.87
10x10x3/8 A500 W	1.62	1.62	2.10	2.48	1.29	1.53
5x5x3/8 A1085 Y	5.19	3.05	5.25	5.50	1.01	1.80
6x6x5/16 A1085 Y	3.02	2.40	3.13	3.12	1.04	1.30
6x6x3/8 A1085 Y	3.95	2.95	3.52	3.52	0.89	1.19
6x6x1/2 A1085 Y	5.79	4.14	4.67	5.12	0.81	1.24

	Predicted Maximum Deformation (in.) $\Delta_{predicted}$		Measured Maximum Deformation (in.) $\Delta_{measured}$		Ratio of Measured-to-Predicted Capacity $\Delta_{measured} : \Delta_{predicted}$	
Test Specimen	**Tens.**	**Comp.**	**Tens.**	**Comp.**	**Tens.**	**Comp.**
7x7x5/16 A1085 Y	2.31	2.18	1.99	2.31	0.86	1.06
7x7x3/8 A1085 Y	2.99	2.74	2.36	2.85	0.79	1.04
7x7x1/2 A1085 Y	4.41	3.90	3.48	4.41	0.79	1.13
8x8x3/8 A1085 Y	2.44	2.40	2.18	2.18	0.89	0.91
8x8x1/2 A1085 Y	3.60	3.48	2.96	3.32	0.82	0.96
10x10x3/8 A1085 Y	1.75	1.74	1.60	1.84	0.92	1.05
5x5x3/8 A1085 R	5.32	3.05	4.91	5.14	0.92	1.69
5x5x3/8 A1085 W	5.36	3.05	4.72	5.27	0.88	1.73
5x5x3/8 A1085 B	5.76	3.05	3.93	5.07	0.68	1.66
6x6x3/8 A1085 R	3.71	2.95	3.96	4.14	1.07	1.40
6x6x3/8 A1085 W	3.98	2.95	3.66	4.04	0.92	1.37
6x6x3/8 A1085 B	4.03	2.95	2.97	3.26	0.74	1.11
8x8x3/8 A1085 R	2.47	2.42	2.68	1.77	1.09	0.73
8x8x3/8 A1085 W	2.51	2.46	2.31	2.28	0.92	0.93
8x8x3/8 A1085 B	2.64	2.54	1.74	2.55	0.66	1.00
8x8x1/2 A1085 R	3.39	3.33	3.31	2.95	0.97	0.89
8x8x1/2 A1085 W	3.66	3.51	2.83	3.28	0.77	0.93
8x8x1/2 A1085 B	3.67	3.52	3.03	3.05	0.83	0.87
5x5x3/8 A1085 Y [S]	3.77	3.05	3.64	3.45	0.97	1.13
7x7x3/8 A1085 Y [S]	2.17	2.18	1.56	1.74	0.72	0.80
8x8x3/8 A1085 Y [S]	1.78	1.77	1.61	1.65	0.91	0.93
5x5x3/8 A1085 Y [C]	5.19	3.05	3.64	7.82	0.70	2.57
7x7x3/8 A1085 Y [C]	2.99	2.74	1.16	4.24	0.39	1.55
8x8x3/8 A1085 Y [C]	2.44	2.40	1.10	3.58	0.45	1.49
5x5x3/8 A1085 Y [NF]	5.19	3.05	7.88	4.34	1.52	1.42
7x7x3/8 A1085 Y [NF]	2.99	2.74	4.08	1.50	1.36	0.55
8x8x3/8 A1085 Y [NF]	2.44	2.40	3.95	1.03	1.62	0.43

Note: Data shown above the line is from Bergendahl (Bergendahl, 2021)

[C] Chevron Compression Dominant Loading Protocol

[NF] Near Fault Tension Dominant Loading Protocol

[S] Short Brace Test

Table 6.3 Summary of Measured and Predicted Behavior

		$\Delta_{measured} : \Delta_{predicted}$ Tension		$\Delta_{measured} : \Delta_{predicted}$ Compression		$\Delta_{measured} : \Delta_{predicted}$ Range	
Loading Protocol	**HSS Specimens**	**Average**	**Standard Deviation**	**Average**	**Standard Deviation**	**Average**	**Standard Deviation**
Symmetric	**All Specimens**	0.90	0.15	1.17	0.30	1.01	0.18
Symmetric	**A500 HSS**	0.95	0.22	1.21	0.31	1.07	0.25
Symmetric	**A1085 HSS**	0.87	0.12	1.15	0.30	0.99	0.14
Symmetric	$b/t_{nom} < \lambda_{HD}$	0.89	0.11	1.28	0.32	1.05	0.15
Symmetric	$b/t_{nom} > \lambda_{HD}$	0.90	0.19	1.05	0.24	0.97	0.20
Symmetric	$KL/r > 100$	0.94	0.14	1.44	0.25	1.14	0.14
Symmetric	$KL/r < 100$	0.87	0.16	0.99	0.17	0.93	0.14
Near Fault	**A1085 HSS**	1.50	0.13	N/A*	N/A*	1.16	0.28
Chevron	**A1085 HSS**	N/A*	N/A*	1.87	0.61	1.10	0.25

* The corresponding loading protocol did not apply tension/compression demands

The predicted versus measured deformation capacities are plotted in Figure 6.47, Figure 6.48, and Figure 6.49, for tension, compression, and deformation range, respectively. Figure 6.47 shows that generally the tensile capacity is slightly overpredicted for the symmetric displacement histories. Figure 6.48 shows that many of measured compressive capacities are significantly larger than the predicted capacities. Figure 6.49 shows that the deformation range is fairly accurate across the dataset.

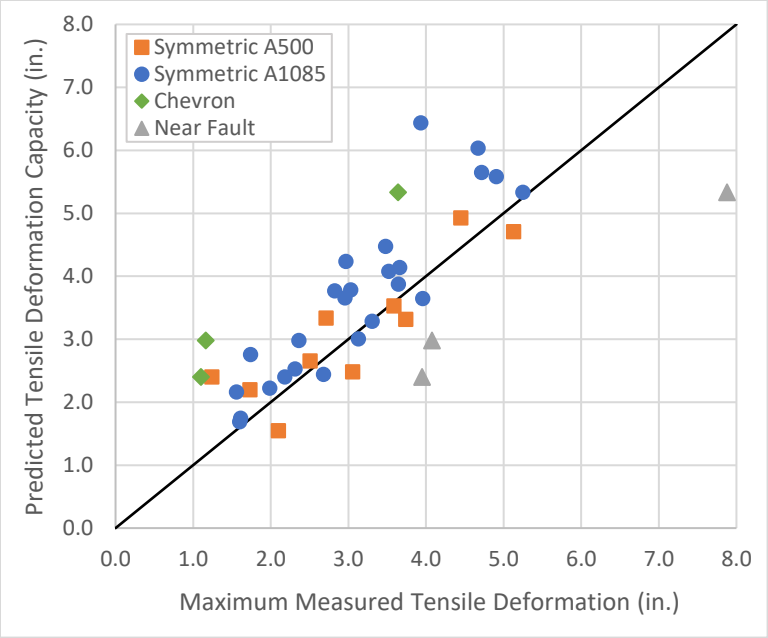

Figure 6.47 Predicted vs. Measured Tensile Deformation Capacity

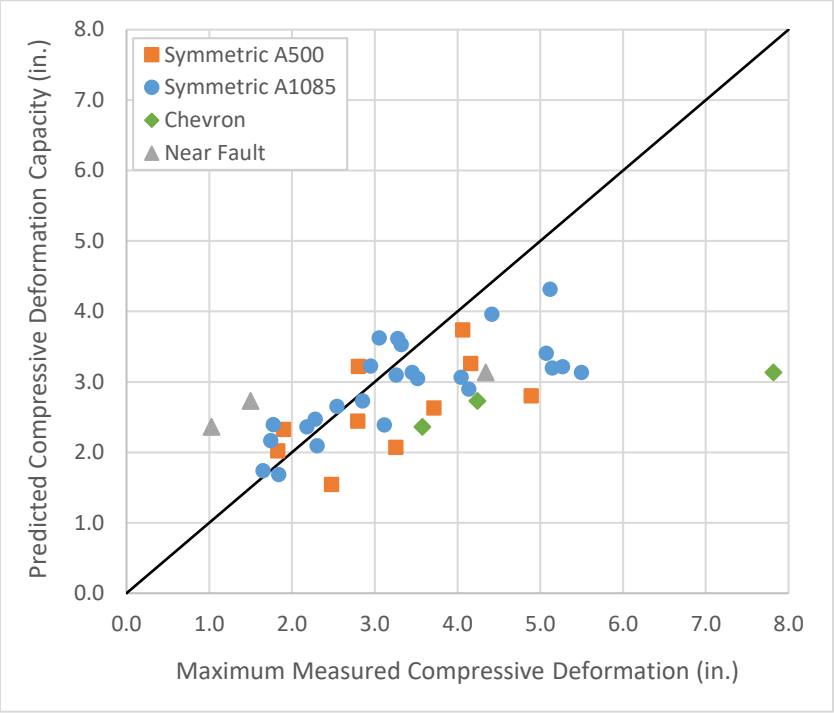

Figure 6.48 Predicted vs. Measured Compressive Deformation Capacity

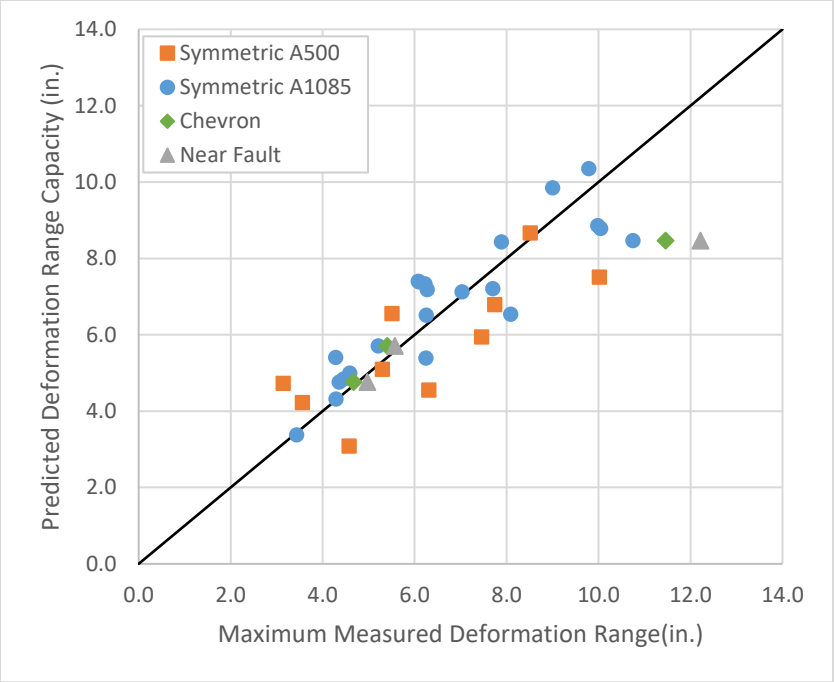

Figure 6.49 Predicted vs. Measured Deformation Range Capacity

As discussed above, three different A1085 HSS shapes were tested using the alternate loading protocols. The chevron loading protocol was compression dominant and intended to represent the behavior of a brace within a SCBF with a chevron configuration. The near-fault loading protocol was tension dominant and intended to represent the pulse-like demands of a near-fault ground motion affected by forward directivity. These loading protocols are detailed in Section 3.5. Due to the tension and compression bias in these loading protocols, the deformation capacity predictions from the nonlinear model are not accurate with the measured deformations.

As expected for the near fault loading protocol, the measured tensile deformation capacity was much larger than predicted. Additionally, the peak measured compressive deformation was much lower than predicted but there was no demand for compressive deformation so a fair comparison cannot be made. As for the chevron loading protocol, the measured compressive deformation capacity was much larger than predicted, however, a fair comparison between the measured and predicted tensile capacity cannot be made because there was no tensile demand.

Although AISC 342 does not specify that the model is for symmetric loading, the comparisons above indicate that it is only accurate for symmetric loading. As shown in Chapter

5, the compressive and tensile deformation capacities are strongly influenced by the displacement history, however, the deformation range was fairly consistent for each of the loading protocols. Although, the predicted tensile and compressive deformation capacities are inaccurate for asymmetric loading, the deformation range provide by the model is quite accurate. For evaluation for asymmetric loading, the use of the deformation range provided by AISC 342 may provide accurate results. A model based on deformation range rather than individual tensile and compressive capacities would provide a better representation of brace deformation capacity.

Evidently, the AISC 342 model is only comparable to the experimental results for the specimens subjected to a symmetric loading protocol. Therefore, the remaining analysis in this subsection will assess only symmetric tests.

The majority of the test specimens did not reach the predicted maximum tensile deformation. Of the 35 specimens subjected to the symmetric loading protocol, only eight (22.9%) reached a greater tensile deformation than predicted. Of the eight that exceeded the predicted tensile deformation, six were within 10% of the predicted value. Many of the significantly overpredicted tensile deformations were due to the model increasing deformation capacity with increased yield strength. This is not consistent with the experimental results which show a negative relationship between yield strength and deformation range. Table 6.3 shows that the average measured to predicted tensile deformation ratio for all symmetric tests was 0.90. Overall, the accuracy of the predicted tensile deformation capacity is quite consistent across the dataset. Although most of the test specimens are within 20% of the predicted tensile deformation, most of the tensile deformations were overpredicted by the nonlinear model provided by AISC 342 which is non-conservative.

Many of the test specimens reached compressive deformations much larger than the predicted maximum compressive deformation. Only one test specimen had a measured-to-predicted compressive deformation ratio of less than 0.80, while twelve had a ratio greater than 1.20. The nonlinear model seems to underestimate the compressive deformation capacity of HSS braces with global slenderness ratios over 80, and more significantly as global slenderness increases. All but one of the test specimens with *KL/r* ratios greater than 80 reached a compressive axial deformation greater than predicted. One of the 5x5x3/8 specimens, achieved a compressive deformation of 1.75 times the predicted deformation – a significant underprediction. The average measured-to-predicted compressive deformation capacity ratio for test specimens

with *KL/r* ratios over 100 was 1.44, while that for *KL/r* ratios less than 100 was 0.99. This indicates that the equation used to predict the maximum compressive deformations is not very accurate at high global slenderness ratios. The majority of previous experimental research on the inelastic behavior of HSS braces was conducted on braces with global slenderness ratios of less than 100 so that may be the reason for the inaccuracy at higher *KL/r* ratios.

For the measured-to-predicted deformation ratios, the standard deviation was much higher for compression (0.31) than tension (0.14) indicating more variation in the accuracy of the compression model. This is largely due to the nonlinear model significantly underestimating the compressive deformation capacity of highly compact HSS braces.

Although the tensile deformations were generally overestimated and the compression deformations were generally underestimated, the predicted deformation range was quite accurate. The average measured-to-predicted deformation range ratio for all of the test specimens subjected to a symmetric loading protocol was 1.01. Although the average is close to 1.0, the average measured-to-predicted deformation range ratio was 1.14 for *KL/r* ratios greater than 100 and 0.93 for *KL/r* ratios less than 100. The predicted deformation range is generally overestimated at lower global slenderness ratios and underestimated at higher global slenderness ratios.

6.3.4 *Recommendations for Nonlinear Modeling of Bracing Members*

Evaluation of the AISC 342 nonlinear model for rectangular HSS braces led to conclusions about the inaccuracies of the model. It was concluded that the nonlinear model significantly underestimates the compressive deformation capacity at higher *KL/r* ratios and slightly overestimates that at lower *KL/r* ratios. Additionally, the predicted tensile deformations were generally overestimated. In cases where the tensile deformation capacity was significantly overestimated, it was because the model increases deformation capacity with increases in yield strength, however, the experimental results showed that the deformation capacity tends to decrease with increase in yield strength. Following these conclusions, the equations used for the AISC nonlinear model were re-evaluated to more accurately predict the experimental data. This

section will provide recommendations for changes in the nonlinear modeling of rectangular HSS bracing members.

A modified model was developed to improve the equations for the n-factor, which determines the maximum deformation capacities. The n-factor for tension and compression are computed separately. The modified model uses the same general form as the AISC 342 equations for n-factors. The coefficients and exponents in modified model were developed by calibrating the equation to the experimental data. The experimental data included in this calibration was all of the braces subjected to the symmetric loading protocol except for the 10x10x3/8 A500 W specimen. This specimen displayed extreme post tearing ductility which skewed the maximum deformations. Thirty-four brace tests were included in the calibration providing a *b/t* range of 9 to 24 and a *KL/r* range of 60 to 127. In Table 6.4, the equations for n-factors are shown for the current and modified models.

Table 6.4 Modified Equations for Calculation of n-factor in AISC 342 Nonlinear Model

	AISC 342	**Modified**
Tension	$n = 4.7\left(\frac{\lambda}{\lambda_{hd}}\right)^{-1.0}\left(\frac{\left(\frac{L_c}{r}\right)}{\sqrt{\frac{E}{F_{ye}}}}\right)^{0.24}$	$n = 3.5\left(\frac{\lambda}{\lambda_{hd}}\right)^{-0.9}\left(\frac{\left(\frac{L_c}{r}\right)}{\sqrt{\frac{E}{F_{ye}}}}\right)^{0.34}$
Compression	$n = 3.0\left(\frac{\lambda}{\lambda_{hd}}\right)^{-1.0}\left(\frac{\left(\frac{L_c}{r}\right)}{\sqrt{\frac{E}{F_{ye}}}}\right)^{1.0}$	$n = 0.83\left(\frac{\lambda}{\lambda_{hd}}\right)^{-0.85}\left(\frac{\left(\frac{L_c}{r}\right)}{\sqrt{\frac{E}{F_{ye}}}}\right)^{1.96}$

Table 6.5 presents the root mean square error for the current and modified models. The modified model has lower root mean square errors for tensile and compressive deformation capacity indicating significant improvement over the current model. Most of the improvement is due to modifications in the compression model.

Table 6.5 RMSE of Modified Models

	Root Mean Square Error	
	AISC 342	**Modified**
Tension	0.632	0.482
Compression	0.983	0.438
Range	1.048	0.815

Although the modified model provides better results, the model still does not work well for the asymmetric displacement histories. In Chapter 5, the investigation into the effect of displacement history showed that displacement history significantly affects the maximum compressive and tensile deformations, but it does not affect the brace deformation range. A model that predicts brace fracture based on deformation range would provide accurate results regardless of displacement history.

Chapter 7. SUMMARY, CONCLUSIONS, AND FUTURE WORK

The inelastic axial deformation of HSS braces is commonly used as the primary yield mechanism in concentrically braced frames. Through yielding in tension and buckling in compression, the brace acts as the main source of energy dissipation. As the brace experiences large axial deformations due to story drift, the midspan forms a plastic hinge and the brace develops local deformations which are followed by brace fracture. Once the brace develops these local deformations (often referred to as cupping), fracture tends to follow shortly after. Therefore, delaying the initiation of local cupping also delays brace fracture. The ability to withstand large axial deformations without brace fracture provides the inelastic deformation capacity needed to assure good seismic performance. The local compactness ratio (*b/t*) and global slenderness ratio (*KL/r*) have a significant impact on the deformation capacity of HSS braces. An HSS brace which is more locally compact and globally slender (low local compactness ratio and high global slenderness ratio) typically exhibits greater deformability. Consequently, non-compact and stocky braces are more prone to early brace fracture.

ASTM A500 is the conventional standard for HSS used in CBFs. In 2013, a new specification for square HSS was introduced – ASTM 1085. Compared to A500 HSS, the A1085 standard has tighter tolerances on geometric requirements and has additional material requirements such as a maximum yield strength and a minimum CVN toughness. As a result, A1085 HSS provides several potential advantages. A tighter tolerance on wall thickness for A1085 results in smaller width-to-thickness ratios than for A500 sections of the same size. Additionally, as a result of stricter requirements for material properties, the expected yield strength ratio, Ry, for A1085 is less than that of A500 members, and this reduces capacity based force demands for the design of other framing elements.

Considering that the A1085 standard is still new to the market, there is an interest in understanding the behavior of A1085 HSS and how it compares to A500. Prior research has indicated that A1085 HSS braces may provide greater ductility than A500, however, limited research has been done to evaluate the cyclic performance of A1085 HSS braces.

To fully realize the benefits of A1085 HSS, a comprehensive research program was undertaken to investigate the cyclic response of A1085 HSS braces. A series of large scale

experiments, as well as material testing, was conducted at the University of Washington Structural Research Lab (UW SRL).

Section 7.1 provides a summary of the experimental research program. Section 7.2 provides conclusions based on the experimental results. Section 7.3 provides recommendations for future research regarding the cyclic performance of HSS braces in CBFs.

7.1 SUMMARY

The experimental research consisted of forty-one cyclic loading component brace tests. Previous research has shown that the inelastic deformation capacity of HSS braces is strongly dependent on the local compactness and global slenderness, so the test specimens were designed to cover a wide range of *b/t* ratios and *KL/r* ratios. The HSS test specimens had *b/t* ratios ranging from of 9 to 25.7, and *KL/r* ratios ranging from about 60 to 127. This range provided braces that meet the compactness limits for SCBFs and OCBFs as well as many that do not meet the requirements for either.

The effect of various parameters on the cyclic response of HSS braces were investigated. The primary study parameters were: (1) type of HSS, i.e., A500C or A1085, (2) HSS producer, (3) global slenderness ratio, *KL/r*, (4) local compactness ratio, *b/t*, and (5) loading protocol, i.e., symmetric or chevron or near fault. The testing was split into four test series with the specimens shown in Table 7.1.

The cyclic response of the brace specimens were analyzed to assess deformation capacity and energy dissipation capacity. Various measures were used to investigate deformation capacity such as maximum compressive and tensile brace axial deformation, deformation range, maximum story drift (assuming 45 degree brace configuration), maximum story drift range, and accumulated axial deformation.

Table 7.1 Summary of Experimental Test Specimens

HSS Shape	Steel Type	Producer	Loading	Brace Length (in.)	*b/t*	*KL/r*
SERIES 1						
5x5x3/8	A500	Yellow	Symmetric	237.5	11.3	127.01
5x5x3/8	A1085	Yellow	Symmetric	237.5	10.3	127.69
6x6x5/16	A500	Red	Symmetric	237.5	17.6	102.81
6x6x5/16	A1085	Yellow	Symmetric	237.5	16.2	103.26
6x6x3/8	A500	Red	Symmetric	237.5	14.2	104.17
6x6x3/8	A1085	Yellow	Symmetric	237.5	13	104.63
6x6x1/2	A500	Red	Symmetric	237.5	9.9	106.50
6x6x1/2	A1085	Yellow	Symmetric	237.5	9	107.47
7x7x5/16	A500	Yellow	Symmetric	237.5	21.1	87.32
7x7x5/16	A1085	Yellow	Symmetric	237.5	19.4	87.64
7x7x3/8	A500	Yellow	Symmetric	237.5	17.1	88.29
7x7x3/8	A1085	Yellow	Symmetric	237.5	15.7	88.62
7x7x1/2	A500	Blue	Symmetric	237.5	12.1	90.30
7x7x1/2	A1085	Yellow	Symmetric	237.5	11	91.00
8x8x3/8	A500	White	Symmetric	237.5	19.9	76.61
8x8x3/8	A1085	Yellow	Symmetric	237.5	18.3	76.86
8x8x1/2	A500	White	Symmetric	237.5	14.2	78.13
8x8x1/2	A1085	Yellow	Symmetric	237.5	13	78.64
10x10x3/8	A500	White	Symmetric	237.5	25.7	60.59
10x10x3/8	A1085	Yellow	Symmetric	237.5	23.7	60.90
SERIES 2						
5x5x3/8	A1085	Red	Symmetric	237.5	10.3	127.69
5x5x3/8	A1085	White	Symmetric	237.5	10.3	127.69
5x5x3/8	A1085	Blue	Symmetric	237.5	10.3	127.69
6x6x3/8	A1085	Red	Symmetric	237.5	13	104.63
6x6x3/8	A1085	White	Symmetric	237.5	13	104.63
6x6x3/8	A1085	Blue	Symmetric	237.5	13	104.63
8x8x3/8	A1085	Red	Symmetric	237.5	18.3	76.86
8x8x3/8	A1085	White	Symmetric	237.5	18.3	76.86
8x8x3/8	A1085	Blue	Symmetric	237.5	18.3	76.86
8x8x1/2	A1085	Red	Symmetric	237.5	13	78.64
8x8x1/2	A1085	White	Symmetric	237.5	13	78.64
8x8x1/2	A1085	Blue	Symmetric	237.5	13	78.64
SERIES 3						
5x5x3/8	A1085	Yellow	Chevron	237.5	10.3	127.69
5x5x3/8	A1085	Yellow	Near Fault	237.5	10.3	127.69
7x7x3/8	A1085	Yellow	Chevron	237.5	15.7	88.62
7x7x3/8	A1085	Yellow	Near Fault	237.5	15.7	88.62
8x8x3/8	A1085	Yellow	Chevron	237.5	18.3	76.86
8x8x3/8	A1085	Yellow	Near Fault	237.5	18.3	76.86
SERIES 4						
5x5x3/8	A1085	Yellow	Symmetric	183.5	10.3	98.66
7x7x3/8	A1085	Yellow	Symmetric	183.5	15.7	68.47
8x8x3/8	A1085	Yellow	Symmetric	183.5	18.3	59.39

7.2 CONCLUSIONS

The conclusions made based on the experimental results and measured specimen properties are summarized here.

- Analysis of the results in this experimental study indicates that ductility and energy dissipation capacity of HSS bracing members are most significantly impacted by the local compactness and global slenderness ratios. Deformation capacity and energy dissipation were shown to increase with decreased local compactness ratios and increased global slenderness ratios. This is consistent with previous research.

- Overall, there was minor variability between the producers of A1085 HSS, however, there was no clear trend between HSS producer and brace performance.

- In the study of various applied displacement protocols, it was evident that the maximum tensile and compressive deformations were highly dependent on displacement history, however, the deformation range was not significantly impacted by displacement history. Therefore, to characterize the seismic response of OCBFs and SCBFs, story drift range should be used, rather than the maximum drift in a single direction.

- Results from material testing showed little correlation with structural response and brace deformation capacity.

- As concluded by Bergendahl (2021), there were no significant differences between the performance of A500 Grade C and A1085 as they both exhibited similar responses. This may be due to the similarities between the measured geometric and material properties of A500 Grade C and A1085 specimens (Bergendahl, 2021). No new data for A500 HSS braces was presented in this paper to draw further conclusions.

- The research shows that identical braces with identical *b/t* ratios provide greater inelastic deformation capacity with longer brace lengths and larger *KL/r* than for shorter braces with smaller *KL/r*. This suggests that more generous *b/t* limits may be permitted if the *KL/r* of the brace is considered by the limit.

- The AISC 342 nonlinear model significantly underestimates the compressive deformation capacity at higher *KL/r* ratios and slightly overestimates that at lower *KL/r* ratios. Additionally, the predicted tensile deformations were generally overestimated. In cases where the tensile deformation capacity was significantly overestimated, it was due to the model's sensitivity to high measured yield strengths.

- The AISC 342 nonlinear model is not accurate for asymmetric displacement histories. A model based on deformation range rather than individual tensile and compressive capacities would provide a better representation of brace deformation capacity and more accurate results regardless of displacement history.

7.3 Recommendations for Future Work

Although this research project provided a thorough investigation into the performance of A1085 HSS braces, the following future research is recommended to further understand the cyclic behavior of HSS braces in braced frames.

- Re-evaluate AISC 341-16 width-to-thickness limits. The results in this study indicated that the current highly-ductile limit is adequate but the moderately-ductile limit is conservative and could be increased while still ensuring adequate brace behavior. Further investigation into the performance of HSS braces with *b/t* ratios in the range of 16-20 could validate an increase in the moderately-ductile width-to-thickness limit.

- Experimental investigation into the cyclic performance of relatively stocky braces. In this study, the *KL/r* ratios ranged from about 60 to 127, however only one specimen that meets the AISC highly ductile limit had a *KL/r* ratio less than 90. To provide a comprehensive evaluation of the width-to-thickness limits for SCBFs and OCBFs, additional research is required to test highly and moderately ductile bracing members with *KL/r* ratios between 40 and 90.

- Consideration of minimum *KL/r* requirements. The experimental results in this research program showed a strong correlation between brace deformation capacity and global slenderness. Currently, there is no minimum *KL/r* requirement in the seismic provisions, but the implementation of one would help ensure ductility in braced frames. Experimental investigation into the cyclic performance of relatively stocky braces would provide the necessary data to reinforce the implementation of minimum *KL/r* limits.

BIBLIOGRAPHY

AISC (2010). "Specification for Structural Steel Buildings." ANSI/AISC 360-10, American Institute of Steel Construction, Chicago, IL.

AISC (2016). "Seismic Provisions for Structural Steel Buildings." ANSI/AISC 341-16, American Institute of Steel Construction, Chicago, IL.

AISC (Draft - 2022). Seismic Provisions for Evaluation and Retrofit of Existing Steel Structural Buildings." AISC 342, American Institute of Steel Construction, Chicago, IL.

ASCE (2017). "Seismic Evaluation and Retrofit of Existing Buildings." ASCE/SEI-17, American Society of Civil Engineers, Reston, VA.

ASTM (2007). "Standard Methods for Notched Bar Impact Testing of Metallic Materials." ASTM E23-07a, ASTM International, West Conshohocken, PA.

ASTM (2017). "Standard Test Methods and Definitions for Mechanical Testing of Steel Products." ASTM A370-17, ASTM International, West Conshohocken, PA.

ATC (1992). "Guidelines for Cyclic Seismic Testing of Components of Steel Structures for Buildings." Report ATC-24, Applied Technology Council, Redwood City, CA.

Bergendahl, W, (2021). “Experimental Investigation to Compare the Cyclic Response of A500 and A1085 HSS Braces.” MS Thesis, University of Washington, Seattle.

Bradley, C. R., Fahnestock, L. A., Hines, E. M., and Sizemore, J. G. (2017). "Full-Scale Cyclic Testing of Low-Ductility Concentrically Braced Frames." Journal of Structural Engineering, 143(6), 04017029.

Fell, B. V., Kanvinde, A. M., Deierlein, G. G., and Myers, A. T. (2009). "Experimental Investigation of Inelastic Cyclic Buckling and Fracture of Steel Braces." Journal of Structural Engineering, 135(1), 19-32.

Gugerli, H. and Goel, S. C. (1982). "Inelastic Cyclic Behavior of Steel Bracing Members." Report UMCE 82R1, University of Michigan, Ann Arbor.

Hsiao, P.-C. (2012). "Seismic Performance Evaluation of Concentrically Braced Frames." Phd Dissertation, University of Washington, Seattle.

Ibarra, S. M. (2018). "Experimental Investigation of Chevron Special Concentrically Braced Frames with a Yielding Beam Plastic Mechanism." MS Thesis, University of Washington, Seattle.

ICBO (1988.) Uniform Building Code. International Conference of Building Officials, Whittier, CA.

Krawinkler, H. (2009). Loading Histories for Cyclic Tests in Support of Performance Assessment of Structural Components.

Lee, S. (1988.) "Seismic Behavior of Hollow and Concrete-Filled Square Tubular Bracing Members, Report UMCE 87-11, University of Michigan, Ann Arbor.

Liu, Z. and Goel, S. C. (1987). "Investigation of Concrete-Filled Steel Tubes under Cyclic Bending and Buckling." PhD Dissertation, University of Michigan, Ann Arbor.

Roeder, C., W., Sen, A. D., Asada, H., Ibarra, S. M., Lehman, D. E., Berman, J. W., Tsai, K. C., Tsai, C. Y., Wu, A. C., Wang, K. J., and Liu, R. (2020). "Inelastic Behavior and Seismic Design of Multistory Chevron-Braced Frames with Yielding Beams." Journal of Constructional Steel Research, v. 167, p. 105817.

Roeder, C., W., Sen, A. D., Terpstra, C., Ibarra, S. M., Liu, R., Lehman, D. E., and Berman, J. W. (2019). "Effect of Beam Yielding on Chevron Braced Frames." Journal of Constructional Steel Research, v. 159, p. 428-441.

Sabelli, R., Roeder, C. W., and Hajjar, J. R. (2013). "Seismic Design of Steel Concentrically Braced Frame Systems." NEHRP Seismic Design Technical Brief No. 8, National Institute of Standards and Technology Engineering Laboratory, Gaithersburg, MD.

Shaback, B., and Brown, T. (2003). "Behaviour of Square Hollow Structural Steel Braces with End Connections Under Reversed Cyclic Axial Loading." Canadian Journal of Civil Engineering, v. 30, p. 745-753.

Swatosh, M. A. (2016), "Seismic Evaluation and Retrofit of Concentrically Braced Frames." MS Thesis, University of Washington, Seattle.

Terpstra, C. (2017). "Impact of Beam Strength on Seismic Performance of Chevron Concentrically Braced Frames." MS Thesis, University of Washington, Seattle.

Tremblay, R. (2002). "Inelastic Seismic Response of Steel Bracing Members." Journal of Constructional Steel Research, v. 58, p. 665-701.

Tremblay, R. (2008). "Inelastic Cyclic Testing of Large Size Steel Bracing Members." The 14th World Conference on Earthquake Engineering, Beijing, China.

Appendix A. TEST SETUP & SPECIMEN DRAWINGS

A.1 REACTION BLOCK DESIGN

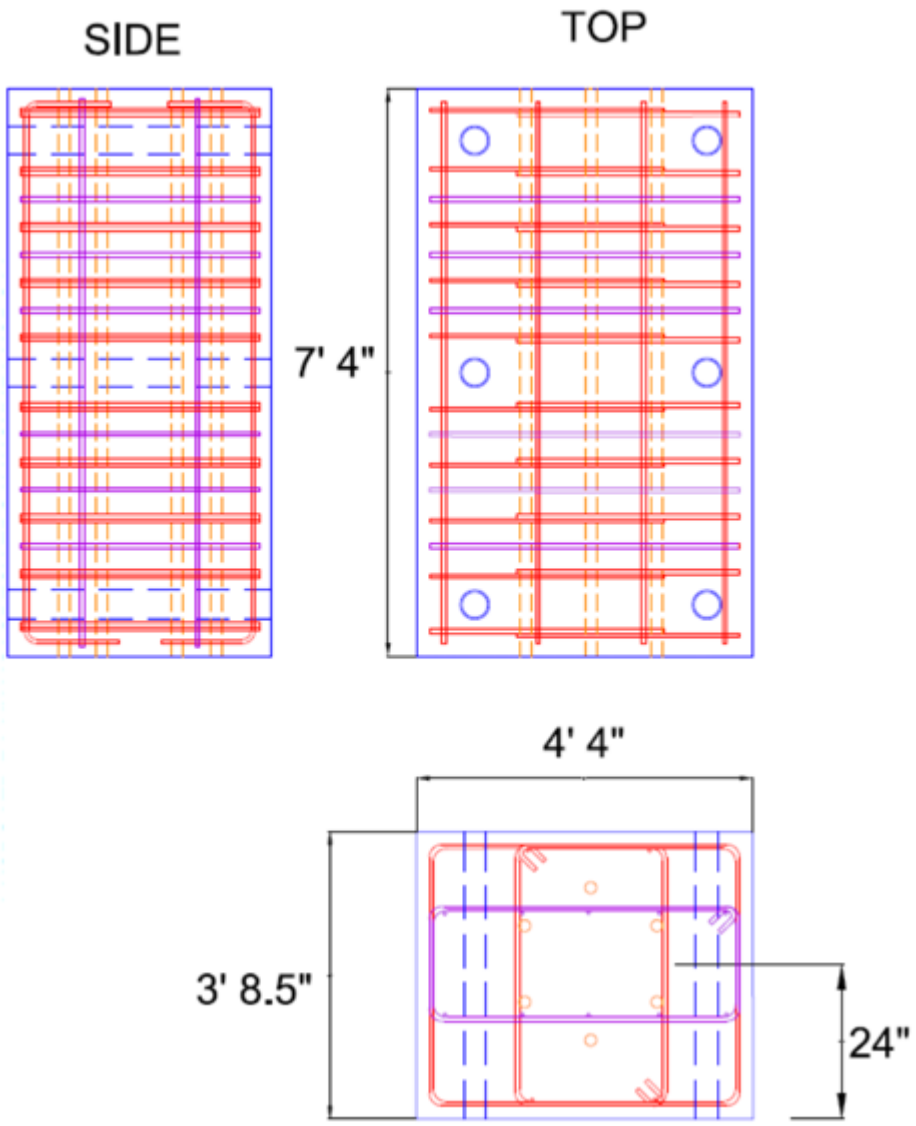

Figure A1.1: Existing Actuator Reaction Block and Rebar Layout – West Actuator

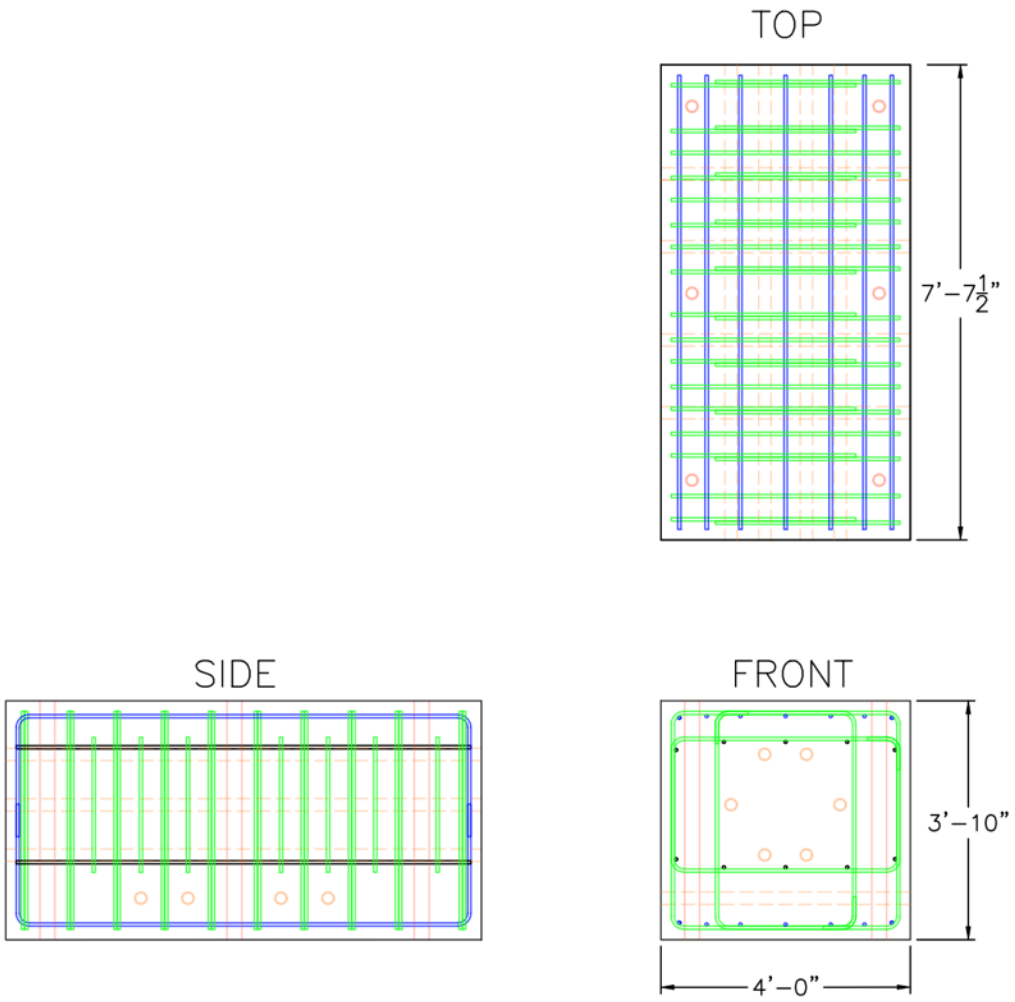

Figure A1.2: Actuator Reaction Block and Rebar Layout – East Actuator

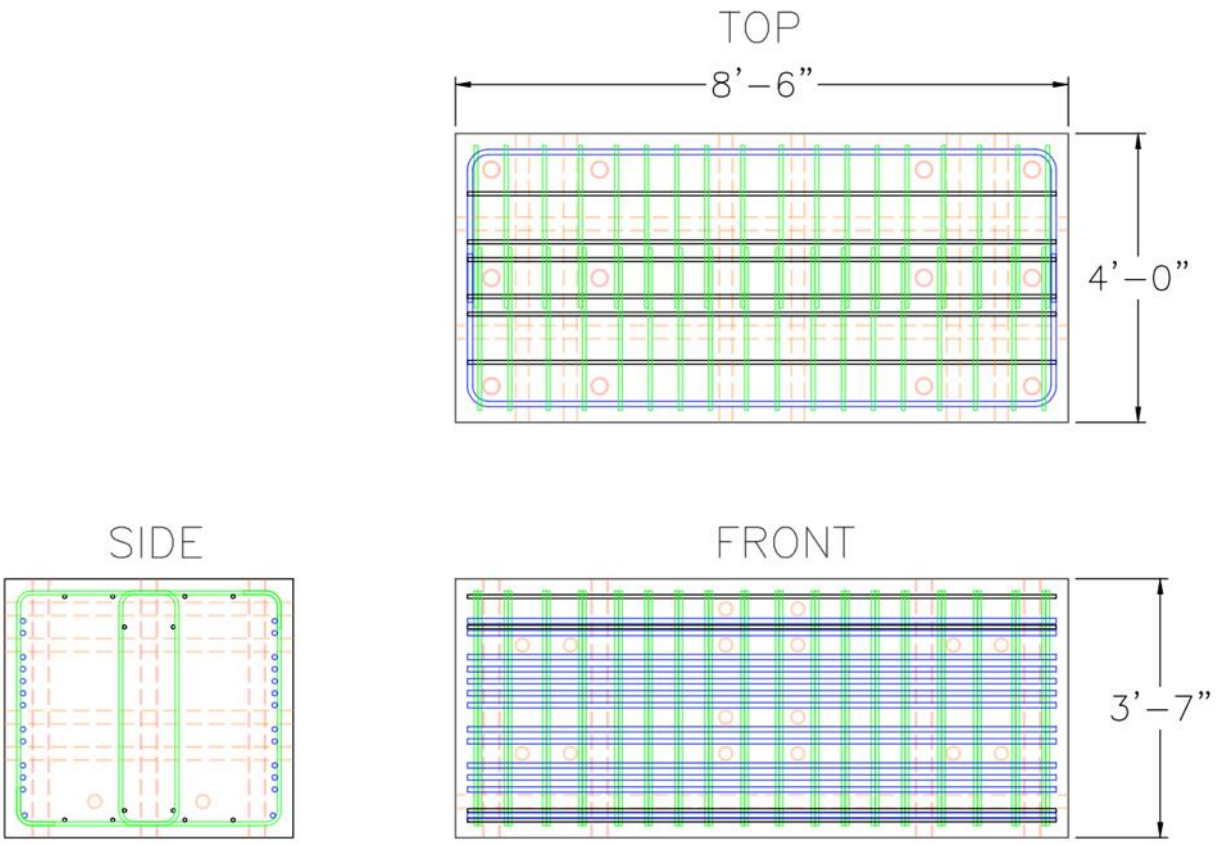

Figure A1.3: End Reaction Block and Rebar Layout

A.2 SLIDING BEAM & CONNECTION PLATE DESIGN

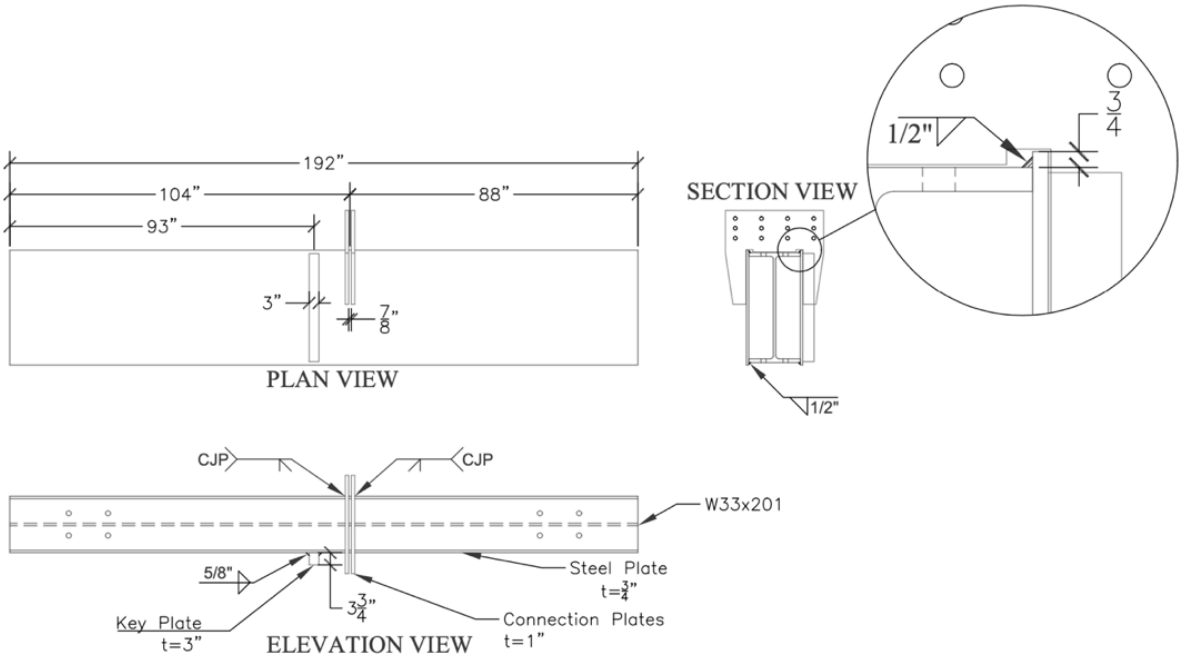

Figure A1.4: Sliding Beam Dimensions

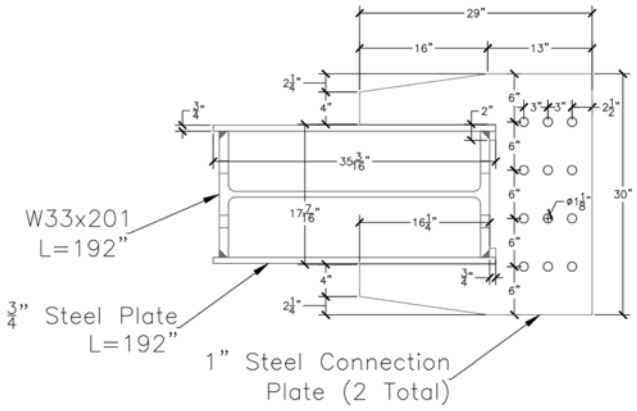

Figure A1.5: Sliding Beam and Connection Plate Cross Section

A.3 ACTUATOR BACKING PLATE DESIGN

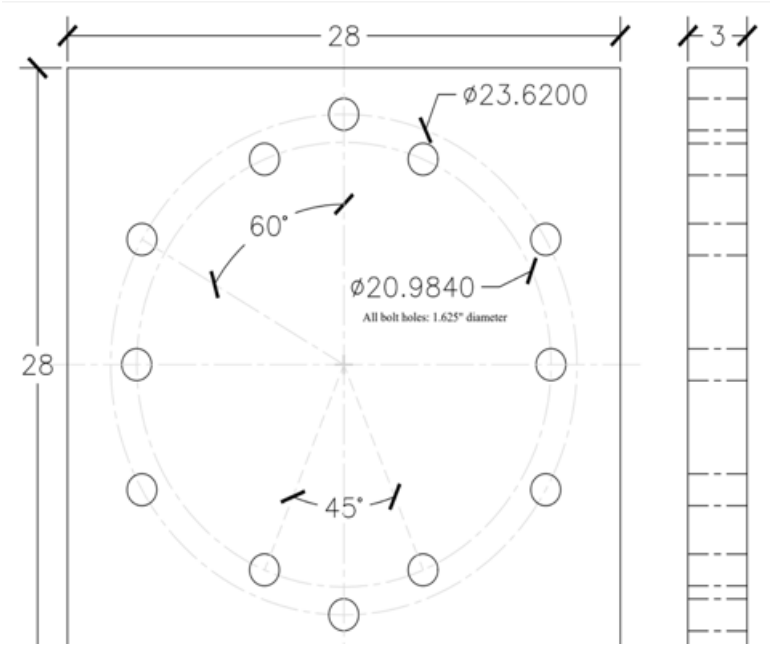

Figure A1.6: Actuator Backing Plate Dimensions

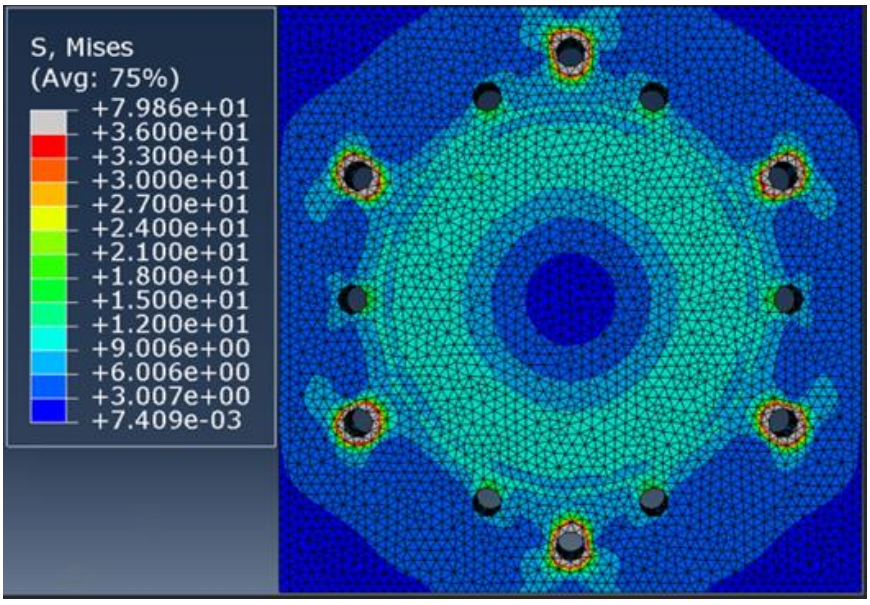

Figure A1.7: Actuator Backing ABAQUS Model

A.4 GUSSET PLATE DESIGN

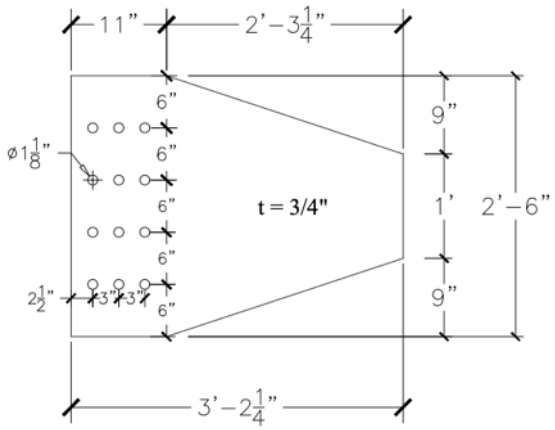

PL – 01

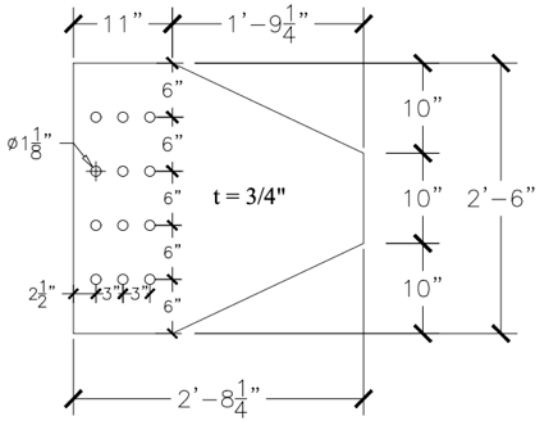

PL – 02

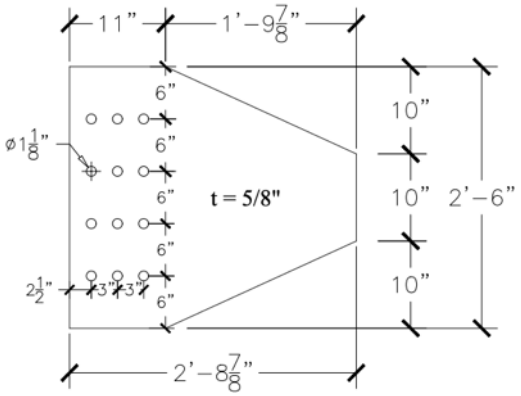

PL – 03

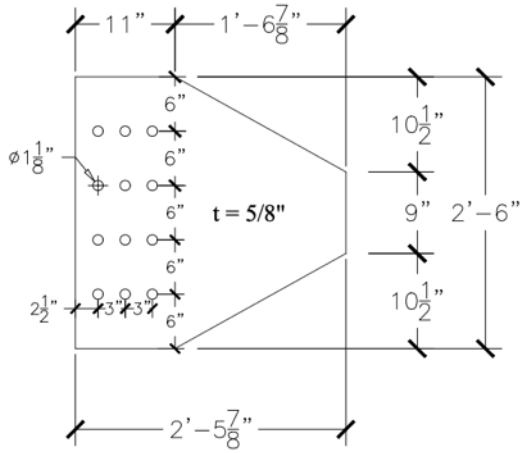

PL – 04

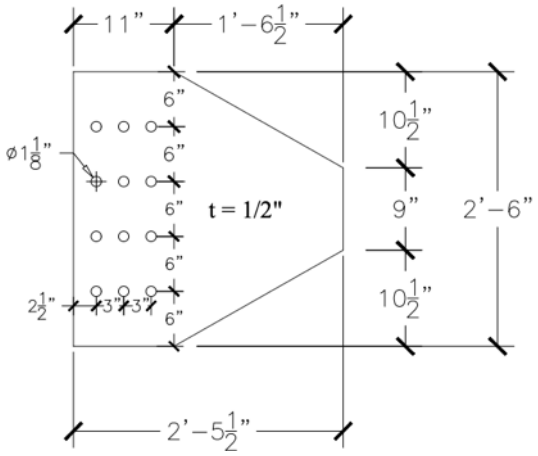

PL – 05

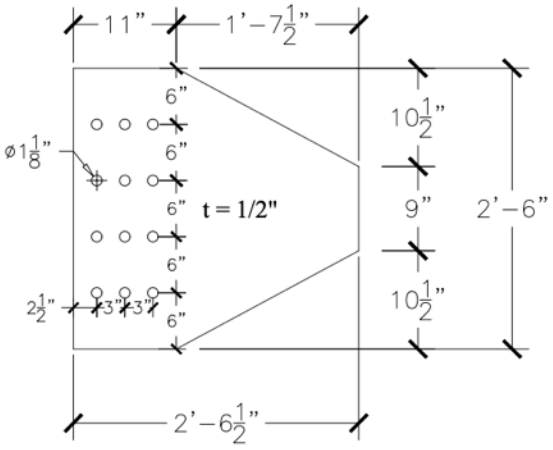

PL – 06

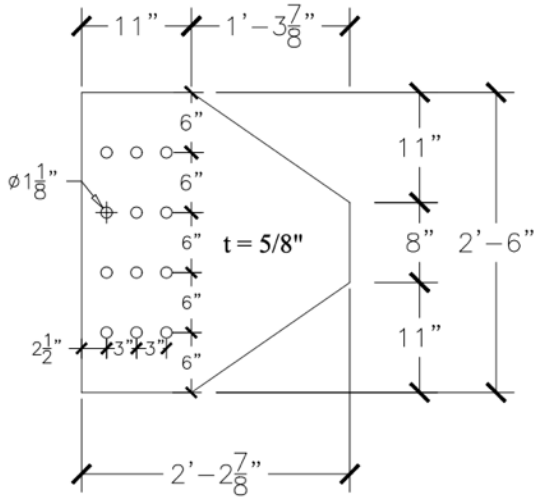

PL – 07

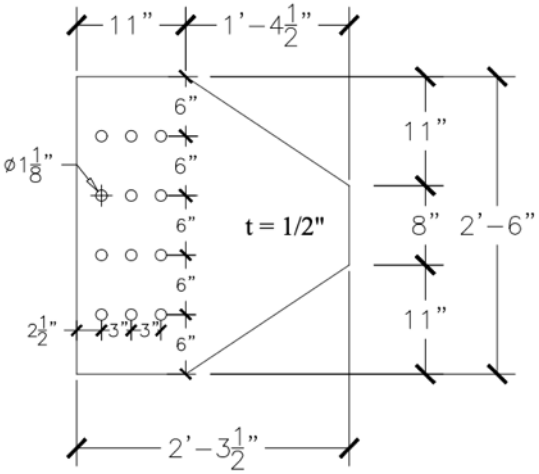

PL – 08

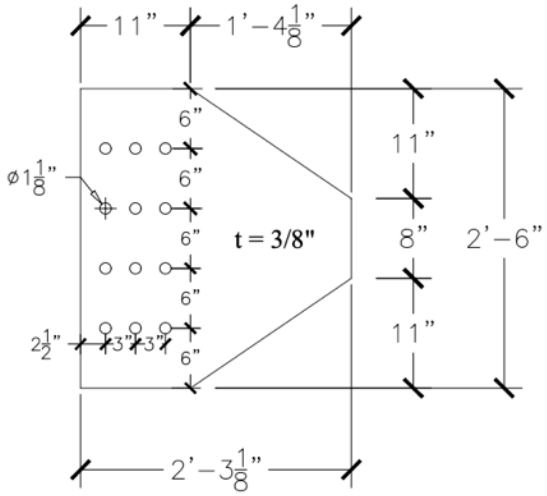

PL – 09

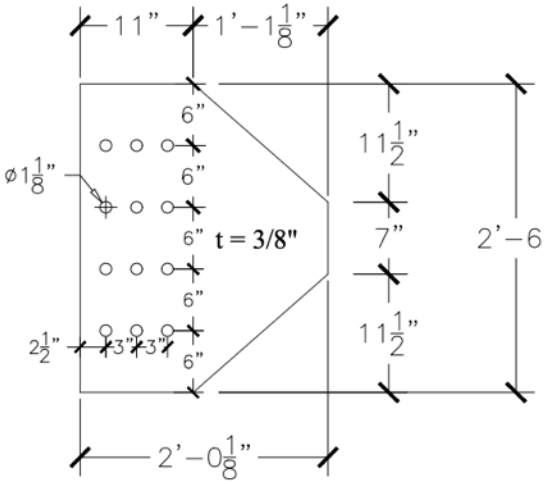

PL – 10

Appendix B. SAMPLE CALCULATIONS

B.1 SLIDING BEAM CALCULATIONS

Sliding Beam Design

$L\_Act := 63\ in$ Distance from 450 kip actuator to center of test specimen

$P\_max := 550\ kip$ Maximum force applied by 450 kip actuator in compression

$M\_u := L\_Act \cdot P\_max = 2887.5\ kip\ ft$ Maximum applied bending moment in sliding beam

$FS := 1.2$
$phi := 0.9$

$$M\_req := \frac{FS \cdot M\_u}{phi} = 3850\ kip\ ft$$

$$V\_req := \frac{(FS \cdot P\_max)}{phi} = 733.3333\ kip$$

W33x201 Sliding Beam

$f\_y := 50\ ksi$

$d\_b := 33.7\ in$

$S\_xb := 686\ in\ in\ in$

$M\_b := S\_xb \cdot f\_y = 2858.3333\ kip\ ft$ Yielding moment capacity of W33x201 beam

$t\_p := \frac{3}{4}\ in$

$$S\_xp := \frac{t\_p \cdot d\_b^{\,2}}{6} = 141.9612\ in^3$$

$M\_p := S\_xp \cdot f\_y = 591.5052\ kip\ ft$ Yielding moment capacity of 0.75" thick steel plate

$M\_sb := M\_b + 2 \cdot M\_p = 4041.3438\ kip\ ft$
$M\_sb = 4041.3438\ kip\ ft$ Total yielding moment capacity of sliding beam

$$FS\_M := \frac{FS \cdot M\_sb}{M\_req} = 1.2596$$

Shear Capacity

$V\_p := 0.6 \cdot f\_y \cdot (t\_p \cdot d\_b) = 758.25\ kip$ Shear capacity of 0.75" thick steel plate

$V\_b := 723\ kip$ Shear capacity of W33x201 beam

$V\_sb := 2 \cdot 0.9 \cdot V\_p + V\_b = 2087.85\ kip$ Total shear capacity of sliding beam

$$FS\_V := \frac{(FS \cdot V\_sb)}{V\_req} = 3.4165$$

Weld Design

$I\_b := 11600\ in^4$

$t\_p := 0.75\ in$

$I\_p := \frac{1}{12} \cdot t\_p \cdot d\_b^3 = 2392.0471\ in^4$

$I\_tot := I\_b + 2 \cdot I\_p = 16384.0941\ in^4$

$t\_f := 1.15\ in$

$b\_f := 15.7\ in$

$Q := \left(\left(d\_b - \frac{t\_f}{2} \right) \cdot (t\_f \cdot b\_f) \right) = 598.0719\ in^3$

$V := 540\ kip$

$q\_tot := \frac{(V \cdot Q)}{I\_tot} = 19.7117\ \frac{kip}{in}$ Shear flow q - distributed to each fillet weld

$q\_i := \frac{q\_tot}{2} = 9.8559\ \frac{kip}{in}$ Shear flow per fillet weld

$phi\_2 := 0.75$

$F\_e := 70\ ksi$

$t\_e := \frac{q\_i}{phi\_2 \cdot 0.60 \cdot F\_e} = 0.3129\ in$ Required effective throat of weld

$v := \frac{t\_e}{\frac{1}{\sqrt{2}}} = 0.4425\ in$ Required length of fillet weld leg

B.2 VERTICAL RESTRAINT CALCULATIONS

Stability Bracing Requirements

Treat brace specimen as a column: AISC Manual 16.1 Appendix 6

Section 6.2: Column Bracing

6.2.2: Nodal Bracing

$Pr := 1000\ kip$ Maximum axial force in column

$Pbr := 0.01 \cdot Pr = 10\ kip$ Required strength of point braces

$Nbr := 4$ Number of brace locations per end: 4 sets of vertical tie downs

$Nrod := 2$ Number of tie down rods per vertical tie down location

Required Strength

$P\_i := \frac{Pbr}{Nbr \cdot Nrod} = 1.25\ kip$ Minimum required clamping force/strength at each tie down

Using 1" 150 ksi Williams Bars: 0.6Pu = 76.5 kips

Required Stiffness

$phi := .75$

$Lbr := 21 \cdot 12\ in$ Unbraced Length (in) of test specimen

$Ebr := \frac{1}{phi} \cdot \left(8 \cdot \frac{Pr}{Lbr}\right) = 42.328\ \frac{kip}{in}$ Required stiffness of the point braces

Bracing at sliding beam end: Assume bottom sliding surface (HSS atop I-Beam connected to floor) is rigid relative to top constraint

$LI := 84\ in$ Horizontal length between clamping bars

$Lsb := 33\ in$ Width of sliding beam

Treating top beam as simply supported - upward force of beam applied at mid-span (worst case)

$E := 29000\ ksi$

1) 6x6x1/4 HSS sections above sliding beam: 4 along length of beam

$I\_1 := 28.6\ in^4$ $A\_1 := 5.24\ in^2$

$I\_1tot := 4 \cdot I\_1 = 114.4\ in^4$ Total moment of inertia of top beams

$Dmax\_1 := \frac{\left(Pbr \cdot LI^3\right)}{48 \cdot E \cdot I\_1tot} = 0.0372\ in$ Maximum deflection of top beams due to bending

$L\_r := 30\ in$ Length of 1" steel threaded rod connecting top and bottom HSS

$A\_r := 0.85\ in^2$ Area of 1" steel rod

$D2 := \frac{\left(Pbr \cdot L\_r\right)}{A\_r \cdot \left(2 \cdot Nbr\right) \cdot E} = 0.0015\ in$ Deflection due to axial elongation of 1" diamenter Williams rods

$B\_1 := \frac{Pbr}{Dmax\_1 + D2} = 258.1246\ \frac{kip}{in}$

$\frac{B\_1}{Ebr} = 6.0982$ Combined stiffness of top beams is adequate: Satisfies requirements

Section 6.3: Beam Bracing - Sliding Beam

6.3.1b: Nodal Bracing

Required Strength: EQ A-6-7

$Mr := 2835\ kip\ ft$ Required flexural strength per LRFD load combinations

$Mr = 34020\ kip\ in$

$Cd := 1.0$

$ho := 33.68\ in - 1.15\ in = 32.53\ in$ Distance between flange centroids

$Prb := \frac{0.02 \cdot Mr \cdot Cd}{ho} = 20.9161\ kip$ Required strength of sliding beam

Beam not subjected to double curvature bending

Required stiffness: EQ A-6-8

$B\_br := \frac{(10 \cdot Mr \cdot Cd)}{Lbr \cdot ho} = 41.5002\ \frac{kip}{in}$ Required stiffness of sliding beam

$L\_sb := 16\ ft = 192\ in$

$I\_sb := 16384\ in^4$ Total moment of inertia of sliding beam (including 3/4" plates but not concrete)

$D\_sb := \frac{\left(Pr \cdot L\_sb^3\right)}{48 \cdot E \cdot I\_sb} = 0.3103\ in$ Displacement of sliding beam from actuators' force

$B\_sb := \frac{Pr}{D\_sb} = 3222.2222\ \frac{kip}{in}$ Stiffness of sliding beam - OK - significantly exceeds required stiffness

B.3 KEYWAY PLATE DESIGN

Keyway Plate Design

$f_y := 36\ ksi$

$t := 3\ in$ Plate thickness

$w := 14\ in$ Plate width

$h := 14\ in$ Plate height

$h_1 := 2.5\ in$ Expected height of contact

$I := \frac{t \cdot w^3}{12} = 686\ in^4$

$W := \frac{t \cdot w^2}{6} = 98\ in^3$

$F := 80\ kip$ Predicted maximum horizontal load applied due to contact between key and keyway

$M := F \cdot h = 1120\ kip\ in$ Maximum bending moment due to applied force

$\sigma_{contact} := \frac{F}{h_1 \cdot t} = 10.6667\ ksi$ Bearing stress at point of contact

$\sigma_{moment} := \frac{M}{W} = 11.4286\ ksi$ Bending stress at base of keyway

Base Weld Design AISC SCM Table 8-4: Eccentrically Loaded Weld Groups Special Case - load not in plane of weld group

$e\_x := 14.375$ Maximum eccentricity of lateral force on keyway (in)

$P := 80$ Potential lateral force (kips)

$C\_1 := 1$ Electrode coefficient strength (E70XX electrodes)

$l\_w := 18$ Weld length (in - base of keyway)

$a := \frac{e\_x}{l\_w} = 0.7986$

$d\_w := 4\ in$ Lateral distance between welds

$k := 0$ Loads not in plane of weld

$C := 1.57$ Coefficient from Table 8-4

$phi := 1$

$D\_min := \frac{P}{phi \cdot C \cdot C\_1 \cdot l\_w} = 2.8309$ Required weld size

(Sixteenths of an inch)

$D := 0.4375$ Try 5/8" weld

$R\_n := C \cdot C\_1 \cdot D \cdot 16 \cdot l\_w = 197.82$ Nominal weld strength (kips)

B.4 CONNECTION DESIGN

Connection Design												
Required force	*Pc*	k	555.0	936.0	676.0	754.0	583.1	493.7	633.1	493.7	418.0	401.7
Yield stress	*Fy*	ksi	50	50	50	50	50	50	50	50	50	50
Tensile strength	*Fu*	ksi	62	62	62	62	62	62	62	62	62	62
Elastic modulus	*E*	ksi	29000	29000	29000	29000	29000	29000	29000	29000	29000	29000
Section	-	-	**HSS10x10x3/8**	**HSS8x8x1/2**	**HSS8x8x3/8**	**HSS7x7x1/2**	**HSS7x7x3/8**	**HSS7x7x5/16**	**HSS6x6x1/2**	**HSS6x6x3/8**	**HSS6x6x5/16**	**HSS5x5x3/8**
Effective length factor	*K*	-	1.0	1.0	1.0	1.0	1.0	1.0	1.0	1.0	1.0	1.0
Length	*L*	in	237.5	237.5	237.5	237.5	237.5	237.5	237.5	237.5	237.5	237.5
Radius of gyration	*r*	in	3.92	3.04	3.1	2.63	2.69	2.72	2.23	2.28	2.31	1.97
Global slenderness ratio	*lambda_g*	-	60.6	78.1	76.6	90.3	88.3	87.3	106.5	104.2	102.8	127.0
Local slenderness ratio	*lambda f*		25.6	14.2	13.9	12	17	21.1	9.31	14.2	17.6	11.9
Highly Ductile b/t limit	*lambda f limit*	-	13.7	13.7	13.7	13.7	13.7	13.7	13.7	13.7	13.7	13.7
Elastic buckling stress	*Fe*	ksi	78.0	46.9	48.8	35.1	36.7	37.5	25.2	26.4	27.1	17.7
Critical stress	*Fcr*	ksi	35.2	32.0	32.6	27.5	28.3	28.6	21.8	22.6	23.1	15.6
Gross area	*Ag*	in2	13.2	14.4	10.4	11.6	8.97	7.59	9.74	7.58	6.43	6.28
Critical buckling force	*Pcr*	k	505	461	335	320	254	217	212	171	148	96
Yield force	*Py*	k	660	720	520	580	449	380	487	379	322	309
Compression-tension force ratio	*beta*	-	0.76	0.64	0.65	0.55	0.57	0.57	0.44	0.45	0.46	0.31
Design overstrength			**1.70**	**2.03**	**2.00**	**2.36**	**2.30**	**2.27**	**2.98**	**2.87**	**2.82**	**4.18**
Brace width	*b*	in	10.000	8.000	8.000	7.000	7.000	7.000	6.000	6.000	6.000	5.000
Brace wall thickness	*t*	in	0.349	0.465	0.349	0.465	0.349	0.291	0.465	0.349	0.291	0.349
Brace splice connection length	*Lc,temp*	in	**22.0**	**18.0**	**17.4**	**14.5**	**15.0**	**15.2**	**12.2**	**12.7**	**12.9**	**10.3**
Design connection length	*Lc,des1*	in	25.0	19.0	20.0	17.0	17.0	18.0	16.0	15.0	15.0	12.0
Gusset plate width	*Bw*		38.666	29.939	31.094	26.630	26.630	27.785	24.475	25.321	25.321	18.856
Gusset plate thickness	*tp*	in	0.40	0.57	0.40	0.51	0.40	0.32	0.47	0.38	0.33	0.38
	tp,des	**in**	**0.750**	**0.750**	**0.625**	**0.625**	**0.500**	**0.500**	**0.625**	**0.500**	**0.375**	**0.375**
Controlling material thickness	*tmin*	in	0.349	0.465	0.349	0.465	0.349	0.291	0.465	0.349	0.291	0.349
Minimum weld size	*wmin*	in	0.19	0.19	0.19	0.19	0.19	0.19	0.19	0.19	0.19	0.19
Design weld size	*w*	in	0.375	0.625	0.500	0.500	0.500	0.500	0.500	0.438	0.438	0.375
Required weld length	*Lc,weld*	in	25.68	16.81	15.18	16.93	13.09	11.09	14.21	12.64	10.72	12.02
	RyFy	ksi	65	65	65	65	65	65	65	65	65	65
Brace end-to-end length	*l*	in	237.5	237.5	237.5	237.5	237.5	237.5	237.5	237.5	237.5	237.5
Global slenderness ratio	*lambda_g*		60.6	78.1	76.6	90.3	88.3	87.3	106.5	104.2	102.8	127.0
Euler buckling stress	*Fe*	ksi	78.0	46.9	48.8	35.1	36.7	37.5	25.2	26.4	27.1	17.7
Critical buckling stress	*Fcr*	ksi	45.9	38.4	37.2	29.9	31.0	31.5	22.1	23.1	23.7	15.6
Expected tensile capacity	***Pt***		**858**	**936**	**676**	**754**	**583**	**493**	**633**	**493**	**418**	**402**
Expected compressive capacity	***Pc***		**690.2**	**597.5**	**441.2**	**396.0**	**316.9**	**272.5**	**245.8**	**199.9**	**174.1**	**109.7**
Weld filler metal capacity		k	1114	1710	1168	1010	1010	1060	950	770	770	534
Weld base metal capacity		k	1483	1502	1187	1344	1009	841	1285	890	742	712
Weld filler metal DCR		-	0.77	0.66	0.57	0.75	0.58	0.46	0.67	0.63	0.54	0.75
Weld base metal DCR		-	0.58	0.62	0.57	0.56	0.58	0.65	0.50	0.55	0.56	0.56

Section	-	-	HSS10x10x3/8	HSS8x8x1/2	HSS8x8x3/8	HSS7x7x1/2	HSS7x7x3/8	HSS7x7x5/16	HSS6x6x1/2	HSS6x6x3/8	HSS6x6x5/16	HSS5x5x3/8
Block shear - shear plane gross	*Agv*	in^2	11.906	11.906	9.922	9.922	7.938	7.938	9.922	7.938	5.953	5.953
Block shear - shear plane net	*Anv*	in^2	8.531	8.531	7.109	7.109	5.688	5.688	7.109	5.688	4.266	4.266
Block shear tension plane	*Ant*	in^2	10.97	10.97	9.14	9.14	7.31	7.31	9.14	7.31	5.48	5.48
Bolt hole size		in	1.125	1.125	1.125	1.125	1.125	1.125	1.125	1.125	1.125	1.125
Gross area		in^2	22.50	22.50	18.75	18.75	15.00	15.00	18.75	15.00	11.25	11.25
Effective area		in^2	19.13	19.13	15.94	15.94	12.75	12.75	15.94	12.75	9.56	9.56
Yield strength		ksi	50	55	55	55	55	55	55	55	55	55
Tensile strength		ksi	65	70	70	70	70	70	70	70	70	70
Elastic modulus	*E*	ksi	29000	29000	29000	29000	29000	29000	29000	29000	29000	29000
Latteral stiffness (12E*I/L^3)			32,222	32,222	32,222	32,222	32,222	32,222	32,222	32,222	32,222	32,222
Gross yield resistance		kip	**1012.5**	**1113.8**	**928.1**	**928.1**	**742.5**	**742.5**	**928.1**	**742.5**	**556.9**	**556.9**
Utilization (brace/gusset)			*85%*	*84%*	*73%*	*81%*	*79%*	*66%*	*68%*	*66%*	*75%*	*72%*
Tensile rupture (net section)		kip	**932.3**	**1004.1**	**836.7**	**836.7**	**669.4**	**669.4**	**836.7**	**669.4**	**502.0**	**502.0**
Utilization (brace/gusset)			*92%*	*93%*	*81%*	*90%*	*87%*	*74%*	*76%*	*74%*	*83%*	*80%*
Bearing		kip	**810**	**891**	**742.5**	**742.5**	**594**	**594**	**742.5**	**594**	**445.5**	**445.5**
Utilization (brace/gusset)			*106%*	*105%*	*91%*	*102%*	*98%*	*83%*	*85%*	*83%*	*94%*	*90%*
Gusset plate block shear		kip	**784.3**	**844.6**	**703.8**	**703.8**	**563.1**	**563.1**	**703.8**	**563.1**	**422.3**	**422.3**
Utilization (brace/gusset)			*109%*	*111%*	*96%*	*107%*	*104%*	*88%*	*90%*	*88%*	*99%*	*95%*
Failure in net shear			1045.7	1126.1	938.4	938.4	750.8	750.8	938.4	750.8	563.1	563.1
Failure in gross shear			1070.2	1160.7	967.3	967.3	773.8	773.8	967.3	773.8	580.4	580.4
Tearout		kip	**998.2**	**1074.9**	**895.8**	**895.8**	**716.6**	**716.6**	**895.8**	**716.6**	**537.5**	**537.5**
Utilization (brace/gusset)			*86%*	*87%*	*75%*	*84%*	*81%*	*69%*	*71%*	*69%*	*78%*	*75%*
Clear distance, edge		in	1.9375	1.9375	1.9375	1.9375	1.9375	1.9375	1.9375	1.9375	1.9375	1.9375
Clear distance, bolt hole		in	1.875	1.875	1.875	1.875	1.875	1.875	1.875	1.875	1.875	1.875
Gusset plate buckling			**981.0**	**1075.7**	**896.4**	**896.4**	**717.1**	**717.1**	**896.4**	**717.1**	**537.9**	**537.9**
Utilization (brace/gusset)			*70%*	*56%*	*49%*	*44%*	*44%*	*38%*	*27%*	*28%*	*32%*	*20%*
Global slenderness ratio	*lambda_g*		20.8	20.8	20.8	20.8	20.8	20.8	20.8	20.8	20.8	20.8
Elastic buckling sterss	*Fe*	ksi	662.5	662.5	662.5	662.5	662.5	662.5	662.5	662.5	662.5	662.5
Critical buckling stress	*Fcr*	ksi	48.4	53.1	53.1	53.1	53.1	53.1	53.1	53.1	53.1	53.1

Section	-	-	HSS10x10x3/8	HSS8x8x1/2	HSS8x8x3/8	HSS7x7x1/2	HSS7x7x3/8	HSS7x7x5/16	HSS6x6x1/2	HSS6x6x3/8	HSS6x6x5/16	HSS5x5x3/8
Bolt limit states												
Bolt type	*Bolt type*	-	A490	A490	A490	A490	A490	A490	A490	A490	A490	A490
Bolt size	*Bolt size*	-	1	1	1	1	1	1	1	1	1	1
Shear location			Shaft	Shaft	Shaft	Shaft	Shaft	Shaft	Shaft	Shaft	Shaft	Shaft
Number of shear planes			2	2	2	2	2	2	2	2	2	2
Surface class		-	Class B	Class B	Class B	Class B	Class B	Class B	Class B	Class B	Class B	Class B
Number of slip planes	n_s	-	2	2	2	2	2	2	2	2	2	2
Number of fillers		-	1	1	1	1	1	1	1	1	1	1
Mean installed bolt pretension to the specified minimum	D_u		1.13	1.13	1.13	1.13	1.13	1.13	1.13	1.13	1.13	1.13
Number of bolts		n	12	12	12	12	12	12	12	12	12	12
Number of bolt rows		n	3	3	3	3	3	3	3	3	3	3
Gross bolt area		in^2	0.785	0.785	0.785	0.785	0.785	0.785	0.785	0.785	0.785	0.785
Net tensile area		in^2	0.606	0.606	0.606	0.606	0.606	0.606	0.606	0.606	0.606	0.606
Minimum bolt pretension		kip	64	64	64	64	64	64	64	64	64	64
Nominal tensile strength		kip	113	113	113	113	113	113	113	113	113	113
Nominal shear strength		kip	84	84	84	84	84	84	84	84	84	84
Mean slip coefficient		-	0.5	0.5	0.5	0.5	0.5	0.5	0.5	0.5	0.5	0.5
Factor for fillers	h_f	-	1	1	1	1	1	1	1	1	1	1
Slip resistance		kip	**867.84**	**867.84**	**867.84**	**867.84**	**867.84**	**867.84**	**867.84**	**867.84**	**867.84**	**867.84**
Utilization (brace/connection)			*99%*	*108%*	*78%*	*87%*	*67%*	*57%*	*73%*	*57%*	*48%*	*45%*
Bolt shear resistance		kip	**1186.92**	**1186.92**	**1186.92**	**1186.92**	**1186.92**	**1186.92**	**1186.92**	**1186.92**	**1186.92**	**1186.92**
Utilization (brace/connection)			*72%*	*79%*	*57%*	*64%*	*49%*	*42%*	*53%*	*42%*	*35%*	*34%*
Gusset plate calculations												
Steel type		-	A572-50	A572-55	A572-55	A572-55	A572-55	A572-55	A572-55	A572-55	A572-55	A572-55
Width min			38.968	29.939	31.094	26.630	26.630	27.785	24.475	23.321	23.321	19.856
Thickness min			0.401	0.368	0.395	0.315	0.398	0.323	0.470	0.384	0.326	0.387
Width		in	**30.000**	**30.000**	**30.000**	**30.000**	**30.000**	**30.000**	**30.000**	**30.000**	**30.000**	**30.000**
Thickness		in	0.750	0.750	0.625	0.625	0.500	0.500	0.625	0.500	0.375	0.375
Unsupported length		in	2.250	2.250	1.875	1.875	1.500	1.500	1.875	1.500	1.125	1.125
Effective length factor	K		2.000	2.000	2.000	2.000	2.000	2.000	2.000	2.000	2.000	2.000
Effective length	L_c		4.500	4.500	3.750	3.750	3.000	3.000	3.750	3.000	2.250	2.250
Second moment of area		in^4	1.055	1.055	0.610	0.610	0.313	0.313	0.610	0.313	0.132	0.132
Radius of gyration		in	0.217	0.217	0.180	0.180	0.144	0.144	0.180	0.144	0.108	0.108
Edge distance parallel		in	2.500	2.500	2.500	2.500	2.500	2.500	2.500	2.500	2.500	2.500
Edge distance perpendicular		in	6.000	6.000	6.000	6.000	6.000	6.000	6.000	6.000	6.000	6.000
Bolt spacing parallel		in	3.000	3.000	3.000	3.000	3.000	3.000	3.000	3.000	3.000	3.000
Bolt spacing perpendicular		in	6.000	6.000	6.000	6.000	6.000	6.000	6.000	6.000	6.000	6.000
Tension stress distribution factor		-	1.000	1.000	1.000	1.000	1.000	1.000	1.000	1.000	1.000	1.000

SAMPLE CONNECTION CALCULATION:

6x6x1/2 A500 HSS

Section Properties

Yield stress	F_y	ksi	50
Tensile strength	F_u	ksi	62
Yield Strength Factor	R_y		1.3
Ultimate Strength Factor	R_t		1.2
Elastic modulus	E	ksi	29000
Effective length factor	K	-	1.0
Length	L	in.	237.5
Radius of gyration	r	in.	2.23
Global slenderness ratio	λ_g	-	106.5
Local slenderness ratio	λ_l	-	9.9
Gross area	A_g	in^2	9.74
Brace width	B	in.	6
Wall thickness	t_{des}	in.	0.465

Expected Forces

$P_y = R_y \cdot F_y \cdot A_y = 1.3 \cdot 50 \cdot 9.74 = 633\ kips$ [Expected Yield Force]

$$4.71 \cdot \sqrt{\frac{E}{R_y F_y}} = 4.71 \cdot \sqrt{\frac{29000}{1.3 \cdot 50}} = 113.4$$

$\frac{KL}{r} = 106.5 < 113.4$

$F_e = \frac{(\pi^2 \cdot E)}{\frac{KL}{r}} = 25.23\ ksi$ [Elastic Critical Stress]

$F_{cr} = 0.658^{\frac{R_y \cdot F_y}{F_e}} \cdot R_y \cdot F_y = 22.13\ ksi$ [Critical Buckling Stress]

$P_{cr} = F_{cr} \cdot A_g = 215.6\ kips$ [Critical Buckling Force]

Weld Design

$L_{c,min} = \frac{P_y}{0.75 \cdot 0.6 \cdot F_u \cdot 4 \cdot t_{des}} = 12.2\ in.$ [Minimum brace connection length]

$L_{c,des} = 15.875\ in.$ [Design brace connection length]

$w_{GP,min} = 2 \cdot B \cdot tan(30) + L_{c,des} = 22.17\ in.$ [Minimum gusset plate width]

$w_{GP,des} = 30\ in.$ [Design gusset plate width]

$t_{GP,min} = \frac{P_y}{55 \cdot 2 \cdot L_{c,des} \cdot tan(30) + B} = 0.52\ in.$ [Minimum gusset plate thickness]

$t_{GP,des} = 0.625\ in.$ [Design gusset plate thickness]

$t_{min} = min(t_{GP,des}, t_{des}) = 0.465\ in.$ [Controlling material thickness]

$w_{min} = \frac{3}{16}\ in.$ [Minimum weld size]

$w_{des} = 0.50\ in.$ [Design fillet weld size]

$n_w = 4$ [Number of fillet welds]

$L_{c,w} = \frac{P_y}{n_w \cdot \Phi \cdot 0.6 \cdot F_{EXX} \cdot 0.707 \cdot w_{des}}$ [Required weld length]

$= \frac{633\ kips}{4 \cdot 0.75 \cdot 0.6 \cdot 70\ ksi \cdot 0.707 \cdot 0.5\ in.} = 14.1\ in.$

$R_f = 0.6 \cdot F_{EXX} \cdot 0.707 \cdot w_{des} \cdot n_w \cdot L_{c,des}$ [Weld filler metal capacity]

$= 0.6 \cdot 70\ ksi \cdot 0.707 \cdot 0.5" \cdot 15.875" = 943\ kips$

$DCR_{Filler\ Metal} = \frac{P_y}{R_f} = \frac{633\ kips}{943\ kips} = 0.67$ [OK]

$R_b = 0.6 \cdot 1.1 \cdot R_y F_y \cdot n_w \cdot w_{des} \cdot L_{c,des}$ [Weld base metal capacity]

$= 0.6 \cdot 1.1 \cdot 1.3 \cdot 50\ ksi \cdot 4 \cdot 0.5" \cdot 15.875" = 1255\ kips$

$DCR_{Base\ Metal} = \frac{P_y}{R_b} = \frac{633\ kips}{11255\ kips} = 0.50$ [OK]

Bolt Design

Bolt Properties

Bolt Type			A490
Shear Location			Shaft
Surface Class			Class B
Number of Bolts	n_b		12
Number of Shear Planes	n_v		2
Number of Slip Planes	n_s		2
Mean Slip Coefficient	c_s		0.5
Number of Fillers	n_f		1
Filler Factor	h_f		1.0
Mean Bolt Pretension Ratio	D_u		1.13
Bolt Size	d_b	in.	1
Minimum Bolt Pretension	$F_{t,b}$	kips	64
Gross Bolt Area	$A_{g,b}$	in^2	0.785
Net Tensile Area	$A_{n,b}$	in^2	0.606
Nominal Tensile Strength	F_{nt}	kips	113
Nominal Shear Strength	F_{nv}	kips	84

$\Phi R_{n,s} = c_s \cdot D_u \cdot h_f \cdot F_{nt} \cdot n_s \cdot n_b$ [Slip Resistance]

$= 0.5 \cdot 1.13 \cdot 1.0 \cdot 64\ kips \cdot 2 \cdot 12 = 868\ kips$

$DCR_{slip} = \frac{P_y}{\Phi R_s} = \frac{633\ kips}{868\ kips} = 0.72$ [OK]

$\Phi R_{n,v} = \Phi \cdot A_{n,b} \cdot F_{nv} \cdot n_v \cdot n_b$ [Bolt Shear Resistance]

$= 0.75 \cdot 0.606\ in^2 \cdot 113\ kips \cdot 2 \cdot 12 = 1187\ kips$

$$DCR_{shear} = \frac{P_y}{\Phi R_n} = \frac{633\ kips}{1187\ kips} = 0.53$$ [OK]

Gusset Plate Design

Gusset Plate Properties

Width	w_{GP}	in.	30
Thickness	t_{GP}	in.	0.625
Yield Strength	$F_{y,GP}$	ksi	55
Tensile Strength	$F_{u,GP}$	ksi	70
Unsupported Length	$L_{u,GP}$	in.	1.875
Effective Length Factor	K_{GP}	-	2
Effective Length	$L_{c,GP}$	in.	3.75
Moment of Inertia	$I_{GP,y}$	in^4	0.61
Radius of Gyration	$r_{GP,y}$	in.	0.18
Bolt Hole Diameter	d_{bh}	in.	1.125
Number of Bolts	n_b		12
Number of Bolt Rows	n_{br}		3
Number of Bolt Columns	n_{bc}		4
Edge Distance - Horizontal	l_{eh}	in.	2.5
Edge Distance - Vertical	l_{ev}	in.	6
Bolt Spacing – Horizontal	l_{bh}	in.	3
Bolt Spacing - Vertical	l_{bv}	in.	6

$$A_{gv} = 2\left(l_{eh} + (n_{br} - 1) \cdot l_{bh} - \frac{d_{bh}}{2}\right) \cdot t_{GP}$$ [Block Shear Plane – Gross Area]

$$= 2 \cdot \left(2.5" + (3 - 1) \cdot 3" - \frac{1.25"}{2}\right) \cdot 0.625" = 9.92\ in^2$$

$$A_{nv} = 2 \cdot \left(\left(l_{eh} - \frac{d_{bh}}{2}\right) + (n_{br} - 1) \cdot (l_{bh} - d_{bh})\right) \cdot t_{GP}$$ [Block Shear Plane – Net Area]

$$= 2 \cdot \left(\left(2.5" - \frac{1.25"}{2}\right) + (3 - 1) \cdot (3" - 1.25")\right) \cdot 0.625 = 7.11\ in^2$$

$$A_{nt} = (l_{bv} - d_{bh}) \cdot \left(\frac{n_b}{n_{br}} - 1\right) \cdot t_{GP}$$ [Block Shear Tension Plane]

$$= (6" - 1.25") \cdot \left(\frac{12}{3} - 1\right) \cdot 0.625" = 9.14\ in^2$$

$A_{g,GP} = w_{GP} \cdot t_{GP} = 30" \cdot 0.625" = 18.75\ in^2$ [Gusset Plate Gross Area]

$A_{e,GP} = \left(w_{GP} - (d_{bh} \cdot n_{bc})\right) \cdot t_{GP}$ [Gusset Plate Net Area]

$= \left(30" - (1.25" \cdot 4)\right) \cdot 0.625" = 15.94\ in^2$

$K_{GP} = \frac{(12 \cdot E \cdot I_{GP,y})}{L_{u,GP}{}^3} = \frac{(12 \cdot 29000\ ksi \cdot 0.61\ in^4)}{(1.875\ in)^3} = 32200 \frac{k}{in}$ [Gusset Plate Lateral Stiffness]

$\Phi R_{n,y} = \Phi \cdot F_{y,GP} \cdot A_{g,GP}$ [Gross Yield Strength]

$= 0.9 \cdot 55\ ksi \cdot 18.75\ in^2 = 928.1\ kips$

$DCR_y = \frac{P_y}{\Phi R_{n,y}} = \frac{633\ kips}{928.1\ kips} = 0.68$ [OK]

$\Phi R_{n,t} = \Phi \cdot F_{u,GP} \cdot A_{n,GP}$ [Tensile Rupture Strength]

$= 0.75 \cdot 70\ ksi \cdot 15.94\ in^2 = 836.7\ kips$

$DCR_t = \frac{P_y}{\Phi R_{n,t}} = \frac{633\ kips}{836.7\ kips} = 0.75$ [OK]

$\Phi R_{n,b} = 1.2 \cdot l_{eh} \cdot t_{GP} \cdot F_u \leq 2.4 \cdot d_b \cdot t_{GP} \cdot F_u$

$= 1.2 \cdot 2.5" \cdot 0.625" \cdot 70\ ksi = 131\ kips > 2.4 \cdot 1" \cdot 0.625" \cdot 70\ ksi = 105\ kips$

$\Phi R_{n,b} = \Phi \cdot 2.4 \cdot t_{GP} \cdot d_b \cdot F_{y,GP} \cdot n_b$ [Bearing Strength]

$= 0.75 \cdot 2.4 \cdot 0.625" \cdot 1" \cdot 55\ ksi \cdot 12 = 742.5\ kips$

$DCR_b = \frac{P_y}{\Phi R_{n,b}} = \frac{633\ kips}{742.5\ kips} = 0.84$ [OK]

$R_{n,bsn} = 0.6 \cdot F_{u,GP} \cdot A_{nv} + 1.0 \cdot F_{u,GP} \cdot A_{nt}$ [Block Shear – Net Section]

$= 0.6 \cdot 70\ ksi \cdot 7.11\ in^2 + 1.0 \cdot 70\ ksi \cdot 9.14\ in^2 = 938.4\ kips$

$R_{n,bsg} = 0.6 \cdot F_{y,GP} \cdot A_{gv} + 1.0 \cdot F_{u,GP} \cdot A_{nt}$ [Block Shear – Gross Section]

$= 0.6 \cdot 55\ ksi \cdot 9.92\ in^2 + 1.0 \cdot 70\ ksi \cdot 9.14\ in^2 = 967.3\ kips$

$\Phi R_{n,bs} = 0.75 \cdot min\left(R_{n,bsn}, R_{n,bsg}\right)$ [Block Shear Strength]

$= 0.75 \cdot 938.4\ kips = 703.8\ kips$

$DCR_{bs} = \frac{P_y}{\Phi R_{n,bs}} = \frac{633\ kips}{703.8\ kips} = 0.89$ [OK]

$l_{c,bh} = l_{bh} - d_{bh} = 3" - 1.25" = 1.875"$ [Clear Distance – Bolt Hole]

$l_{c,e} = l_{eh} - \frac{d_{bh}}{2} = 2.5" - \frac{1.125"}{2} = 1.94"$ [Clear Distance – Edge]

$$\Phi R_{n,to} = \Phi 1.2 \cdot F_{u,GP} \cdot t_{GP} \left(l_{c,e} \left(\frac{n_b}{n_{br}} \right) + l_{c,bh} \left(\frac{n_b}{n_{br}} \right) (n_{br} - 1) \right) \quad \text{[Tearout Strength]}$$

$$= 0.75 \cdot 1.2 \cdot 70\ ksi \cdot 0.625" \left(1.94" \left(\frac{12}{3} \right) + 1.875" \left(\frac{n_b}{n_{br}} \right) (3 - 1) \right) = 895.8\ kips$$

$$DCR_{to} = \frac{P_y}{\Phi R_{n,to}} = \frac{633\ kips}{895.8\ kips} = 0.70 \quad \text{[OK]}$$

$$\lambda_g = \frac{l_{c,GP}}{r_{GP,y}} = \frac{3.75"}{0.18"} = 20.8 \quad \text{[Global Slenderness Ratio]}$$

$$F_{e,GP} = \frac{(\pi^2 \cdot E)}{\lambda_g{}^2} = \frac{(\pi^2 \cdot 29000\ ksi)}{20.8^2} = 662.5\ ksi \quad \text{[Elastic Critical Stress]}$$

$$4.71\sqrt{\frac{E}{F_{y,GP}}} = 4.71\sqrt{\frac{29000\ ksi}{55\ ksi}} = 108.2 \qquad \lambda_g < 108.2$$

$$F_{cr,GP} = 0.658^{\left(\frac{E}{F_{y,GP}}\right)} \cdot F_{y,GP} \quad \text{[Critical Buckling Stress]}$$

$$= 0.658^{\left(\frac{29000\ ksi}{55\ ksi}\right)} \cdot 55\ ksi = 53.1\ ksi$$

$$\Phi R_{n,bk} = \Phi \cdot A_{g,GP} \cdot F_{cr,GP} \quad \text{[Gusset Plate Buckling Strength]}$$

$$= 0.9 \cdot 18.75\ in^2 \cdot 53.1\ ksi = 896.4\ kips$$

$$DCR_{bk} = \frac{P_{cr}}{\Phi R_{n,bk}} = \frac{215.6\ kips}{896.4\ kips} = 0.27 \quad \text{[OK]}$$

B.5 NET SECTION REINFORCEMENT DESIGN

Net Section Reinforcement Plate Design

HSS Shape	Thickness (in.)	Width (in.)	Length (in.)	Weld Size (in.)
10x10x3/8	3/8	5.25	24	1/4
8x8x1/2	3/8	5.25	24	1/4
8x8x3/8	3/8	4.25	20	1/4
7x7x1/2	3/8	4.25	20	1/4
7x7x3/8	3/8	4.25	20	1/4
7x7x5/16	3/8	3.25	18	1/4
6x6x1/2	3/8	3.25	18	1/4
6x6x3/8	3/8	3.25	18	1/4
6x6x5/16	3/8	3.25	18	1/4
5x5x3/8	3/8	2.75	16	1/4

SAMPLE NET SECTION REINFORCEMENT CALCULATION:

6x6x1/2 A500 HSS

Section Properties

Yield stress	F_y	ksi	50
Tensile strength	F_u	ksi	62
Yield Strength Factor	R_y		1.3
Ultimate Strength Factor	R_t		1.2
Elastic modulus	E	ksi	29000
Gross area	A_g	in^2	9.74
Brace width	B	in.	6
Wall thickness	t_{des}	in.	0.465
Gusset Plate Width	w_{GP}	in.	0.625
Workable Flat Width	w_f	in.	3.75

$w_s = w_{GP} + 0.125" = 0.625" + 0.125" = 0.75"$ [Slot Width]

$A_{nb} = A_g - 2 \cdot t_{des} \cdot w_s$ [Net Area at Slot]

$= 9.74\ in^2 - 2 \cdot 0.465" \cdot 0.75" = 9.04\ in^2$

$w_{f,a} = w_f - 2 \cdot \frac{w_{des}}{16} = 3.75" - 2 \cdot \frac{4}{16} = 3.25"$ [Available Flat Width]

$b_{cp} = 3.25"$ [Design Cover Plate Width]

$t_{cp} = 0.375"$ [Design Cover Plate Thickness]

$A_{cp} = b_{cp} \cdot t_{cp} = 1.22\ in^2$ [Cover Plate Area]

$L_{cp} = 18"$ [Design Cover Plate Length]

$\underline{x} = \frac{(B^2+2B^2)}{4(2B)} = \frac{(3\cdot(6\ in.)^2)}{4\cdot(2\cdot 6\ in)} = 2.25"$ [Connection Eccentricity]

$U = 1 - \frac{\underline{x}}{L_{cp}} = 1 - \frac{2.25"}{18"} = 0.875"$ [Shear Lag Factor]

Net Section Rupture Limit State

$A_e = U(A_{nb} + 2 \cdot A_{cp})$ [Section Effective Net Area]

$= 0.875(9.04\ in^2 + 2 \cdot 1.22\ in^2) = 10.1\ in^2$

$\frac{A_g}{A_e} = \frac{9.74\ in^2}{10.1\ in^2} = 0.97$ [OK: $A_e > A_g$]

Longitudinal Weld Design

Cover Plate & Fillet Weld Properties

Yield stress	$F_{y,cp}$	ksi	50
Yield Strength Factor	$R_{y,cp}$		1.1
Cover Plate Width	b_{cp}	in.	3.25
Cover Plate Thickness	t_{cp}	in.	0.375
Cover Plate Area	A_{cp}	in^2	1.22
Cover Plate Length	L_{cp}	in.	18
Weld Size	*D*	16ths of an in.	4

Weld Length	L_w	in.	16
Weld Electrode Strength	F_{EXX}	ksi	70
Number of Welds per Plate	n_w		2

$P_{y,cp} = R_{y,cp} \cdot F_{y,cp} \cdot A_{cp}$ [Expected Cover Plate Yield Force]

$= 1.1 \cdot 50\ ksi \cdot 1.22\ in^2 = 67\ kips$

$\Phi R_{n,w} = 1.392 \cdot D \cdot \frac{L_w}{2} \cdot n_w$ [Cover Plate Weld Strength]

$$= 1.392 \cdot 4 \cdot \frac{18"}{2} \cdot 2 = 100.2\ kips$$

$DCR_w = \frac{P_{y,cp}}{\Phi R_{n,w}} = \frac{67\ kips}{100.2\ kips} = 0.67$ [OK: $\Phi R_{n,w} > P_{y,cp}$]

Net Section Reinforcement Plate Design

Test Specimen	$Thickness$ **(in.)**	$Width$ **(in.)**	**Length (in.)**	**Weld Size (in.)**
6x6x1/2 A500 R	3/8	3.25	18	1/4

B.6 AISC 342 NONLINEAR ANALYSIS PROCEDURE – 5X5X3/8 A1085 Y HSS

Material and Geometric Properties

$$E = 29000\ ksi$$

$$A_g = 6.58\ in^2$$

$$F_{ye} = R_y F_y = 1.25 \cdot 50\ ksi = 62.5\ ksi$$

$$L_c = K \cdot L_b = 1.0 \cdot 237.5\ in = 237.5\ in.$$

$$r = 1.86\ in.$$

$$F_e = \frac{\pi^2 E}{\left(\frac{L_c}{r}\right)^2} = 17.55\ ksi$$

$$F_{cre} = \left(0.658^{\left(\frac{F_{ye}}{F_e}\right)}\right) \cdot F_{ye} = 15.39\ ksi$$

$$\lambda = \frac{b}{t} = 10.3$$

$$\lambda_{hd} = 0.65 \cdot \sqrt{\frac{E}{F_{ye}}} = 0.65 \cdot \sqrt{\frac{29000\ ksi}{62.5\ ksi}} = 14.0$$

Expected strengths and yield deformations

$$P_{ye} = F_{ye} \cdot A_g = 62.5\ ksi \cdot 6.58\ in^2 = 411.3\ k$$

$$P_{ce} = F_{cre} \cdot A_g = 15.39\ ksi \cdot 6.58\ in^2 = 101.3\ k$$

$$\Delta_T = \frac{(P_{ye} \cdot L_c)}{A_g \cdot E} = \frac{(411.3\ k \cdot 237.5\ in.)}{6.58\ in^2 \cdot 29000\ ksi} = 0.51\ in.$$

$$\Delta_C = \frac{(P_{ce} \cdot L_c)}{A_g \cdot E} = \frac{(101.3\ k \cdot 237.5\ in.)}{6.58\ in^2 \cdot 29000\ ksi} = 0.13\ in$$

Nonlinear Analysis

For tension of a rectangular HSS brace:

$$n = 4.7 \cdot \left(\frac{\lambda}{\lambda_{hd}}\right)^{-0.99} \cdot \left(\frac{\left(\frac{L_c}{r}\right)}{\sqrt{\frac{E}{F_{ye}}}}\right)^{0.24} = 4.7 \cdot \left(\frac{10.3}{14.0}\right)^{-0.99} \left(\frac{\left(\frac{237.5\ in.}{1.86\ in.}\right)}{\sqrt{\frac{29000\ ksi}{62.5\ ksi}}}\right)^{0.24} = 9.76$$

For compression of a rectangular HSS brace:

$$n = 3.0 \cdot \left(\frac{\lambda}{\lambda_{hd}}\right)^{-0.96} \cdot \left(\frac{\left(\frac{L_c}{r}\right)}{\sqrt{\frac{E}{F_{ye}}}}\right)^{1.0} = 3.0 \cdot \left(\frac{10.3}{14.0}\right)^{-0.96} \cdot \left(\frac{\left(\frac{237.5\ in.}{1.86\ in.}\right)}{\sqrt{\frac{29000\ ksi}{62.5\ ksi}}}\right)^{1.0} = 23.88$$

For tension of a rectangular HSS brace:

$$d = n \cdot \Delta_T = 9.76 \cdot 0.53\ in. = 5.00\ in.$$

$$f = 1.0$$

$$f \cdot P_{ye} = 1.0 \cdot P_{ye} = 1.0 \cdot 411.3\ k = 411.3\ k$$

Acceptance Criteria:

IO: $1.5 \cdot \Delta_T = 1.5 \cdot 0.51\ in. = 0.77\ in.$

LS: $0.7 \cdot n \cdot \Delta_T = 0.7 \cdot 9.76 \cdot 0.51\ in. = 3.50\ in$

CP: $n \cdot \Delta_T = 9.76 \cdot 0.51\ in. = 5.00\ in.$

For compression of a rectangular HSS brace:

$$d = n \cdot \Delta_C = 23.88 \cdot 0.13\ in. = 3.01\ in.$$

$$f = 0.2$$

$$f \cdot P_{ce} = 0.2 \cdot P_{ce} = 0.2 \cdot 101.3\ k = 20.3\ k$$

Acceptance Criteria:

IO: $1.5 \cdot \Delta_C = 1.5 \cdot 0.13\ in. = 0.19\ in.$

LS: $0.7 \cdot n \cdot \Delta_C = 0.7 \cdot 23.88 \cdot 0.13\ in. = 2.11\ in.$

CP: $n \cdot \Delta_C = 23.88 \cdot 0.13\ in. = 3.10\ in.$

Action	Modeling Parameters		Performance Level Criteria		
	d (in.)	$f \cdot P\ (k)$	IO (in.)	LS (in.)	CP (in.)
Tension	5.00	411.3	0.77	3.50	5.00
Compression	3.01	20.3	0.19	2.11	3.01

Modelling Parameters and Predicted Performance

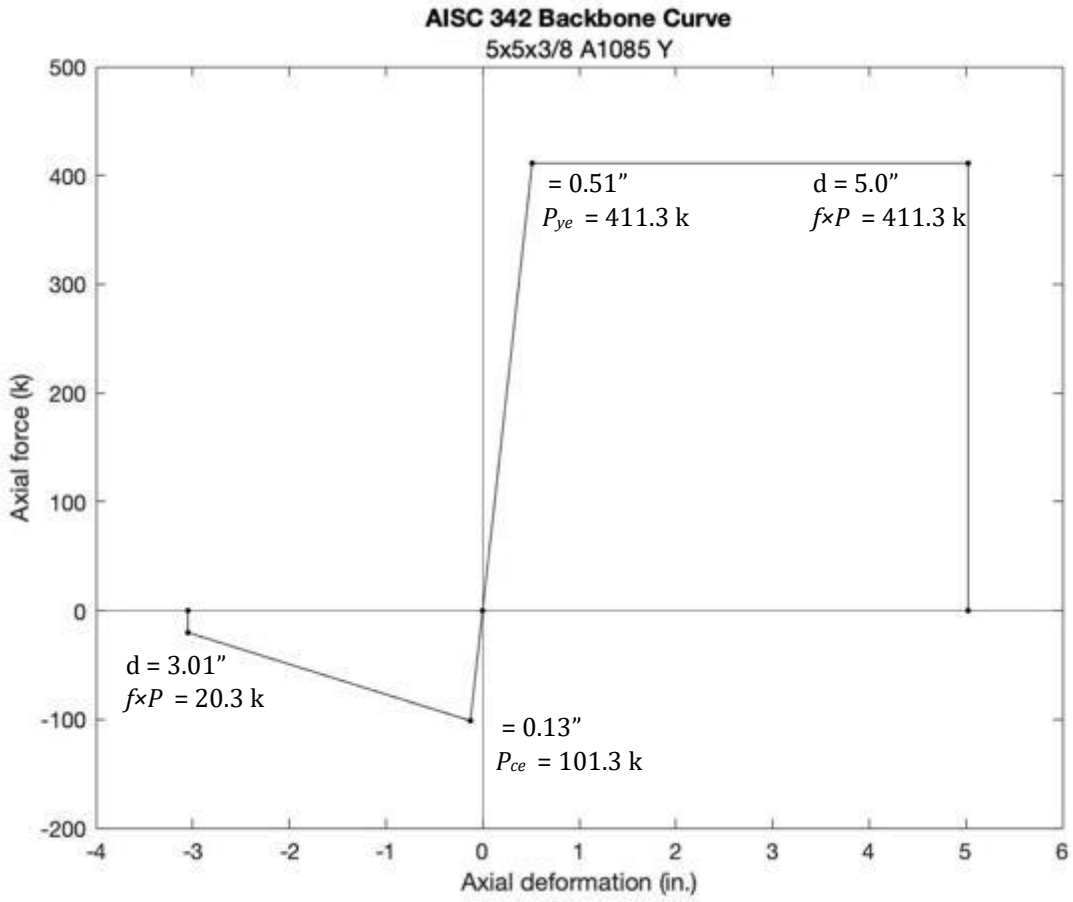
AISC 342 Backbone Curve
5x5x3/8 A1085 Y
= 0.51”
P_{ye} = 411.3 k
d = 5.0”
$f \times P$ = 411.3 k
d = 3.01”
$f \times P$ = 20.3 k
= 0.13”
P_{ce} = 101.3 k
Axial force (k)
Axial deformation (in.)
500
400
300
200
100
0
-100
-200
-4
-3
-2
-1
0
1
2
3
4
5
6

Appendix C. APPENDIX 3: MATERIAL PROPERTIES

C.1 TENSION COUPON INFORMATION AND RESULTS

			Measured Thickness				Measured Width				Cross Sectional	Yield		Ultimate		Initial Gauge	Final Gauge	% Elongation	
Producer	Material	Shape	1 (in)	2 (in)	3 (in)	Avg (in)	1 (in)	2 (in)	3 (in)	Avg (in)	Area (in^2)	Stress (ksi)	Average (ksi)	Stress (ksi)	Average (ksi)	Length (in)	Length (in)	% Elongation	Average
RED	A1085	8x8x1/2	0.458	0.457	0.457	0.457	1.506	1.504	1.501	1.504	0.688	ERROR	58.54	63.99	64.27	2.1746	2.925	34.51	34.43
			0.457	0.457	0.457	0.457	1.499	1.5	1.498	1.499	0.685	58.54		64.54		2.1524	2.892	34.36	
RED	A1085	8x8x3/8	0.366	0.366	0.366	0.366	1.495	1.495	1.496	1.495	0.547	59.08	61.2	73.39	75.42	2.1509	2.872	33.53	32.44
			0.365	0.366	0.364	0.365	1.5	1.502	1.499	1.500	0.548	63.32		77.45		2.2033	2.894	31.35	
RED	A1085	6x6x3/8	0.368	0.368	0.368	0.368	1.5	1.501	1.501	1.501	0.552	60.78	60.405	74.78	74.29	2.145	2.858	33.24	33.26
			0.367	0.367	0.367	0.367	1.5	1.501	1.5	1.500	0.551	60.03		73.80		2.1227	2.829	33.27	
RED	A1085	5x5x3/8	0.367	0.367	0.369	0.368	1.492	1.494	1.495	1.494	0.549	68.78	68.815	77.61	77.52	1.9807	2.6691	34.76	34.92
			0.367	0.367	0.368	0.367	1.499	1.499	1.499	1.499	0.551	68.85		77.43		2.0146	2.7213	35.08	
BLUE	A500	7x7x3/8	0.344	0.341	0.342	0.342	1.502	1.502	1.502	1.502	0.514	59.8	59.04	68.77	68.49	1.9999	2.72177	36.10	35.92
			0.343	0.343	0.343	0.343	1.502	1.503	1.503	1.503	0.515	58.28		68.21		2.004	2.7203	35.74	
BLUE	A1085	8x8x1/2	0.501	0.5	0.498	0.500	1.5	1.498	1.497	1.498	0.749	67.27	66.355	71.06	70.51	1.9886	2.7582	38.70	39.56
			0.497	0.497	0.496	0.497	1.5	1.5	1.5	1.500	0.745	65.44		69.95		1.997	2.8043	40.43	
BLUE	A1085	8x8x3/8	0.374	0.373	0.374	0.374	1.502	1.502	1.501	1.502	0.561	69.23	68.235	72.10	71.63	2.004	2.7548	37.47	37.18
			0.376	0.377	0.376	0.376	1.501	1.502	1.502	1.502	0.565	67.24		71.15		2.0236	2.7704	36.90	
BLUE	A1085	6x6x3/8	0.374	0.374	0.375	0.374	1.501	1.501	1.501	1.501	0.562	68.55	69.05	73.21	73.59	1.9982	2.6959	34.92	34.75
			0.373	0.373	0.375	0.374	1.501	1.502	1.501	1.501	0.561	69.55		73.98		2.002	2.6944	34.59	
BLUE	A1085	5x5x3/8	0.377	0.377	0.376	0.377	1.495	1.496	1.496	1.496	0.563	78.35	78.145	87.65	87.62	2.001	2.5596	27.92	27.90
			0.379	0.379	0.38	0.379	1.499	1.499	1.499	1.499	0.569	77.94		87.59		2.0007	2.5585	27.88	
WHITE	A1085	8x8x1/2	0.487	0.486	0.486	0.486	1.502	1.502	1.501	1.502	0.730	66.15	66.15	73.12	73.08	2.012	2.8685	42.57	42.02
			0.487	0.488	0.489	0.488	1.498	1.499	1.5	1.499	0.732	ERROR		73.03		2.0222	2.861	41.48	
WHITE	A1085	8x8x3/8	0.368	0.368	0.366	0.367	1.492	1.492	1.491	1.492	0.548	63.12	63.185	70.93	70.67	1.9926	2.8056	40.80	40.55
			0.371	0.372	0.372	0.372	1.506	1.506	1.505	1.506	0.560	63.25		70.42		2.0125	2.8234	40.29	
WHITE	A1085	6x6x3/8	0.375	0.375	0.375	0.375	1.499	1.5	1.5	1.500	0.562	68.32	67.66	74.00	73.22	2	2.7428	37.14	37.53
			0.375	0.375	0.374	0.375	1.495	1.496	1.497	1.496	0.561	67		72.43		2.0054	2.766	37.93	
WHITE	A1085	5x5x3/8	0.37	0.369	0.371	0.370	1.499	1.498	1.497	1.498	0.554	69.19	69.525	74.46	75.03	2.0002	2.772	38.59	38.06
			0.367	0.366	0.367	0.367	1.497	1.497	1.498	1.497	0.549	69.86		75.59		2.018	2.7755	37.54	

			Measured Thickness				Measured Width				Cross Sectional	Yield		Ultimate		Initial Gauge	Final Gauge	% Elongation	
Producer	Material	Shape	1 (in)	2 (in)	3 (in)	Avg (in)	1 (in)	2 (in)	3 (in)	Avg (in)	Area (in^2)	Stress (ksi)	Average (ksi)	Stress (ksi)	Average (ksi)	Length (in)	Length (in)	% Elongation	Average
YELLOW	A500	5x5x3/8	0.344	0.344	0.344	0.344	1.497	1.498	1.497	1.497	0.515	65.07	65.38	72.48	71.86	2.07	2.71	30.95	30.79
			0.344	0.343	0.342	0.343	1.499	1.496	1.497	1.497	0.514	65.69		71.23		2.10	2.74	30.63	
YELLOW	A1085	5x5x3/8	0.366	0.362	0.358	0.359	1.502	1.502	1.5	1.501	0.539	65.34	66.04	74.84	74.62	1.79	2.37	32.18	32.83
			0.363	0.361	0.362	0.362	1.496	1.496	1.495	1.496	0.541	66.74		74.40		1.85	2.47	33.48	
RED	A500	6x6x5/16	0.29	0.29	0.289	0.290	1.498	1.497	1.498	1.498	0.434	60.2	57.37	74.23	72.77	2.06	2.78	34.77	34.65
			0.289	0.289	0.289	0.289	1.492	1.492	1.491	1.492	0.431	54.54		71.32		2.08	2.80	34.52	
YELLOW	A1085	6x6x5/16	0.309	0.309	0.308	0.309	1.505	1.504	1.504	1.504	0.464	62.62	62.07	71.72	71.93	2.05	2.77	35.07	34.11
			0.306	0.305	0.306	0.306	1.492	1.493	1.492	1.492	0.456	61.52		72.14		2.07	2.75	33.15	
RED	A500	6x6x3/8	0.353	0.353	0.354	0.353	1.496	1.496	1.495	1.496	0.528	62.43	61.19	76.46	76.36	2.06	2.78	35.42	35.36
			0.352	0.354	0.355	0.354	1.494	1.494	1.494	1.494	0.528	59.95		76.27		2.04	2.76	35.31	
YELLOW	A1085	6x6x3/8	0.369	0.367	0.368	0.368	1.496	1.497	1.497	1.497	0.551	66.9	66.81	72.85	72.64	2.05	2.68	31.08	31.86
			0.37	0.371	0.368	0.370	1.498	1.498	1.498	1.498	0.554	66.72		72.43		2.06	2.73	32.64	
RED	A500	6x6x1/2	0.466	0.462	0.459	0.462	1.495	1.495	1.494	1.495	0.691	63.59	62.84	68.30	67.05	2.06	2.71	31.46	33.48
			0.457	0.46	0.461	0.459	1.493	1.494	1.495	1.494	0.686	62.09		65.81		2.07	2.81	35.49	
YELLOW	A1085	6x6x1/2	0.487	0.484	0.483	0.485	1.504	1.502	1.503	1.503	0.728	67.6	67.85	71.61	71.96	2.07	-	-	34.88
			0.486	0.485	0.487	0.486	1.52	1.522	1.521	1.521	0.739	68.1		72.31		2.06	2.78	34.88	
YELLOW	A500	7x7x5/16	0.29	0.293	0.289	0.291	1.496	1.497	1.498	1.497	0.435	61.76	62.71	70.14	70.02	2.06	2.64	28.53	31.16
			0.294	0.292	0.292	0.293	1.497	1.497	1.498	1.497	0.438	63.66		69.89		2.07	2.76	33.79	
YELLOW	A1085	7x7x5/16	0.303	0.304	0.304	0.304	1.495	1.496	1.495	1.495	0.454	57.14	57.695	64.08	64.13	LASER EXT ISSUE			33.12
			0.302	0.302	0.302	0.302	1.498	1.502	1.502	1.501	0.453	58.25		64.18		2.08	2.77	33.12	
YELLOW	A500	7x7x3/8	0.341	0.341	0.342	0.341	1.495	1.496	1.495	1.495	0.510	62.03	61.35	71.80	72.19	2.10	2.74	30.59	30.76
			0.342	0.342	0.341	0.342	1.493	1.494	1.493	1.493	0.510	60.67		72.57		2.07	2.71	30.93	
YELLOW	A1085	7x7x3/8	0.366	0.365	0.369	0.367	1.497	1.498	1.498	1.498	0.549	62.19	61.89	70.19	70.07	2.12	2.79	31.32	31.32
			0.362	0.363	0.365	0.363	1.491	1.492	1.491	1.491	0.542	61.58		69.94		LASER EXT ISSUE			
BLUE	A500	7x7x1/2	0.457	0.457	0.457	0.457	1.496	1.496	1.496	1.496	0.684	58.09	57.82	69.14	69.14	2.10	2.73	29.90	29.60
			0.457	0.455	0.455	0.456	1.495	1.496	1.497	1.496	0.682	57.54		69.14		2.09	2.71	29.30	
YELLOW	A1085	7x7x1/2	0.48	0.483	0.478	0.480	1.495	1.496	1.495	1.495	0.718	63.74	64.38	71.98	71.68	2.06	2.75	33.25	32.70
			0.486	0.486	0.486	0.486	1.495	1.496	1.497	1.496	0.727	65.01		71.37		2.08	2.75	32.15	
WHITE	A500	8x8x3/8	0.345	0.345	0.345	0.345	1.5	1.499	1.499	1.499	0.517	66.02	66.19	75.67	76.52	2.03	2.75	35.18	34.44
			0.348	0.348	0.346	0.347	1.49	1.492	1.492	1.491	0.518	66.36		77.36		2.06	2.75	33.69	
YELLOW	A1085	8x8x3/8	0.341	0.342	0.341	0.341	1.497	1.496	1.499	1.497	0.511	60.61	60.37	73.69	72.12	2.04	2.75	35.08	34.20
			0.342	0.344	0.343	0.343	1.494	1.495	1.495	1.495	0.513	60.12		70.55		2.08	2.77	33.33	
WHITE	A500	8x8x1/2	0.46	0.462	0.46	0.461	1.498	1.499	1.499	1.499	0.690	65.92	65.47	72.04	72.01	2.09	2.78	33.12	34.27
			0.457	0.457	0.457	0.457	1.495	1.495	1.494	1.495	0.683	65.02		71.98		2.08	2.82	35.43	
YELLOW	A1085	8x8x1/2	0.481	0.484	0.482	0.482	1.492	1.493	1.493	1.493	0.720	62.26	64.42	74.53	75.43	2.11	2.80	32.83	32.23
			0.485	0.484	0.484	0.484	1.498	1.495	1.495	1.496	0.725	66.57		76.33		2.08	2.74	31.64	
WHITE	A500	10x10x3/8	0.349	0.349	0.35	0.349	1.494	1.494	1.495	1.494	0.522	60.93	59.02	70.61	69.45	2.11	2.75	30.11	34.20
			0.349	0.349	0.349	0.349	1.494	1.494	1.494	1.494	0.521	57.11		68.30		2.07	2.86	38.29	
YELLOW	A1085	10x10x3/8	0.362	0.363	0.371	0.365	1.498	1.498	1.499	1.498	0.547	58.07	58.34	70.47	73.76	2.06	2.77	34.22	34.94
			0.36	0.362	0.364	0.362	1.495	1.497	1.495	1.496	0.541	58.61		77.05		2.08	2.83	35.66	

C.2 YIELD STRENGTH PROPERTIES

HSS Section	Measured Yield Stress $F_{y,m}$ (ksi)	Measured Yield Strength Ratio $R_{y,meas}$	Expected Yield Stress $F_{y,nom}R_{y,nom}$ (ksi)
5x5x3/8 A500 Y	65.38	1.31	65
5x5x3/8 A1085 Y	66.04	1.32	62.5
6x6x5/16 A500 R	57.37	1.15	65
6x6x5/16 A1085 Y	62.07	1.24	62.5
6x6x3/8 A500 R	61.19	1.22	65
6x6x3/8 A1085 Y	66.81	1.34	62.5
6x6x1/2 A500 R	62.84	1.26	65
6x6x1/2 A1085 Y	67.85	1.36	62.5
7x7x5/16 A500 Y	62.71	1.25	65
7x7x5/16 A1085 Y	57.70	1.15	62.5
7x7x3/8 A500 Y	61.35	1.23	65
7x7x3/8 A1085 Y	61.89	1.24	62.5
7x7x1/2 A500 B	57.82	1.16	65
7x7x1/2 A1085 Y	64.38	1.29	62.5
8x8x3/8 A500 W	66.19	1.32	65
8x8x3/8 A1085 Y	60.37	1.21	62.5
8x8x1/2 A500 W	65.47	1.31	65
8x8x1/2 A1085 Y	64.42	1.29	62.5
10x10x3/8 A500 W	59.02	1.18	65
10x10x3/8 A1085 Y	58.34	1.17	62.5
5x5x3/8 A1085 R	68.82	1.38	62.5
5x5x3/8 A1085 W	69.53	1.39	62.5
5x5x3/8 A1085 B	78.145	1.56	62.5
6x6x3/8 A1085 R	60.405	1.21	62.5
6x6x3/8 A1085 W	67.66	1.35	62.5
6x6x3/8 A1085 B	69.05	1.38	62.5
8x8x3/8 A1085 R	61.2	1.22	62.5
8x8x3/8 A1085 W	63.185	1.26	62.5
8x8x3/8 A1085 B	68.235	1.36	62.5
8x8x1/2 A1085 R	58.54	1.17	62.5

C.3 CHARPY V-NOTCH TEST RESULTS

Temperature	40 deg F				Sub-Size: 7.5 mm	
Setting	Energy (120 ft-lbs)				Sub-Size: 5 mm	
			CVN Specimen Size	Absorbed Energy (ft-lbs)		
Producer	Material	Shape	Thickness (mm)	Individual	Average	
YELLOW	A500	5x5x3/8	7.5	11.5	12.8	
				12.5		
				14.5		
YELLOW	A1085	5x5x3/8	7.5	19.5	18.8	
				20.5		
				16.5		
RED	A500	6x6x5/16	5	42	40.8	
				41		
				39.5		
YELLOW	A1085	6x6x5/16	5	21	23.0	
				22.5		
				25.5		
RED	A500	6x6x3/8	7.5	40	42.5	
				47		
				40.5		
YELLOW	A1085	6x6x3/8	7.5	11	18.7	
				23		
				22		
RED	A500	6x6x1/2	10	120	120.0	120+
				120		120+
				120		120+
YELLOW	A1085	6x6x1/2	10	27	27.8	
				24.5		
				32		
YELLOW	A500	7x7x5/16	5	17.5	15.7	
				17.5		
				12		
YELLOW	A1085	7x7x5/16	5	21	18.5	
				22		
				12.5		
YELLOW	A500	7x7x3/8	7.5	13.5	14.3	
				15.5		
				14		
YELLOW	A1085	7x7x3/8	7.5	18.5	17.3	
				16.5		
				17		
BLUE	A500	7x7x1/2	10	45.5	42.0	
				42.5		
				38		
YELLOW	A1085	7x7x1/2	10	29	28.7	
				29		
				28		
WHITE	A500	8x8x3/8	7.5	73	65.5	
				62		
				61.5		
YELLOW	A1085	8x8x3/8	7.5	8.5	8.5	
				7		
				10		
WHITE	A500	8x8x1/2	10	49.5	67.3	
				81		
				71.5		
YELLOW	A1085	8x8x1/2	10	45	40.3	
				38		
				38		
WHITE	A500	10x10x3/8	7.5	120	120.0	120+
				120		120+
				120		120+
YELLOW	A1085	10x10x3/8	7.5	20	20.7	
				20.5		
				21.5		
Yellow	A1085	8x8x1/2	10	98.5	89.5	
				102		
				68		
White	A500	8x8x1/2	10	120	103.3	120+
				120		120+
				70		

Temperature	40 deg F				Sub-Size: 7.5 mm	
Setting	Energy (120 ft-lbs)				Sub-Size: 5 mm	
			CVN Specimen Size	Absorbed Energy (ft-lbs)		
Producer	Material	Shape	Thickness (mm)	Individual	Average	
YELLOW	A500	7x7x1/2	10	15.5	15.17	
				15		
				15		
RED	A1085	8x8x1/2	10	120	120.00	120+
				120		120+
				120		120+
RED	A1085	8x8x3/8	7.5	47	58.33	
				61		
				67		
RED	A1085	6x6x3/8	7.5	43	40.50	
				36		
				42.5		
RED	A1085	5x5x3/8	7.5	20	23.17	
				28.5		
				21		
BLUE	A500	7x7x3/8	7.5	76	76.17	
				70.5		
				82		
BLUE	A500	7x7x5/16	5	39.5	38.83	
				37		
				40		
BLUE	A1085	8x8x1/2	10	120	120.00	120+
				120		120+
				120		120+
BLUE	A1085	8x8x3/8	7.5	120	120.00	120+
				120		120+
				120		120+
BLUE	A1085	6x6x3/8	7.5	120	120.00	120+
				120		120+
				120		120+
BLUE	A1085	5x5x3/8	7.5	38.5	30.67	
				29		
				24.5		
WHITE	A1085	8x8x1/2	10	120	120.00	120+
				120		120+
				120		120+
WHITE	A1085	8x8x3/8	7.5	79.5	70.50	
				68		
				64		
WHITE	A1085	6x6x3/8	7.5	85	82.67	
				78		
				85		
WHITE	A1085	5x5x3/8	7.5	65	76.83	
				71.5		
				94		

C.4 WALL THICKNESS MEASUREMENTS

		Wal Thickness Measurements (in.)																	
HSS Section	**Steel Type / Producer**	**S Top 1**	**S Top 2**	**S Bot 1**	**S Bot 2**	**SW 1**	**SW 2**	**SE 1**	**SE 2**	**N Top 1**	**N Top 2**	**N Bot 1**	**N Bot 2**	**NW 1**	**NW 2**	**NE 1**	**NE 2**	**Average Measured Thickness**	**Specified Design Thickness**
10X10X3/8	**A500 W**	0.349	0.351	0.351	0.352	0.350	0.349	0.348	0.349	0.344	0.346	0.342	0.344	0.342	0.343	0.345	0.346	**0.347**	**0.349**
	A1085 Y	0.367	0.369	0.365	0.366	0.367	0.366	0.365	0.366	Plasma Cut - Inaccurate Measurements								**0.366**	**0.375**
8X8X1/2	**A500 W**	0.464	0.462	0.461	0.460	0.460	0.461	0.463	0.459	Plasma Cut - Inaccurate Measurements								**0.461**	**0.465**
	A1085 R	0.467	0.468	0.462	0.465	0.463	0.466	0.468	0.465	0.464	0.466	0.469	0.467	0.463	0.464	0.462	0.464	**0.465**	**0.500**
	A1085 W	0.498	0.497	0.499	0.498	0.500	0.501	0.498	0.499	0.498	0.497	0.499	0.498	0.500	0.501	0.498	0.499	**0.499**	**0.500**
	A1085 B	0.499	0.495	0.502	0.499	0.499	0.502	0.501	0.500	0.502	0.501	0.504	0.502	0.500	0.503	0.500	0.501	**0.501**	**0.500**
	A1085 Y	0.488	0.491	0.491	0.489	0.487	0.485	0.484	0.487	Plasma Cut - Inaccurate Measurements								**0.488**	**0.500**
8X8X3/8	**A500 W**	0.351	0.350	0.350	0.347	0.348	0.349	0.348	0.350	0.351	0.350	0.350	0.351	0.350	0.351	0.350	0.350	**0.350**	**0.349**
	A1085 R	0.368	0.385	0.367	0.368	0.367	0.368	0.366	0.366	0.366	0.369	0.365	0.367	0.366	0.370	0.367	0.365	**0.368**	**0.375**
	A1085 W	0.375	0.375	0.376	0.377	0.375	0.374	0.375	0.377	0.370	0.372	0.372	0.372	0.375	0.374	0.373	0.376	**0.374**	**0.375**
	A1085 B	0.372	0.374	0.373	0.376	0.375	0.376	0.375	0.377	0.371	0.374	0.377	0.380	0.377	0.378	0.374	0.376	**0.375**	**0.375**
	A1085 Y	0.373	0.369	0.372	0.369	0.370	0.368	0.367	0.369	Plasma Cut - Inaccurate Measurements								**0.370**	**0.375**
7X7X1/2	**A500 B**	0.468	0.469	0.471	0.472	0.460	0.457	0.457	0.460	0.471	0.470	0.469	0.471	0.455	0.460	0.454	0.457	**0.464**	**0.465**
	A1085 Y	0.484	0.485	0.486	0.480	0.485	0.486	0.483	0.485	0.482	0.483	0.481	0.485	0.484	0.483	0.483	0.484	**0.484**	**0.500**
7X7X3/8	**A500 Y**	0.342	0.340	0.343	0.341	0.340	0.342	0.342	0.341	0.340	0.342	0.343	0.340	0.343	0.343	0.346	0.343	**0.342**	**0.349**
	A1085 Y	0.365	0.367	0.364	0.364	0.366	0.364	0.361	0.362	0.367	0.365	0.363	0.363	0.370	0.369	0.364	0.364	**0.365**	**0.375**
7X7X5/16	**A500 Y**	0.285	0.283	0.293	0.295	0.290	0.286	0.290	0.292	0.289	0.290	0.290	0.292	0.294	0.294	0.294	0.288	**0.290**	**0.291**
	A1085 Y	0.298	0.296	0.302	0.304	0.307	0.302	0.307	0.311	0.303	0.303	0.312	0.306	0.307	0.306	0.310	0.310	**0.305**	**0.313**
6X6X1/2	**A500 R**	Plasma Cut - Inaccurate Measurements								0.481		0.477		0.480		0.479		**0.479**	**0.465**
	A1085 Y	Plasma Cut - Inaccurate Measurements								0.491		0.495		0.492		0.486		**0.491**	**0.500**
6X6X3/8	**A500 R**									0.369		0.364		0.366		0.368		**0.367**	**0.349**
	A1085 R	0.367	0.368	0.373	0.375	0.371	0.374	0.369	0.363	0.370	0.374	0.373	0.370	0.375	0.374	0.372	0.375	**0.371**	**0.375**
	A1085 W	0.376	0.378	0.376	0.378	0.375	0.375	0.377	0.378	0.376	0.378	0.377	0.377	0.375	0.376	0.377	0.378	**0.377**	**0.375**
	A1085 B	0.374	0.378	0.378	0.380	0.382	0.381	0.382	0.383	0.380	0.379	0.380	0.380	0.383	0.384	0.374	0.374	**0.380**	**0.375**
	A1085 Y	Plasma Cut - Inaccurate Measurements								0.372		0.373		0.375		0.374		**0.373**	**0.375**
6X6X5/16	**A500 R**	0.303		0.304		0.305		0.307		Plasma Cut - Inaccurate Measurements								**0.305**	**0.291**
	A1085 Y	0.312		0.314		0.315		0.309		Plasma Cut - Inaccurate Measurements								**0.313**	**0.313**
5X5X3/8	**A500 Y**									0.362		0.360		0.358		0.358		**0.360**	**0.349**
	A1085 R	0.371	0.376	0.374	0.375	0.372	0.376	0.377	0.376	0.375	0.374	0.375	0.377	0.374	0.375	0.377	0.375	**0.375**	**0.375**
	A1085 W	0.370	0.370	0.372	0.371	0.379	0.375	0.375	0.373	0.375	0.371	0.372	0.378	0.377	0.374	0.375	0.376	**0.374**	**0.375**
	A1085 B	0.379	0.381	0.385	0.381	0.377	0.379	0.382	0.381	0.382	0.384	0.375	0.380	0.383	0.383	0.381	0.380	**0.381**	**0.375**
	A1085 Y	Plasma Cut - Inaccurate Measurements								0.379		0.380		0.371		0.375		**0.376**	**0.375**

C.5 CORNER RADIUS MEASUREMENTS

HSS Section	Steel Type / Producer	Corner Radius Measurments (in.)								Average Radius (in.)
10X10X3/8	**A500 W**	0.69	0.72	0.69	0.72	0.81	0.81	0.84	0.84	**0.77**
	A1085 Y	0.88	0.88	0.88	0.88	0.94	0.88	0.91	0.90	**0.89**
8X8X1/2	**A500 W**	0.88	0.84	0.91	0.88	0.88	0.91	0.91	0.91	**0.89**
	A1085 R	1.00	1.03	1.03	1.03	1.00	1.00	1.03	1.03	**1.02**
	A1085 W	1.03	0.84	0.81	1.03	1.03	0.94	1.03	0.94	**0.96**
	A1085 B	0.94	1.19	1.16	1.00	1.00	1.19	0.94	1.19	**1.07**
	A1085 Y	1.13	1.16	1.16	1.16	1.13	1.13	1.16	1.13	**1.14**
8X8X3/8	**A500 W**	0.66	0.69	0.81	0.78	0.78	0.81	0.97	0.91	**0.80**
	A1085 R	0.78	0.81	0.84	0.88	0.69	0.75	0.81	0.78	**0.79**
	A1085 W	0.69	0.75	0.81	0.81	0.75	0.75	0.84	0.78	**0.77**
	A1085 B	1.00	0.88	0.72	0.91	0.91	0.84	0.84	0.75	**0.86**
	A1085 Y	1.06	1.09	1.13	1.09	1.00	1.03	1.06	1.03	**1.06**
7X7X1/2	**A500 B**	0.84	0.81	0.84	0.88	1.00	1.03	1.06	1.09	**0.95**
	A1085 Y	1.03	1.03	1.09	1.13	0.97	1.00	1.06	1.06	**1.05**
7X7X3/8	**A500 Y**	0.78	0.81	0.81	0.78	0.84	0.88	0.88	0.88	**0.83**
	A1085 Y	0.84	0.84	0.88	0.94	0.97	0.97			**0.91**
7X7X5/16	**A500 Y**	0.72	0.75	0.66	0.69	0.63	0.66	0.59	0.59	**0.66**
	A1085 Y	0.69	0.72	0.72	0.63	0.63	0.63			**0.67**
6X6X1/2	**A500 R**	1.09	1.13	1.13	1.09	0.84	0.88	0.88	0.84	**0.98**
	A1085 Y	0.84	0.84	0.88	0.81	0.81	0.81			**0.83**
6X6X3/8	**A500 R**	0.66	0.63	0.81	0.84	0.66	0.66	0.88	0.88	**0.75**
	A1085 R	0.69	0.72	0.75	0.69	0.69	0.78	0.69	0.75	**0.72**
	A1085 W	0.75	0.78	0.81	0.81	0.78	0.81	0.84	0.75	**0.79**
	A1085 B	0.78	0.81	0.84	0.81	0.78	0.94	0.81	0.88	**0.83**
	A1085 Y	0.75	0.75	0.69	0.66	0.75	0.75	0.69	0.69	**0.71**
6X6X5/16	**A500 R**	0.56	0.59	0.63	0.63	0.56	0.56	0.59	0.59	**0.59**
	A1085 Y	0.56	0.59	0.66	0.69	0.75	0.72	0.72	0.72	**0.68**
5X5X3/8	**A500 Y**	0.72	0.72	0.75	0.78	0.81	0.78			**0.76**
	A1085 R	0.75	0.75	0.78	0.75	0.78	0.78	0.81	0.75	**0.77**
	A1085 W	0.72	0.75	0.75	0.69	0.72	0.69	0.69	0.78	**0.72**
	A1085 B	0.63	0.78	0.66	0.81	0.69	0.81	0.72	0.78	**0.73**
	A1085 Y	0.69	0.72	0.69	0.78	0.75	0.75			**0.73**

Appendix D. MATLAB SCRIPTS

D.1 Data Trimming Script

```
%% INPUT INFORMATION %%
%Raw Data File Name
raw_data = 'Output Data.txt';  %enter raw data file name

%Brace Info
fy = 50;              %Approx yield stress of specimen
Ry = 1.3;              %Ry_A500 = 1.3  Ry_A1085 = 1.25
A_s = 13.2;            %Area of steel

%Trimming Tolerances
tol1 = 0.00000;        %For targets 1-3
tol2 = 0.00000;        %For targets 4-6
tol3 = 0.00000;        %For targets > 6

%New Data File name
new_data_file_name = '10x10x3_8_A1085_Y_Trim.txt';

%%%%%% END DATA INPUT
%%%%%%%%%%%%%%%%%%%%%%%%%%%%%%%%%%%%%%%%%%%%%%%%%%%%%%%%%%%%%



%% Load data
data = readmatrix(raw_data);

n = size(data,1);              %number of rows
m = size(data,2);              %number of columns



%% Find Peaks
small_Act_Disp = -1*data(:,9);   % 350k actuator displacement
point = data(:,6);              % Data count

[pks,loc] = findpeaks(small_Act_Disp,point,'MinPeakProminence',.1,'MinPeakDistance',500);
peaks = [pks, loc];             % Find peaks and corresponding data count

t = size(peaks,1);              % Number of rows in peaks table

for i = 1:t                     % Formatting of data in table
   count(i) = [i]';
end
idx = count.';
```

```
for i = 1:t                    % Format target displacements in table
   target(i) = ceil(idx(i)/2);
end
target = target.';
peaks = [idx, pks, loc, target];

%% Add column for target displacement to data matrix
for i = 1:n-1
   for j = 1:t-1
      if data(i,6) > loc(j)
         data(i,40) = target(j);
      end
   end
end

for i = 1:n-1
   if data(i,6) < loc(1)
      data(i,40) = 1;
   end
end

%% Remove unwanted data during holds
delete = zeros(n,1);
j = 1;

% Assign tolerances 1,2,3 manually to delete data during holds
for e = 1:n-1
   if  data(e,40) <= 3                    % Trimming  first 3 targets
      diff = abs(data(e,9) - data(e-1,9));
      if diff < tol1
         delete(j,1) = e;
         j = j+1;
      end

   elseif (4 <= data(e,40)) && (data(e,40) <= 6)   %Trimming next targets
      diff = abs(data(e,9) - data(e-1,9));
      if diff < tol2
         delete(j,1) = e;
         j = j+1;
      end
   else
      diff = abs(data(e,9) - data(e-1,9));       % Trimming other targets
      if diff < tol3
         delete(j,1) = e;
         j = j+1;
      end
   end
end
delete = delete(1:j-1,1);
```

```
data([delete],:)= [];                % Delete rows of data during holds


%% Write trimmed data to a new file, use for corrections
%     Make sure trimming parameters are working properly before exporting
%     trimmed data
%         Modify  tolerances, cycle numbers, etc if necessary
%
%           Format: 'SizexSizexThick_ness_Material_Trim'

writematrix(data, new_data_file_name)  %Write trimmed data to new text file
```

D.2 DATA CORRECTION SCRIPT

```
%% INPUT INFORMATION
%%%%%%%%%%%%%%%%%%%%%%%%%%%%%%%%%%%%%%%%%%%%%%%%%%%%%%%%%%%%%%%%%%%%%%%%

%Trimmed Data File Name
input_data = '10x10x3_8_A1085_Y_Trim.txt';  %enter raw data file name

%Instrument Location Info
Dist_SP_SGPs = 10;    %Distance between gusset plate transverse string pots
GP_t = 0.75;              %Gusset plate width (in)
GP_Gap = 3*GP_t;          %Gap between gusset and connection plates
GP_ecc = 0.375;           %Gusset plate eccentricity (in)

NGP_SP_distx = 2;       %Horizontal distance from east face of brace to string pot - North
NGP_SP_disty = 2.875;   %Longitudinal distance from end of brace to string pot end - North

SGP_SP_distx = 2;       %Horizontal distance from east face of brace to string pot - South
SGP_SP_disty = 2.875;   %Longitudinal distance from end of brace to string pot end - South

brace_width = 10;       %Width of test specimen (in)

%Trimming Tolerances
tol1 = 0.0025;        % South Gusset Plate 1
tol2 = 0.0025;        % South Gusset Plate 2
tol3 = 0.01;          % Axial Displacement
tol4 = 0.1;           % Out of Plane Displacement

%New Data File name
new_data_file_name = '10x10x3_8_A1085_Y_Trim_Corr.txt';
```

```
%%%%%% END DATA INPUT
%%%%%%%%%%%%%%%%%%%%%%%%%%%%%%%%%%%%%%%%%%%%%%%%%%%%%%%%%%%%%%%%%

%% Load data
data = readmatrix(input_data);

n = size(data,1);          % Number of rows
m = size(data,2);          % Number of columns

for i = 1:n                % Set up indexing
   data(i,6) = i;
end

%% Trim Gusset Plate Data
% Makes processing data easier
% South Gusset Plate 1
j = 1;
delete = zeros(n,1);
for i = 1:n-1
   diff = abs(data(i,13)-data(i+1,13));   % Trim spikes in data
   if diff > tol1                         % Assign tolerance 1 manually
      delete(j,1) = i;
      j = j+1;
   end
end
delete = delete(1:j-1,1);
data([delete],:)= [];

%South Gusset Plate 2
n = size(data,1);
j = 1;
delete2 = zeros(n,1);
diff = zeros(n,1);
for i = 1:n-1
   diff = abs(data(i,23)-data(i+1,23));   % Trim spikes in data
   if diff > tol2                         % Assign tolerance 2 manually
      delete2(j,1) = i;
      j = j+1;
   end
end
delete2 = delete2(1:j-1,1);
data([delete2],:)= [];


%% Correct for Rigid Body Rotation

count = data(:,6);                  % Data count - used for indexing
small_Act_Disp = -1*data(:,9);      % 350k actuator displacement
small_Act_Load = -1*data(:,8);      % 350k actuator load
```

```
SP_Trans_SGP1 = data(:,13);        % Gusset plate displacement - base
SP_Trans_C1 = data(:,15);          % Brace OOP displacement - center 1
SP_Long_Brace = data(:,17);        % Brace axial displacement
SP_Long_Tot = data(:,18);          % Total axial dispalcement
SP_Trans_SGP2 = data(:,23);        % Gusset plate displacement - end
SP_Trans_C2 = data(:,24);          % Brace OOP displacement - center 2
Target = data(:,40);               % Target displacement number

n = size(data,1);                  % Create indexing vector
for i = 1:n
   count(i) = [i]';
end
idx = count.';


for i = 1:n

   if SP_Trans_SGP1(i) > SP_Trans_SGP2(i)   % Correct axial displacement data if gusset plate is
rotated
      data(i,41) = SP_Long_Brace(i);

   else
      SGP_Trans_Mvmt(i) = SP_Trans_SGP2(i) - SP_Trans_SGP1(i);     %Difference between transverse
movement of gusset plate string pots

      SGP_Rotation(i) = atand(SGP_Trans_Mvmt(i) / Dist_SP_SGPs);  %Calculate rotation angle of south
gusset plate
      SGP_CCW_Rot(i) = 360 - SGP_Rotation(i);       %CCW rotation to new SP location

      % Assuming CR at mid-point of GP gap
      NGP_dist_CRx = brace_width/2 - GP_ecc + NGP_SP_distx; %Horiz distance from center of rot. -
North
      NGP_dist_CRy = GP_Gap/2 + NGP_SP_disty; %Longitudinal distance from center of rot to SP -
North

      SGP_dist_CRx = brace_width/2 - GP_ecc + SGP_SP_distx; %Horiz distance from center of rot. -
South
      SGP_dist_CRy = GP_Gap/2 + SGP_SP_disty; %Longitudinal distance from center of rot to SP -
South

      NewDist_N_CRtoSP_y(i) = NGP_dist_CRx * sind(SGP_CCW_Rot(i)) + NGP_dist_CRy *
cosd(SGP_CCW_Rot(i));
            %Calculate new longitudinal distance from CR to string pot-North

      RB_Mvmt_N(i) = NewDist_N_CRtoSP_y(i) - NGP_dist_CRy;
            %Change in longitudinal distance between CR and SP - North

      NewDist_S_CRtoSP_y(i) = SGP_dist_CRx * sind(SGP_CCW_Rot(i)) + SGP_dist_CRy *
cosd(SGP_CCW_Rot(i));
```

```
            %Calculate new longitudinal distance from CR to string pot-South

        RB_Mvmt_S(i) = NewDist_S_CRtoSP_y(i) - SGP_dist_CRy;
            %Change in longitudinal distance between CR and SP - South

        Total_RB_AxialEff(i) = RB_Mvmt_N(i) + RB_Mvmt_S(i);

        data(i,41) = SP_Long_Brace(i) - Total_RB_AxialEff(i);
    end

end


%% Trim Axial Displacement Data
%Redefine Data Vectors
Corrected_Long_Brace = data(:,41);
small_Act_Load = -1*data(:,8);
small_Act_Disp = -1*data(:,9);

j = 1;
delete3 = zeros(n,1);
diff = zeros(n,1);
for i = 1:n-4
    diff(i) = abs(Corrected_Long_Brace(i) - Corrected_Long_Brace(i+1));
    if diff(i) > tol3          % Remove spikes in axial disp. data
        delete3(j,1) = i;      % Set tolerance manually
        j = j+1;
    end
end
delete3 = delete3(1:j-1,1);
data([delete3],:)= [];


%% Trim OOP Displacement Data
SP_Trans_C1 = data(:,15);
SP_Trans_C2 = data(:,24);
SP_Trans_SGP1 = data(:,13);
Brace_OOP_Disp = (SP_Trans_C1 + SP_Trans_C2)/2 - SP_Trans_SGP1;
        % Calculate brace OOP displacement at center
j = 1;
n = size(data,1);
delete4 = zeros(n,1);
diff = zeros(n,1);
for i = 2:n           % Trim data to remove spikes in OOP disp. data
    diff(i) = abs(Brace_OOP_Disp(i) - Brace_OOP_Disp(i-1));
    if diff(i) > tol4 && i < n-6 %Keep Last few data points!
        delete4(j,1) = i;
        j = j+1;
        Brace_OOP_Disp(i) = (SP_Trans_C1(i)+SP_Trans_C2(i))/2;
    end
```

```
end
delete4 = delete4(1:j-1,1);
data([delete4],:)= [];


%% Axial Displacement Corrections
%Recreate idx vector
n = size(data,1);
count = data(:,6);
for i = 1:n
    count(i) = [i]';
end
idx = count;

%Calculate the corrections made
Corrected_Long_Brace = data(:,41);
SP_Long_Brace = data(:,17);
Corrections = Corrected_Long_Brace - SP_Long_Brace;

SP_Long_Brace = data(:,17);
SP_Long_Tot = data(:,18);

%% Write corrected data to a new file, use for test summary
% %% Write trimmed + corrected data to a new file, use for data analysis
%     % Make sure corrections  are working properly before exporting
%         % Modify  brace, gusset, eccentricity, string pot locations, etc
%
%           % Format: 'SizexSizexThick_ness_Material_Trim_Corr'
%
% writematrix(data,new_data_file_name)  %Write corrected data to new text file
```

Appendix E. ADDITIONAL TABLES AND FIGURES

E.1 RELATIONSHIP BETWEEN *B/T* AND *KL/R*

This section will provide a series of figures that plot the global slenderness ratio, *KL/r*, versus the local compactness ratio, *b/t*. The specimens in these figures show the A1085 HSS specimens from the yellow producer subjected to the symmetric loading protocol. The plotted points are grouped based on various measures of brace deformability – axial deformation range, story drift range, and maximum story drift. The figures have lines to group the specimens based on the respective measure of deformability. These lines were drawn empirically based on the experimental data. If a specimen is above a line, it reached an axial deformation greater than the respective line.

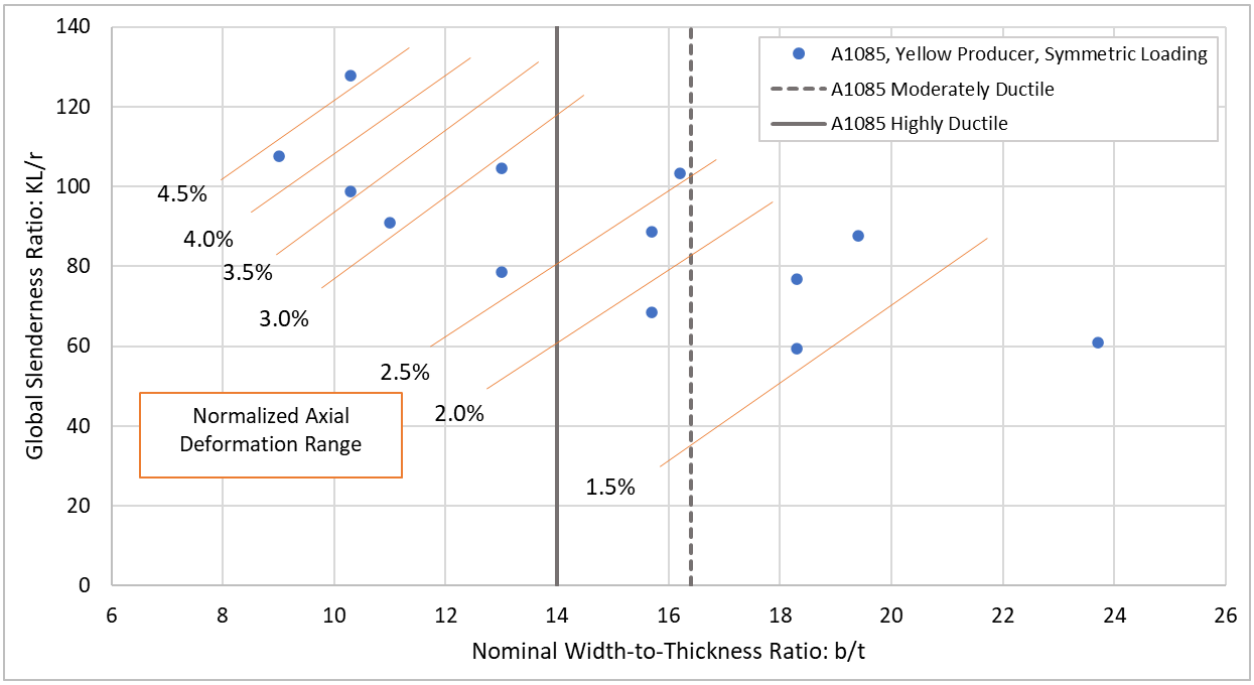

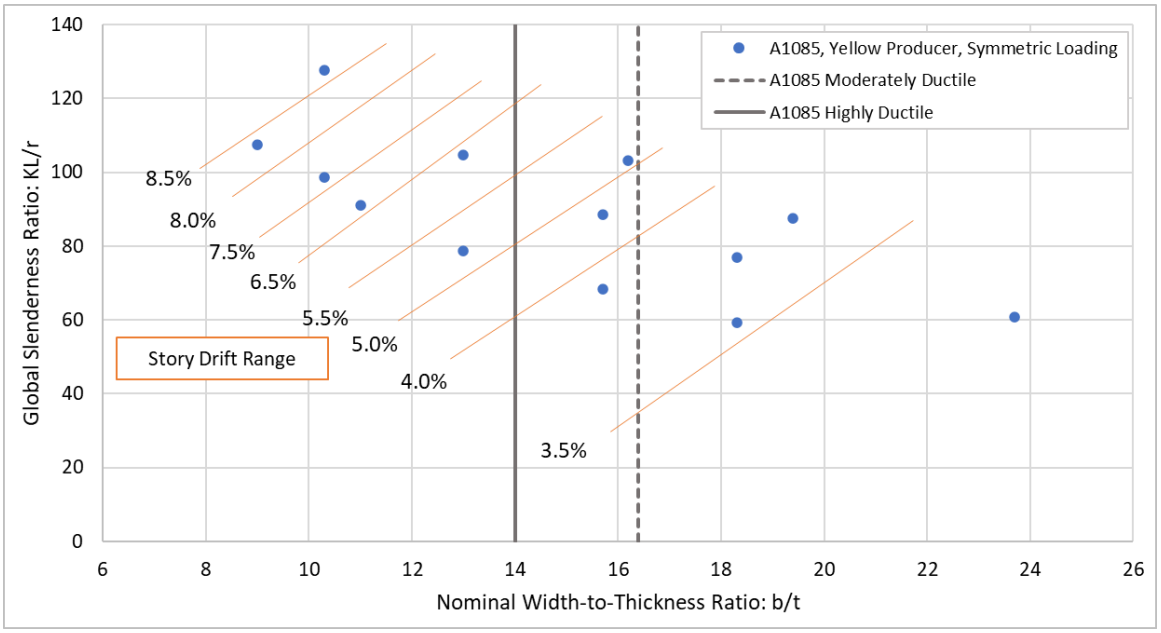
A1085, Yellow Producer, Symmetric Loading
A1085 Moderately Ductile
A1085 Highly Ductile
Story Drift Range
8.5%
8.0%
7.5%
6.5%
5.5%
5.0%
4.0%
3.5%
Global Slenderness Ratio: KL/r
Nominal Width-to-Thickness Ratio: b/t
0
20
40
60
80
100
120
140
6
8
10
12
14
16
18
20
22
24
26

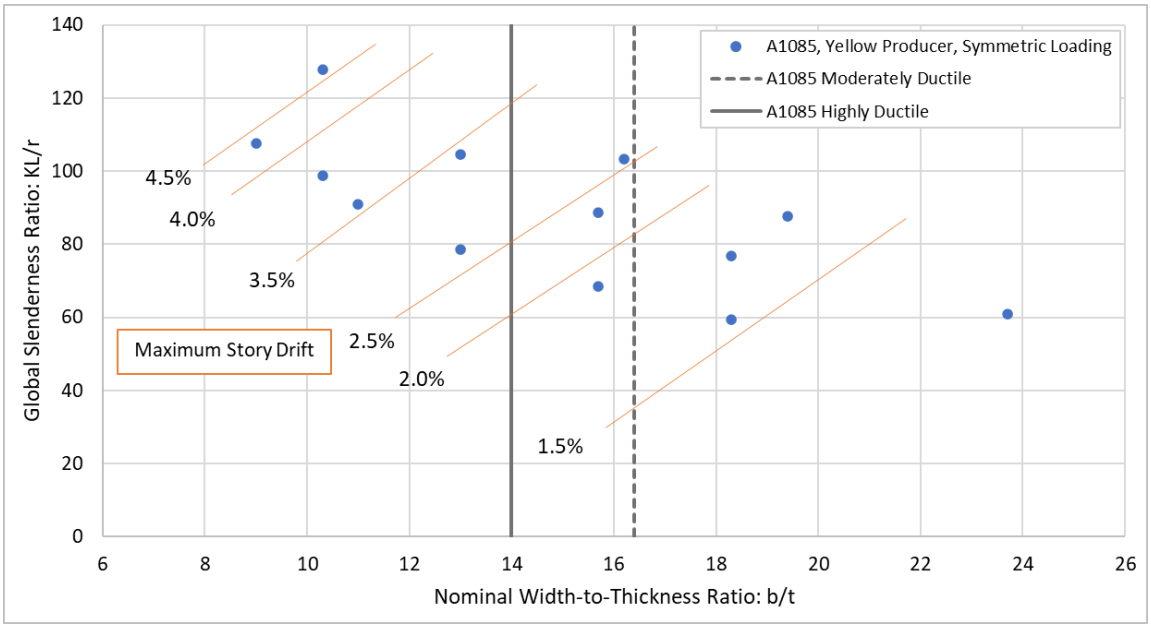
A1085, Yellow Producer, Symmetric Loading
A1085 Moderately Ductile
A1085 Highly Ductile
Maximum Story Drift
4.5%
4.0%
3.5%
2.5%
2.0%
1.5%
Global Slenderness Ratio: KL/r
Nominal Width-to-Thickness Ratio: b/t
0
20
40
60
80
100
120
140
6
8
10
12
14
16
18
20
22
24
26

E.2 MAXIMUM MEASURED AVERAGE STRAIN

The measured strain provided in the table below was measured using two optotrak targets placed 3” north and south of the center of the brace. For two main reasons, the strains shown are the maximum measured strains but not necessarily the maximum actual strains. First, the optotrak targets often popped off due to large cupping deformations so strains could not be measured after that. Second, the plastic hinge was not always located directly at the center of the brace so the specimens the 6” gauge length did not capture the maximum actual strains in some cases.

Test Specimen	Maximum Measured Average Strain	Maximum Strain/Measured Yield Strain
5x5x3/8 A500 Y	error	error
5x5x3/8 A1085 Y	0.1963	87.1
6x6x5/16 A500 R	0.0438	19.3
6x6x5/16 A1085 Y	0.0463	23.4
6x6x3/8 A500 R	0.0282	13.2
6x6x3/8 A1085 Y	0.0394	18.7
6x6x1/2 A500 R	0.2238	97.1
6x6x1/2 A1085 Y	0.1499	69.2
7x7x5/16 A500 Y	0.0063	2.7
7x7x5/16 A1085 Y	0.0170	7.9
7x7x3/8 A500 Y	0.0317	15.9
7x7x3/8 A1085 Y	0.0319	15.1
7x7x1/2 A500 B	0.1240	58.1
7x7x1/2 A1085 Y	0.0699	35.1
8x8x3/8 A500 W	0.0108	4.9
8x8x3/8 A1085 Y	0.0197	8.6
8x8x1/2 A500 W	0.0343	16.5
8x8x1/2 A1085 Y	0.0400	17.7
10x10x3/8 A500 W	0.0159	7.1
10x10x3/8 A1085 Y	0.0107	5.3
5x5x3/8 A1085 R	0.1805	89.7
5x5x3/8 A1085 W	0.1938	81.7
5x5x3/8 A1085 B	0.1011	42.2
6x6x3/8 A1085 R	0.0961	35.7
6x6x3/8 A1085 W	0.0912	43.8
6x6x3/8 A1085 B	0.0961	41.2
8x8x3/8 A1085 R	0.0143	6.0
8x8x3/8 A1085 W	0.0167	7.9
8x8x3/8 A1085 B	error	error
8x8x1/2 A1085 R	0.0530	22.5

8x8x1/2 A1085 W	0.0457	22.6
8x8x1/2 A1085 B	0.0447	19.6
5x5x3/8 A1085 Y [C]	0.1483	64.8
5x5x3/8 A1085 Y [NF]	0.2158	94.7
7x7x3/8 A1085 Y [C]	0.0088	3.9
7x7x3/8 A1085 Y [NF]	0.0549	25.7
8x8x3/8 A1085 Y [C]	0.0024	1.1
8x8x3/8 A1085 Y [NF]	0.0283	13.6
5x5x3/8 A1085 Y [S]	0.1405	67.5
7x7x3/8 A1085 Y [S]	0.0228	10.0
8x8x3/8 A1085 Y [S]	0.0058	2.7

E.3 AXIAL DEFORMATION INCLUDING CONNECTION REGION

The axial brace deformation used in throughout this document was measured from brace end-to-end. Additional deformation occurs in the connection region which contributes to the system deformation capacity. Deformation in the connection region occurs through yield of the gusset plate, bolt bearing, as well as bolt slip. The table below shows the total system deformation range which was measured from connection plate to connection plate. The table also includes the brace axial deformation and the ratio of system-to-brace axial deformation range. The deformations shown in the table are normalized by the initial brace length, *L*. Much of the variation in the ratio of system-to-brace axial deformation range is due to the varying severity of bolt slip during testing.

Test Specimen	Brace Axial Deformation Range (%)	System Axial Deformation Range (%)	Ratio of System-to-Brace Axial Deformation Range
5x5x3/8 A500 Y	4.22	4.38	1.04
5x5x3/8 A1085 Y	4.53	4.68	1.03
6x6x5/16 A500 R	2.65	2.67	1.01
6x6x5/16 A1085 Y	2.63	2.70	1.03
6x6x3/8 A500 R	3.14	3.24	1.03
6x6x3/8 A1085 Y	2.96	3.12	1.05
6x6x1/2 A500 R	3.59	3.96	1.10
6x6x1/2 A1085 Y	4.12	4.31	1.04
7x7x5/16 A500 Y	1.50	1.53	1.02
7x7x5/16 A1085 Y	1.81	1.88	1.04
7x7x3/8 A500 Y	2.23	2.27	1.02
7x7x3/8 A1085 Y	2.20	2.29	1.04
7x7x1/2 A500 B	3.26	3.39	1.04
7x7x1/2 A1085 Y	3.32	3.43	1.03
8x8x3/8 A500 W	1.32	1.38	1.04
8x8x3/8 A1085 Y	1.84	1.84	1.00
8x8x1/2 A500 W	2.32	2.58	1.11
8x8x1/2 A1085 Y	2.64	2.76	1.04
10x10x3/8 A500 W	1.93	1.98	1.03
10x10x3/8 A1085 Y	1.45	1.52	1.05
5x5x3/8 A1085 R	4.23	4.39	1.04
5x5x3/8 A1085 W	4.20	4.39	1.04
5x5x3/8 A1085 B	3.79	3.96	1.05
6x6x3/8 A1085 R	3.41	3.52	1.03
6x6x3/8 A1085 W	3.24	3.34	1.03
6x6x3/8 A1085 B	2.62	2.74	1.04
8x8x3/8 A1085 R	1.87	2.09	1.11
8x8x3/8 A1085 W	1.93	2.01	1.04
8x8x3/8 A1085 B	1.80	1.88	1.04
8x8x1/2 A1085 R	2.63	2.76	1.05
8x8x1/2 A1085 W	2.57	2.72	1.06
8x8x1/2 A1085 B	2.56	2.67	1.04
5x5x3/8 A1085 Y [C]	4.82	5.13	1.06
5x5x3/8 A1085 Y [NF]	5.14	5.36	1.04
7x7x3/8 A1085 Y [C]	2.28	2.37	1.04
7x7x3/8 A1085 Y [NF]	2.35	2.39	1.02
8x8x3/8 A1085 Y [C]	1.97	2.04	1.03
8x8x3/8 A1085 Y [NF]	2.10	2.20	1.05
5x5x3/8 A1085 Y [S]	3.87	4.05	1.05
7x7x3/8 A1085 Y [S]	1.80	1.92	1.07
8x8x3/8 A1085 Y [S]	1.78	1.90	1.07

E.4 EVALUATION OF B/T LIMITS

In Spring of 2022, new compactness limits were proposed for seismic design of SCBFs and OCBFs in AISC 341-22. The figures below show the story drift range and maximum story drift plotted against the normalized b/t ratio. Vertical lines indicate the current and proposed b/t limits. The experimental data from this research indicates that the current highly ductile limit is adequate and the moderately ductile in conservative.

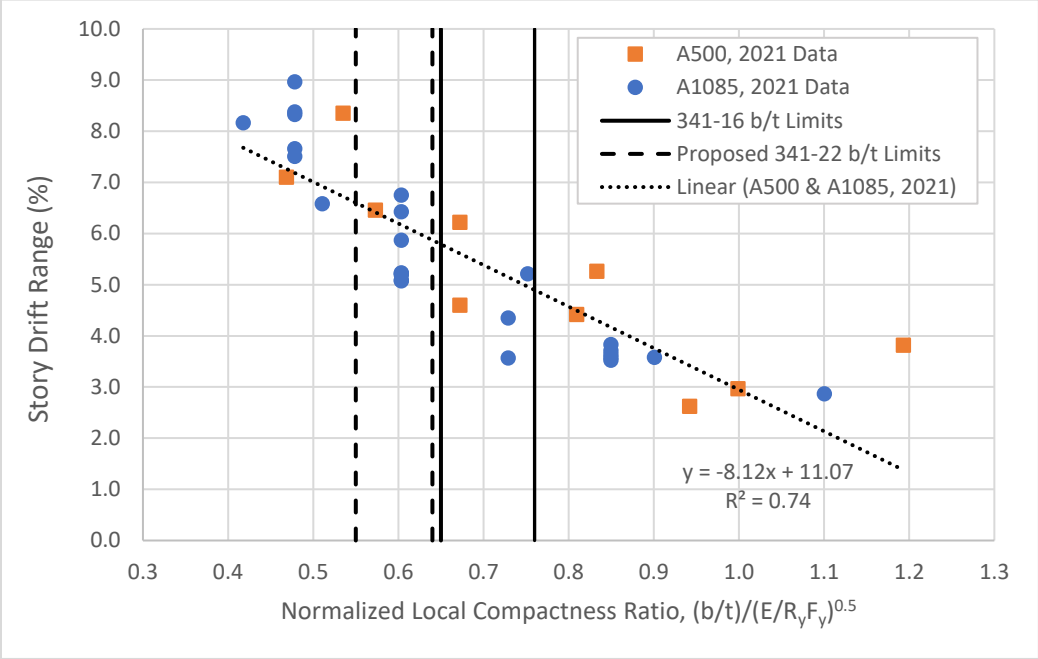

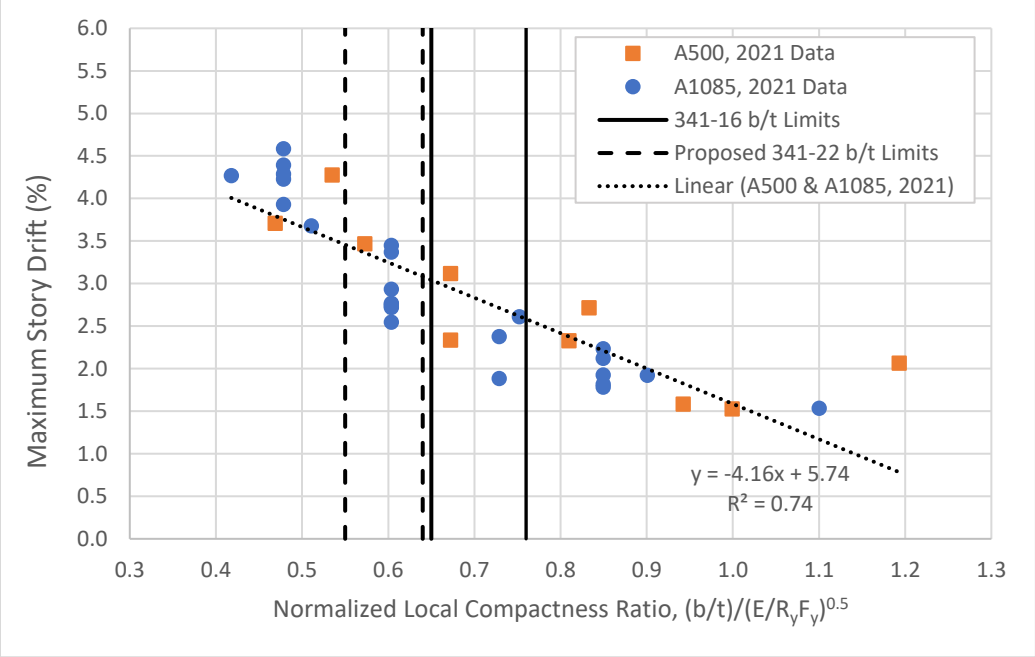
A500, 2021 Data
A1085, 2021 Data
341-16 b/t Limits
Proposed 341-22 b/t Limits
Linear (A500 & A1085, 2021)
y = -4.16x + 5.74
R² = 0.74
Maximum Story Drift (%)
Normalized Local Compactness Ratio, (b/t)/(E/RyFy)0.5
6.0
5.5
5.0
4.5
4.0
3.5
3.0
2.5
2.0
1.5
1.0
0.5
0.0
0.3
0.4
0.5
0.6
0.7
0.8
0.9
1.0
1.1
1.2
1.3

Appendix F. BRACE TEST REPORTS

This appendix includes test reports for all 41 brace tests that were completed as part of this experimental research study. Each test report includes qualitative and quantitative information recorded during testing. The reports provide information such as brace properties, brace performance, key observations, performance plots, and test photos. Table F.1 below shows the test specimens in the order that the reports are presented.

Table F.1 Test Specimens

HSS Shape	ASTM Specification	Producer	Brace Length (in.)	Loading Protocol
5x5x3/8	A500	Yellow	237.5	Symmetric
5x5x3/8	A1085	Yellow	237.5	Symmetric
6x6x5/16	A500	Red	237.5	Symmetric
6x6x5/16	A1085	Yellow	237.5	Symmetric
6x6x3/8	A500	Red	237.5	Symmetric
6x6x3/8	A1085	Yellow	237.5	Symmetric
6x6x1/2	A500	Red	237.5	Symmetric
6x6x1/2	A1085	Yellow	237.5	Symmetric
7x7x5/16	A500	Yellow	237.5	Symmetric
7x7x5/16	A1085	Yellow	237.5	Symmetric
7x7x3/8	A500	Yellow	237.5	Symmetric
7x7x3/8	A1085	Yellow	237.5	Symmetric
7x7x1/2	A500	Blue	237.5	Symmetric
7x7x1/2	A1085	Yellow	237.5	Symmetric
8x8x3/8	A500	White	237.5	Symmetric
8x8x3/8	A1085	Yellow	237.5	Symmetric
8x8x1/2	A500	White	237.5	Symmetric
8x8x1/2	A1085	Yellow	237.5	Symmetric
10x10x3/8	A500	White	237.5	Symmetric
10x10x3/8	A1085	Yellow	237.5	Symmetric
5x5x3/8	A1085	Red	237.5	Symmetric
5x5x3/8	A1085	White	237.5	Symmetric
5x5x3/8	A1085	Blue	237.5	Symmetric
6x6x3/8	A1085	Red	237.5	Symmetric
6x6x3/8	A1085	White	237.5	Symmetric
6x6x3/8	A1085	Blue	237.5	Symmetric
8x8x3/8	A1085	Red	237.5	Symmetric
8x8x3/8	A1085	White	237.5	Symmetric
8x8x3/8	A1085	Blue	237.5	Symmetric
8x8x1/2	A1085	Red	237.5	Symmetric
8x8x1/2	A1085	White	237.5	Symmetric

8x8x1/2	A1085	Blue	237.5	Symmetric
5x5x3/8	A1085	Yellow	237.5	Chevron
5x5x3/8	A1085	Yellow	237.5	Near Fault
7x7x3/8	A1085	Yellow	237.5	Chevron
7x7x3/8	A1085	Yellow	237.5	Near Fault
8x8x3/8	A1085	Yellow	237.5	Chevron
8x8x3/8	A1085	Yellow	237.5	Near Fault
5x5x3/8	A1085	Yellow	183.5	Symmetric
7x7x3/8	A1085	Yellow	183.5	Symmetric
8x8x3/8	A1085	Yellow	183.5	Symmetric

5x5x3/8 A500 Y Brace Test Summary

Test Name: 5x5x3/8 A500 Y
Test Date: 3/17/21

Brace Properties

Measured Yield Stress (ksi)	65.38
Measured Ultimate Stress (ksi)	71.86
Yield Load (kips)	416.8
Critical Buckling Load (kips)	96.2
Percent Elongation - 2" (%)	30.79
CVN Width (mm)	7.5
CVN Absorbed Energy (ft-lbs)	12.8
Brace Length (in)	237.5

Area (in^2)	6.18
Moment of Inertia (in^4)	21.7
Corner Radius (in)	0.76
Thickness - Nominal (in)	0.349
Thickness - Measured (in)	0.36
Brace Compactness Ratio (*b/t*) - Nominal	11.3
Brace Compactness Ratio (*b/t*) - Measured	9.67
Global Slenderness ratio (*KL/r*)	127

Specimen Performance

Test Event	Axial Brace Displacement (in)	Target Displacement (in) (Cycle)	Force (kips)	$P / P_{Yield/Critical}$	
Peak Tension Load	1.92	2.25 (1)	432.5	1.04	Y
B1: Initial Global Buckling	-0.18	0.25 (1)	-95.3	-0.99	C
B2: Moderate Global Buckling	-1.0553	1.25 (1)	-56.3	-0.13	C
B3-T: Local Cupping	-4.38	4.75 (2)	-19.5	-0.05	C
B3-C: Striations & Tearing	4.89	5.25 (1)	386.0	0.93	Y
B4: Brace Fracture	5.13	5.75 (1)	116.0	0.28	Y

Key Observations

Cycle #	Displacement	Observations
15-16	1.75”	Bolt slip at first tension cycle - loud bang. SP_SGP_E fell off specimen, replaced immediately.
17-18	2.25”	Banging sounds observed during tension cycles, near peak tension Comp. cycle 1 - SP_L_Br caught on Optotrak string, fixed, use hold data for brace axial displacement here!
27-28	4.75”	Minor cupping observed at peak compressive cycles
29-30	5.25”	Cupping at peak compressive cycles, major cupping at cycle 30. Striations observed at peak tensile displacements.
31-32	5.75”	Fracture at first tension cycle!

Test Results

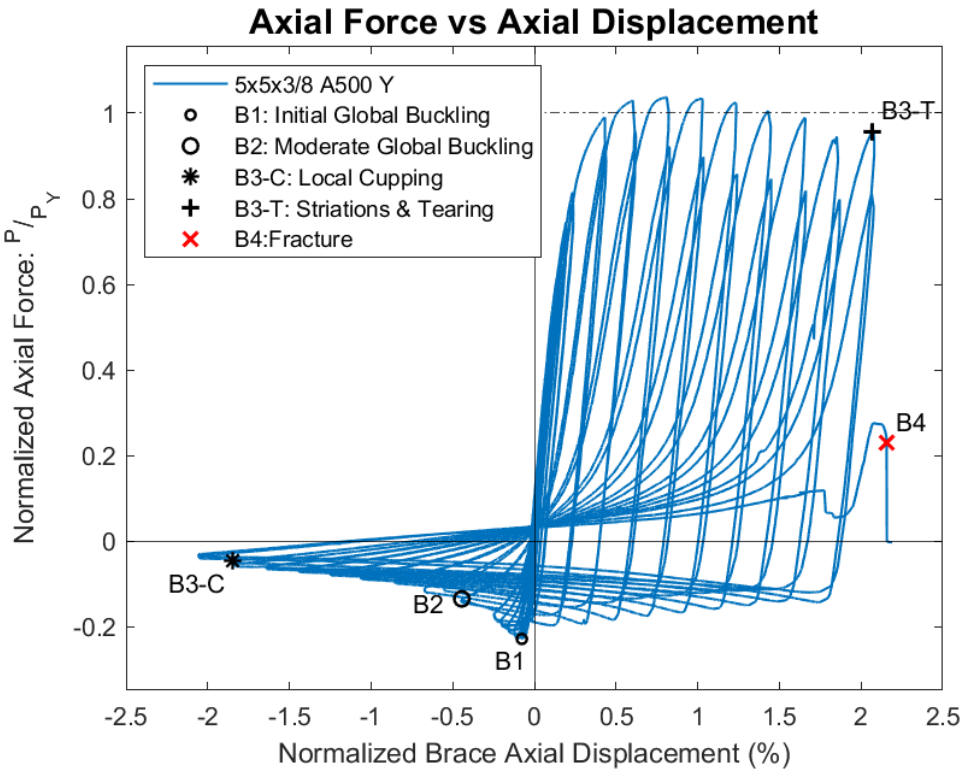

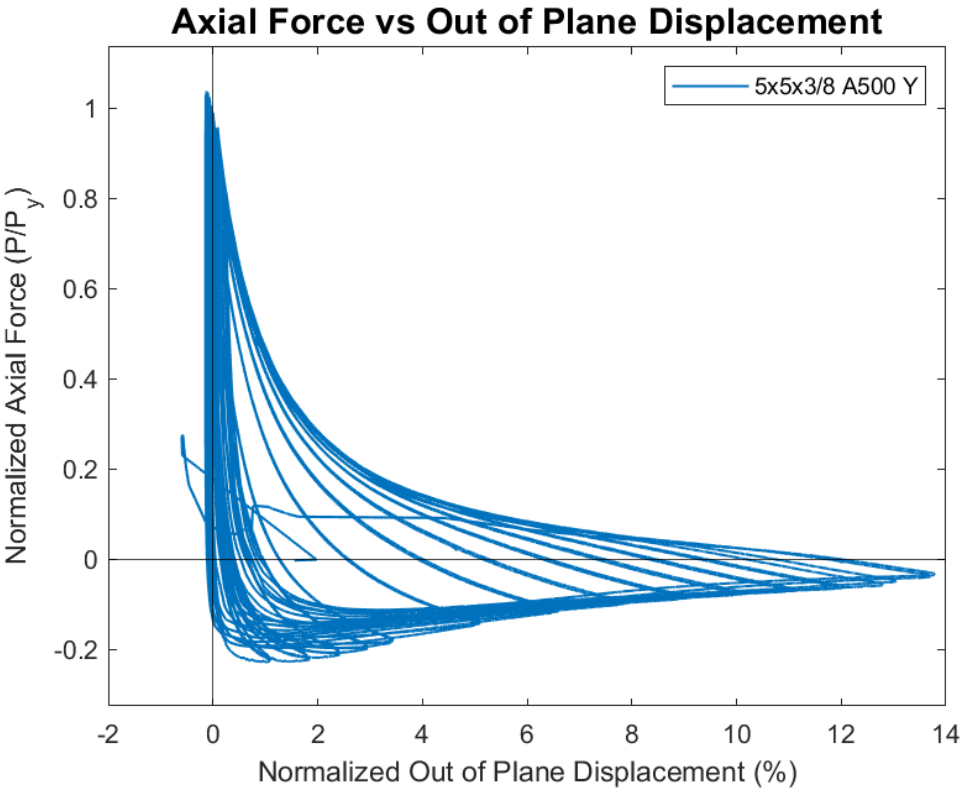

Photos

Moderate cupping at center of brace: 5.25” cycles

Peak out of plane displacement: 5.25” cycles

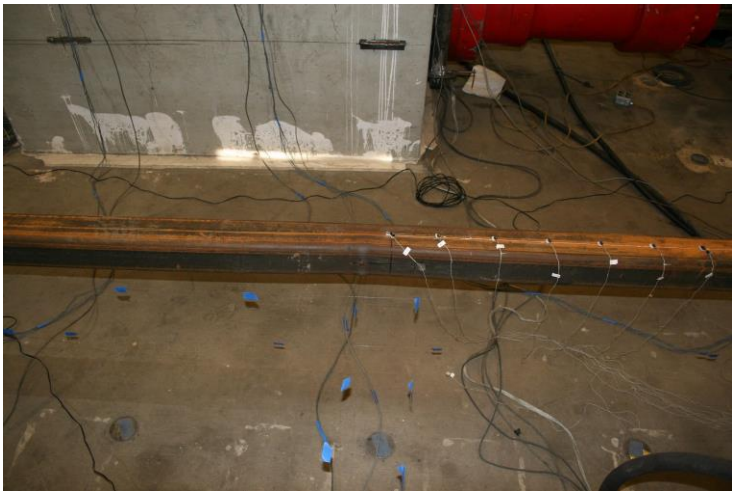

Striations at center of brace: 5.25” cycles

Specimen fractured in tension during first 5.75” cycle

5x5x3/8 A1085 Y Brace Test Summary

Test Name: 5x5x3/8 A1085 Y
Test Date: 4/2/21

Brace Properties

Measured Yield Stress (ksi)	66.04
Measured Ultimate Stress (ksi)	74.62
Yield Load (kips)	435.7
Critical Buckling Load (kips)	101.3
Percent Elongation - 2" (%)	32.83
CVN Width (mm)	7.5
CVN Absorbed Energy (ft-lbs)	18.8
Brace Length (in)	237.5

Area (in²)	6.58
Moment of Inertia (in⁴)	22.8
Corner Radius (in)	0.729
Thickness - Nominal (in)	0.375
Thickness - Measured (in)	0.376
Brace Compactness Ratio (*b/t*) - Nominal	10.3
Brace Compactness Ratio (*b/t*) - Measured	9.42
Global Slenderness ratio (*KL/r*)	127.7

Specimen Performance

Test Event	Axial Brace Displacement (in)	Target Displacement (in) (Cycle)	Force (kips)	$P / P_{Yield/Critical}$	
Peak Tension Load	1.83	2.25 (1)	443.6	1.02	Y
B1: Initial Global Buckling	-0.19	0.25 (1)	-98.4	0.97	C
B2: Moderate Global Buckling	-1.26	1.25 (1)	-57.5	0.57	C
B3-T: Local Cupping	-5.01	5.25 (1)	-17.6	0.17	C
B3-C: Striations & Tearing	4.43	5.75 (2)	76.0	0.17	Y
B4: Brace Fracture	5.25	5.75 (2)	116.7	0.27	Y

Key Observations

Cycle #	Displacement (in.)	Observations
11-12	0.75	Bolt slip first tension cycle - North gusset plate. Knocking/banging sounds when specimen in tension occurred during this cycle and beyond
15-16	1.75	Bolt slip first tension cycle - South gusset plate
27-28	4.75	Minor cupping observed at peak compressive displacements at the center of the specimen - east face
29-30	5.25	Moderate cupping observed at first peak compressive displacement Major cupping observed at second peak compressive displacement - cycle 30
31-32	5.75	Brace survived first tensile displacement - cycle 31 Major cupping observed at first peak compressive displacement - cycle 31 Brace tearing and fracture - second tensile displacement - cycle 32

Test Results

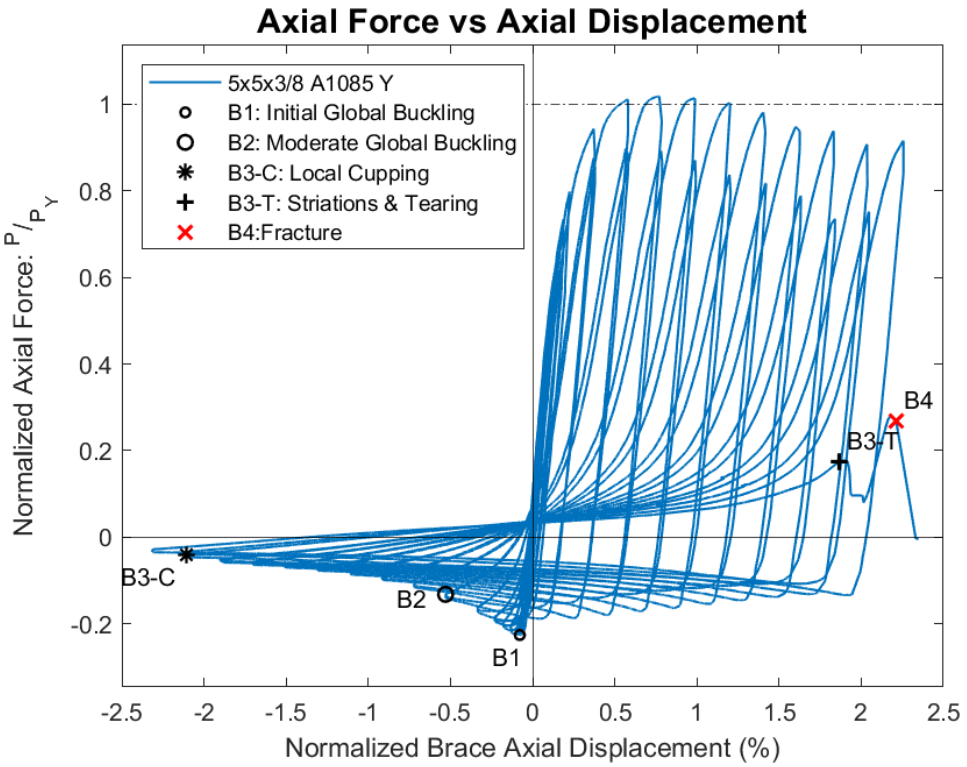

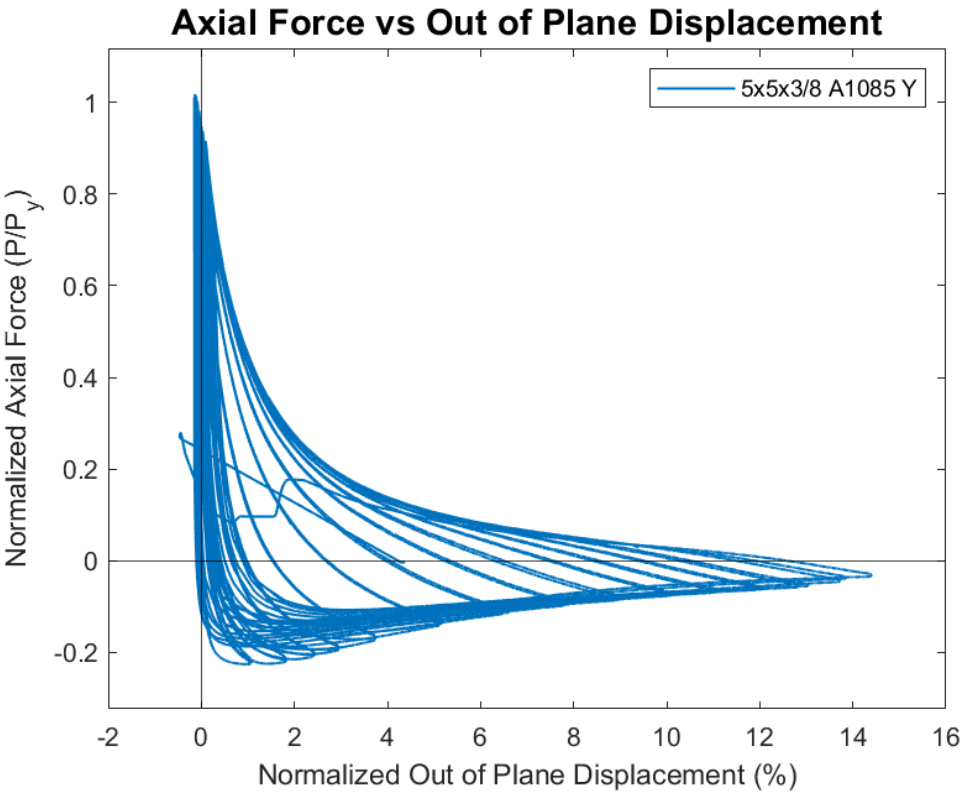

Photos

Development of Tearing in Tension - 2nd cycle at 5.75”

Brace Fracture: 2nd Cycle at 5.75”

Peak Out of Plane Displacement: 5.75” Cycles

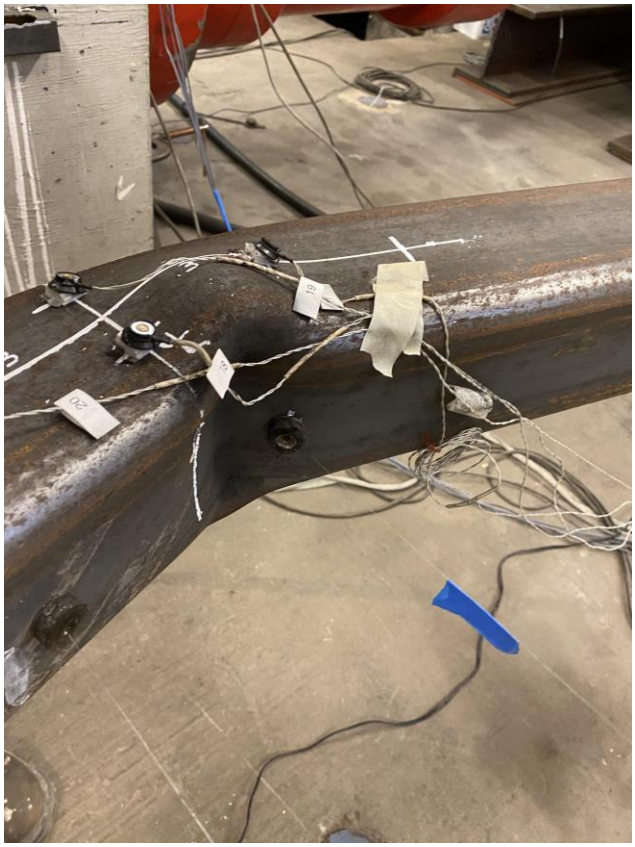

Cupping at Center of Specimen: 5.25” Cycles

6x6x5/16 A500 R Brace Test Summary

Test Name: 6x6x5/16 A500 R
Test Date: 4/7/2021

Brace Properties

Measured Yield Stress (ksi)	57.37	**Area (in²)**	6.43
Measured Ultimate Stress (ksi)	72.77	**Moment of Inertia (in⁴)**	34.3
Yield Load (kips)	386.6	**Corner Radius (in)**	0.59
Critical Buckling Load (kips)	152.7	**Thickness - Nominal (in)**	0.291
Percent Elongation - 2" (%)	34.65	**Thickness - Measured (in)**	0.305
CVN Width (mm)	5	**Brace Compactness Ratio (*b/t*) - Nominal**	17.6
CVN Absorbed Energy (ft-lbs)	40.8	**Brace Compactness Ratio (*b/t*) - Measured**	15.80
Brace Length (in)	237.5	**Global Slenderness ratio (*KL/r*)**	102.8

Specimen Performance

Test Event	Axial Brace Displacement (in)	Target Displacement (in) (Cycle)	Force (kips)	$P / P_{Yield/Critical}$	
Peak Tension Load	1.85	2.25 (1)	409.7	1.06	Y
B1: Initial Global Buckling	-0.22	0.25 (1)	-125.8	0.82	C
B2: Moderate Global Buckling	-1.79	1.75 (1)	-52.8	0.35	C
B3-T: Local Cupping	-2.72	2.75 (2)	-30.1	0.20	C
B3-C: Striations & Tearing	2.45	3.25 (2)	252.0	0.65	Y
B4: Brace Fracture	2.93	3.75 (1)	99.6	0.26	Y

Key Observations

Cycle #	Displacement (in.)	Observations
15-16	1.75	Bolt slip at first tension cycle (15): ~⅛" Bolt slip at north and south gusset plates Knocking/banging sounds in tension - observed in all future cycles
19-20	2.75	Minor cupping observed at first compressive displacement - minimal at East/West faces Local cupping observed at second compressive displacement - center of cupping: 4.5" north of brace center
21-22	3.25	Major cupping at first and second peak compressive displacements Tearing began to occur when specimen in tension during second cycle 22 After tearing in specimen - buckling direction switched to east due to tearing initiating on the east face of the specimen. Out of plane string pots at quarter points and center of specimen out of range (cycle 22)
23-24	3.75	Specimen fractured in tension during first cycle (23)

Test Results

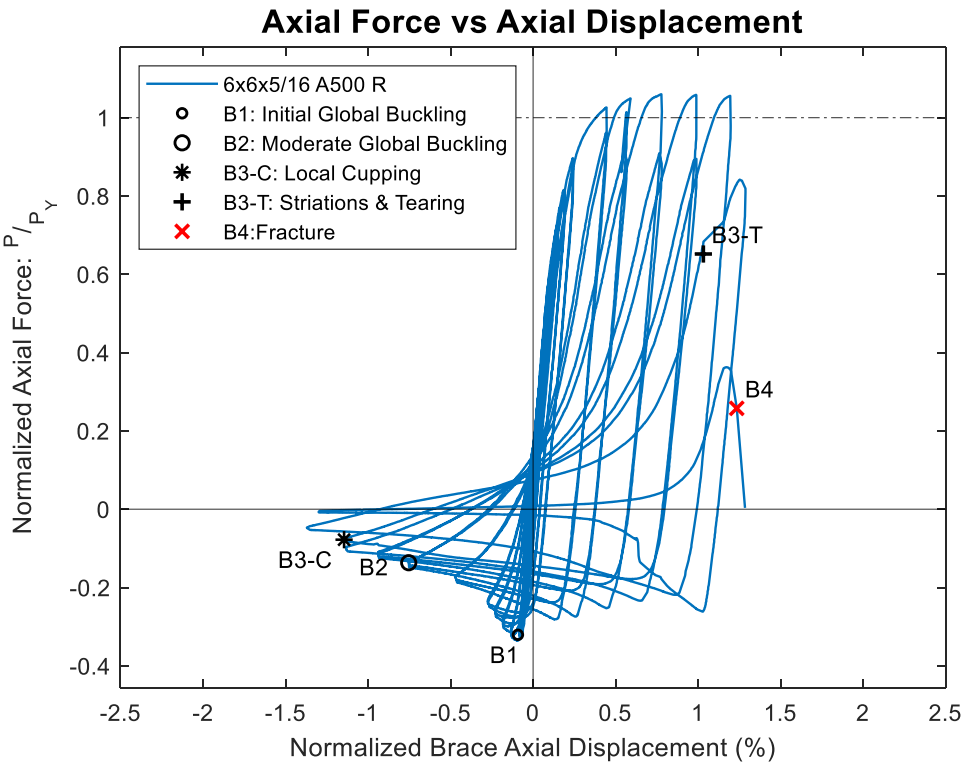

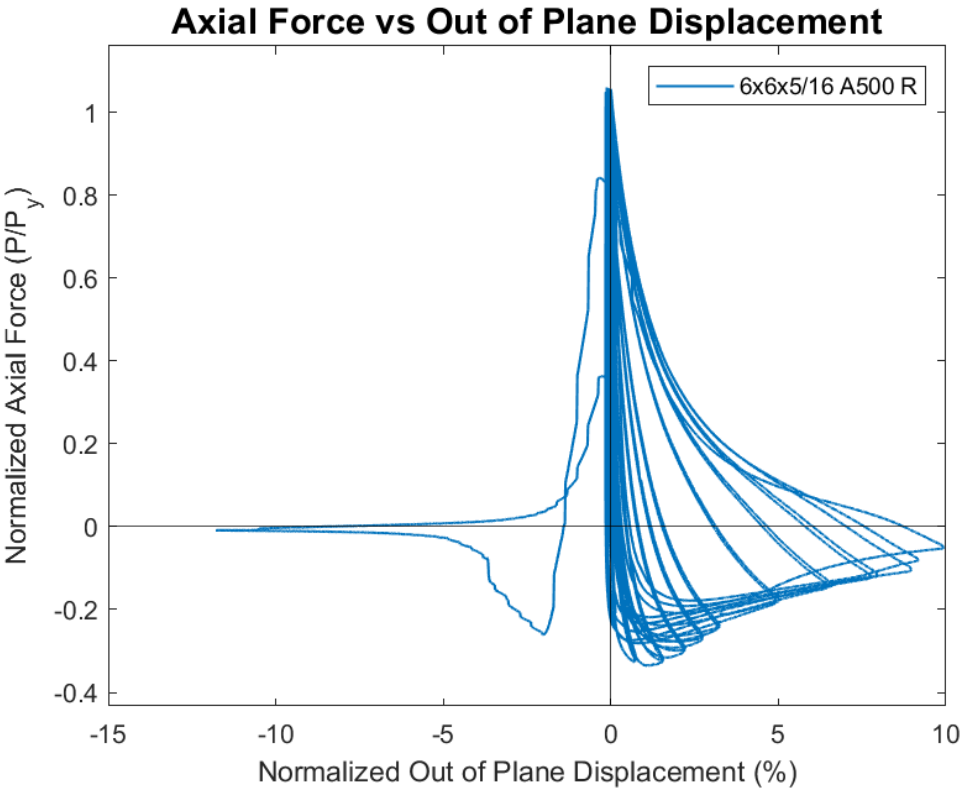

Photos

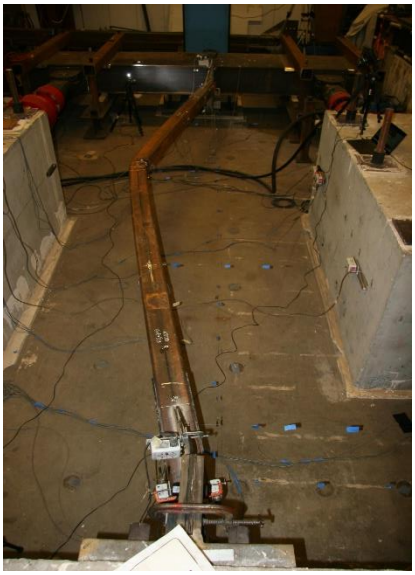

Peak Out of Plane Displacement (West): 3.25” Cycle 1

Peak Out of Plane Displacement (East): 3.25” Cycle 2

Fractured Specimen: 3.75” Displacement Cycle 1 - Tension Displacement

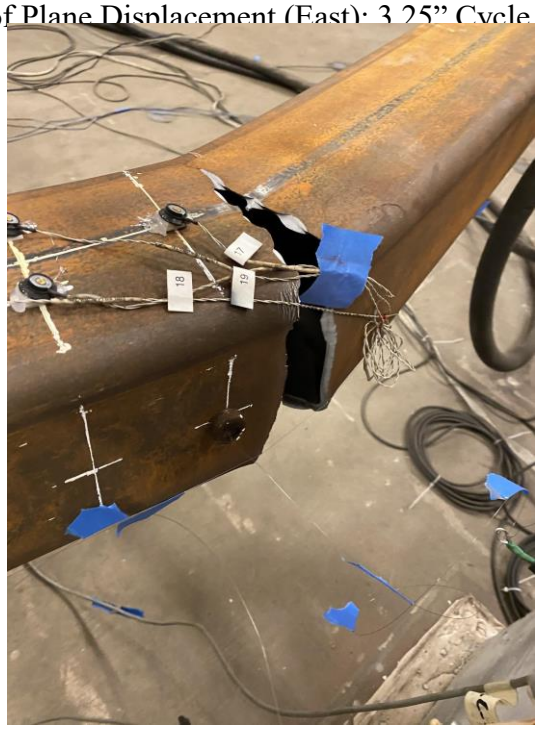

Tearing in Specimen: Cycle 2 at 3.25”

6x6x5/16 A1085 Y Brace Test Summary

Test Name: 6x6x5/16 A1085 Y
Test Date: 4/28/2021

Brace Properties

Measured Yield Stress (ksi)	62.07
Measured Ultimate Stress (ksi)	71.92
Yield Load (kips)	426.4
Critical Buckling Load (kips)	1110.2
Percent Elongation - 2" (%)	34.11
CVN Width (mm)	5
CVN Absorbed Energy (ft-lbs)	23
Brace Length (in)	237.5

Area (in^2)	6.87
Moment of Inertia (in^4)	36.3
Corner Radius (in)	0.676
Thickness - Nominal (in)	0.313
Thickness - Measured (in)	0.313
Brace Compactness Ratio (*b/t*) - Nominal	16.2
Brace Compactness Ratio (*b/t*) - Measured	14.85
Global Slenderness ratio (*KL/r*)	103.3

Specimen Performance

Test Event	Axial Brace Displacement (in)	Target Displacement (in) (Cycle)	Force (kips)	$P / P_{Yield/Critical}$	
Peak Tension Load	1.90	2.25 (1)	456.4	1.07	Y
B1: Initial Global Buckling	-0.18	0.25 (1)	-139.8	0.13	C
B2: Moderate Global Buckling	-1.63	1.75 (1)	-64.0	0.06	C
B3-T: Local Cupping	-2.56	2.75 (2)	-33.5	0.03	C
B3-C: Striations & Tearing	2.46	3.25 (2)	272.0	0.64	Y
B4: Brace Fracture	3.13	3.75 (1)	123.0	0.29	Y

Key Observations

Cycle #	Displacement (in)	Observations
9-10	0.625	Bolt slip - T1 - north and south gusset plates Knocking/racking sounds observed in tension - future cycles too Similar to previous cycles otherwise
17-18	2.25	Minimal local cupping at C2 peak compressive displacement (~1/16”)
19-20	2.75	Minor local cupping (¼”) at C1 peak Moderate cupping at C2 peak - centered 1.5” north of center
21-22	3.25	Major cupping at C1 Tearing observed at T2 near peak tensile displacement Major cupping at C2 post-tearing
23-24	3.75	Fracture at T1!

Test Results

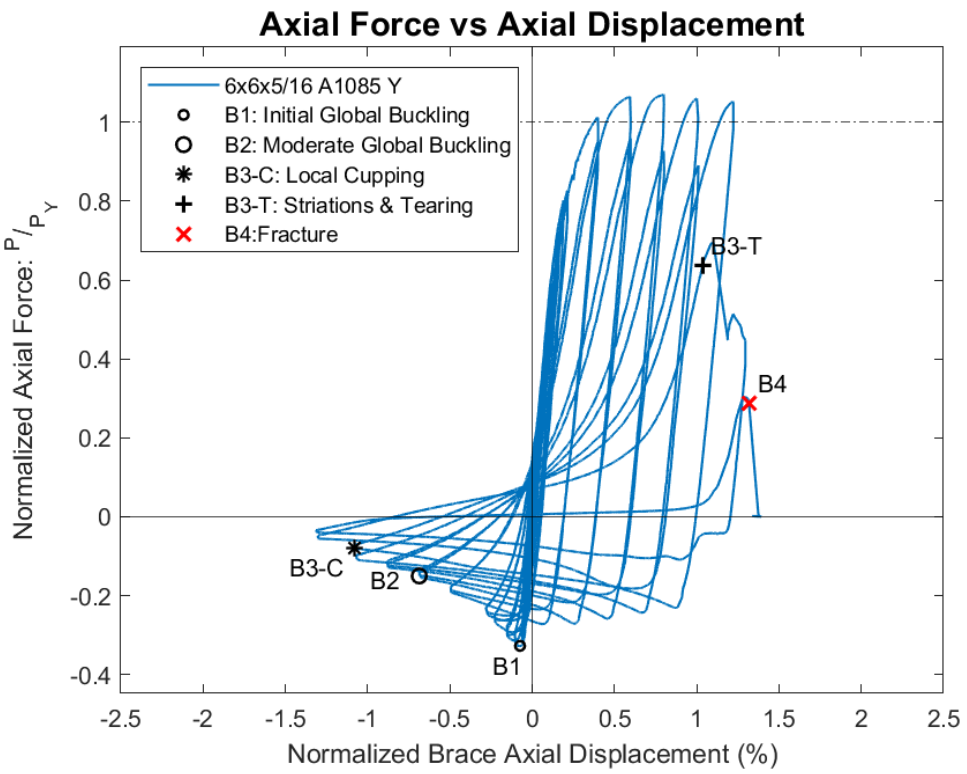

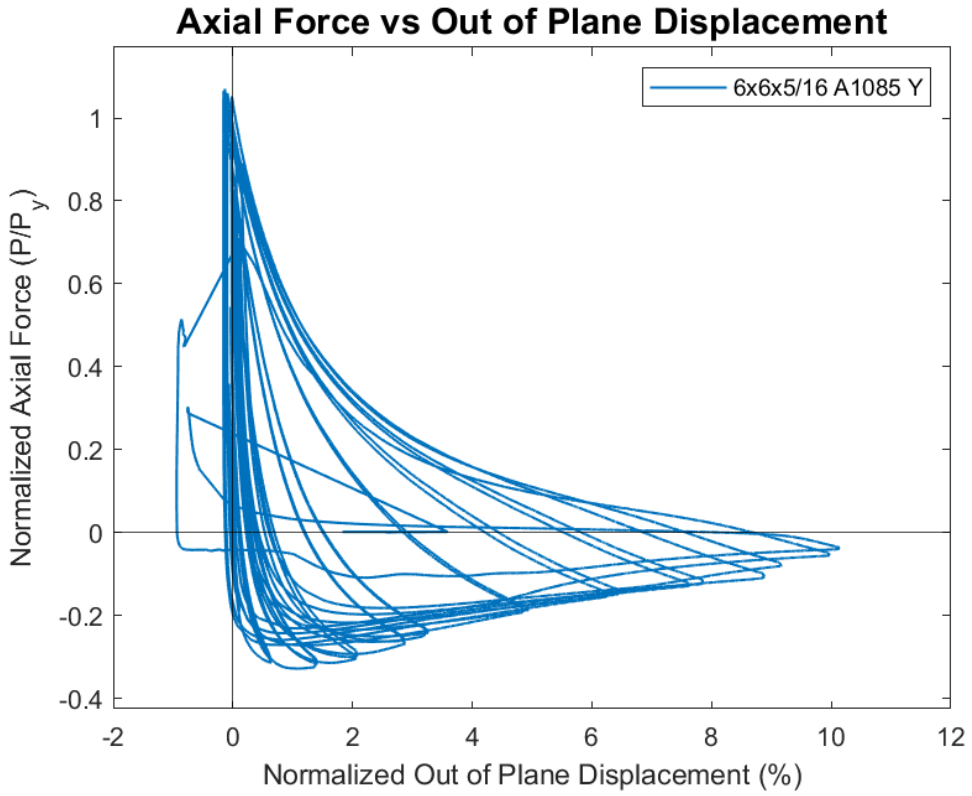

Photos

Cupping at Center of Specimen: 3.25” Cycle 1 C

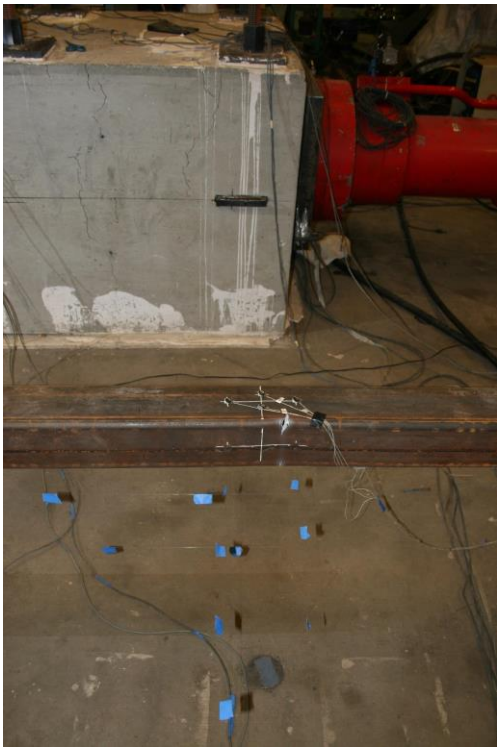

Initiation of Tearing: 3.25” Cycle 2 T

Cupping at Center of Specimen: 3.25” Cycle 2 C

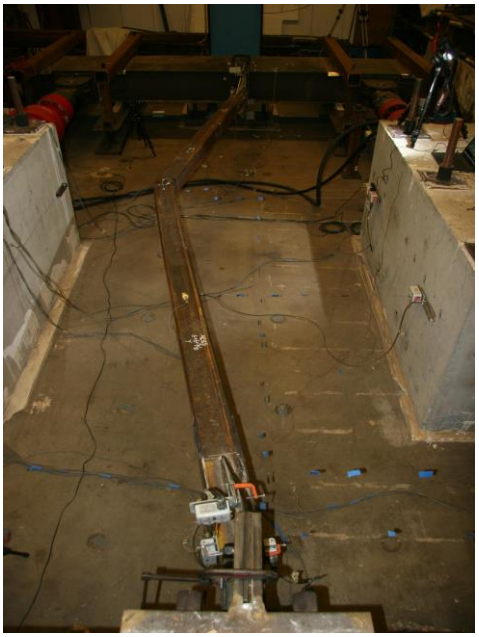

Peak Out of Plane Displacement: 3.25” Cycles

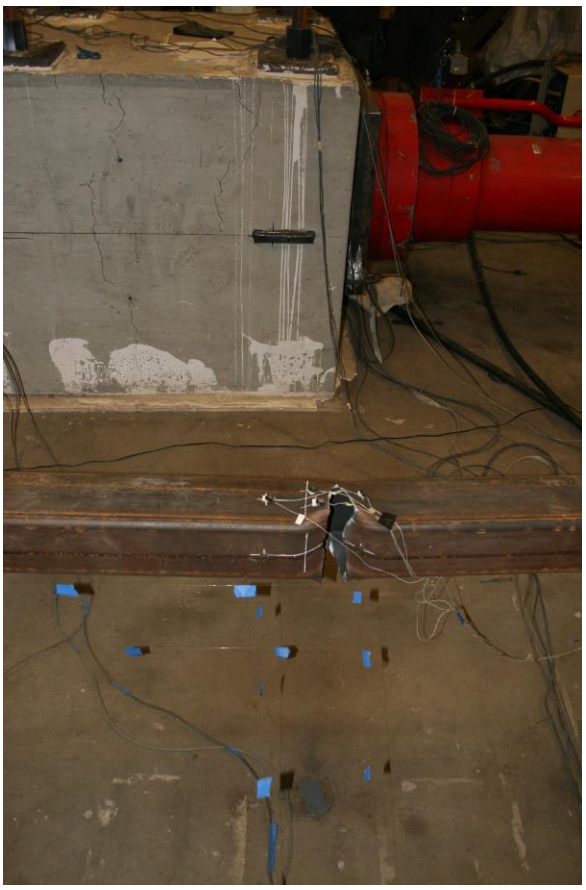

Tearing Prior to Fracture: 3.75” Cycle 1 T

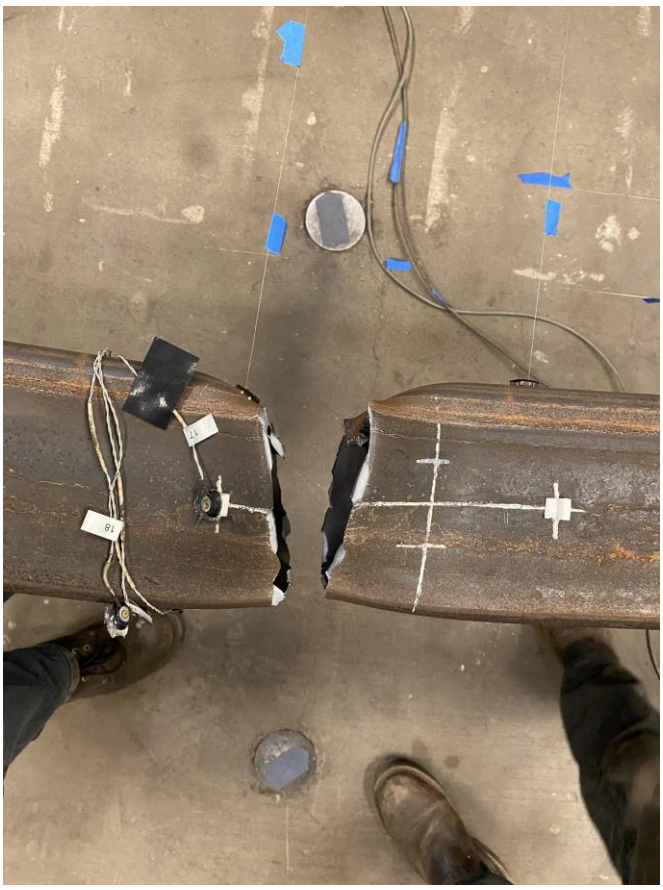

Fractured Specimen: 3.75” Cycle 1 T

6x6x3/8 A500 R Brace Test Summary

Test Name: 6x6x3/8 A500 R
Test Date: 4/22/2021

Brace Properties

Measured Yield Stress (ksi)	61.19
Measured Ultimate Stress (ksi)	76.36
Yield Load (kips)	487.7
Critical Buckling Load (kips)	175.2
Percent Elongation - 2" (%)	35.36
CVN Width (mm)	7.5
CVN Absorbed Energy (ft-lbs)	42.5
Brace Length (in)	237.5

Area (in²)	7.58
Moment of Inertia (in⁴)	39.5
Corner Radius (in)	0.75
Thickness - Nominal (in)	0.349
Thickness - Measured (in)	0.367
Brace Compactness Ratio (*b/t*) - Nominal	14.2
Brace Compactness Ratio (*b/t*) - Measured	12.26
Global Slenderness ratio (*KL/r*)	104.2

Specimen Performance

Test Event	Axial Brace Displacement (in)	Target Displacement (in) (Cycle)	Force (kips)	P / $P_{Yield/Critical}$	
Peak Tension Load	1.78	2.25 (1)	511.0	1.05	Y
B1: Initial Global Buckling	-0.19	0.25 (1)	-168.7	0.96	C
B2: Moderate Global Buckling	-1.75	1.75 (1)	-72.0	0.41	C
B3-T: Local Cupping	-3.16	3.25 (2)	-43.5	0.25	C
B3-C: Striations & Tearing	3.23	3.75 (2)	428.0	0.88	Y
B4: Brace Fracture	3.74	4.25 (1)	190.0	0.39	Y

Key Observations

Cycle #	Displacement (in.)	Observations
9-10	0.625	Bolt slip South Gusset Plate, T1
13-14	1.25	Bolt slip North Gusset Plate, T1 Cracking/racking noises in tension
21-22	3.25	Minor cupping observed (~⅛") - C1 Increased cupping observed (~⅜") - C2
23-24	3.75	Major cupping ~1.5" north of center - C1 Small striations in top East corner at the center of brace - T2 Major cupping observed - C2
25-26	4.25	Tearing & Fracture - T1

Test Results

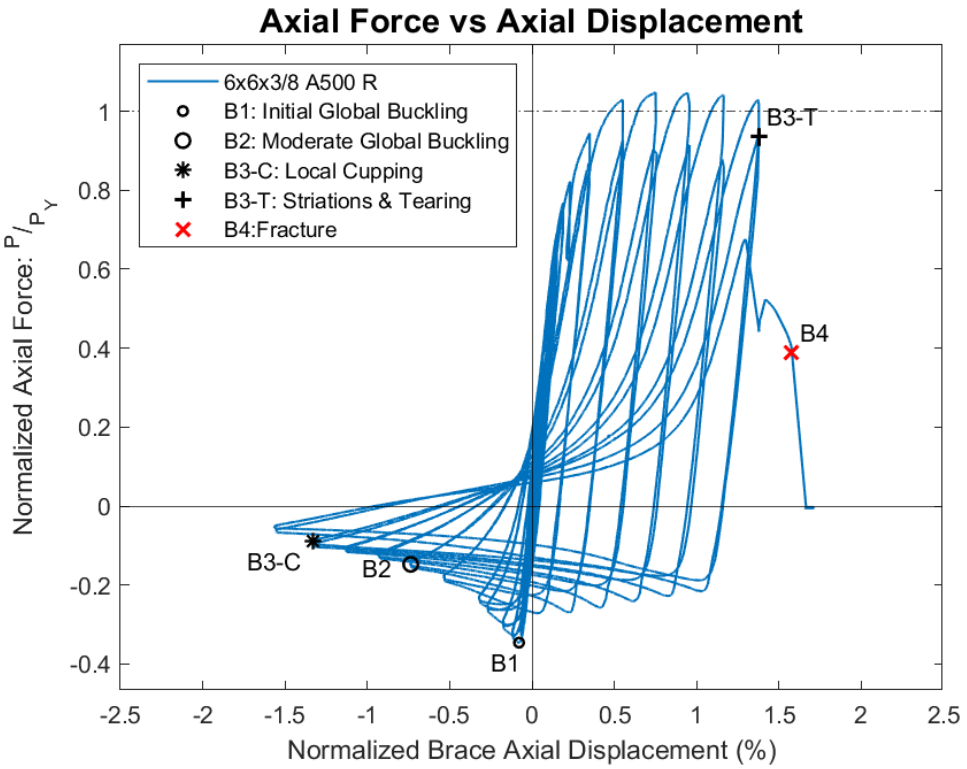

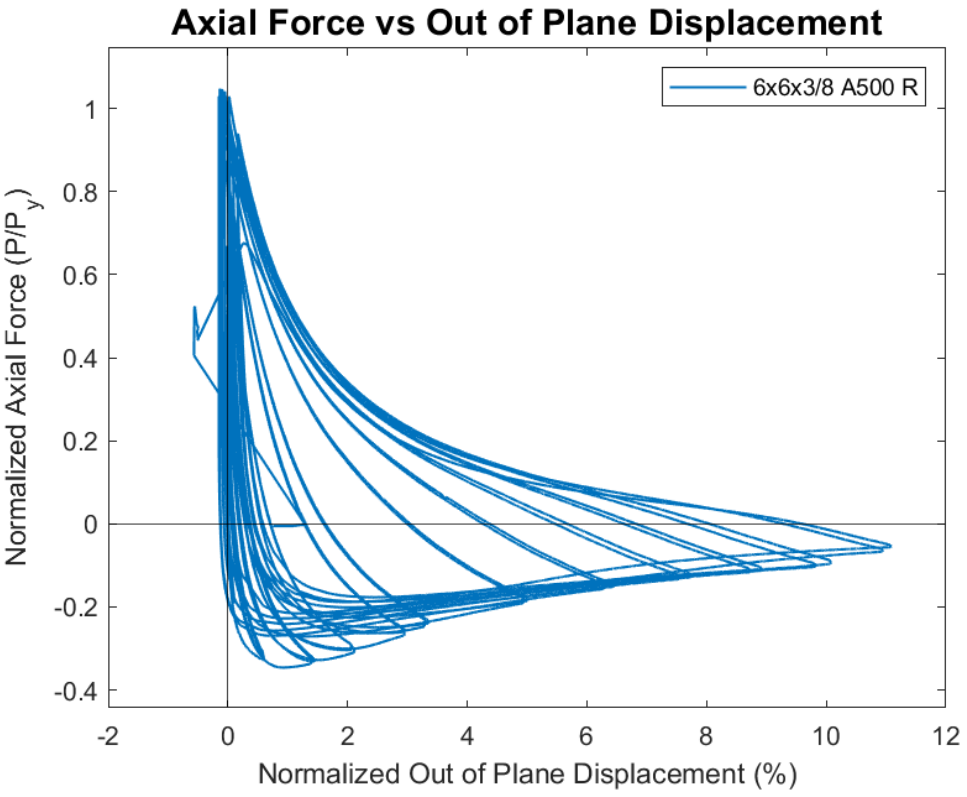

Photos

Peak Out of Plane Displacement: 3.75” Cycles

Initial Striations at Center of Specimen: 2nd Cycle at 3.75”

Cupping at Center of Specimen: 3.75” Cycle

Fractured Specimen: First Cycle at 4.25”

6x6x3/8 A1085 Y Brace Test Summary

Test Name: 6x6x3/8 A1085 Y
Test Date: 4/23/2021

Brace Properties

Measured Yield Stress (ksi)	66.81
Measured Ultimate Stress (ksi)	72.64
Yield Load (kips)	539.8
Critical Buckling Load (kips)	185.4
Percent Elongation - 2" (%)	31.86
CVN Width (mm)	7.5
CVN Absorbed Energy (ft-lbs)	18.7
Brace Length (in)	237.5

Area (in²)	8.08
Moment of Inertia (in⁴)	41.6
Corner Radius (in)	0.715
Thickness - Nominal (in)	0.375
Thickness - Measured (in)	0.375
Brace Compactness Ratio (*b/t*) - Nominal	13
Brace Compactness Ratio (*b/t*) - Measured	12.19
Global Slenderness ratio (*KL/r*)	104.6

Specimen Performance

Test Event	Axial Brace Displacement (in)	Target Displacement (in) (Cycle)	Force (kips)	$P / P_{Yield/Critical}$	
Peak Tension Load	1.76	2.25 (1)	547.9	1.01	Y
B1: Initial Global Buckling	-0.15	0.25 (1)	-180.0	0.97	C
B2: Moderate Global Buckling	-1.63	1.75 (1)	-81.0	0.44	C
B3-T: Local Cupping	-3.06	3.25 (2)	-40.4	0.22	C
B3-C: Striations & Tearing	2.70	3.75 (2)	196.4	0.36	Y
B4: Brace Fracture	0.55	3.75 (2)	-25.2	0.14	C

Key Observations

Cycle #	Displacement (in)	Observations
7-8	0.5	Bolt slip: N & S gusset plates - Cycle T1 Similar OOP displacement as previous cycles
21-22	3.25	Minor cupping at C1 peak compressive displacement (~¼") Moderate cupping at C2 peak Center of cupping ~1" south of center
23-24	3.75	Major cupping at C1 peak Tearing at T2 - did not fracture! Tearing in east/top/bottom faces Specimen fractured as it was put into compression - C2 Ductile tearing of west face - fractured

Test Results

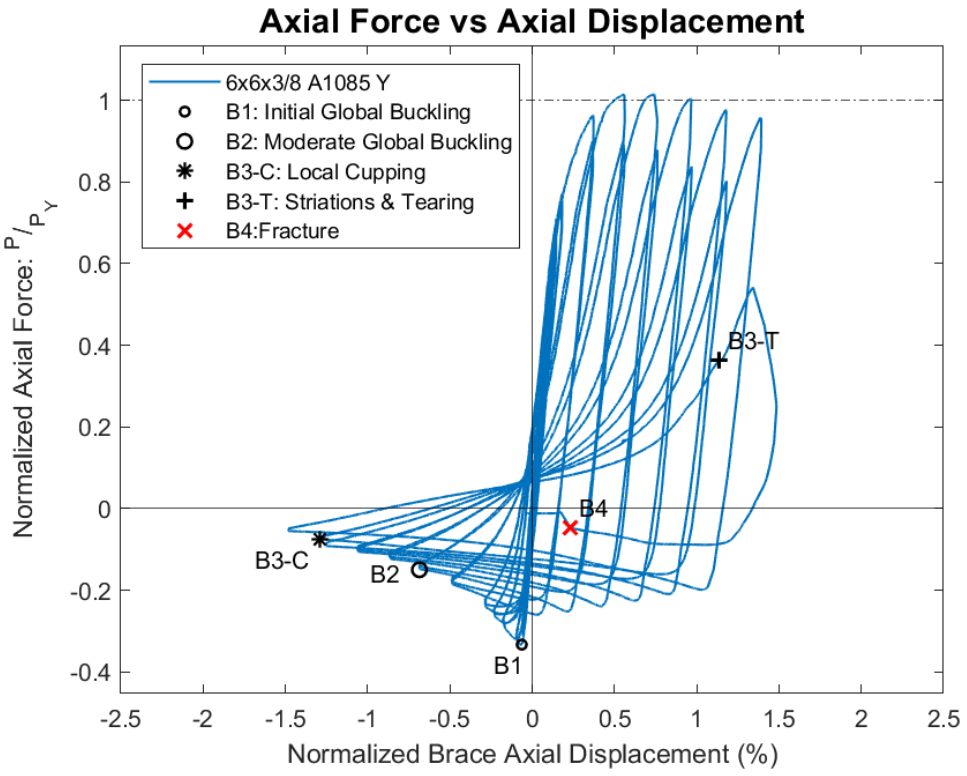

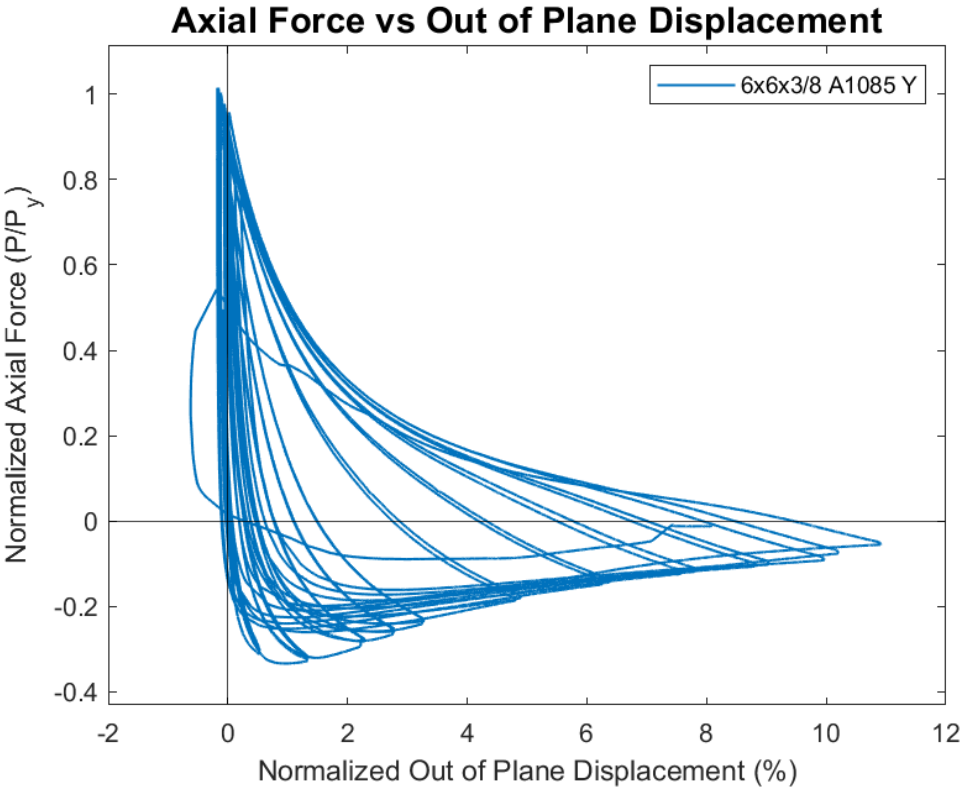

Photos

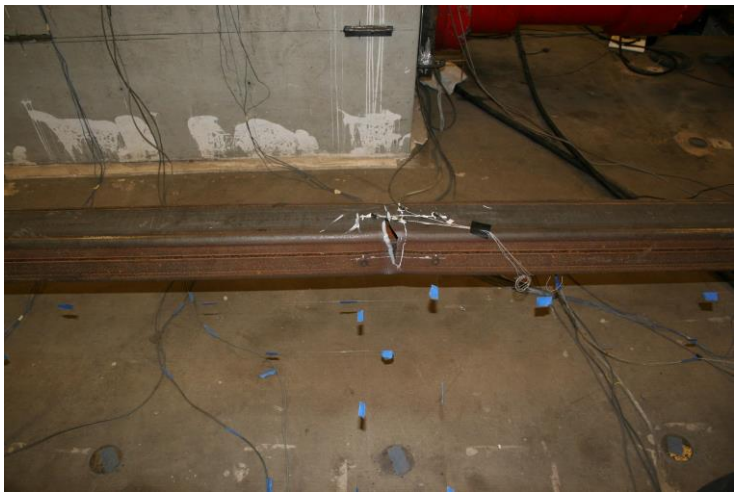

Tearing at Center of Specimen: First Cycle at 3.75”

Ductile Fracture of Specimen in Compression at 3.75”

Cupping at Center of Specimen: 3.75” Cycle 1

Fractured Specimen

6x6x1/2 A500 R Brace Test Summary

Test Name: 6x6x1/2 A500 R
Test Date: 4/30/2021

Brace Properties

Measured Yield Stress (ksi)	62.84
Measured Ultimate Stress (ksi)	67.05
Yield Load (kips)	630.5
Critical Buckling Load (kips)	215.6
Percent Elongation - 2" (%)	33.48
CVN Width (mm)	10
CVN Absorbed Energy (ft-lbs)	120+
Brace Length (in)	237.5

Area (in²)	9.74
Moment of Inertia (in⁴)	48.3
Corner Radius (in)	0.984
Thickness - Nominal (in)	0.465
Thickness - Measured (in)	0.479
Brace Compactness Ratio (*b/t*) - Nominal *	9.9
Brace Compactness Ratio (*b/t*) - Measured	8.42
Global Slenderness ratio (*KL/r*)	106.5

Specimen Performance

Test Event	Axial Brace Displacement (in)	Target Displacement (in) (Cycle)	Force (kips)	$P / P_{Yield/Critical}$	
Peak Tension Load	1.24	2.25 (1)	646.2	1.02	Y
B1: Initial Global Buckling	-0.18	0.375 (1)	-218.7	1.01	C
B2: Moderate Global Buckling	-1.20	1.25 (1)	-111.0	0.51	C
B3-T: Local Cupping	-3.58	3.75 (2)	-44.0	0.20	C
B3-C: Striations & Tearing	3.78	4.25 (1)	492.0	0.78	Y
B4: Brace Fracture	0.20	4.75 (1)	-43.3	0.20	C

Key Observations

Cycle #	Displacement (in)	Observations
9-10	0.625	Bolt slip - T1 - north and south gusset plates Knocking/racking of bolts in tension - observed in future cycles
21-22	3.25	Minor cupping at C1 & C2 peak (~1/4”)
23-24	3.75	Cupping at C1 peak (~⅝”) Cupping at C2 peak (~¾”) VERY hot to touch at center - C2 - much warmer than previous tests
25-26	4.25	Striations observed at T1: East side corners Major cupping at C1 & C2 peak Minor tearing observed at T2
27-28	4.75	Tearing at T1: Tore through half of the brace (East side) Complete fracture in C1 at before reaching peak displacement!

Test Results

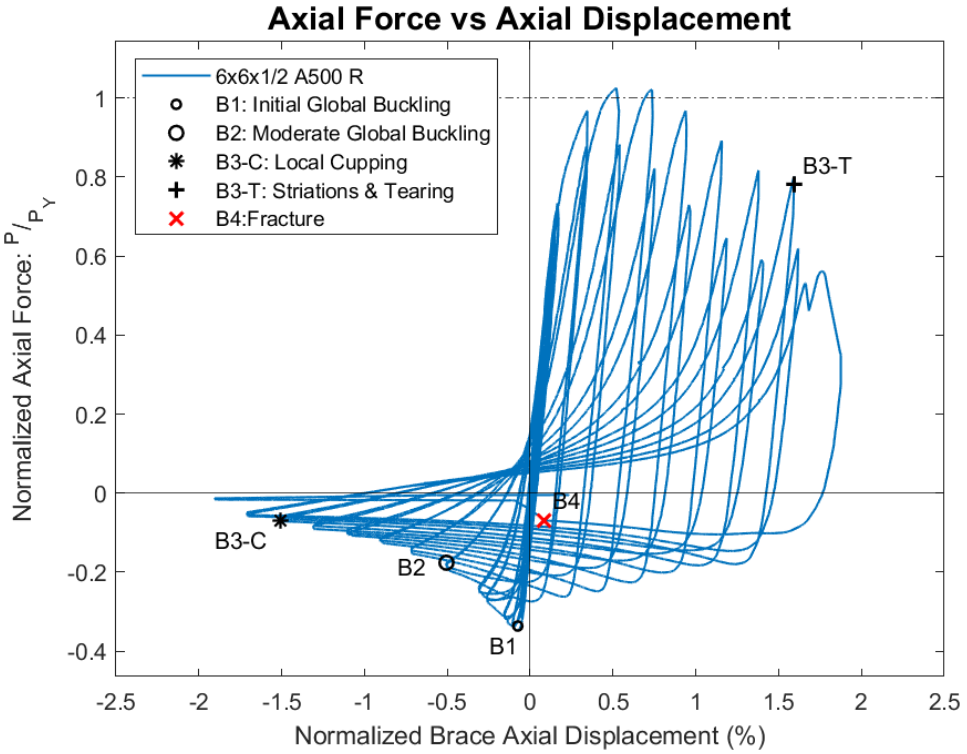

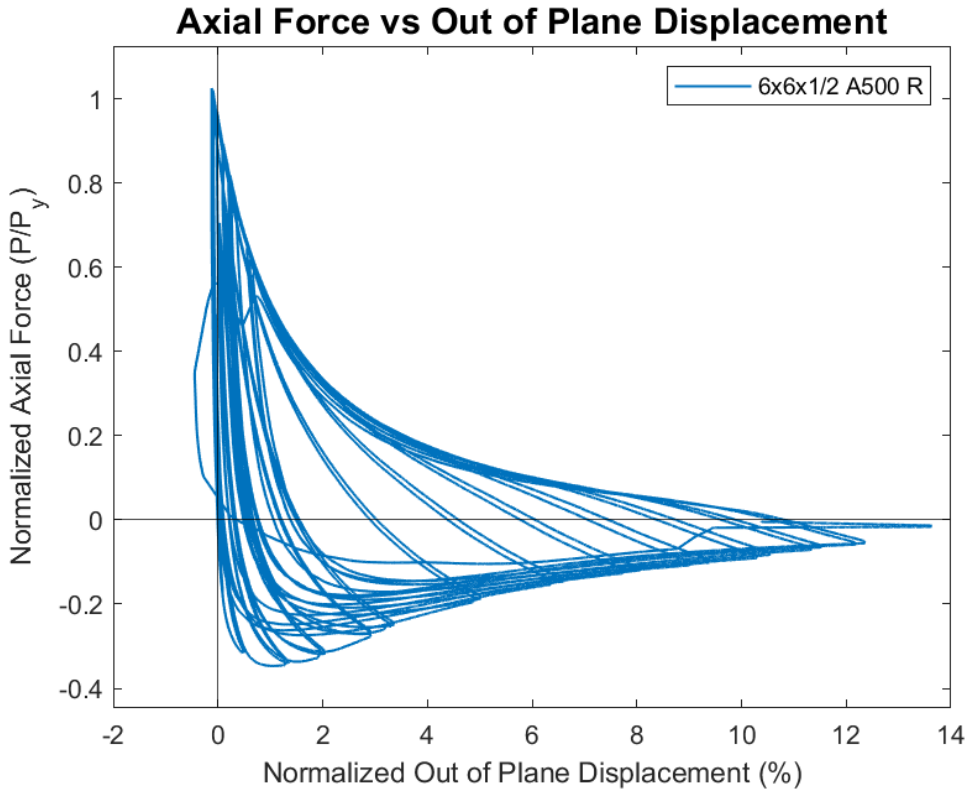

Photos

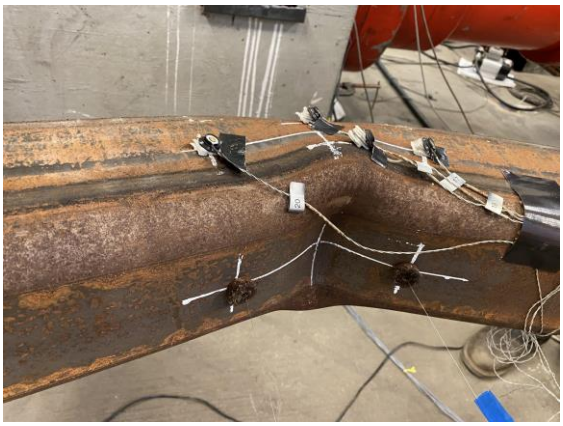

Cupping at Center of Brace: 3.75” Cycles

Initiation of Brace Tearing: 4.25” Cycle 2

Brace Tearing: 4.75” Cycle 1

Peak Out of Plane Displacement: 4.25” Cycles

Fractured Specimen: After Cycle 1 at 4.75”

6x6x1/2 A1085 Y Brace Test Summary

Test Name: 6x6x1/2 A1085 Y
Test Date: 5/6/2021

Brace Properties

Measured Yield Stress (ksi)	67.85	**Area (in²)**	10.36
Measured Ultimate Stress (ksi)	71.96	**Moment of Inertia (in⁴)**	50.5
Yield Load (kips)	683.2	**Corner Radius (in)**	0.833
Critical Buckling Load (kips)	225.0	**Thickness - Nominal (in)**	0.5
Percent Elongation - 2" (%)	34.48	**Thickness - Measured (in)**	0.486
CVN Width (mm)	10	**Brace Compactness Ratio (*b/t*) - Nominal**	9
CVN Absorbed Energy (ft-lbs)	27.8	**Brace Compactness Ratio (*b/t*) - Measured**	8.92
Brace Length (in)	237.5	**Global Slenderness ratio (*KL/r*)**	107.5

Specimen Performance

Test Event	Axial Brace Displacement (in)	Target Displacement (in) (Cycle)	Force (kips)	$P / P_{Yield/Critical}$	
Peak Tension Load	1.61	2.25 (1)	727.2	1.06	Y
1: Initial Global Buckling	-0.19	0.375 (1)	-218.6	0.97	C
2: Moderate Global Buckling	-1.75	1.75 (1)	-109.2	0.49	C
3-T: Local Cupping	-4.13	4.25 (2)	-51.6	0.23	C
3-C: Striations & Tearing	4.49	5.25 (1)	626.6	0.92	Y
4: Brace Fracture	4.67	5.75 (1)	200.0	0.29	Y

Key Observations

Cycle #	Displacement (in.)	Observations
7-8	0.5	Bolt slip N & S gusset plates- T1
23-24	3.75	Minor cupping - C2 (~⅛")
25-26	4.25	Minor cupping - C1 (~¼") Moderate cupping - C2 (~½"), Center of cupping: ½" north of center
27-28	4.75	Cupping at C1 peak: ~1" Major Cupping at C2 peak Difficult to measure cupping at C1 and C2 due to significant local deformations at the top and bottom corners - fold in and up
29-30	5.25	Striations at center - T1 peak displacement Major cupping at C1 peak - very deep Fractured at T2 before reaching peak tensile displacement

Test Results

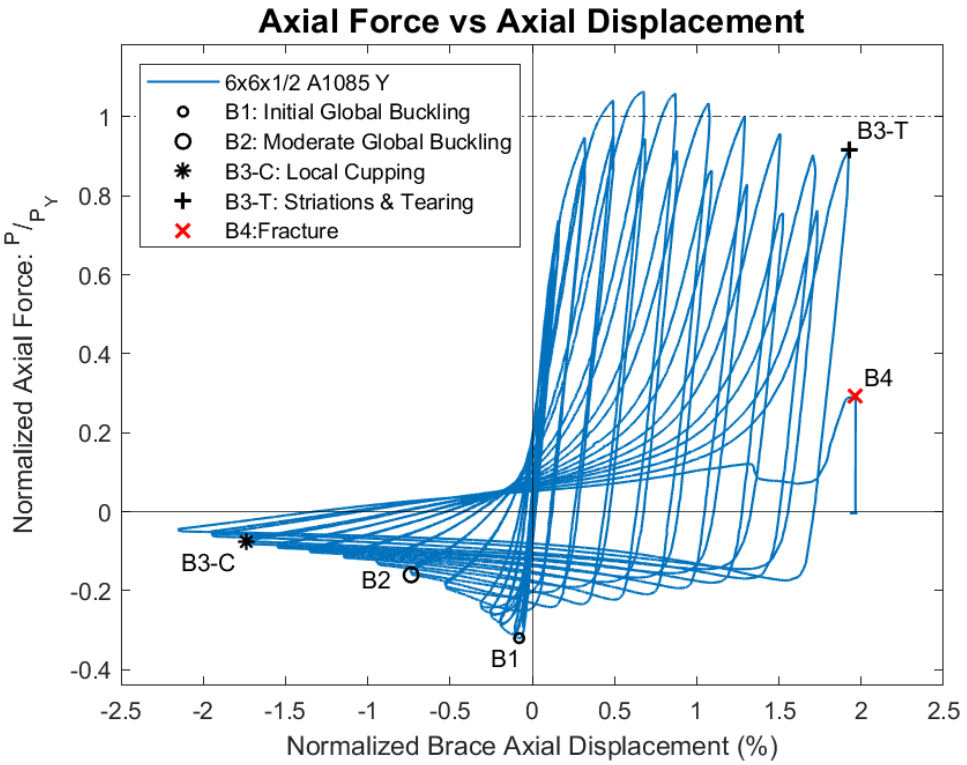

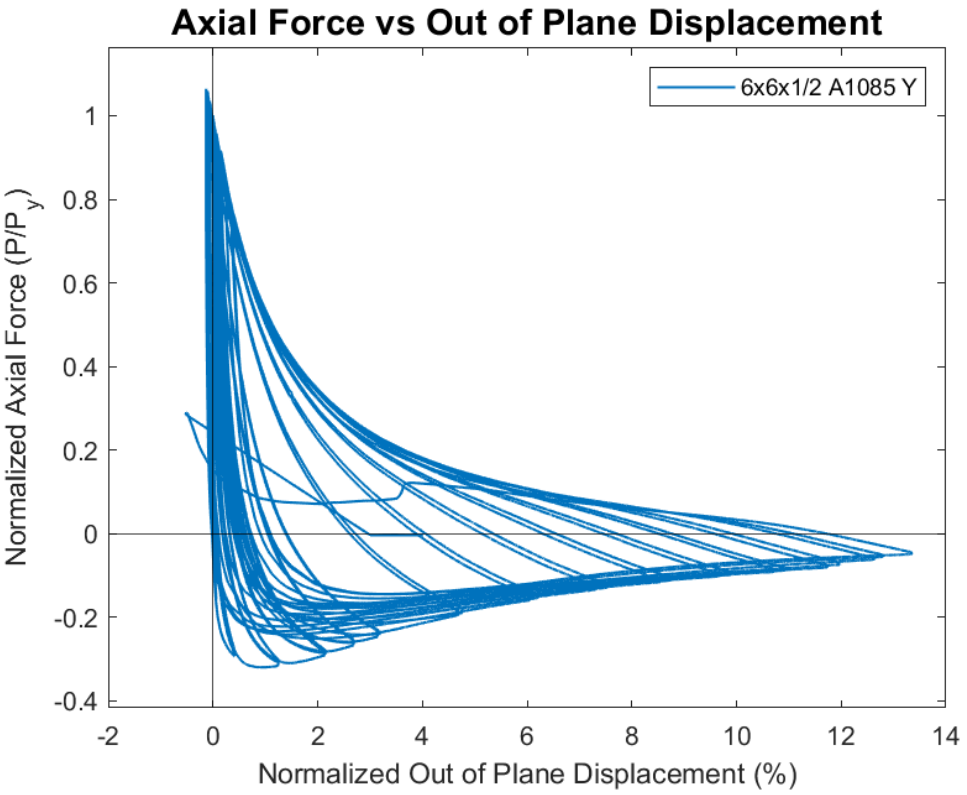

Photos

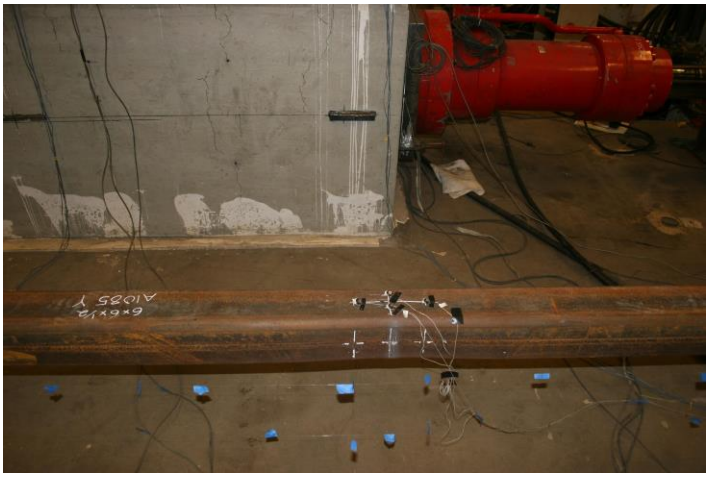

Development of Striations in Tension: First 5.25” Cycle

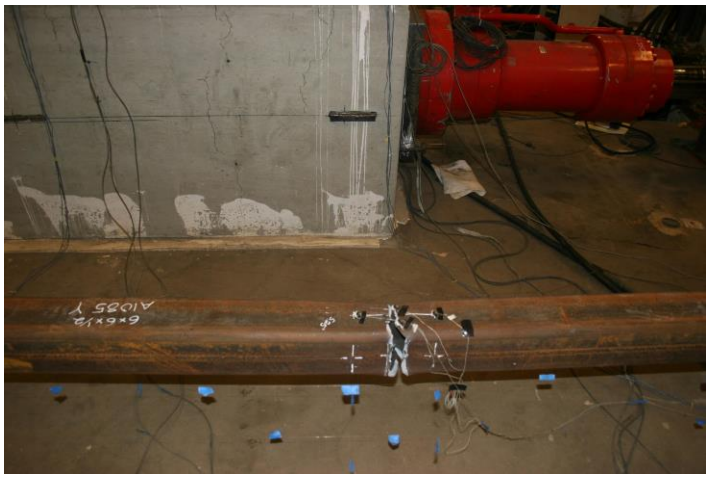

Tearing at Center of Specimen: Second 5.25” Cycle

Cupping at Center of Specimen: 4.75” Cycles

Fractured Specimen: Second Cycle at 5.25”

Peak Out of Plane Displacement: 5.25” Cycle

7x7x5/16 A500 Y Brace Test Summary

Test Name: 7x7x5/16 A500 Y
Test Date: 5/19/2021 - 11:00 AM

Brace Properties

Measured Yield Stress (ksi)	62.71
Measured Ultimate Stress (ksi)	70.02
Yield Load (kips)	474.3
Critical Buckling Load (kips)	239.1
Percent Elongation - 2" (%)	31.16
CVN Width (mm)	5
CVN Absorbed Energy (ft-lbs)	15.7
Brace Length (in)	237.5

Area (in²)	7.59
Moment of Inertia (in⁴)	56.1
Corner Radius (in)	0.66
Thickness - Nominal (in)	0.291
Thickness - Measured (in)	0.29
Brace Compactness Ratio (*b/t*) - Nominal	21.1
Brace Compactness Ratio (*b/t*) - Measured	19.59
Global Slenderness ratio (*KL/r*)	87.3

Specimen Performance

Test Event	Axial Brace Displacement (in)	Target Displacement (in) (Cycle)	Force (kips)	$P / P_{Yield/Critical}$	
Peak Tension Load	1.23	1.75 (1)	496.6	1.05	Y
B1: Initial Global Buckling	-0.21	0.375 (1)	-209.8	0.88	C
B2: Moderate Global Buckling	-1.65	1.75 (1)	-58.6	0.25	C
B3-T: Local Cupping	-1.82	1.75 (1)	-54.5	0.23	C
B3-C: Striations & Tearing	1.04	2.25 (1)	323.3	0.68	Y
B4: Brace Fracture	1.73	2.25 (1)	193.0	0.41	Y

Key Observations

Cycle #	Displacement (in.)	Observations
7-8	0.5	Bolt slip T1 - N & S gusset plates Minor OOP buckling displacement
13-14	1.25	Similar to previous cycles No visible cupping observed & still cold at center
15-16	1.75	Moderate cupping observed - C1 (~1” deep) at C1. Cupping centered about 6” south of center Major cupping observed at C2 peak compressive displacement (1.75” deep) with significant vertical bending of top and bottom sides of tube at the location of cupping
17-18	2.25	Fractured in tension prior to reaching T1 peak displacement

Test Results

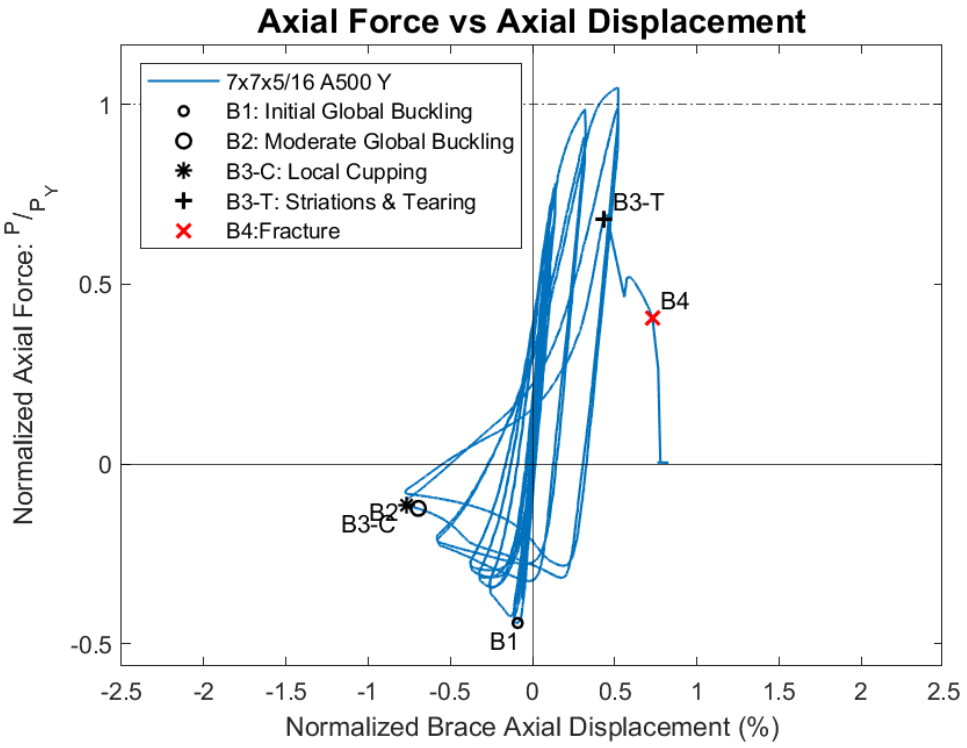

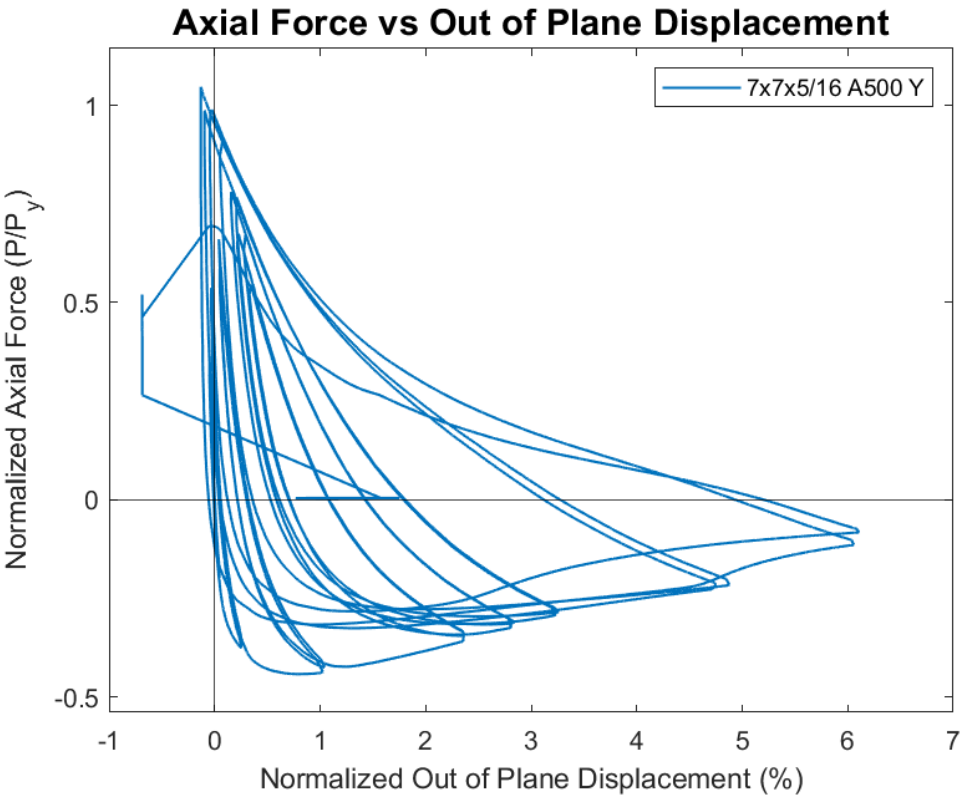

Photos

Cupping at Center of Specimen: 1.75” Cycle 1 & 2 C

Fractured Specimen: 2.25” Cycle 1 T

Initial Striations at Center of Specimen: 2.25” Cycle 1 T

Tearing at Center of Specimen: 2.25” Cycle 1 T

7x7x5/16 A1085 Y Brace Test Summary

Test Name: 7x7x5/16 A1085 Y
Test Date: 5/20/2021 - 2:30 PM

Brace Properties

Measured Yield Stress (ksi)	57.7
Measured Ultimate Stress (ksi)	64.13
Yield Load (kips)	456.5
Critical Buckling Load (kips)	251.7
Percent Elongation - 2" (%)	33.12
CVN Width (mm)	5
CVN Absorbed Energy (ft-lbs)	18.5
Brace Length (in)	237.5

Area (in^2)	8.12
Moment of Inertia (in^4)	59.6
Corner Radius (in)	0.667
Thickness - Nominal (in)	0.313
Thickness - Measured (in)	0.305
Brace Compactness Ratio (*b/t*) - Nominal	19.4
Brace Compactness Ratio (*b/t*) - Measured	18.58
Global Slenderness ratio (*KL/r*)	87.6

Specimen Performance

Test Event	Axial Brace Displacement (in)	Target Displacement (in) (Cycle)	Force (kips)	$P / P_{Yield/Critical}$	
Peak Tension Load	1.72	2.25 (1)	478.1	1.05	Y
B1: Initial Global Buckling	-0.21	0.375 (1)	-201.5	0.80	C
B2: Moderate Global Buckling	-1.69	1.75 (1)	-81.2	0.32	C
B3-T: Local Cupping	-1.74	1.75 (2)	-56.3	0.22	C
B3-C: Striations & Tearing	1.35	2.25 (2)	264.7	0.58	Y
B4: Brace Fracture	1.99	2.75 (1)	146.1	0.32	Y

Key Observations

Cycle #	Displacement (in)	Observations
5-6	0.375	Minor OOP buckling displacement Bolt Slip - South Gusset Plate T2
11-12	0.75	Bolt Slip - North Gusset Plate T1
15-16	1.75	Minor cupping observed C1 peak displacement (~⅛") Moderate cupping observed C2 peak displacement (~1") Center of cupping: 4" North of center
17-18	2.25	Major cupping observed C1 peak displacement (~2") Tore through east, top, and bottom faces of specimen at cupping location Major cupping observed C2 peak displacement (~2")
19-20	2.75	Fractured in first tension cycle before reaching peak displacement

Test Results

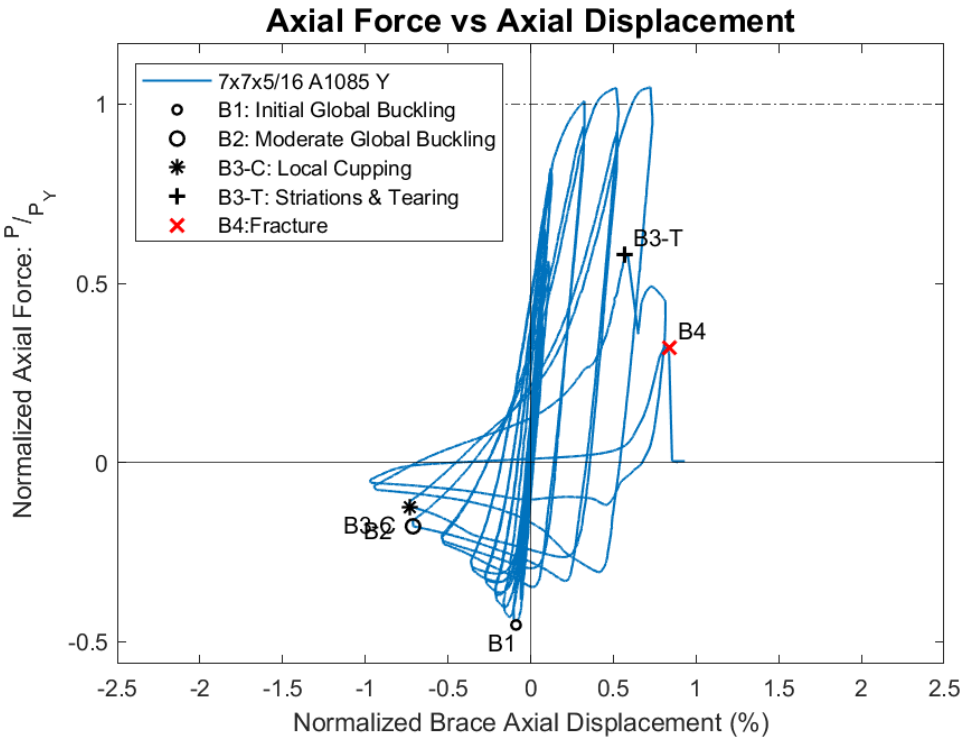

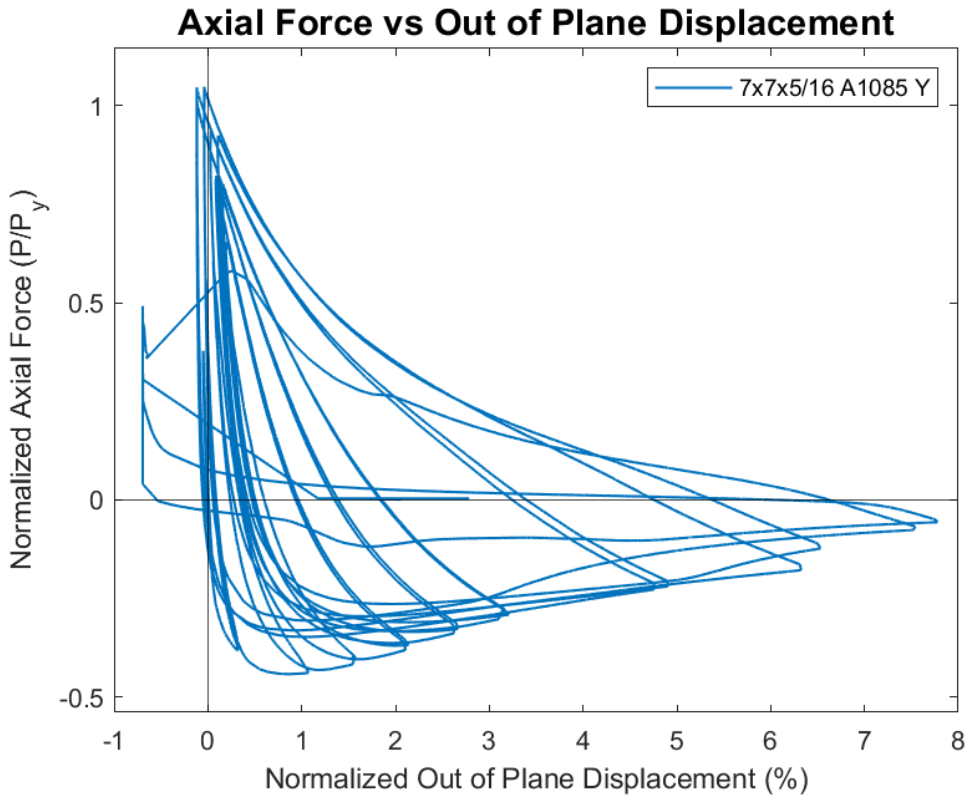

Photos

Cupping at Center of Specimen: 2.25” Cycles 1 and 2 C

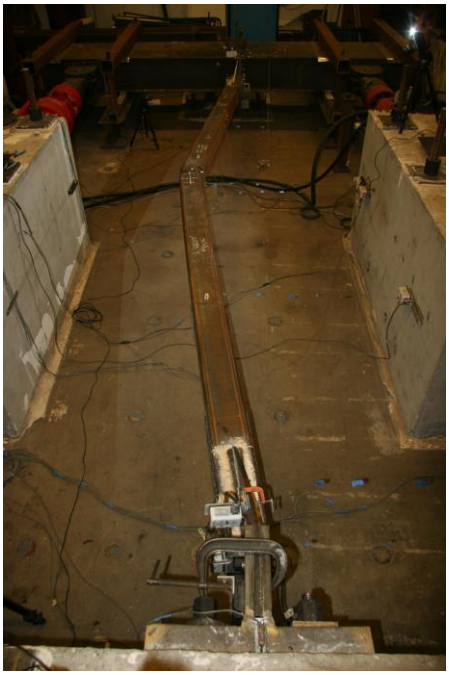

Peak out of Plane Displacement: 2.25” Cycles 1 & 2 C

Fractured Specimen: 2.75” Cycle 1 T

Development of Striations at Center of Specimen: 2.25” Cycle 2 T

Tearing Through Specimen: 2.25” Cycle 2 T

7x7x3/8 A500 Y Brace Test Summary

Test Name: 7x7x3/8 A500 Y
Test Date: 5/25/2021 - 2:00 PM

Brace Properties

Measured Yield Stress (ksi)	61.35
Measured Ultimate Stress (ksi)	72.19
Yield Load (kips)	539.3
Critical Buckling Load (kips)	277.9
Percent Elongation - 2" (%)	30.76
CVN Width (mm)	7.5
CVN Absorbed Energy (ft-lbs)	14.3
Brace Length (in)	237.5

Area (in^2)	8.97
Moment of Inertia (in^4)	68.7
Corner Radius (in)	0.832
Thickness - Nominal (in)	0.349
Thickness - Measured (in)	0.342
Brace Compactness Ratio (*b/t*) - Nominal	17.1
Brace Compactness Ratio (*b/t*) - Measured	15.60
Global Slenderness ratio (*KL/r*)	88.3

Specimen Performance

Test Event	Axial Brace Displacement (in)	Target Displacement (in) (Cycle)	Force (kips)	$P / P_{Yield/Critical}$	
Peak Tension Load	1.70	2.25 (1)	570.9	1.06	Y
B1: Initial Global Buckling	-0.26	0.375 (1)	-231.8	0.83	C
B2: Moderate Global Buckling	-1.76	1.75 (1)	-99.5	0.36	C
B3-T: Local Cupping	-2.23	2.25 (2)	-60.7	0.22	C
B3-C: Striations & Tearing	1.65	2.75 (2)	237.8	0.44	Y
B4: Brace Fracture	-1.82	2.75 (2)	-5.4	0.02	C

Key Observations

Cycle #	Displacement (in)	Observations
7-8	0.5	Bolt slip T1 - North and South Gusset Plates Similar out of plane buckling displacement as previous cycles
17-18	2.25	Minor cupping observed at C1 peak displacement (~3/16” deep) Cupping observed at C2 peak displacement (~¾”) Center of cupping: 3” north of center
19-20	2.75	Major cupping observed at C1 peak displacement (~2+”) Tearing observed at T2 peak displacement - through east, top, and bottom faces of specimen Brace fractured in compression in cycle 2, at about 1.5” displacement

Test Results

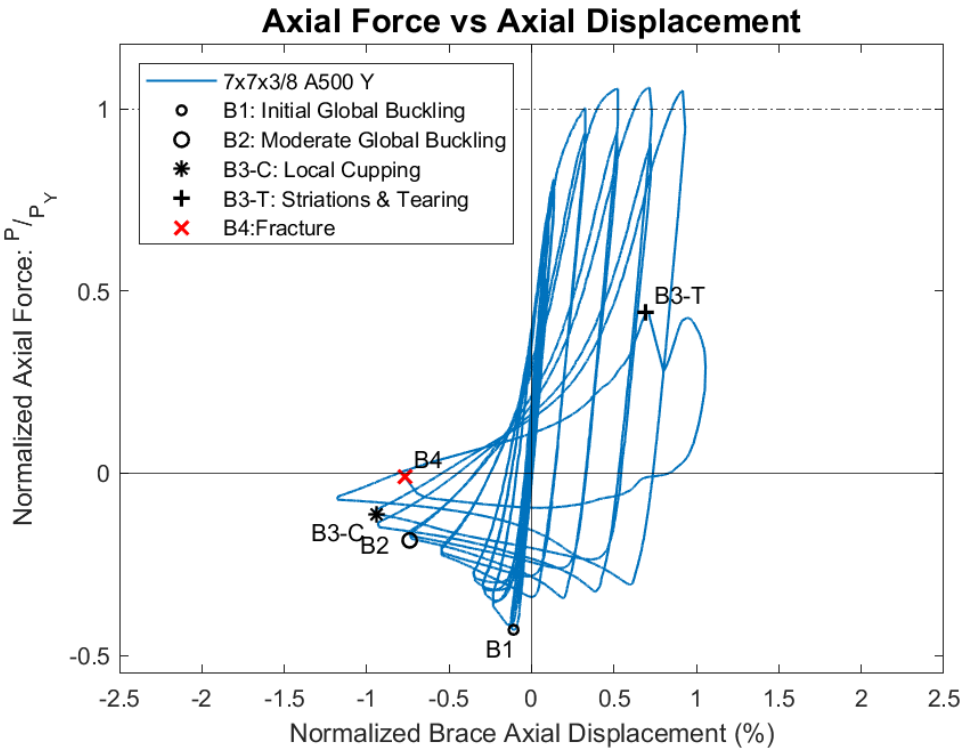

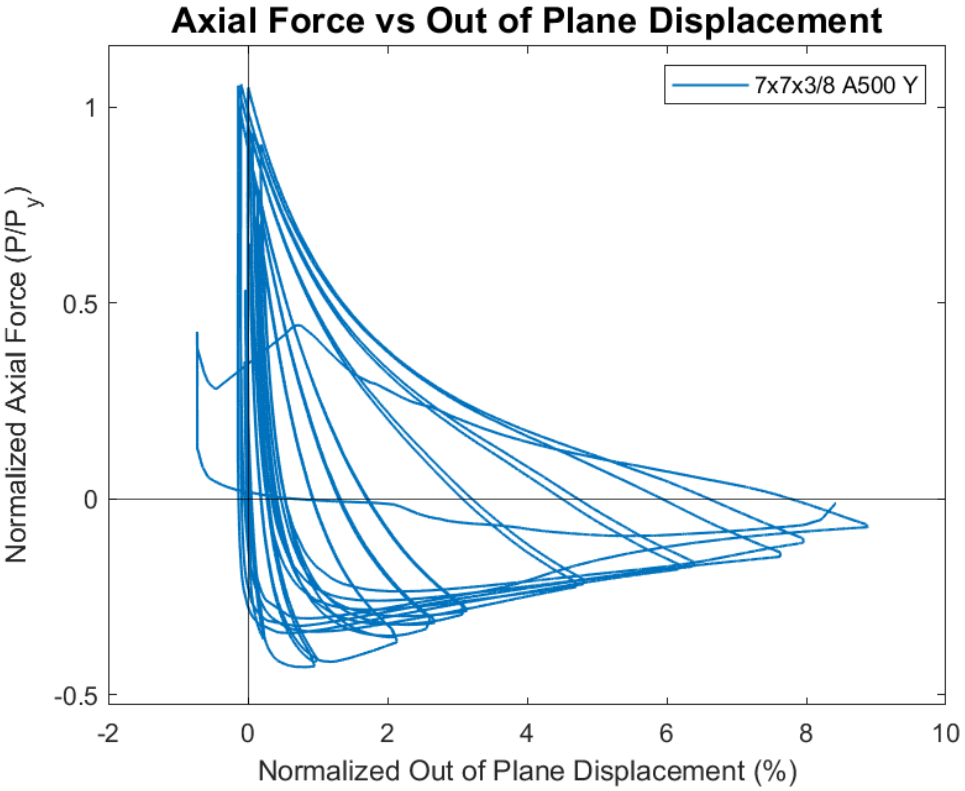

Photos

Cupping at Center of Specimen: 2.75” Cycle 1 C

Initiation of Tearing at Center of Specimen: 2.75” Cycle 2 T

Tearing Through Center of Specimen: 2.75” Cycle 2 T

Fractured Specimen: 2.75” Cycle 2 C

7x7x3/8 A1085 Y Brace Test Summary

Test Name: 7x7x3/8 A1085 Y
Test Date: 5/27/2021 - 2:15 PM

Brace Properties

Measured Yield Stress (ksi)	61.89	**Area (in²)**	9.58
Measured Ultimate Stress (ksi)	70.07	**Moment of Inertia (in⁴)**	68.7
Yield Load (kips)	577.1	**Corner Radius (in)**	0.906
Critical Buckling Load (kips)	292.2	**Thickness - Nominal (in)**	0.375
Percent Elongation - 2" (%)	31.32	**Thickness - Measured (in)**	0.365
CVN Width (mm)	7.5	**Brace Compactness Ratio (*b/t*) - Nominal**	15.7
CVN Absorbed Energy (ft-lbs)	17.3	**Brace Compactness Ratio (*b/t*) - Measured**	14.21
Brace Length (in)	237.5	**Global Slenderness ratio (*KL/r*)**	88.6

Specimen Performance

Test Event	Axial Brace Displacement (in)	Target Displacement (in) (Cycle)	Force (kips)	$P / P_{Yield/Critical}$	
Peak Tension Load	1.53	1.75 (1)	615.9	1.07	Y
B1: Initial Global Buckling	-0.27	0.375 (1)	-254.9	0.87	C
B2: Moderate Global Buckling	-1.82	1.75 (1)	-106.0	0.36	C
B3-T: Local Cupping	-2.27	2.25 (1)	-82.6	0.28	C
B3-C: Striations & Tearing	1.44	2.75 (2)	234.0	0.41	Y
B4: Brace Fracture	2.36	3.25 (1)	152.5	0.26	Y

Key Observations

Cycle #	Displacement (in)	Observations
5-6	0.375	Minor bolt slip T1: North and South gusset plates Minor OOP buckling displacement
9-10	0.625	Major bolt slip T1: North and South gusset plates
17-18	2.25	Minor cupping observed C1 peak displacement (~⅜" deep) Moderate/Major cupping observed C2 peak displacement (1.5") Cupping centered 2" North of center
19-20	2.75	Major cupping C1 peak displacement (2") Tearing through east, top, and bottom faces of brace at T2 peak Major cupping at C2 peak displacement - similar to C1
21-22	3.25	Brace fracture in cycle T1 before reaching target displacement

Test Results

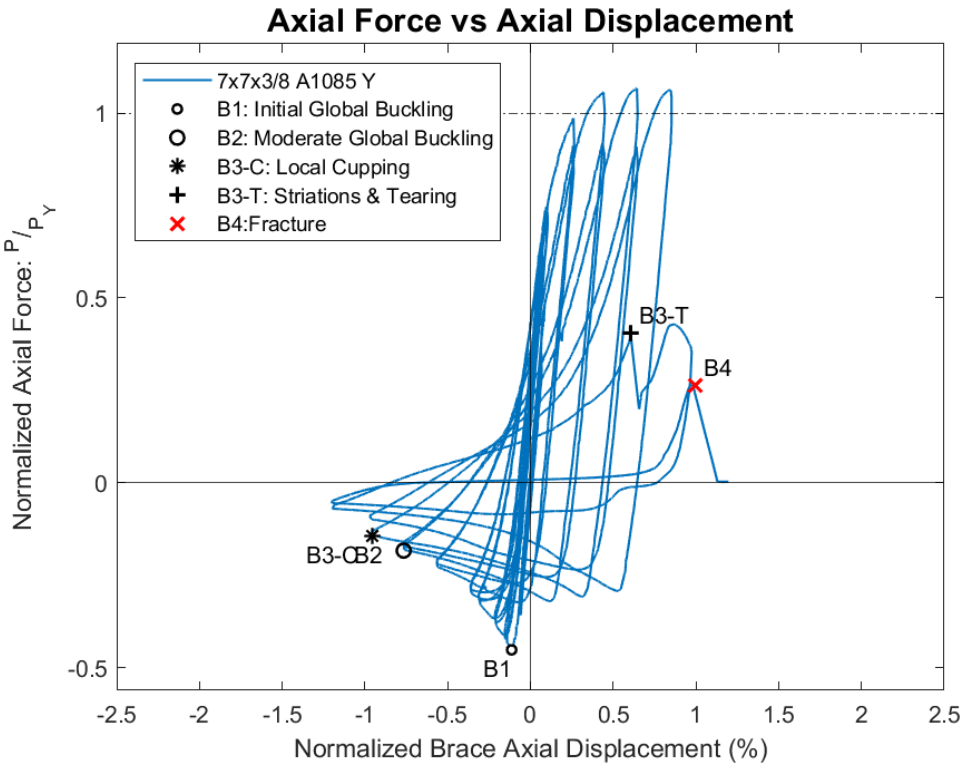

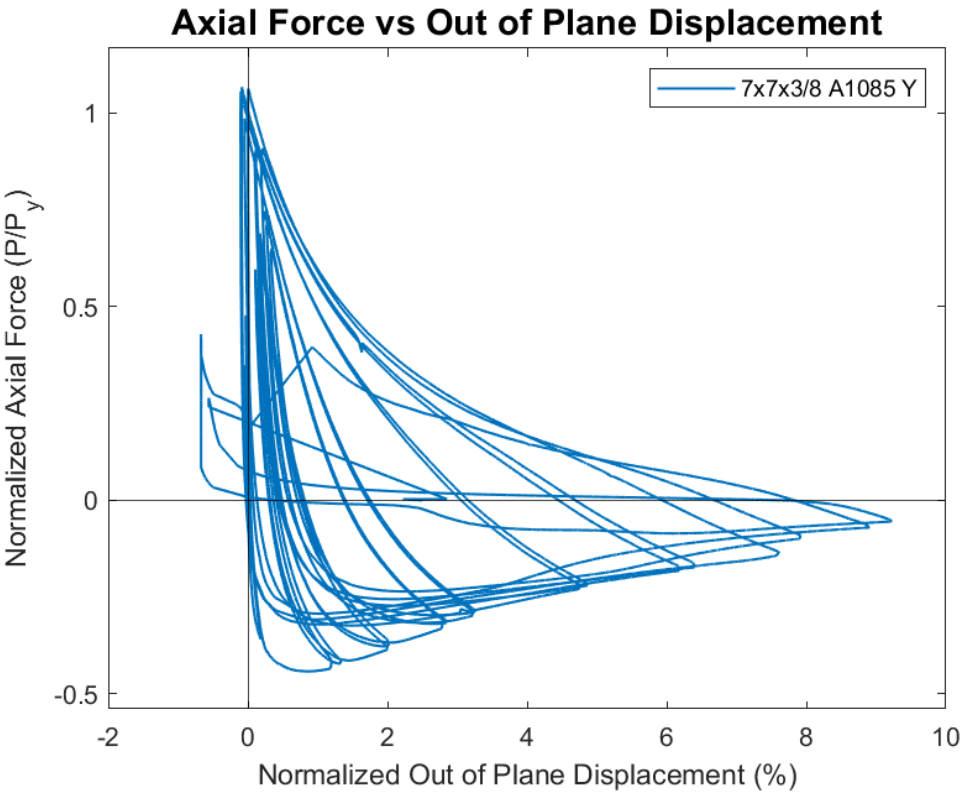

Photos

Cupping at Center of Specimen: 2.75” Cycles 1 & 2 C

Tearing Through Specimen: 2.75” Cycle 2 T

Initiation of Tearing at Center of Specimen: 2.75” Cycle 2 T

Fractured Specimen after 3.25” Displacement - Cycle 1 T

7x7x1/2 A500 B Brace Test Summary

Test Name: 7x7x1/2 A500 B
Test Date: 6/9/2021 - 1:00 PM

Brace Properties

Measured Yield Stress (ksi)	57.82
Measured Ultimate Stress (ksi)	69.14
Yield Load (kips)	669.3
Critical Buckling Load (kips)	347.3
Percent Elongation - 2" (%)	29.6
CVN Width (mm)	10
CVN Absorbed Energy (ft-lbs)	42
Brace Length (in)	237.5

Area (in²)	11.6
Moment of Inertia (in⁴)	80.5
Corner Radius (in)	0.945
Thickness - Nominal (in)	0.465
Thickness - Measured (in)	0.464
Brace Compactness Ratio (*b/t*) - Nominal	12.1
Brace Compactness Ratio (*b/t*) - Measured	11.01
Global Slenderness ratio (*KL/r*)	90.3

Specimen Performance

Test Event	Axial Brace Displacement (in)	Target Displacement (in) (Cycle)	Force (kips)	$P / P_{Yield/Critical}$	
Peak Tension Load	1.64	1.75 (1)	710.4	1.06	Y
B1: Initial Global Buckling	-0.22	0.375 (1)	-278.8	0.80	C
B2: Moderate Global Buckling	-1.75	1.75 (1)	-124.0	0.36	C
B3-T: Local Cupping	-3.17	3.25 (2)	-77.2	0.22	C
B3-C: Striations & Tearing	3.27	4.25 (1)	594.0	0.89	Y
B4: Brace Fracture	3.59	4.25 (2)	186.0	0.28	Y

Key Observations

Cycle #	Displacement (in)	Observations
11-12	0.75	Bolt slip T1 - North & South gusset plates
21-22	3.25	Minor cupping at C1 peak displacement - (~⅛") Minor cupping at C2 peak displacement - (¼")
23-24	3.75	Cupping at C1 peak displacement - (¾") Location of cupping: ~1" North of center Major cupping at C2 peak displacement - (½") Unpredicted actuator behavior near peak tensile displacements - actuators not in sync, 1" difference in displacement near target peak
25-26	4.25	Same unpredicted actuator behavior near peak tensile displacement Striations observed near peak displacement – T1

		Major cupping at C1 peak displacement - (2.5”) Fractured during T2 near peak displacement

Test Results

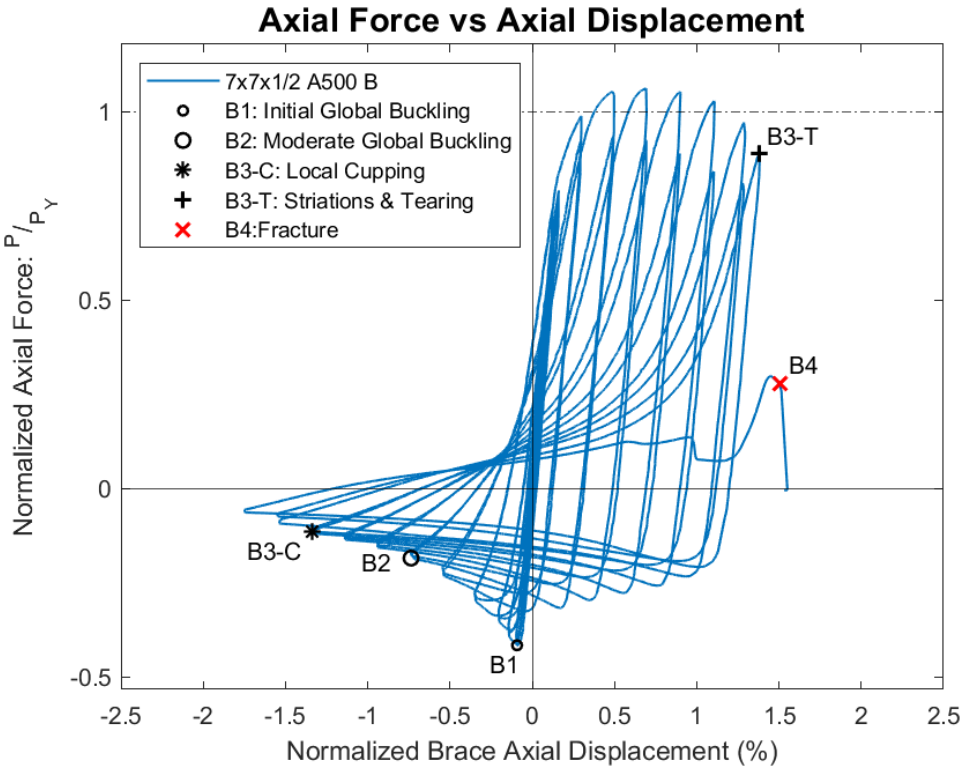

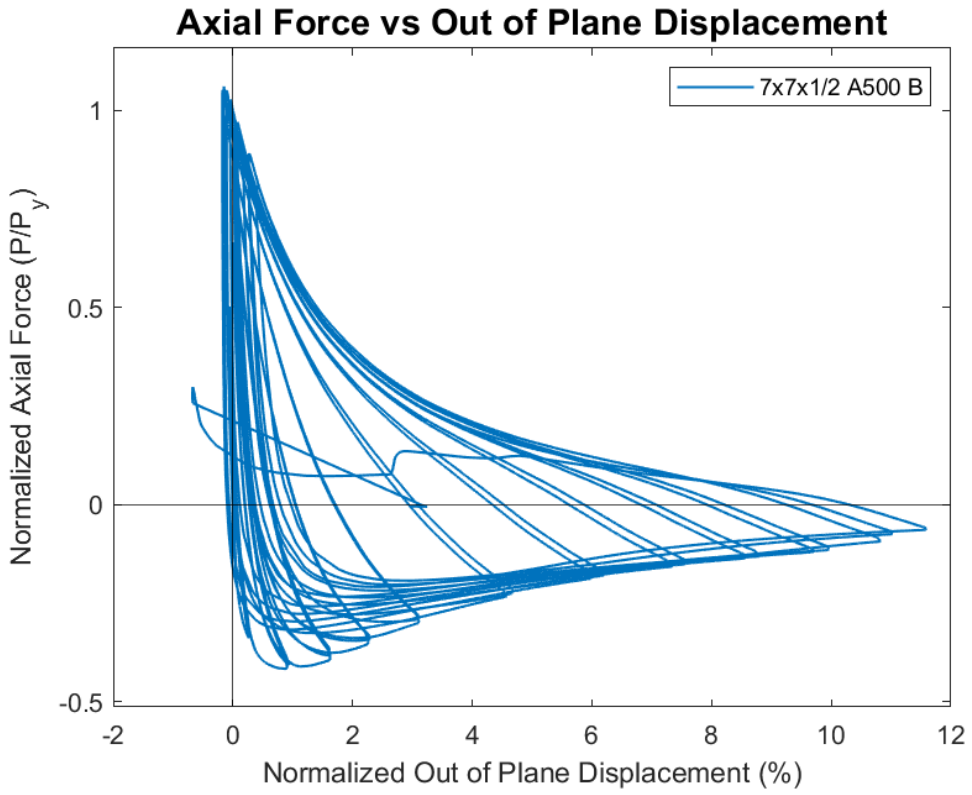

Photos

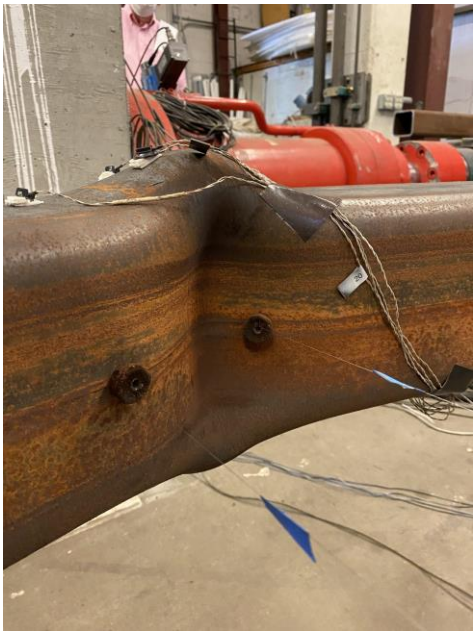

Cupping at Center of Brace: 3.75” Cycles

Development of Striations at Center of Brace: 4.25” Cycle 1 T

Tearing at Center of Specimen: 4.25” Cycles

Fractured Specimen

7x7x1/2 A1085 Y Brace Test Summary

Test Name: 7x7x1/2 A1085 Y
Test Date: 6/4/2021 - 11:30 AM

Brace Properties

Measured Yield Stress (ksi)	64.375	**Area (in²)**	12.4
Measured Ultimate Stress (ksi)	71.68	**Moment of Inertia (in⁴)**	84.7
Yield Load (kips)	772.7	**Corner Radius (in)**	1.047
Critical Buckling Load (kips)	363.6	**Thickness - Nominal (in)**	0.5
Percent Elongation - 2" (%)	32.7	**Thickness - Measured (in)**	0.484
CVN Width (mm)	10	**Brace Compactness Ratio (*b/t*) - Nominal**	11
CVN Absorbed Energy (ft-lbs)	28.7	**Brace Compactness Ratio (*b/t*) - Measured**	10.14
Brace Length (in)	237.5	**Global Slenderness ratio (*KL/r*)**	91

Specimen Performance

Test Event	Axial Brace Displacement (in)	Target Displacement (in) (Cycle)	Force (kips)	$P / P_{Yield/Critical}$	
Peak Tension Load	1.44	2.25 (1)	805.1	1.04	Y
B1: Initial Global Buckling	-0.32	0.375 (1)	-305.7	0.84	C
B2: Moderate Global Buckling	-1.87	1.75 (1)	-141.9	0.39	C
B3-T: Local Cupping	-3.38	3.25 (2)	-80.2	0.22	C
B3-C: Striations & Tearing	3.19	4.25 (1)	760.0	0.98	Y
B4: Brace Fracture	3.48	4.25 (2)	270.0	0.35	Y

Key Observations

Cycle #	Displacement (in)	Observations
7-8	0.5	Bolt slip T1: North and South gusset plates
21-22	3.25	Minor cupping at C1 peak displacement (~3/16”) Cupping at C2 peak displacement (~⅜”) Cupping location: 2” North of brace center
23-24	3.75	Cupping at C1 peak displacement (1”) Cupping at C2 peak displacement (1.25”) Very hot at center of specimen
25-26	4.25	Striations observed at T1 peak displacement Major cupping at C1 peak displacement (~1.75”) Fracture at T2 near peak displacement

Test Results

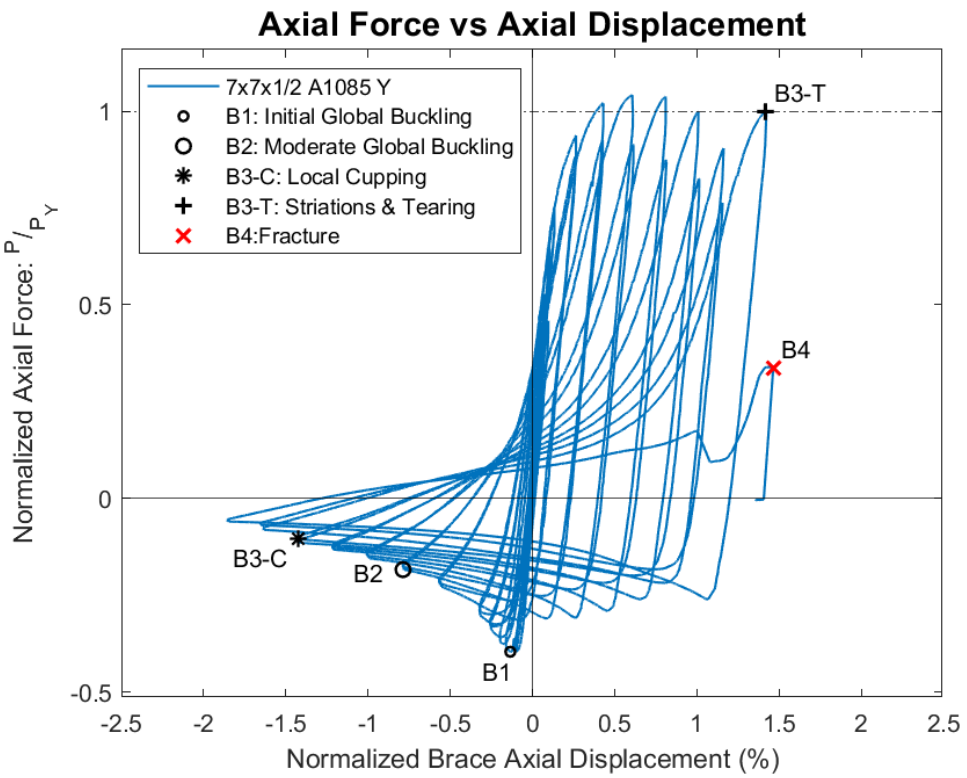

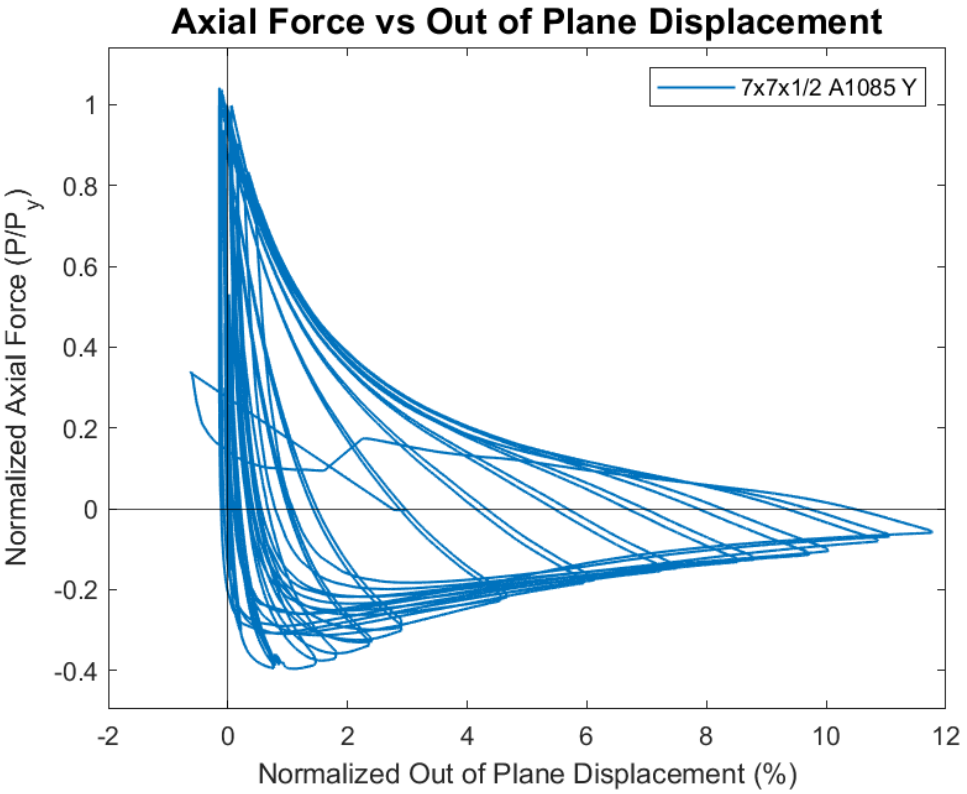

Photos

Cupping at Center of Specimen: 3.75” Cycles 1 & 2 C

Closeup of Cupping: 4.25” Cycle 1 C

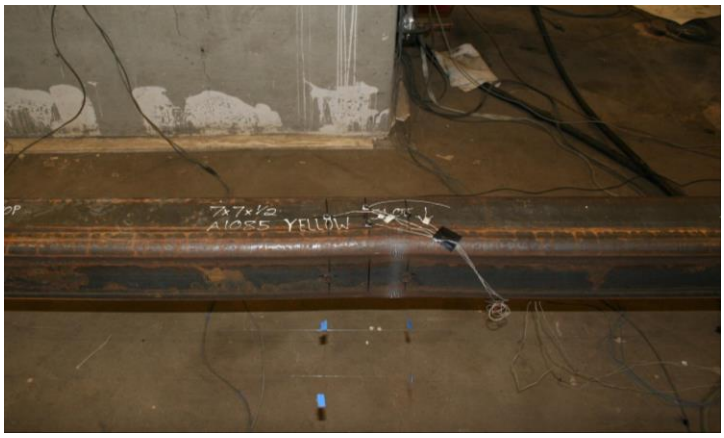

Development of Striations at Center of Specimen: 4.25” Cycle 1 T

Fractured Specimen after 4.25” Displacement - Cycle 2 T

8x8x3/8 A500 W Brace Test Summary

Test Name: 8x8x3/8 A500 W
Test Date: 6/11/2021 - 1:00 PM

Brace Properties

Measured Yield Stress (ksi)	66.19
Measured Ultimate Stress (ksi)	76.52
Yield Load (kips)	690.3
Critical Buckling Load (kips)	387.0
Percent Elongation - 2" (%)	34.44
CVN Width (mm)	7.5
CVN Absorbed Energy (ft-lbs)	65.5
Brace Length (in)	237.5

Area (in^2)	10.4
Moment of Inertia (in^4)	100
Corner Radius (in)	0.801
Thickness - Nominal (in)	0.349
Thickness - Measured (in)	0.35
Brace Compactness Ratio (*b/t*) - Nominal	19.9
Brace Compactness Ratio (*b/t*) - Measured	18.28
Global Slenderness ratio (*KL/r*)	76.6

Specimen Performance

Test Event	Axial Brace Displacement (in)	Target Displacement (in) (Cycle)	Force (kips)	$P / P_{Yield/Critical}$	
Peak Tension Load	1.06	1.75 (1)	702.7	1.02	Y
B1: Initial Global Buckling	-0.28	0.5 (1)	360.0	-0.93	C
B2: Moderate Global Buckling	-1.89	1.75 (1)	-75.0	0.19	C
B3-T: Local Cupping	-1.33	1.25 (2)	-134.0	0.35	C
B3-C: Striations & Tearing	0.96	1.75 (2)	614.0	0.89	Y
B4: Brace Fracture	1.24	2.25 (1)	310.6	0.45	Y

Key Observations

Cycle #	Displacement (in)	Observations
9-10	0.625	Bolt slip at North and South gusset plates - T1 String pot measuring total longitudinal displacement fell off during bolt slip, replaced immediately
13-14	1.25	Cupping observed at C2 peak displacement - (¾")
15-16	1.75	Major cupping at C1 peak displacement (1.75") Striations and minor tearing specimen at T2 peak displacement Major cupping at C2 peak displacement (2")
17-18	2.25	Specimen fractured near T1 peak displacement

Test Results

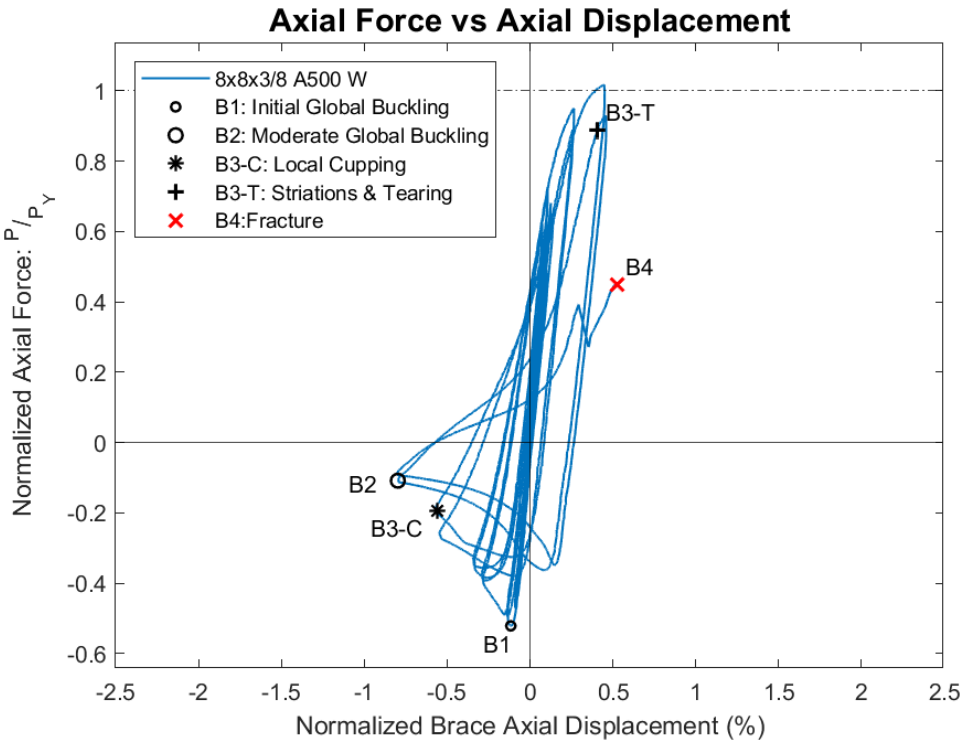

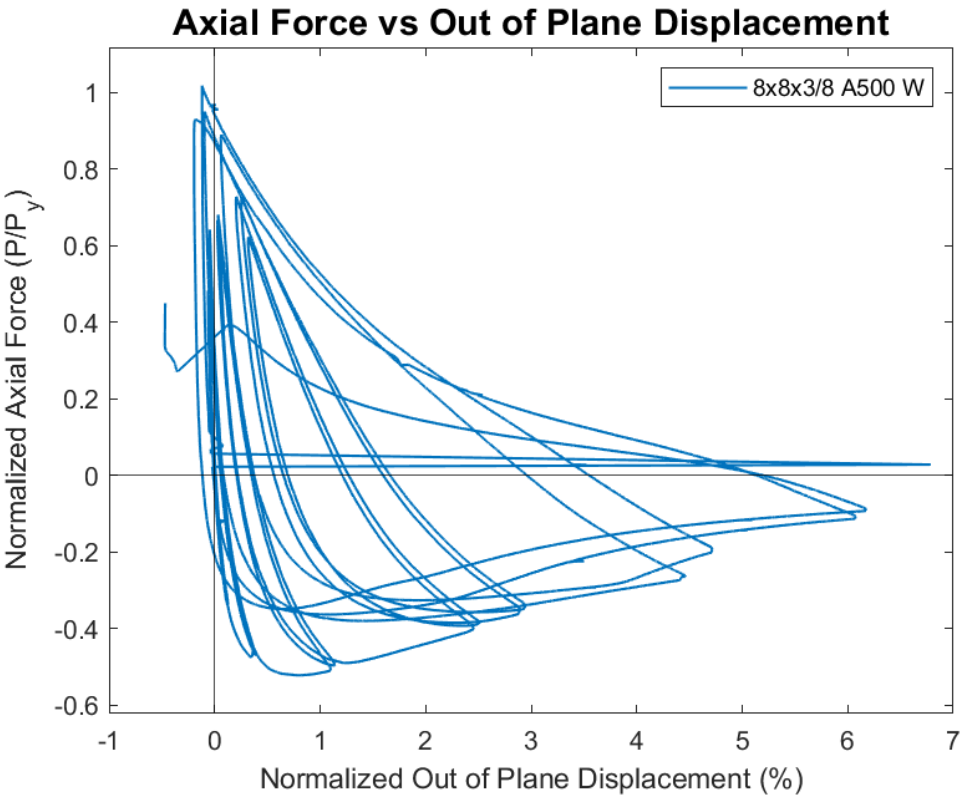

Photos

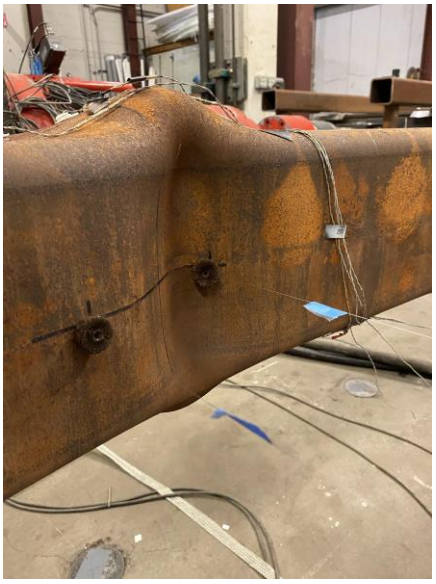

Cupping at Center of Specimen: 1.75” Cycle 1 C

Initiation of Striations and Tearing: 1.75” Cycle 2 T

Cupping after Initial Tearing: 1.75” Cycle 2 C

Tearing at Center Immediately Prior to Fracture: 2.25” Cycle 1 T

8x8x3/8 A1085 Y Brace Test Summary

Test Name: 8x8x3/8 A1085 Y
Test Date: 6/15/2021 - 1:00 PM

Brace Properties

Measured Yield Stress (ksi)	60.37	**Area (in²)**	11.1
Measured Ultimate Stress (ksi)	72.12	**Moment of Inertia (in⁴)**	106
Yield Load (kips)	661.2	**Corner Radius (in)**	1.06
Critical Buckling Load (kips)	404.3	**Thickness - Nominal (in)**	0.375
Percent Elongation - 2" (%)	34.2	**Thickness - Measured (in)**	0.37
CVN Width (mm)	7.5	**Brace Compactness Ratio (*b/t*) - Nominal**	18.3
CVN Absorbed Energy (ft-lbs)	8.5	**Brace Compactness Ratio (*b/t*) - Measured**	15.89
Brace Length (in)	237.5	**Global Slenderness ratio (*KL/r*)**	76.86

Specimen Performance

Test Event	Axial Brace Displacement (in)	Target Displacement (in) (Cycle)	Force (kips)	$P / P_{Yield/Critical}$	
Peak Tension Load	1.29	1.75 (1)	672.6	1.02	Y
B1: Initial Global Buckling	-0.31	0.5 (1)	-328.8	0.81	C
B2: Moderate Global Buckling	-2.17	1.75 (1)	-62.8	0.16	C
B3-T: Local Cupping	-1.68	1.75 (2)	-110.8	0.27	C
B3-C: Striations & Tearing	1.68	2.25 (2)	534.0	0.81	Y
B4: Brace Fracture	2.18	2.75 (1)	180.0	0.27	Y

Key Observations

Cycle #	Displacement (in)	Observations
7-8	0.5	Minor bolt slip T1: North and South gusset plates Minor out of plane buckling displacement observed in compression
15-16	1.75	Minor cupping at C1 peak displacement (~⅛" deep) Cupping at C2 peak displacement (¾") Center of local cupping - 3.5" North of center
17-18	2.25	Major cupping at C1 peak displacement (2") Tearing through east/bottom faces - T2 peak displacement Major cupping at C2 peak displacement (2.25")
19-20	2.75	Fracture at T1 prior to peak displacement (~2.25" displacement)

Test Results

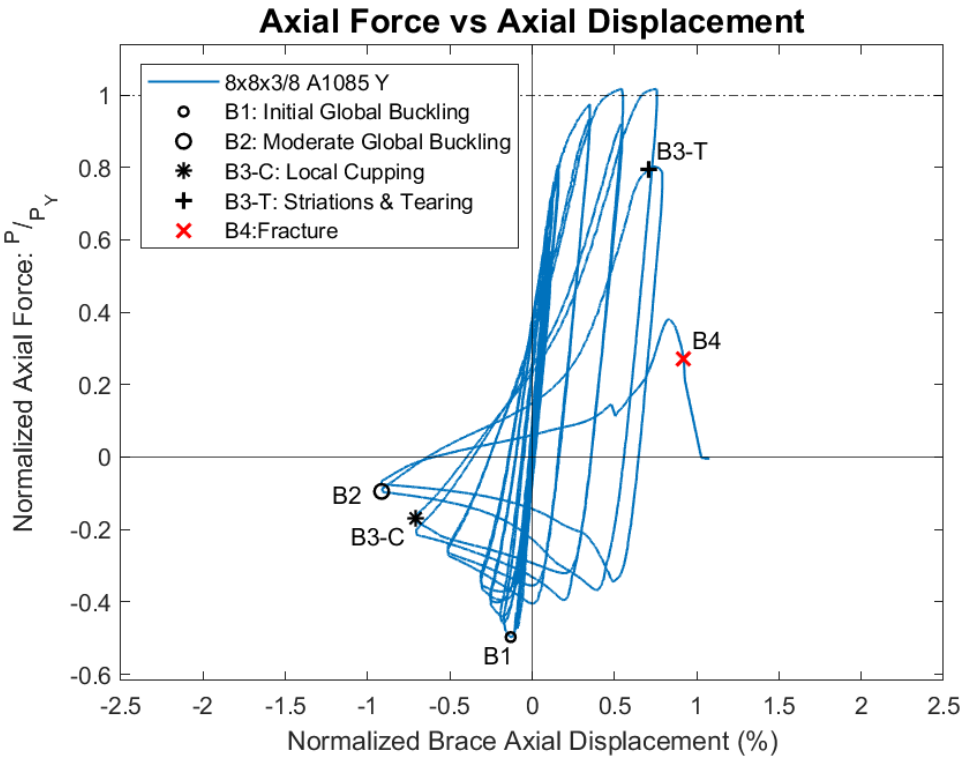

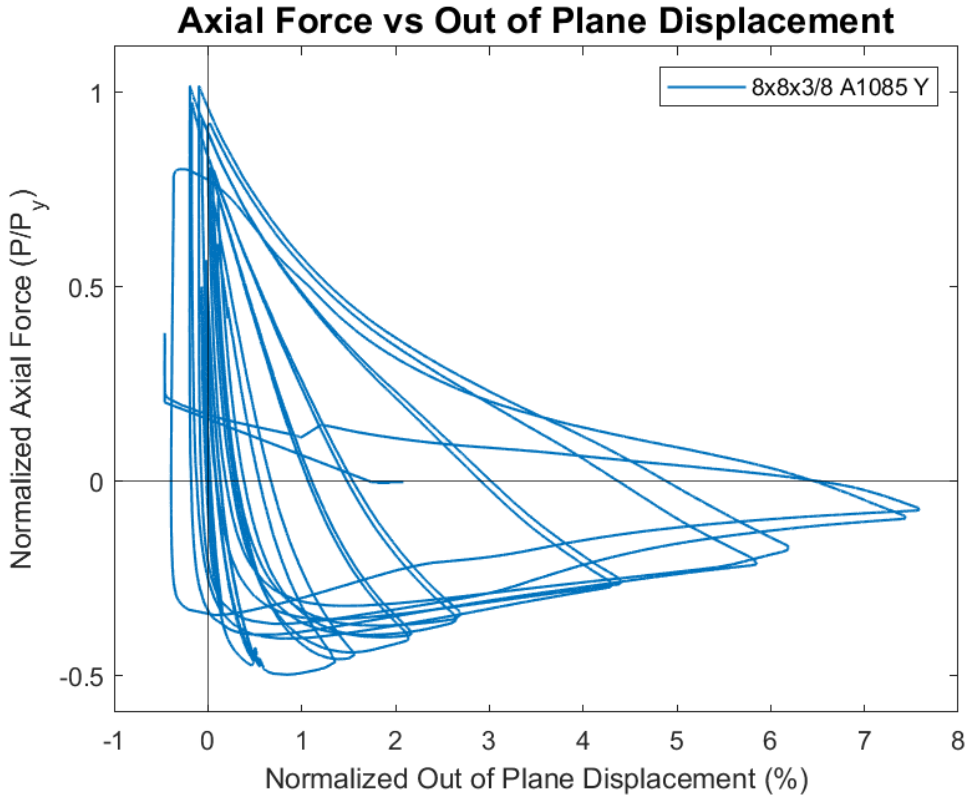

Photos

Cupping at Center of Specimen: 2.25” Cycle 1 C

Development of Striations and Tearing: 2.25” Cycle 2 T

Post-Tearing cupping at Center of Specimen: 2.25” Cycle 2 C

Fractured Specimen during 2.75” Cycle 1 T

8x8x1/2 A500 W Brace Test Summary

Test Name: 8x8x1/2 A500 W
Test Date: 6/23/21 & 7/2/21

Brace Properties

Measured Yield Stress (ksi)	65.47
Measured Ultimate Stress (ksi)	72.01
Yield Load (kips)	876.2
Critical Buckling Load (kips)	491.2
Percent Elongation - 2" (%)	33.12
CVN Width (mm)	10
CVN Absorbed Energy (ft-lbs)	67.3
Brace Length (in)	237.5

Area (in²)	13.5
Moment of Inertia (in⁴)	125
Corner Radius (in)	0.887
Thickness - Nominal (in)	0.465
Thickness - Measured (in)	0.461
Brace Compactness Ratio (*b/t*) - Nominal	14.2
Brace Compactness Ratio (*b/t*) - Measured	13.51
Global Slenderness ratio (*KL/r*)	78.125

Specimen Performance

Test Event	Axial Brace Displacement (in)	Target Displacement (in) (Cycle)	Force (kips)	P / $P_{Yield/Critical}$	
Peak Tension Load	1.17	1.75 (1)	906.0	1.03	Y
B1: Initial Global Buckling	-0.33	0.625 (1)	-434.7	0.88	C
B2: Moderate Global Buckling	-2.04	2.25 (1)	-165.4	0.34	C
B3-T: Local Cupping	-2.05	2.25 (2)	-148.7	0.30	C
B3-C: Striations & Tearing	2.32	3.25 (1)	842.4	0.96	Y
B4: Brace Fracture	2.54	3.25 (2)	270.0	0.31	Y

Key Observations

Cycle #	Displacement (in)	Observations
5-6	0.375	Stopped test after 1 full cycle due to unexpected actuator behavior Re-started test on 7/2/21 - Start with 0.375" Cycle 2 - Initial brace tensile force = 88 kip (From end of cycle 1) Bolt slip T2 - N & S GP
17-18	2.25	Very minor cupping (~⅛" deep, global) C1 Local Cupping observed at peak displacement C2 (½" deep)
19-20	2.75	Cupping at C1 peak displacement ~1.75" deep Major cupping at C2 peak displacement ~2.75" deep
21-22	3.25	Striations and tearing at peak displacement T1 - Tore halfway through Direction of buckling switched to East in compression, Brace fractured in tension - T1 at about 3" displacement

Test Results

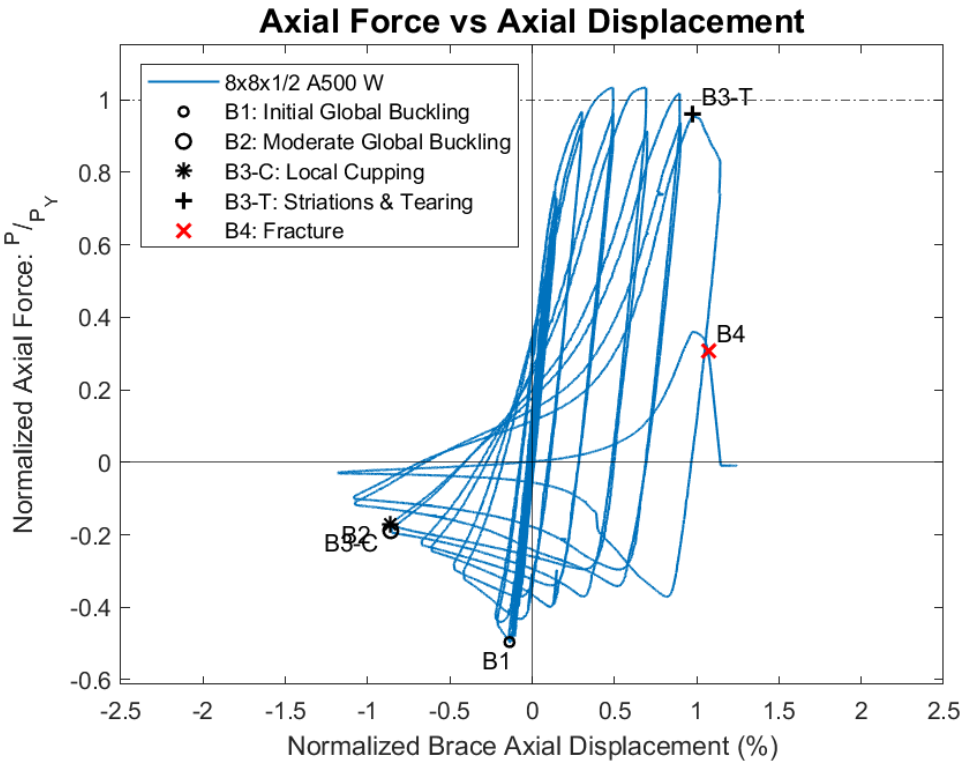

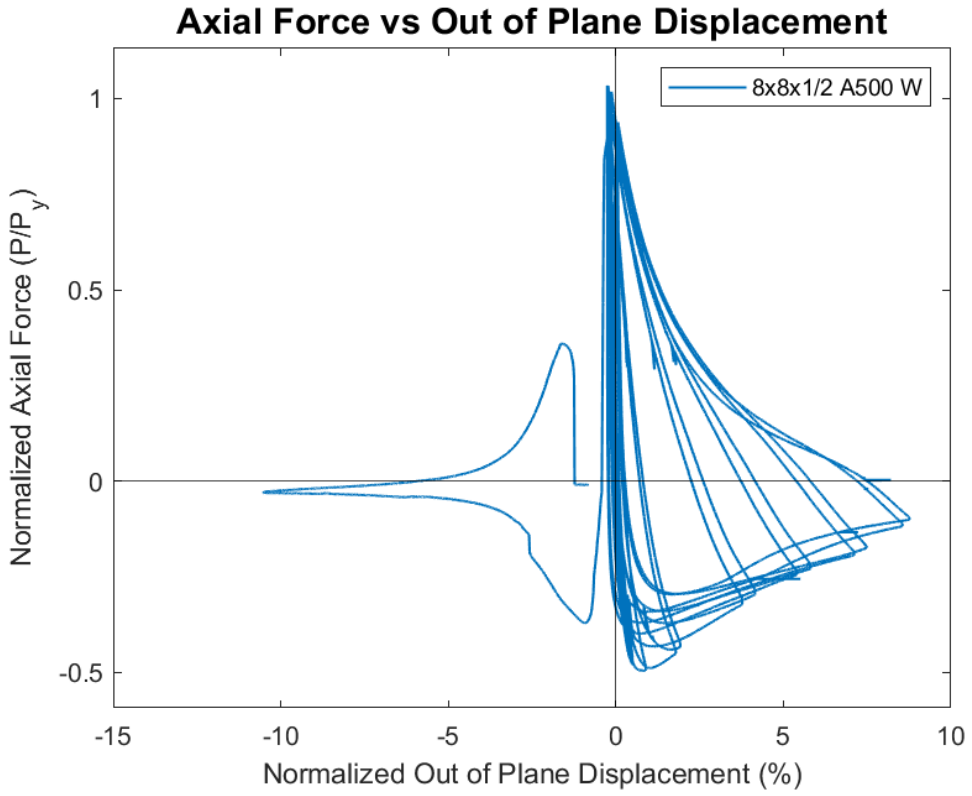

Photos

Cupping at Center of Specimen:
2.25” Cycle 2 C

Initiation of Striations and Tearing: 3.25” Cycle 1 T

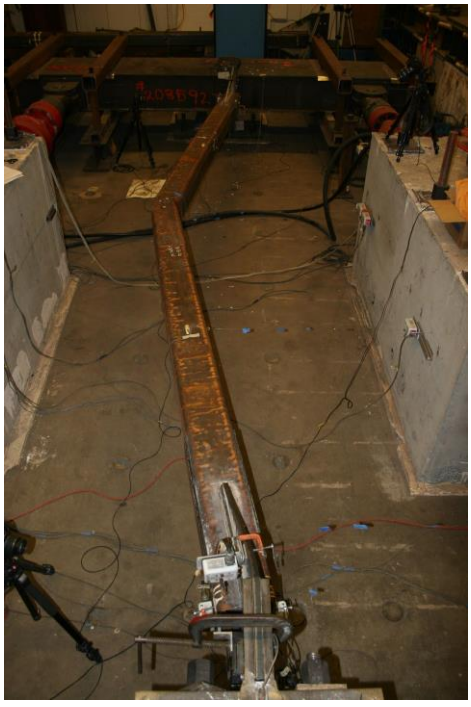

Peak Lateral Displacement: West
2.75” Cycles 1 & 2 C

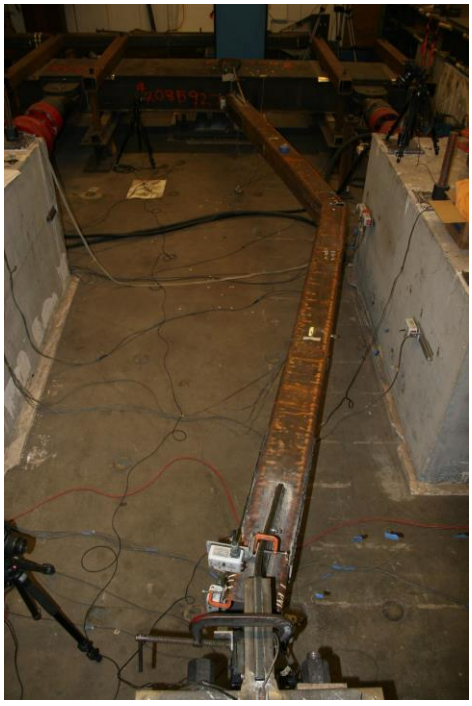

Peak Lateral Displacement: East
3.25” Cycle 1 C

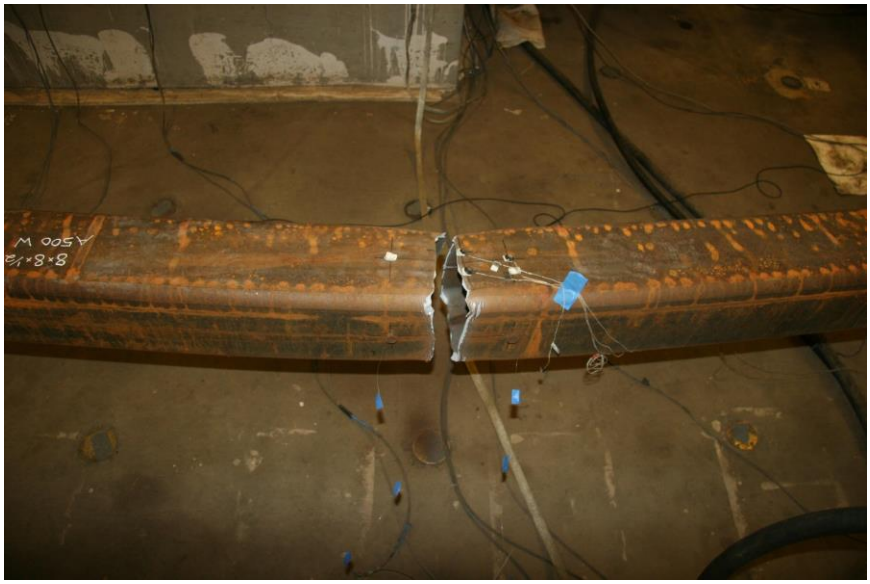

Fractured Specimen: 3.25” Cycle 1 T

Tearing at Center of Specimen: 3.25” Cycle 1 C

8x8x1/2 A1085 Y Brace Test Summary

Test Name: 8x8x1/2 A1085 Y
Test Date: 7/8/21 - 10:00 AM

Brace Properties

Measured Yield Stress (ksi)	64.42
Measured Ultimate Stress (ksi)	75.43
Yield Load (kips)	905.4
Critical Buckling Load (kips)	511.4
Percent Elongation - 2" (%)	32.23
CVN Width (mm)	10
CVN Absorbed Energy (ft-lbs)	40.3
Brace Length (in)	237.5

Area (in^2)	14.4
Moment of Inertia (in^4)	131
Corner Radius (in)	1.141
Thickness - Nominal (in)	0.5
Thickness - Measured (in)	0.488
Brace Compactness Ratio (*b/t*) - Nominal	13
Brace Compactness Ratio (*b/t*) - Measured	11.72
Global Slenderness ratio (*KL/r*)	78.64

Specimen Performance

Test Event	Axial Brace Deformation (in)	Target Displacement (in) (Cycle)	Force (kips)	$P / P_{Yield\|Critical}$	
Peak Tension Load	1.43	2.25 (1)	921.9	1.02	Y
1: Initial Global Buckling	-0.32	0.625 (1)	-418.2	0.82	C
2: Moderate Global Buckling	-2.10	2.25 (2)	-158.3	0.31	C
3-T: Local Cupping	-2.58	2.75 (1)	-131.4	0.26	C
3-C: Striations & Tearing	2.41	3.25 (2)	875.0	0.97	Y
4: Brace Fracture	2.96	3.75 (1)	309.8	0.34	Y

Key Observations

Cycle #	Displacement (in)	Observations
3-4	0.25	Bolt Slip - NGP T1
5-6	0.375	Bolt Slip - SGP T1
9-10	0.625	Global Buckling observed - C1
19-20	2.75	Minor cupping observed at C1 peak displacement (~⅝" deep) Cupping observed at C2 peak displacement (~1.5" deep) Location of cupping: Center of specimen
21-22	3.25	Cupping observed at C1 peak displacement (~2" deep) Development of striations at corners - T2 peak Cupping observed at C2 peak displacement (~2.25" deep)
23-24	3.75	Specimen fractured at ~3.4" actuator displacement - T1

Test Results

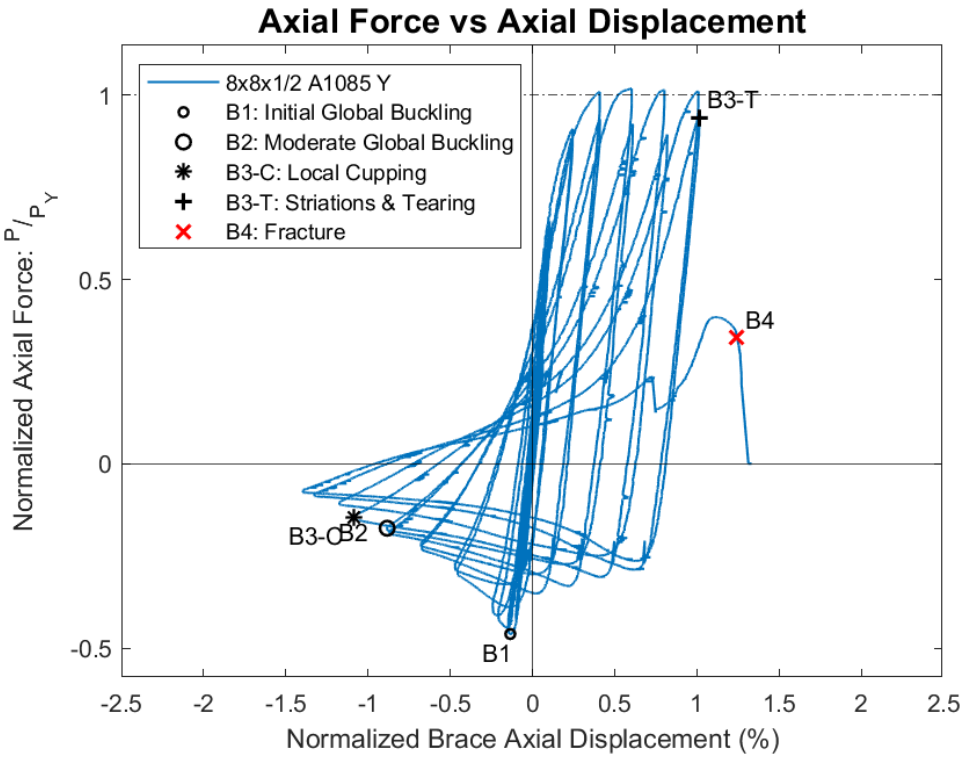

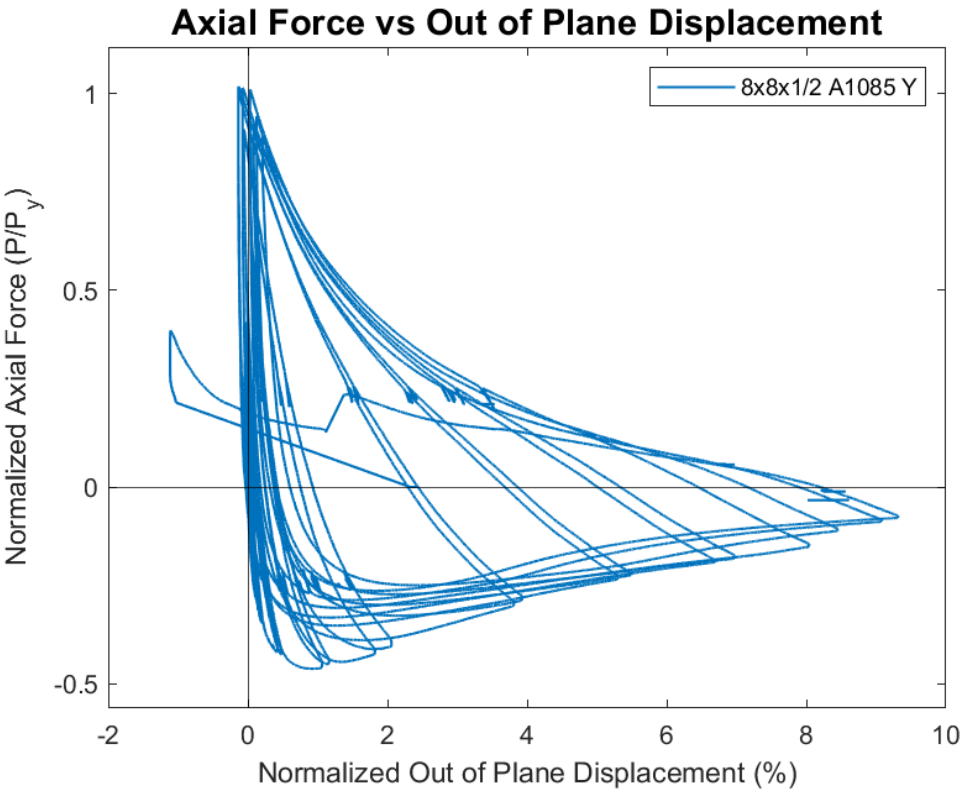

Photos

Cupping at Center of Specimen: 3.25” Cycles 1 & 2

Initiation of Striations and Tearing: 3.25” Cycle 1 T

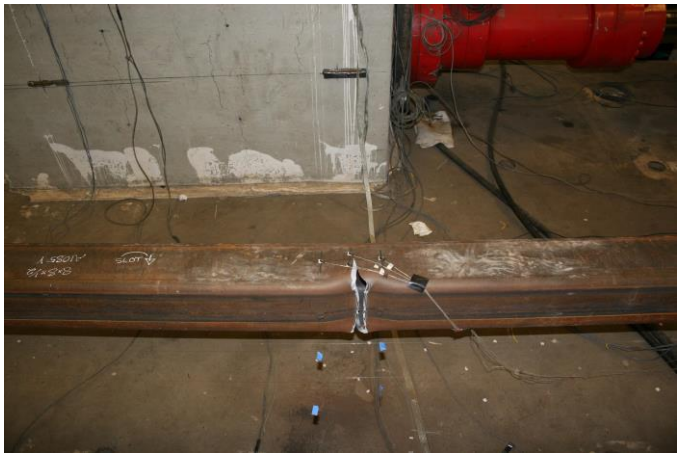

Tearing at Center of Specimen: 3.25” Cycle 1 T

Fractured Specimen: 3.75 Cycle 1 T

10x10x3/8 A500 W Brace Test Summary

Test Name: 10x10x3/8 A500 W
Test Date: 7/6/2021 - 11:00 AM

Brace Properties

Measured Yield Stress (ksi)	59.02	**Area (in²)**	13.2
Measured Ultimate Stress (ksi)	69.45	**Moment of Inertia (in⁴)**	202
Yield Load (kips)	774.6	**Corner Radius (in)**	0.766
Critical Buckling Load (kips)	605.3	**Thickness - Nominal (in)**	0.349
Percent Elongation - 2" (%)	34.2	**Thickness - Measured (in)**	0.347
CVN Width (mm)	7.5	**Brace Compactness Ratio (*b/t*) - Nominal**	25.7
CVN Absorbed Energy (ft-lbs)	120+	**Brace Compactness Ratio (*b/t*) - Measured**	24.40
Brace Length (in)	237.5	**Global Slenderness ratio (*KL/r*)**	60.6

Specimen Performance

Test Event	Axial Brace Displacement (in)	Target Displacement (in) (Cycle)	Force (kips)	$P / P_{Yield/Critical}$	
Peak Tension Load	0.94	1.75 (1)	785.4	1.01	Y
B1: Initial Global Buckling	-0.48	0.75 (1)	-480.1	0.79	C
B2: Moderate Global Buckling	N/A	N/A	N/A	N/A	C
B3-T: Local Cupping	-1.35	1.25 (1)	-174.0	0.29	C
B3-C: Striations & Tearing	0.94	1.75 (1)	785.4	1.01	Y
B4: Brace Fracture	2.12	2.75 (1)	176.5	0.23	Y

Key Observations

Cycle #	Displacement (in)	Observations
3-4	0.25	Bolt slip NGP - T2
7-8	0.5	Bolt slip SGP - T1
9-10	0.625	Global buckling observed
13-14	1.25	Cupping observed at C1 peak displacement (1.25” Deep) Location of cupping: 2.5” South of Center Cupping observed at C2 peak displacement (1-⅞” Deep)
15-16	1.75	Minor striations observed at corners - T1 peak Cupping observed at C1 peak displacement (2.5” deep) Tearing at top and bottom corners of east wall at T2 peak Cupping observed at C2 peak displacement (2.5” deep)

17-18	2.25	Tearing propagated across east, top, and bottom walls at T1 peak Cupping observed at C1 peak displacement (2.75” deep) Tearing continued to propagate during T2, but specimen did not fracture - only west flange remained intact Similar cupping behavior observed during C2 peak displacement
19-20	2.75	Specimen fractured during T1 cycle at an actuator displacement of about 2.5”

Test Results

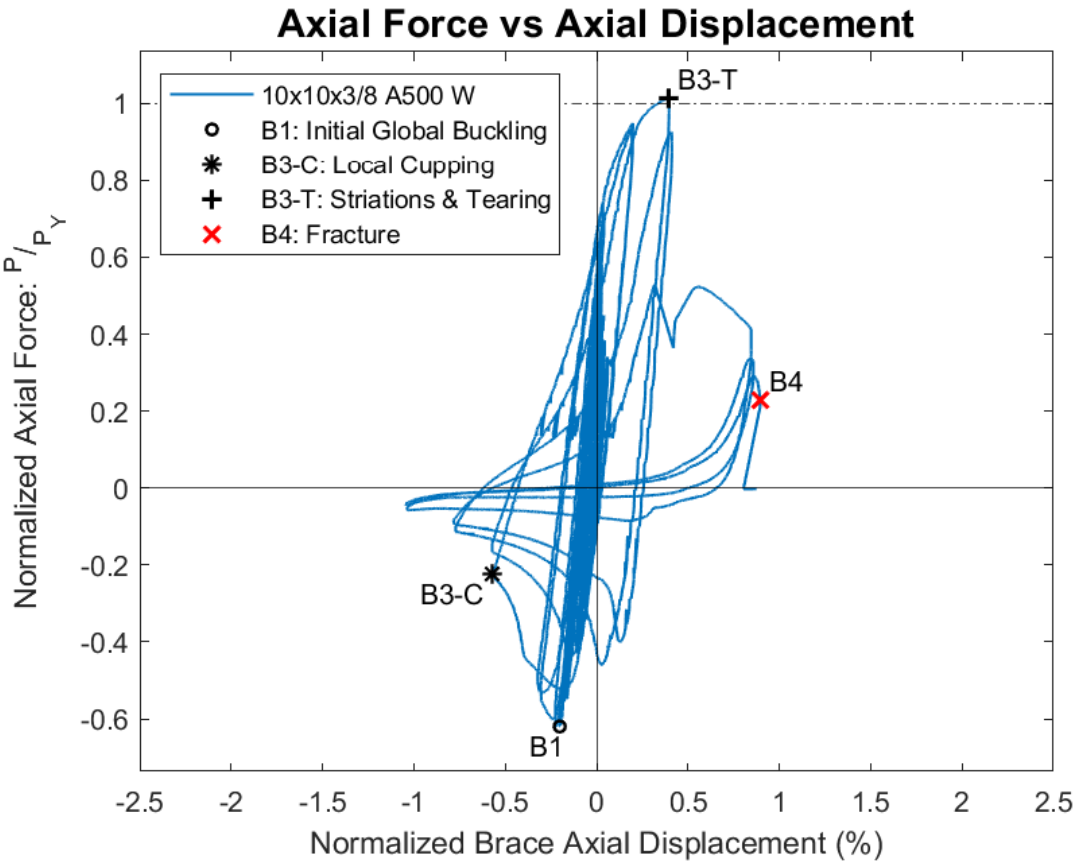

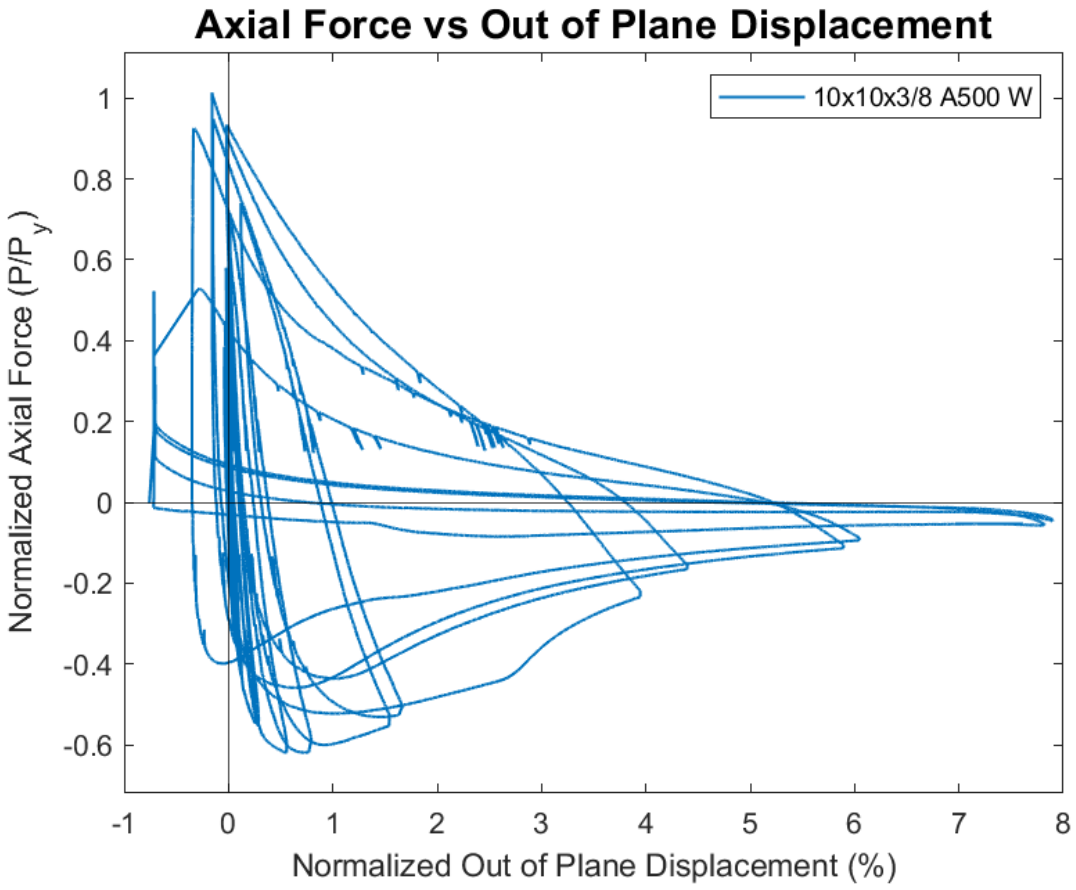

Photos

Cupping at Center of Specimen: 1.25” Cycle 1 C

Initiation of Striations and Tearing: 1.75” Cycle 1 T

Cupping after Initial Tearing at Corners: 1.75” Cycle 2 C

Propagation of Tearing at Center: 2.25” Cycle 1 T

Cupping After Tearing Through Cross Section: 2.25 Cycles 1 & 2 C

Specimen Immediately Before Fracture: 2.75” Cycle 1 T

10x10x3/8 A1085 Y Brace Test Summary

Test Name: 10x10x3/8 A1085 Y
Test Date: 7/7/21 - 11:00 AM

Brace Properties

Measured Yield Stress (ksi)	58.34
Measured Ultimate Stress (ksi)	73.76
Yield Load (kips)	802.9
Critical Buckling Load (kips)	627.9
Percent Elongation - 2" (%)	34.94
CVN Width (mm)	7.5
CVN Absorbed Energy (ft-lbs)	20.7
Brace Length (in)	237.5

Area (in²)	14.1
Moment of Inertia (in⁴)	214
Corner Radius (in)	0.766
Thickness - Nominal (in)	0.375
Thickness - Measured (in)	0.366
Brace Compactness Ratio (*b/t*) - Nominal	23.7
Brace Compactness Ratio (*b/t*) - Measured	23.14
Global Slenderness ratio (*KL/r*)	60.90

Specimen Performance

Test Event	Axial Brace Displacement (in)	Target Displacement (in) (Cycle)	Force (kips)	$P / P_{Yield/Critical}$	
Peak Tension Load	1.03	1.75 (1)	812.8	1.01	Y
B1: Initial Global Buckling	-0.45	0.75 (1)	-507.6	0.81	C
B2: Moderate Global Buckling	N/A	N/A	N/A	N/A	C
B3-T: Local Cupping	-1.15	1.25 (1)	-214.0	0.34	C
B3-C: Striations & Tearing	1.03	1.75 (1)	812.5	1.01	Y
B4: Brace Fracture	1.60	2.25 (1)	280.0	0.35	Y

Key Observations

Cycle #	Displacement (in)	Observations
5-6	0.375	Bolt Slip - North and South GPs - T1
11-12	0.75	Initial global buckling observed - C1
13-14	1.25	Cupping observed at C1 peak displacement (1” Deep) Location of cupping - 10” south of center Cupping observed at C2 peak displacement (1.75” Deep)
15-16	1.75	Striations observed at T1 peak displacement Cupping observed at C1 peak displacement (2.5” deep) Tearing propagated halfway through cross section at T2 Cupping observed at C2 peak displacement (2.5” deep)
17-18	2.25	Fracture during T1 at an actuator displacement of about 1.95”

Test Results

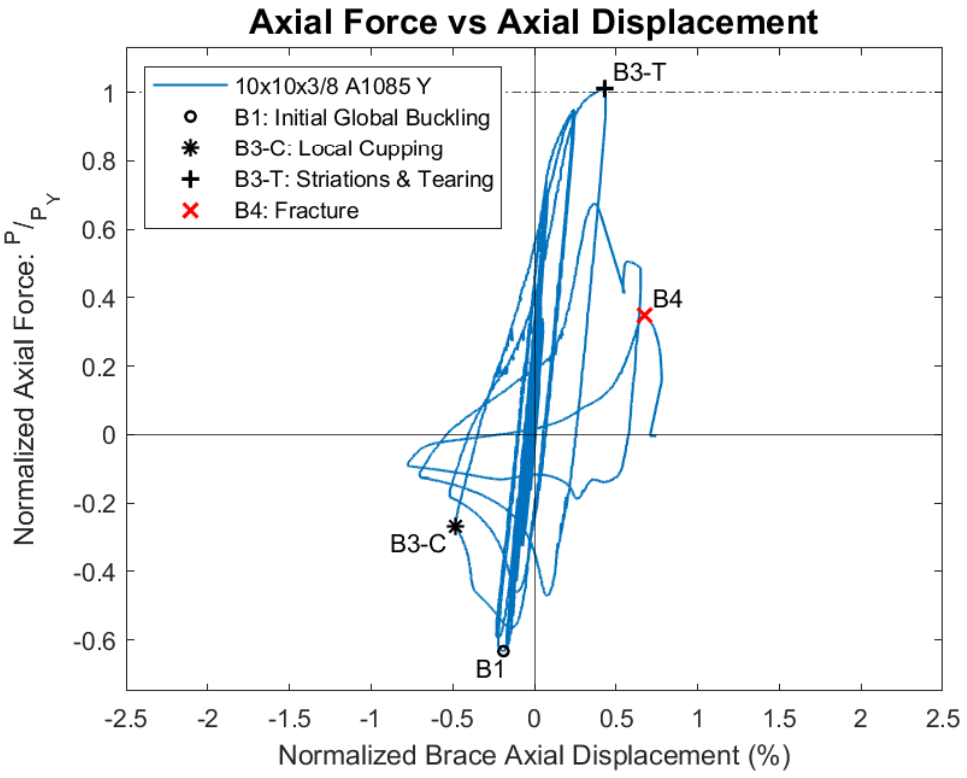

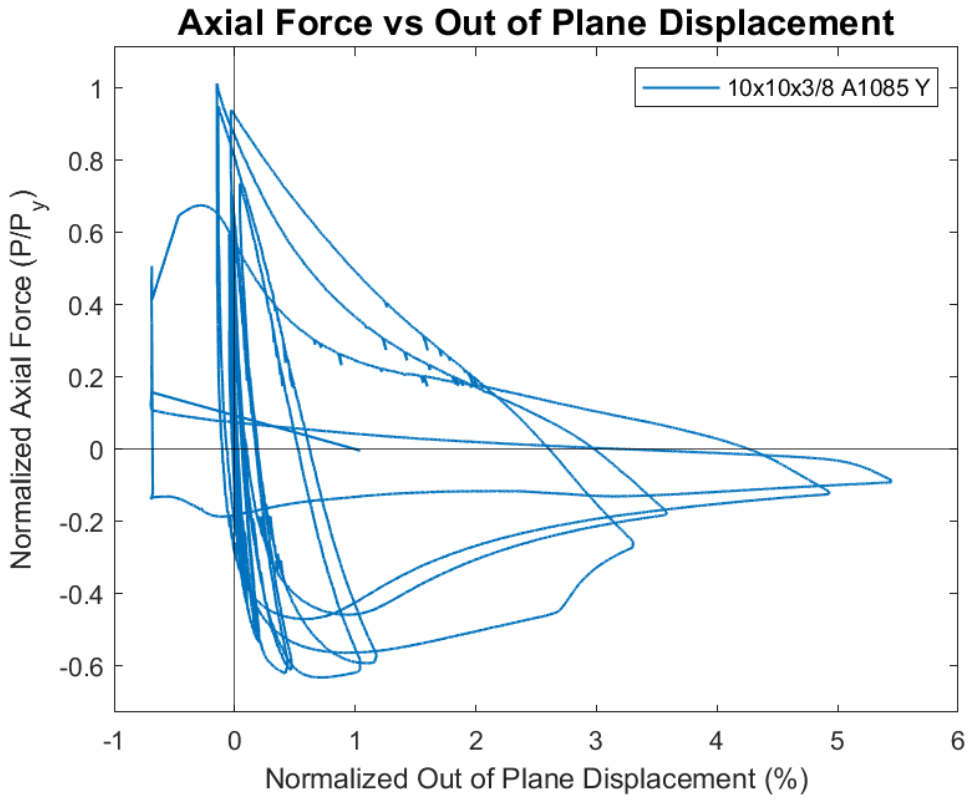

Photos

Cupping at Center of Specimen: 1.25” Cycle 1 C

Development of Striations at Corners: 1.75” Cycle 1 T

Cupping at Center of Specimen After Tearing: 2.25” Cycle 2 C

Tearing Across East Wall: 1.75” Cycle 2 T

Fractured Specimen: 3.75 Cycle 1 T

Cross Section of Fractured Specimen After Testing

5x5x3/8 A1085 R Brace Test Summary

Test Name: 5x5x3/8 A1085 R
Test Date: 7/20/21

Brace Properties

Measured Yield Stress (ksi)	68.82	**Area (in²)**	6.58
Measured Ultimate Stress (ksi)	77.52	**Moment of Inertia (in⁴)**	22.8
Yield Load (kips)	452.80	**Corner Radius (in)**	0.770
Critical Buckling Load (kips)	101.3	**Thickness - Nominal (in)**	0.375
Percent Elongation - 2" (%)	34.92	**Thickness - Measured (in)**	0.375
CVN Width (mm)	7.5	**Brace Compactness Ratio (*b/t*) - Nominal**	10.3
CVN Absorbed Energy (ft-lbs)	23.17	**Brace Compactness Ratio (*b/t*) - Measured**	9.23
Brace Length (in)	237.5	**Global Slenderness ratio (*KL/r*)**	127.7

Specimen Performance

Test Event	Axial Brace Deformation (in)	Target Displacement (in) (Cycle)	Force (kips)	$P / P_{Yield \mid Critical}$	
Peak Tension Load	1.72	2.25 (1)	456.59	1.01	Y
B1: Initial Global Buckling	-0.13	0.25 (1)	-114.23	1.13	C
B2: Moderate Global Buckling	-0.34	1.25 (1)	-104.77	1.03	C
B3-C: Local Cupping	-4.14	4.25 (1)	-29.08	0.29	C
B3-T: Striations & Tearing	4.21	5.75 (2)	108.50	0.24	Y
B4: Brace Fracture	4.91	5.75 (2)	125.28	0.28	Y

Key Observations

Cycle #	Displacement (in.)	Observations
5-6	0.375	Initial global buckling, first compression cycle
7-8	0.5	Bolt slip at south gusset plate, first tension cycle
9-10	0.625	Moderate out of plane buckling, first compression cycle
11-12	0.75	Bolt slip at north gusset plate, first tension cycle
25-26	4.25	Minor cupping observed in both compression cycles (~1/8" deep)
29-30	5.25	Cupping developing at 2" south of the brace midspan Cupping observed to be ~1" deep
31-32	5.75	Fracture during first tension cycle at ~5.4" displacement

Test Results

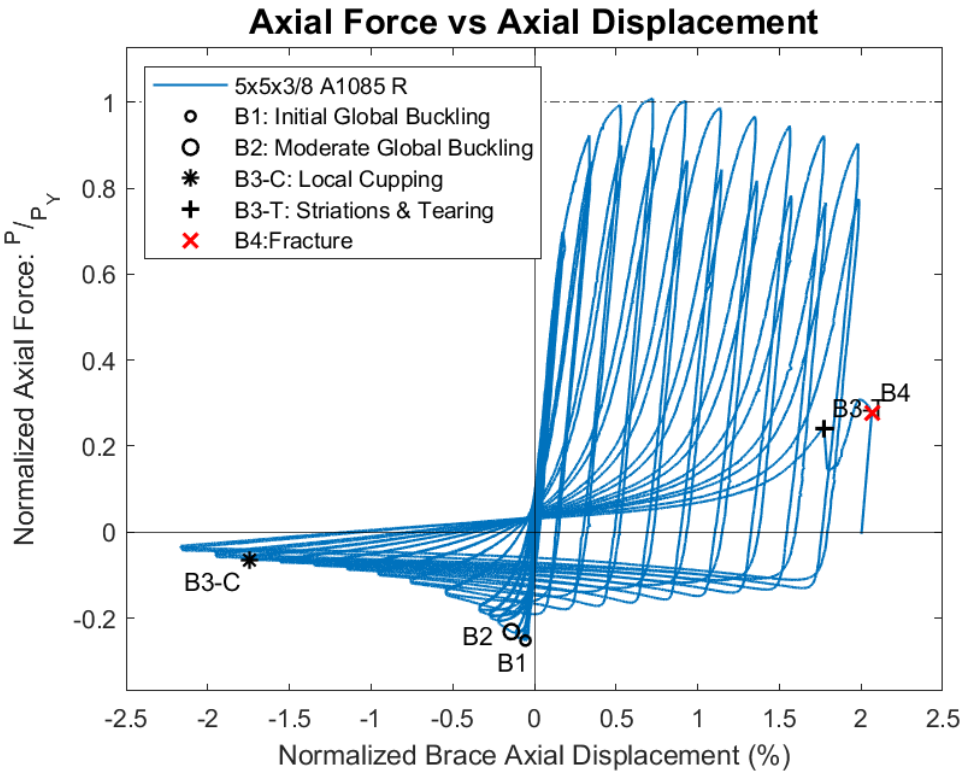

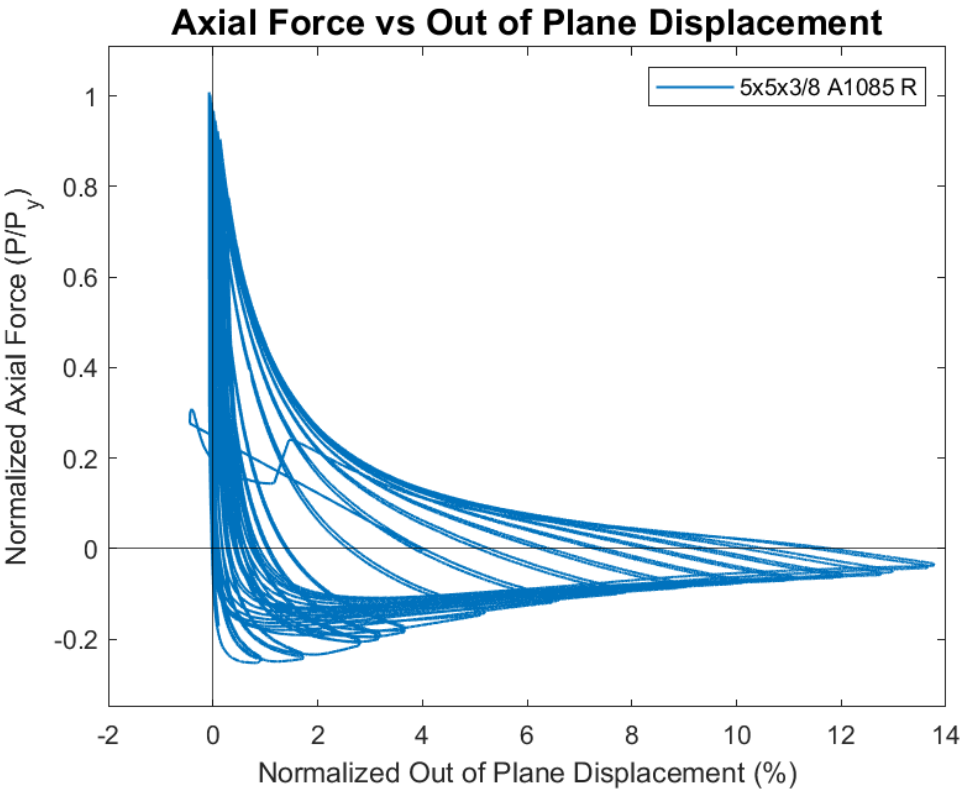

Photos

Moderate cupping at center of brace: 5.25” cycles

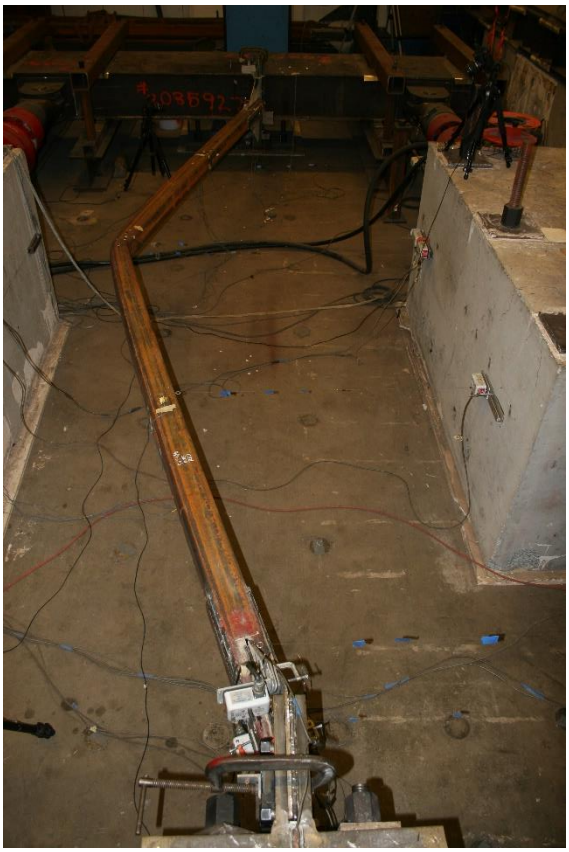

Peak out of plane displacement: 5.25” cycles

Tearing beginning to develop at center of brace: 5.75” cycles

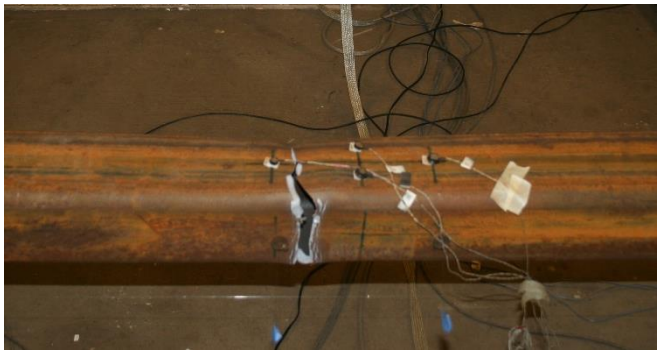

Fracture in tension during first 5.75” cycle

5x5x3/8 A1085 W Brace Test Summary

Test Name: 5x5x3/8 A1085 W
Test Date: 8/23/21

Brace Properties

Measured Yield Stress (ksi)	69.53	**Area (in²)**	6.58
Measured Ultimate Stress (ksi)	75.03	**Moment of Inertia (in⁴)**	22.8
Yield Load (kips)	456.3	**Corner Radius (in)**	0.723
Critical Buckling Load (kips)	101.3	**Thickness - Nominal (in)**	0.375
Percent Elongation - 2" (%)	38.06	**Thickness - Measured (in)**	0.374
CVN Width (mm)	7.5	**Brace Compactness Ratio (*b/t*) - Nominal**	10.3
CVN Absorbed Energy (ft-lbs)	76.83	**Brace Compactness Ratio (*b/t*) - Measured**	9.50
Brace Length (in)	237.5	**Global Slenderness ratio (*KL/r*)**	127.7

Specimen Performance

Test Event	Axial Brace Deformation (in)	Target Displacement (in) (Cycle)	Force (kips)	$P / P_{Yield \mid Critical}$	
Peak Tension Load	1.54	2.25 (1)	468.27	1.03	Y
B1: Initial Global Buckling	-0.14	0.25 (1)	-110.19	1.09	C
B2: Moderate Global Buckling	-0.39	0.625 (1)	-102.85	1.02	C
B3-C: Local Cupping	-4.27	4.25 (1)	-30.11	0.30	C
B3-T: Striations & Tearing	4.01	5.25 (2)	165.21	0.36	Y
B4: Brace Fracture	2.05	5.25 (2)	-22.98	-0.05	Y

Key Observations

Cycle #	Displacement	Observations
3-4	0.25	Initial global buckling
7-8	0.5	Bolt slip at north gusset plate during first tension cycle
9-10	0.625	Bolt slip at south gusset plate, first tension cycle
25-26	4.25	Initial cupping observed at first peak compression, very minor ~1/16” deep Cupping ~3/16” deep, second peak compression Cupping developed at 1” south of brace midspan
27-28	4.75	Cupping ~0.5” deep, first peak compression Cupping ~0.75” deep, second peak compression
29-30	5.25	Cupping ~1” deep, first peak compression Tore thru top, bottom, and east walls during second tension cycle Fractured as brace buckled in second compression cycle

Test Results

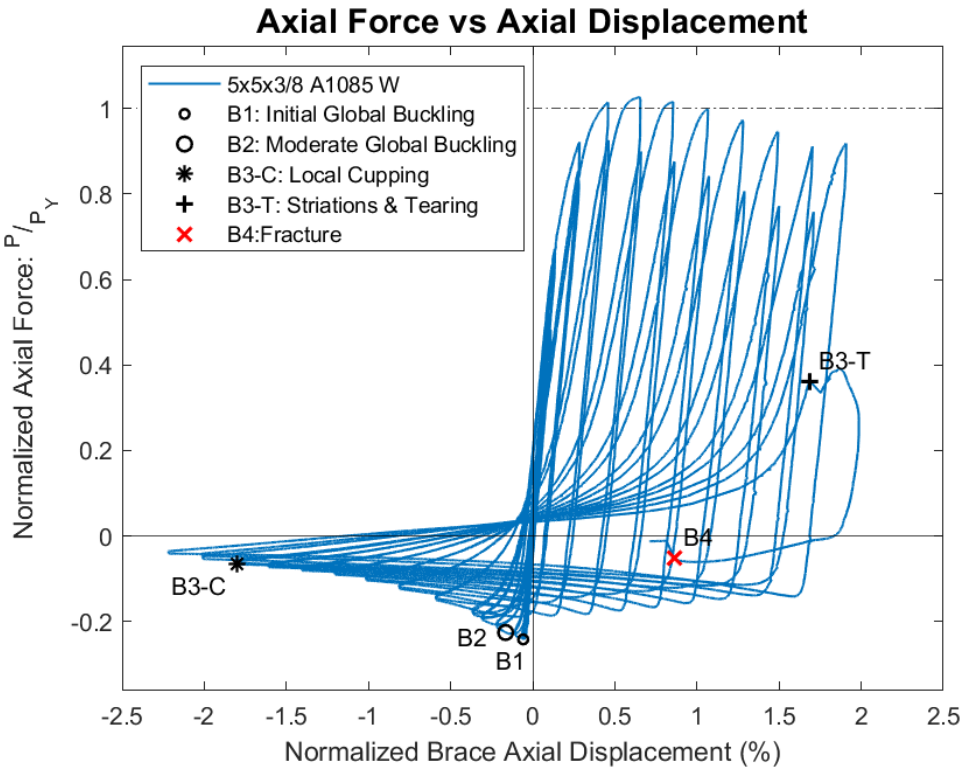

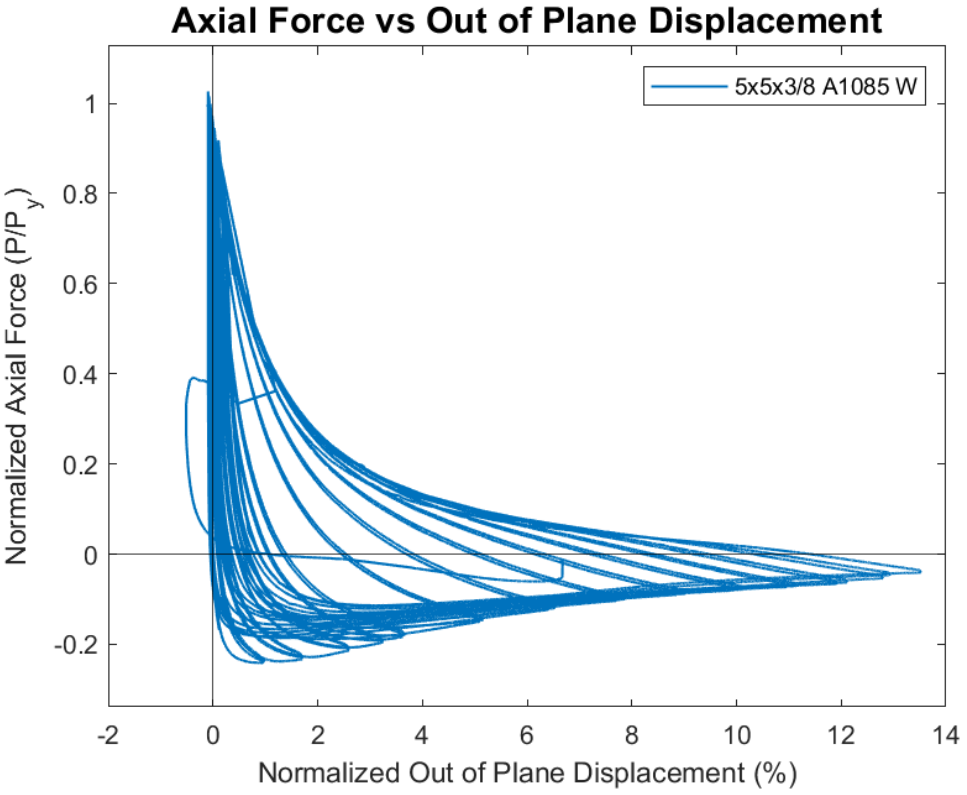

Photos

Moderate cupping at center of brace: 5.25” cycles

Peak out of plane displacement: 5.25” cycles

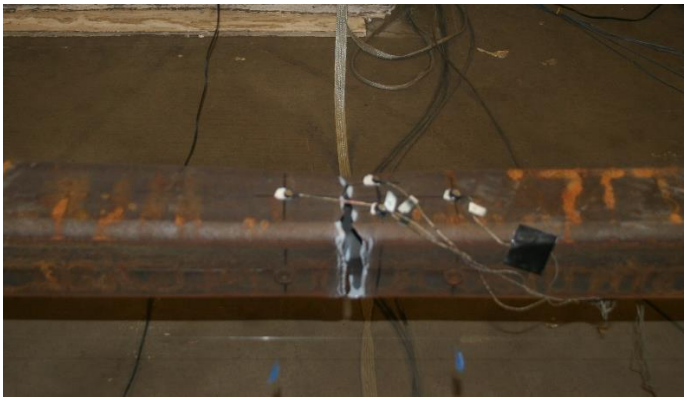

Specimen tearing during second tension cycle at 5.25”

Fracture thru west wall in compression: 5.25” cycles

5x5x3/8 A1085 B Brace Test Summary

Test Name: 5x5x3/8 A1085 B
Test Date: 8/25/21

Brace Properties

Measured Yield Stress (ksi)	78.15	**Area (in²)**	6.58
Measured Ultimate Stress (ksi)	87.63	**Moment of Inertia (in⁴)**	22.8
Yield Load (kips)	522.4	**Corner Radius (in)**	0.734
Critical Buckling Load (kips)	101.3	**Thickness - Nominal (in)**	0.375
Percent Elongation - 2" (%)	27.90	**Thickness - Measured (in)**	0.381
CVN Width (mm)	7.5	**Brace Compactness Ratio (*b/t*) - Nominal**	10.3
CVN Absorbed Energy (ft-lbs)	30.67	**Brace Compactness Ratio (*b/t*) - Measured**	9.27
Brace Length (in)	237.5	**Global Slenderness ratio (*KL/r*)**	127.7

Specimen Performance

Test Event	Axial Brace Deformation (in)	Target Displacement (in) (Cycle)	Force (kips)	$P / P_{Yield \mid Critical}$	
Peak Tension Load	1.66	2.75 (1)	538.20	1.03	Y
B1: Initial Global Buckling	-0.15	0.25 (1)	-126.44	1.25	C
B2: Moderate Global Buckling	-0.38	0.5 (1)	-110.61	1.09	C
B3-C: Local Cupping	-3.95	3.75 (1)	-33.70	0.33	C
B3-T: Striations & Tearing	3.70	4.75 (2)	332.25	0.64	Y
B4: Brace Fracture	3.74	5.25 (1)	117.50	0.22	Y

Key Observations

Cycle #	Displacement (in.)	Observations
		The brace began buckling east (the opposite of the intended direction) String pots were adjusted accordingly
3-4	0.25	Initial global buckling, first compression cycle
5-6	0.375	Bolt slip at north gusset plate, first tension cycle
7-8	0.5	Moderate out of plane buckling, first compression cycle
9-10	0.625	Bolt slip at south gusset plate, first tension cycle
17-18	2.25	Brace out of plane buckling switched directions (now buckling west) Transverse string pots at the brace midspan were moved to the other side Longitudinal string pots were moved to other side to avoid obstruction
23-24	3.75	Very minor initial cupping observed at first peak compression Cupping ~1/8” deep, second peak compression

		Cupping developed at 2.5” south of brace midspan
25-26	4.25	Cupping ~3/8” deep, first peak compression Cupping ~3/4” deep, second peak compression
27-28	4.75	Cupping ~1” deep, first peak compression Tore thru 3/4 walls during second tension cycle Buckled east after tearing, second compression cycle
29-30	5.25	Fracture during first tension cycle!

Test Results

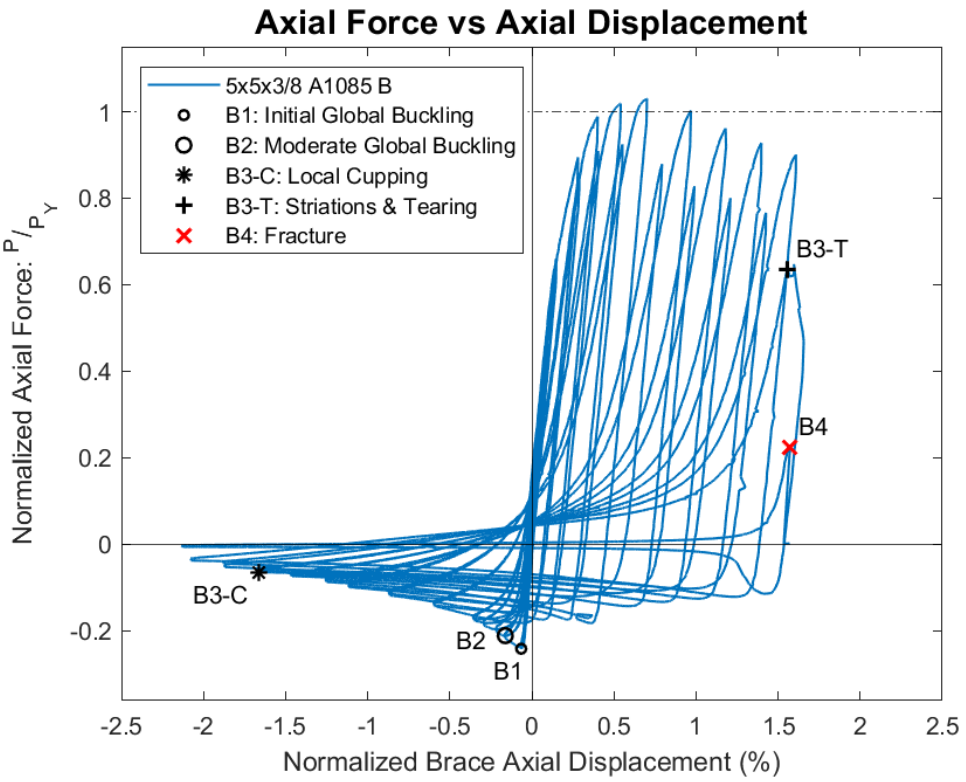

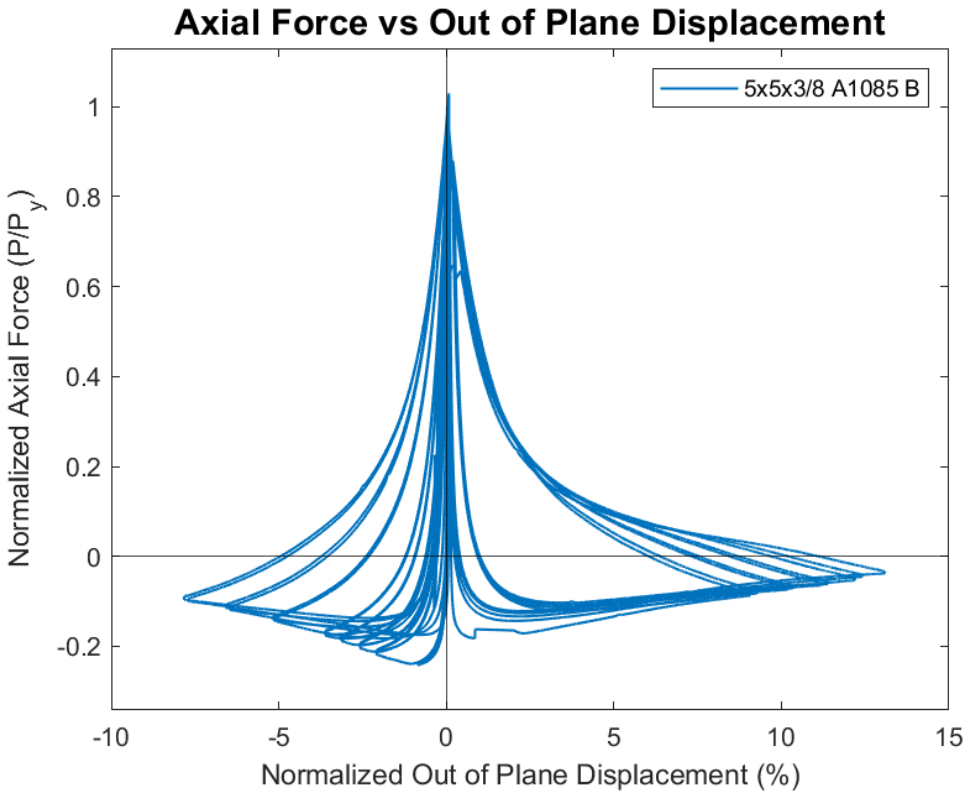
Axial Force vs Out of Plane Displacement
5x5x3/8 A1085 B
Normalized Axial Force (P/P_y)
1
0.8
0.6
0.4
0.2
0
-0.2
-10
-5
0
5
10
15
Normalized Out of Plane Displacement (%)

Photos

Moderate cupping at center of brace: 4.75” cycles

Tearing thru three walls: 4.75” cycles

Specimen buckling eastward after tearing: 4.75” cycle 2

Specimen buckling westward: 4.75” cycle 1

6x6x3/8 A1085 R Brace Test Summary

Test Name: 6x6x3/8 A1085 R
Test Date: 8/9/21

Brace Properties

Measured Yield Stress (ksi)	60.41	**Area (in²)**	8.08
Measured Ultimate Stress (ksi)	74.29	**Moment of Inertia (in⁴)**	41.6
Yield Load (kips)	482.87	**Corner Radius (in)**	0.719
Critical Buckling Load (kips)	185.27	**Thickness - Nominal (in)**	0.375
Percent Elongation - 2" (%)	33.26	**Thickness - Measured (in)**	0.371
CVN Width (mm)	7.5	**Brace Compactness Ratio (*b/t*) - Nominal**	13
CVN Absorbed Energy (ft-lbs)	40.5	**Brace Compactness Ratio (*b/t*) - Measured**	12.30
Brace Length (in)	237.5	**Global Slenderness ratio (*KL/r*)**	104.63

Specimen Performance

Test Event	Axial Brace Deformation (in)	Target Displacement (in) (Cycle)	Force (kips)	$P / P_{Yield \mid Critical}$	
Peak Tension Load	1.78	2.25 (1)	521.04	1.08	Y
B1: Initial Global Buckling	-0.19	0.25 (1)	-178.82	0.97	C
B2: Moderate Global Buckling	-0.53	0.75 (1)	-147.64	0.80	C
B3-C: Local Cupping	-3.09	3.25 (1)	-51.03	0.28	C
B3-T: Striations & Tearing	2.99	4.25 (2)	107.57	0.22	Y
B4: Brace Fracture	3.96	4.25 (2)	125.10	0.26	Y

Key Observations

Cycle #	Displacement	Observations
5-6	0.375	Initial global buckling, first compression cycle
9-10	0.625	Bolt slip at north gusset plate, first tension cycle
11-12	0.75	Moderate out of plane buckling, C1
21-22	3.25	Initial cupping observed at 2” north of brace midspan at first peak compression Cupping ~3/16” deep at second peak compression
23-24	3.75	Cupping ~5/8” deep at first peak compression Cupping ~1.25” deep at second peak compression
25-26	4.25	Cupping ~1.5” deep at first peak compression Fracture at second peak tension!

Test Results

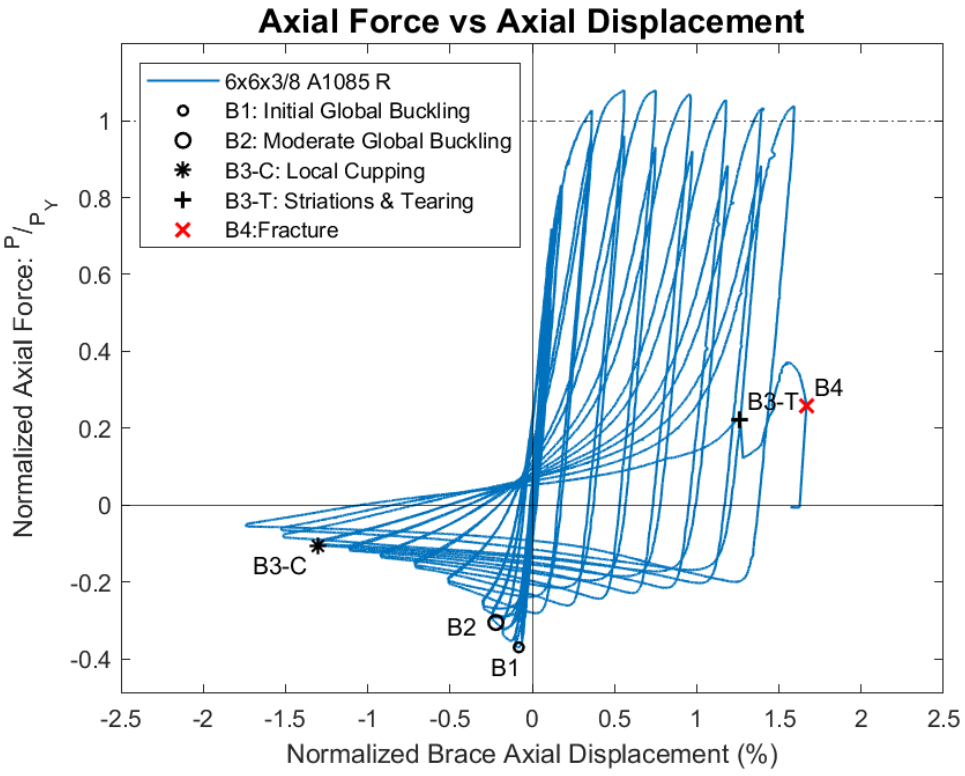

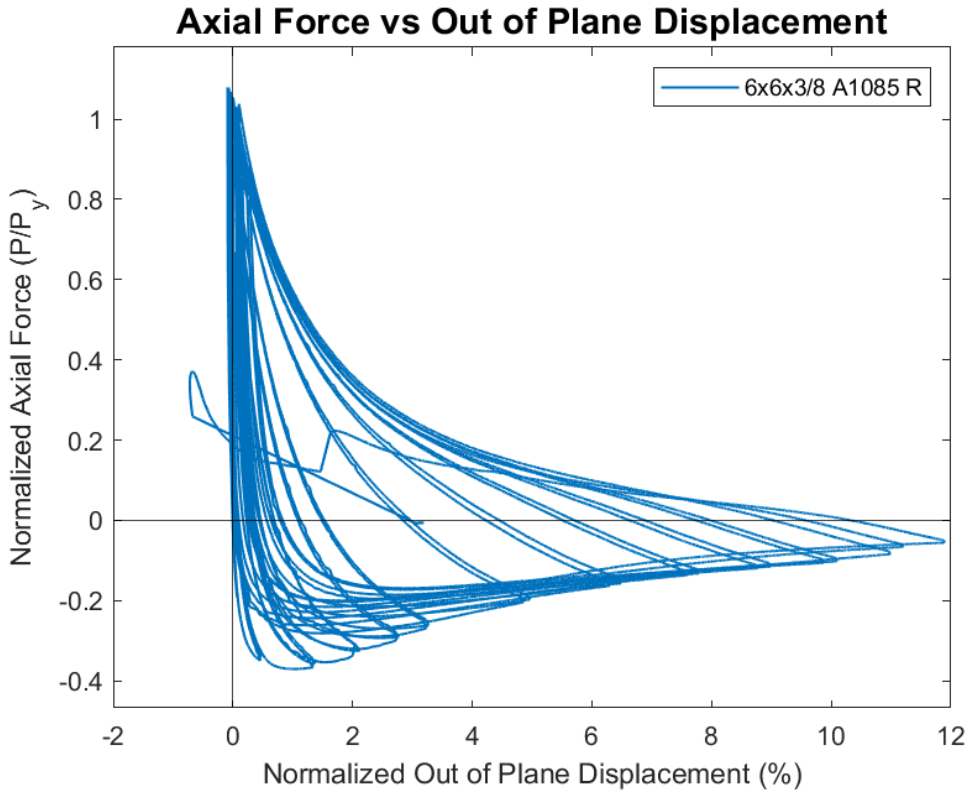

Photos

Moderate cupping at center of brace: 4.25” cycles

Peak out of plane displacement: 4.25” cycles

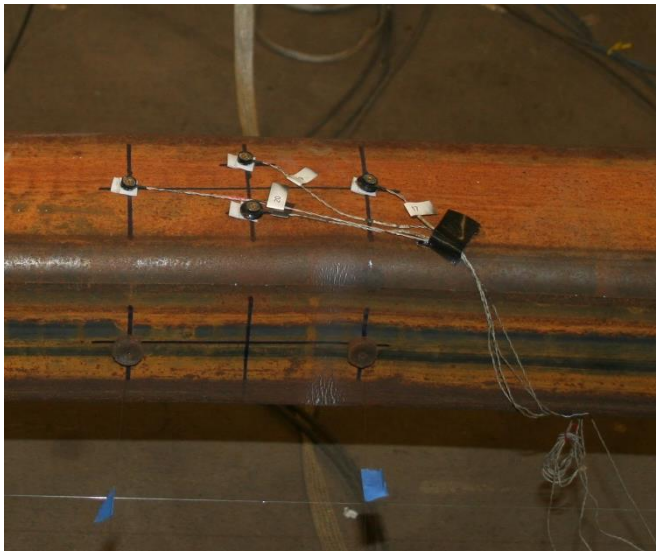

Striations beginning to develop at center of brace: 4.25” cycles

Specimen fractured in tension during first 4.25” cycle

6x6x3/8 A1085 W Brace Test Summary

Test Name: 6x6x3/8 A1085 W
Test Date: 8/13/21

Brace Properties

Measured Yield Stress (ksi)	67.66	**Area (in²)**	8.08
Measured Ultimate Stress (ksi)	73.22	**Moment of Inertia (in⁴)**	41.6
Yield Load (kips)	549.61	**Corner Radius (in)**	0.793
Critical Buckling Load (kips)	185.27	**Thickness - Nominal (in)**	0.375
Percent Elongation - 2" (%)	37.53	**Thickness - Measured (in)**	0.377
CVN Width (mm)	7.5	**Brace Compactness Ratio (*b/t*) - Nominal**	13
CVN Absorbed Energy (ft-lbs)	82.67	**Brace Compactness Ratio (*b/t*) - Measured**	11.74
Brace Length (in)	237.5	**Global Slenderness ratio (*KL/r*)**	104.63

Specimen Performance

Test Event	Axial Brace Deformation (in)	Target Displacement (in) (Cycle)	Force (kips)	$P / P_{Yield \mid Critical}$	
Peak Tension Load	1.26	1.75 (1)	549.5	1.00	Y
B1: Initial Global Buckling	-0.23	0.375 (1)	-185.8	1.00	C
B2: Moderate Global Buckling	-0.57	0.625 (1)	-148.4	0.80	C
B3-C: Local Cupping	-3.17	3.25 (1)	-47.8	0.26	C
B3-T: Striations & Tearing	3.05	4.25 (1)	370.1	0.68	Y
B4: Brace Fracture	1.44	4.25 (1)	-22.5	-0.04	Y

Key Observations

Cycle #	Displacement	Observations
5-6	0.375	Bolt slip at south gusset plate, first tension cycle Initial global buckling, first compression cycle
7-8	0.5	Bolt slip at north gusset plate, first tension cycle
9-10	0.625	Moderate out of plane buckling, first compression cycle
21-22	3.25	Initial cupping observed to be Cupping ~1/8” deep, first peak compression Cupping ~3/8” deep, second compression cycle Cupping developed at 1” north of brace midspan
23-24	3,75	Cupping ~1” deep, first peak compression Cupping ~1.25” deep, second peak compression
25-26	4.25	Tore ~80% thru brace, one corner remaining, first tension cycle Fractured as brace buckling going into first compression cycle

Test Results

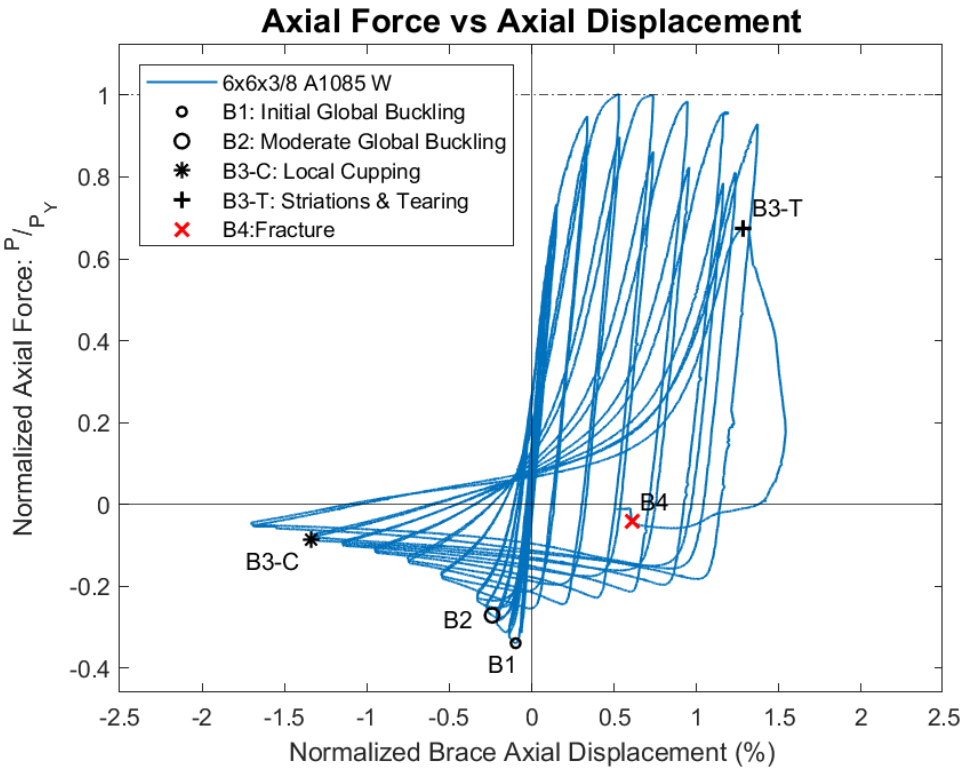

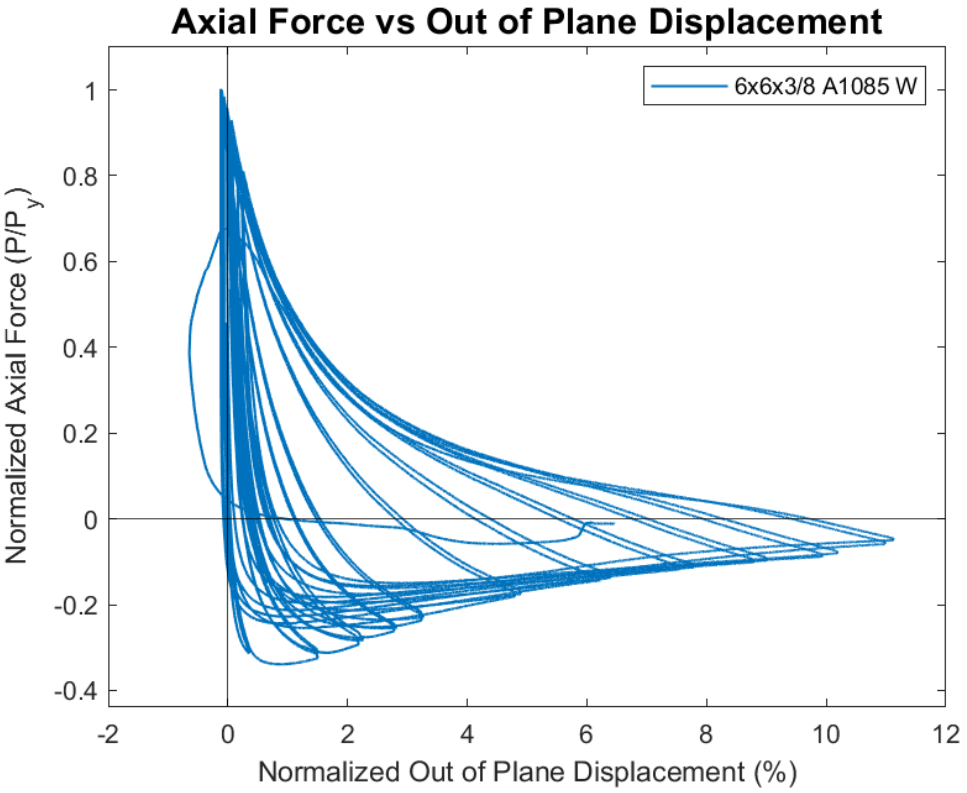

Photos

Fracture as brace buckled in compression: 4.25” cycles

Moderate cupping at center of brace: 3.75” cycles

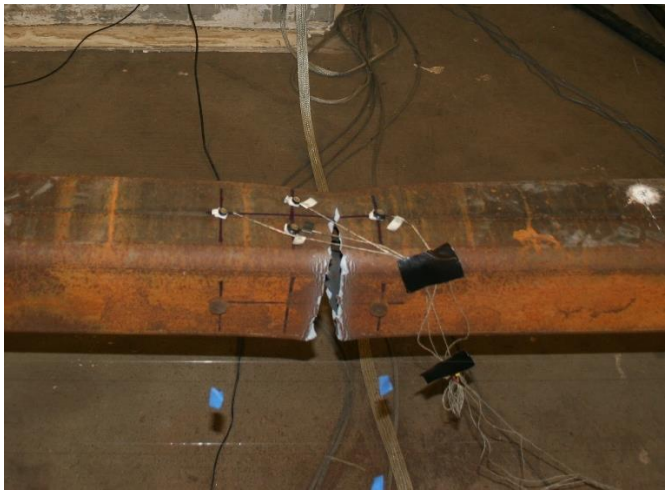

Specimen tore thru 3 walls in tension during first 4.25” cycle

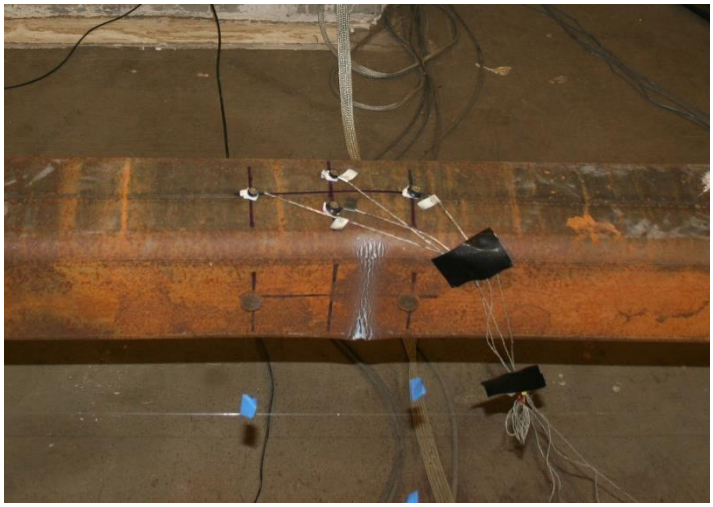

Tearing beginning to develop at center of brace: 4.25” cycles

6x6x3/8 A1085 B Brace Test Summary

Test Name: 6x6x3/8 A1085 B
Test Date: 7/27/21

Brace Properties

Measured Yield Stress (ksi)	69.05	**Area (in²)**	8.08
Measured Ultimate Stress (ksi)	73.59	**Moment of Inertia (in⁴)**	41.6
Yield Load (kips)	565.4	**Corner Radius (in)**	0.832
Critical Buckling Load (kips)	185.3	**Thickness - Nominal (in)**	0.375
Percent Elongation - 2" (%)	34.75	**Thickness - Measured (in)**	0.380
CVN Width (mm)	7.5	**Brace Compactness Ratio (*b/t*) - Nominal**	13
CVN Absorbed Energy (ft-lbs)	120+	**Brace Compactness Ratio (*b/t*) - Measured**	11.41
Brace Length (in)	237.5	**Global Slenderness ratio (*KL/r*)**	104.63

Specimen Performance

Test Event	Axial Brace Deformation (in)	Target Displacement (in) (Cycle)	Force (kips)	$P / P_{Yield \mid Critical}$	
Peak Tension Load	1.62	2.25 (1)	581.67	1.03	Y
B1: Initial Global Buckling	-0.18	0.325 (1)	-177.88	0.96	C
B2: Moderate Global Buckling	-0.55	0.625 (1)	-151.97	0.82	C
B3-C: Local Cupping	-2.30	2.25 (2)	-60.18	0.32	C
B3-T: Striations & Tearing	2.13	3.75 (1)	156.46	0.28	Y
B4: Brace Fracture	2.97	3.75 (1)	181.96	0.32	Y

Key Observations

Cycle #	Displacement (in.)	Observations
5-6	0.375	Initial global buckling, first compression cycle
7-8	0.5	Bolt slip at south gusset plate, first tension cycle
9-10	0.625	Moderate out of plane buckling, first compression cycle
11-12	0.75	Bolt slip at north gusset plate, first tension cycle
17-18	2.25	Initial cupping observed to be ~1/8” deep, second compression cycle
19-20	2.75	Cupping developed at 3” south of brace midspan Cupping ~0.75” deep at first peak compression Cupping ~1” deep at second peak compression
21-22	3.25	Cupping ~1.5” deep at first peak compression Cupping ~1.5” deep at second peak compression Wrinkling observed at brace midspan at second peak compression
23-24	3.75	Fracture during first tension cycle!

Test Results

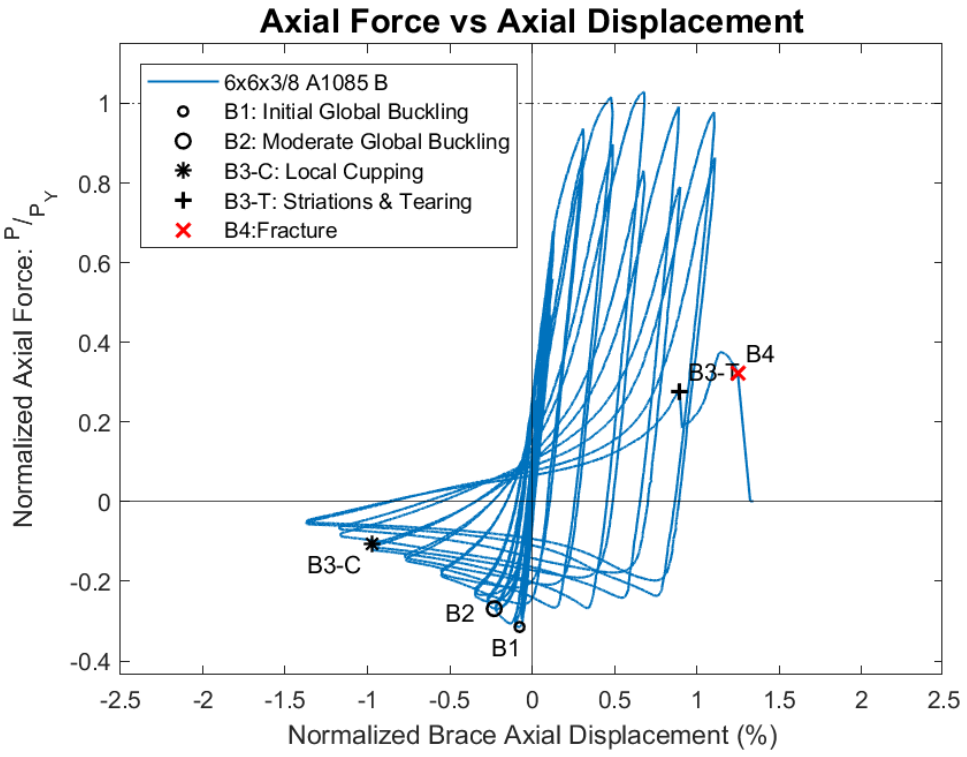

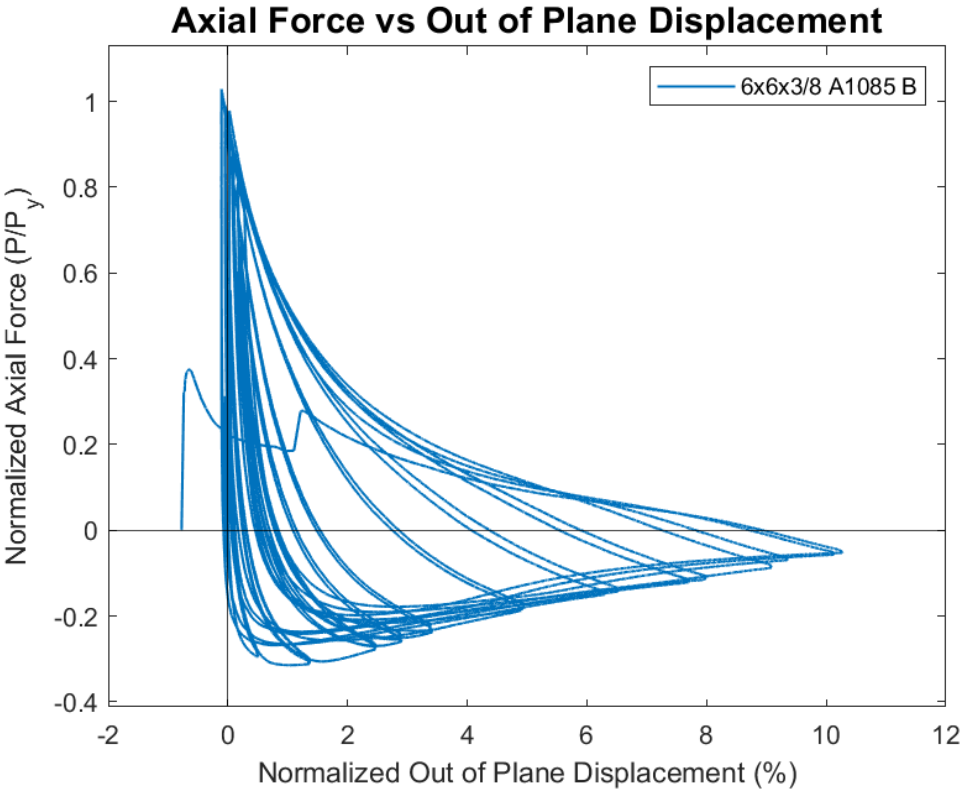

Photos

Moderate cupping at center of brace: 3.25” cycles

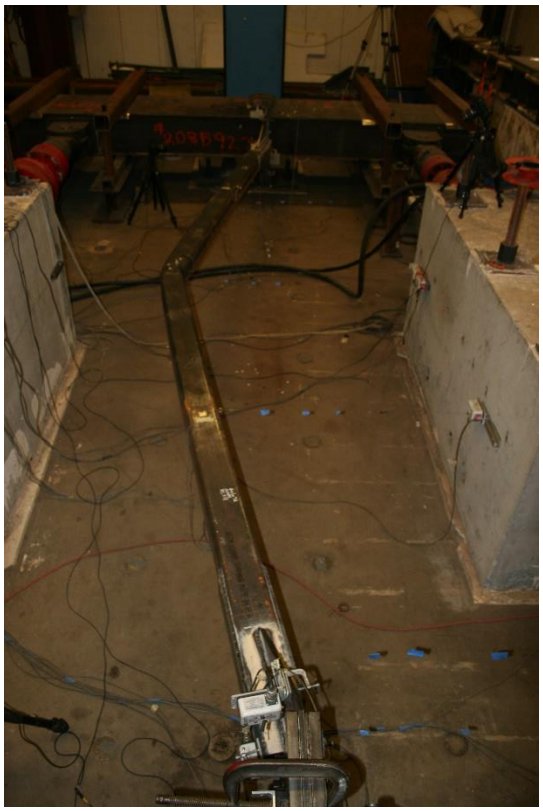

Peak out of plane displacement: 3.25” cycles

Striations develop at center of brace: 3.25” cycles

Specimen fractured in tension during first 3.75” cycle

8x8x3/8 A1085 R Brace Test Summary

Test Name: 8x8x3/8 A1085 R
Test Date: 9/8/21

Brace Properties

Measured Yield Stress (ksi)	61.20
Measured Ultimate Stress (ksi)	75.42
Yield Load (kips)	666.64
Critical Buckling Load (kips)	404.31
Percent Elongation - 2" (%)	32.44
CVN Width (mm)	7.5
CVN Absorbed Energy (ft-lbs)	58.33
Brace Length (in)	237.5

Area (in²)	11.1
Moment of Inertia (in⁴)	106
Corner Radius (in)	0.793
Thickness - Nominal (in)	0.375
Thickness - Measured (in)	0.368
Brace Compactness Ratio (*b/t*) - Nominal	18.3
Brace Compactness Ratio (*b/t*) - Measured	17.43
Global Slenderness ratio (*KL/r*)	76.86

Specimen Performance

Test Event	Axial Brace Deformation (in)	Target Displacement (in) (Cycle)	Force (kips)	$P / P_{Yield \mid Critical}$	
Peak Tension Load	1.98	2.25 (1)	660.41	0.99	Y
B1: Initial Global Buckling	-0.12	0.5 (1)	-323.69	0.80	C
B2: Moderate Global Buckling	-0.69	1.25 (1)	-205.42	0.51	C
B3-C: Local Cupping	-1.27	1.75 (1)	-146.10	0.36	C
B3-T: Striations & Tearing	2.06	2.25 (2)	630.72	0.95	Y
B4: Brace Fracture	2.68	2.75 (1)	95.06	0.14	Y

Key Observations

Cycle #	Displacement	Observations
5-6	0.375	Bolt slip at north gusset plate: all tension and compression cycles (continued throughout test)
7-8	0.5	Initial global buckling, first compression cycle
13-14	1.25	Moderate global out of plane buckling
15-16	1.75	Initial minor cupping: ~1/8" deep, first peak compression Cupping: ~5/8" deep, second peak compression
17-18	2.25	Cupping: ~1.75" deep, first peak compression Minor tearing observed on east corners at second peak tension Cupping: ~2" deep, second peak compression
19-20	2.75	Fracture! First tension cycle

Test Results

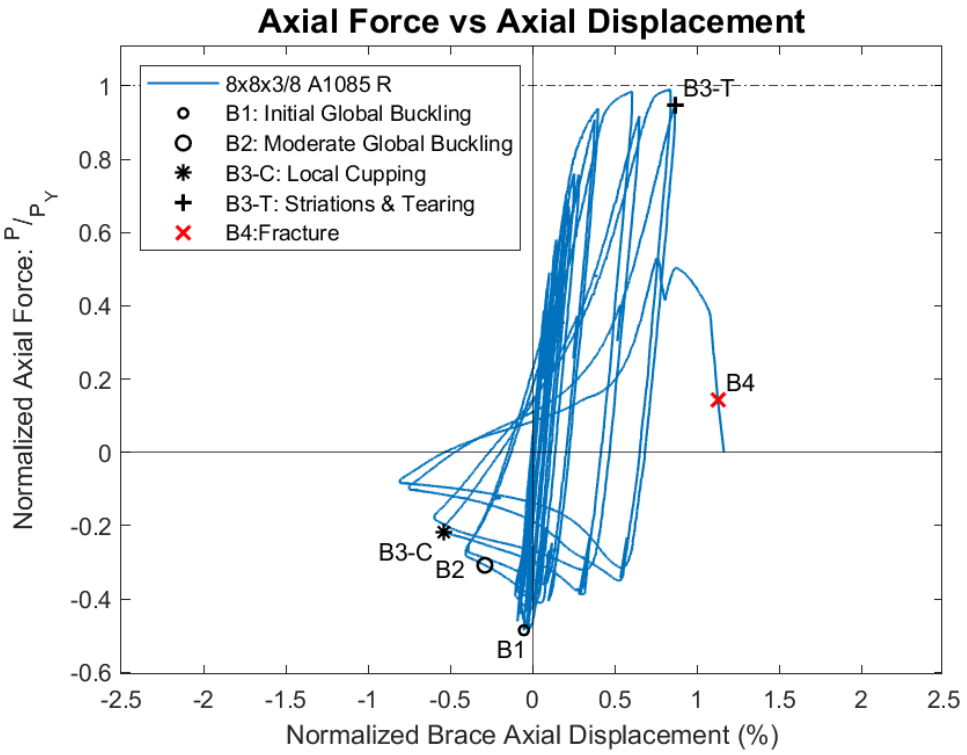

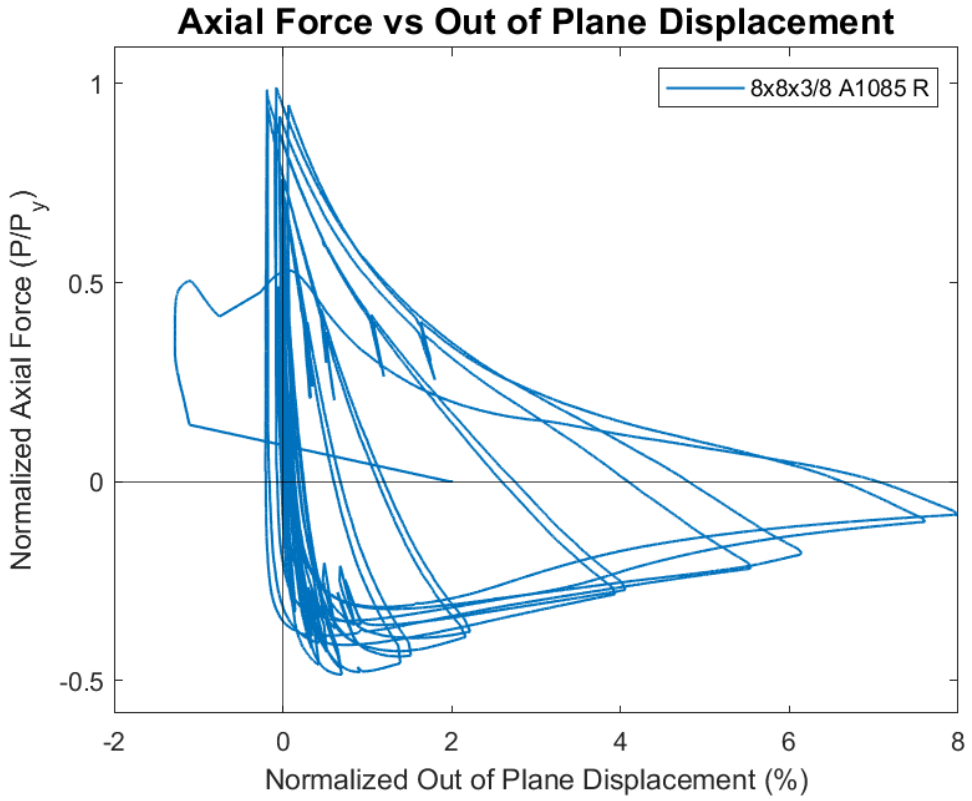

Photos

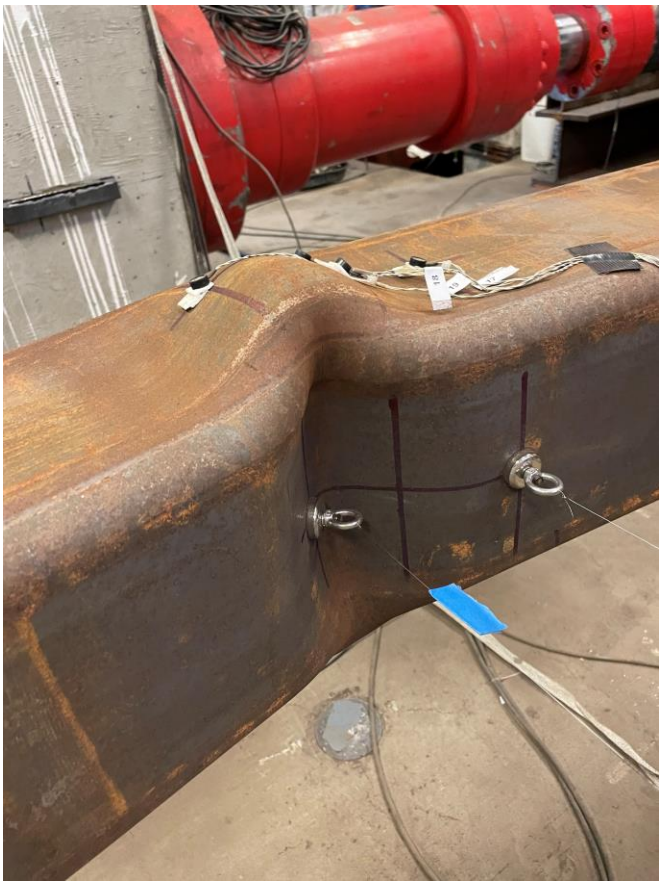

Severe cupping at center of specimen: 2.25” C2

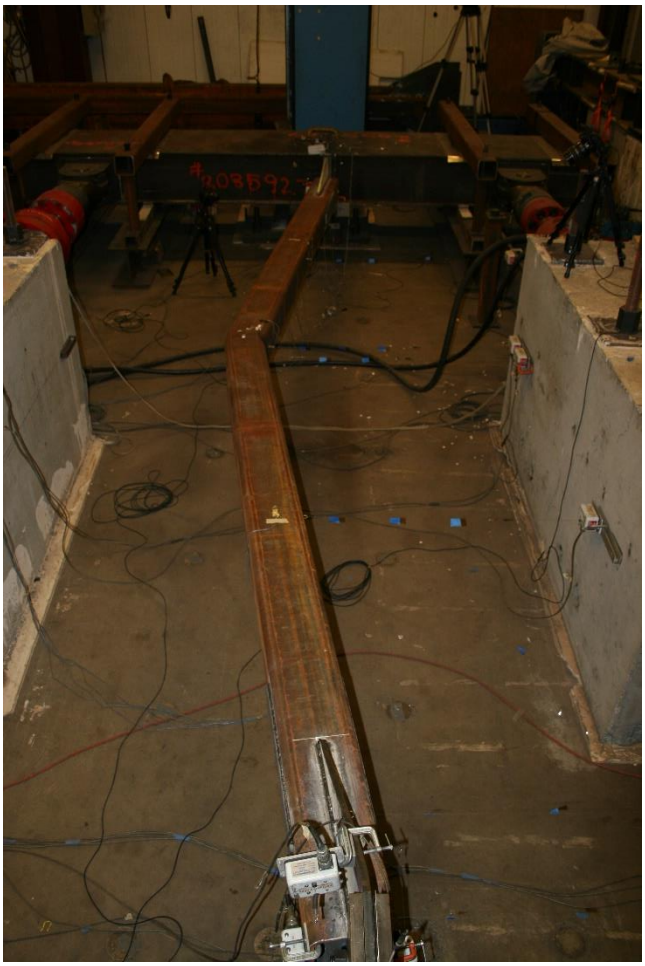

Maximum out of plane displacement: 2.25” cycles

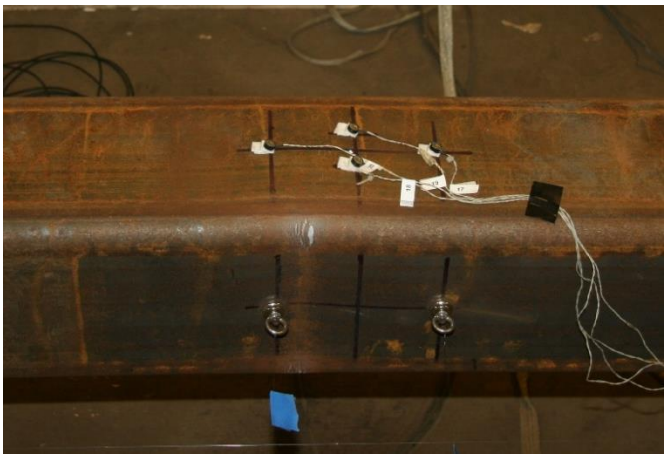

Striations/tearing initiating at the corners: 2.25” T1

Specimen fractured at first 2.75” tension cycle

8x8x3/8 A1085 W Brace Test Summary

Test Name: 8x8x3/8 A1085 W
Test Date: 9/13/21

Brace Properties

Measured Yield Stress (ksi)	63.19	**Area (in²)**	11.1
Measured Ultimate Stress (ksi)	70.67	**Moment of Inertia (in⁴)**	106
Yield Load (kips)	699.48	**Corner Radius (in)**	0.773
Critical Buckling Load (kips)	404.31	**Thickness - Nominal (in)**	0.375
Percent Elongation - 2" (%)	40.55	**Thickness - Measured (in)**	0.374
CVN Width (mm)	7.5	**Brace Compactness Ratio (*b/t*) - Nominal**	18.3
CVN Absorbed Energy (ft-lbs)	70.5	**Brace Compactness Ratio (*b/t*) - Measured**	17.26
Brace Length (in)	237.5	**Global Slenderness ratio (*KL/r*)**	76.86

Specimen Performance

Test Event	Axial Brace Deformation (in)	Target Displacement (in) (Cycle)	Force (kips)	P / P$_{Yield\ |\ Critical}$	
Peak Tension Load	1.21	1.75 (1)	711.95	1.02	Y
B1: Initial Global Buckling	-0.24	0.5 (1)	-361.03	0.89	C
B2: Moderate Global Buckling	-0.78	1.25 (1)	-219.76	0.54	C
B3-C: Local Cupping	-1.66	1.75 (1)	-148.96	0.37	C
B3-T: Striations & Tearing	1.70	2.25 (2)	673.74	0.96	Y
B4: Brace Fracture	2.31	2.75 (1)	180.37	0.26	Y

Key Observations

Cycle #	Displacement	Observations
7-8	0.5	Bolt slip at south gusset plate, first tension cycle Initial global buckling, first compression cycle
9-10	0.625	Bolt slip at north gusset plate, first tension cycle
13-14	1.25	Moderate global out of plane buckling, first compression cycle
15-16	1.75	Initial minor cupping: ~1/8” deep, first peak compression Cupping: ~5/8” deep, second peak compression Cupping observed at 3.5” north of brace midspan
17-18	2.25	Cupping: ~1.5” deep, first peak compression Striations/minor tearing on corners of east wall, second tension cycle Cupping: ~2” deep, second peak compression
19-20	2.75	Fracture during first tension cycle!

Test Results

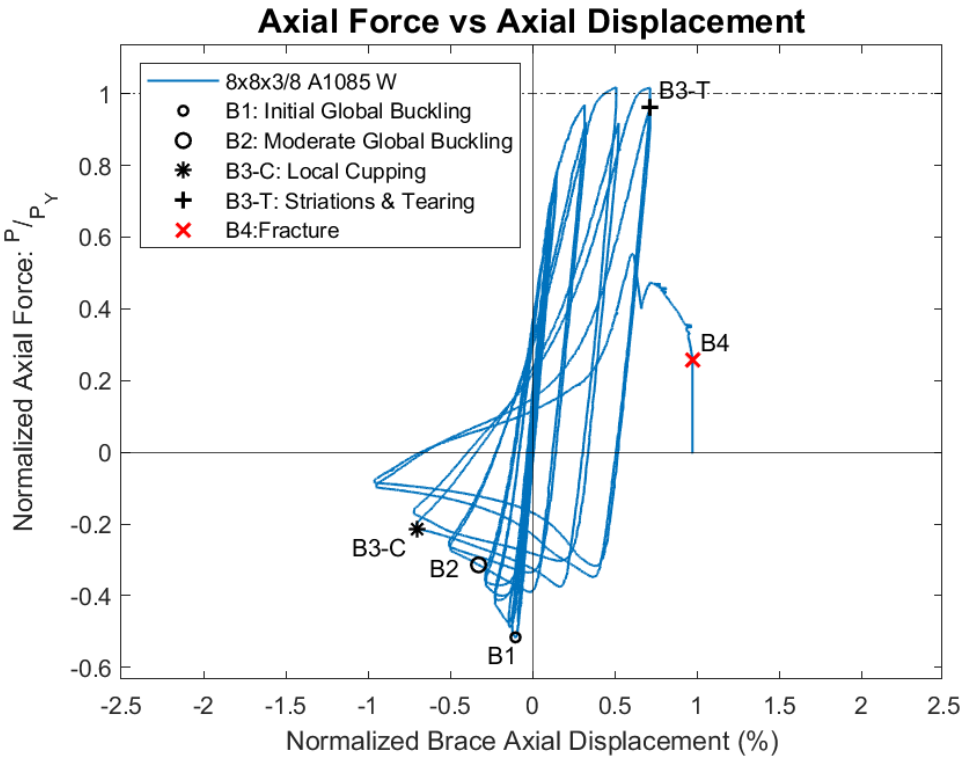

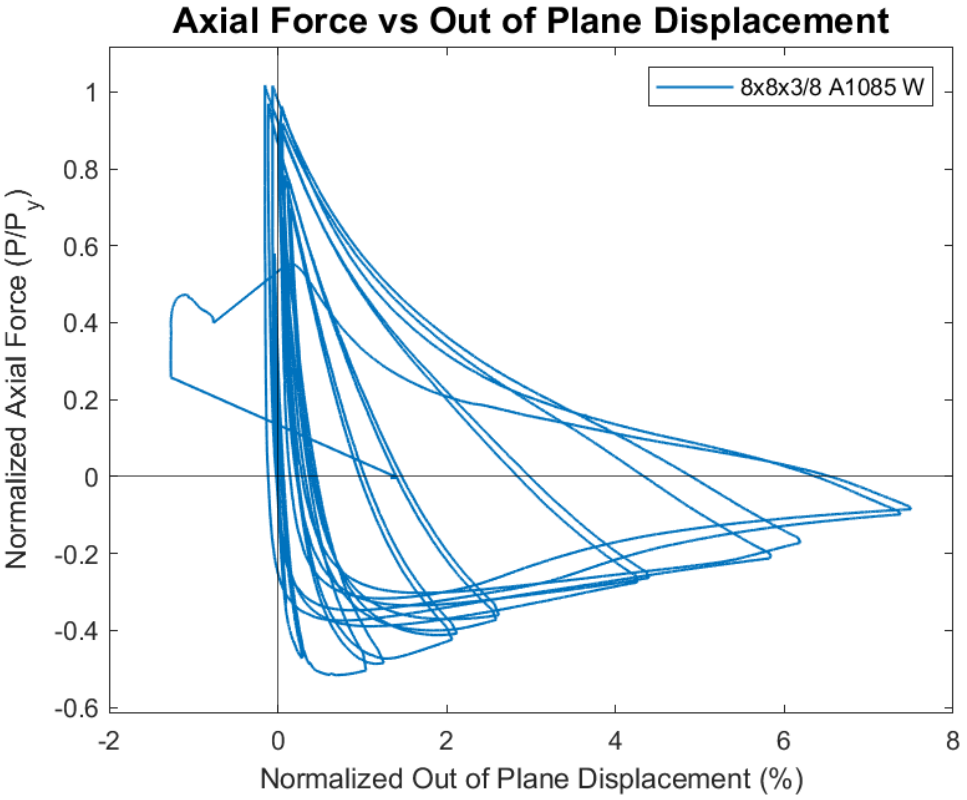

Photos

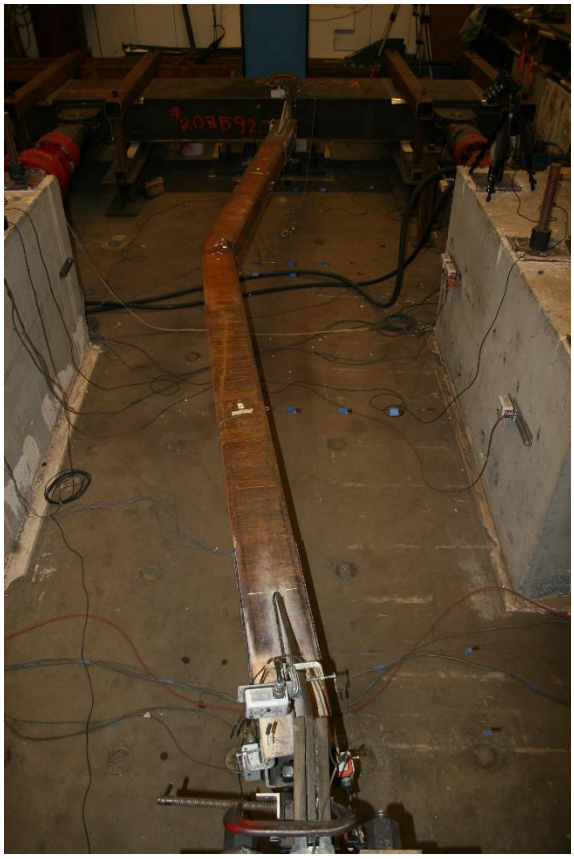

Maximum out of plane displacement: 2.25” cycles

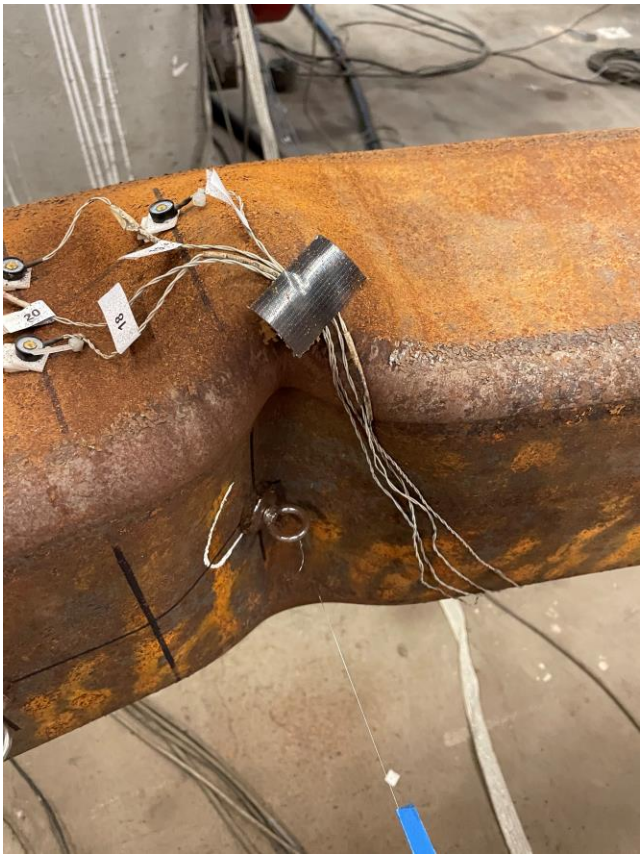

Major cupping at the center of the brace: 2.25” cycles

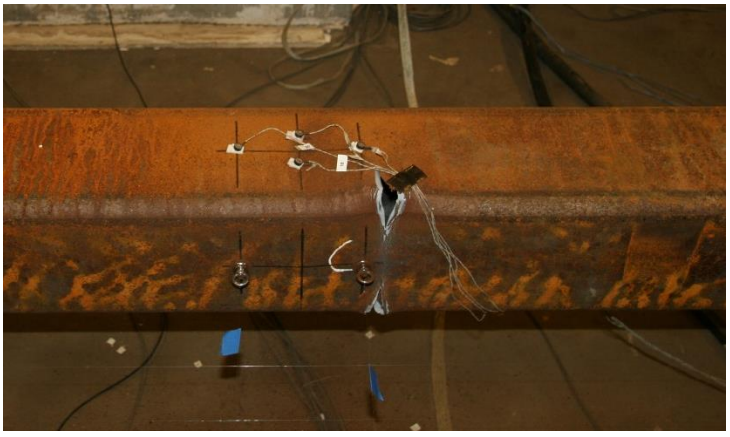

Tearing at corners on the east wall: 2.75” disp.

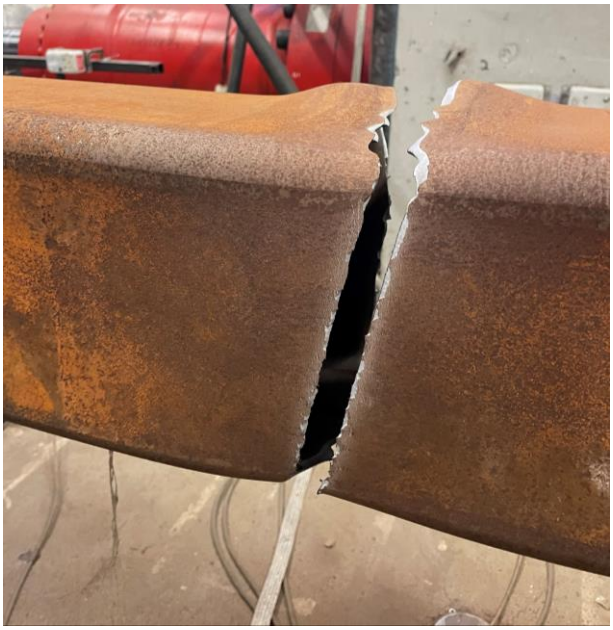

Specimen fractured at first cycle of 2.75” disp.

8x8x3/8 A1085 B Brace Test Summary

Test Name: 8x8x3/8 A1085 B
Test Date: 9/3/21

Brace Properties

Measured Yield Stress (ksi)	68.24	**Area (in²)**	11.1
Measured Ultimate Stress (ksi)	71.63	**Moment of Inertia (in⁴)**	106
Yield Load (kips)	757.41	**Corner Radius (in)**	0.855
Critical Buckling Load (kips)	404.31	**Thickness - Nominal (in)**	0.375
Percent Elongation - 2" (%)	37.18	**Thickness - Measured (in)**	0.375
CVN Width (mm)	7.5	**Brace Compactness Ratio (*b/t*) - Nominal**	18.3
CVN Absorbed Energy (ft-lbs)	120+	**Brace Compactness Ratio (*b/t*) - Measured**	16.77
Brace Length (in)	237.5	**Global Slenderness ratio (*KL/r*)**	76.86

Specimen Performance

Test Event	Axial Brace Deformation (in)	Target Displacement (in) (Cycle)	Force (kips)	$P / P_{Yield \mid Critical}$	
Peak Tension Load	1.40	2.25 (1)	763.00	1.01	Y
B1: Initial Global Buckling	-0.34	0.625 (1)	-363.94	0.90	C
B2: Moderate Global Buckling	-1.06	1.25 (1)	-249.06	0.62	C
B3-C: Local Cupping	-1.34	1.25 (2)	-212.34	0.53	C
B3-T: Striations & Tearing	1.26	2.25 (2)	561.86	0.74	Y
B4: Brace Fracture	1.74	2.75 (1)	170.63	0.23	Y

Key Observations

Cycle #	Displacement	Observations
7-8	0.5	Bolt slip at north and south gusset plates, first tension cycle *Bolt slip occurred in tension and compression throughout testing
9-10	0.625	Initial global buckling
13-14	1.25	Moderate global buckling, first compression cycle Very minor cupping: ~1/8” deep, second peak compression
15-16	1.75	Cupping: ~0.75” deep, first peak compression Cupping: ~1.5” deep, second peak compression
17-18	2.25	Striations observed at first peak tension Cupping: ~2” deep, first peak compression Tore halfway thru brace during second tension cycle
19-20	2.75	Fracture during first tension cycle!

Test Results

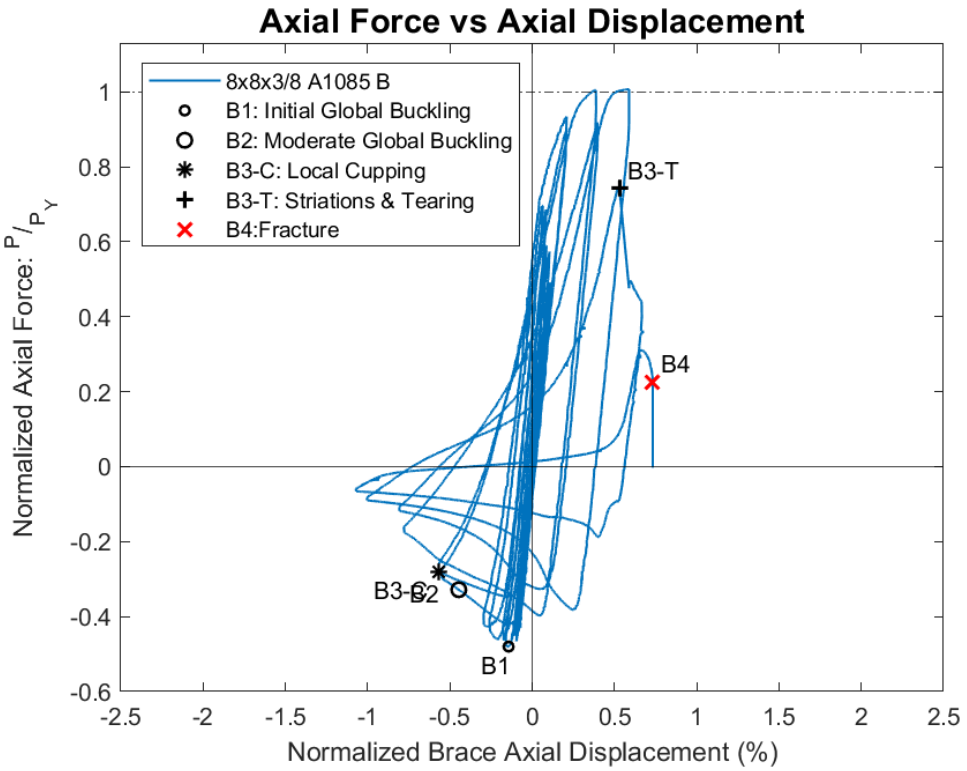

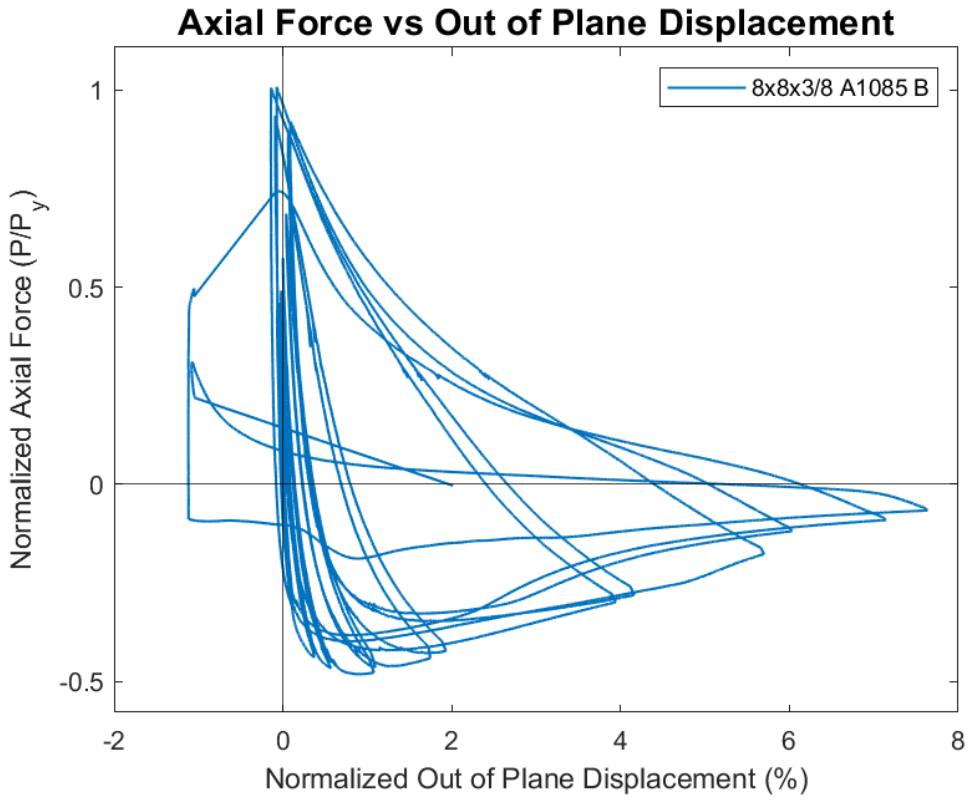

Photos

Cupping at the center of the brace: 2.25” cycles

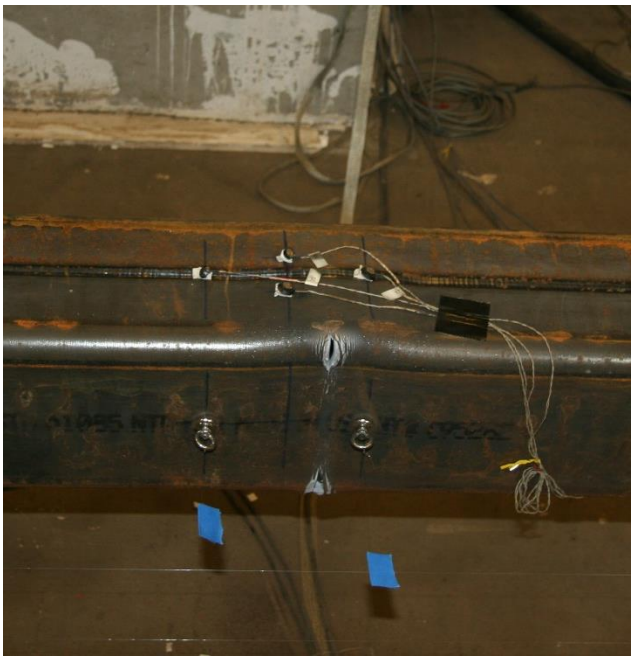

Tearing at center of brace: 2.25” cycles

Cupping at the center after tearing: 2.25” cycle 2

Large residual local deformations following fracture

8x8x1/2 A1085 R Brace Test Summary

Test Name: 8x8x1/2 A1085 R
Test Date: 10/13/21

Brace Properties

Measured Yield Stress (ksi)	58.54	**Area (in²)**	14.4
Measured Ultimate Stress (ksi)	64.27	**Moment of Inertia (in⁴)**	131
Yield Load (kips)	783.97	**Corner Radius (in)**	1.02
Critical Buckling Load (kips)	511.41	**Thickness - Nominal (in)**	0.500
Percent Elongation - 2" (%)	34.43	**Thickness - Measured (in)**	0.465
CVN Width (mm)	10	**Brace Compactness Ratio (*b/t*) - Nominal**	13
CVN Absorbed Energy (ft-lbs)	120+	**Brace Compactness Ratio (*b/t*) - Measured**	12.83
Brace Length (in)	237.5	**Global Slenderness ratio (*KL/r*)**	78.64

Specimen Performance

Test Event	Axial Brace Deformation (in)	Target Displacement (in.) (Cycle)	Force (kips)	$P / P_{Yield \mid Critical}$	
Peak Tension Load	1.37	1.75 (1)	819.18	1.04	Y
B1: Initial Global Buckling	-0.13	0.625 (1)	-425.29	0.83	C
B2: Moderate Global Buckling	-0.57	1.25 (1)	-275.55	0.54	C
B3-C: Local Cupping	-1.45	1.75 (1)	-176.30	0.34	C
B3-T: Striations & Tearing	2.35	2.75 (1)	793.50	1.01	Y
B4: Brace Fracture	3.31	3.75 (1)	168.32	0.21	Y

Key Observations

Cycle #	Displacement (in.)	Observations
7-8	0.5	Bolt slip at north gusset plate, first compression cycle (bolt slip occurred in tension and compression throughout test)
11-12	0.75	Initial global buckling, first compression cycle
13-14	1.25	Moderate global buckling, first compression cycle Initial minor cupping: ~1/16” deep, second peak compression
15-16	1.75	Cupping: ~1/8” deep, first peak compression Cupping: ~1/4” deep, second peak compression
17-18	2.25	Cupping: ~1” deep, first peak compression Cupping: ~1.5” deep, second peak compression Cupping observed at midspan of brace

19-20	2.75	Striations observed at first peak tension Cupping: ~2” deep, first peak compression Tearing developed at corners of east wall, second tension cycle Cupping: ~2” deep, second peak compression
21-22	3.25	Tore thru east, top and bottom walls, first tension cycle Cupping: ~2.25” deep, first peak compression Cupping: ~2.25” deep, second peak compression
23-24	3.75	Fracture! First tension cycle

Test Results

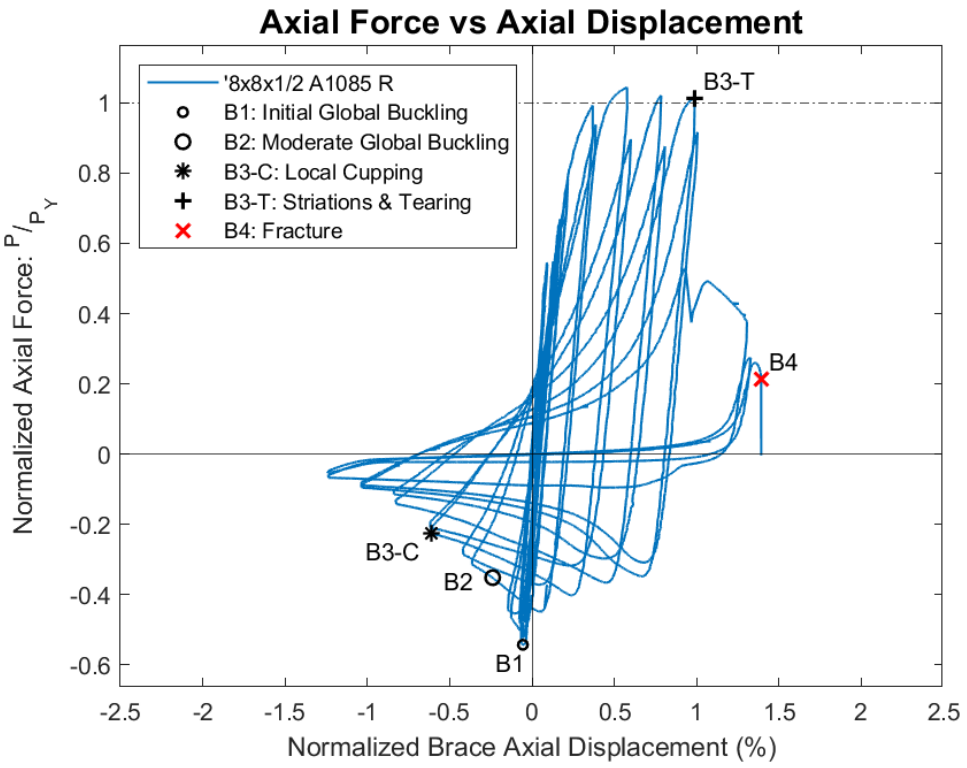

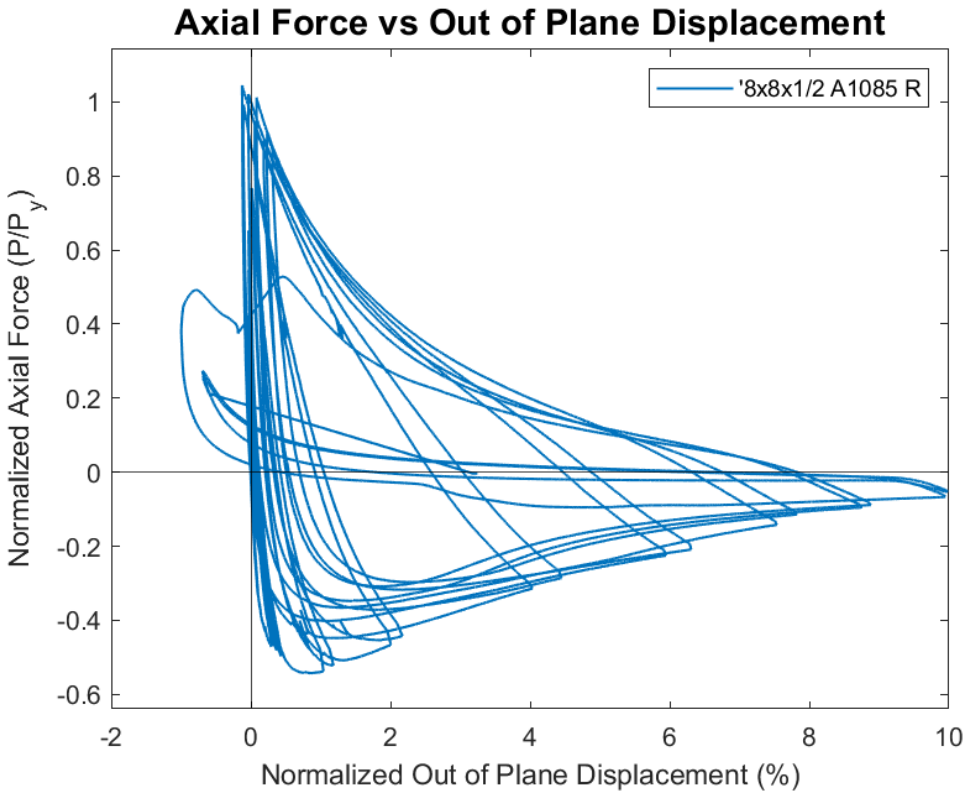
Axial Force vs Out of Plane Displacement
'8x8x1/2 A1085 R
Normalized Axial Force (P/P_y)
Normalized Out of Plane Displacement (%)
1
0.8
0.6
0.4
0.2
0
-0.2
-0.4
-0.6
-2
0
2
4
6
8
10

Photos

Major cupping prior to tearing: 2.75” cycles

Cupping after specimen tore halfway thru: 3.25” cycles

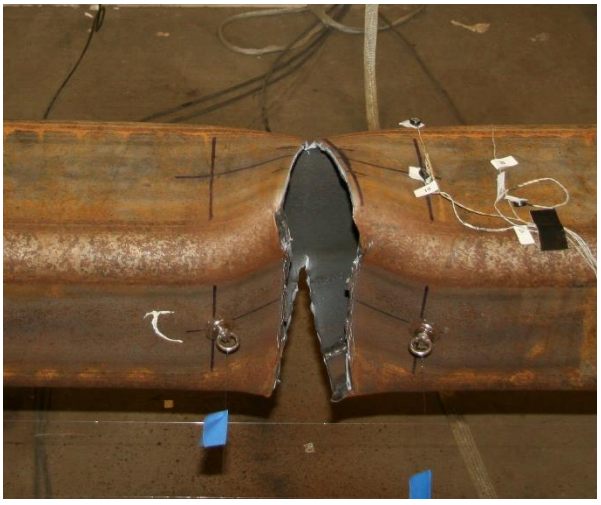

Specimen partially torn at incipient fracture: 3.75” T1

Fracture at the center of the specimen: 3.75” T1

8x8x1/2 A1085 W Brace Test Summary

Test Name: 8x8x1/2 A1085 W
Test Date: 10/20/21

Brace Properties

Measured Yield Stress (ksi)	66.15
Measured Ultimate Stress (ksi)	73.08
Yield Load (kips)	950.65
Critical Buckling Load (kips)	511.41
Percent Elongation - 2" (%)	42.02
CVN Width (mm)	10
CVN Absorbed Energy (ft-lbs)	120+
Brace Length (in)	237.5

Area (in²)	14.4
Moment of Inertia (in⁴)	131
Corner Radius (in)	0.957
Thickness - Nominal (in)	0.500
Thickness - Measured (in)	0.499
Brace Compactness Ratio (*b/t*) - Nominal	13
Brace Compactness Ratio (*b/t*) - Measured	12.20
Global Slenderness ratio (*KL/r*)	78.64

Specimen Performance

Test Event	Axial Brace Deformation (in)	Target Displacement (in) (Cycle)	Force (kips)	$P / P_{Yield \mid Critical}$	
Peak Tension Load	1.40	2.25 (1)	964.72	1.01	Y
B1: Initial Global Buckling	-0.35	0.625 (1)	-446.26	0.87	C
B2: Moderate Global Buckling	-0.95	1.25 (1)	-299.87	0.59	C
B3-C: Local Cupping	-1.75	1.75 (2)	-202.80	0.40	C
B3-T: Striations & Tearing	2.38	3.25 (1)	943.50	0.99	Y
B4: Brace Fracture	2.83	3.75 (1)	221.34	0.23	Y

Key Observations

Cycle #	Displacement (in.)	Observations
7-8	0.5	Bolt slip at north gusset plate: T1, C1, T2, C2
9-10	0.625	Initial global buckling, C1
13-14	1.25	Moderate global buckling, C1
15-16	1.75	Initial minor cupping: ~1/16” deep, C2
17-18	2.25	Cupping: ~1/8” deep, ~8” tall, C1 Cupping: ~1/4” deep, ~8.25” tall, C2
19-20	2.75	Cupping: ~0.75” deep, ~9.25” tall, C1 Cupping: ~1.75” deep, ~10.5” tall, C2 Cupping at 3” north of brace midspan
21-22	3.25	Striations/minor tearing at corners of east wall, T1 Cupping: ~2” deep, ~11” tall, C1 Tore thru east, top, and bottom walls, T2
23-24	3.75	Fracture! T1 at ~3.3” actuator displacement

Test Results

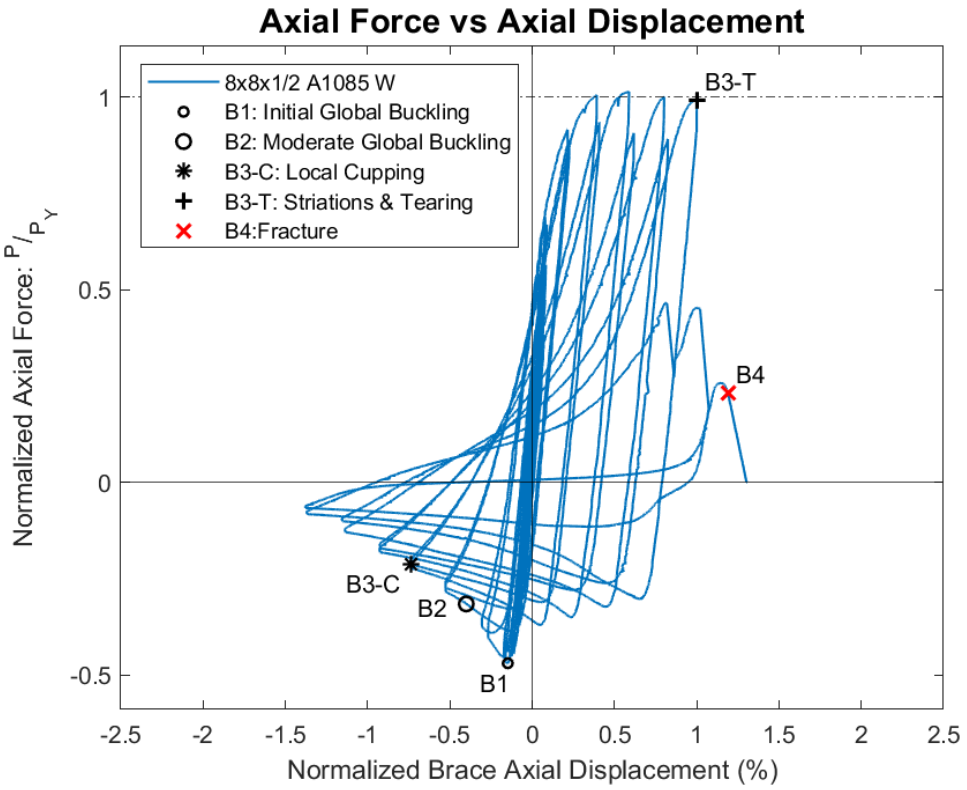

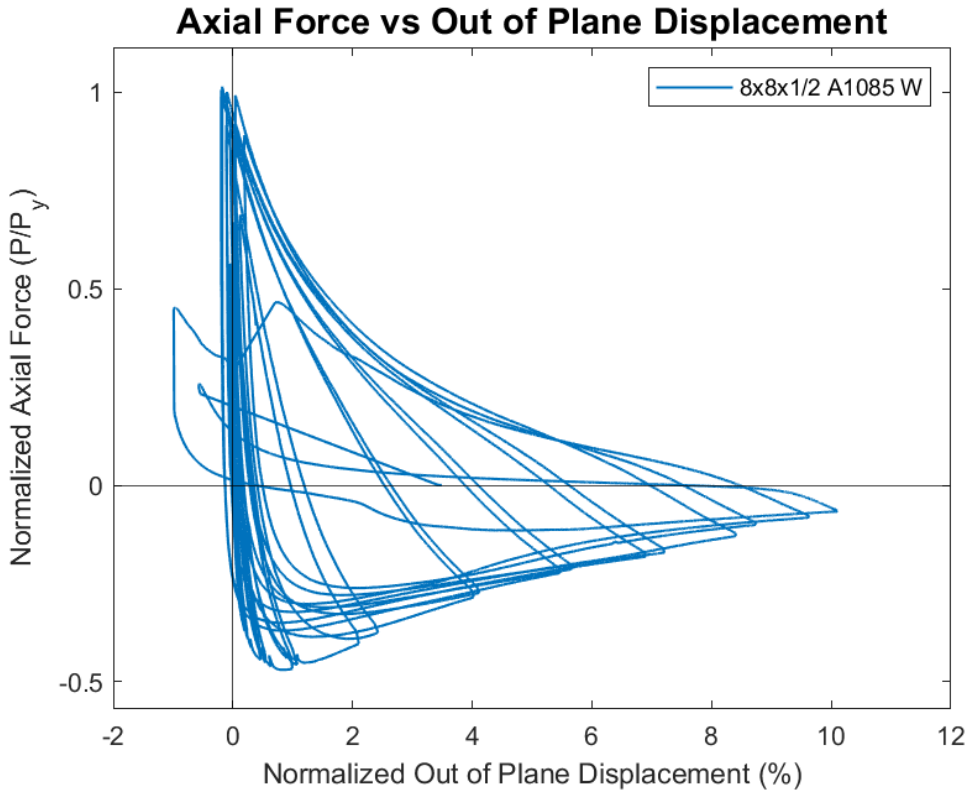

Photos

Max out of plane displacement: 3.25” C2

‘Kaldestad effect’ on outside face of brace while buckling

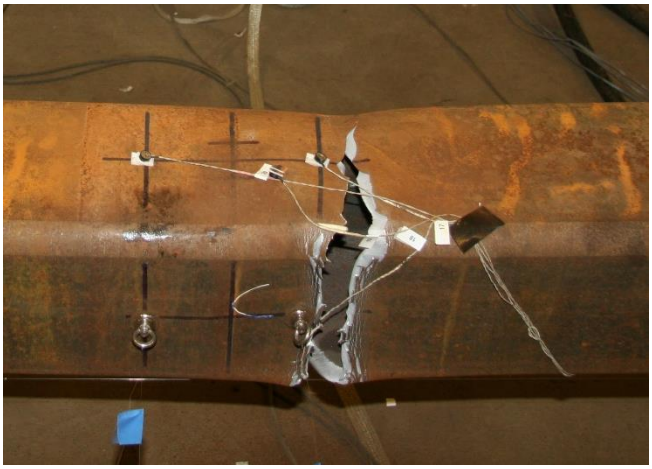

Specimen torn thru 3 walls: 3.25” T2

Specimen fractured at first 3.75” tension cycle

8x8x1/2 A1085 B Brace Test Summary

Test Name: 8x8x1/2 A1085 B
Test Date: 9/15/21

Brace Properties

Measured Yield Stress (ksi)	66.36	**Area (in²)**	14.4
Measured Ultimate Stress (ksi)	70.51	**Moment of Inertia (in⁴)**	131
Yield Load (kips)	957.42	**Corner Radius (in)**	1.074
Critical Buckling Load (kips)	511.41	**Thickness - Nominal (in)**	0.500
Percent Elongation - 2" (%)	39.56	**Thickness - Measured (in)**	0.501
CVN Width (mm)	10	**Brace Compactness Ratio (*b/t*) - Nominal**	13
CVN Absorbed Energy (ft-lbs)	120+	**Brace Compactness Ratio (*b/t*) - Measured**	11.68
Brace Length (in)	237.5	**Global Slenderness ratio (*KL/r*)**	78.64

Specimen Performance

Test Event	Axial Brace Deformation (in)	Target Displacement (in) (Cycle)	Force (kips)	$P / P_{Yield \mid Critical}$	
Peak Tension Load	1.21	1.75 (1)	938.58	0.98	Y
B1: Initial Global Buckling	-0.12	0.75 (1)	-478.57	0.94	C
B2: Moderate Global Buckling	-0.70	1.25 (1)	-318.58	0.62	C
B3-C: Local Cupping	-1.39	1.75 (1)	-221.39	0.43	C
B3-T: Striations & Tearing	2.40	3.25 (1)	694.01	0.72	Y
B4: Brace Fracture	2.20	3.25 (1)	11.80	0.01	Y

Key Observations

Cycle #	Displacement (in.)	Observations
5-6	0.375	Bolt slip at north gusset plate during first compression cycle (bolt slip occurred in tension and compression throughout test)
11-12	0.75	Initial global buckling, first compression cycle
13-14	1.25	Bolt slip at south gusset plate Moderate global buckling, first compression cycle
15-16	1.75	The smaller actuator reached its capacity causing it to lag the larger actuator by ~0.2". This occurred at ~1.60" during the first tension cycle. The test was held while the hydraulic pump pressure was increased. Testing continued smoothly Initial minor cupping: ~1/16" deep, first peak compression

		Cupping: ~1/8” deep, second peak compression
17-18	2.25	Cupping: ~3/8” deep, ~8.5” tall, first peak compression Cupping: ~1” deep, second peak compression Cupping observed at 1” north of brace midspan
19-20	2.75	Cupping: ~1.75” deep, ~8.5” tall, first peak compression Cupping: ~2” deep, second peak compression
21-22	3.25	Tore thru halfway thru brace during first tension cycle Tearing continued thru west wall while buckling in second compression cycle Fractured during second tension cycle!

Test Results

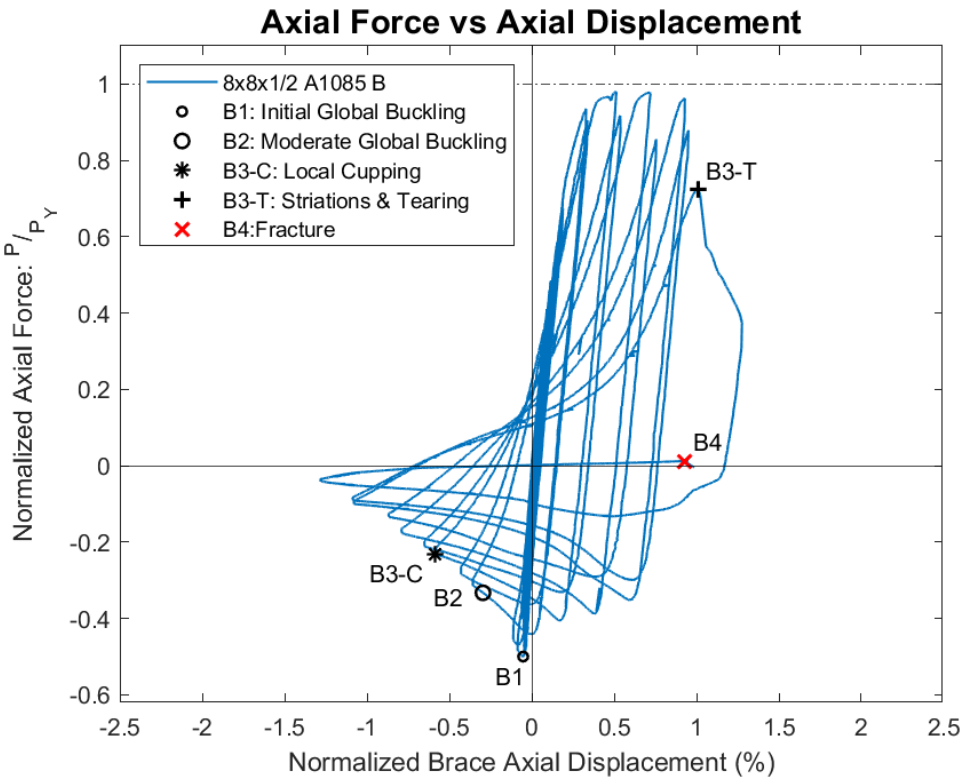

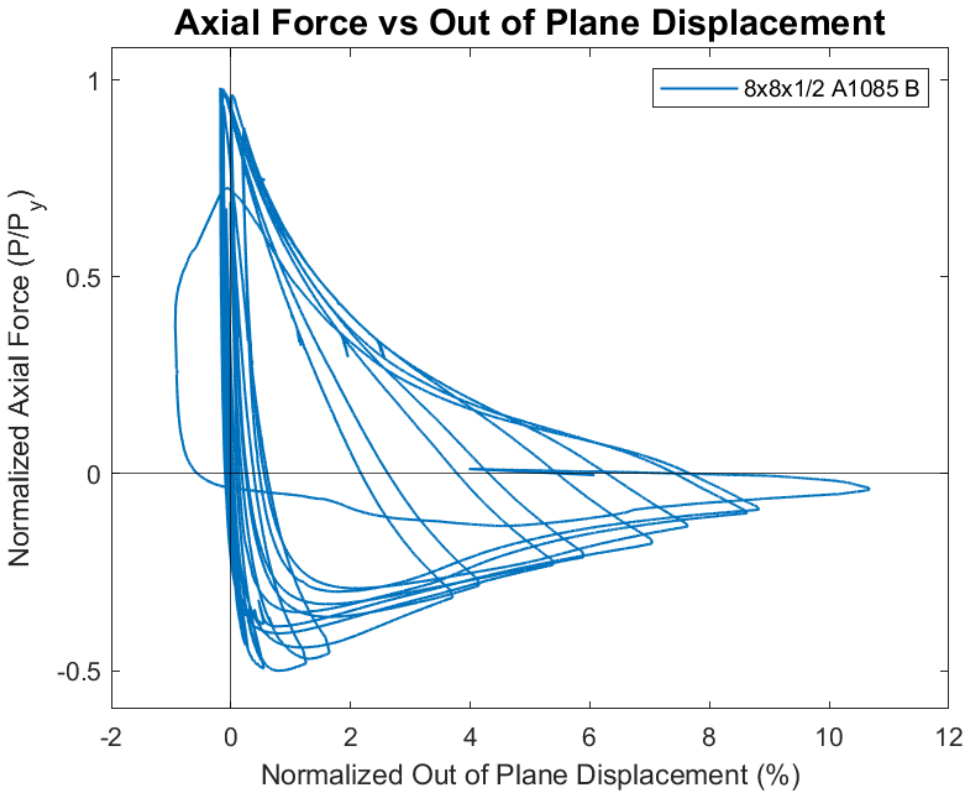
Axial Force vs Out of Plane Displacement
8x8x1/2 A1085 B
Normalized Axial Force (P/P_y)
Normalized Out of Plane Displacement (%)
1
0.5
0
-0.5
-2
0
2
4
6
8
10
12

Photos

Maximum out of plane displacement: 3.25” C1

Cupping at center of specimen: 2.75” C2

Specimen tearing halfway thru cross-section: 3.25” T1

Tearing thru west wall while buckling: 3.25” C1

5x5x3/8 A1085 Y Chevron Brace Test Summary

Test Name: 5x5x3/8 A1085 Y - Chevron
Test Date: 10/26/21

Brace Properties

Measured Yield Stress (ksi)	66.04	**Area (in²)**	6.58
Measured Ultimate Stress (ksi)	74.62	**Moment of Inertia (in⁴)**	21.7
Yield Load (kips)	435.7	**Corner Radius (in)**	0.729
Critical Buckling Load (kips)	101.3	**Thickness - Nominal (in)**	0.375
Percent Elongation - 2" (%)	32.83	**Thickness - Measured (in)**	0.376
CVN Width (mm)	7.5	**Brace Compactness Ratio (*b/t*) - Nominal**	10.3
CVN Absorbed Energy (ft-lbs)	18.8	**Brace Compactness Ratio (*b/t*) - Measured**	9.42
Brace Length (in)	237.5	**Global Slenderness ratio (*KL/r*)**	127.7

Specimen Performance

Test Event	Axial Brace Deformation (in)	Target Displacement (in) (Cycle)	Force (kips)	$P / P_{Yield \mid Critical}$	
Peak Tension Load	3.53	4.00 T (1)	409.06	0.94	Y
B1: Initial Global Buckling	-0.19	0.375 C (1)	-93.31	0.92	C
B2: Moderate Global Buckling	-0.35	0.625 C (1)	-87.30	0.86	C
B3-C: Local Cupping	-7.74	8.25 C (11)	-20.60	0.20	C
B3-T: Striations & Tearing	3.23	4.5 T (1)	168.22	0.39	Y
B4: Brace Fracture	3.64	4.5 T (1)	125.02	0.29	Y

Key Observations

Cycle #	Displacement (in.)	Observations
5-6	0.375 C	Initial global buckling, C1
9-10	0.625 C	Moderate global buckling, C1
29-30	7.50 C	Slightly starting to cup: <1/16” deep, C2
31-40	8.25 C	Actuator could not move farther than 8.25” in compression 10 cycles ran at this displacement Cupping: ~1/16” deep, every cycle Center of brace got slightly warmer No development of striations, tearing or cupping
41	0.5 T, 8.25 C	Cupping: ~1/8” deep
42	1.0 T, 8.25 C	Cupping: ~1/8” deep

43	1.5 T, 8.25 C	Bolt slip, north gusset plate Cupping: ~1/8” deep, peak compression
44	2.0 T, 8.25 C	Cupping: ~3/16” deep, peak compression
45	2.5 T, 8.25 C	Cupping: ~3/16” deep, peak compression
46	3.0 T, 8.25 C	Cupping: ~3/8” deep, peak compression
47	3.5 T, 8.25 C	Cupping: ~0.75” deep, peak compression
48	4.0 T, 8.25 C	Visual necking at center of brace in tension, no striations Cupping: ~1.25” deep, peak compression SP_Long_C1 popped off near peak compression
49	4.5 T, 8.25 C	Fracture! In tension at ~3.8” actuator displacement

Test Results

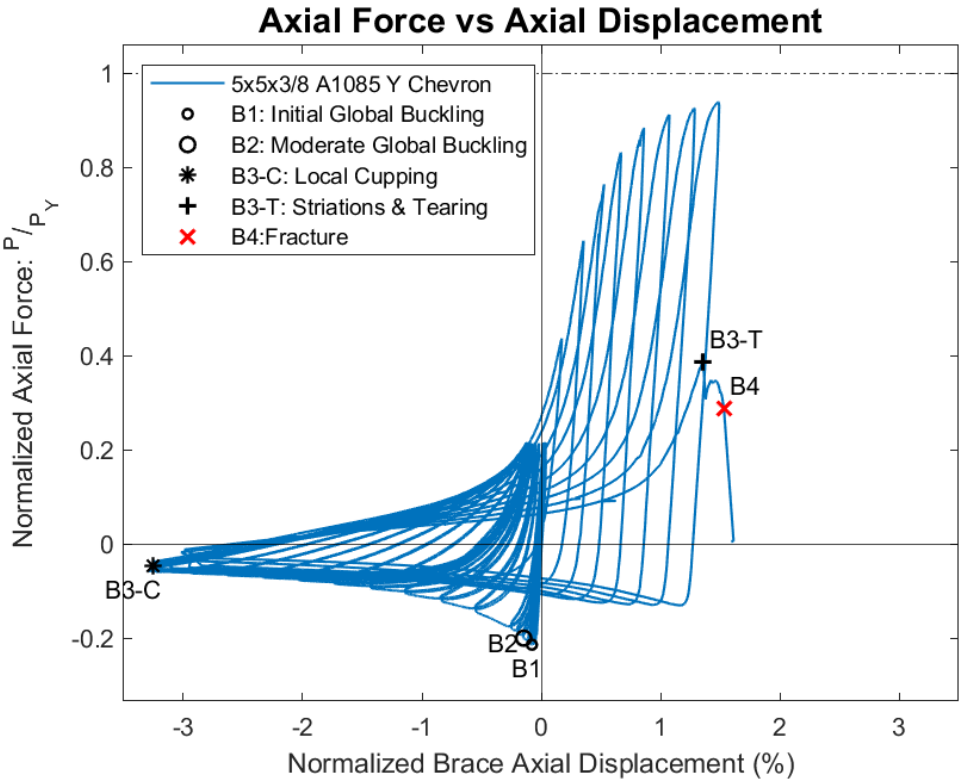

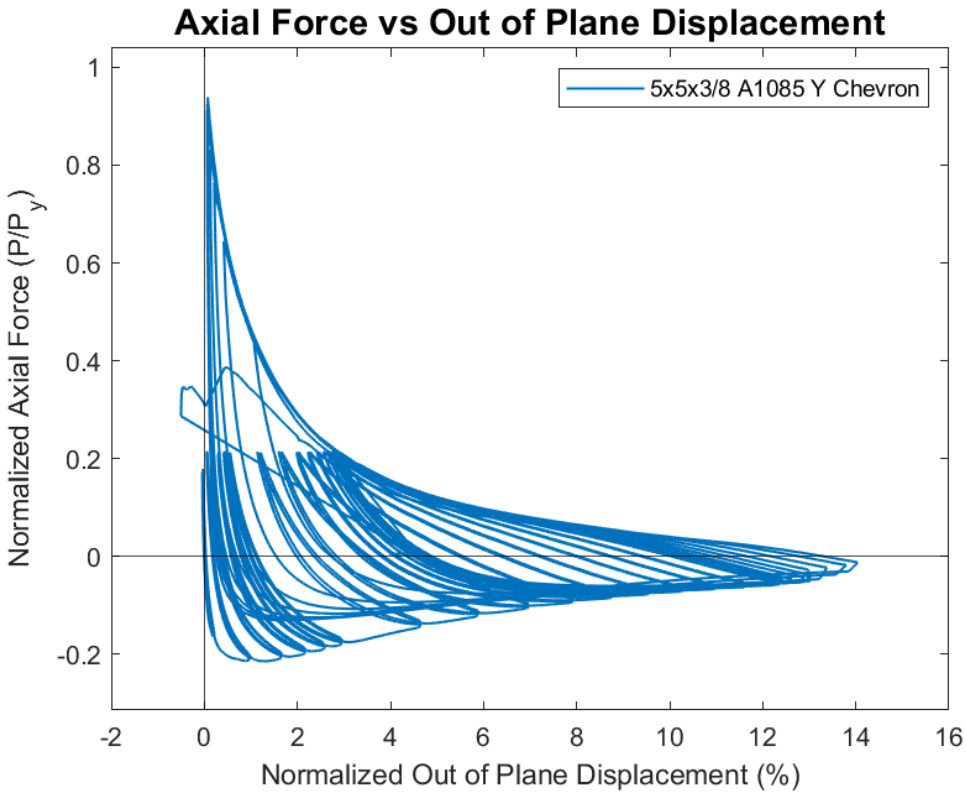
Axial Force vs Out of Plane Displacement
5x5x3/8 A1085 Y Chevron
Normalized Axial Force (P/P_y)
Normalized Out of Plane Displacement (%)
1
0.8
0.6
0.4
0.2
0
-0.2
-2
0
2
4
6
8
10
12
14
16

Photos

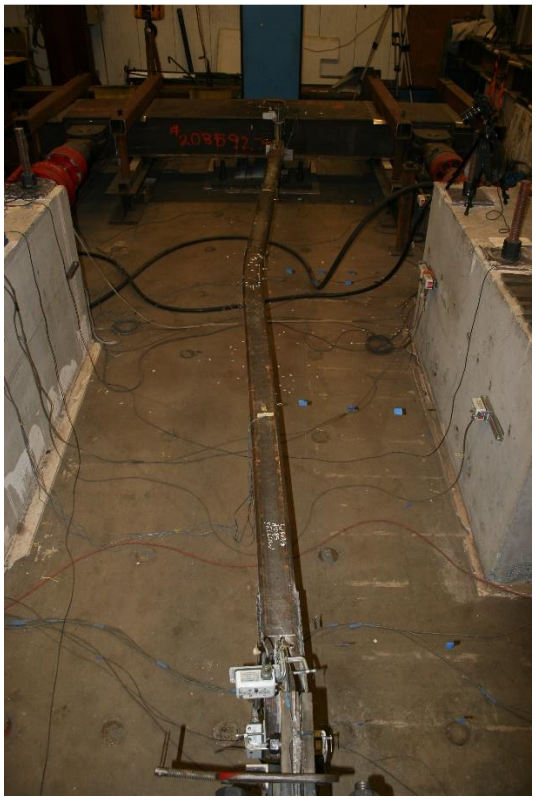

Specimen at a tension load equal to $P_{critical}$: Cycle 40

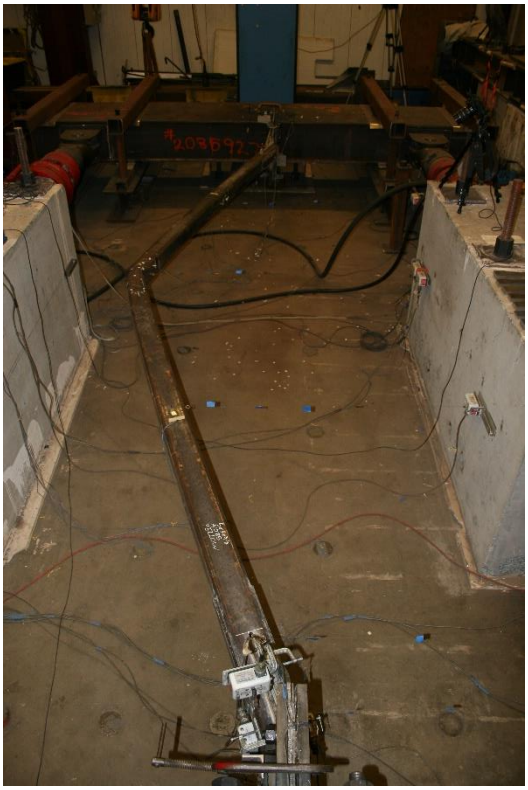

Maximum out of plane displacement: Cycle 48

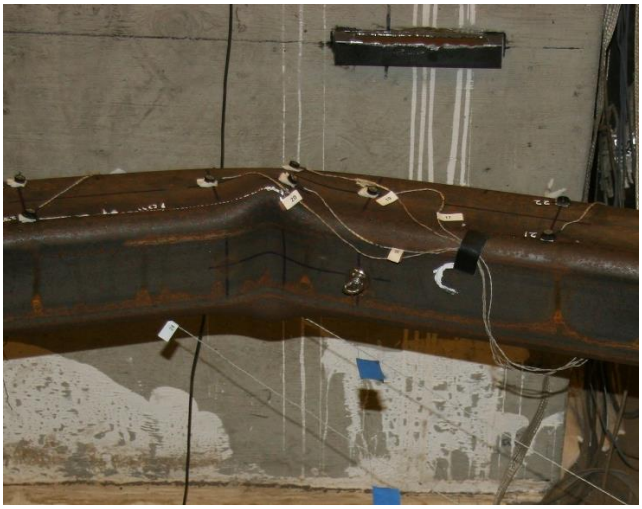

Cupping at peak out of plane displacement: Cycle 48

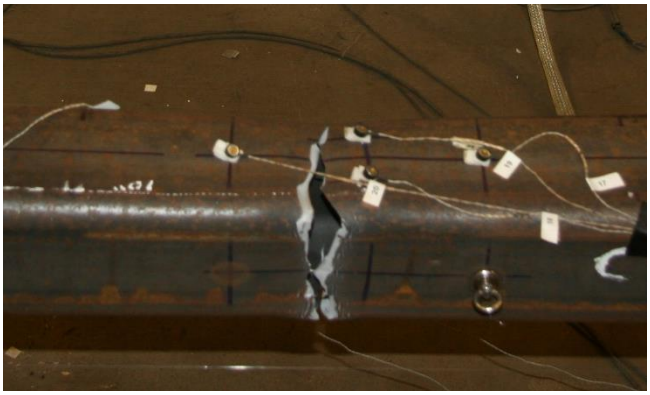

Tearing across the center of the brace: cycle 49

5x5x3/8 A1085 Y – Near Fault Brace Test Summary

Test Name: 5x5x3/8 A1085 Y – Near Fault
Test Date: 10/28/21

Brace Properties

Measured Yield Stress (ksi)	66.04	**Area (in²)**	6.58
Measured Ultimate Stress (ksi)	74.62	**Moment of Inertia (in⁴)**	21.8
Yield Load (kips)	435.7	**Corner Radius (in)**	0.729
Critical Buckling Load (kips)	101.3	**Thickness - Nominal (in)**	0.375
Percent Elongation - 2" (%)	32.83	**Thickness - Measured (in)**	0.376
CVN Width (mm)	7.5	**Brace Compactness Ratio (*b/t*) - Nominal**	10.3
CVN Absorbed Energy (ft-lbs)	18.8	**Brace Compactness Ratio (*b/t*) - Measured**	9.42
Brace Length (in)	237.5	**Global Slenderness ratio (*KL/r*)**	127.7

Specimen Performance

Test Event	Axial Brace Deformation (in)	Target Displacement (in) (Cycle)	Force (kips)	P / $P_{Yield\ |\ Critical}$	
Peak Tension Load	3.16	3.56 (1)	464.24	1.07	Y
B1: Initial Global Buckling	-0.18	-1.19 (1)	-95.36	0.94	C
B2: Moderate Global Buckling	-0.36	-1.19 (1)	-88.92	0.88	C
B3-C: Local Cupping	-2.62	-2.38 (27)	-25.32	0.25	C
B3-T: Striations & Tearing	6.64	8.31 (34)	37.97	0.09	Y
B4: Brace Fracture	7.88	8.31 (34)	84.58	0.19	Y

Key Observations

Cycle #	Displacement	Observations
0.5	-1.19”	Initial global buckling, Moderate global buckling OOP Displacement ≈ 9.75”
1	3.56”	Bolt slip Brace yielding and strain hardening in tension
26.5	-2.38”	Initial cupping: ~1/16” deep
29.5	-3.56”	Cupping: ~1/8” deep Center of brace is hot to touch
30.5	-3.56”	Cupping: ~1/4” deep
31	7.72”	Necking observed at center of brace in tension
31.5	-4.16”	Cupping: ~3/4” deep

32	7.72”	Necking observed at center of brace in tension No visible striations or tearing
32.5	-4.16”	Cupping: ~1.25” deep Cupping concentrated at 2.5” south of center of brace
33	8.31”	Striations and necking observed at center of brace in tension
33.5	-4.75”	Cupping: ~1.25” deep Center of brace is SUPER hot to touch
34	8.31”	Fracture at actuator displacement of about 8” in tension

Test Results

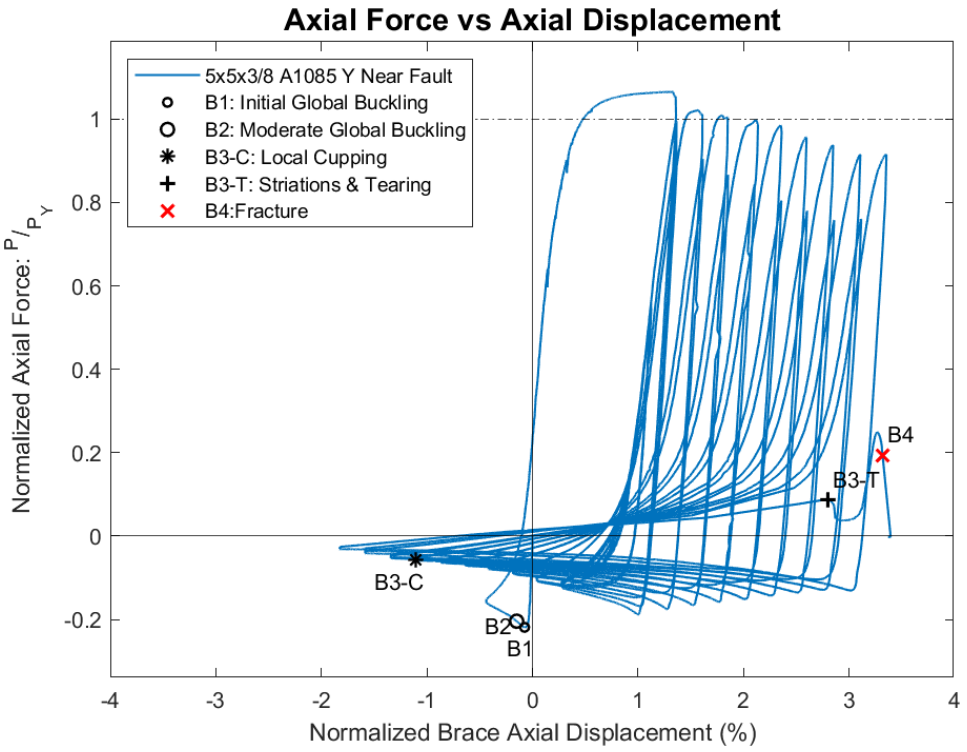

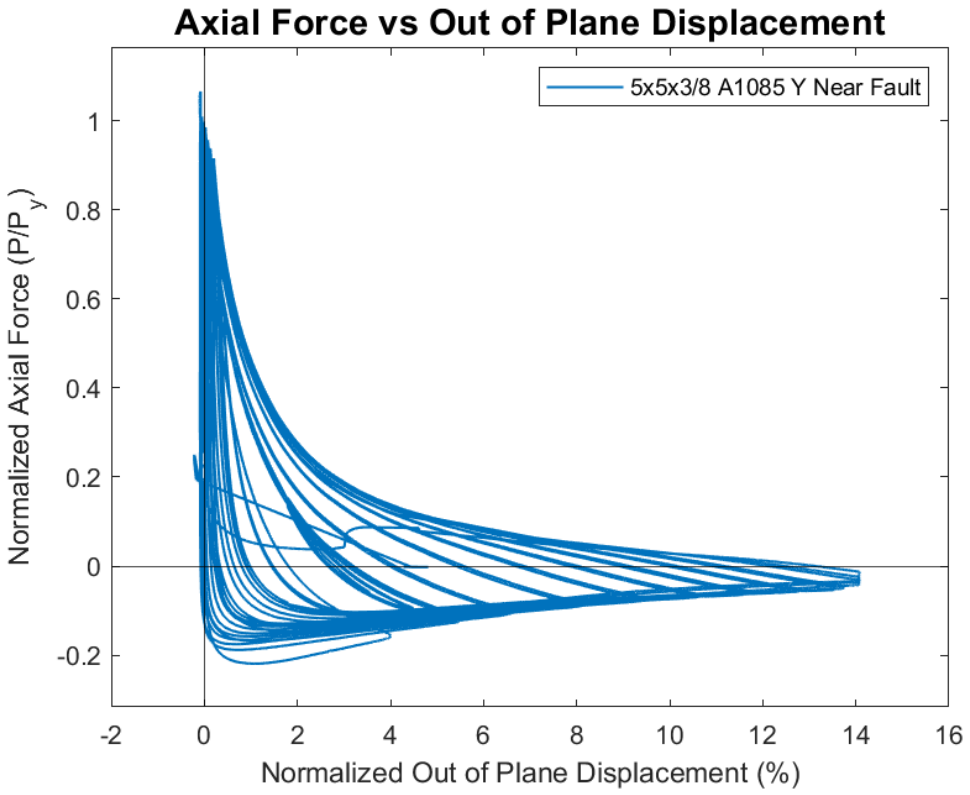
Axial Force vs Out of Plane Displacement
5x5x3/8 A1085 Y Near Fault
Normalized Axial Force (P/P_y)
Normalized Out of Plane Displacement (%)
1
0.8
0.6
0.4
0.2
0
-0.2
-2
0
2
4
6
8
10
12
14
16

Photos

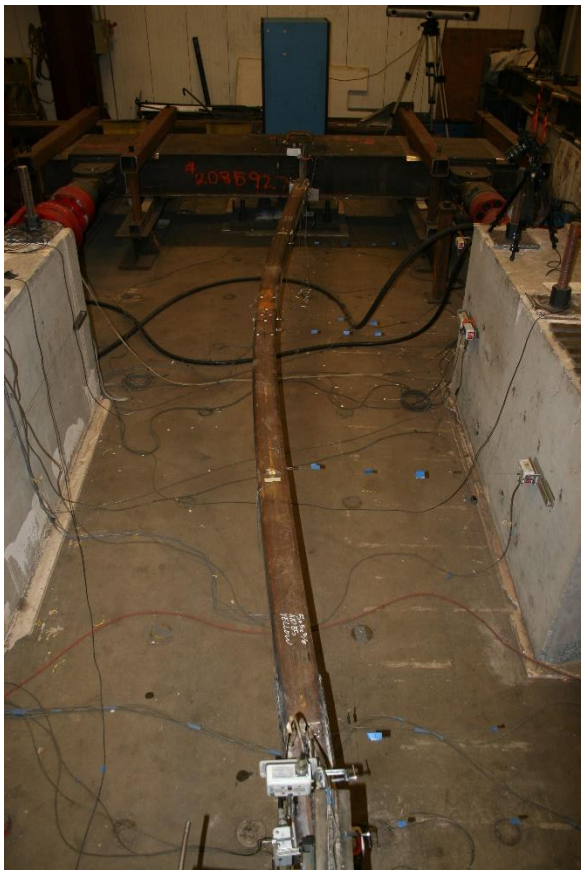

Moderate global buckling at first peak compression cycle

Max out of plane displacement: Cycle 33.5

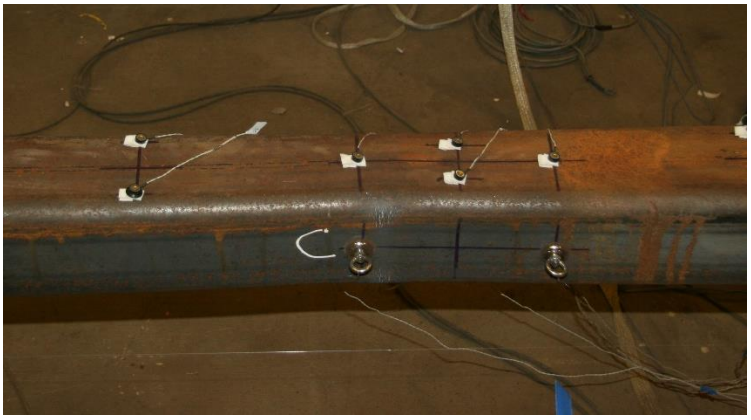

Specimen showing necking and striations: Cycle 33 tension

Brace fractured in tension at cycle 34

7x7x3/8 A1085 Y - Chevron Brace Test Summary

Test Name: 7x7x3/8 A1085 Y - Chevron
Test Date: 11/9/21

Brace Properties

Measured Yield Stress (ksi)	61.89	**Area (in²)**	9.58
Measured Ultimate Stress (ksi)	70.7	**Moment of Inertia (in⁴)**	68.7
Yield Load (kips)	577.1	**Corner Radius (in)**	0.906
Critical Buckling Load (kips)	292.2	**Thickness - Nominal (in)**	0.375
Percent Elongation - 2" (%)	31.32	**Thickness - Measured (in)**	0.365
CVN Width (mm)	7.5	**Brace Compactness Ratio (*b/t*) - Nominal**	15.7
CVN Absorbed Energy (ft-lbs)	17.3	**Brace Compactness Ratio (*b/t*) - Measured**	14.21
Brace Length (in)	237.5	**Global Slenderness ratio (*KL/r*)**	127

Specimen Performance

Test Event	Axial Brace Deformation (in)	Target Displacement (in) (Cycle)	Force (kips)	$P / P_{Yield \mid Critical}$	
Peak Tension Load	0.01	-	258.3	0.45	Y
B1: Initial Global Buckling	-0.23	0.5 (1)	-257.4	0.88	C
B2: Moderate Global Buckling	-0.74	1.50 (1)	-186.1	0.64	C
B3-C: Local Cupping	-2.01	2.25 (2)	-106.3	0.36	C
B3-T: Striations & Tearing	0.09	4.50 (2)	256.6	0.44	Y
B4: Brace Fracture	1.16	5.25 (1)	127.1	0.22	Y

Key Observations

Cycle #	Displacement	Observations
7-8	0.5”	Initial global buckling
13-14	1.50”	Moderate global buckling
17-18	3.00”	Cupping: ~1/8” deep, C1 & C2
19-20	3.75”	Cupping: ~0.5” deep, C1 Cupping: ~1” deep, C2
21-22	4.50”	Cupping: ~1.5” deep, C1 Striations/very minor tearing at east corners, T2 Cupping: ~1.5” deep, C2
23	5.25”	Fracture! T1 at actuator displacement of 1.13” T

Test Results

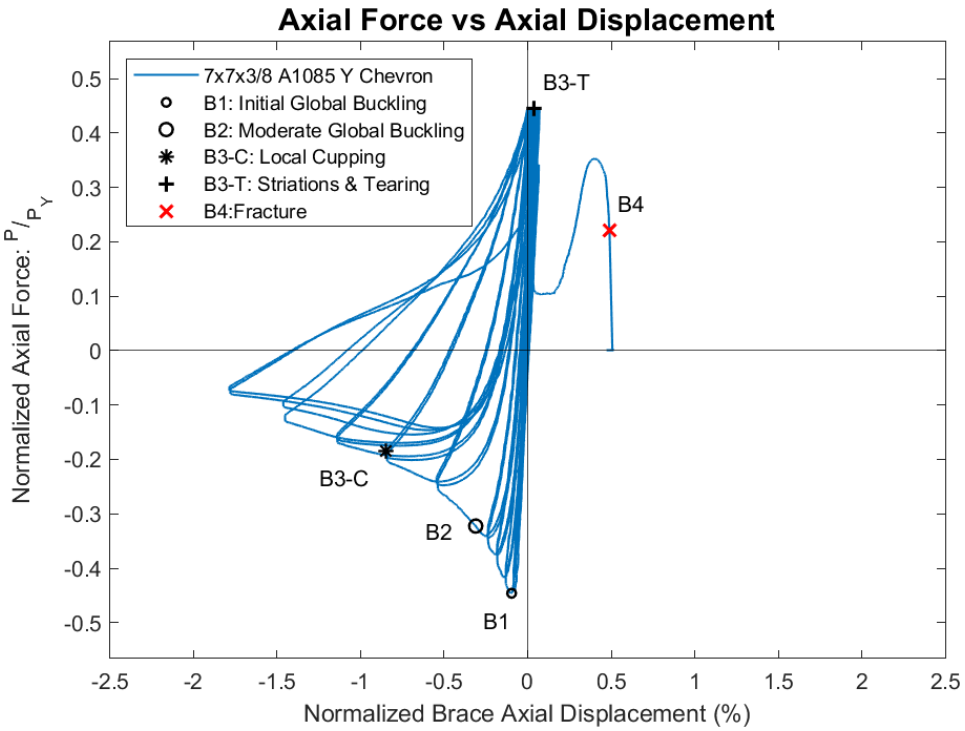

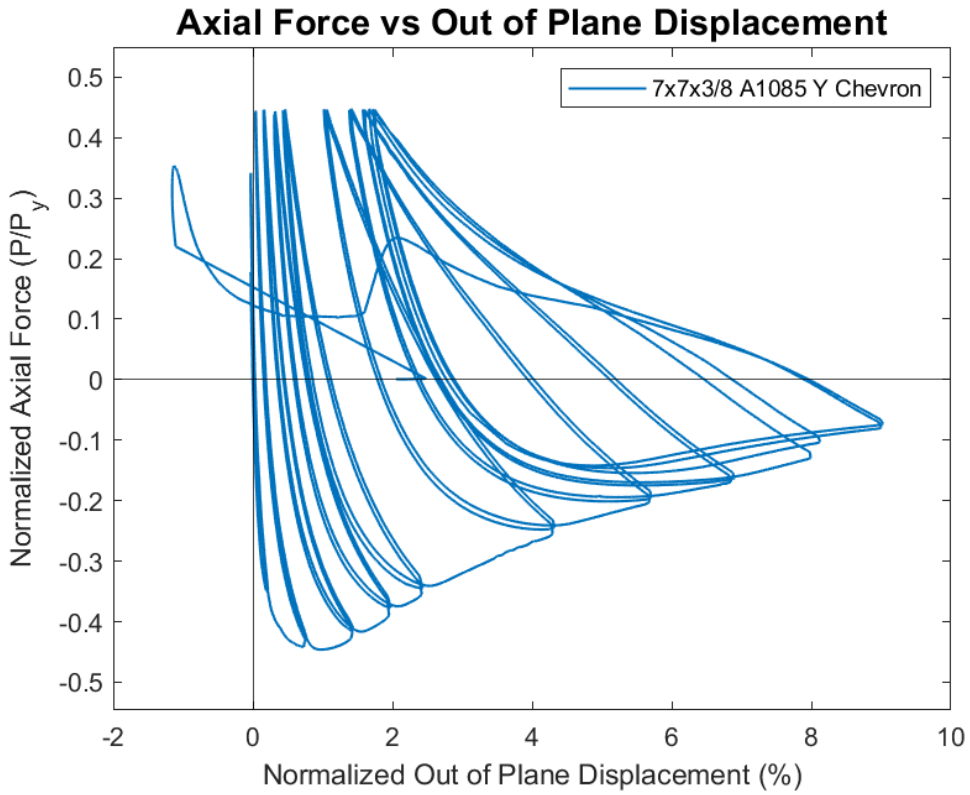

Photos

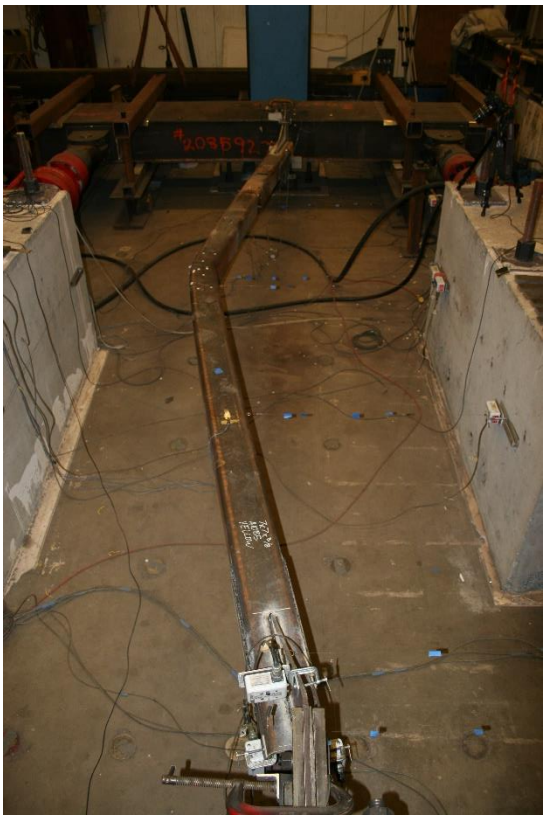

Maximum out of plane displacement: cycle 22

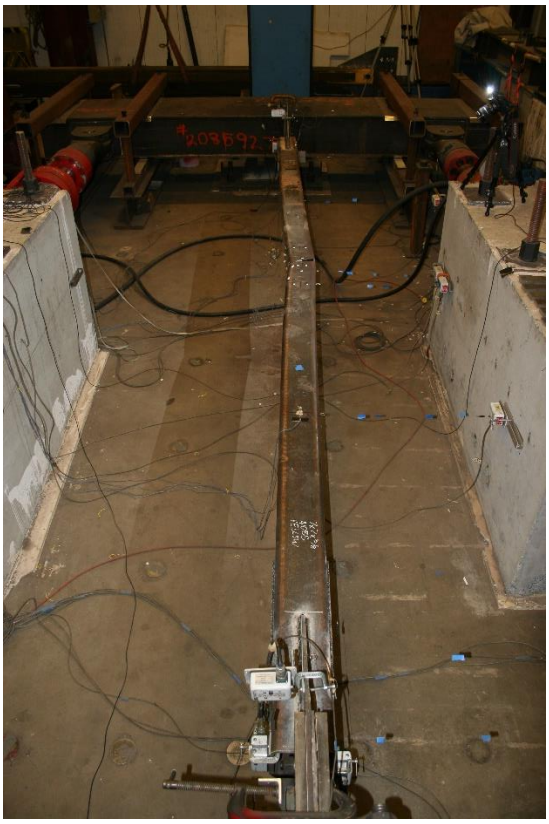

Specimen moving out of plane in opposite direction of buckling while tearing at midspan: cycle 23

Moderate cupping in plastic hinge region: cycle 23

Tearing at the center of the specimen: cycle 23

7x7x3/8 A1085 Y – Near Fault Test Summary

Test Name: 7x7x3/8 A1085 Y – Near Fault
Test Date: 11/3/21

Brace Properties

Measured Yield Stress (ksi)	61.89	**Area (in²)**	9.58
Measured Ultimate Stress (ksi)	70.07	**Moment of Inertia (in⁴)**	68.7
Yield Load (kips)	577.1	**Corner Radius (in)**	0.906
Critical Buckling Load (kips)	292.2	**Thickness - Nominal (in)**	0.375
Percent Elongation - 2" (%)	31.32	**Thickness - Measured (in)**	0.365
CVN Width (mm)	7.5	**Brace Compactness Ratio (*b/t*) - Nominal**	15.7
CVN Absorbed Energy (ft-lbs)	17.3	**Brace Compactness Ratio (*b/t*) - Measured**	14.21
Brace Length (in)	237.5	**Global Slenderness ratio (*KL/r*)**	88.6

Specimen Performance

Test Event	Axial Brace Deformation (in)	Target Displacement (in) (Cycle)	Force (kips)	$P / P_{Yield \mid Critical}$	
Peak Tension Load	2.74	3.56 (1)	670.9	1.16	Y
B1: Initial Global Buckling	-0.23	-1.19 (1)	-255.2	0.87	C
B2: Moderate Global Buckling	-0.72	-1.19 (1)	-188.7	0.65	C
B3-C: Local Cupping	-0.27	0 (18.5)	-98.7	0.34	C
B3-T: Striations & Tearing	3.32	4.75 (22)	194.3	0.34	Y
B4: Brace Fracture	4.08	4.75 (22)	185.8	0.32	Y

Key Observations

Cycle #	Displacement	Observations
0.5	-1.19”	Initial global buckling, moderate global buckling
1	3.56”	Yielding and strain hardening in large tension cycle
1.5	0.59”	The direction of out of plane buckling flipped to going east, instrumentation was adjusted accordingly
17	3.56”	Brace did not fully straighten back out until this cycle
18.5	0”	Initial minor cupping on west wall, , ~1/16” deep
19.5	-0.59”	Cupping: ~1/4” deep
20.5	-0.59”	Cupping: ~1” deep Cupping concentrated at center of brace
21.5	-1.19”	Severe cupping: ~1.75” deep, ~9.75” tall
22	4.75”	Fracture at actuator displacement = 4.63” T

Test Results

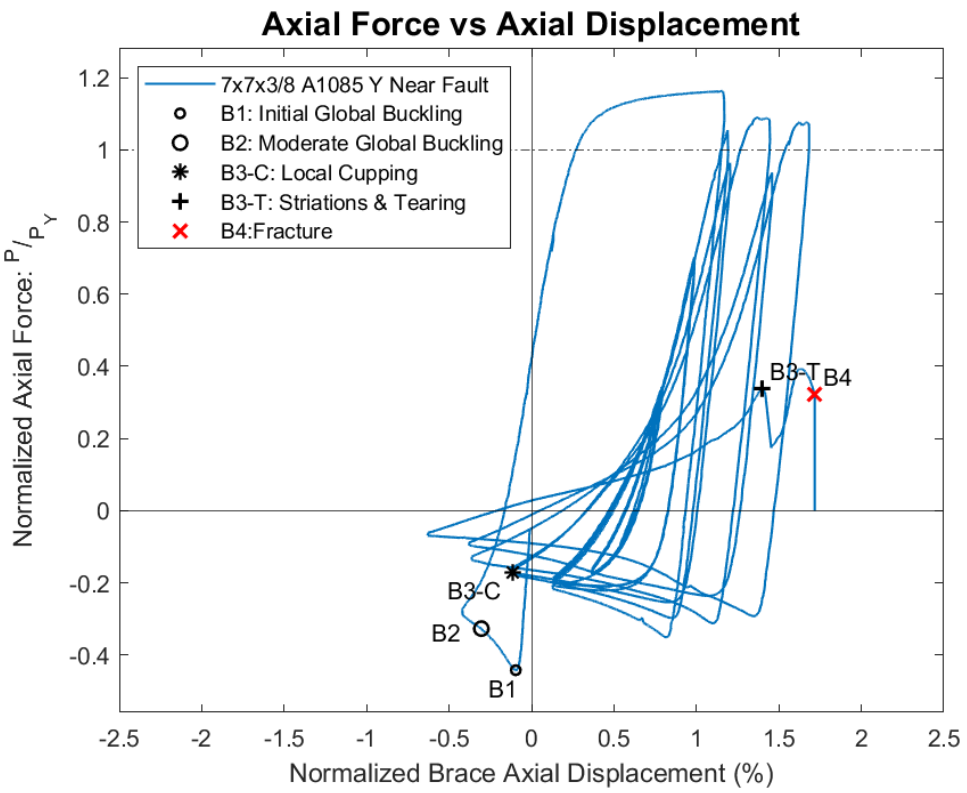

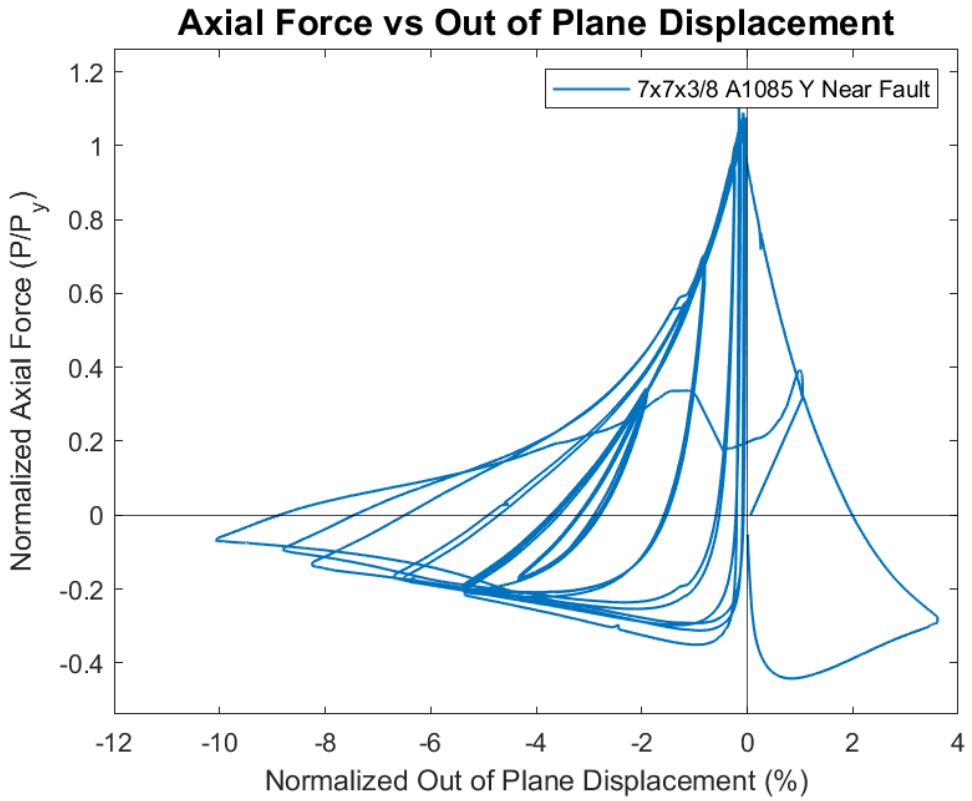

Photos

First peak compression, specimen buckling west east: cycle 21.5

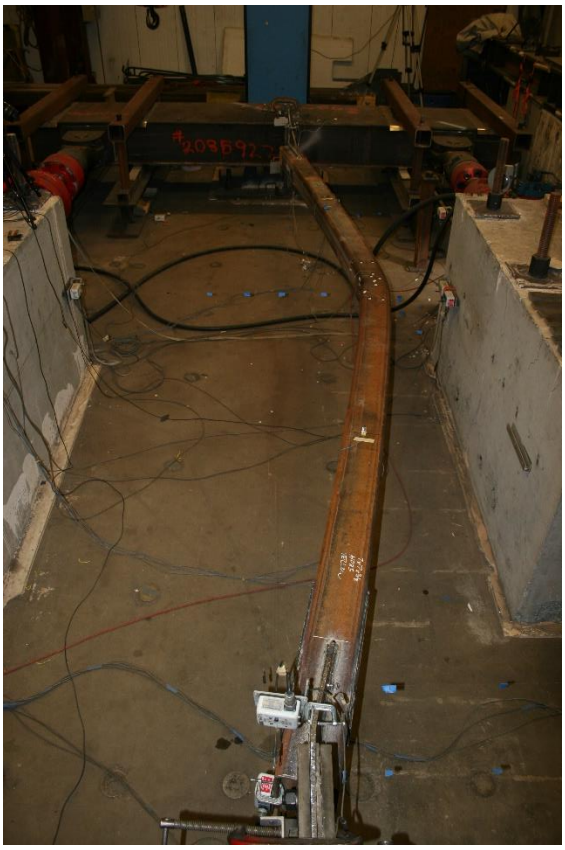

Max out of plane displacement, specimen buckling

Severe cupping at the center of the specimen: cycle 21.5

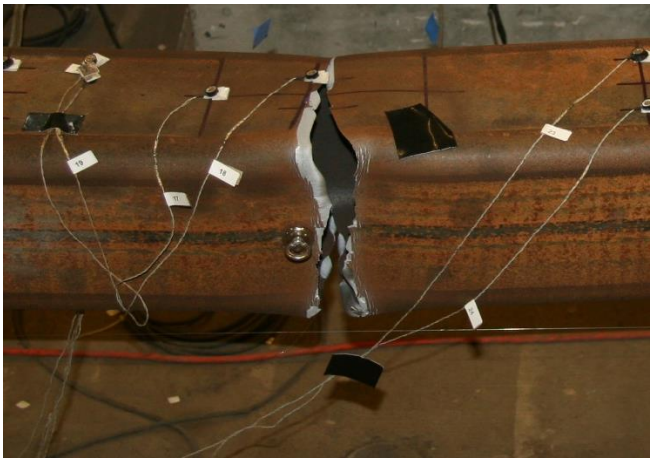

Specimen at incipient fracture: cycle 22

8x8x3/8 A1085 Y - Chevron Brace Test Summary

Test Name: 8x8x3/8 A1085 Y - Chevron
Test Date: 11/15/21

Brace Properties

Measured Yield Stress (ksi)	60.37	**Area (in²)**	11.1
Measured Ultimate Stress (ksi)	72.12	**Moment of Inertia (in⁴)**	106
Yield Load (kips)	661.2	**Corner Radius (in)**	1.06
Critical Buckling Load (kips)	404.3	**Thickness - Nominal (in)**	0.375
Percent Elongation - 2" (%)	34.2	**Thickness - Measured (in)**	0.370
CVN Width (mm)	7.5	**Brace Compactness Ratio (*b/t*) - Nominal**	18.3
CVN Absorbed Energy (ft-lbs)	8.5	**Brace Compactness Ratio (*b/t*) - Measured**	15.89
Brace Length (in)	237.5	**Global Slenderness ratio (*KL/r*)**	76.86

Specimen Performance

Test Event	Axial Brace Deformation (in)	Target Displacement (in) (Cycle)	Force (kips)	P / $P_{Yield\ |\ Critical}$	
Peak Tension Load	0.08	-	332.9	0.50	Y
B1: Initial Global Buckling	-0.27	0.5 (1)	-320.7	0.79	C
B2: Moderate Global Buckling	-1.06	1.50 (1)	-213.6	0.53	C
B3-C: Local Cupping	-2.03	2.25 (1)	-139.2	0.34	C
B3-T: Striations & Tearing	0.14	3.75 (2)	320.6	0.48	Y
B4: Brace Fracture	1.10	4.50 (1)	86.5	0.13	Y

Key Observations

Cycle #	Displacement (in.)	Observations
7-8	0.5	Initial global buckling, C1
13-14	1.50	Moderate global buckling, C2
15-16	2.25	Initial minor cupping: ~1/8” deep, C1 & C2
17-18	3.00	Cupping: ~0.5” deep, ~8.75” tall, C1 Cupping: ~1.25” deep, 10” tall, C2 Cupping at 5” north of center of brace
19-20	3.75	Cupping: ~1.75” deep, ~10.75” tall, C1 Tearing at the corners of the East wall, T2 Cupping: ~1.75” deep, ~11” tall, C2 Wrinkling observed in cupping region, C2
21	4.50	Fracture! T1 at actuator displacement of 1.09” T

Test Results

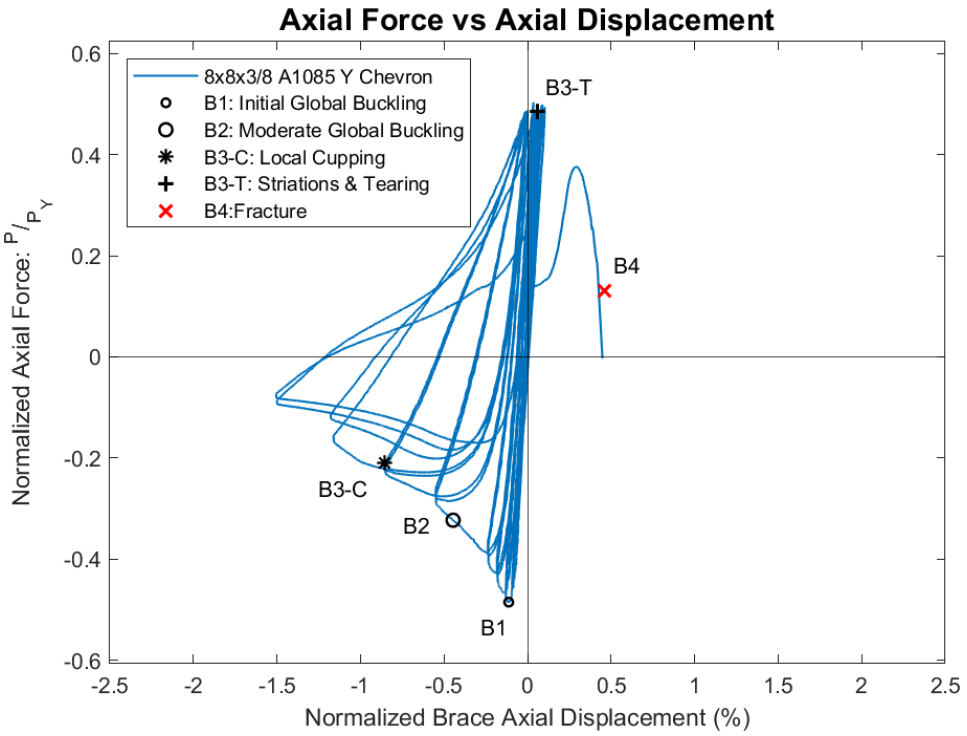

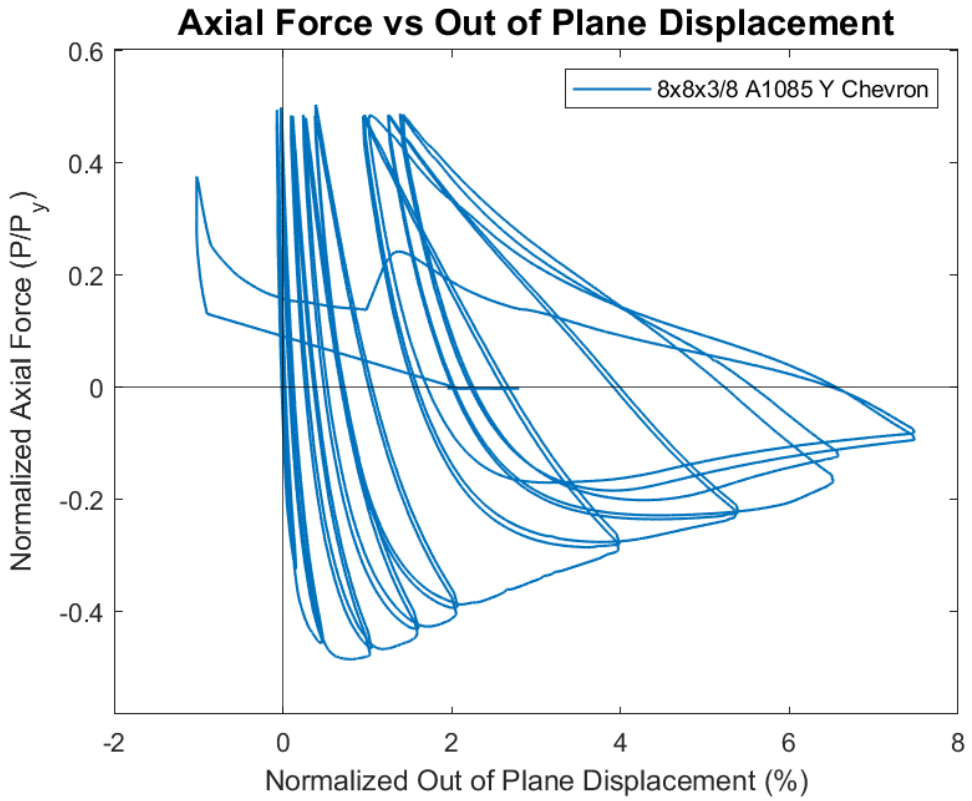

Photos

Maximum out of plane displacement: Cycle 20

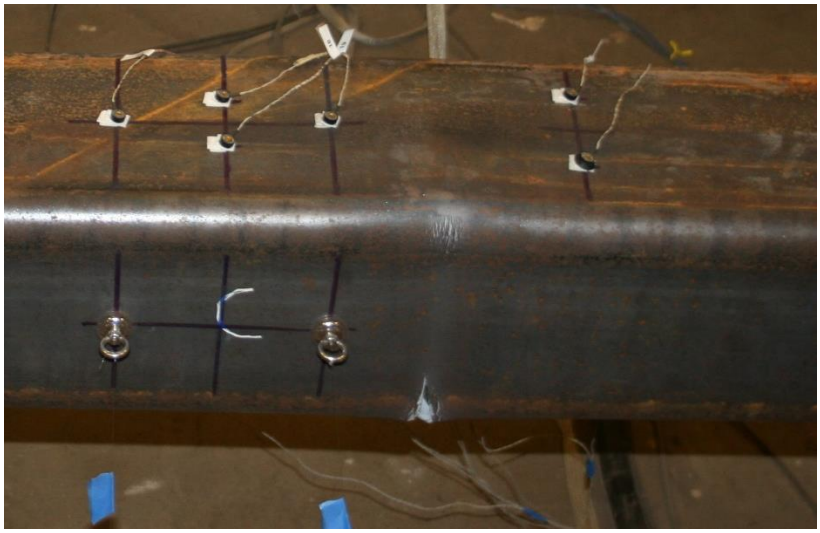

Striations and tearing at the corners of the east wall: Cycle 20

Development of tearing across the brace section: cycle 21

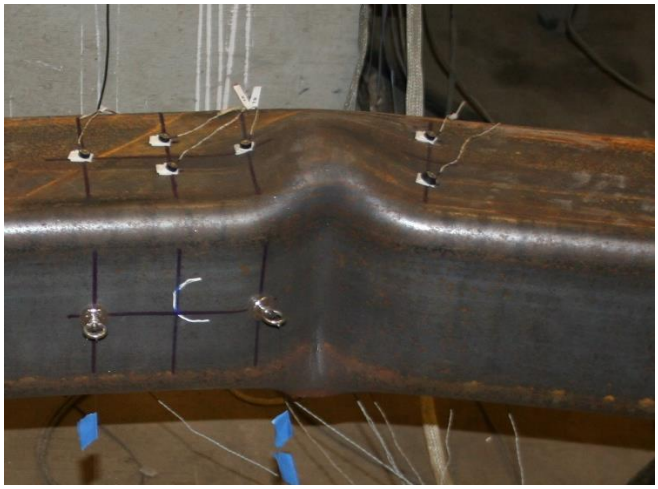

Major cupping at brace midspan: cycle 20

8x8x3/8 A1085 Y – Near Fault Brace Test Summary

Test Name: 8x8x3/8 A1085 Y – Near Fault
Test Date: 11/17/2021

Brace Properties

Measured Yield Stress (ksi)	60.37	**Area (in²)**	11.1
Measured Ultimate Stress (ksi)	72.12	**Moment of Inertia (in⁴)**	106
Yield Load (kips)	661.2	**Corner Radius (in)**	1.06
Critical Buckling Load (kips)	404.3	**Thickness - Nominal (in)**	0.375
Percent Elongation - 2" (%)	34.2	**Thickness - Measured (in)**	0.370
CVN Width (mm)	7.5	**Brace Compactness Ratio (*b/t*) - Nominal**	18.3
CVN Absorbed Energy (ft-lbs)	8.5	**Brace Compactness Ratio (*b/t*) - Measured**	15.89
Brace Length (in)	237.5	**Global Slenderness ratio (*KL/r*)**	76.86

Specimen Performance

Test Event	Axial Brace Deformation (in)	Target Displacement (in) (Cycle)	Force (kips)	$P / P_{Yield \mid Critical}$	
Peak Tension Load	3.10	3.56 (1)	716.3	1.08	Y
B1: Initial Global Buckling	-0.31	1.19 (1)	-308.4	0.76	C
B2: Moderate Global Buckling	1.38	0.59 (1.5)	-194.3	0.48	C
B3-C: Local Cupping	0.13	0 (17.5)	-126.6	0.31	C
B3-T: Striations & Tearing	3.25	4.16 (20)	352.5	0.53	Y
B4: Brace Fracture	3.95	4.16 (20)	132.1	0.20	Y

Key Observations

Cycle #	Displacement	Observations
0.5	-1.19”	Initial global buckling
1	3.56”	Bolt slip at north and south gusset plates Specimen experienced excessive yielding during large tensile displacement
1.5	0.59”	Moderate global buckling
17.5	0”	Initial minor cupping: ~1/8” deep
18.5	0”	Cupping: ~0.75” deep, 9” tall
19.5	-0.59”	Cupping: ~1.75” deep, 11” tall
20	4.16”	Fracture at peak tensile displacement

Test Results

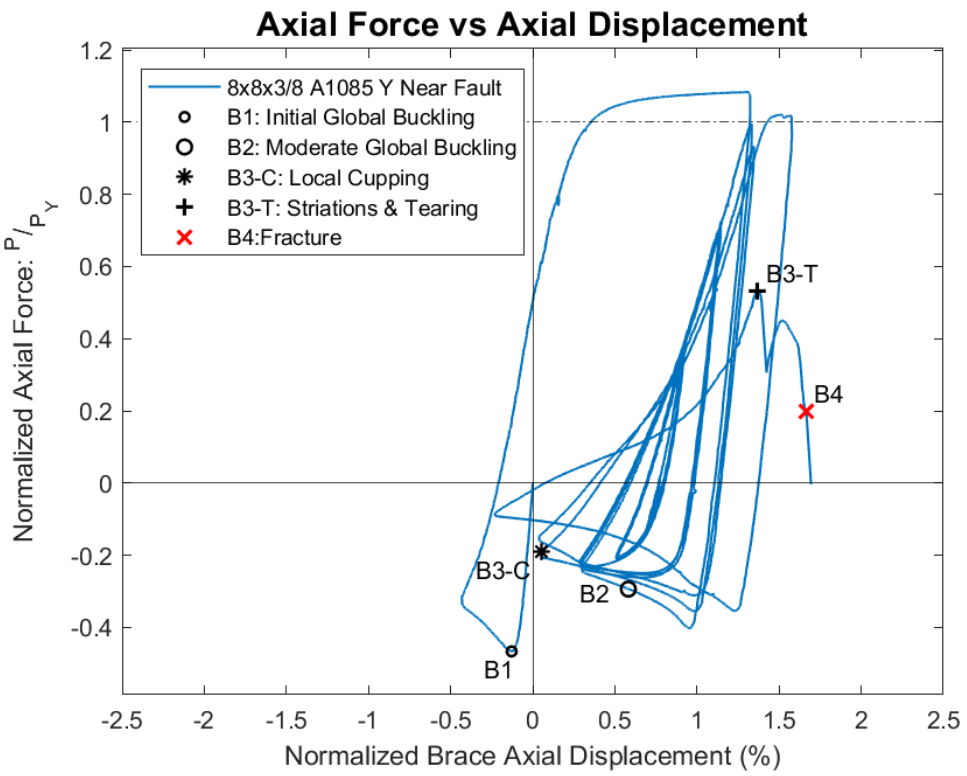

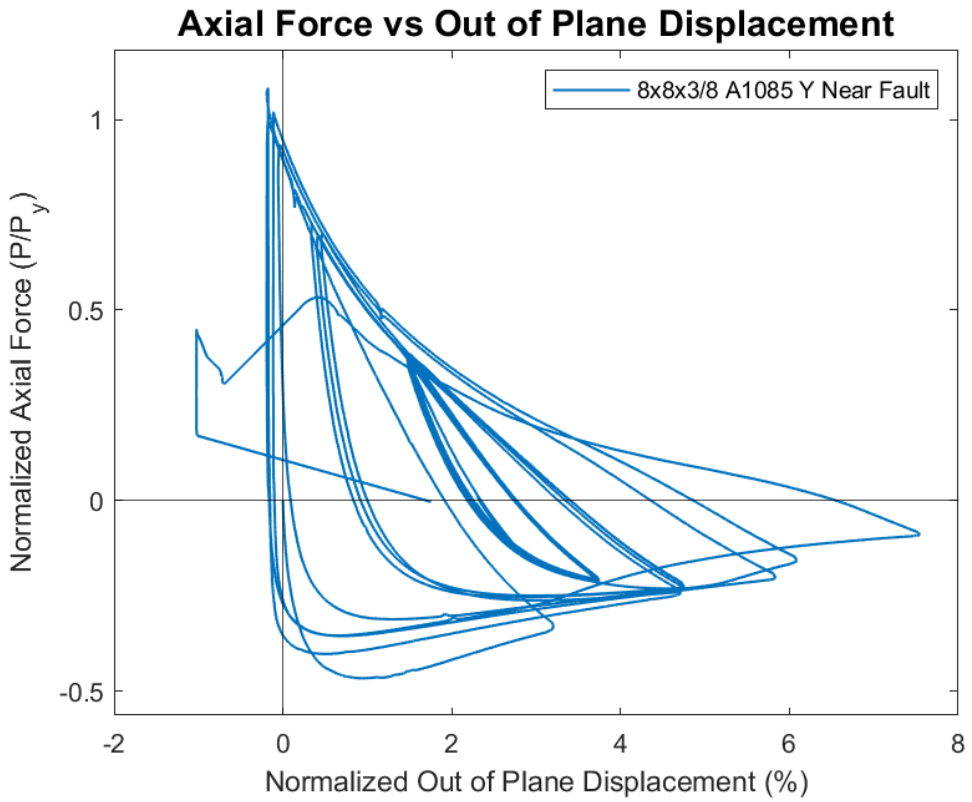

Photos

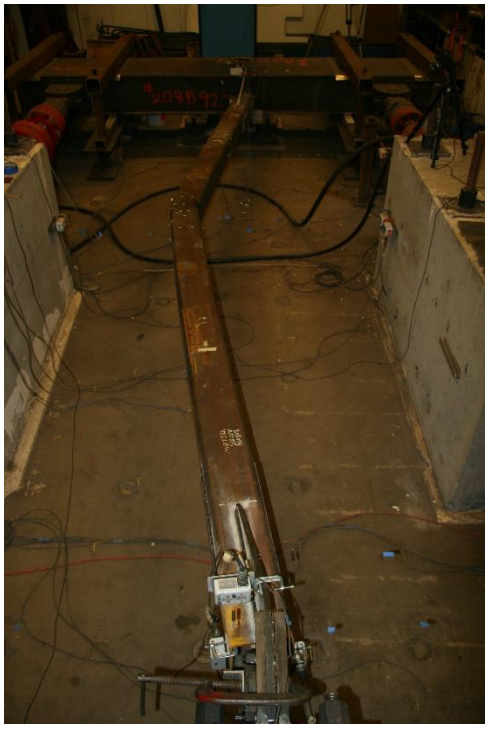

Max out of plane displacement: cycle 19.5

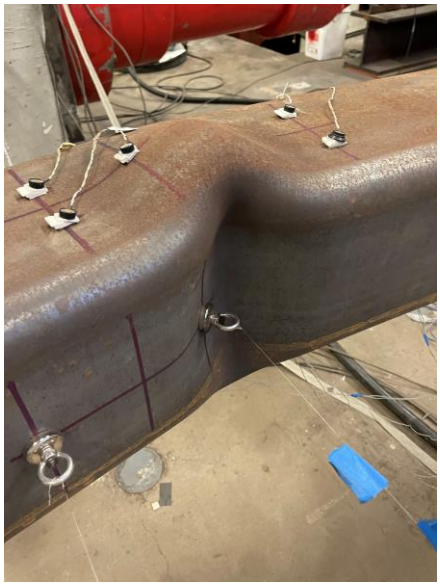

Major cupping during final compression cycle prior to fracture

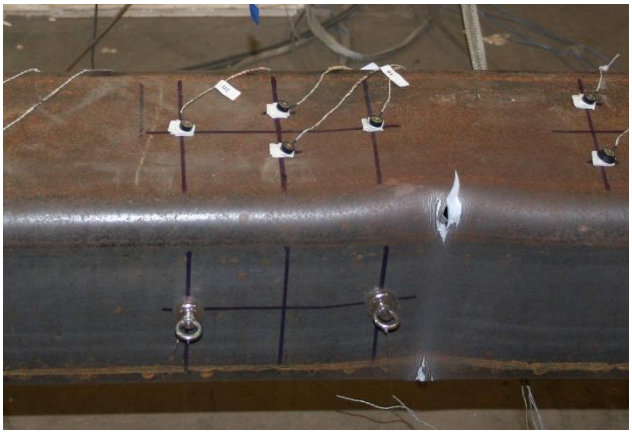

Initiation of tearing ~5” north of center of brace: cycle 20

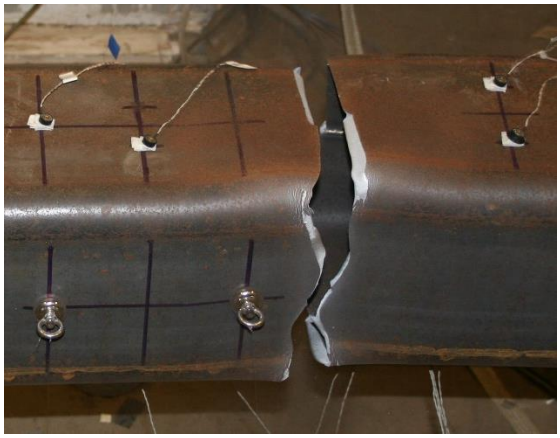

Fracture at ~ 4.00” displacement: cycle 20

5x5x3/8 A1085 Y "Short" Brace Test Summary

Test Name: 5x5x3/8 A1085 Y - Short
Test Date: 12/10/2021

Brace Properties

Measured Yield Stress (ksi)	66.04	**Area (in²)**	6.58
Measured Ultimate Stress (ksi)	74.62	**Moment of Inertia (in⁴)**	22.8
Yield Load (kips)	435.7	**Corner Radius (in)**	0.729
Critical Buckling Load (kips)	101.3	**Thickness - Nominal (in)**	0.375
Percent Elongation - 2" (%)	32.83	**Thickness - Measured (in)**	0.375
CVN Width (mm)	7.5	**Brace Compactness Ratio (*b/t*) - Nominal**	10.3
CVN Absorbed Energy (ft-lbs)	18.8	**Brace Compactness Ratio (*b/t*) - Measured**	9.42
Brace Length (in)	237.5	**Global Slenderness ratio (*KL/r*)**	127

Specimen Performance

Test Event	Axial Brace Deformation (in)	Target Displacement (in) (Cycle)	Force (kips)	$P / P_{Yield \mid Critical}$	
Peak Tension Load	1.37	1.738 (1)	438.58	1.01	Y
B1: Initial Global Buckling	-0.19	0.290 (1)	-140.80	0.83	C
B2: Moderate Global Buckling	-0.41	0.579 (1)	-113.70	0.67	C
B3-C: Local Cupping	-2.32	2.511 (1)	-43.27	0.26	C
B3-T: Striations & Tearing	3.30	3.670 (1)	388.63	0.89	Y
B4: Brace Fracture	3.64	4.056 (1)	78.10	0.18	Y

Key Observations

Cycle #	Displacement (in.)	Observations
5-6	0.290	Initial global buckling
9-10	0.483	Bolt slip at the north gusset plate, T1
11-12	0.579	Moderate global buckling, C1
21-22	2.511	Initial minor cupping: ~1/16" deep, C1 Cupping: ~1/8" deep, C2 Cupping observed at the center of the specimen
23-24	2.897	Cupping: ~3/16" deep, C1 Cupping: ~1/4" deep, C2
25-26	3.284	Cupping: ~5/8" deep, C1 Cupping: ~3/4" deep, C2

27-28	3.670	Striations observed on the corners of the east wall, T1 Cupping: ~1” deep, C1 Tore halfway thru, T2 Cupping: ~1.5” deep, C2
29	4.056	Fracture! at actuator displacement = 3.83”, T1

Test Results

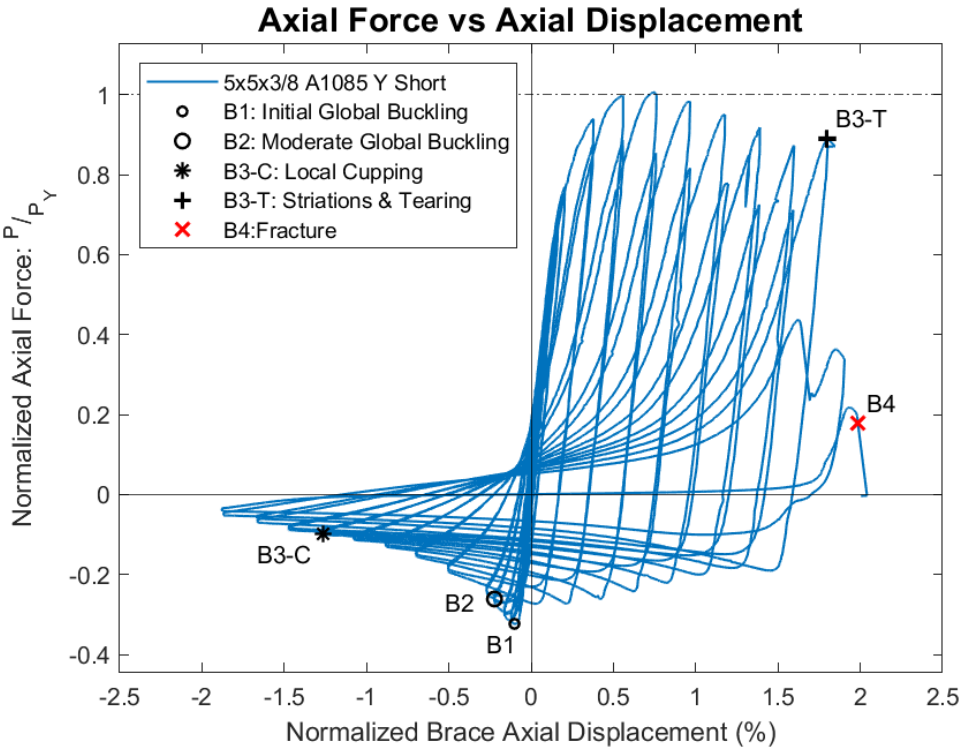

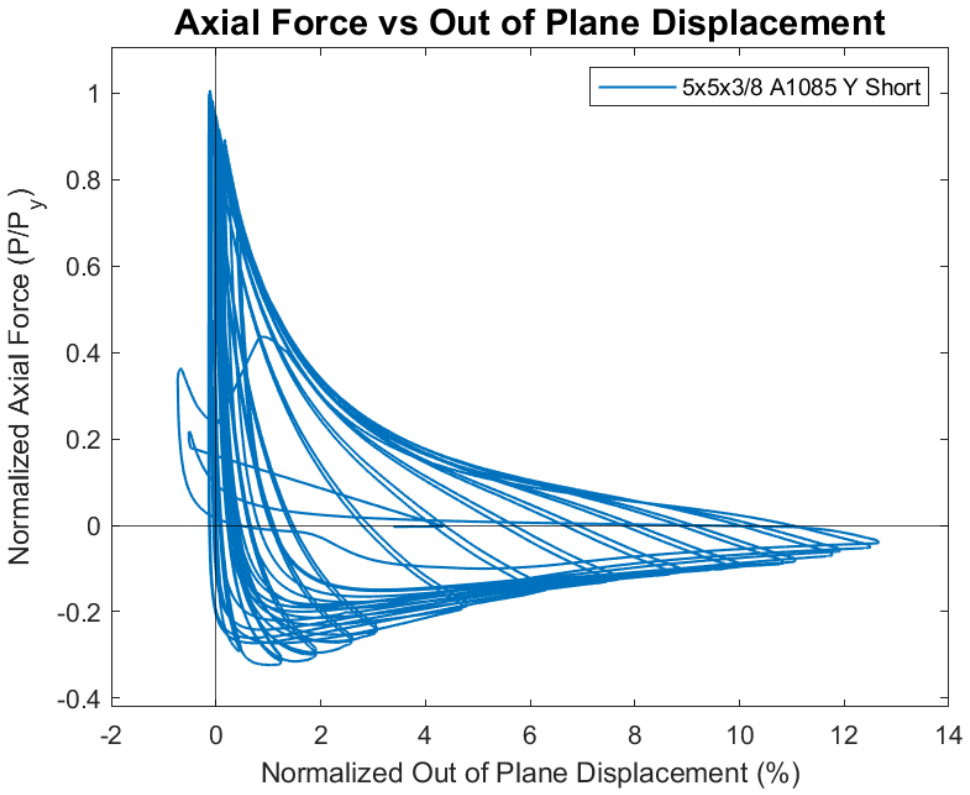

Photos

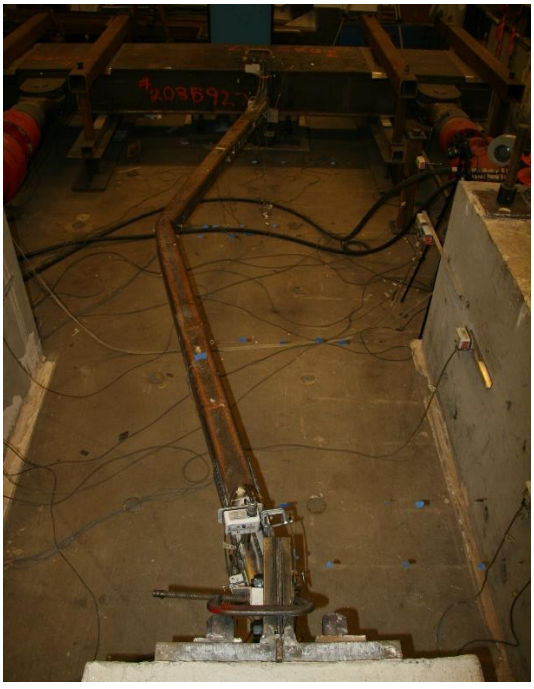

Maximum out of plane displacement: cycle 27

Major cupping at center of brace: cycle 27

Specimen tore thru east, bottom, and top walls: cycle 28

Fracture at the center of the brace: cycle 29

7x7x3/8 A1085 Y Short Brace Test Summary

Test Name: 7x7x3/8 A1085 Y - Short
Test Date: 12/14/2021

Brace Properties

Measured Yield Stress (ksi)	61.89	**Area (in²)**	9.58
Measured Ultimate Stress (ksi)	70.07	**Moment of Inertia (in⁴)**	68.7
Yield Load (kips)	577.1	**Corner Radius (in)**	0.906
Critical Buckling Load (kips)	292.2	**Thickness - Nominal (in)**	0.375
Percent Elongation - 2" (%)	31.32	**Thickness - Measured (in)**	0.365
CVN Width (mm)	7.5	**Brace Compactness Ratio (*b/t*) - Nominal**	15.7
CVN Absorbed Energy (ft-lbs)	17.3	**Brace Compactness Ratio (*b/t*) - Measured**	14.21
Brace Length (in)	183.5	**Global Slenderness ratio (*KL/r*)**	88.6

Specimen Performance

Test Event	Axial Brace Deformation (in)	Target Displacement (in) (Cycle)	Force (kips)	$P / P_{Yield \mid Critical}$	
Peak Tension Load	1.20	1.738 (1)	617.5	1.07	Y
B1: Initial Global Buckling	-0.23	0.386 (1)	-327.9	0.84	C
B2: Moderate Global Buckling	-0.84	0.966 (1)	-193.6	0.50	C
B3-C: Local Cupping	-1.33	1.352 (1)	-145.0	0.37	C
B3-T: Striations & Tearing	1.12	1.738 (2)	473.6	0.82	Y
B4: Brace Fracture	1.56	2.125 (1)	104.8	0.18	Y

Key Observations

Cycle #	Displacement (in.)	Observations
7-8	0.386	Initial global buckling, C1
9-10	0.483	Large bolt slip, north gusset plate: T1, C1, T2
11-12	0.579	Minor bolt slip, north gusset plate: T1
13-14	0.966	Moderate global buckling, C1
15-16	1.352	Cupping: ~1/8” deep, ~7.25” tall, C1 ~1/2” deep, ~7.75” tall, C2
17-18	1.738	Cupping: ~1.25” deep, C1 Tore thru east bottom corner. Striations on east top corner. T2 Cupping: ~1.5” deep; Wrinkling observed in cupping region, C2
19	2.125	Fracture! T1 at actuator displacement of 1.89” T

Test Results

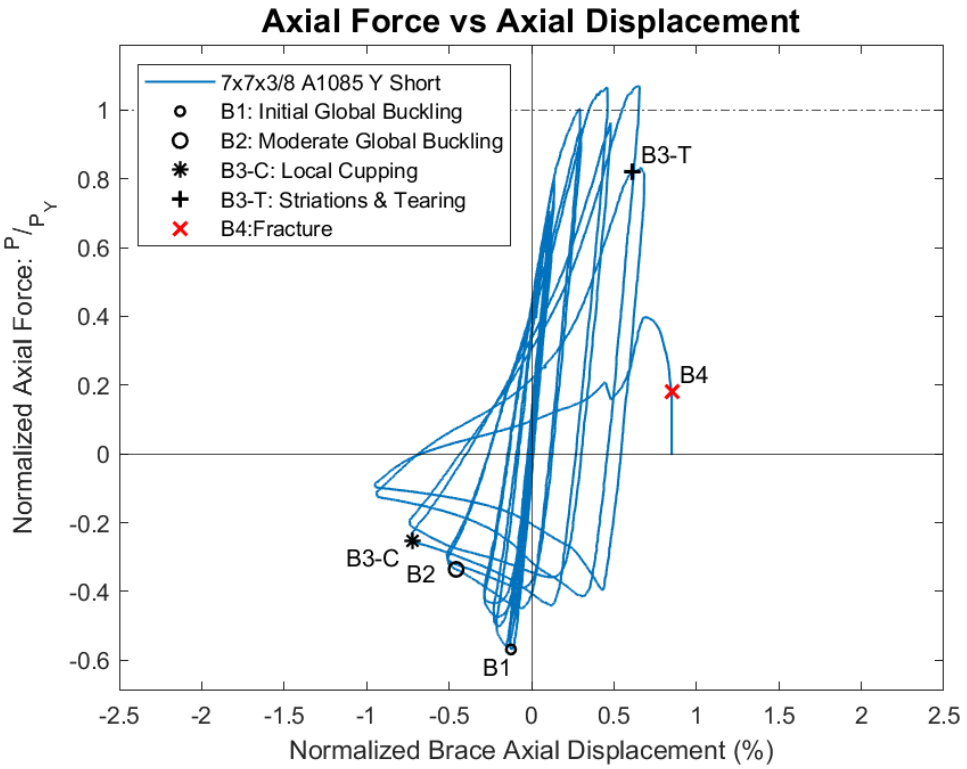

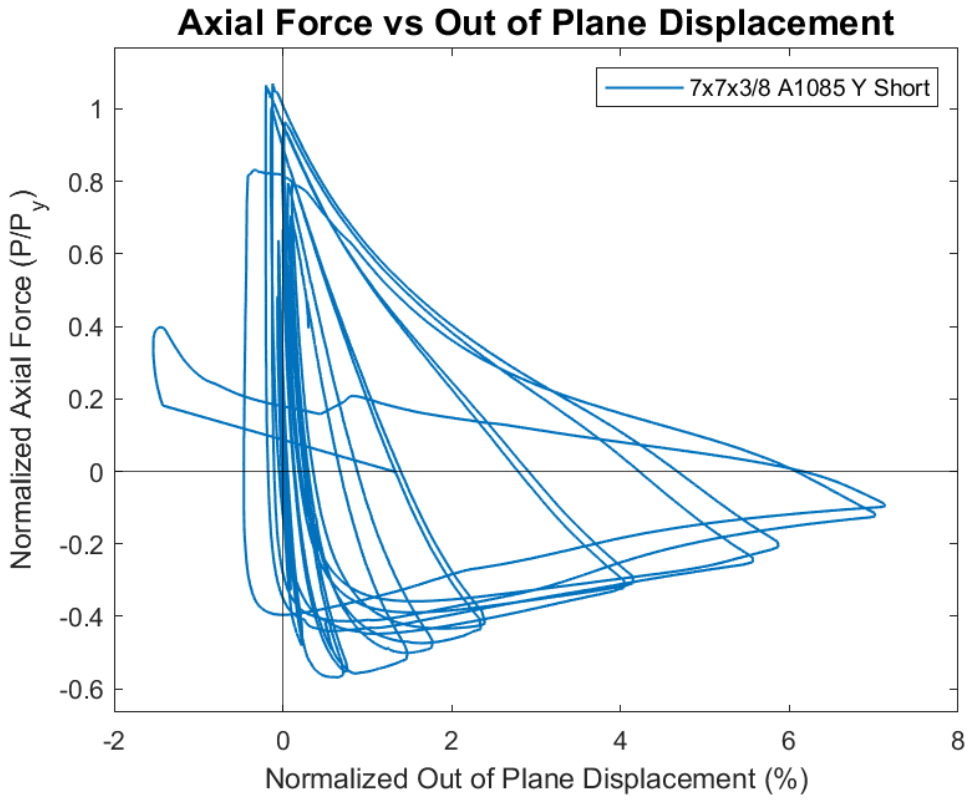

Photos

Initial tearing on east wall: cycle 17

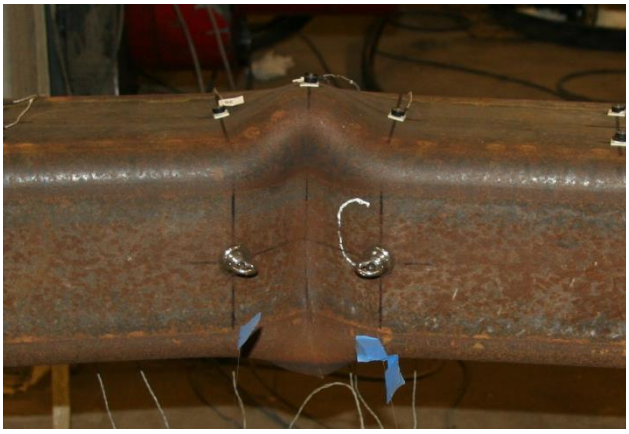

Major cupping at center of brace: cycle 17

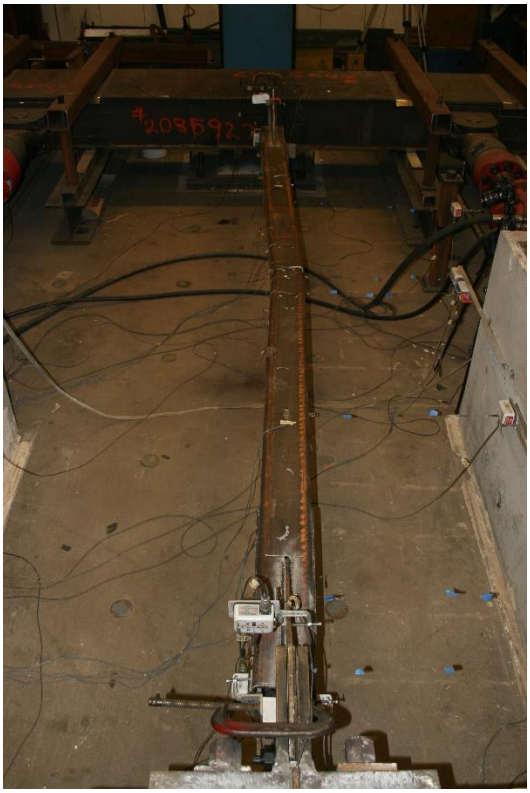

Brace tearing at incipient fracture: cycle 19

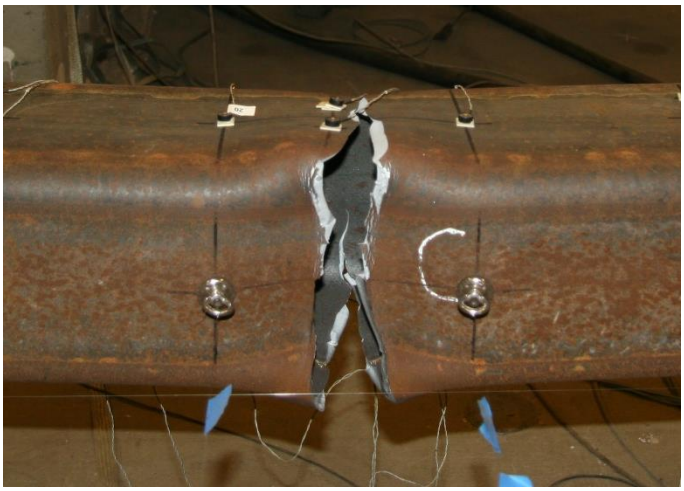

Brace tearing at incipient fracture: cycle 19

8x8x3/8 A1085 Y - Short Brace Test Summary

Test Name: 8x8x3/8 A1085 Y - Short
Test Date: 12/17/21

Brace Properties

Measured Yield Stress (ksi)	60.37
Measured Ultimate Stress (ksi)	72.12
Yield Load (kips)	661.2
Critical Buckling Load (kips)	404.3
Percent Elongation - 2" (%)	34.2
CVN Width (mm)	7.5
CVN Absorbed Energy (ft-lbs)	8.5
Brace Length (in)	183.5

Area (in^2)	11.1
Moment of Inertia (in^4)	106
Corner Radius (in)	1.06
Thickness - Nominal (in)	0.375
Thickness - Measured (in)	0.370
Brace Compactness Ratio (*b/t*) - Nominal	18.3
Brace Compactness Ratio (*b/t*) - Measured	15.89
Global Slenderness ratio (*KL/r*)	76.86

Specimen Performance

Test Event	Axial Brace Deformation (in)	Target Displacement (in) (Cycle)	Force (kips)	$P / P_{Yield \mid Critical}$	
Peak Tension Load	0.92	1.352 (1)	666.4	1.01	Y
B1: Initial Global Buckling	-0.29	0.483 (1)	-393.6	0.78	C
B2: Moderate Global Buckling	-0.88	1.352 (1)	-212.1	0.42	C
B3-C: Local Cupping	-1.24	1.352 (1)	-157.5	0.31	C
B3-T: Striations & Tearing	1.32	1.738 (1)	663.1	1.00	Y
B4: Brace Fracture	1.61	2.125 (1)	124.2	0.19	Y

Key Observations

Cycle #	Displacement (in.)	Observations
9-10	0.483	Minor bolt slip, south gusset plate: T1, C1, T2 Initial global buckling: C1
13-14	0.966	Bolt slip, north gusset plate: T1
15-16	1.352	Moderate Global Buckling: C1 Cupping, ~0.5” deep: C1 Cupping, ~1.5” deep: C2 Cupping observed at 3” south of center
17-18	1.738	Striations at east corners: T1 Cupping, ~2” deep: C1 Tore thru east, top, and bottom walls: T2 Did not measure cupping due to tearing: C2
19	2.125	Fracture at actuator displacement of 1.85” T

Test Results

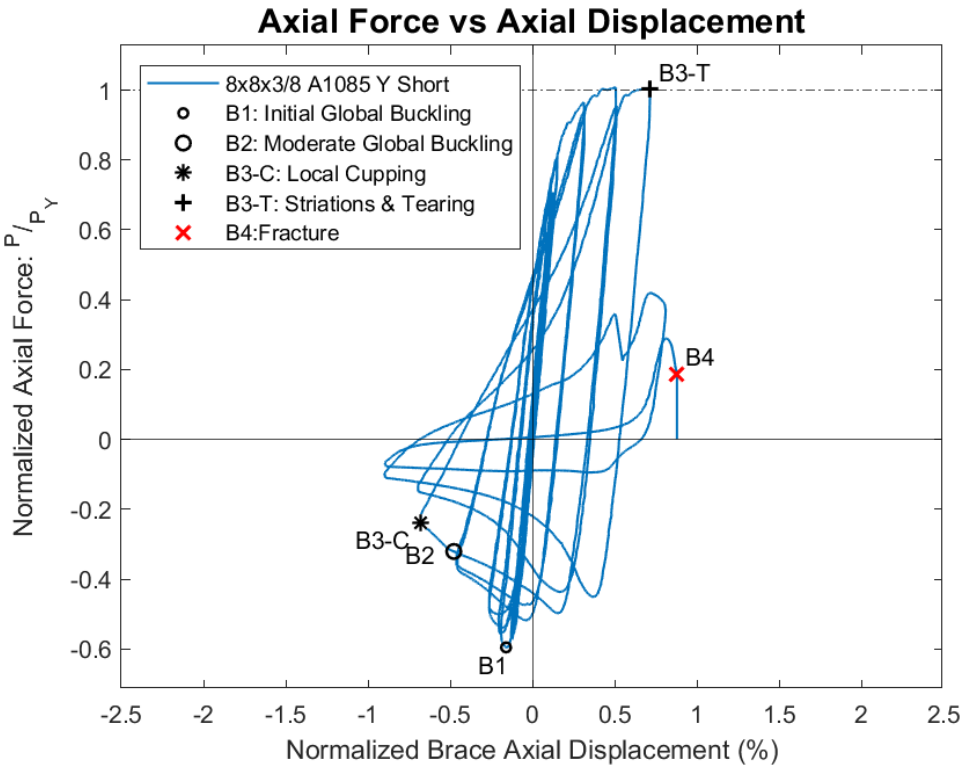

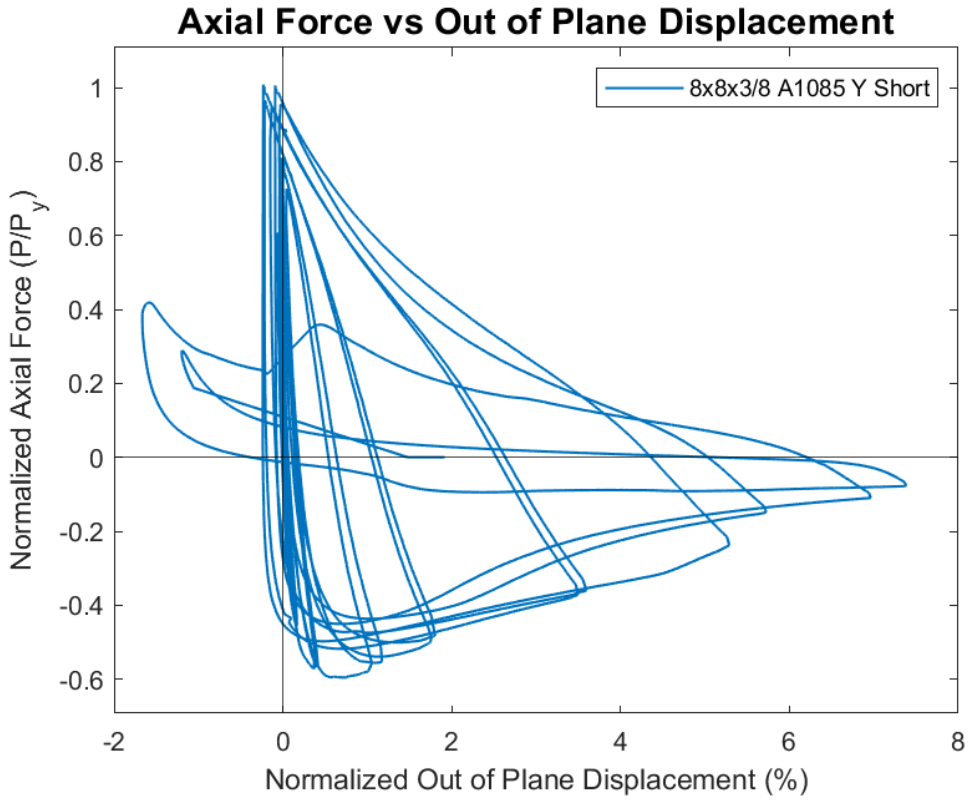

Photos

Maximum out of plane displacement: cycle 18

Striations forming on the corners of the east wall: cycle 17

Cupping and wrinkling following tearing: cycle 18

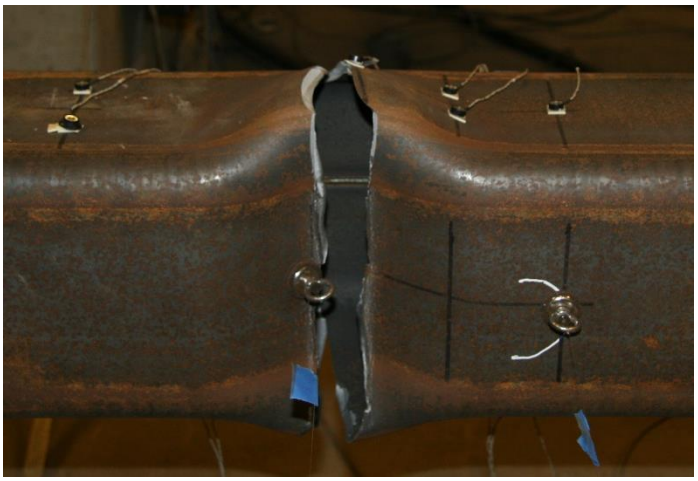

Tearing opening at incipient fracture: cycle 19